A. Weiss, T. Abel, V. Hill

The First Stars

Proceedings of the MPA/ESO Workshop held at Garching, Germany, 4-6 August 1999

Springer

Berlin Heidelberg New York
Barcelona Budapest Hong Kong
London Milan Paris
Santa Clara Singapore Tokyo

Preface

The First Stars mark the transition between the dark ages of the Universe and the appearance of the sky as we know it. They are enigmatic entities: neither their formation process, their initial mass function, nor their existence in the present universe are known with any certainty. On the other hand, one thing is certain – they did exist! It appeared to be a good idea to organize a meeting to try to address all these open questions, the main incentive for our plan being the wealth of abundance data about ultra-metal-poor halo stars, naturally thought to be closest to *The First Stars.*

It turned out, to our surprise, that the subject was interesting to a much larger community than we thought. In the end, instead of the 70 attendees expected, over 110 were present, with equal representation from the various fields involved: spectroscopic observations, stellar evolution, nucleosynthesis, star formation, galaxy evolution, structure formation. It appeared that this first meeting on *The First Stars* was held at a very opportune time to allow the different fields, where large progress has just been made in recent years, to interact and to exchange their views and results. This was an important aspect of the meeting: it gave us a coherent overview of the current knowledge – which probably is far less incomplete than we thought – about *The First Stars*. Indeed, during the meeting, several ideas, which have been around for some time, appeared to become questionable, probably the most important being those concerning age–metallicity relations ("Are the first stars the oldest or the most metal-poor ones?"), and where to find them ("Are some first stars forming right now in dwarf galaxies?").

The organizers were gratified by the excellent attendance, the very encouraging remarks concerning the meeting which they received both during and after the workshop, the excellent reviews and fascinating contributed talks and posters, as well as the friendly and constructive atmosphere during these three days. We thank all participants for making *The First Stars* the success it was.

The meeting would not have been possible in this form without the help and cooperation of many people, among them the members of the local and scientific organizing committees, and the conference secretary C. Rickl. Additional help came from M. Depner, C. Stoffer, M. Reuter, G. Wimmersberger and A. Stuiber, as well as support from the organizers of the first MPA/ESO-meeting (1998), T. Banday and M. Bartelmann. We wish to thank all of them.

Since the meeting took place immediately before Wednesday, August 11, 1999 – the day of the last total solar eclipse of the 20th century with the eclipse path running almost exactly through MPA and ESO – many participants remained in Garching to watch this event and to celebrate it with local colleagues. Unfortunately, the weather was very unpleasant and most of the eclipse was hidden behind thick rain clouds (the party, however, took place nevertheless). The LOC regrets this very much – however, this was the only thing we could not organize...

Garching, February 2000

Achim Weiss
Tom Abel
Vanessa Hill

The First Stars:

Local Organizing Committee:
A. Weiss (chair), V. Hill (co-chair), T. Abel, J. Bergeron, M.A.T. Groenewegen, C. Rickl, E. Tolstoy, S.D.M. White

Scientific Organizing Committee:
T. Abel, T. Beers, J. Bergeron, A. Burkert, C. Chiosi, H. Ferguson, T. Gehren, V. Hill, K. Nomoto, M. Rees, A. Renzini, S. Ryan, E. Tolstoy, A. Weiss, S.D.M. White, R. Wyse

Contents

Part I

The First Stars – Introduction and Context

Population III by Popular Demand – Progress and Previews

Timothy C. Beers

Department of Physics & Astronomy, Michigan State University,
E. Lansing, MI 48824 USA

Abstract. I discuss the ongoing search for stars of the Milky Way which have been referred to as members of Population III. Following a discussion of possible definitions for these stars, I consider the reasons why astronomers have undertaken this search, and list some of the numerous astrophysical uses of the extremely metal-poor stars which have been found along the way. I then review survey techniques which have been used in the past, and provide an update on plans for future investigations. Finally, the question of when one might consider the search for Population III FINISHED is addressed.

1 Introduction

The most metal-deficient stars in the Milky Way provide astronomers with a wealth of information on the early epochs of galaxy formation, the nature and interplay of various stellar populations, and even on the chemical composition of the (nearly) metal-free Universe shortly after the Big Bang. Since the topic of this meeting is the FIRST STARS to have formed in the Universe, in this brief review I consider several fundamental questions which must be addressed in order to make progress in our understanding of these objects: (1) What is a Population III star?, (2) Why search for Population III stars?, (3) How should we search for Population III stars?, and finally, (4) When do we stop the search for Population III Stars?

2 What IS a Population III Star?

Population III is a term which has taken on a variety of meanings in the past, as astronomers have refined their picture of early star formation in the Universe. Population III means different things to different people ! Among the definitions which have been employed:

- A star with metal abundance which is significantly less than the lowest abundance globular clusters ([Fe/H] ~ -2.5)
- A star of "pure" Big Bang composition – H, He, Li, and precisely ZERO heavier elements
- A star which was born within the first $10^6 - 10^7$ years following the Big Bang (independent of its metal abundance)

- A star which is no longer "living," but which was formed very early in the history of the Universe and *imprinted* telltale signs of its previous existence in the elemental abundance patterns of presently observable stars

If we take this last definition for a Population III star, it must be acknowledged that we will never be able to point our telescopes to a given position on the sky and directly examine the properties of the first stars to have formed in the Galaxy. For the theoretician, this is not particularly troublesome. For the observer, this is less than satisfactory. Since there is not a single star known to date which is widely agreed upon as being a member of Population III, we still have the luxury of choosing a working definition of what these objects might be. Exercising the unlimited optimism of the observational astronomer, I propose the following working definition for a *detectable* Population III star:

A Population III star is a presently-surviving (i.e., $\tau_{\rm ms} \geq 14$ Gyr) member of the very FIRST generation of stars born in the Galaxy, from gas of primordial abundance. In other words, a truly ZERO metal abundance star (for all intents and purposes, a star with a measurable atmospheric abundance [Fe/H]≤ -6.0).

Note that this definition implies a very specific set of requirements:

- The FMF (First Mass Function) must extend to include low mass stars with sufficiently long main-sequence lifetimes that survivors might be identifiable at present
- Pollution of a stellar atmosphere (either by intrinsic or extrinsic mechanisms) with metallic species subsequent to a star's formation cannot be effective (else we would never measure a star's atmospheric metal abundance satisfying the definition)

This definition is useful because it is testable. If, over the course of the extensive searches described below, astronomers still find themselves without a single Population III star to point their telescopes at, then we will have learned that one or both of the above requirements must not have been met in nature.

3 Why Search for Population III Stars?

Unfortunately, we cannot yet answer this question with the old standby "because they are there," as we don't yet know that ! However, even a completely unsuccessful search for Population III stars rewards astronomers with insight into a wide variety of astrophysical issues. From spectroscopic and photometric information gleaned from the "rejects" of searches for Population III stars one can extract nuggets of precious information. For example:

- The nature of the halo Metallicity Distribution Function (MDF) – how low can we go?
- Abundances of heavy metal species in the SECOND generation of stars
- Measurements of the primordial lithium abundance and limits on the flux of early Galactic cosmic rays
- Direct measurements of the elemental yields of early Type II supernovae, and the opportunity to unravel their mass distribution
- Identification of the astrophysical site(s) of the s-process(es)
- The nucleosynthesis products of the first AGB stars
- Identification of the astrophysical site(s) of the r-process(es?)
- Efficiency of mixing processes in the early Galaxy
- Measurement of elemental species (such as Zn) which are used to explore gas abundances along lines of sight toward distant QSOs
- Estimation of hard lower limits on the age of the Galaxy and the Universe from the use of light- and heavy-element chronometers
- Evidence for the existence and nature of the metal-weak tail of the thick disk of the Galaxy
- Measures of the halo and thick disk velocity ellipsoids, and their alteration with Galactocentric distance
- Examination of kinematic constraints on the so-called "counter-rotating high halo" and other evidence, such as kinematic substructure, of past and present mergers of the Galaxy with smaller satellites

Many of the above issues are discussed in this volume. In this review I discuss the stars which form the observational database upon which such investigations are based.

4 How Should We Search for Population III Stars?

Ever since astronomers realized that extremely metal-poor stars are rare, but identifiable, members of the presently observable Milky Way, we have been working hard to devise effective survey strategies to ferret them out in ever increasing numbers. Quite independent of the techniques applied, there emerge two fundamental "barriers" which must be overcome in order for a search to be successful:

- A successful survey technique must maximize the "effective yield" (EY) of interesting candidates, so that large amounts of telescope time are not wasted obtaining follow-up observations of stars which turn out not to be of interest
- A successful survey technique must be applied to a large fraction of (at least) the high Galactic latitude sky, so as to obtain a significant increase in the numbers of recognized extremely metal-poor stars

For the purposes of this discussion, let us define the effective yield of a given survey as:

$$\mathrm{EY} = \frac{[\#\ \text{stars with [Fe/H]} \leq -2.0]}{[\text{total}\ \#\ \text{of targeted stars}]} \tag{1}$$

For an efficient follow-up campaign, an "ideal" EY would be higher than 50%. This has not yet been achieved, but should be possible with concentrated effort. Past experience suggests that it is often difficult to obtain sufficient telescope time for the demonstration and refinement of a new survey technique (especially when one is confined to shared, rather than private, observatories). The end result is that compromises are made in the EY of the survey. This is a most unfortunate reality.

The "sky coverage barrier" has resulted in surveys which require many years, if not decades, to come to fruition. This is a particularly acute problem when one is relying on shared facilities. My involvement with the HK survey, for example, began in 1983 (as an exercise in learning a spectrographic data reduction software package in those pre-IRAF/MIDAS days we would all like to forget). Over the past (gasp) 16 years, the follow-up efforts from the HK survey have expanded to involve over 30 astronomers working with $\sim$ 15 different telescope/detector combinations, with the final total number of (medium-resolution) spectroscopic observations reaching roughly 5000 stars. I am extremely grateful for the patience of those collaborators who have "stayed the course" throughout this long journey. We have succeeded in identifying over 100 stars with $\mathrm{[Fe/H]} < -3.0$, a few stars near $\mathrm{[Fe/H]} = -4.0$, and of course, many other interesting stars of somewhat higher abundance.

Within the next 2-3 years, ALL of the presently-recognized stars with abundances $\mathrm{[Fe/H]} < -3.0$ will be observed at high resolution (and presumably with exquisite signal-to-noise ratios) with new-generation telescopes. This is a sobering statement ! I address what might be done about this state of affairs in a separate contribution to this volume.

4.1 Searches in the Past

Before we consider new strategies in the search for Population III stars, it is instructive to consider the approaches which have been employed in the past. Space precludes a complete discussion, but a list of previously-applied survey techniques would include the following.

"Informed Serendipity." This term (first used in this context by John Norris), refers to the targeting of a small number of candidate stars with characteristics which are suggestive of the most extreme metal-poor stars. For example, the discovery that G64-12 is a main-sequence dwarf with abundance $\mathrm{[Fe/H]} \sim -3.5$ came from an investigation of stars with the largest known space motions [9]. The most metal-deficient giant yet known, CD$-$38:245, with [Fe/H] ~ -4.0 [5], came from a limited follow-up of stars identified from the Slettebak & Brundage [24] prism survey, and noted by them as having "a continuous spectrum" but shown by Graham & Slettebak [16] to have colors typical of a rather late-type star. In spite of great observational effort since then, there are presently only a handful of stars known with metallicities at or below [Fe/H] $= -3.5$. "Informed Serendipity" is a powerful technique.

High Proper Motion Samples. Spectroscopic surveys of stars selected to have high proper motions have provided roughly 10% of the known stars with [Fe/H] ≤ -2.0. Examples of such surveys include the lists of Luyten proper motion stars in the southern hemisphere studied by Ryan & Norris [23], and the Giclas proper motion sample in the northern hemisphere investigated by Carney et al. [10] . Unfortunately, the EY of these surveys is not particularly high.

Wide-Field Objective-Prism Surveys. Photographic objective-prism surveys over large areas of sky, based on widened spectra and a visual selection technique, have provided the majority of the presently known extremely metal-poor stars. One example is the survey of Bond [6,7], which resulted in the identification of samples of metal-poor stars that continue to be discussed in the modern literature, but which only contained a relatively small number of stars with [Fe/H] at or below -2.5, leading Bond to ask "Where Is Population III?" [8].

George Preston suggested a slightly modified version of this approach, employing an interference filter in the focal plane, used in combination with the objective prism. This effort, now known as the HK survey (formerly referred to in the literature as the Preston-Shectman survey), was able to go several magnitudes deeper than the Bond survey, and has been described in detail in Beers et al. [1–3]. This technique has been successful in the identification of roughly 1000 halo stars with [Fe/H] < -2.0, and has provided the majority of targets of immediate interest for high-resolution spectroscopic study with the new-generation 8m-class telescopes (such as VLT, SUBARU, and GEMINI) which are now coming online.

Based on numbers presented in Table 1 of [3], the EY of the HK survey is on the order of 22%, so roughly twice that of proper-motion selected samples, but still at least a factor of two smaller than the ideal case. The careful reader of this table will note a rather wide variation in EY among the groups which carried out the spectroscopic follow-up campaigns. This variation arises, in the main, because not all groups were in a position to conduct a photometric pre-selection of the original HK survey candidates prior to obtaining spectroscopy, a filtering process which can effectively eliminate stars which are either too hot or too cool to be of interest. When a photometric pre-filtering *was* done (e.g., the BPS and ANU groups), the HK survey achieved an EY of $\sim 32\%$.

We are presently obtaining digital scans of the HK survey plates using the APM facility in Cambridge. Color calibrations of direct sky survey plates in the northern and southern hemisphere are expected to be completed shortly as well. With this data in hand, we should be able to recover a large fraction of the cooler metal-deficient stars on the HK survey plates which were missed during the visual selection procedure. Preliminary results of an artificial neural network analysis of this data has been presented in [21]. All indications are that the EY resulting from this procedure should reach close to 50%.

4.2 Searches in the Future

How can we do better? There are a number of surveys which are just getting underway that hold the promise of dramatically increasing the numbers of known extremely metal-poor stars, and, perhaps, will result in the discovery of a *bona-fide* Population III star.

The Hamburg/ESO Survey. The Hamburg/ESO Stellar Survey (HES) described by Christlieb et al. (this volume, and references therein) is based on automated scans of *unwidened* wide-field objective-prism plates, covers essentially the entire southern Galactic cap, and reaches a limiting magnitude of $B \sim 17 - 17.5$, 1-1.5 magnitudes fainter than that reached by the HK survey. Since each one magnitude interval in limiting magnitude results in an increase in survey volume of a factor of 4, one might expect the HES to eventually identify on the order of $\sim 5 - 10$ times as many extremely metal-poor stars as the HK survey. Of course, eventually one reaches distances where the rapidly falling density profile of the stellar component of the halo limits the increase in the numbers of interesting stars to be detected at fainter apparent magnitudes. The real advantage of the HES over the HK survey is due to the quality of the prism spectra, their greater wavelength coverage, and the automated selection criteria. These advantages assure that low-metallicity candidates can be selected without the introduction of a metallicity-temperature bias, a further limitation of the (visual) HK survey. As a result, the expected EY of interesting metal-poor stars from the HES survey should be substantially higher than that of the HK survey. Tests of the EY are presently being conducted.

Broad-Band Colorimetric Surveys. Since we believe that Population III stars (according to the above definition) are most likely to be found in the halo of the Galaxy, it makes sense to conduct surveys for possible candidates *in situ*. One efficient way to do this is by a careful pre-selection of stars which are, for example, main-sequence dwarfs near the tip of the halo turnoff, and that exhibit colors consistent with a complete (or nearly complete) absence of heavy metals in their atmospheres. Accurate broad-band photometry is now becoming a reality for literally hundreds of millions of stars with the advent of the Sloan Digital Sky Survey (SDSS). As described in [18], properly combined filter observations of faint halo stars should be able to readily separate stars with abundance [Fe/H] ≤ -2.0 from those above this value. Although there is expected to be little sensitivity to metallicity below –3.0, the large lists of candidate metal-poor stars to be generated from SDSS will provide very attractive targets for future study. The EY of the SDSS lists of metal-poor stars has yet to be determined, and tests of the variation of the EY with apparent magnitude (due to the greater photometric errors for the fainter stars, and to the potential intrusion of large numbers of fainter stars of normal metal abundance into the sample) have yet to be carried out, but all present indications at present are encouraging.

Low mass M-type stars potentially comprise the *dominant* stellar component of the Milky Way halo, yet only recently has their nature come under scrutiny. Because of their great numbers, and under the assumption that the FMF does not change significantly at low abundances, the sdM stars provide excellent samples for examination of subtle variations in the halo MDF as a function of distance, and in the search for Population III. At present only a handful of sdMs are known with [Fe/H] ≤ -1.0, mostly from spectroscopic examination of high proper-motion catalogs [13]. However, Gizis [14] has shown that sdMs can be readily recognized from inspection of various two-color planes (e.g., $J - H$ *vs.* $H - K$), and further, that reliable estimates of abundance can be obtained from moderate-resolution spectroscopic analysis of their molecular bands (CaH, TiO) in the spectral region $6300 \leq \lambda \leq 7200$ Å . It has been estimated that on the order of 15,000 sdMs with [Fe/H] ≤ -1.0 can be identified from follow-up spectroscopy of candidates selected from the recently-initiated 2Mass survey [15]. We await the initiation of a dedicated spectroscopic follow-up campaign in order to test the EY of this approach.

Narrow-Band Colorimetric Surveys. McWilliam and collaborators have begun exploring the use of a narrow-band filter, centered on the stellar CaII H and K lines to obtain CCD photometry of stars, and thereby select extremely metal-poor stars by the lack of strength in these resonance lines [19]. The first application of this technique to stars in the Galactic bulge and in nearby dwarf galaxies appears quite promising. Again, the crucial issue will be the demonstration of a useful EY for this approach.

Wide-Field Spectroscopic Surveys. Single-slit spectroscopic follow-up of the large numbers of newly-identified candidate extremely metal-poor stars from the surveys described above would be a daunting observational task. Fortunately, a far more efficient follow-up technique is now feasible. The pioneering work of Watson and Parker has given the astronomical community the FLAIR II wide-field spectrograph, now in operation at the UK Schmidt in Australia. Recent approval of the AAT Board for preparation of a robotic fiber positioning system for the FLAIR II instrument will result in a new six-degree field (6DF) instrument to be in place in late 1999 [25]. By early 2000, it is anticipated that the 6DF will be in routine operation. With the benefit of a CCD upgrade, and some 150 active fibers, acceptable integration times will yield ~ 2 Å resolution spectra of stellar sources down to $B = 16.5$. One interesting challenge remains: filling all the fibers on the 6DF with useful target stars ! Clearly, the optimal approach is to combine catalogues extracted from projects with similar wavelength and resolution requirements. The large numbers of stars to come from the digital HK survey, the HES, the southern-most (and brighter) stars from the SDSS, as well as additional proper-motion selected stars, suggest themselves. The sdM stars, owing to their lack of flux in the blue, would probably have to be undertaken as a separate survey. Obviously, developing a similar instrument to the 6DF to be used on northern-hemisphere Schmidt telescopes should be given high priority as well.

There is little doubt that the search for Population III stars will reach a pinnacle with the successful operation of planned space-based survey instruments such as GAIA [12]. The possibility of obtaining medium-resolution spectroscopy (as well as proper motions, and accurate astrometry) for up to 10^7 stars down to 17th magnitude will revolutionize Galactic astronomy in virtually every way. Assuming a successful mission, one might predict an EY approaching 100%.

4.3 Are We Looking in the Right Place?

The results of the HK survey indicate that the lowest abundance stars which are presently to be found in the Galaxy terminate at around [Fe/H] $= -4.0$, well above the metallicity we would associate with true Population III [3]. However, it must be kept in mind that the HK survey only identifies halo stars no greater than 5-10 kpc from the Sun (for giants; 1 kpc is the approximate limit for main-sequence turnoff stars in the halo). It may well be the case that such locally-selected samples of stars are not representative subsets of the most metal-deficient stars to be found in the Galaxy. One additional complication has now become clear – the thick disk of the Galaxy (which has a space density up to 50 times that of the halo component in the solar neighborhood) does indeed possess a metal-weak tail (see Chiba, this volume, and references therein), at least down to [Fe/H] ~ -2.0. The effect of these local "contaminants" from the thick disk may artificially boost the apparent numbers of metal-poor stars in the solar neighborhood to such a degree that extrapolations of the MDF based on local samples may in fact be using an incorrect "normalization," and we may have to contend with problems of interpretation.

Tests of whether or not the local volume is a fair subsample will only come when samples of much fainter stars, located 10's of kpc away, become available. Some information is potentially available from the existing samples, based on their kinematics. One could, for example, test if the MDF of stars on orbits which take them well outside the solar neighborhood differs greatly from that of stars which are confined to several kpc away. As some have speculated [20], if the epoch of ultra metal-poor star formation precedes the dissipative formation of galaxies (as is likely if early generation stars are the sources of the ionizing background radiation at $z > 5$), then the most metal-deficient stars may fact be distributed rather similarly to the dark matter itself, i.e., with a much broader spatial distribution than the majority of luminous halo stars. If this is the case, searches for Population III will only succeed when they probe the VERY faint stars in the outskirts of the Galaxy.

4.4 Are We Looking for the Right Thing?

Thus far, our discussion has been predicated on the assumption that the surface abundances of heavy elements in low-mass halo stars do not change over time (the second of our requirements for a "detectable" Population III star). There is evidence now accumulating to suggest that this may in fact *not* be true.

4.5 Intrinsic Pollution

New stellar evolution models for extremely metal-poor stars [11] suggest that enhanced mixing at the time of helium-core flash may result in the conversion of some quite metal-deficient stars into carbon-enhanced stars, a mechanism which might explain the fact that ~25% of the stars in the HK survey with [Fe/H] ≤ -3.0 exhibit strong C and N features in their spectra [22]. The tantalizing possibility is that ALL low mass stars with [Fe/H] ≤ -4.0 undergo this conversion, which means that in order to find the stars of Population III, we should be searching for the most metal-deficient CARBON stars in the Galaxy. The HES discussed above is able to preferentially select such stars based on the presence of strong CH G-bands in their spectra, hence a dedicated follow-up of these candidates may prove quite interesting.

4.6 Extrinsic Pollution

Other mechanisms by which stars which were born with [Fe/H] ≤ -6.0 might be missed in present-day searches for Population III have been discussed in the literature. One idea [26,17] is that, over their extended lifetimes, Population III stars which repeatedly pass through the gradually more metal-enriched ISM of the Galactic disk could accrete sufficient amounts of heavier metals onto their atmospheres to boost their observed atmospheric abundances to [Fe/H] > -4.0. We now have sufficiently large samples of metal-poor stars to test such a hypothesis. For example, one might compare the MDF of main-sequence dwarfs (which to first order should retain evidence of the accreted material on their surfaces) with that of evolved giants (which should mix the accreted material because of their convective envelopes) – the expectation being that the dwarf MDF should be truncated and lack a tail at lower metallicity when compared to the giant MDF. Another test would be to compare the abundance distribution of main-sequence dwarfs which populate "plunging" orbits, and hence spend a tiny fraction of their time passing through the Galactic disk (and do so at high velocity) with that of similar stars which spend their lifetimes on orbits which continually bathe them with disk ISM, hence maximizing the possibility for accretion. Large catalogs of metal-poor stars with available space motions [4] should provide useful samples for such an investigation.

5 When Do We Stop the Search for Population III Stars?

Now seems an appropriate time to consider the longer-term prospect for conducting searches for evidence of the elusive Population III. Below I consider four possible "termination points."

5.1 Now?

I am asked all of the time whether or not we have identified a sufficiently large number of extremely metal-poor stars already. The answer I give is always the same, a resounding "NO !". The samples we have assembled over the past two decades have certainly opened investigations which may in fact resolve a number of the long-standing questions of early Galactic nucleosynthesis. However, as soon as one moves beyond the most obvious questions, and begins to subdivide the existing samples of extremely metal-poor stars based on, for example, (1) their kinematics and orbital families, (2) their light- and heavy-element abundance patterns, or (3) their present evolutionary states, it becomes obvious that the individual subsamples are going to be far too small to obtain adequate descriptions of general patterns.

As mentioned above, the blue-sensitive, high resolving-power spectrographs such as UVES on the VLT-UT2, HDS on SUBARU, and HROS on GEMINI, will shortly provide astronomers with high-resolution data for the entire sample of Galactic stars which are known at $[Fe/H] < -3.0$. If, at the end of this time, we expect to have unanswered questions about the nature of the early Galaxy as revealed by observations of the most metal-deficient stars (and who does *not* expect this?), there will exist a need for at least another several hundred stars with $[Fe/H] \leq -3.0$. Given the minimum several-year lead time which is required to assemble such samples, now is the time to re-double our efforts.

5.2 In the Near Future, ∼5–10 Years?

The next decade will be a transition period for studies the first stellar populations of the Galaxy. Large surveys of the type I have described above should be brought to completion by this time. This will not happen automatically, of course. As a community, it is important that we utilize the survey telescopes of the future – the 4m class telescopes of today – to obtain the medium-resolution spectroscopy and photometry which is required to fully exploit the dedicated searches for Population III. We encourage telescope time allocation committees to consider the "fast rather than faint" model for assigning access to those who wish to pursue the long-term follow-up observations which will be needed to make significant progress.

One can safely predict an explosion of detailed understanding of the elemental abundances of first- and second-generation stars from the data flow generated by 8m-10m class telescopes. The era of space-based survey missions will be upon us, and ground-based surveys will have less and less impact on the continued searches for Population III, at least for stars of apparent magnitude < 17.

5.3 In the Distant Future, ∼10–15 Years?

GAIA, and other missions (such as SIM) will be well underway, and perhaps completed. One might speculate that astronomers, by this time, should have intimate knowledge of the nature of the early Galaxy, and Universe. Perhaps this will be so. Experience suggests, however, that the deluge of new information acquired will show us the "mistakes of the past" and suggest interesting new avenues for future observational campaigns.

5.4 Never

Never is a long time, but I suspect that the search for Population III, and the knowledge obtained about the nature of the extremely metal-poor stars of the Milky Way, will continue to amuse, delight, perplex, and hopefully, enlighten astronomers for a long time to come. This is where the smart money is going.

References

1. Beers, T.C., Preston, G.W., Shectman, S.A. (1985) AJ 90, 2089
2. Beers, T.C., Preston, G.W., Shectman, S.A. (1992) AJ 103, 1987
3. Beers, T.C. (1999) Third Stromlo Symposium: The Galactic Halo, eds. B. Gibson, T. Axelrod, M. Putman (ASP, San Francisco), 165, p. 206
4. Beers, T.C., Chiba, M., Yoshii, Y., Platais, I., Hanson, R.B., Fuchs, B., Rossi, S. (1999) AJ, submitted
5. Bessel, M.S., Norris, J.E. (1984) ApJ 285, 622
6. Bond, H.E. (1970) ApJS 22, 117

7. Bond, H.E. (1980) ApJS 44, 517
8. Bond, H.E. (1981) ApJ 248, 606
9. Carney, B.W., Peterson, R.C. (1981) ApJ 245, 238
10. Carney, B.W., Latham, D.W., Laird, J.B., Aguilar, L.A. (1994) AJ 107, 2240
11. Fujimoto, M., Aikawa, M., Iben, I., Jr. (1999) Third Stromlo Symposium: The Galactic Halo, eds. B. Gibson, T. Axelrod, M. Putman (ASP, San Francisco), 165, p. 243
12. Gilmore, G.F. et al. (1998) SPIE 3350, 541
13. Gizis, J., Reid, N. (1996) AJ 111, 365
14. Gizis, J. (1997) AJ 113, 806
15. Gizis, J. (1998) private communication
16. Graham, J.A., Slettebak, A. (1973) AJ 78, 295
17. Iben, I., Jr. (1983) Mem. Soc. Astr. Italiana 54, 311
18. Lenz, DD., Newberg, H.J., Rosner, R., Richards, G.T., Stoughton, C. (1998) ApJS 119, 121
19. McWilliam, A. (1998) private communication
20. Rees, M.J. (1998) Space Science Reviews, 84,43
21. Rhee, J., Beers, T.C., Irwin, M., (1999) BAAS 31, p. 971
22. Rossi, S., Beers, T.C., Sneden, C. (1999) Third Stromlo Symposium: The Galactic Halo, eds. B. Gibson, T. Axelrod, M. Putman (ASP, San Francisco), 165, p. 268
23. Ryan, S.G., Norris, J.E. (1991) AJ 101, 1835
24. Slettebak, A., Brundage, R.K. (1971) AJ 76, 338
25. Watson, F. (1998) AAO Newsletter, 85, 11
26. Yoshii, Y. (1981) A&A 97, 280

Did the Universe Start at Zero Metallicity?

Karsten Jedamzik

Max-Planck-Institut für Astrophysik, 85740 Garching, Germany

Abstract. Standard Big Bang nucleosynthesis predicts an essentially zero primordial metallicity. I speculate on possible metal (i.e. nucleon number $A \geq 12$) production in scenarios of inhomogeneous Big Bang nucleosynthesis. It is conceivable, though not necessarily probable, that some primordial metallicity is synthesized if a small fraction of all cosmic baryons reside in very high-density regions. Such conditions could possibly result from the evaporation of some baryon-number carrying soliton prior to the epoch of Big Bang nucleosynthesis.

It is widely accepted that an era of big bang nucleosynthesis (hereafter; BBN) between cosmic temperatures $T \sim 1$ MeV and $T \sim 10$ keV is the production site of the bulk of ^{4}He and ^{3}He, a good fraction of ^{7}Li, and essentially all ^{2}H observed in nebulae and stars in the present universe. Generally good agreement between observationally inferred primordial abundances and theoretical predictions for ^{2}H, ^{4}He, and ^{7}Li may be obtained within a standard homogeneous BBN scenario with baryon-to-photon ratio η in the range $2 \times 10^{-10} - 6 \times 10^{-10}$ [1] (most likely towards the upper end of this range), though details of the observational determination of primordial abundances and the question about consistency within a standard BBN scenario remain under investigation. Primordial conditions as envisioned in a standard BBN scenario yield only production of minute amounts of isotopes with nucleon number $A > 7$. For a baryon-to-photon ratio of $\eta \approx 4 \times 10^{-10}$ synthesis of a ^{12}C mass fraction of only $X_{^{12}C} \approx 5 \times 10^{-15}$ results. There is also production of trace amounts of ^{6}Li, ^{9}Be, and ^{11}B, with typical mass fractions $\sim 10^{-16} - 10^{-13}$. In contrast to stellar nucleosynthesis, the three-body triple alpha process is not operative in standard BBN, mainly due to the small densities ($\sim 10^{-5}$g/cm^3 at $T \approx 100$ keV) and short expansion time (~ 100 s). A potentially different way of bridging between light and "heavy" ($A \geq 12$) elements across the mass eight gap is via the reaction sequence ^{7}Be $\rightarrow$ ^{11}C $\rightarrow$ ^{11}B $\rightarrow$ ^{12}C. This reaction chain is, nevertheless, ineffective in a standard BBN since build-up of ^{7}Be occurs late at $T \sim 50 - 100$ keV where Coulomb barrier effects prevent further processing of this isotope into heavier ones.

One may pose the following question: *Which alternative BBN scenarios would give substantial initial metal production, without violating observational constraints on the light elements?* Here "metal"refers to isotopes with nucleon number $A \geq 12$ and by the term "substantial " it is meant that production would result in abundance which could either be directly observable in the not-to-distant future within the atmospheres of metal-poor stars, or would be sufficient for the operation of the CNO cycle within the first stars ($X_{CNO} > 10^{-10}$). The only scenario for pre-stellar production of metals known to the author is a BBN scenario characterized by an inhomogeneous baryon distribution. Such inhomogeneities in the baryon-to-photon ratio may result from the out-of-equilibrium dynamics of the early universe prior to the BBN era, as possibly during a first-order QCD phase transition ($T \approx 100$ MeV) or an era of inhomogeneous electroweak baryogenesis ($T \approx 100$ GeV). Another possibility may be the creation of baryon "lumps" via the evaporation of baryon number carrying solitons formed in the early universe, such as strange quark matter nuggets or B-balls. Given the wide variety of possibilities and the large intrinsic uncertainties of scenarios for the generation of baryon number fluctuations in the early universe, it is probably best to initially regard the question about primordial abundance yields and possible metallicity production in inhomogeneous BBN scenarios disconnected from the speculative mechanism for the creation of baryon number fluctuations.

In the past, there have been a number of investigations of the evolution of pre-existing η fluctuations from high cosmic temperatures ($T \approx 100$ GeV) through the epoch of BBN [2], and of the resulting BBN abundance yields [3]. Baryon number fluctuations only impact BBN yields if they survive complete dissipation by neutron diffusion before the epoch of weak freeze-out at $T \approx 1$ MeV. This is the case for fluctuations containing baryon number in excess of $N_b \gtrsim 10^{35}(\eta_h/10^{-4})^{-1/2}$, where η_h is the baryon-to-photon ratio within the fluctuation, corresponding to a baryon mass of $M_b \gtrsim 10^{-22}M_\odot(\eta_h/10^{-4})^{-1/2}$. For reference, the baryon mass contained within the QCD- and electroweak horizon are $\sim 10^{-8}M_\odot$ and $\sim 10^{-18}M_\odot$, respectively. The evolution of fluctuations after the epoch of weak freeze-out, for a large part of parameter space, is characterized by differential neutron-proton diffusion resulting in high-density, proton-rich and low-density, neutron-rich regions. It had been suggested that such scenarios may not only result in consistency between observationally inferred and theoretically predicted primordial abundances for much larger horizon-average baryon-to-photon ratios than $\eta \approx 4 \times 10^{-10}$, but also lead to a possible efficient r-process nucleosynthesis [4] in the neutron-rich regions. When all dissipative and hydrodynamic processes during inhomogeneous BBN are treated properly, one finds that, except for a fairly small parameter space, the average η in inhomogeneous BBN scenarios may not be larger than in standard BBN due to overabundant ^{7}Li and/or ^{4}He synthesis [5]. A detailed investigation of possible r-process nucleosynthesis in the neutron-rich regions shows that an r-process is utterly ineffective in inhomogeneous BBN [6]. This is mostly due to r-process yields being a sensitive function of the local baryon-to-photon ratio in the neutron-rich region, which generically is too low in inhomogeneous BBN.

Nevertheless, BBN metal synthesis via p- and α-burning reactions of cosmologically interesting magnitude may occur if a small fraction, f_b, of the cosmic baryons reside in regions with very high baryon-to-photon ratio, $\eta_h \geq 10^{-4}$ [7]. Whereas inhomogeneous BBN scenarios are typically plagued by overproduction of ^{7}Li, the comparatively early production of ^{7}Be (which would decay into ^{7}Li) in regions with $\eta_h \geq 10^{-4}$ allows for a further processing of ^{7}Be into heavier isotopes. The net nucleosynthesis of such regions are a ^{4}He mass fraction $Y_p \approx 0.36$, some metals, and virtually no ^{2}H, ^{3}He, and ^{7}Li. A baryon-to-photon ratio $\eta \approx 10^{-4}$ is interesting as it presents the asymptotic value attained after partial dissipation of initially very high-density regions $\eta_i \gg 10^{-4}$ by the action of neutrino heat conduction at temperature $T \gg 1$ MeV, for a wide part of parameter space. Baryon "lumps" with initial baryon-to-photon ratio η_i and baryonic mass less than $M_b \leq 10^{-14} M_\odot \eta_i$ will have evolved to an asymptotic $\eta_f \approx 10^{-4}$ by the time of weak freeze-out. They are further almost unaffected by neutron diffusion during BBN provided their mass exceeds $M_b \gtrsim 10^{-19} M_\odot$. In this case horizon-averaged BBN abundance yields may be determined by an appropriate average of the yields of two homogeneous universes, one at $\eta_h \approx 10^{-4}$ and one at η_l, close to the observationally inferred value for a standard BBN scenario. The resultant cosmic average metallicity in such an inhomogeneous scenario may be approximated by

$$[\mathrm{Z}] \sim -6.5 + \log_{10}(f_b/10^{-2}) + 2\log_{10}(\eta_h/10^{-4}) \,, \tag{1}$$

where [Z] denotes the logarithm of $\mathrm{X}_{A\geq 12}$ relative to the solar value ($\mathrm{X}_\odot \approx 2 \times 10^{-2}$). The most stringent constraint on the fraction of baryons residing in high η regions comes from a possible overproduction of ^{4}He, with a change $\Delta Y_p \approx 0.12 f_b$ relative to a homogeneous BBN at η_l, allowing for $f_b \sim 10^{-2} - 3 \times 10^{-2}$, and [Z]$\sim -6$, possibly even larger for $\eta_h > 10^{-4}$. Given $\eta_h \approx 10^{-4}$, a nucleosynthetic signature is given by [O/C] ~ 1.3 and [C/$Z_{A\geq 28}$] ~ -1.5. For $\eta_h \gg 10^{-4}$, synthesis of mostly iron-group elements results.

In conclusion, it is possible, though not necessarily probable, that the universe "started" with some initial metallicity if a small fraction of the cosmic baryon number existed in high-density regions at the epoch of BBN, This metallicity may be large enough to have the first stars operate on the CNO-cycle, even though it probably would fall below the metallicities observed in the currently most metal-poor stars ([Z] ~ -5) known.

References

1. for recent reviews cf. K. A. Olive, G. Steigman, and T. P. Walker, astro-ph/9905320; S. Burles, K. M. Nollett, and M. S. Turner, astro-ph/9903300.
2. J. H. Applegate, C. J. Hogan, and R. J. Scherrer (1987) Phys. Rev. D **35** 1151; A. Heckler and C. J. Hogan (1993) Phys. Rev. D **47** 4256; K. Jedamzik and G. M. Fuller (1994) Astrophys. J. **423** 33.
3. for a review cf. R. A. Malaney and G. J. Mathews (1993), Phys. Rep. **229** 145.
4. J. H. Applegate (1988) Phys. Rep. **163** 141.
5. K. Jedamzik, G. M. Fuller, and G. J. Mathews (1994) Astrophys. J. **423** 50; K. Kainulainen, H. Kurki-Suonio, and E. Shivola (1999) Phys. Rev. D **5908** 3505, and references therein.
6. T. Rauscher, J. H. Applegate, J. J. Cowan, F. K. Thielemann, and M. Wiescher (1994) Astrophys. J. **429** 499.
7. K. Jedamzik, G. M. Fuller, G. J. Mathews, and T. Kajino (1994) Astrophys. J. **422** 423.

Death of Stellar Baryonic Dark Matter

Katherine Freese[1], Brian Fields[2], and David Graff[3]

[1] University of Michigan, Dept. of Physics, Ann Arbor, MI 48109-1120
[2] Ohio State University, Astronomy Dept., Columbus, OH 43210
[3] University of Illinois, Astronomy Dept., Urbana, IL 61801-3080

Abstract. The nature of the dark matter in the haloes of galaxies is one of the outstanding questions in astrophysics. All stellar candidates, until recently thought to be likely baryonic contributions to the Halo of our Galaxy, are shown to be ruled out. Faint stars and brown dwarfs are found to constitute only a few percent of the mass of the Galaxy. Stellar remnants, including white dwarfs and neutron stars, are shown to be very constrained as well. High energy gamma-rays observed in HEGRA data place the strongest constraints, $\Omega_{WD} < 3 \times 10^{-3} h^{-1}$, where h is the Hubble constant in units of 100 km s^{-1} Mpc^{-1}. Hence one is left with several unanswered questions: 1) What are MACHOs seen in microlensing surveys? 2) What is the dark matter in our Galaxy? Indeed a nonbaryonic component in the Halo seems to be required.

1 Introduction

The nature of the dark matter in the haloes of galaxies is an outstanding problem in astrophysics. Over the last several decades there has been great debate about whether this matter is baryonic or must be exotic. Many astronomers believed that a stellar or substellar solution to this problem might be the most simple and therefore most plausible explanation. However, in the last few years, these candidates have been ruled out as significant components of the Galactic Halo. I will discuss limits on these stellar candidates, and argue for my personal conviction that: *Most of the dark matter in the Galactic Halo must be nonbaryonic.*

Until recently, stellar candidates for the dark matter, including faint stars, brown dwarfs, white dwarfs, and neutron stars, were extremely popular. However, recent analysis of various data sets has shown that faint stars and brown dwarfs probably constitute no more than a few percent of the mass of our Galaxy [1–6]. Specifically, using Hubble Space Telescope and parallax data, we showed that faint stars and brown dwarfs contribute no more than 1% of the mass density of the Galaxy. Microlensing experiments (the MACHO [8], [9] and EROS [10]) experiments), which were designed to look for Massive Compact Halo Objects (MACHOs), also failed to find these light stellar objects and ruled out substellar dark matter candidates in the $(10^{-7} - 10^{-2}) M_{\odot}$ mass range.

Recently white dwarfs have received attention as possible dark matter candidates. Interest in white dwarfs has been motivated by microlensing events interpreted as being in the Halo, with a best fit mass of $\sim 0.5 M_\odot$. However, I will show that stellar remnants including white dwarfs and neutron stars are extremely problematic as dark matter candidates. A combination of excessive infrared radiation, mass budget issues and chemical abundances constrains the abundance of stellar remnants in the Halo quite severely, as shown below. Hence, white dwarfs, brown dwarfs, faint stars, and neutron stars are either ruled out or extremely problematic as dark matter candidates. Thus the puzzle remains, What are the 14 MACHO events that have been interpreted as being in the Halo of the Galaxy? Are some of them actually located elsewhere, such as in the LMC itself? These questions are currently unanswered. As regards the dark matter in the Halo of our Galaxy, one is driven to nonbaryonic constituents as the bulk of the matter. Possibilities include supersymmetric particles, axions, primordial black holes, or other exotic candidates.

In this talk I will focus on the arguments against stellar remnants as candidates for a substantial fraction of the dark matter, as white dwarfs in particular have been the focus of attention as potential explanations of microlensing data. For a discussion of limits on faint stars and brown dwarfs, see earlier conference proceedings by Freese, Fields, and Graff ([6] and [7]).

2 White Dwarfs

Stellar remnants (white dwarfs and neutron stars) face a number of problems and issues as dark matter candidates: 1) infrared radiation; 2) IMF (initial mass function); 3) baryonic mass budget; 4) element abundances.

We find that none of the expected signatures in the above list of a significant white dwarf component in the Galactic Halo are seen to exist.

2.1 Constraints from multi-TeV γ-rays seen by HEGRA

The mere existence of multi-TeV γ-rays seen in the HEGRA experiment places a powerful constraint on the allowed abundance of white dwarfs. This arises because the progenitors of the white dwarfs would produce infrared radiation that would prevent the γ-rays from getting here. The γ-rays and infrared photons would interact via $\gamma\gamma \to e^+e^-$.

Multi-TeV γ-rays from the blazar Mkn 501 at a redshift z=0.034 are seen in the HEGRA detector. The cross section for (1-10)TeV γ-rays peaks at infrared photon energies of (0.03-3)eV. Photons in this energy range would be produced in abundance by the progenitor stars to white dwarfs and neutron stars. By requiring that the optical depth due to $\gamma\gamma \to e^+e^-$ be less than one for a source at $z = 0.034$ we limit the cosmological density of stellar remnants [14] to $\Omega_{\rm WD} \leq (1-3) \times 10^{-3} h^{-1}$. This constraint is quite robust and model independent, as it applies to a variety of models for stellar physics, star formation rate and redshift, mass function, and clustering.

2.2 Mass Budget Issues

Contribution of Machos to the Mass Density of the Universe: (based on work by Fields, Freese, and Graff [15]) There is a potential problem in that too many baryons are tied up in Machos and their progenitors (Fields, Freese, and Graff). We begin by estimating the contribution of Machos to the mass density of the universe. Microlensing results [8] predict that the total mass of Machos in the Galactic Halo out to 50 kpc is $M_{\rm Macho} = (1.3-3.2)\times 10^{11} M_\odot$. Now one can obtain a "Macho-to-light" ratio for the Halo by dividing by the luminosity of the Milky Way (in the B-band), $L_{MW} \sim (1.3-2.5)\times 10^{10} L_\odot$, to obtain $(M/L)_{\rm Macho} = (5.2-25) M_\odot/L_\odot$. From the ESO Slice Project Redshift survey [16], the luminosity density of the Universe in the B band is $\mathcal{L}_B = 1.9 \times 10^8 h\ L_\odot\ {\rm Mpc}^{-3}$. If we assume that the M/L which we defined for the Milky Way is typical of the Universe as a whole, then the universal mass density of Machos is

$$\Omega_{\rm Macho} \equiv \rho_{\rm Macho}/\rho_c = (0.0036 - 0.017)\, h^{-1} \tag{1}$$

where the critical density $\rho_c \equiv 3H_0^2/8\pi G = 2.71 \times 10^{11}\, h^2\, M_\odot\ {\rm Mpc}^{-3}$.

We will now proceed to compare our $\Omega_{\rm Macho}$ derived in Eq. 1 with the baryonic density in the universe, $\Omega_{\rm B}$, as determined by primordial nucleosynthesis. To conservatively allow for the full range of possibilities, we will adopt $\Omega_{\rm B} = (0.005 - 0.022)\ h^{-2}$. Thus, if the Galactic halo Macho interpretation of the microlensing results is correct, Machos make up an important fraction of the baryonic matter of the Universe. Specifically, the central values give

$$\Omega_{\rm Macho}/\Omega_{\rm B} \sim 0.7\,. \tag{2}$$

However, the lower limit on this fraction is considerably less restrictive,

$$\frac{\Omega_{\rm Macho}}{\Omega_{\rm B}} \geq \frac{1}{6} h \geq \frac{1}{12}\,. \tag{3}$$

Mass Budget constraints from Machos as Stellar Remnants: White Dwarfs or Neutron Stars In general, white dwarfs, neutron stars, or black holes all came from significantly heavier progenitors. Hence, the excess mass left over from the progenitors must be added to the calculation of $\Omega_{\rm Macho}$; the excess mass then leads to stronger constraints. Typically we find the contribution of Macho progenitors to the mass density of the universe to be $\Omega_{\rm prog} = 4\Omega_{\rm Macho} = (0.016 - 0.08)h^{-1}$. The central values of all the numbers now imply $\Omega_{\rm prog} \sim 3\Omega_B$, which is obviously unacceptable. One is driven to the lowest values of $\Omega_{\rm Macho}$ and highest value of Ω_B to avoid this problem.

2.3 On Carbon and Nitrogen

The overproduction of carbon and/or nitrogen produced by white dwarf progenitors is one of the greatest difficulties faced by a white dwarf dark matter scenario, as first noted by Gibson and Mould [17]. Stellar carbon yields for zero metallicity stars are quite uncertain. Still, according to the yields by [21], a star of mass $2.5M_{\odot}$ will produce about twice the solar enrichment of carbon. However, stars in our galactic halo have carbon abundance in the range $10^{-4} - 10^{-2}$ solar. Hence the ejecta of a large population of white dwarfs would have to be removed from the galaxy via a galactic wind.

However, carbon abundances in intermediate redshift Lyα forest lines have recently been measured to be quite low, at the $\sim 10^{-2}$ solar level [18], for Lyα systems at $z \sim 3$ with column densities $N \geq 3 \times 10^{15}\,\mathrm{cm}^{-2}$ (for lower column densities, the mean C/H drops to $\sim 10^{-3.5}$ solar [19].

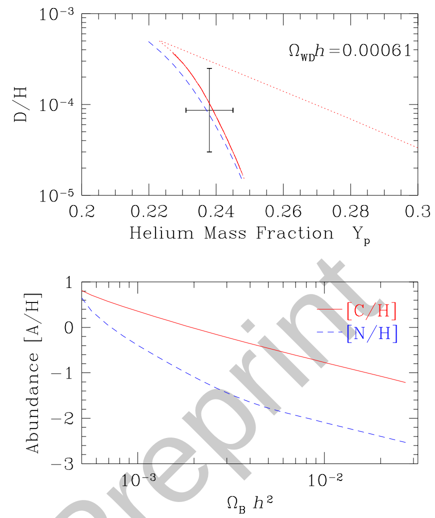

Fig. 1. (taken from Fields, Freese, and Graff 1999): **(a)** The D/H abundances and helium mass fraction Y for models with $\Omega_{\mathrm{WD}}h = 6.1 \times 10^{-4}$, $h = 0.7$, and IMF peaked at $2M_{\odot}$. The short-dashed curve shows the initial abundances and the error bars the range of D and He measurements. The other three curves show the changes in primordial D and He as a result of white dwarf production. The solid one is for the full chemical evolution model, the dotted one for instantaneous recycling, and the long-dashed one for the burst model. This is the absolute minimum Ω_{WD} compatible with cosmic extrapolation of white dwarf Machos if Machos are contained only in spiral galaxies with luminosities similar to the Milky Way. **(b)** CNO abundances produced in the same model as **a**, here plotted as a function of Ω_B. The CN abundances are presented relative to solar via the usual notation of the form $[\mathrm{C/H}] = \log_{10} \frac{\mathrm{C/H}}{(\mathrm{C/H})_{\odot}}$. The C and N production in particular are greater than 1/10 solar.

In order to maintain carbon abundances as low as 10^{-2} solar, only about 10^{-2} of all baryons can have passed through the intermediate mass stars that were the predecessors of Machos [15]. Such a fraction can barely be accommodated for the remnant density predicted from our extrapolation of the Macho group results, and would be in conflict with $\Omega_{\rm prog}$ in the case of a single burst of star formation. Note that stars heavier than $4M_\odot$ may replace the carbon overproduction problem with nitrogen overproduction [21,22].

Using the yields described above, we calculated the C and N that would result from the stellar processing for a variety of initial mass functions for the white dwarf progenitors. We used a chemical evolution model based on a code described in Fields & Olive [23] to obtain our numerical results. Our results are presented in the figure.

In the figure, we make the parameter choices that are in agreement with D and He^4 measurements (see the discussion below) and are the least restrictive when comparing with the Lyα measurements. We take an initial mass function (IMF) sharply peaked at $2M_\odot$, so that there are very few progenitor stars heavier than $3M_\odot$ (this IMF is required by D and He^4 measurements). In addition (see the figures in Fields, Freese, and Graff [20]) we have considered a variety of other parameter choices. By comparing with the observations, we obtain the limit, $\Omega_{\rm WD} h \leq 2 \times 10^{-4}$. As a caveat, note that it is possible that carbon never leaves the (zero metallicity) white dwarf progenitors, so that carbon overproduction is not a problem [24].

2.4 Deuterium and Helium

Because of the uncertainty in the C and N yields from low-metallicity stars, we have also calculated the D and He^4 abundances that would be produced by white dwarf progenitors. These are far less uncertain as they are produced farther out from the center of the star and do not have to be dredged up from the core. Panel a) in the figure displays our results. Also shown are the initial values from big bang nucleosynthesis and the (very generous) range of primordial values of D and He^4 from observations. From D and He alone, we can see that the white dwarf progenitor IMF must be peaked at low masses, $\sim 2M_\odot$. We obtain $\Omega_{\rm WD} \leq 0.003$.

3 Conclusions

A Zero Macho Halo? The possibility exists that the 14 microlensing events that have been interpreted as being in the Halo of the Galaxy are in fact due to some other lensing population. One of the most difficult aspects of microlensing is the degeneracy of the interpretation of the data, so that it is currently impossible to determine whether the lenses lie in the Galactic Halo, or in the Disk of the Milky Way, or in the LMC. In particular, it is possible that the LMC is thicker than previously thought so that the observed events are due to self-lensing of the LMC. All these possibilities are being investigated. More data are required in order to identify where the lenses are.

Microlensing experiments have ruled out baryonic dark matter objects in the mass range $10^{-7}M_\odot$ all the way up to $10^{-2}M_\odot$. In this talk I discussed the heavier possibilities in the range $10^{-2}M_\odot$ to a few $M_\odot$. Brown dwarfs and faint stars are ruled out as significant dark matter components; they contribute no more than 1% of the Halo mass density. Stellar remnants are not able to explain the dark matter of the Galaxy either; none of the expected signatures of stellar remnants, i.e., infrared radiation, large baryonic mass budget, and C,N, and He^4 abundances, are found observationally.

Hence, in conclusion,

1) Nonbaryonic dark matter in our Galaxy seems to be required, and

2) The nature of the Machos seen in microlensing experiments and interpreted as the dark matter in the Halo of our Galaxy remains a mystery. Are we driven to primordial black holes [25] [26], nonbaryonic Machos (Machismos?), mirror matter Machos ([27]) or perhaps a no-Macho Halo?

References

1. Bahcall, J.N., Flynn,. C., Gould, A., & Kirkahos, S., 1994, ApJ, 435, L51
2. Graff, D.S., & Freese, K. 1996a, ApJ, 456, L49
3. Graff, D.S., & Freese, K. 1996b, ApJ, 467, L65
4. Méra, D., Chabrier, G., & Schaeffer, R. 1996, Europhys. Lett., 33, 327
5. Flynn, C., Bahcall, J., & Gould, A. 1996, ApJ, 466, L55
6. Freese,K., Fields, B., & Graff, D., "What are Machos? Limits on Stellar Objects as the Dark Matter of Our Halo," Conf. Proc. of the Int'l Workshop on Aspects of Dark Matter in Astro and Particle Physics, Heidelberg, Germany, astro-ph/9901178
7. Freese, K., Fields, B., & Graff, D., 1999, astro-ph/9904401
8. Alcock, C., et al. 1996, ApJ, 461, 84
9. Alcock, C., et al. 1997a, ApJ, 486, 697
10. Ansari, R., et al. 1996, A&A, 314, 94
11. Axelrod, T., MACHO experiment, talk presented at Aspen, June 1997
12. Gates, E., Gyuk, G., & Turner, M.S. 1996, PRD, 53, 4138
13. Konopelko, A.K., Kirk, J.G., Stecker, F.W., & Mastichiadis, A. 1999, astro-ph/9904057
14. Graff, D.S., Freese, K., Walker, T.P., & Pinsonneault, M.H. 1999, in press, ApJ Lett, astro-ph/9903181
15. Fields, B., Freese, K., & Graff, D., 1998, New Astron, 3, 347
16. Zucca, E., et al. 1997, A&A, 326, 477
17. Gibson, B.K., & Mould, J.R., 1997, ApJ, 482, 98
18. Songaila, A., & Cowie, L.L. 1996, AJ, 112, 335
19. Lu, L., Sargent, W.L.W., Barlow, T.A., & Rauch, M. 1998, astro-ph/9802189
20. Fields, B., Freese, K., & Graff, D., 1999, in press, ApJ
21. van den Hoek, L.B., & Groenewegen, M.A.T. 1997, A&AS, 123, 305
22. Lattanzio, J.C. & Boothroyd, A.I., 1997 astro-ph/9705186
23. Fields, B.D., & Olive, K.A. 1998, ApJ, 506, 177
24. Chabrier, G. 1999, ApJ Lett, in press; astro-ph/9901145
25. Carr, B. 1994, ARAA, 32, 531
26. Jedamzik, K. 1997, Phys. Rev. D, 55, 5871
27. Mohapatra, R.N., & Teplitz, V.L. 1999, astro-ph/9902085

Part II

Observations of Extremely Metal-Poor Galactic Stars

Abundances of the Light Elements in the Ultra-Metal-Poor Stars

François Spite[1]

[1] Observatoire de Paris, Section de Meudon
[2] DASGAL, UMR 8633 du CNRS, F-92195 Meudon CEDEX, France

Abstract. Since no Pop III stars have been observed, the only way for finding the abundances of light elements in the first stars is to extrapolate the abundance trend found in objects of increasing ages, and in this procedure, the ultra metal-poor stars carry an exceptional weight. The examination of the trends of the light element abundances shows that a number of problems are unsolved, and the VLT will certainly bring a useful contribution.

1 Introduction: abundances in the first stars. Methodology

No Population III star has been observed yet [7]. Several scenarios have been proposed in order to explain the scarcity of such stars (e. g. [29,11,56], see also [3]). Failing anything bettter, the abundances of the elements in the primitive stars of our Galaxy are evaluated by the extrapolation of the trend of the abundances observed in objects of more and more advanced ages. But since the age of objects and in particular the age of unevolved (or only slightly evolved stars) is difficult to determine, the parameter used is the metallicity. There is no theoretical argument for a strict correlation between age and metallicity, since the time scale of a local enrichment is much smaller than the time scale of the general enrichment of the Galaxy [22]. And also, the Galaxy may be built from small independent accreted systems. Indeed, the observed values of metallicity and age in the stars of our Galaxy [20], are widely scattered around a mean relation for individual stars (see the fig. 1 of [18]). However, the fit of the model to a mean relation is quite satisfactory, and it is clear that a part of the scatter is due to the systematic shift in metallicity between stars of low and high galactocentric distances. Part of the scatter is also due to errors in age and metallicity determinations. A way to go deeper in the analysis, is to use the abundance ratios of the abundances of two elements : most of the abundance errors cancel out in the determination of the ratio of the abundances of two elements. And it is indeed observed that the behavior of abundance ratios is much better defined. If, among stars of the same metallicity, a given ratio shows a spread larger than expected according to the errors, this spread provides some (more or less indirect) information about the nucleosynthesis of these elements. For example Ryan et al. [46]

have shown that among very metal-poor stars, the strontium (Sr) shows wide variations, and these authors suggest that the Sr-poor stars are second generation stars. Indeed, the simplest way to explain the lack of Sr, is to assume that the progenitor of the elements found in a low-metal Sr-poor star was without iron-peak elements (without seed nuclei), and therefore unable to produce Sr by neutron-capture. This iron-free progenitor would probably be a Pop III star, and the Sr-poor stars would then be second generation (primitive) stars. The other point about this spread is that the very old, very metal-poor stars, are built from the ejecta of only a few (or even of a single) supernova, and not from well mixed (homogeneized) ejecta. The analysis of the production of Pop III stars by Audouze & Silk [3] predicts simultaneously a large scatter in abundances and a lower limit of the observed metallicity hardly smaller than [Fe/H] = - 4.0 (as indeed observed). Let us recall the square bracket notation: $[X] = \log X_* - \log X_\odot$.

Therefore, the analysis of both the trend, and the scatter around the trend, of the abundances (or abundances ratios) of the elements, in stars of decreasing metallicity is a valuable tool for the evaluation of the abundances in the first stars. Obviously, the ultra metal-poor stars carry a considerable weight in such an evaluation.

Another indirect tool, useful as a check, is the determination of the Galactic gradient, since the central part of the Galaxy is more processed relative to the external parts (which are therefore somewhat more primitive).

The literature about this topic is enormous, and I have to apologize for not beeing able to quote, in this brief review, all the authors who have made significant contributions in this field.

2 Deuterium

Deuterium should be an ideal illustration of the method. In the classical scenario, it is produced in the Big Bang Nucleosynthesi (BBN), and its later production in galaxies is negligible. On the contrary, it is largely destroyed: the nucleus of D is very fragile and is easily destroyed in stars (and even in brown dwarfs), producing some ^{3}He. Its evolution in galaxies is in principle quite straightforward: in fact, D is controversial.

The abundance is generally given by number of atoms, or, exceptionnally, by mass as X_2 (see for example Tosi [55]). In our Galaxy, it is found that the young objects show some scatter (not understood) of deuterium abundance : D/H ranges from 0.5 to 4 10^{-5} [60] in the interstellar gas. In the local ISM, [34] finds a smaller range: 1.2 to 2 10^{-5}.

The solar system provides 2.1 $\pm$ 0.5 10^{-5} for the protosolar abundance [24], and clearly different values, ranging from 2 to 3.6 10^{-5} (or even 5 10^{-5}) have been found for the atmosphere of Jupiter [60], leading to suspect [45] some alteration of the initial ratio.

The observable old stars have rather deep convective envelopes, leading to D destruction: it has been checked that the abundance of D is low (upper limit) in these old stars [52].

Deuterium is observed in distant extragalactic gas, absorbing the light of more distant objects. This high redshift gas, of low metallicity, is old (redshift up to z = 3.57). Different abundances have been found by different teams, the range reaching sometimes an order of magnitude.

The reason for such differences are not clearly known, but it has to be noted that only small regions of the gas are sampled in each measurement by the narrow light beam of the distant source, and the differences (somehow reminiscent of those found in the gas in our Galaxy) may be the reflect of a local gradient produced for example by radiation pressure. It is very difficult to assign a value to the D/H ratio in the extragalactic gas as long as the source of the differences between the determinations is not understood. A general broad trend is however proposed by Lemoine et al. [33] and is illustrated in their figure 1, but the new very low measurement of Molaro et al. [37] makes this trend even more uncertain. Finally, the primordial D/H value, is not well defined. Anyhow, in the first stars, the proportion of D, relative to the bulk of H and He, is very small. But even at this low value, D has influenced the formation of the first stars, by helping the cooling of the contracting gas, and by providing the first nuclear reactions in the core for ALL stars (including the brown dwarfs).

3 The ^{3}He isotope

This isotope is produced in the Big Bang. It happens that it is virtually not observable in the spectra of stars. It is predicted to be produced in low mass stars, and a high abundance is found in some planetary nebulae, but more generally, the predicted significant production of ^{3}He by the stars in the Galaxy is not observed, and the abnormally low $^{12}C/^{13}C$ ratio measured in low-mass giants suggests an additional mixing during stellar evolution, which would destroy ^{3}He (cf. [17]).

In the local interstellar medium, the ratio ^{3}He/H is around 2.5 10^{-5} (Gloeckler and Geiss [25]). In the Galactic ISM (H II regions), it seems independent of metallicity and age, defining a plateau [6]. This independence is checked by a similar independence of the galactocentric distance.

In the solar system, the ratio is 1.5 10^{-5} (meteorites, Jupiter), not incompatible, within errors, with the value found from the H II regions.

It is not measured in old unevolved objects.

The extrapolation, using galactic evolution models [55], is rather easy (the case of a plateau is the simplest one), but the value remains uncertain, since the behavior of ^{3}He is not fully understood. The proportion of ^{3}He in the first stars is small anyway, preventing the isotope from influencing strongly the formation of the first stars.

4 Helium: ^{4}He

He is produced in the Big Bang and in the stars: all stars produce some He internally, some expel it, enriching the interstellar medium, sometimes at early times (before SN explosion in the case of the WR stars), sometimes later (stellar wind in evolved low-mass stars).

The abundances of He, relative to H, are quoted by the ratio y of the number of atoms, or by the mass-ratio Y with $Y \approx 4y/(1+4y)$.

In young stars [38] Y = 0.28-0.29

In young B stars [35] Y = 0.285

In the Hyades, from Hipparcos data (ESA 1997 [21]) it is found [41] that Y = 0.26 (or more precisely 0.006 less than the Sun which has an initial value of 0.266, when evaluated homogeneoulsy in the same grid of models used by these authors).

Interstellar gas: in Orion, Y is found to be 0.257 [5], again less than the Sun. In the solar system, the initial value for the Sun is Y = 0.27 (current value in external layers around 0.25).

No direct spectroscopic measurements can be made in old stars, but from the application of the stellar pulsation theory (RR Lyrae) and from the HR diagram of globular cluster, a value around Y = 0.23 is found.

The blue compact galaxies (BCG) are objects including a starburst which illuminates a rather primitive gas. Some doubts have however been raised about the fact that the starburst, currently observed in these objects, is really the first one [1,48]. Anyhow, the He abundance may be plotted versus the metallicity (measured here by the abundance of oxygen), and the resulting trend provides (by extrapolation to a zero O abundance) a rather well defined value of the primordial He, but various corrections have to be applied, and different authors find different observations and/or results: $Y_p = 0.228$ [40] or 0.244 [30]. The small difference [49] is important for comparison with the predictions of the primordial nucleosynthesis (see their figure 1), but is not essential in the processus of formation of the first stars.

5 Lithium

The ^{6}Li isotope:

This isotope is important, not by itself, but for defining the status of ^{7}Li : the isotope ^{6}Li is indeed more fragile than ^{7}Li, so that the fact that ^{6}Li is present in a few old metal-poor stars ([14] and references therein, [28]) suggests that ^{7}Li is only slightly (if at all) depleted in these stars.

The ^{7}Li isotope:

The Big Bang Nucleosynthesis predicts the production of this isotope. It is also produced by Cosmic Rays, and possibly in some supernovae (ν-process), by novae, by evolved low-mass stars. The nucleus is fragile, destroyed by proton fusion in the internal layers of stars, and preserved in the (observed) external layers. But any mixing of the external and internal layers will deplete the preserved lithium, decreasing its observed abundance.

The ^{7}Li abundance is known in young objects of our Galaxy. In the interstellar gas, the abundance is different in different directions (clouds): for example there is a factor of more than one order of magnitude between the cloud towards ρ Oph and the cloud towards ζ Oph [31,32]. This is reminiscent of the spread observed for D/H. The high value of the interstellar abundance would be around log ε(Li) $= 3.5 \pm 0.4$. In the young stars and young clusters, the abundance is log ε(Li) = 3.3- 3.0.

In the meteorites of the solar system the abundance is log ε(Li) = 3.31. In the solar photosphere, the value is currently log ε(Li) = 1.16 [53]. The difference between the proto-solar and solar values is attributed to a depletion of Li in the external layers of the sun: for example [59] explains this depletion (and the behavior of ^{3}He) by the combination of convection, slow mixing and diffusion.

In old metal-poor stars, it happens that the Li abundance is extraordinarily uniform, independent of temperature (for $T_{\rm eff} \geq 5700$ K) and [Fe/H] $\leq$ -1.4: these stars define a two-dimensional plateau, and this plateau is valid for stars considered as very old, either because they have a halo kinematics, or are ultra metal-poor [12], or Sr-poor [51]. Out of a sample of more than 100 stars, only 5 or 6 are Li-poor (binaries? other anomaly?) and another star would be Li-rich (iron anomaly? red giant contamination? other?). The spread of the Li abundances of the other stars is small, so small that it can be explained entirely by the expected determination errors (Ryan et al. [47]). Such a small spread is exceptional. The Sr/Fe is admittedly quite exceptionnal in the other way, but all trends in stellar abundances, and moreover even in abundance ratios, have a significant spread, too large for being explained by the determination errors. The abnormally small Li spread has to be explained.

Little is known about Li in other galaxies. In the LMC, the SN 1987A has enabled the measurement of an upper limit of Li abundance in the interstellar gas. The Li is found [26] to have, in young supergiants, the same behavior as in the young supergiants of the Galaxy.

Two possible interpretations of the plateau:

1- A high primordial abundance, and a significant but uniform depletion

2- A low primordial abundance, and a depletion so small that the differences induced by metallicity and/or mass are negligible, the plateau remains thin and flat [50].

The first interpretation provides a good fit of the predictions of a slow mixing to the observations of Li in the population I (e.g. [42,58]), but not very good for the Pop II. It is not clearly understood why the physical processes (rotationnally induced mixing, diffusion, etc.) become less efficient (or inefficient) in Pop II stars, although [13] has noted that the structure of Pop II stars is different from the structure in Pop I stars.

One possible discrimination between the two interpretations is about the spread of Li: real or due to errors? In order to discriminate, it is necessary to push the accuracy of Li abundances. Abundances in stars are in principle found by fitting a computed synthetic spectrum to the observed stellar spectrum. However, this is a multi-parameter fit, so that uncertainties remain. One independent constraint is helpful in increasing the accuracy: the stellar color, accurately measured by stellar photometry. The calibration of the observable (color) into the physiscal parameter T_{eff} is however a delicate matter, and the choice of one or another calibration results in significant differences in abundances. Recently, Ryan et al. [47] analyzed a sample in a way enabling a significant decrease of both systematic and random errors, reaching a very small scatter of Li abundances around the plateau, scatter entirely explained by the formal computed errors. A small slope of Li versus Fe/H remains, but is easily explained by the expected progressive production of Li by the Cosmic Rays.

So that the data indicate that:

- either the depletion of Li is identical in different stars (different metallicities, different masses, different rotational histories), and this is improbable at first sight, unless some feedback processus is stabilising the lithium abundance

- or the depletion is small, by some inhibiting or compensating effects, so small that its variations are insignificant. In this interpretation, the abundance of the plateau, extrapolated to very low metallicty, is therefore the primordial abundance.

According to the second interpretation, the lithium abundance in the first stars is about $\log \varepsilon(\mathrm{Li}) = 2.24$ dex (in the T_{eff} scale chosen by Bonifacio and Molaro [9]), but higher, by a factor up to 10 in the first interpretation. The problems raised by these two interpretations are discussed with great insight by Cayrel [14].

It has to be noted that the second interpretation requires a large ^{7}Li production by stars, novae (and supernovae?), and this production is not yet clearly understood. Some moderate- mass stars produce Li in the red giant and AGB phases. A recent detection of a Li-rich giant in a cluster [27] provides new information about the exact phase of Li production in giants.

In addition to "old" Pop II stars defined by low metallicity, we can consider the Sr-poor stars. The *s*-process elements, such as Sr, are produced by neutron bombardment of seed nuclei (nuclei of the iron peak), so that the absence of Sr in metal-poor stars has been interpreted by the absence of seed nuclei in the precursors of these stars (Ryan [46]): these iron- free precursors had then to be made of primordial material. The Li abundance, in the Sr-poor stars, happens to be very similar to the abundance of the normal metal-poor stars of the plateau. One more check can be made, using the parameters of the Galactic orbits of the stars as a proxy for ages: the behavior of Li is essentially the same as the one found when using the metallicity.

The Li abundances in metal-poor stars have been determined, using classical model atmospheres. Using 3-D convection in his improved model, [2] derived an abundance lower by a factor ot about 2. But for a completely reliable value of the Li abundance, the computation should take into account also the NLTE effects, which will compensate at least partly the 3-D effect.

Anyhow, the proportion of lithium in the primordial matter is small relative to the bulk of matter made of H and He, but this small amount of metal may have some influence on the cooling of the contracting clouds which are forming the first stars, and it is, after D, the first element to be burned in nuclear reactions in the center of the stars.

6 Beryllium

Be is produced by Cosmic Rays, it is not supposed to be produced in stars, and a very small amount may be produced in the Big Bang nucleosynthesis. The nucleus of Be is fragile and is destroyed in the internal layers of the stars, but it is less fragile than lithium. Be is observable in stars from the ground: there are two lines in a very crowded region in the UV, near the limit of transparence of the terrestrial atmosphere.

The abundance of Be in the Pop I stars is similar to the abundance in the solar system, with some spread. The solar abundance is $\log \varepsilon(\mathrm{Be}) = 1.15$, lower than the meteoritic abundance (1.42), and Be is classically supposed to be depleted by a factor of about 2 (but see [4]). In Pop II stars, the Be abundance decreases with the iron abundance: the slope of the relation [Be/H] versus [Fe/H] is not very different from one, [36,8,23] but there is a significant spread, somewhat larger than the estimated errrors, indicating inhomogeneous production of Be by the Cosmic Rays. The relation goes on straight through the very metal-poor stars, and no plateau is observed, but, according to [54], the plateau predicted by the inhomogeneous BBN should show up only at metallicities around [Fe/H] = -4 (and even lower for the standard BBN). Unfortunately, the measurement of extremely low Be abundances (extremely faint lines) in such scarce (and therefore faint) ultra metal-poor stars is extremely difficult.

The observations, currently limited to a metallicity of [Fe/H] = -3 (but the VLT + UVES will hopefully do better!), do not show yet any evidence of a Be plateau: the Be abundance in the first stars is currently expected to be not larger than the abundance of the Big Bang, i. e. larger than 10^{-17} for the SBBN and 10^{-14} for the IBBN (Orito et al. [39]). The influence of Be is therefore expected to be very small in the formation of the first stars.

7 Boron

Boron is produced by the Cosmic Rays, and it may be produced in supernovae by neutrino spallation of ^{12}C (the ν-process of Woosley et al. [61]). There are two isotopes, and the production processes do not provide the same isotopic ratios (and even the low energy cosmic rays do not provide the same ratio as the classical Cosmic Rays [57]). The current observations are not able to constrain strongly the production processes [44]. The nucleus of B is fragile and is destroyed in the internal layers of the stars, but it is less fragile than B (and *a fortiori* than lithium).

The abundance of B in the Pop I stars is similar to the abundance found in the solar system and in the Sun itself: the meteoritic abundance is log ε(Be) = 2.78. The abundance decreases with the iron abundance [19,43] the slope is about one, similar to the behavior of Be, so that the ratio Be/B is constant. Some spread is observed, also suggesting inhomogeneities in the production by Cosmic Rays. A plateau is neither expected nor observed. The B abundance in the first stars is therefore very small and is not supposed to have a great influence in the formation of the first stars.

8 Conclusion

The abundances of the light elements in the first stars are derived from the extrapolation of the trend of the abundances in stars of increasing ages, and in this way, the data obtained for the ultra metal poor stars have a major weight. On the observational side, the VLT, UVES, FLAMES, GIRAFFE will provide essential data. At the same time an effort towards a rigorous interpretation of the spectra will be necessary. Some problems about the abundances of the first stars (and about the primordial abundances) require an accuracy of stellar abundance determination, which is at the limit of its current possibilities. Better calibrations (e. g. through interferometric measurements), better treatment of convection, (e. g. 3-D models), NLTE computations etc...will soon provide the awaited progresses

References

1. Aloisi A., Tosi M., Greggio L. (1999) AJ **118**, 302
2. Asplund M., Nordlund A., Trampedach R., Stein R. (1999), A&A 346, L17
3. Audouze J., Silk J. (1995), ApJ 451, L49
4. Balachandran S., Bell R. A. (1998), Nature 392, 791
5. Baldwin J. A., Ferland G. J., Martin P. G. et al. (1991), ApJ 374, 580
6. Balser D. S., Rood R. T., Bania T. M. (1999), ApJ 522, L73
7. Beers T. C. (1999), this volume
8. Boesgaard A. M., Deliyannis C. P., King J. R. et al. (1999), AJ 117, 1549
9. Bonifacio P., Molaro P. (1997), MNRAS 285, 847
10. Castilho B., Spite F., Barbuy B. et al. (1999), A&A 345, 249
11. Cayrel R. (1986), A&A 168, 81
12. Cayrel R. (1996), A&ARv 7, 217
13. Cayrel R. (1998), in: "Primordial Nuclei and their Galactic evolution", ISSI workshop, eds. N. Prantzos, M. Tosi, R. von Steiger, Space Sci. Rev. 84, 145

14. Cayrel R. (1999a), in: LiBeB, Cosmic Rays and related X- and Gamma-Rays, eds. R. Ramaty, E. Vangioni-Flam, M. Cassé, K. Olive, ASP Conf. Ser. 171, p. 261
15. Cayrel R., Spite M., Spite F. et al. (1999b), A&A 343, 923
16. Charbonnel C. (1998a), in: "Primordial Nuclei and their Galactic evolution", ISSI workshop, eds. N. Prantzos, M. Tosi, R. von Steiger, Space Sci. Rev. 84, 199
17. Charbonnel C., Do Nascimento J. D., Jr. (1998), A&A 336, 915
18. Chiappini et al. (1997), ApJ 477, 765
19. Duncan D. K., Primas F. Rebull L. M. et al. (1997), ApJ 488, 438
20. Edvardsson B., Andersen J., Gustafsson B., Lambert D. L., Nissen P. E., Tomkin J. (1993), A&A 27, 101
21. ESA, (1997), The Hipparcos and Tycho Catalogues, ESA SP-1200
22. Fuhrmann K., (1999) this volume
23. García López J. R. (1999), in: "LiBeB Cosmic Rays and related X- and Gamma-Rays", eds. R. Ramaty, E. Vangioni-Flam, M. Cassé, K. Olive., ASP Conf. Ser. 171, p. 77
24. Geiss J., Gloeckler G. (1998), in: "Primordial Nuclei and their Galactic evolution", ISSI workshop, eds. N. Prantzos, M. Tosi, R. von Steiger, Space Sci. Rev. 84, 239
25. Gloeckler G., Geiss J. (1998), in: "Primordial Nuclei and their Galactic evolution", ISSI workshop, eds. N. Prantzos, M. Tosi, R. von Steiger, Space Sci. Rev. 84, 275
26. Hill V. (1999), A&A 345, 430
27. Hill V., Pasquini L., (1999), A&A 348, L21
28. Hobbs L. M., Thorburn J. A., Rebull L. M. (1999), ApJ 523, 797
29. Iben I., Jr (1967), ApJ 147, 650
30. Izotov Y. I., Thuan T. X. (1998), ApJ 500, 188
31. Lemoine M., Ferlet R., Vidal-Madjar A.et al. (1993), A&A 269, 469
32. Lemoine M., Ferlet R., Vidal-Madjar A. (1995), A&A 298, 879
33. Lemoine M., Audouze J., Ben Jaffel L. et al. (1999), New Astr. 4, 231
34. Linsky J. L. (1998), in: "Primordial Nuclei and their Galactic evolution", ISSI workshop, eds. N. Prantzos, M. Tosi, R. von Steiger, Space Sci. Rev. 84, 185
35. McErlean N. D., Lennon D. J., Dufton P. L. (1999), A&A 349, 553
36. Molaro P., Bonifacio P., Castelli F., Pasquini L. (1997), A&A 319, 593
37. Molaro P., Bonifacio P., Centurion M., Vladilo G. (1999), A&A 349, L13
38. Nissen P. E. (1983), in "ESO Workshop on Primordial Helium", Garching, p. 163
39. Orito M., Kajino T., Boyd R. N., Mathews G. J. (1997), ApJ 488, 515
40. Pagel B. E. J., Simonson E. A., Terlevich R. J., Edmunds M. G. (1992), MNRAS 255, 325
41. Perryman M. A., Brown A. G. A., Lebreton Y. et al. (1998), A&A 331, 81
42. Pinsonneault M. H., Narayan V. K., Steigman G., Walker T. P. (1998), in: Cool stars, stellar systems and the Sun, 10th Cambridge Workshop, eds. Donahue, J. A. Bookbinder, ASP Conf. Ser. 154, San Francisco, p. 959
43. Primas F. Duncan D. K., Peterson R. C., Thorburn J. A. (1999), A&A 34, 545
44. Rebull L. (1999) this volume
45. Reeves H. (1998), in: "Primordial Nuclei and their Galactic evolution", ISSI workshop, eds. N. Prantzos, M. Tosi, R. von Steiger, Space Sci. Rev. 84, 319

46. Ryan S. G., Norris J. E., Bessell M. S. (1991), AJ 102, 303
47. Ryan S. G., Norris J. E., Beers T. C. (1999), ApJ 523, 654
48. Schulte-Ladbeck R. (1999), this volume
49. Skillman E. D., Terlevich E., Terlevich R. (1998), in: "Primordial Nuclei and their Galactic evolution", ISSI workshop, eds. N. Prantzos, M. Tosi, R. von Steiger, Space Sci. Rev. 84, 105
50. Spite F., Spite M. (1982), A&A 115, 357
51. Spite F., Spite M. (1993), A&A 279, L9
52. Spite M., Spite F., Maillard J.-P. (1983), A&A 128, 252
53. Steenbock W., Holweger H. (1984), A&A 130, 319
54. Suzuki T. K., Yoshi Y., Kajino T. (1999), ApJ 522, L125
55. Tosi M. (1998), in: "Primordial Nuclei and their Galactic evolution", ISSI workshop, eds. N. Prantzos, M. Tosi, R. von Steiger, Space Sci. Rev. 84, 207, 207
56. Tsujimoto T., Shigeyama T., Yoshii Y. (1999), ApJ 519, L63
57. Vangioni-Flam E., Cassé M., Fields B. D., Olive K. A. (1996), ApJ 468, 199
58. Vauclair S. (1998a), Space Sci. Rev. 85, 71
59. Vauclair S. (1998b), in: "Primordial Nuclei and their Galactic evolution", ISSI workshop, eds. N. Prantzos, M. Tosi, R. von Steiger, Space Sci. Rev. 84, 265
60. Vidal-Madjar A., Ferlet R., Lemoine M. (1998), in: "Primordial Nuclei and their Galactic evolution", ISSI workshop, eds. N. Prantzos, M. Tosi, R. von Steiger, Space Sci. Rev. 84, 297
61. Woosley S. E., Hartmann D. H.., Hoffman R. D.,Haxton W. C. (1990), ApJ 356, 272

Heavy Elements in Very Metal-Poor Stars

Sean G. Ryan

Physics Department, The Open University, Walton Hall MK7 6AA, UK

Abstract. Metal-poor stars provide information on the characteristics and chemical evolution of the halo population of the Galaxy, the first epoch of star formation and Galaxy formation (not just locally but with relevance to high-redshift objects), and big bang nucleosynthesis. This paper looks at recent developments in this subject. A more comprehensive review, including a discussion of the reliability of abundance measurements, field star vs globular cluster differences, and a report on Li, can be found elsewhere [69].

1 Introduction

Halo stars constitute the oldest and most extended stellar population *known* in the Galaxy, and have the lowest metallicities. Hence they provide the first data in the sequence of Galactic chemical evolution (GCE). Fig. 1(a-c) shows the metallicity distributions of 36 halo globular clusters (Laird et al. [38]), 373 halo field stars [39,71] and 34 damped Lyman-α systems (DLAs [65]). Not only are the field and cluster metallicity distributions comparable, they are *lower* in metallicity than the DLAs having redshifts $z \sim$ 1–3. That is, very metal poor stars are amongst the lowest metallicity objects in the known universe. There is ongoing debate about what the DLAs really are, possibilities including:

- spiral disks/protodisks/thick disks (e.g. [90,40])
- dwarf galaxies [63,64]
- ejecta from dwarf galaxies [61].

In examining Galactic stars, we have the advantage of studying objects with reasonably well understood histories and physical states, whose spectra are not blended, and whose abundances, which are measurable for many elements, are unaffected by depletion onto dust grains.

The value of halo stars for studying early epochs of the universe may be further illustrated by considering metallicity-redshift space. Fig. 1(d-f) shows a number of Galactic and high-redshift objects, along with three GCE models assuming outflow, no outflow (closed box) and inflow for Galaxy formation assumed to begin at redshift $z = 5$ [21]. (A Hubble constant $H_0 = 50$ km s^{-1} Mpc^{-1} and flat cosmology [$q_0 = 0.5$] were used to establish the age-redshift relation.) The disk star sequence and bulge of the Galaxy are based on the observations of Edvardsson et al. [22] and Sadler et al. [74]. The high-redshift objects are the DLAs from Pettini et al. [65] binned in redshift, Molaro et al. [51] and Lu et al. [40], a region corresponding to

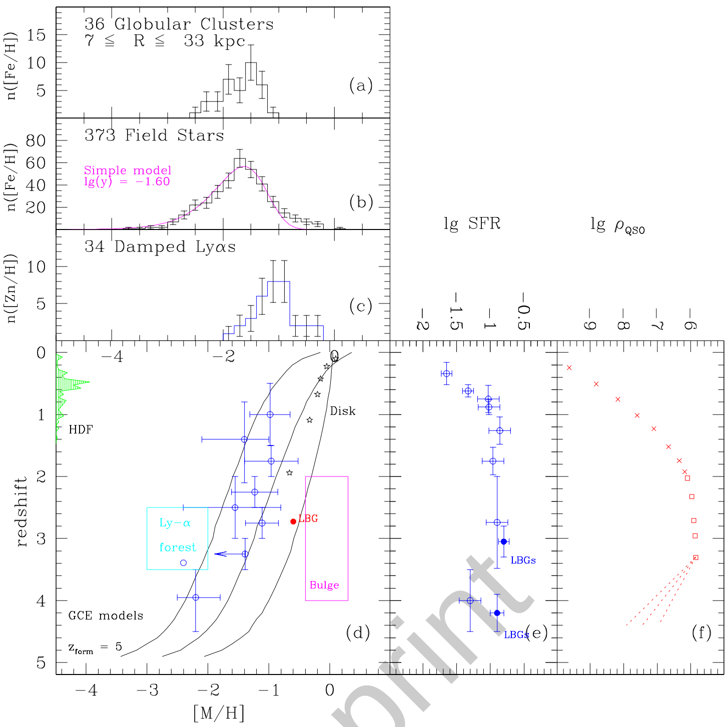

Fig. 1. Metallicity distributions of **(a)** Galactic halo globular clusters, **(b)** Galactic halo field stars, and **(c)** Damped Lyman-α quasar absorption line systems. **(d)** Galactic and high-redshift objects in the redshift–metallicity plane, the former located at their redshift of formation (assuming $H_0 = 50$ km s^{-1} Mpc^{-1}). *solid curves* = GCE models; *open circles* = DLAs; *stars* = disk star sequence; *solid circle* = LBG. **(e)** Star formation history of extragalactic objects. **(f)** Quasar density distribution. (See text for discussion)

the Lyman-α forest [29], and one Lyman break galaxy (LBG) from Pettini et al. [66]. The redshift distribution in the Hubble Deep Field [11] is shown as an inset against the vertical axis. In adjoining panels are the extinction-corrected star formation rate [83] and the quasar space density [89] whose steep fall at redshift $z > 3.5$ indicates that these objects were still forming prior to this epoch, presumably along with galaxies. Several points can be noted.

• The overlapping of high redshift and Galactic objects in this epoch-metallicity plane (redshift translates to epoch), e.g. the LBG and the Galactic bulge, and the Lyman-α forest and metal poor stars, emphasises that these objects provide complementary views on the formation and evolution of galaxies. No one class should be considered in isolation from the others.

• Galactic stars with [Fe/H] < -3, corresponding to $z \gtrsim 4$–5, uniquely probe the earliest star formation events. A high level of detail is achievable because many elements can be measured in well understood objects. Furthermore, the elements in these objects owe their existence to very few previous generations of stars, possibly only one [72]. They mark the beginning of GCE, and as such will be the main topic of this review.

2 How Many Supernovae Make a Population II Star?

One GCE model which considers individual generations of stars is [75] stochastic model. This has only one free parameter, the mean number of enrichments prior to the termination of star formation, μ. Applied to halo field stars, it gives a reasonable fit to the globular cluster distribution, implying a mean of ten enrichments per fragment [71]. With the mean metallicity of the halo globular clusters being [Fe/H] $\simeq -1.5$, this suggested that a single event could enrich a fragment to [Fe/H] $\simeq -2.5$.

Truran [87] argued that the atmospheres of second generation stars would contain r- but no s-process isotopes, whereas subsequent generations would contain both types. Although it was not clear at which metallicity this would be achieved, it forced people to think about the first few generations of stars.[1] Large star-to-star variations in the neutron-capture abundances of stars with [Fe/H] < -2.5 (e.g. [25]) suggested that prior nucleosynthesis involved small numbers of supernovae (SN). Related observations of Sr led Ryan et al. [72] to consider stochastic enrichment and to calculate the metallicity produced by a single supernova as [Fe/H] $= -3.8$, based on a typical SN II progenitor mass of 25 $M_\odot$ and an assumed primordial cloud mass of 10^6 $M_\odot$.[2] This coincided with the observed huge abundance variations of strontium, and was consistent with the lowest stellar metallicities.[3]

Star-to-star differences in neutron-capture element abundances at the lowest metallicities also required that chemical inhomogeneities existed around the time these stars were forming. [3] showed further that mixing timescales in the halo were sufficiently long that inhomogeneities of this type would not be erased on the timescale over which stars would form, supporting the

[1] It is uncertain that we will actually see a clear division between r- and s-process elements in second versus third generation stars, because most neutron-capture elements have contributions from both the s- and r-process.

[2] The SN mass was a compromise between higher mass stars being rarer and lower mass stars having lower yields. The cloud mass was based on large globular clusters, giant molecular clouds, and the collapse of metal poor gas.

[3] The vanishing of Sr in some stars at this metallicity suggested to me, at the time, that Truran's mechanism was possibly being observed, and that genuine second generation stars were being identified. However, more recent data on Ba has altered my views on this; see Footnote 1 and later sections of this paper.

proposition that the progeny of the first supernovae would be found around this metallicity. Mounting examples of neutron-capture element variations from star to star (e.g. [57,48,68,73]) strengthened the view that the most metal-poor stars exhibit the ejecta of very small numbers of supernova.

The need to integrate small numbers of supernova with GCE models led Ryan et al. [73] to examine the enrichment by a single SN in a primordial cloud. Adopting the supernova remnant (SNR) model of [16], they calculated the cloud mass with which the SN ejecta would mix as

$$m_{\rm ISM} = 3.4 \times 10^4 E_{51}^{0.95} n_0^{-0.10} \zeta_m^{-0.15} (\beta C_{06})^{-1.29} \quad {\rm M}_\odot,$$

where E, n, ζ, and βC_{06} refer to the explosion energy, cloud density, cloud metallicity, and shock speed in appropriate units. The main features of this result were:

- the mass of gas enriched is almost independent of the cloud characteristics (n, ζ) and depends strongly (almost linearly) on the energy of the SN;
- the typical enriched mass of the cloud would be 7×10^4 M$_\odot$;
- the typical metallicity following this first enrichment would be [Fe/H] = -2.7, matching (perhaps coincidentally) the changes in the behaviour of iron-peak and neutron-capture elements and the lowest metallicity globular clusters.

Many other GCE models have been developed that incorporate the initial mass function, the mass-dependence of stellar lifetimes, the mass- and metallicity-dependence of supernova and stellar-wind yields, and more. New ones have been forthcoming that include SNR physics and inhomogeneous mixing (e.g. [76,88,31,2]). It will be possible to use observed abundances to constrain the model inputs. As stars at these low abundances are believed to be second generation stars, of particular interest will be the shape of the IMF of their progenitors (Population III stars!), the mass limits for the production of SN of Population III stars, and the yields of individual Population III objects.

3 Intermediate-Mass Elements

Measurements of O are presented in Fig. 2, which isolates giants from dwarfs, and shows separately the abundances derived from the forbidden lines [O I], near-infrared triplet O I, and ultraviolet OH lines.

Results for the infra-red triplet have been inconsistent. Abia & Rebolo [1] found a progressive increase in the overabundance, but subsequent studies found different results, arguing inconsistencies between different lines [41], $T_{\rm eff}$ dependences, and errors in the $T_{\rm eff}$ scale and equivalent widths. The most recent studies used the UV OH lines, Israelian et al. [33] and Boesgaard et al. [10] finding almost identical trends towards high O overabundances in the most metal-poor stars. Note that although Bessell et al. [9] concluded that their OH line measurements were consistent with [4] giants, [9] dwarfs

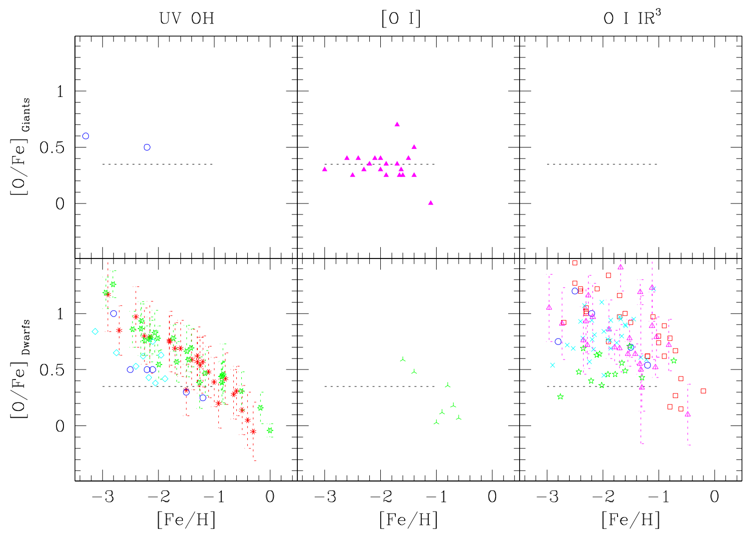

Fig. 2. Oxygen in metal poor field stars. *circles:* Bessell, Sutherland & Ruan 1991; *filled triangles:* Barbuy 1988; *diamonds:* Nissen et al. 1994; *six-pointed stars:* Boesgaard et al. 1999; *asterisks:* Israelian, García Lopéz & Rebolo 1998; *inverted 'Y's:* Spite & Spite 1991; *squares:* Abia & Rebolo 1989; *crosses:* Tomkin et al. 1992; *five-pointed stars:* King 1993; *open triangles:* Cavallo, Pilachowski & Rebolo 1997

and [54] almost fit the recent OH trend, albeit displaced by $\simeq -0.3$ dex. [26] warns of the difficulty of fitting the continuum near the UV OH lines for the more metal-rich stars, the need for accurate molecular line parameters, and the need to apply NLTE corrections for the high-excitation O I triplet. The lack of agreement between measurements of the triplet (Fig. 2) attests to the difficulties in using these lines.

Barbuy's finding that O behaves like the α-elements was attractive under the paradigm that copious production of Fe in SN Ia was responsible for the decrease in $[\alpha/\mathrm{Fe}]$ at $[\mathrm{Fe/H}] > -1$. However, O and the α elements are formed separately, so their yields relative to Fe do not have to exhibit the same dependence on metallicity. The difficulty posed by the observations is that current stellar models predict O and α to evolve together, and do not show high overabundances of [O/Fe] (e.g. [84]). It is not sufficient to claim that the Fe yields could be wrong, for while they *could* be wrong, the OH observations require that $[\mathrm{O}/\alpha]$ is also strongly dependent upon metallicity, and that is not seen in the models either. So, if the theoretical yields are to fit the OH line data, significantly higher O production will be required, irrespective of what changes are made to Fe.

Carbon and nitrogen measurements in very metal-poor stars [34] generally give approximately solar ratios. However, there have also been significant numbers of C-rich stars found at the lowest iron abundances [7]. While one of these, CS 22892-052, has huge r-process element overabundances [78,79], the majority exhibit s-process patterns [58,5,60]. The high C abundances are not predicted by theoretical yields of supernovae (e.g. Timmes et al. [84]), but might be explained by enrichment of the early halo by mass loss from high mass Population III stars which have synthesized C via the triple-alpha process and mixed it to their surfaces (e.g. [44]). The frequency of C-rich stars and their tendency to be accompanied by s-process rather than r-process heavy element signatures (suggestive of AGB star evolution rather than supernovae) will be important to understanding their origin. (Note, however, that not all C-rich stars exhibit heavy element anomalies [59]).

The α-elements (Mg, Si, Ca) have fairly uniform overabundances relative to iron extending down to the lowest metallicities [72,57,48,73]. Recent studies have begun to concentrate on star-to-star variations, with [36,13,55] identifying stars with low [α/Fe] ratios, predominantly retrograde kinematics, and young ages. The low [α/Fe] ratios are reminiscent of those proposed by [46] and [24] for star formation in dwarf galaxies where star formation ceased before metallicities typical of Galactic disk stars were reached, so that the appearance of SN Ia would lead to low [α/Fe] ratios even at metallicities typical of halo stars.[4] Similarly, the dual halo models of [92], based on globular clusters, and [56], based on field stars, fit with the characteristics of the stars now observed. Clearly there is still much to learn about the Galactic halo by exploiting relative abundances.

4 The Iron-Peak Elements

The iron-peak elements most easily observed in very metal-poor stars are Sc, Ti, Cr, Mn, Fe, Co, and Ni. For stars with [Fe/H] > -2.5, most of these species exhibit solar abundance ratios. One exception is Mn, which is underabundant by $\sim$0.3 dex in halo stars. A second exception is Ti, which is believed to be produced in the same region of stars as the other iron-peak elements, but whose abundance appears more like the α-elements[5]. McWilliam et al. [48] and Ryan et al. [73] showed that Mn and Cr become very underabundant in stars with [Fe/H < -2.5, while in the same objects Co becomes overabundant. These changes were not predicted by supernova computations.

The iron-peak species are synthesised deep in the star, close to the mass-cut. Efforts to understand the abundance trends have focussed on the possible

[4] A possible conflict is raised by the work of [37] who propose that the SN Ia mechanism would have lower efficiency at [Fe/H] < -1 due to the weaker winds in metal-deficient stars.

[5] Truran (1999, private communication) reports that the experimental ^{44}Ti(α,p)^{47}V rate is five times higher than the theoretical one used in previous nucleosynthesis calculations, so the theoretical yields of some iron-peak elements will be subject to revision.

α-rich freeze-out [91,48], the location of the mass-cut [53]), and the dependence of yields on stellar mass, metallicity, and neutron excess [53,30]. The explanation must not distort the [X/Fe] ratios of species such as Mg, Si, and Ca which are formed well outside the mass-cut; this is particularly challenging for explanations which alter the Fe yield! Progress may increase when 3D hydrodynamical models provide more realistic treatments of the supernova explosion (e.g. [52]). Observational evidence for mixing of material from the mass-cut to the photosphere [82,23] provides additional clues and constraints as we seek more realistic supernova models.

5 Neutron-Capture Elements

Spite & Spite [80] showed that the Ba in halo stars owed its origin primarily to the r-process. [87] argued that the s-process should be viewed as a secondary process while the r-process was primary, and thus that first generation — Population III — stars would not execute the s-process. [25] showed that the neutron-capture elements exhibited abundance patterns more consistent with the r-process than the s-process. [48] extended the Ba and Eu comparison to the lowest metallicities ([Fe/H] $= -4$), confirming the existence of r-process (rather than s-process) ratios.

In a small number of cases, spectral line profiles allow constraints to be placed on the isotope ratios. [43] obtained observations of this effect, and in HD 140283, at [Fe/H] $= -2.6$, inferred an s-process rather than r-process pattern for Ba. This result was unexpected given the r-process framework that had been established over the preceeding nearly 20 years. In contrast, Gacquer & Francois (1998, private communication) find an r-process signature for this star.

The reliance almost solely on Ba and Eu as diagnostics of the s- vs r-process fractions has been diminished by *HST* data for other important neutron-capture elements having UV spectra. Included in this list are Ag, Pt, Os, and Pb [20,19,77].

Gilroy et al. [25] also found that neutron-capture elements showed significant star-to-star variations in the most metal poor objects ([Fe/H] $\lesssim -2.5$), building upon cases reported earlier during the decade. The variations are greatest for Sr, where ranges of a factor of more than 100 were found amongst dwarfs [72] and giants [57]. Moreover, as Figure 3(a,b) shows, such extreme variations are *not* shared by Ba, which exhibits a fairly steady trend towards lower [Ba/Fe] at lower [Fe/H].

Reconciling Sr and Ba is a challenge. If the r-process alone is responsible for their synthesis in very metal-poor halo stars, then Fig. 3(a,b) tells us that the r-process cannot be universal. Whilst there is no theoretical reason why it *must* be universal, halo star neutron-capture element abundance patterns generally resemble the r-process contribution in the sun (e.g. [25,48,17,79]). We seek a source of additional Sr in the lowest metallicity objects involving

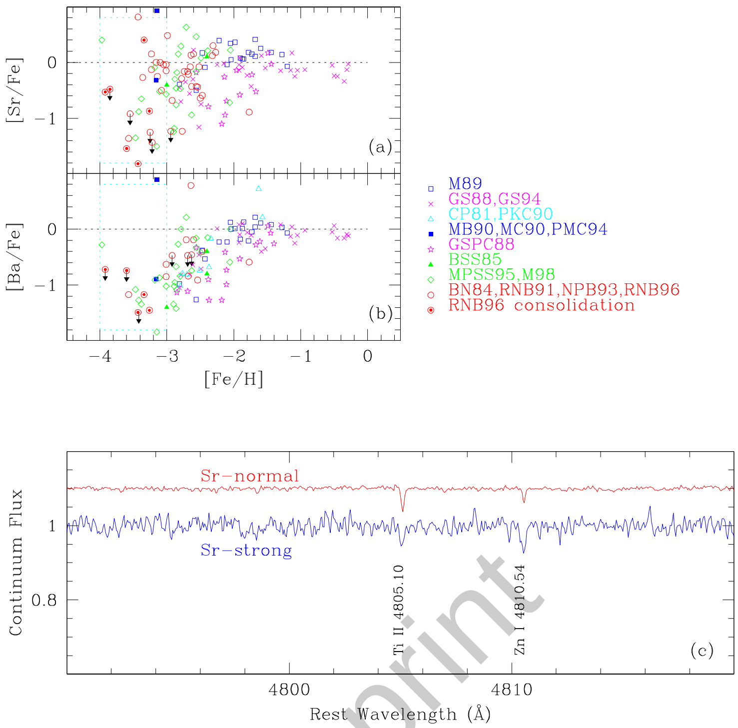

Fig. 3. (a) and (b) Abundances of Sr and Ba in halo stars. The dashed box outlines the same region of [X/Fe] and [Fe/H] in each plot. Whereas [Sr/Fe] exhibits a range by a factor of more than 100, [Ba/Fe] has a well-behaved trend towards lower values at the lowest [Fe/H]. **(c)** Spectra of Fe and Zn lines in Sr-rich (lower) and Sr-normal (upper) stars. The investigation of other low-atomic-number neutron-capture elements indicates that these too are overabundant in the Sr-rich stars, as expected for a low-neutron-exposure process [70].

low neutron exposures that synthesise only species around the atomic number of Sr since other species near Sr are also enhanced in the high-Sr stars ([73,70], see Fig. 3(c)). The weak s-process produces primarily low atomic-numbered neutron-capture species, and would be active in normal high mass (>15 $M_\odot$) stars, but the lack of seed nuclei and a suitable neutron source would severely hamper this in low metallicity stars. It may be necessary to look for a low-neutron-exposure r-process [31].

The change in [Ba/Fe] and [Eu/Fe] for stars with [Fe/H] < -2 suggests that these species are not produced abundantly in the most massive metal-poor supernovae. Mathews & Cowan [45] associated their production with 10–11 $M_\odot$ stars. Although the evolution in their models is now seen to be too steep, the concept of low-mass stars being responsible has survived, and a more gradual emergence is seen in the models of [86] which use a mass range 8–10 $M_\odot$ for the process. Travaglio et al. also treat the enrichment of the cloud inhomogeneously, along the lines described in §2 of this review (also [31]).

Assuming that the neutron-capture elements in the atypical r-process-rich star, CS 22892-052, are present in the same proportions as the r-process contribution in the sun, [18] derive an age of 17±4 Gyr, based on the radioactive Th abundance. This is consistent with current estimates of globular cluster ages from isochrone fitting, of around $12.8^{+4.2}_{-2.8}$ Gyr [15]. Improved data and GCE models will hopefully reduce the errors to provide a chronometer of better accuracy than the globular cluster technique.

6 Final Comments

Stars with [Fe/H] < -3 formed at the earliest epochs of star formation, corresponding to redshifts $z \gtrsim 4$. They formed from gas clouds enriched by single supernovae, and hence allow us to investigate the first (Population III) stars which enriched primordial (big bang) material with heavy elements. Even though that stellar population was small in number and no surviving example has been detected today, it is still possible to investigate its mass function and evolution via the nucleosynthetic yields frozen into the next generation of stars, the extremely metal-poor Population II stars.

References

1. Abia, C. & Rebolo, R. 1989, ApJ, 347, 186
2. Argast, D. & Samland, M. 1999, The Galactic Halo: from Globular Clusters to Field Stars, 35th Liège Int. Astroph. Coll., in press
3. Audouze, J. & Silk, J. 1995, ApJ, 451, L49
4. Barbuy, B. 1988, A&A, 191, 121
5. Barbuy, B. Cayrel, R., Spite, M., Beers, T. C., Spite, F., Nordstrom, B. & Nissen, P. E. 1997, A&A, 317, L63
6. Barbuy, B., Spite, F., & Spite, M. 1985, A&A, 144, 343
7. Beers, T. C., Preston, G. W. & Shectman, S. A. 1992, AJ, 103, 1987
8. Bessell, M. S. & Norris, J. E. 1984, ApJ, 285, 622
9. Bessell, M. S., Sutherland, R. S. & Ruan, K. 1991, ApJ, 383, L71
10. Boesgaard, A. M., King, J. R., Deliyannis, C. P. & Vogt, S. S. 1999, AJ, 117, 492
11. Bouwens, R., Broadhurst, T., & Silk, J. 1998, ApJ, 506, 557
12. Carney, B. W. & Peterson, R. C. 1981, ApJ, 245, 238
13. Carney, B. W., Wright, J. S., Sneden, C., Laird, J. B., Aguilar, L. A. & Latham, D. W. 1997, AJ, 114, 363
14. Cavallo, R. M., Pilachowski, C. A. & Rebolo, R. 1997, PASP, 109, 226

15. Chaboyer, B. 1999, The Galactic Halo: from Globular Clusters to Field Stars, 35^{th} Liège Int. Astroph. Coll., in press
16. Cioffi, D. F., McKee, C. F. & Bertschinger, E. 1988, ApJ, 334, 252
17. Cowan, J. J., Burris, D. L., Sneden, C., McWilliam, A. & Preston, G. W. 1995, ApJ, 439, L51
18. Cowan, J. J., McWilliam, A., Sneden, C., & Burris, D. L. 1997, ApJ, 480, 246
19. Cowan, J. J., Sneden, C., Truran, J. W. & Burris, D. L. 1996, ApJ, 460, L115
20. Crawford, J. L., Sneden, C., King, J. R., Boesgaard, A. M. & Deliyannis, C. P. 1998, AJ, 116, 2489
21. Edmunds, M. G. & Phillipps, S. 1997, MNRAS, 292, 733
22. Edvardsson, B., Andersen, J., Gustafsson, B., Lambert, D. L., Nissen, P. E. & Tomkin, J. 1993, A&A, 275, 101
23. Fassia, A., Meikle, W. P. S., Geballe, T. R., Walton, N. A., Pollaco, D. L., Rutten, R. G. M. & Tinney, C. 1998, MNRAS, 299, 150
24. Gilmore, G. & Wyse, R. F. G. 1991, ApJ, 367, L55
25. Gilroy, K. K., Sneden, C., Pilachowski, C. A. & Cowan, J. J. 1988, ApJ, 327, 298
26. Gratton, R. 1999, The Galactic Halo: from Globular Clusters to Field Stars, 35^{th} Liège Int. Astroph. Coll., in press
27. Gratton, R. G. & Sneden, C. 1988, A&A, 204, 193
28. Gratton, R. & Sneden, C. 1994, A&A, 287, 927
29. Hellsten, U., Dave, R., Hernquist, L., Weinberg, D. H. & Katz, N. 1997, ApJ, 487, 482
30. Hix, W. R. & Thielemann, K.-F. , 1996, ApJ, 460, 869
31. Ishimaru, Y. & Wanajo, S. 1999a, ApJ, 511, L33
32. Ishimaru, Y. & Wanajo, S. 1999b, MPA/ESO Workshop on the First Stars, Garching 1999, in press.
33. Israelian, G., García López, R. & Rebolo, R. 1998, ApJ, 507, 805
34. Israelian, G. & Rebolo, R. 1999, The First Stars, MPA/ESO Workshop, Garching August 1999, in press
35. King, J. R. 1993, AJ, 106, 1206
36. King, J. R. 1997, AJ, 113, 2302
37. Kobayashi, C., Tsuijmoto, T., Nomoto, K. Hachisu, I. & Kato, M. 1998, ApJ, 503, L155
38. Laird, J. B., Carney, B. W. & Latham, D. W. 1988b, AJ, 95, 1843
39. Laird, J. B., Rupen, M. P., Carney, B. W. & Latham, D. W. 1988a, AJ, 96, 1908
40. Lu, L., Sargent, W. L. W., Barlow, T. A., Churchill, C. W. & Vogt, S. S. 1996, ApJS, 107, 475
41. Magain, P. 1988, The Impact of Very High S/N Spectroscopy on Stellar Physics, ed. G. Cayrel de Strobel & M. Spite (Dordrecht, Kluwer), 485
42. Magain, P. 1989, A&A, 209, 211
43. Magain, P. 1995, A&A, 297, 686
44. Marigo, P. 1999, MPA/ESO Workshop on The First Stars, Garching August 1999, in press
45. Mathews, G. J. & Cowan, J. J. 1990, Nature, 345, 491
46. Matteucci, F. & Brocato, E. 1990, ApJ, 365, 539
47. McWilliam, A., 1998, AJ, 115, 1640
48. McWilliam, A., Preston, G. W., Sneden, C. & Searle, L. 1995, AJ, 109, 2757

49. Molaro, P. & Bonifacio, P. 1990, A&A, 236, L5
50. Molaro, P. & Castelli, F. 1990, A&A, 228, 426
51. Molaro, P., D'Odorico, S., Fontana, A., Savaglio, S. & Vladilo, G. 1996, A&A, 308, 1
52. Müller, E., Fryxell, B. & Arnett, D. 1991, A&A, 251, 505
53. Nakamura, T., Umeda, Nomoto, K., Thielemann, F.-K. & Burrows, I. 1999, ApJ, in press (astro-ph/9809307)
54. Nissen, P. E., Gustafsson, B., Edvardsson, B., & Gilmore, G. 1994, A&A, 285, 440
55. Nissen, P. E. & Schuster, W. M. 1997, A&A, 326, 751
56. Norris, J. E. 1994, ApJ, 431, 645
57. Norris, J. E., Peterson, R. C. & Beers, T. C. 1993, ApJ, 415, 797
58. Norris, J. E., Ryan, S. G. & Beers, T. C. 1997a, ApJ, 488, 350
59. Norris, J. E., Ryan, S. G. & Beers, T. C. 1997b, ApJ, 489, L169
60. Norris, J. E., Ryan, S. G., Beers, T. C. & Aoki, W. 2000, in prep.
61. Nulsen, P. E. J., Barcons, X. & Fabian, A. C. 1998, MNRAS, 301, 168
62. Peterson, R., Kurucz, R. L., & Carney, B. W. 1990, ApJ, 350, 173
63. Pettini, M., Boksenberg, A. & Hunstead, R. W. 1990, ApJ, 348, 48
64. Pettini, M., Ellison, S. L., Steidel, C. C. & Bowen, D. V. 1999a, ApJ, 510, 576
65. Pettini, M., Smith, L. J., King, D. L. & Hunstead, R. W. 1997, ApJ, 486, 665
66. Pettini, M., Steidel, C. C., Adelberger, K. L., Dickinson, M. & Giavalisco, M. 1999b, preprint
67. Primas, F., Molaro, P., & Castelli, F. 1994, A&A, 290, 885
68. Ryan, S. G. 1996, ASP Conf.Ser. 92, 113
69. Ryan, S. G. 2000, The Galactic Halo: from Globular Clusters to Field Stars, 35^{th} Liège Int. Astroph. Coll., in press
70. Ryan, S. G., Blake, L., Norris, J. E. & Beers, T. C. 2000, in preparation
71. Ryan, S. G. & Norris, J. E. 1991, AJ, 101, 1865
72. Ryan, S. G., Norris, J. E. & Bessell, M. S. 1991, AJ, 102, 303
73. Ryan, S. G., Norris, J. E., & Beers, T. C. 1996, ApJ, 471, 254
74. Sadler, E. M., Rich, R. M. & Terndrup, D. M. 1996, AJ 112, 171
75. Searle, L. 1977 In: Tinsley, B. M. & Larson, R. B. (eds) The Evolution of Galaxies and Stellar Populations, Yale Uni. Obs., New Haven, p.219
76. Shigeyama, T. & Tsujimoto, T. 1998, ApJ, 507, L135
77. Sneden, C., Cowan, J. J., Burris, D. L. & Truran, J. W. 1998, ApJ, 496, 235
78. Sneden, C., Preston, G. W., McWilliam, A. & Searle, L. 1994, ApJ, 431, L27
79. Sneden, C., McWilliam, A., Preston, G. P., Cowan, J. J., Burris, D. L. & Armosky, B. J., 1996, ApJ, 467, 819
80. Spite, M. & Spite, F. 1978, A&A, 67, 23
81. Spite, M. & Spite, F. 1991, A&A, 252, 689
82. Stathakis, R. A. 1996, PhD Thesis, Sydney Uni.
83. Steidel, C. C., Adelberger, K. L., Giavalisco, M., Dickinson, M. & Pettini, M., 1999, astro-ph/9811399
84. Timmes, F. X., Woosley, S. E., & Weaver, T. A. 1995, ApJS, 98, 617
85. Tomkin, J., Lemke, M., Lambert, D. L. & Sneden, C. 1992, AJ, 104, 1568
86. Travaglio, C., Galli, D., Gallino, R., Busso, M., Ferrini, F. & Straniero, O. 1999, ApJ, 521, 691
87. Truran, J. W. 1981, A&A, 97, 391
88. Tsujimoto, T. & Shigeyama, T. 1998, ApJ, 508, L151

89. Warren, S. J., Hewett, P. C. & Osmer, P. S. 1994, ApJ, 421, 412
90. Wolfe, A. M., Turnshek, D. A., Smith, H. E. & Cohen, R. D. 1986, ApJS, 61, 249
91. Woosley, S. E. & Hoffman, R. D. 1992, ApJ, 395, 202
92. Zinn, R. 1993, ASP.Conf.Ser, 48, 38

Finding the First Stars: The Hamburg/ESO Objective Prism Survey

Norbert Christlieb[1], Dieter Reimers[1], Lutz Wisotzki[1], Johannes Reetz[2], Thomas Gehren[2], and Timothy C. Beers[3]

[1] Hamburger Sternwarte, Germany
[2] Universitäts-Sternwarte München, Germany
[3] Department of Physics & Astronomy, Michigan State University, U.S.A.

1 The Hamburg/ESO survey

The Hamburg/ESO survey (HES, [4]) is an objective-prism survey for bright quasars based on IIIa-J plates taken with the ESO Schmidt telescope and its $4°$ prism. It covers the total southern extragalactic sky ($\delta < +2\overset{\circ}{.}5$; $|b| \gtrsim 30°$). All 380 Schmidt plates (effective area $\sim$ 7 000 square degrees) have been taken, and have been digitized and reduced in Hamburg. The spectral range of the HES plates is $3200\,\text{Å} < \lambda < 5300\,\text{Å}$, with a seeing-limited spectral resolution of 15 Å at Hγ. This makes it possible to efficiently exploit the stellar content of the survey.

Among other interesting objects (e.g. white dwarfs, carbon stars, and field horizontal branch A-type stars; [2]), extremely metal-poor stars can be selected by automated procedures in the digital database of the HES. With its magnitude range of $12 \gtrsim B_J \gtrsim 17.5$, the HES is more than one magnitude deeper than the HK survey of Beers et al. [1]. Moreover, it covers regions in the sky that are not covered by the HK survey. In result, the HES can increase the total survey volume for metal-poor stars by more than a factor of 4 compared to the HK survey alone.

2 Selection of metal-poor Stars

We select metal-poor stars in the HES by means of automatic spectral classification [3]. As a training set, we use an extensive grid of model atmospheres converted to objective prism spectra. The grid covers the following parameter range: $5200\,\text{K} < T_{\text{eff}} < 6800\,\text{K}$ (200 K steps), $2.2 < \log g < 4.6$ (0.8 dex steps) and $-0.3 > [\text{Fe/H}] > -3.6$ (-0.3 dex steps). Any object brightness can be simulated by adding the appropriate amount of gaussian noise. For automatic classification we apply a Bayes rule which employs feature vectors $\boldsymbol{x}$ containing a large set of automatically detected spectral features, e.g. equivalent widths of stellar absorption lines, line indices, broad band colours, and narrow band colours equivalent to Strömgren $uvb\beta$. Class-conditional probabilitiy distributions $p(\boldsymbol{x}|\Omega_i)$ are modelled by multivariate normal distributions.

In a simulation we investigated the effective yield (EY) of our selection, in dependence of B magnitude. Since we currently concentrate our efforts on metal-poor *turnoff* stars, we slightly modify the definition of EY given by Beers (this volume):

$$\mathrm{EY}(y) = \frac{\#\ \text{stars with [Fe/H]} \leq y \text{ and } \log g \geq 4.0}{\text{total}\ \#\ \text{of selected stars}} \tag{1}$$

We used $\sim 30\,000$ spectra in each magnitude bin, distributed in [Fe/H] according to a metallicity distribution function derived from the catalogue of Beers et al. [1].

The result is shown in Fig. 1. Note that sample completeness and EY are complementary. If the selection is optimized towards high EY, the completeness is $\sim 60\,\%$ for $B < 16.5$ mag. If a completeness of $\sim 90\,\%$ is desired, EYs are typically by a factor 2 lower.

Our results will be verified by spectroscopic follow-up observations in an upcoming observing run at the ESO-NTT.

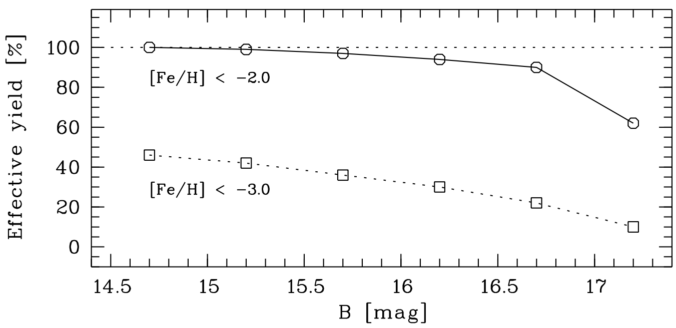

Fig. 1. Effective yield of metal-poor turnoff stars selected by automatic classification in the HES, determined by simulations.

References

1. Beers T.C., Preston G.W., Shectman S.A. (1992) A search for stars of very low metal abundance. II. AJ 103:1987
2. Christlieb N. (2000) The stellar content of the Hamburg/ESO objective prism survey, PhD thesis, University of Hamburg
3. Christlieb N., Graßhoff G. et al. (1998) Automatic spectral classification. In: Balderjahn I. et al. (Eds.) Classification, Data Analysis, and Data Highways. Springer, Berlin, 16–23.
4. Wisotzki L., Köhler T. et al. (1996) The Hamburg/ESO survey for bright QSOs I. Survey design and candidate selection procedure. A&AS 115:227

Copper and Zinc Abundances in Metal-Poor Stars

Francesca Primas[1], Eric Brugamyer[2], Chris Sneden[2], Jeremy R. King[3], Timothy C. Beers[4], Ann M. Boesgaard[5], and Constantine P. Deliyannis[6]

[1] European Southern Observatory, Karl-Schwarzschild str.2, 85748 Garching, Germany
[2] Department of Astronomy, University of Texas at Austin, USA,
[3] Department of Physics & Astronomy, University of Nevada at Las Vegas, USA,
[4] Department of Physics & Astronomy, Michigan State University, USA,
[5] Department of Astronomy, University of Hawaii, USA,
[6] Department of Astronomy, Indiana State University, USA

Abstract. We present preliminary results of our recent effort devoted to the determination of copper and zinc abundances in a large sample of stars of the Galactic halo. By adding several new data points at very low metallicity, we aim at better constraining the [Cu/Fe] and [Zn/Fe] trends below [Fe/H]= -2.5. The very few Cu and Zn data points currently available below this metallicity [11], are not sufficient to draw firm conclusions. A deeper knowledge of the nucleosynthetic origin of these two elements is necessary to clarify whether copper and zinc should be considered the heaviest of the iron-group elements, or the lightest of the neutron-capture elements.

1 Introduction

By study of the observed trends and possible intrinsic dispersions of elemental abundance ratios in metal-poor stars it is possible to uncover information about the degree of homogenization of the early Galaxy (mixing processes) and to test theoretical model predictions (e.g. Type II supernovae yields). One basic ingredient for a correct interpretation of abundance trends is a deep knowledge of the nucleosynthetic origin of each element under investigation. For the elements copper and zinc this knowledge is still uncertain.

Falling just beyond the iron-peak (Z_{Cu}=29, Z_{Zn}=30), there has always been some question as to whether it is more proper to assign these species to the iron-group elements, or to consider them as the lightest of the neutron-capture elements. Traditionally, Cu has been thought to be produced via s-process neutron-capture reactions, but it can also be manufactured in explosive Ne-burning [12]. Zinc is formed in explosive Si-burning. The possibility that zinc may also be produced in relatively large quantities by a low density "α-rich freeze-out" during Si-burning [13] makes its nucleosynthetic origin even more uncertain.

Knowledge of the correlation of [Zn/Fe] with [Fe/H] is crucial for studies of Damped Ly-α systems (DLAs), as those studies use zinc as a surrogate for estimation of the overall metallicity in the line-of-sight gas clouds. In the Milky Way Zn has always been found to exhibit solar ratios, relative to other elemental species, over a wide range of metallicities. Thus, observations of super-solar [Zn/Fe] or [Zn/Cr] ratios in DLAs has been usually explained by invoking selective dust depletion for Fe and Cr. However, it remains possible that the observed Zn over-abundance may be intrinsic to its stellar nucleosynthesis, since the dust depletion hypothesis seems inconsistent with other elemental ratios [6].

The [Cu/Fe] trend with metallicity is equally important since copper is one of several elements of the iron-group known to display a significant departure in the [element/Fe] ratio in metal-poor stars. It had been previously thought that the elements in the vicinity of iron exist in their solar ratios over a wide range in metallicity. Recently, however, previously unnoticed trends of iron-peak elements (e.g., Cr, Mn, and Co) have been discovered below [Fe/H]$\simeq -2.5$ [7,9]. The interpretation of the observed departures of Cr, Mn, Co, and Cu from their solar ratios suggests that a distinct phase of nucleosynthesis must have occurred before the Galaxy reached that metallicity.

Despite a very detailed knowledge on several other elemental abundance patterns, very few spectroscopic analyses have been devoted to study Cu and Zn abundances in metal-poor stars. The currently available observations of Cu and Zn in the Galactic halo [10,11] show a possible decline in [Cu/Fe] ratios with decreasing metallicities and no anomaly in [Zn/Fe]. *But* no star below ~ -2.7 has ever been subjected to a detailed abundance study.

2 The Observed Sample

Copper and zinc abundances are usually observed via their neutral atomic transitions in the optical: at 5105Å and 5782Å for copper and at 4722Å and 4810Å for zinc. The paucity of data points available at low metallicities (especially for copper) arises from the fact that the lines become vanishingly weak as the overall metal abundance decreases. Thus, in order to make progress at low abundances, we decided to target *for the first time* the resonance Cu I lines in the near-UV ($\lambda\lambda$ 3247 and 3274).

Combined observational efforts were carried out at McDonald Observatory ($R \sim 60,000$ resolving power and S/N$\geq$100) and at the ESO La Silla Observatory, where CASPEC at the 3.6m telescope has been used to observe in the near-UV at a resolving power of $R \sim 27,000$. Because of technical problems with CASPEC, only the brightest (i.e. more metal-rich objects, [Fe/H]~ -1.0) could be observed, with typical S/N ratios of the order of 50. However, by taking advantage of the availability of $N \sim 20$ spectra obtained at Keck I equipped with HIRES (originally obtained for beryllium studies [2]) we have considerably enlarged the sample of stars observed in the near-UV at lower metallicities. These spectra are characterized by a resolving power of R$\sim$ 45,000, and S/N much higher that 100 at the wavelengths of interest.

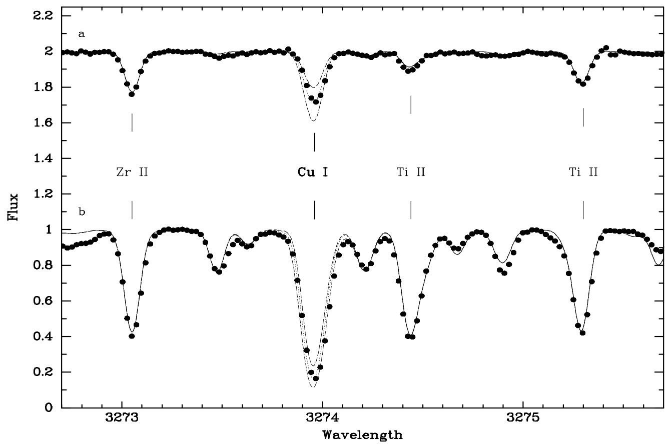

Fig. 1. Spectrum synthesis fit of the $\lambda3274$ region for BD $+20^{\circ}3603$ (a; [M/H]$=-2.2$) and HD 76932 (b; [M/H]$=-1.0$), both observed at KECK I with HIRES

A total sample of $N \sim 100$ objects has been observed, spanning the metallicity range $-3.0 \leq$ [Fe/H] ≤ -0.7. The overlap with the samples previously analyzed by Sneden and collaborators amounts to 20% at most. At the moment, we have reduced and analyzed about half of the available spectra.

3 The Analysis

Copper and zinc abundances were determined by measuring the equivalent widths of the lines that fall in the optical, and by using spectrum syntheses in the near-UV. For these purposes, the programs WIDTH, SYNTHE and the published Kurucz grid of model atmospheres [5] were employed. The atomic parameters of the optical transitions were taken from [11], while the line list for synthesizing a small region around each of the Cu I resonance lines was originally taken from [5] compilations. Some changes to the *gf*-values of a few specific lines (copper excluded) were made based on the comparison of synthetic solar spectra generated with the Holweger & Muller [3] solar model atmosphere to the Solar Flux Atlas [4]. Hyperfine splitting of the Cu I lines was accounted for, with the component wavelengths and relative strengths taken from Kurucz' world-wide-web database.

At this preliminary stage of the analysis, physical parameters (T_{eff}, logg, and [Fe/H]) of the stars were taken from the literature, after a careful inspection of the studies employing high resolution and high S/N data. For the sample of stars observed at Keck, we used the physical parameters previously determined by Boesgaard et al. [2], based on their "Carney et al." temperature scale.

Figure 1 shows a small spectral region around the redder Cu I line for two of the stars observed with HIRES at Keck. The best-fit syntheses are overplotted (dotted lines). The dashed lines represent syntheses computed with a ± 0.2 dex (for BD $+20°3603$, spectrum *a*) and ± 0.5 (for HD 76932, spectrum *b*) variation in copper. This is to show that at higher metallicities the line approaches complete saturation, thus becoming unreliable.

Average error bars have been assigned to each data point (cf Fig. 2a,b, lower right corners): ± 0.10 dex in [Fe/H], and ± 0.14 dex in the copper and zinc estimates. The latter was estimated by taking into account the sensitivity of Cu and Zn abundances to changes in T_{eff}, logg, and [Fe/H].

4 Results and Future Prospects

Our final derived [Cu/Fe] ratios are presented in Fig. 2a as a function of the overall stellar metallicities. As expected from previous studies, we find copper to be under-abundant compared to iron, a result which strengthens the attribution of its production to secondary nucleosynthesis processes. However, the copper abundances determined from the resonance lines (filled circles) do not show significant variations with decreasing overall metallicity (remaining always about [Cu/Fe] ~ -1.0) – a somewhat surprising result which needs to be investigated in more detail. It may be due to systematic differences between the abundance indicators we have employed, or it may also suggest a more complicated nucleosynthetic origin of the element.

Similarly, most of the Zn data points confirm the previously detected solar ratio of [Zn/Fe] over a large interval in overall metallicity (see Fig. 2b). However, the few extremely metal-poor stars in our sample do seem to indicate a rise in the [Zn/Fe] ratio at the lowest metallicities, for which observational errors can be excluded as a plausible cause. This, if confirmed, would increase the likelihood that the α-rich freeze-out is at work for this element. Of course, this rising trend of [Zn/Fe] would have to be taken into account by those who make use of observed Zn abundance as a substitute for other metallicity estimators, such as Fe or Cr.

By completing the analysis of the entire sample, and by adding some more Zn determinations at the lowest metallicities, we will soon achieve a much more complete and detailed picture. Because of the large spectral coverage available in our studies, we will also analyze Ni, and some of the other heavy elements such as Sr. If both Ni and Zn are products of the α-rich freeze-out in early Galactic nucleosynthesis, then any Ni excess will be matched by copious amounts of Zn. Similarly, if Cu and Zn were produced mainly by an s-process, then Sr should also be dominated by s-process nucleosynthesis [1], which is inconsistent with what McWilliam et al. [7] have found so far. If we are able to better constrain the supernova yield of each element, it will then be possible to use this information, together with the large number of

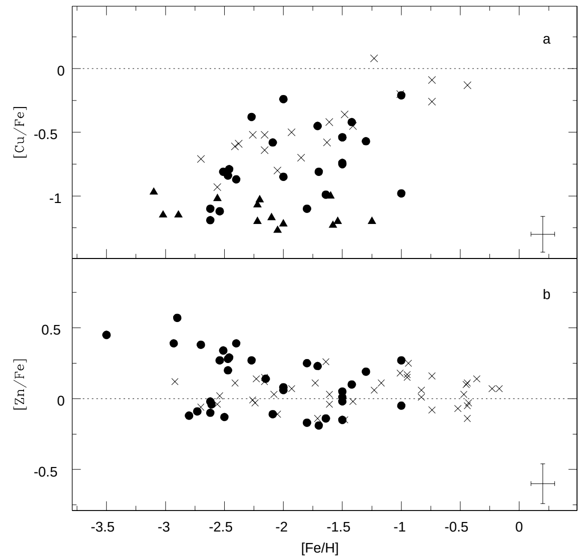

Fig. 2. a) [Cu/Fe] versus [Fe/H] as derived from [11] (*crosses*) and this analysis (*filled circles* represent abundances derived from the λ5105Å and/or λ5782Å lines; *filled triangles* represent abundances derived from the near-UV resonance lines). b) [Zn/Fe] vs/ [Fe/H] as derived by [11] (*crosses*) and this analysis (*filled circles*). The dashed lines represent the solar ratios.

Zn determinations in DLAs [8] to trace the increase of heavy elements in the universe from the epoch of Galaxy formation to the present.

References

1. Baraffe, I., Takahashi, K. (1993) A&A 280, 476
2. Boesgaard, A., Deliyannis, C., et al. (1999) AJ 117, 1549
3. Holweger, H., Muller, E. (1974) Sol. Phys. 39, 19
4. Kurucz, R., Furenlid, I., et al. (1984) Solar Flux Atlas from 296 to 1300 nm. Cambridge: Harvard University Press
5. Kurucz, R. (1993) CD-ROM #13
6. Lu, L., Sargent, W., (1996) ApJS 107, 475
7. McWilliam, A., Preston, G., et al. (1995) AJ 109, 2757
8. Pettini, M., Smith, L., et al. (1997) ApJ 486, 665
9. Ryan, S., Norris, J., et al. (1996) ApJ 471, 254
10. Sneden, C., Crocker, D. (1988) ApJ 335, 406
11. Sneden, C., Gratton, R., et al. (1991) A&A 246, 354
12. Woosley, S., Weaver, T. (1980) ApJ 238, 1017
13. Woosley, S., Hoffman, R. (1992) ApJ 395, 202

CNO Abundances in Metal-Poor Unevolved Stars

Garik Israelian, Ramón J. García López, and Rafael Rebolo

Instituto de Astrofísica de Canarias, E-38200 La Laguna, Tenerife, Spain

Abstract. We present a study of C, N, and O abundances for 24 unevolved metal-poor stars with metallicities in the range $-0.3<$ [Fe/H]< -3. New C and N abundances have been measured using high resolution spectroscopy of the CH and NH bands at 3145 and 3360 Å, respectively. We also discuss the oxygen abundances obtained by Israelian et al. [10] for these stars and delineate the early Galactic evolution of these elements.

1 Introduction

Knowledge of CNO abundances in metal-poor stars is very important because of what it can tell us about the history of element production by stars, and what types of stars have been mainly responsible for this production. The surface abundances of CNO are also signatures of internal nucleosynthesis and mixing between the core and outer layers of the star. Mixing is expected to occur when a star becomes a red giant following the exhaustion of hydrogen in the core (the so called "first dredge-up"). The key property of H burning through the CNO cycles is that the total number of CNO nuclei is conserved.

Important results have been obtained from the analysis of CNO molecular bands and atomic lines ([17] and references therein) in the spectra of unevolved halo stars. However, such analyses have been either based on high resolution spectra of small samples (less than 10) or low/intermediate resolution spectra of large samples ($\sim$ 100) of stars. We are studying CNO abundances from high resolution spectra of more than 40 halo dwarfs. In this paper we report preliminary results based on 24 halo dwarfs discussed by [10].

2 Observations

The observations were carried out in different runs using the UES ($R = \lambda/\Delta\lambda \sim 50000$) of the 4.2-m WHT at the Observatorio del Roque de los Muchachos (La Palma), and the UCLES ($R \sim 60000$) of the 3.9-m AAT. The final signal-to-noise ratio (S/N) varies for the different echelle orders, being in the range 30–100 for most of the stars.

3 Analysis

A grid of LTE, plane-parallel, constant flux, and blanketed model atmospheres provided by Kurucz [11], computed with ATLAS9 without overshooting, and interpolated for given values of $T_{\rm eff}$, $\log g$, and [Fe/H] was used. Details on the analysis of the OH lines have been presented in [10]. We have derived carbon abundances from the CH band at 3145 Å using the list of [11]. Nitrogen abundances have been derived from the NH band at 3360 Å using the atomic and molecular data from Norris (1999, private communication). Synthetic spectra were computed with the WITA3 code by Pavlenko [13]. Effective temperatures ($T_{\rm eff}$) for our stars were estimated using the Alonso et al. [2] calibrations versus $V-K$ and $b-y$ colors, which were derived applying the infrared flux method, and cover a wide range of spectral types and metal content. Metallicities were adopted from literature values obtained from high resolution spectra. Gravities were derived using the accurate parallaxes measured by *Hipparcos* (ESA [7]) . These gravity values are larger by 0.28 dex in average than the values adopted in our previous analysis of OH lines [10]. This implies a mean small reduction of 0.09 dex in the oxygen abundances inferred in the latter paper, which does not affect the previously observed linear relationship between [O/Fe] and [Fe/H].

3.1 Oxygen

Type II SNe are expected to produce significant amounts of oxygen. Iron is produced in both, Type II and in Type I SNe. Since the latter come from longer lifetime progenitors, it has been argued for a long time that oxygen must be overabundant in very old stars. Evidence for high [O/Fe] ratios in many metal-poor stars has been reported during the last decades. Oxygen abundances derived from near-UV OH lines for 24 metal-poor stars have been presented recently [10]. It has been shown that the [O/Fe] ratio of metal-poor stars increases from 0.6 to 1 between [Fe/H]$=-1.5$ and -3.0 with a slope of -0.31 ± 0.11 (Fig. 1). Contrary to the previously accepted picture, new oxygen abundances, derived from low-excitation OH lines, agreed well with those derived from high-excitation lines of the O I IR triplet at 7774 Å. The comparison with oxygen abundances derived from the measurements of the IR triplet by Tomkin et al. [15] showed a mean difference of 0.00 ± 0.11 dex for the stars in common.

Israelian et al. [10] found four dwarfs (HD 22879, HD 76932, HD 103095 and HD 134169) in their sample for which oxygen abundances had been previously derived using [O I]. They synthesized the forbidden oxygen line for these stars adopting the same set of stellar parameters than for the OH analysis, the gf value given by Lambert (1978) and the equivalent widths provided in the literature for the λ 6300 Å line. The estimated abundances were in reasonable agreement with those derived from OH but still slightly lower. The abundances found using *Hipparcos* gravities are in better agreement, which

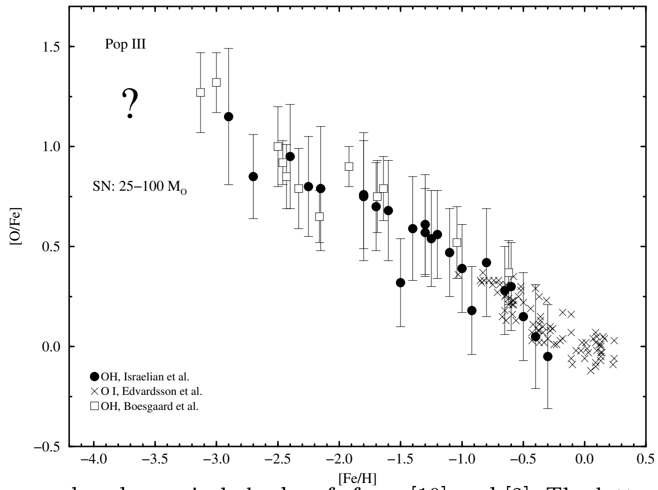

Fig. 1. Oxygen abundances in halo dwarfs from [10] and [3]. The latter have been corrected to our s stellar parameters scale.

strongly suggests that a reliable gravity scale may indeed be key to explain the discrepancies on oxygen abundances from forbidden and permitted lines in unevolved metal-poor stars. Recently, Fulbright & Kraft [9] have reported relatively low oxygen abundances from the [O I] line in two metal-poor subgiants, BD +23 3130 and BD +37 1458. Their analysis is based on gravities derived from LTE ionization balance. However, it has been shown recently that gravities derived using this technique in metal-poor stars do not agree with the gravities inferred from accurate *Hipparcos* parallaxes [1], which casts a shadow upon analyses of very metal-poor stars based on gravities derived from the ionization balance. Errors of 0.5 dex in log g have a significant effect on the interpretation of the forbidden line. Its sensitivity to gravity and the extreme difficulty of measuring lines of just a few mÅ in a spectral region where there are many telluric lines suggest that their results should be taken with caution.

Boesgaard et al. [3] have obtained high quality Keck spectra of several metal-poor stars in the near UV, and recently concluded their analysis of a different set of OH lines. They find very good agreement with our results, and basically the same dependence of [O/Fe] versus metallicity. The mean difference in oxygen abundance for ten stars in common with [10] is 0.00±0.06 dex when the differences in stellar parameters are taken into account.

Chemical evolution models of the early Galaxy where stellar lifetimes are taken into account and assuming that Type Ia SN appear at a Galactic age of 30 million years can also explain the evolution of oxygen delineated in Fig. 1 [5]. The evolution of oxygen proposed in this paper also helps to understand the evolution of ^{6}Li versus [Fe/H] and the ^{6}Li/Be ratio at low metallicities in the framework of standard Galactic Cosmic Ray Nucleosynthesis [8]. In addition, [14] have proposed that a delay between the effective deposition times into the ISM of Fe and O (only a fraction of which condensed in oxyde grains) can explain a linear trend of [O/Fe].

3.2 Carbon

It is commonly accepted that intermediate mass stars ($3M_\odot < M < 10M_\odot$) are the main source of Galactic C [17]. It has been shown [12,4,15] that [C/Fe] is approximately zero independently of [Fe/H]. Note that all these studies were based on the 4300 Å feature of CH. [15] have demonstrated that C I at ~ 9100 Å provides an average [C/Fe]=+0.3±0.2, whereas the CH band provides [C/Fe]=−0.1±0.2. We confirm earlier results that [C/Fe]~0 in the wide range of [Fe/H] (Fig. 2).

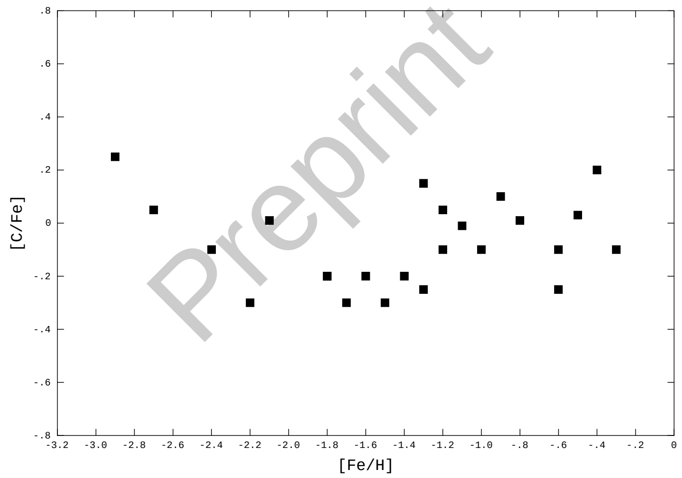

Fig. 2. Carbon abundances in halo dwarfs. Typical error bar is 0.3 dex.

3.3 Nitrogen

The isotope ^{14}N is synthesized from ^{12}C and ^{16}O through the CNO cycles in the H-burning layer. Observations of the NH band at 3360 Å have allowed many investigators to delineate the Galactic evolution of N down to [Fe/H]~ −2.8. [16] used high resolution spectra of 8 disk and 6 halo stars (−0.3 < [Fe/H]< −2.3) and found [N/Fe]≃ −0.25. [12] and [4] obtained

[N/Fe]= -0.67 ± 0.14 (intermediate resolution spectra of 116 stars) and [N/Fe]= -0.11 ± 0.06 (low resolution spectra of 76 stars), respectively. However, we should stress that this band is blended with Ti and Sc lines and it is preferable to use high resolution spectra in order to avoid any systematics due to the overabundance of Ti (α-element) and Sc in metal-poor stars. We confirm previous results that [N/Fe] is constant in a wide range of [Fe/H].

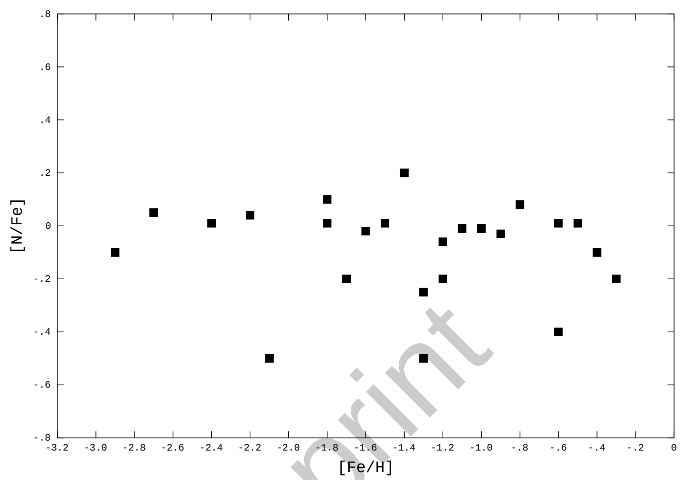

Fig. 3. Nitrogen abundances in halo dwarfs. Typical error bar is 0.2 dex.

4 Concluding remarks

We have derived carbon, nitrogen and oxygen abundances for a sample of metal-poor unevolved stars. [C/Fe] and [N/Fe] ratios appear to be constant, independently of metallicity, in the range 0.3 >[Fe/H]> -3.0, while the [O/Fe] ratio increases from approximately 0 to 1. Carbon and nitrogen abundances show larger scatter than oxygen at a given metallicity, which could reflect the larger variety of stellar production sites for these elements. Work is in progress to derive CNO abundances for a larger sample of unevolved metal-poor stars using other features in the optical and IR spectral regions, which should in principle allow a reliable estimate of the Galactic evolution of these elements.

References

1. Allende Prieto, C., García López, R. J., Lambert, D. L., & Gustafsson, B. (1999) ApJ (in press)
2. Alonso, A., Arribas, S., & Martinez-Roger, C. (1996) A& AS **313**, 873
3. Boesgaard, A.M., King, J.R., Deliyannis, C. P., Vogt, S.S. (1999) AJ **117**, 492
4. Carbon, D., Barbuy, B., Kraft, R., Friel, E. and Suntzeff, N. (1987) PASP **99**, 335
5. Chiappini, C., Matteucci, F., Beers, T.C., Nomoto, K. (1999) ApJ **515**, 226
6. Edvardsson, B., Andersen, J., Gustafsson, B., Lambert, D. L., Nissen, P. E., & Tomkin, J. (1993) A&A **275**, 101
7. ESA 1997, The Hipparcos and Tycho Catalogues, ESA SP-1200
8. Fields, B.D., Olive, K.A. (1999) ApJ **516**, 797
9. Fulbright, J. and Kraft, R. (1999) AJ **118**, 527
10. Israelian, G., García López, R. J., & Rebolo, R. (1998) ApJ **507**, 805
11. Kurucz, R. (1992) CD ROMs, Atlas9 Stellar Atmospheres Programs, SAO, Cambridge
12. Laird, J. (1985) ApJ **289**, 556
13. Pavlenko, Ya. V. (1991) Soviet Ast. **35**, 212
14. Ramaty, R., Vangioni-Flam, E., Casse, M. and Olive, K. (1999) PASP **111**, 651
15. Tomkin, J., Lemke, M., Lambert, D. L., & Sneden, C. (1992) AJ **104**, 1568
16. Tomkin, J. and Lambert, D. (1984) ApJ **279**, 220
17. Wheeler, J., Sneden, C., and Lambert, D. (1989) ARA&A **27**, 279

CHCN Very Metal-Poor Stars: Are These the Missing Pop III ?

Vanessa Hill[1], Beatriz Barbuy[2], François Spite[3], Monique Spite[3], Roger Cayrel[3], Birgitta Nordström[4], and Timothy C. Beers[5]

[1] ESO, Karl-Schwarzschild-Str. 2, D-85748 Garching, Germany
[2] Universidade de São Paulo, CP 3386, São Paulo 01060-970, Brazil
[3] DASGAL, Observatoire de Paris-Meudon, F-92195 Meudon Cedex, France
[4] Niels Bohr Institute for Astronomy, Physics & Geophysics, Copenhagen University, Juliane Maries Vej 30, DK-2100 Copenhagen, Denmark
[5] Michigan State University, Department of Physics & Astronomy, East Lansing, MI 48824, USA

Abstract. We have carried out a new analysis of two of the most extreme CH/CN very metal poor giants (originally discovered as part of the ongoing Beers Preston & Shectman HK survey [2]) with high resolution spectroscopy to determine the precise chemical composition of these objects, paying special attention to the heavy s and r neutron-capture elements. The results of this study are presented and discussed in terms of the possible origins for these objects: mass-transfer from a binary companion or intrinsic evolutionary stage of evolved Pop III stars ?

We have carried out a revised analysis and derivation of heavy-element (Z>35) abundances in the very metal-poor CH/CN-strong stars CS 22948-27 and CS 29497-34, originally discovered as part of the ongoing HK survey and previously analyzed by Barbuy et al. [1]. These stars show among the highest C and N enhancements relative to Fe known ([C/Fe]=+2. and +2.5, with [Fe/H]=−2.47 and −2.90 respectively), which results in very strong CH, C_2 and CN bands. The blending of lines, particularly in the blue, presents a great problem for abundance derivation from atomic lines. Nevertheless, by making use of spectrum synthesis fitting and using especially computed atmosphere models, it has been possible to derive the abundances of the neutron-capture heavy elements Sr, Y, Ba, La, Ce, Pr, Nd, Eu, and Dy. Details about the method and analysis can be found in [5].

The abundance patterns of the neutron-capture elements in CS 22948-27 and CS 29497-34 appear to be intermediate between a r-process (as indicated by a high Eu abundance) and a s-process enrichment patterns (Fig. 1). The s-process contribution might be well due to a mass-transfer episode from an evolved companion star, although our radial velocity measurements show no significant variations, i.e., no indications of binarity (but the accuracy and temporal baseline are not sufficient to exclude this hypothesis either).

At first inspection, the huge carbon enhancements found in CS 22948-27 and CS 29497-34 suggest a scenario, originally proposed by Iben [3], which induces a very efficient production of carbon in zero-metal stars of moderate mass. The carbon may then be violently mixed [4], also producing large amounts of nitrogen, and bringing these elements to the stellar surface. This scenario, however, would predict a $^{12}C/^{13}C$ ratio near the equilibrium value, whereas our present measurements provide a significantly larger value. Also, the presence of metals has to be explained. [4] propose accretion from interstellar clouds, but any stellar wind would make this accretion rather inefficient. Moreover, the high observed Eu/Fe ratio would restrict the accretion specifically to those clouds which themselves possess high Eu/Fe ratios – a very improbable process.

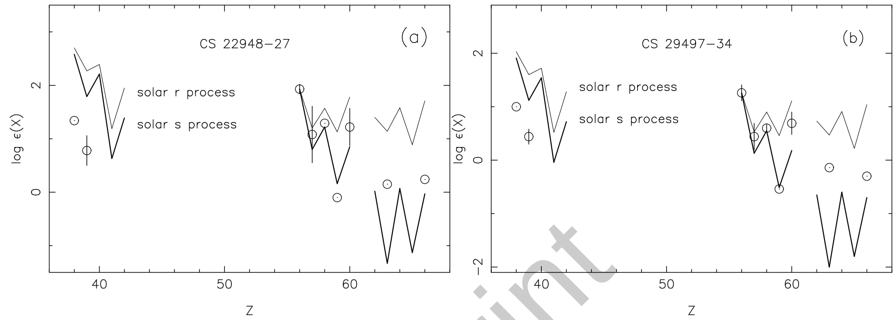

Fig. 1. Observed abundance pattern of the neutron-capture elements compared to the solar s- (thick line) and r-process (thin line) patterns, normalized to Ba (Z = 56), as in [6]. The standard deviations were computed when more than two lines were measured, and the error bars are indicated accordingly.

Our present observations of these two stars suggest that these giants are not Pop III stars, polluted either by internal or external processes, but rather, they are very metal-poor stars, enhanced in C, N and s-process elements (and Eu) either because the matter which formed these stars happened to be enriched in these elements, or by mass transfer from an evolved companion.

The full understanding of these very metal-poor and C,N-rich stars, revealed to be numerous in the HK survey, clearly warrants detailed investigation through the analysis of a much larger sample.

References

1. Barbuy B., Cayrel R., Spite M., Beers T.C., Spite F., et al. 1997, A&A **317**, L63
2. Beers T.C., Preston G.W., Shectman S.A. (1992), AJ **103**, 1987
3. Iben I. Jr. 1982, ApJ **260**, 821
4. Fujimoto M.Y., Aikawa M., Iben I. Jr. 1999, in 3rd Stromlo Symposium: The Galactic Halo, ASP Conf. Ser. **666**, 247
5. Hill V., Barbuy B., Spite F., Spite M., Cayrel R., et al., 1999 (A&A in press)
6. Sneden C., McWilliam A., Preston G.W., Cowan J.J., Burris D.L., Armosky B.J. 1996, ApJ **467**, 819

Preliminary Abundance Ratios in an Extremely Metal-Poor Binary Star

Birgitta Nordström[1], Eric Depagne[2], Monique Spite[2], François Spite[2], Vanessa Hill[3], Roger Cayrel[2], and Timothy C. Beers[4]

[1] Niels Bohr Institute for Astronomy, Physics & Geophysics, Copenhagen University, Juliane Maries Vej 30, DK-2100 Copenhagen, Denmark
[2] DASGAL, Observatoire de Paris-Meudon, F-92195 Meudon Cedex, France
[3] ESO, Karl-Schwarzschild-Str. 2, D-85748 Garching, Germany
[4] Michigan State University, Department of Physics & Astronomy, East Lansing, MI 48824, USA

Abstract. The orbital elements of CS 22873-139 have been revisited and preliminary abundance ratios in this extremely metal poor binary star with [Fe/H] ≈ -3.6 are given.

1 Introduction

CS22873-139 is a very metal poor double-lined binary star ([Fe/H] ≈ -3.6), which is located near the main sequence turn-off. Only a few such stars are known. It is therefore interesting to determine the elemental abundance ratios in this star and we report here about work in progress. The orbital elements of this system have been studied by [2], who found a period of 19.165 days and a mass ratio of $0.86 < M_A/M_B < 0.90$.

Preston proposed that this star is an intermediate age object accreted from a low luminosity satellite of the Milky Way. The ratios of the abundances of the different elements could be a test of this hypothesis.

2 Observations and Radial Velocity Measurements

The observations were carried out with the ESO Multi-Mode Instrument (EMMI), at the NTT, and with the CASPEC spectrograph at the ESO 3.6m telescope. The resolution is 50000 for EMMI spectra and 16000 for CASPEC spectra. Moreover some spectra for radial velocities have been obtained with the new spectrograph FEROS at the ESO 1.5m telescope in July and August 1999. The orbital elements could be improved with these new observations. We find an eccentricity of 0.20 while Preston found 0.26. The period is 19.163 days, very similar to the previous value and the most probable mass ratio is $0.76 < M_A/M_B < 0.80$ (Fig. 1).

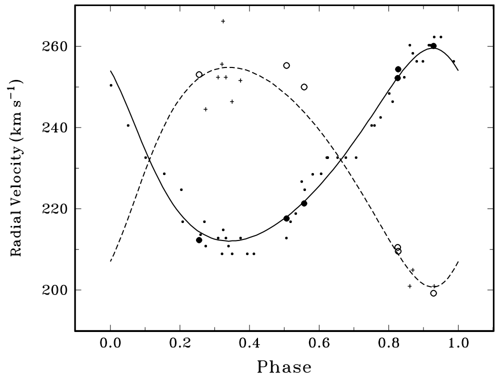

Fig. 1. Radial velocity curves of the two components of CS22873-139. Small dots and plusses: Preston's observations. Large dots and circles: our new observations.

3 Analysis

The models used in the analysis of the stars have been interpolated in the grid of Edvardsson et al. [1] computed with an updated version of the MARCS code. The temperature of the primary star is strongly constrained by the profile of the wings of the hydrogen lines. The difference between the temperature of the components A and B has been estimated for a mass ratio of 0.78, from the isochrone of VandenBerg et al. [3] computed for 12 Gyrs and [Fe/H]=-2.3. We found that the temperature of the brightest component is about 6300K and that $\Delta \mathrm{Teff}_{\mathrm{A,B}} \approx 1300$K. The results of the analysis are given in Table 1.

Two abundance anomalies are striking: first the very low abundance of strontium, and second the rather low abundance of magnesium ([Mg/Fe]≈ 0.0 instead of +0.4 as expected in very metal poor stars) associated with a strong overabundance of titanium (an element which may be considered like magnesium and calcium as an α element). The spectrum is compatible with a normal lithium abundance $\mathrm{A_{Li}} = 2.05$.

Table 1. Abundances of the different elements in CS 22873-139 A and B

[Fe/H]	-3.60			$\mathrm{A_{Li}}$	2.05
[Mg/Fe]	+0.02	[Ca/Fe]	+0.30	[Ti/Fe]	+1.00
[Al/Fe]	-0.60	[Sc/Fe]	+0.36	[Sr/Fe]	< -1.7

References

1. Edvardsson B., Andersen J., Gustafsson B., et al., 1993, A&A 275, 101
2. Preston G., 1994, AJ 108, 2267
3. VandenBerg D.A., Swenson F.J., Rogers F.J., et al., 1997, in preparation.

Three Very Metal-Poor, Extremely Wide Binaries

Christine Allen, Arcadio Poveda, and M.A. Herrera

Instituto de Astronomía, UNAM. Apdo. Postal 70-264, México D.F. 04510

1 Introduction

In a recent investigation [1] we have identified over a hundred wide, common proper-motion binaries belonging to the old disk, the thick disk or the halo of the Galaxy. These systems were found by searching for common proper-motion companions to the high-velocity, metal-poor primaries of the lists of Schuster et al. [3,4]. For these stars, Strömgren photometry has allowed the determination of metallicities, distances and, in many cases, individual ages. The values obtained for the metallicities and ages of a number of these stars place them among the oldest, most metal-poor stars of the Galaxy. For the purposes of this work, we concentrate our attention on those stars with [Fe/H] < -2.00 as representatives of the very early stellar population of our Galaxy.

Table 1. Principal properties of the three binaries

	W1828 (Hip 15396)	G15-10 (Hip 74199)	G40-14 (–)
V_p (km s^{-1})	417.5	306.7	413.1
V_{gc}	229.4	248.4	256.0
E (100 km_2 s^{-2})	-1163.1	-1131.5	-1095.8
h (10 kpc km s^{-1})	-143.8	30.4	- 113.9
$R_{\min}$ (kpc)	7.6	1.1	2.9
$R_{\max}$ (kpc)	9.6	15.6	16.4
$\lvert z_{\max}\rvert$ (kpc)	5.2	7.1	1.4
Eccentricity	0.12	0.87	0.70
[Fe/H]	- 2.05	- 2.14	- 2.34
Age (Gy)	20.9	–	20.3
$\langle a \rangle$	55410	125073	32232

2 Results and discussion

Among 48 stars with [Fe/H] < -2.00 present in the lists of Schuster et al. we have found only three wide binaries. Table 1 lists the main properties of these systems. The listed distances, ages and metallicities were taken from Schuster et al.

We note the remarkably large separations of these three binaries. For comparison, we calculate the fraction of extremely wide binaries ($\langle a \rangle >$ 20 000 AU) among a complete sample extracted from the wide binaries ($\langle a \rangle > 25$ AU) of the solar vicinity [2]. The probability of randomly obtaining in three trials three extremely wide binaries out of a population with a typical frequency of 2.5% is about 10^{-5}. Also remarkable is that two of the galactic orbits are retrograde, while the third is only marginally direct.

The persistence of the duplicity for very old systems, like the stars in Table 1, is an intriguing problem. Their galactic orbits show that these systems spend most of the time far from the galactic plane, which is where most of the massive perturbers are located. Their high space velocities also contribute to making the rare encounters relatively ineffective for their disruption.

3 Summary and conclusions

We stress that the binaries were selected from our list of 123 systems only by the criterion that their primaries should have [Fe/H] < -2.00. The three binaries found by this selection criterion turned out to have extreme properties, which can be summarized as follows: 1. Two of the binaries have strongly retrograde orbits, while the third is only marginally direct. 2. The separations, and hence the expected major semiaxes, of all three binaries are extremely large. 3. Two systems have individual age determinations; both turn out to be very old (≈ 20 Gy), among the oldest in Schuster et al.'s lists. 4. The peculiar velocities are quite large ($V_p > 300$ km s^{-1}). 5. Although the galactocentric velocities are moderate, the distances from the galactic plane reached by these systems, $z_{\max}$, are large, which clearly places them among the halo population.

Acknowledgment. We acknowledge partial financial support for this work from Conacyt, through Grant Nr. 25502-E

References

1. Allen, C., Poveda, A. & Herrera, M. A. 1999, A&A in press.
2. Poveda, A., Herrera, M. A., Allen, C., Cordero, G. & Lavalley, C. 1994, Rev. Mex. Astron. Astrof. 28, 43.
3. Schuster, W. J. & Nissen, P. E. 1988, Astron. Astrop. Suppl, 73, 225.
4. Schuster, W. J. Parrao, L. & Contreras, M. E. 1993, Astron. Astrop. Suppl, 97, 951.

And if Thick-Disk Stars Were the First Stars?

Klaus Fuhrmann

Universitäts-Sternwarte München

Abstract. Observational evidence for a *multi-component* Galactic halo and the absence of any one-to-one age-metallicity relation implies that the mere finding of an ultra metal-poor star must be considered as a weak argument for a "first star" in terms of age. The Milky Way's *thick-disk* population, by contrast, is identifiable as an extremely old population and as such most appropriate to provide *reliable* constraints on the age of the Galaxy.

1 First Stars: Is Metallicity *per se* of Relevance?

There is a lively interest in the search for *first stars* that results from their expected imprints of the Big Bang nucleosynthesis, the hope for a better understanding of structure formation, or – no less exciting – to constrain the age of the Galaxy. With respect to the nucleosynthesis of the first stars a zero metallicity for elements heavier than LiBeB is presumably most favourable for a pristine composition, though large dedicated surveys have not yet found any such objects (Beers 1999, this volume). From the viewpoint of stellar interior calculations it is likewise important to investigate the physical processes at Z=0. If, however, one is interested in the earliest *epochs* of astration, metallicity is no longer a primary characteristic. Among the many related examples we mention the dwarf spheroidal Leo I which shows the presence of a substantial population with ages of $\sim$3 Gyr at a metallicity [Fe/H]~ -2.0 [11], whereas the prominent globular cluster 47 Tuc, by contrast, is about $\sim$10 billion years older, but with a more than tenfold metal abundance.

Thus, to pin down the age of the Galaxy the restriction to metal-poor halo stars of either the field or globular clusters is by no means a basic requirement. What is, instead, important is the unequivocal identification of *the* ancient stellar population(s) in the Galaxy, which has become rather difficult for "the halo" since there is now overwhelming evidence that this is a multi-component entity (cf. e.g. [12,9], and references therein). Even more, although the bulk of the halo stars has an old mean age, blue metal-poor field stars [13], or, perhaps more convincing, the Sagittarius dwarf merger [8] remind us that accretion of young or intermediate-age populations is also a non-negligible phenomenon in the Galactic outskirts. Likewise, not all halo stars share the ~ -0.4 dex metal deficiency of iron-peak vs α-elements (cf. [3,10]), which, if simple accretion is not the underlying mechanism, implies the existence of a couple of Gyr *younger* halo stars (cf. [7]).

With these drawbacks in mind we shall therefore follow here another line of evidence by presenting observational results for an *individual* identification of nearby field stars of the Milky Way's *thick disk*, which show up as extremely old objects. It is then argued that this population was most likely formed at a high star formation rate and is presumably as old as the ancient Galactic halo. As such, the thick-disk population would be particularly appropriate to impose the most reliable constraints on the age of the Galaxy.

2 Field Stars of the Solar Neighborhood

The data we present in what follows are based on a sample of about 100 nearby F and G dwarfs, part of which are long-lived. The restriction to stars of the solar neighborhood has several reasons, one is rather practical and results from the fact that we are aiming at high-resolution, high-signal-to-noise spectroscopy with $\lambda/\Delta\lambda \sim$60000 and S/N$\geq$ 200. More important, however, is the wish to compare the spectroscopically derived, i.e. model-atmosphere-dependent, stellar parameters with the solid astrometric parallaxes from the Hipparcos satellite. This comparison provides invaluable information on the stellar surface gravities, effective temperatures, metallicities and radii. In combination with stellar evolutionary tracks, the Hipparcos data also allow for fairly accurate mass and age determinations for nearby *field* stars in evolved stages. For certain candidates this can in fact be very precise as has recently been demonstrated by Dravins et al. [4] for the closest subgiant β Hyi.

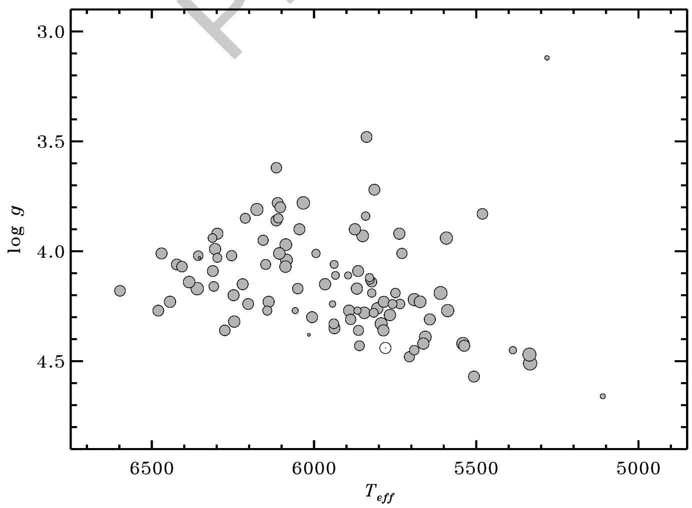

Fig. 1. The sample of nearby field stars in the T_{eff}-$\log g$ *Kiel diagram*. Circle diameters are in proportion to the derived metallicities

In Fig. 1 we display the relevant sample of stars in the T_{eff}-$\log g$ *Kiel diagram*, wherein each star is depicted in proportion to its derived metallicity. Details of the analyses and the tabulated stellar parameters are given in Fuhrmann ([5], 2000 in preparation). Here we restrict ourselves mentioning that the very good match of the spectroscopic and astrometric distances as illustrated in Fig. 2 provides much confidence in the applied spectroscopic methods and is also a useful sieve for a number of outliers (depicted by open circles), such as spectroscopic binaries. It is important to note that the 2.8% systematic discrepancy in Fig. 2 corresponds to a mere $\sim$0.02 dex in $\Delta \log g$ and that the diagram reveals the principal potential of accurate distance determinations for F and G dwarfs – even on Galactic (kpc) scales – once a high-resolution + high-signal-to-noise spectrum is available.

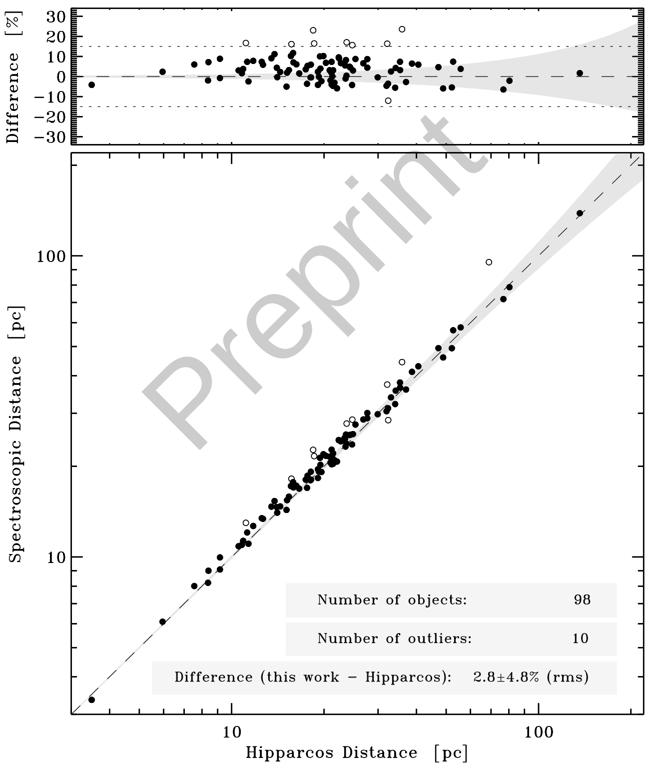

Fig. 2. Comparison of the spectroscopic versus astrometric distance scale. The Hipparcos data have typical parallax errors of 1 mas, as illustrated by the shaded wedge. Individual uncertainties of the spectroscopic data should not exceed 15% (dotted curve in the upper panel), with no dependence on distance. The spectroscopic distances result in *higher* values by 2.8% on average, and a statistical *rms* error of 4.8%. Outliers (e.g. spectroscopic binaries) are marked by open circles

3 First stars in the Galaxy: *Thick Disk* Versus *Halo*

The presumably most important aspect of the analyzed sample of nearby F and G stars in Fig. 1 is that stars of both disk populations can be identified *individually* at a high confidence level. In Fig. 3 we show the updated version of the relevant diagram that reveals the abundance, abundance ratio, and age characteristics of the analyzed stars (excluding already the outliers of Fig. 2). In addition, the peculiar velocities of the stars $v_{pec} = (U^2 + V^2 + W^2)^{1/2}$ vs [Mg/H] are displayed in Fig. 4. Note that, while ideally all stellar aspects should be considered simultaneously, it is the age distribution that provides the most important clue for the distinctness of thick- and thin-disk stars. In fact, in the course of the work the paucity of stars with ages between approximately 9 to 12 Gyr was noticed relatively early and finally led to the suggestion that thick-disk stars represent an entirely very old population, separated from the thin disk by a significantly reduced rate, or even a hiatus, in star formation. The backbone for the principal feasibility of meaningful age determinations of *individual* field stars is certainly the Hipparcos data. But there is also considerable progress in the stellar interior calculations, as described in [2] , in particular with respect to the efficiency of the convective energy transport. Thus age determinations can nowadays indeed be very accurate – at least differentially.

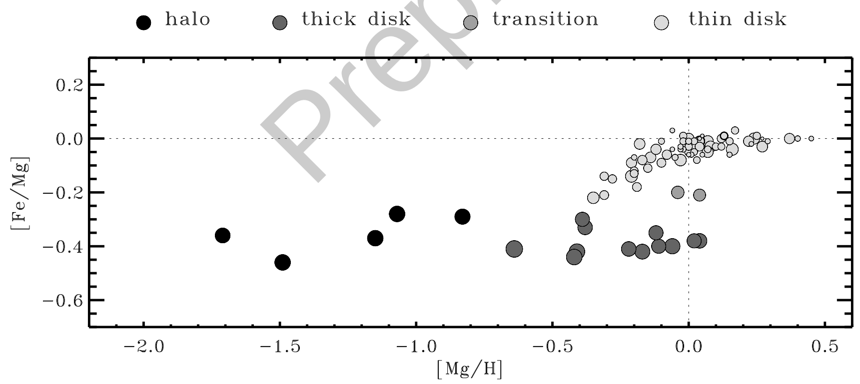

Fig. 3. Abundance ratios [Fe/Mg] vs [Mg/H]. Circle diameters are in proportion to the stellar ages. Different *stellar populations* are given with various grayscale symbols as indicated in the legend on top, and are based on chemistry, kinematics and age

Although most of our sample stars are "normal" thin-disk stars, and, accordingly, the number of investigated nearby halo and thick-disk stars is yet very small, there is currently much evidence that the thick-disk population is not detectably younger compared to ancient halo field stars. HD 84937, for

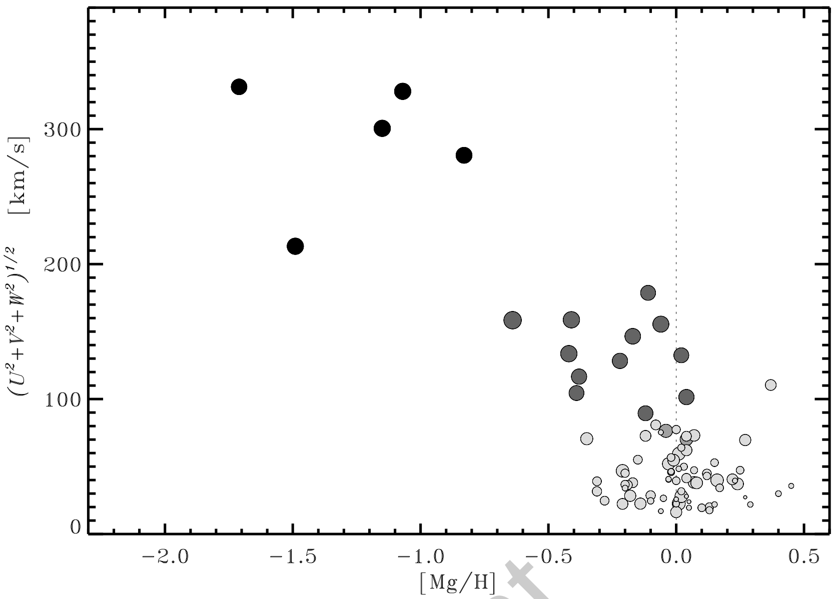

Fig. 4. Peculiar velocities $v_{pec} = (U^2 + V^2 + W^2)^{1/2}$ of the nearby F and G stars versus metallicity. Grayscaling and symbol sizes have the same meaning as in Fig. 3

instance, the halo turnoff star at [Mg/H]~ -1.7 in Fig. 3, is presumably coeval ($\sim$ 13 Gyr) to 72 Her and HD 221830, the two most metal-rich thick-disk stars in this diagram.

Hence, it is most obviously *not* the amount of metals that determines the age. If, however, both thick-disk and old halo stars are indistinguishably coeval, their distinct kinematic properties make Gilmore's [6] suggestion of two, *parallel*, evolutionary paths, namely "halo-to-bulge" and "thick disk-to-thin disk", a very appealing scenario. In this case, and since we can find more than a hundred thick-disk F and G field stars within 50 pc, i.e. tracers with very accurate Hipparcos data, a precise age determination of this population (notably subgiants) is extremely rewarding. This task is particularly promising since both the modeling of the stellar atmospheres and the stellar interior calculations of thick-disk stars can be very differential with respect to the Sun. A peek at Fig. 5, where we compare a tracing of the Moon (=reflected sunlight) with the thick-disk star 72 Her (T_{eff}/log g/[Fe/H]/[Fe/Mg] $= 5735/4.24/-0.34/-0.38$) is quite obvious in this respect. Note, in particular, the Mg I line $\lambda 5711$ which is of equal strength in both stars (as it holds true for presumably all the α-elements).

In other words, 72 Her is a star of approximately solar effective temperature, only $\sim$0.2 dex more evolved in log g, and has a metal content that is

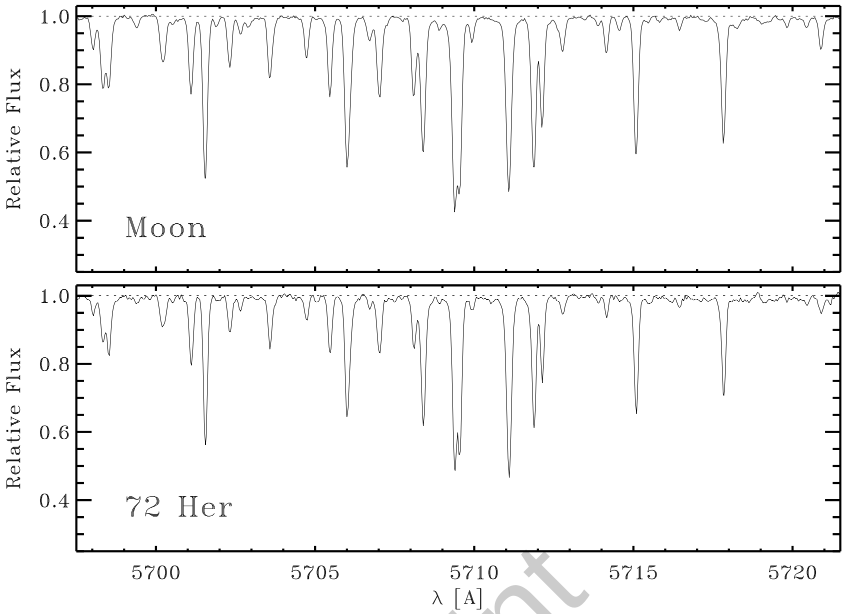

Fig. 5. Spectral portion of a Moon (reflected sunlight) spectrum compared to the nearby thick-disk star 72 Her. The latter is at [Fe/H]$= -0.34$ dex, but has approximately *solar magnesium* abundance (cf. the absorption line $\lambda5711$ which is Mg I). Note that 72 Her may actually be as old as $\sim$13 Gyr

partly solar and partly only a factor two off. At a distance of 14 pc its absolute visual magnitude is also very well known. Hence one may put forward the question: *are there well-founded arguments – except for the notoriously ill-determined helium abundance – to distrust differential analyses of stars like this?*

In the case of the halo star HD 84937 ($6353/4.03/-2.07/-0.36$), for a counter-example, we register an iron abundance about one hundredth of the solar value and a turnoff stage of evolution, which – as a result of the star's low metallicity – is $\sim$600 K hotter than the Sun. The accuracy of the effective temperature determination is thereby more contestable, as is the abundance determination, for which a more or less disjunct set of lines is mandatory for stars in this metallicity range. Further, the Hipparcos-based luminosity of HD 84937 (d=80 pc) is also less accurate by a factor of four compared to 72 Her. The disadvantage for a precise age determination of 72 Her is, of course, that it has not yet reached its turnoff position. Though this is the case for the related HD 221830 ($5749/4.19/-0.36/-0.38$), one would ideally like to have a nearby thick-disk subgiant for that purpose. In that case, the stellar parameters and stellar interior calculations would certainly supercede the achievable accuracy for *any* known halo star.

This last point is important to keep in mind. Indeed, the Hipparcos data enable age determinations of nearby *field* stars that are also more reliable than *any* of the existing globular cluster data (recall the example of β Hyi mentioned above). With (i) negligible uncertainties in distance and (ii) low interstellar absorption, hence reliable absolute visual magnitudes, with (iii) accurate, purely spectroscopic stellar parameters and (iv) detailed information on elemental abundances and abundance ratios, there can be no doubt that nearby field stars possess an enormous potential. Of course, it has repeatedly been mentioned that for reasonable age determinations of field halo stars only a handful of them with reliable Hipparcos parallaxes exist in the solar neighborhood. But there is more than ten times as many nearby thick-disk stars. For a meaningful constraint on the age of the Galaxy by virtue of this population one of the important questions is then: was the feedback of the massive stars already there, while the low mass stars were still forming? The mixing timescale for the first generation of stars may actually be on the order of $\sim 3 \times 10^6$ yr [1]. But can we expect *large* amounts of metal-enrichment *and* locking in long-lived stars within, say, $\sim 10^8$ yr? The data of Fig. 3, with considerable [Fe/Mg] deficiencies *up to solar metallicity* and the subsequent age gap to thin-disk stars are most likely the fingerprints of a high star formation rate for the thick disk. This might in fact imply that some, if not all, of the nowadays observable objects of this population were there right from the very early phase of our Galaxy.

References

1. Audouze, J., Silk, J. (1995) ApJ 451, L49
2. Bernkopf, J. (1998) A&A 332, 127
3. Carney, B.W. (1999) ASP Conf. Ser. 165, 230
4. Dravins, D., Lindegren, L., VandenBerg, D.A. (1998) A&A 330, 1077
5. Fuhrmann, K. (1998) A&A 338, 161
6. Gilmore, G. (1995) IAU Symp. 164, 99
7. Gilmore, G., Wyse, R.F.G. (1998) AJ 116, 748
8. Ibata, R.A., Gilmore, G., Irwin, M. (1994) Nat 370, 194
9. Johnston, K.V. (1999) ASP Conf. Ser. 165, 64
10. Laird, J.B. (1999) ASP Conf. Ser. 165, 248
11. Lee, M.G., et al. (1993) AJ 106, 1420
12. Majewski, S.R. (1999) ASP Conf. Ser. 165, 76
13. Preston, G.W., Beers, T.C., Shectman, S.A. (1994) AJ 108, 538

Gravities of Metal-Poor Halo Dwarfs and the Age of the Universe

Andreas J. Korn and Thomas Gehren

Universitäts-Sternwarte München (USM), Scheinerstr. 1, 81679 München

Abstract. We report on the methodology of an ongoing project to determine accurate stellar parameters ($T_{\rm eff}$, $\log g$, [Fe/H], [α/Fe]) for a number of metal-poor halo stars located *at the turnoff* (TO). With the aid of *shift-free* unified stellar evolutionary models we envision to derive *absolute* ages for these stars. Their ages will set stringent lower limits to the age of the Galaxy and the Universe.

Ingredients needed

Despite the fact that "[Fe/H] is a clock without hands" (Simon White, this conference), low-mass low-metallicity stars at the turnoff cannot be young objects. To derive their ages to within $\Delta t \sim 1-2$ Gyr we need:

1. high-quality spectra (R $\sim$ 40 000, S/N $\sim$ 200)
2. reliable effective temperatures ($\Delta T_{\rm eff} \sim 50$ K)
3. reliable surface gravities ($\Delta \log g \sim 0.1$ dex)
   1., 2. & 3. $\Rightarrow$ accurate abundances (Δ[X/H] $\sim$ 0.1 dex) and
4. state-of-the-art evolutionary tracks respectively isochrones.

Naturally, points 2 and 3 entail the full complexity of model atmospheres (empirical vs. theoretical) and line formation (LTE vs. NLTE).

1 Spectra

We have obtained spectra of local halo TO stars down to 11.5$^{\rm th}$ magnitude using FOCES [1] on the Calar Alto 2.2m telescope. According to [2] they have photometric metallicities [m/H] between -2.2 (HD 84937) and -3.5 (G 64-12). The spectra have $R = 40\,000$ and cover the wavelength range of 3900 – 9000 Å. For the fainter targets the required S/N ratio is achieved by coadding individual exposures.

2 Effective Temperatures

Together with $\log g$ from Mg Ib (see Section 3), $T_{\rm eff}$ derived from fitting Balmer profiles yields results fully compatible with HIPPARCOS parallaxes (cf. [3]). In the framework of the convection theory by [4] a *single* α parameter ($\alpha_{\rm CM} \sim 0.8$) is capable of fulfilling the constraints of both stellar structure and Balmer profile fitting (cf. Section 4). The typical uncertainty of this step is 50 K for spectra with S/N ratios of $\sim$ 200.

3 Gravities

Balancing Fe I and Fe II in LTE has been shown to yield gravities that are incompatible with HIPPARCOS for stars hotter than the Sun [3,5]. The *strong line method* (using pressure-broadened lines of Mg Ib) becomes inapplicable below $[m/\mathrm{H}] \sim -2.4$ due to the weakening of the spectral features [5]. For the most metal-poor stars we therefore concentrate our efforts on
- the Fe I/II ionization equilibrium (numerous yellow lines) and
- the Ca I/II ionization equilibrium (Ca I λ4226 vs. Ca II $\lambda\lambda$8498/8542/8662).

Both Fe I and Ca II are subject to strong NLTE effects which are currently under investigation. After calibration an internal accuracy for $\log g$ of 0.05 to 0.1 dex ought to be within reach of a *differential* analysis with respect to the Sun.

4 Evolutionary models

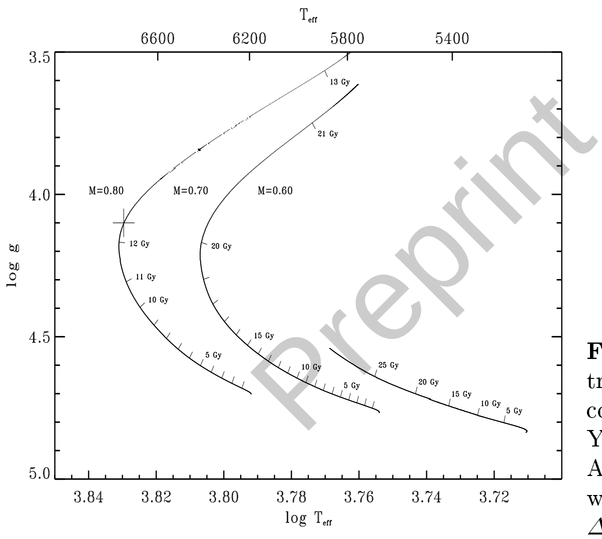

Fig. 1. Evolutionary tracks by Bernkopf (priv. comm.) for [Fe/H]$=-3$, Y$=0.23$ and $[\alpha/\mathrm{Fe}]=+0.4$. A fictitious TO star with $\Delta T_{\mathrm{eff}}=50\,\mathrm{K}$ and $\Delta \log g=0.05$ is indicated.

The stellar evolutionary calculations by [6] include convection according to [4] and gravitational diffusion. Model atmospheres are taken into account as the surface boundary condition.
With $\Delta \log g \sim 0.05$ dex an accuracy of $\Delta t \sim 1$ Gyr will become feasible, far more accurate than what can currently be achieved by cosmological methods.

References

1. Pfeiffer, Frank, Baumüller, Fuhrmann & Gehren, 1998, A&AS, 130, 381
2. Carney, Latham, Laird & Aguilar, 1994, AJ, 107, 2240
3. Fuhrmann, 1998, A&A, 338, 161
4. Canuto & Mazzitelli, 1991, ApJ, 370, 295
5. Fuhrmann, 1998, A&A, 330, 626
6. Bernkopf, 1998, A&A, 332, 127

Kinematical Properties of Very Metal-Deficient Stars Based on a Large Unbiased Sample

Masashi Chiba

National Astronomical Observatory, Mitaka, Tokyo 181-8588, Japan

Abstract. We briefly describe the kinematics of about 1200 metal-deficient stars in the solar neighborhood, based on the recently completed catalog selected without kinematic bias. We stress here that the stellar halo possesses internal subcomponents characterized by different kinematics and density distribution. The implications of the current data for the formation of the Galaxy are also discussed.

1 Introduction

Kinematical and chemical information of metal-deficient stars provide us the early dynamic condition of the Galaxy under which they were formed, because the relaxation time required to mix up their initial phase-space distribution exceeds the age of the Galaxy. Thus, such metal-deficient stars are a useful probe of how disk-type galaxies like our own have developed their characteristic structures while changing the dynamical state with time. Based on this motivation, we have conducted the assembly and analysis of the large, non-kinematically selected sample of metal-deficient stars in the solar neighborhood [1,3]. Here we report the basic kinematical properties of our sample stars, and attempt to clarify the possible picture of the Galaxy formation which confronts with the observational data.

2 The Sample

The Beers et al. catalog, consisting of about 2000 stars below [Fe/H]$= -0.6$, includes updated stellar positions, newly-derived homogeneous distance estimates, revised radial velocities, and refined metal abundances. Moreover, a subset of about 1200 stars in the catalog contains available proper motions from a variety of recently completed proper motion catalogs, including the Hipparcos Catalogue and other ground-based catalogs [1]. Here we adopt the 1203 stars in the current work, for which the full three-dimensional velocity components are calculable. We remark that this is the largest sample of metal-deficient stars having available proper motions among any non-kinematically selected samples.

3 Results

3.1 Kinematics

Metal-deficient stars in the solar neighborhood are characterized by a radially elongated velocity ellipsoid and small systematic rotation. Specifically, for the stars with [Fe/H]≤ -2.2 located near the Galactic plane $|Z| < 1$ kpc, the velocity dispersions in the (U, V, W) velocity components read $(141\pm11, 108\pm9, 94\pm8)$ km s^{-1}, in reasonable agreement with previous results. The shape of the velocity ellipsoid remains basically unchanged as long as [Fe/H]≤ -1.7. In Fig. 1 , we show the mean rotational velocity $< V_\phi >$ as a function of [Fe/H]. It is clearly seen that the rotational properties change discontinuously at [Fe/H]$\simeq -1.7$: for [Fe/H]< -1.7, there is no obvious systematic variation of $< V_\phi >$ with decreasing [Fe/H], in contrast to the stars for [Fe/H]> -1.7. Thus, contrary to the monolithic collapse scenario by Eggen et al. [4], the formation of the halo to disk may undergo in a discontinuous manner. Also, the metal-deficient stars at $|Z| < 1$ kpc show a rather large prograde rotation of $< V_\phi >= 30-50$ km s^{-1}, and $< V_\phi >$ decreases if more stars at larger heights are considered, thereby indicating the vertical gradient of $< V_\phi >$. This suggests that the halo formation is *not* entirely chaotic as expected from dissipationless merging/accretion of fragments (Searle & Zinn [7]), but is affected by some sort of coherent process, possibly involving energy dissipation of gas.

We note that in contrast to Carney et al. [2] who utilized the kinematically biased sample, we find no evidence for the retrograde rotation of the halo stars at large distances from the plane. The outer halo appears to show *no* net rotation.

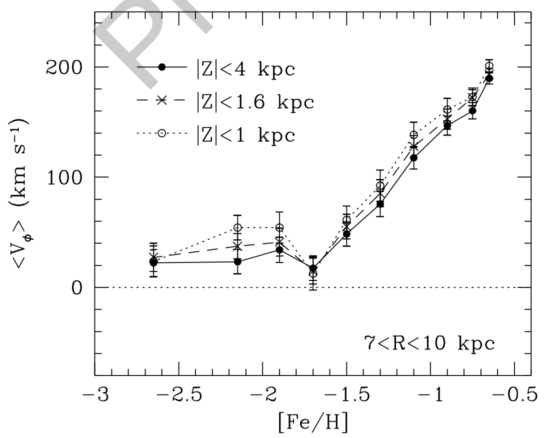

Fig. 1. Distribution of the mean rotational velocity $< V_\phi >$ vs. [Fe/H]

We also derive the orbital motions of the sample stars in a gravitational potential of the Galaxy including the dark halo. Using the analytic Stäckel potential [8], we compute the orbital eccentricities, e, defined as $e = (r_{ap} - r_{pr})/(r_{ap}+r_{pr})$, where r_{ap} and r_{pr} denote the apo- and peri-galactic distances, respectively Fig. 2 shows the relation between [Fe/H] and e. As is evident, metal-deficient stars have a diverse range in e, i.e., there is no correlation between [Fe/H] and e, in contrast to the finding by ELS.

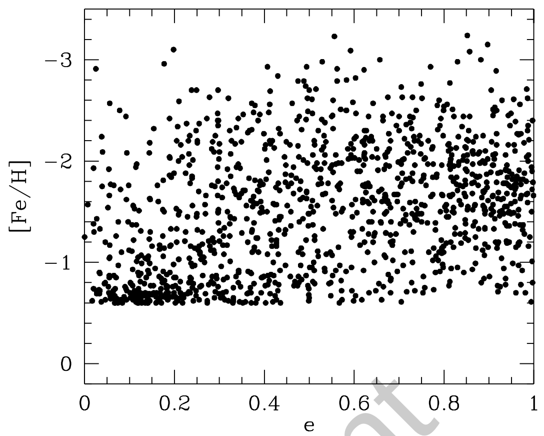

Fig. 2. The relation between [Fe/H] and e of the sample stars

3.2 Is There a Very Metal-Weak Thick Disk?

It has been discussed by previous researchers that low-e, low-[Fe/H] stars found here may belong to the metal-weak tail of the rapidly rotating thick disk that dominates at [Fe/H]$= -0.6$ to -1, and that the disk component may have an extended metallicity distribution even below [Fe/H]$= -2$. This may imply that the thick disk is formed by the dynamical heating of the pre-existing thin disk when a satellite galaxy falls into the disk [6]. To assess this point, we investigate the frequency distributions of both V_ϕ and e, based on a Monte Carlo model of a mixture of two Gaussian velocity distributions for the separate components of halo and disk, where the latter is assumed to comprise the fraction F and rotate rapidly at 200 km s^{-1}. We find that for [Fe/H]≤ -2.2, the disk fraction F is zero, although about 20% of the stars in this abundance range have $e < 0.4$. Thus, low-e, low-[Fe/H] stars belong to the halo component. In the intermediate abundance range $-1.7 <$[Fe/H]≤ -1, we estimate $F = 0.3$ Fig. 3 shows the dependence of F on [Fe/H], demonstrating that very metal-deficient stars are dominated by halo-like kinematics. Thus we conclude that the formation of the thick disk component occurred *subsequent to* the halo formation.

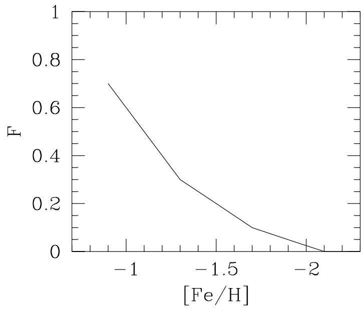

Fig. 3. Fraction of the thick disk at $|Z| < 1$ kpc as a function of [Fe/H]

3.3 Global Density Distribution of the Halo

Although our sample stars are located near the Sun, the orbits of these stars show large excursions in the Galactic space. Thus, their local kinematics convey the information on global dynamics and structure of the halo [5]. In other words, the nearby stars occupy a large volume of the phase space defined in the three isolating integrals of motion I_i, $i = 1, 2, 3$. Following these strategies, Sommer-Larsen & Zhen [8]) developed the maximum likelihood method for recovering the global density distribution of the halo, and applied it to their 118 halo stars available then. We apply the method to our larger sample of 355 stars with [Fe/H]≤ -1.8 and derive the global density distribution, as shown in Fig. 4 The lack of stars at small R but large Z is due to incompleteness. Besides this region, it is found that the outer part of the halo at $R > 15$ kpc appears to be round, in agreement with SLZ, whereas the inner part shows a highly flat density distribution. Fits of elliptical contours to the equidensity contours read that the axial ratio q is as large as 0.9 at $R \simeq 20$ kpc but is about 0.65 at $R < 15$ kpc, where q decreases smoothly with decreasing R. Thus, the halo can be described as nearly spherical and no net rotation at the outer part, and highly flat and prograde rotation (with a vertical gradient) at the inner part.

4 Implications for the Galaxy Formation

The current results set constraints on the scenarios for the formation of the Galaxy. The absence of a correlation between [Fe/H] and e suggests that the Galaxy has not experienced a free-fall monolithic collapse (ELS) unless otherwise there remain no low-e, low-[Fe/H] stars after collapse. Alternatively, the halo may have been assembled from merging/accretion of numerous fragments (SZ), but our finding of the finite vertical gradient of $< V_\phi >$ needs another explanation. Also, the result that the halo possesses internal subcomponents in both kinematics and spatial structure may not be explained neither by the ELS nor SZ hypothesis alone: the formation of the inner halo

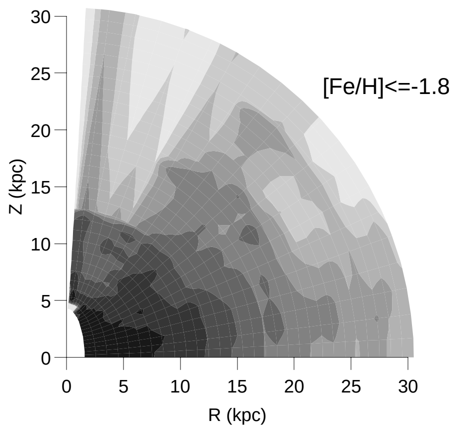

Fig. 4. Equidensity contours for the reconstructed halo in the (R, Z) plane

involves a dissipative process, not a dissipationless merging of fragments nor heating of the proto-disk, so that we require the hybrid picture, ELS plus SZ.

We go on to ask whether the ELS plus SZ picture is a natural consequence of the currently favored CDM theory of galaxy formation. According to the simulation work (Bekki & Chiba, this volume), the clumps of stars formed in local density fluctuations merge together in a dissipationless manner, and the debris shows the nearly spherical, outer halo. Then, as a result of merging of small clumps, some number of more massive clumps are developed, where each clump contains both metal-deficient stars formed earlier and gas accreted from surroundings. When the last merging event between the largest clumps occurs in a dissipative manner, the stars inside them are spread over the inner part of the halo, producing a flat density distribution, whereas a large fraction of gas end up in the center of the Galaxy and form the bulge. Therefore, the CDM theory may reproduce, at least qualitatively, the overall kinematic properties of the metal-deficient stars via both dissipationless and dissipative mergings of subgalactic clumps at the outer and inner halo, respectively.

The author is grateful to T. C. Beers, Y. Yoshii, I. Platais, R. B. Hanson, B. Fuchs, S. Rossi, and K. Bekki for collaboration.

References

1. Beers, T. C., et al. 1999, AJ, in preparation
2. Carney, B. W., et al. 1996, AJ, 112, 668
3. Chiba, M., Beers, T. C., & Yoshii, Y. 1999, AJ, in preparation
4. Eggen, O. J., Lynden-Bell, D., & Sandage, A. R. 1962, ApJ, 136, 748 (ELS)
5. May, A. & Binney, J. 1986, MNRAS, 221, 857
6. Quinn, P. J., Hernquist, L., & Fullagar, D. P. 1993, ApJ, 403, 74
7. Searle, L. & Zinn, R. 1978, ApJ, 225, 357 (SZ)
8. Sommer-Larsen, J., & Zhen, C. 1990, MNRAS, 242, 10 (SLZ)

Part III

The First Stars – Evolution and Nucleosynthesis

The Peculiar Evolutionary Behaviour of Population III Stars

Vittorio Castellani[1]

University of Pisa, Physics Department, I56100 Pisa, Italy

Abstract. The role of metal deficient stars in the scenario of galactic evolution is shortly recalled and the origin of their peculiar evolutionary behaviour is discussed to the light of the physical ingredients governing stellar structures. On this basis we define as Pop III all the metal deficient stars which are predicted to succeed in self producing carbon during their H burning phase. One finds that such Pop III stars are mainly characterised by a *decreased* upper limit for the appearance of electron degeneracy in the core of H-shell burning structures and by an *increased* upper limit for the occurrence of degenerate CO cores, both these occurrences being the result of the increased efficiency of pp burning. As a consequence, in Pop III one finds an increased probability for C detonation events. Further dynamic instabilities either at the He flash or during the AGB evolution are recalled, discussing the open problems still affecting the present knowledge of Pop III stellar structures.

1 Metal Deficient Stars: Why and Where?

The relevance of metal deficient stellar structures in the scenario of galactic nuclear evolution follows the theoretical evidence that matter forming our Universe emerged from the Big Bang with an amount of heavy elements definitely smaller than Z= 10^{-10} (see, e.g. [1]). Accordingly, one cannot escape the conclusion that the first step of that long history of stellar nucleosynthesis which led to actual abundances was performed by structures with no or very few metals.

More in general, one finds that metal deficient structures can play a relevant role in several cosmological problems. Following [4] one may shortly quote that:

- Faint objects and/or dark remnants could contribute to the "*missing mass*"
- Light could contribute to the 3 K background
- Heat could have re-ionised the Universe
- He yield could have produced pseudo primordial He abundances
- Heavy elements yield could have contribute to pregalactic Z-enrichment

Therefore one is interested in theoretical predictions concerning both metal deficient, massive stars, which already disappeared but injecting light and fresh nuclei in the cosmic space, possibly leaving compact dark remnants, and metal deficient low mass stars, which can be still alive in the present Universe.

The scarce observational evidence for surviving metal deficient stars has prompted in the past the popular conjecture of an Initial Mass Function (IMF) shifted toward large masses in comparison with the IMF for more metal rich stellar populations. However, the investigation by Palla et al. [19] on the radiative opacity of metal free mixtures has largely deprived such a conjecture of his supposed physical basis.

In this context, it may be worth to recall that in any case the evidence for metal deficient stars is expected to be a very poor one. Assuming negligible gas consumption, one finds that to enrich the galactic gas from Z=10^{-7} to the present abundance of heavy elements (Z$\sim 10^{-2}$) one needs a total amount of heavy elements 10^5 times larger than that in Z=10^{-7} mixture. As an order of magnitude, adopting the most simple assumptions of constant IMF and constant Supernovae yields, one finds that stellar populations with $10^{-7} \leq Z \leq 10^{-2}$ must be 10^5 times more abundant than less metal rich stars and, as a results, that one expects no more than 1 star with Z$\leq 10^{-7}$ out of 10^5 more metallic stars.

The problem of the actual IMF of metal deficient (hereinafter MD) stars is well outside the scope of this paper. Here we only notice that the often referred *"statistically significant lack of Pop III stars"* among disk stars [2] can be removed by simply assuming that the first steps of nuclear evolution of galactic matter occurred in the halo [3], as one could expect on very general grounds. Therefore the only meaningful discussion about the IMF of metal deficient stellar populations should rely on the metallicity distribution of stars over the whole galactic structure.

2 MD Structures: the Pioneering Era

The first approach to the structure of metal deficient stars dates back to the early '70s with some historical papers exploring the case Z=0, putting in this way the basis for all the incoming investigations. Ezer & Cameron [13] investigated zero metal MS stars in the range 5 to 200 $M_\odot$. The following year Ezer [12] presented the evolution of a 3 $M_\odot$ model from the MS phase till the exhaustion of central He. Castellani & Paolicchi [7] finally extended these investigations to the range of low masses, down to 0.8 $M_\odot$. To be quoted in this period also an investigation by Wagner [21] on low mass stars in the range Z= $10^{-6} - 10^{-8}$.

To understand the peculiarity of these zero metal structures one has to remind that the behaviour of a stellar structure is governed by three physical ingredients, namely:

- Equation of State (EOS)
- Radiative opacity
- Energy generation

When passing from "normal" Pop II structures ($Z \sim 10^{-3} - 10^{-4}$) to Pop III stars, both EOS and Opacity are scarcely affected by the lack of metals. On the contrary, the energy generation is "decapitated" since the lack of C nuclei does not allow CNO burning. The consequences of such an occurrence can be easily predicted when taking into account a theoretical evidence often not widely recognised, namely that *the luminosity of a MS structure is essentially governed by the stellar mass and NOT by the efficiency of nuclear reactions.* As a consequence, stars which are normally powered by CNO burning must raise their internal temperatures to obtain the required output of energy from pp burning only.

Such an occurrence can be clearly detected in Fig.1, where we report the central temperature of MS stars as a function of the stellar mass for selected assumptions about the star metallicities. As expected, one finds that the smaller masses (normally powered by pp burning only) are practically unaffected by the amount of metals. However, when increasing the stellar mass the increase of central temperatures in $Z=10^{-4}$ models is early damped by the ignition of CNO burning. Decreasing the metallicity the damping becomes progressively less efficient, practically vanishing when $Z=10^{-10}$. The parallel behaviour of central densities is shown in the same Fig.1, where one finds that extremely MD stars have the peculiarity of continuously increasing the central densities when increasing the mass, unlike all the more metallic models.

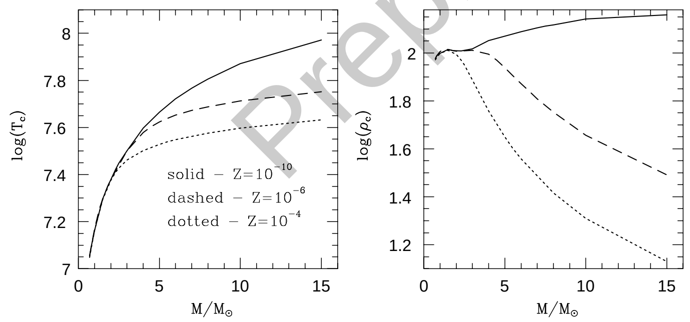

Fig. 1. Central temperatures (left) and densities (right) for MS stars as a function of the stellar mass and for the labelled values of the star metallicity.

As a relevant point, one finds that zero metal MS structures more massive than $\sim 10\ M_\odot$ raise their internal temperatures up to the threshold of 10^8 K, where the (cosmological) He is burned into C, and fresh self-produced carbon nuclei allow the onset of CNO burning. As a consequence, zero metal MS stars above $\sim 10\ M_\odot$ keep central temperatures near the threshold of 10^8 K, and the production of energy is mainly governed by the amount of self-produced C: larger the mass, larger this amount.

Moving from MS structures to more advanced evolutionary phases, one already knows that all "normal" stars, as Pop II stars are, increase their requirement of energy, thus increasing central temperatures, and even low mass stars around the Turn Off point are by now dominated by CNO burning. Not surprisingly, one finds that low mass, zero metal stars during the post MS phases reach in all case the threshold of 10^8 K, thus starting producing carbon: stars in the range of masses M$\sim$ 2.5-7.0 $M_\odot$ appear already significatively powered by CNO burning when the abundance of central H is still of the order of X_c $\sim$0.30, whereas less massive stars must wait till the last phases of H exhaustion at the centre. We conclude that ALL zero metal stars share the common peculiarity of experiencing self-production of C, either in the Zero Age MS (larger masses) or in later phases of central H burning. According to the available computations we will discuss later on, this is also the case for Z=10^{-10}, whereas no star with Z=10^{-6} experiences such a self-enrichment of C.

Such an evidence offers the opportunity of a natural definition of Population III: *One can define as Pop III stars all the structures which share the common peculiarity of experiencing self-production of C sometime during their H burning evolution.* According to such a definition, we will regard as Pop III all the stellar structures with metallicity below a not yet well defined upper limit between Z=10^{-10} and Z=10^{-6}. In the following sections we will present in more details available theoretical expectations concerning these structures, separately discussing

i) the evolutionary features of Pop III low mass stars which can be still (nuclearly) alive and, ii) the structure and the fate of more massive stars which already disappeared from the present Universe.

3 Living Pop III Stars (Low Masses)

After the pioneering era, the chronological history of the investigations on this issue runs as follows:

→D'Antona [11] followed the H-burning evolution of 0.9 and 1.0 $M_\odot$ with Z=0, disclosing the typical evolution of low mass stars BUT with much lower luminosity at the RG tip. Oscillations of nuclear energy outputs L_{pp}, L_{CNO} and $L_{3\alpha}$ were possibly regarded as numerical. However, the occurrence of some sort of instability was confirmed by

→Guenter & Demarque [16], who followed the evolution of a 0.9 $M_\odot$, Z=0 model till the ignition of the H burning shell, when a growing convective instability stopped the computations. The issue was clarified after seven years, with the work by

→Fujimoto, Iben & Hollowell [14] who discussed the case of a 1.0 $M_\odot$, Z=0 model, disclosing the occurrence at the exhaustion of central H of a convective thermal runaway, followed by multiple runaways all along RGB evolution. Moreover, these authors found evidences for a very strong He flash, with a mixing which should enrich the stellar surface with CNO elements ($X_{CNO} \sim 0.004$: see also [17]) but not with Fe. Low mass Pop III models were further investigated by

→Cassisi & Castellani [5], who presented a grid of models covering the range of masses from 0.7 to 15 $M_\odot$ for the case $Z=10^{-10}$.

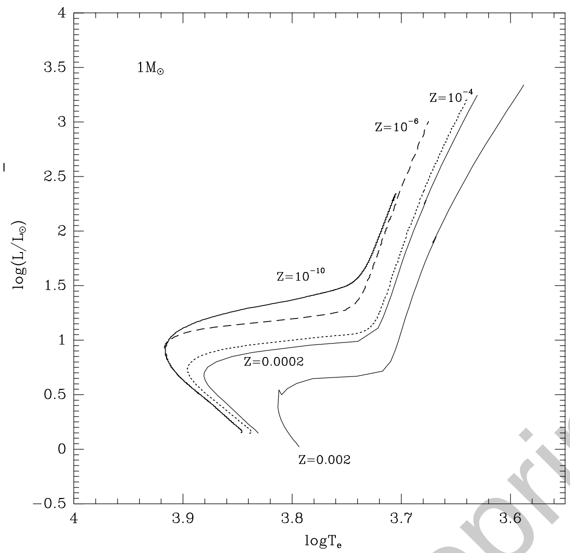

Fig. 2. The evolutionary paths of 1.0 $M_\odot$ models for the labelled values of the adopted metallicity

Low masses, which develop a degenerate He core during H shell burning phases, were followed till the onset of the He flash, more massive stars till the later phases of He shell burning around a degenerate CO core or till the carbon ignition. Fig.2 compares the evolutionary paths of 1.0 $M_\odot$ models as computed for the various labelled assumptions about the metallicity.

As shown in Fig.3, according to these computations one finds that the *"Transition Mass"*, i.e., the upper mass limit for electron degeneracy decreases from $M_T \sim 1.5 M_\odot$ at $Z=10^{-4}$ down to $M_T \sim 1.1 M_\odot$ at $Z=10^{-10}$. As a relevant consequence, one predicts that a true Pop II with $Z=10^{-4}$ develops RG branches after only 0.7 Gyr, whereas a population with $Z=10^{-10}$ must wait about 5 Gyr before doing the same. An occurrence to be taken into account when predicting the run of integrated colours with the population age. Note that such a decrease is the simple consequence of Pop III structures being hotter and, thus, less affected by electron degeneracy. The following phases of He burning have been studied by

→Cassisi, Castellani & Tornambé [6], who investigated $Z=10^{-10}$ He burning stars to predict HB structures for ages in the range 7 to 15 Gyr. One finds that old Pop III populations should have no or very few RR Lyrae pulsators

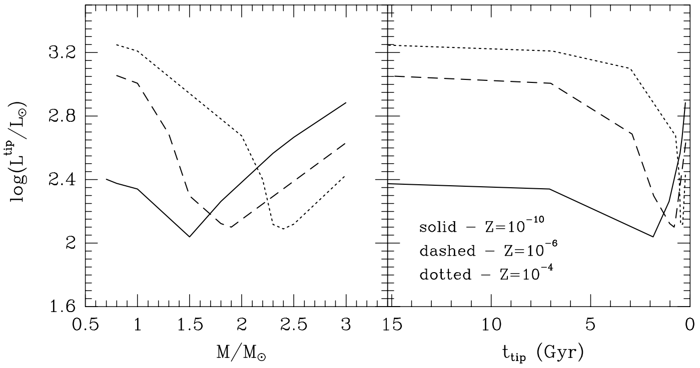

Fig. 3. The star luminosity at the He ignition as a function of the stellar mass (left) or of the cluster age (right) across the *Red Giant Transition Phase*. Because of electron degeneracy, low masses have large He cores and, thus, large luminosities. Increasing the mass, degeneracy vanishes and both He core and luminosity decrease, till increasing again because of the growing of central convection

(Fig.4), an occurrence which gives a warning against the use of these variables as metallicity tracers. As a further relevant point, one finds that AGB models at the first He reignition at the end of the quiescent He shell burning undergo a violent He-shell flash ($L_{He} \sim 10^8 L_\odot$) which, in turn, triggers an even stronger H-shell flash which in few seconds injects in the stellar envelope no less than 10^{48} ergs, possibly ejecting a nuclearly processed envelope. However, the dynamics of this process needs further investigation.

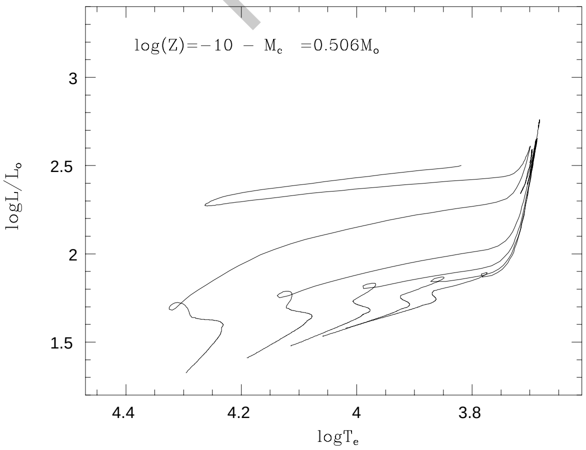

Fig. 4. Pop III HB models for a cluster age t=15 Gyr all along their central He burning evolution remain hotter than the RR Lyrae instability strip (logTe$\sim$3.85)

To close this section, we only notice that Z=10^{-10} models in [5] do not show any evidence of the thermal runaways found in the previous investigations at the exhaustion of central H. Recent numerical experiments (Cassisi, private communication) indicate that this is the consequence of the small but still not negligible amount of metals in their Z=10^{-10} models, which succeeds in producing a small amount of CNO burning which, in turn, smoothes the self-enrichment of carbon, damping the quoted runaways.

4 Massive Pop III Structures

As expected, massive Pop III structures have relatively short lifetimes. As a consequence one is dealing with stellar structures which have already disappeared from our Universe. However, their memory is still present, since they represent the first important step governing the long nuclear staircase which provided the Universe of heavy elements. To have light on the peculiar behaviour of such Pop III structures one has to bear in mind two quite elementary points, namely;

- According to Schwarzschild's criterion, convection occurs everywhere in the structure the radiative gradient ∇_{rad} is larger than the adiabatic one ∇_{ad}, and
- In stellar interiors the adiabatic gradient is nearly constant ($\nabla_{ad} \sim 0.4$) whereas the radiative gradient is proportional to the local flux of energy.

By recalling that Pop III MS structures are in all cases much more supported by pp burning than normal structures do and that pp burning is much less dependent on the temperature than CNO, it follows that the central region where the energy is produced is larger, then the energy flux is locally smaller and one can predict that Pop III MS structures must have peculiarly smaller convective cores, if any. As a matter of the fact, this is what was found since the early investigations on that matter (see, e.g., [10,8].

Such a peculiarity is well represented in Fig.5, which shows the extension of the central convective cores as a function of the central H abundance for Pop III stars for the selected labelled mass values. One finds, e.g., that a 5.0 $M_{\odot}$ Pop III (Z=10^{-10}) model starts its H burning evolution with a convective core of 0.73 $M_{\odot}$ against the 1.41 $M_{\odot}$ of the corresponding Z=10^{-4} model. As a further peculiarity, Fig.5 shows that during central H burning all stars undergo an episode of rapid growing of the convective instability not experienced by normal stars. One may easily understand that this episode marks the onset of CNO burning via the already quoted self-enrichment of Carbon. Fig.6 compares the evolutionary paths of 5.0 $M_{\odot}$ models as computed for the various labelled assumptions about the metallicity. One should notice that the (Z=10^{-10}) model till the exhaustion of central He remain hotter than $\log T_{\rm e} = 4.4$.

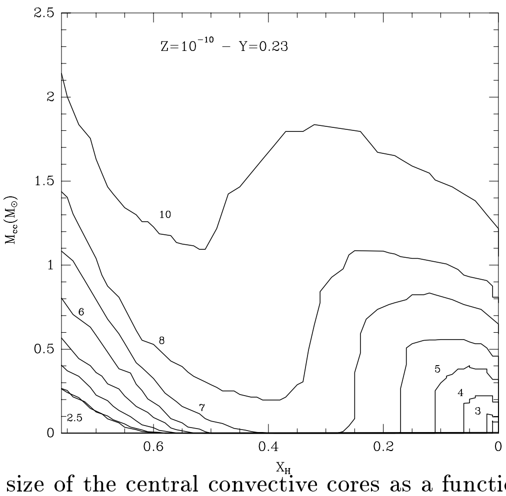

Fig. 5. The size of the central convective cores as a function of the central abundance of H (X_c) for $Z=10^{-10}$ and for the various labelled stellar masses

According to well known prescriptions of stellar evolution, a relevant consequence of the smaller convective cores is that one expects *an increase of the upper mass limit (M^{up}) for the occurrence of degenerate CO cores at the end of central He burning.* Thus in Pop III stars the range of stellar masses which can, at least in principle, end their life with the carbon detonation is expected to be larger. This is confirmed by detailed computations [5]. As shown in Fig.7, the value of M^{up}, which is now a bit larger than 5.5 $M_\odot$, at the beginning of the galactic history was larger than 7.0 $M_\odot$.

As well known, mass loss can prevent the detonation by lowering the actual stellar mass below the Chandrasekhar limit before this limit is reached by the growing (electron degenerate) CO stellar core. The evidence that Pop III stars not only leave a larger room for carbon detonation but also that possibly they suffer a smaller amount of mass loss drive to the conclusion that in this populations carbon detonation is, at least, much more probable, with possible relevant outcomes on the history of galactic enrichment of iron.

To close this section, one has finally to notice that Chieffi & Tornambé [9], investigating the evolutionary behaviour of a 5.0 $M_\odot$ Pop III model, brought to the light an unexpected features of zero metals models in their advanced phases of evolution (Asymptotical Giant Branch). By definition, intermediate mass stars after the exhaustion of central He develop an electron degenerate CO core which grows with time until reaching the bottom of the H-rich stellar envelope. As early recognised by Schwarzschild & Harm [20] and deeply investigated by Iben (see references in [18]) at this phase a "normal" star undergo a series of alternative ignitions of the H or He burning shells. As a relevant point, one finds that such *thermal pulsating* structures are expected to experience the *"third dredge up"*, i.e., an episode of mixing bringing for the

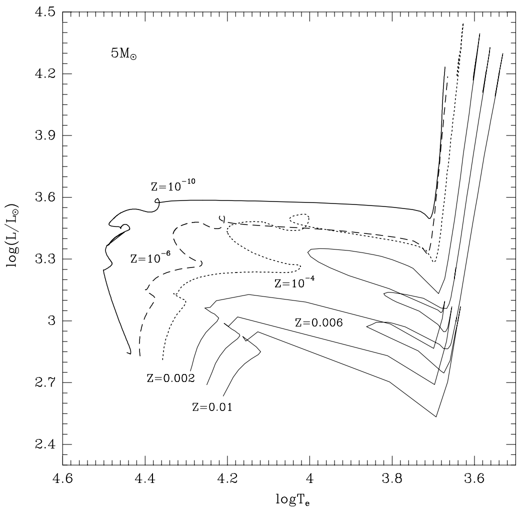

Fig. 6. The evolutionary paths of 5.0 M$_\odot$ models for the labelled values of the adopted metallicity

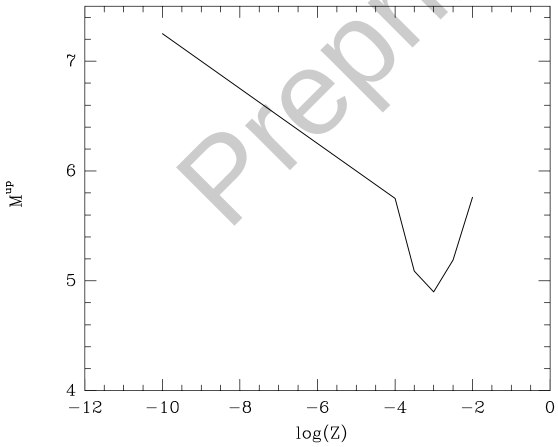

Fig. 7. The predicted values of M^{up} as a function of stellar metallicity

first time at the stellar surface the products of the He burning. Unexpectedly, one finds that zero metal stars escape this phenomenon, and both H and He burning shells appear able to quietly burn at the same time. An occurrence which has been further carefully investigated [15].

5 Conclusions

One finds that Pop III stars do have a peculiar evolutionary behaviour and that this peculiarity is essentially grounded on the lacking contribution of CNO burning to the energy requirements of a stellar structure. As a consequence, the upper limit for low mass stars (with electron degenerate He core) is decreased and the upper limit for intermediate stars (with electron degenerate CO cores) is increased.

This peculiar evolutionary behaviour appears, it may be, sufficiently well understood. We have reasonable predictions about the expected observational features of Pop III star surviving in the present Universe and, in the meantime, we understand that C detonation could have been of increased relevance in such a population, because of the increased value of M^{up} and, possibly, for a decreased efficiency of mass loss. However, further investigations are expected about the final fate of low mass AGB stars as well as about the development of the He flash in Pop III but not zero metal stars.

By defining as "Pop III" those stellar structures which in their H burning phase experience CNO burning via self produced carbon, further investigations should be devoted to assess the upper Z limit for these Pop III structures, as well as to investigate the variations of the evolutionary behaviour within these Pop III limits. Bearing in mind that the first 10 $M_\odot$ of iron mixed throughout the Galaxy (i.e., the very first dozens of Supernovae) have already raised an original zero metal mixture up to and above $Z=10^{-10}$.

References

1. Applegate, J.H., Hogan, C.J., Scherrer, R.J., . (1988) ApJ **329**, 572
2. Bond, H.E. (1981) ApJ **248**, 606
3. Caloi, V., Castellani, V. (1984) in *Frontiers of Astronomy and Astrophysics*, p.94, R.Pallavicini ed., Florence
4. Carr, B.J., Bond, J.R., Arnett, W.D. (1984) ApJ **277**, 445
5. Cassisi S., Castellani, V. (1993) ApJS **88**, 509
6. Cassisi, S., Castellani, V., Tornambé, A. (1996) ApJ **459**, 298
7. Castellani, V., Paolicchi, P. (1975) Astrophys. Sp. Sci. **35**, 175
8. Castellani, V., Chieffi, A., Tornambé A. (1983) ApJ **272**, 249
9. Chieffi A., Tornambé A. (1984) ApJ **287**, 745
10. Chiosi, C. (1983) Mem. Soc. Astron. It. **54**, 251
11. D'Antona, F. (1982) A&A **115**, L1
12. Ezer,D. (1972) Astrophys. Spa. Sci. **18**, 226
13. Ezer, D., Cameron, A.G.W. (1971) Astrophys. Spa. Sci. **14**, 399
14. Fujimoto, M.Y., Iben, I.Jr., Hollowell, D. (1990) ApJ **349**, 580
15. Fujimoto, M.Y., Iben, I.Jr., Chieffi, A., Tornambé, A. (1984) ApJ **287**, 749
16. Guenther, D.B., Demarque, P. (1983) A&A **118**, 262
17. Hollowell, D., Iben, I.Jr., Fujimoto, M.Y. (1990) ApJ **351**, 245
18. Iben, I.Jr., Renzini, A. (1983) ARA&A **21**, 271
19. Palla, F., Salpeter E.E., Stahler S.W. (1983) ApJ **271**, 632
20. Schwarzschild, M., Harm, R. (1965) ApJ **142**, 855
21. Wagner, R. (1974) ApJ **191**, 173

Evolution of Pop III Stars

Cesare Chiosi

University of Padua, Department of Astronomy, Vicolo Osservatorio 5, 35122 Padua, Italy

Abstract. In this paper, first we summarize the many reasons that over the years led to introduce the concept of Pop-III stars. Second, we shortly cast the problem of their mass-scale and initial mass function. Third, we highlight the distinct behavior of zero-metal stars with respect to those of normal and low metal content, and concisely discuss their inner structure and path on the HR diagram in the mass range 0.9 to 100 $M_\odot$ limited to core H- and He-burnings. Finally, we draw some general remarks on the stellar ejecta as a function of the chemical composition, and present some preliminary results concerning the ejecta from massive Pop-III stars due to stellar winds during the early stages.

1 Introduction

The standard Big Bang Nucleosynthesis [73] predicts that no elements heavier than ^{7}Li should exist in the gas mixture in which the first stars are generated. These stars, named Pop-III objects, are expected to have structure and evolution distinct from those in which traces of heavier elements like carbon are present.

The existence of Pop-III stars has been invoked for many different reasons among which we recall:
(1) The gap between the cosmological abundances ($Z \simeq 10^{-10} - 10^{-12}$) and those *observed* in the lowest metallicity Pop-II stars ($Z \simeq 10^{-4} - 10^{-3}$) that should be filled by Pop-III objects.
(2) The severe scarcity of metal-poor stars in the solar vicinity relative to predictions from simple models of chemical evolution [104] which is otherwise known as the G-Dwarf problem. Among other explanations, the most obvious one is that there was a pristine generation of massive stars that synthesized and ejected the first heavy elements in the Universe.
(3) The oxygen anomaly or enhancement of α-elements in galactic metal-poor stars [92].
(4) The existence of extremely metal-poor stars showing s-process elements in their envelopes [101]. The increasing observational evidence for metal-deficient stars (as low as $Z \leq 10^{-6}$) populating the galactic halo [67,68,71], [82,93].
(5) The missing mass in clusters of galaxies and galactic haloes [106] formed by their dark remnants.
(6) The generation of the 3K background radiation and/or distortion in its spectrum [59,84,87,83,21].

(7) The re-ionization of the Universe [35,50,98,99] and the starting engine for the formation of the first galaxies [74,55,51,21,98,75].
(8) The contaminants of the intergalactic medium as inferred from metallic absorption lines in the Ly-α forest seen in quasar light [33,94].
(9) The cosmological helium abundance [96].
(10) The formation of massive Black Holes [103].

This short, and badly incomplete list clearly shows how much interest has been attributed over the years towards the idea of a very early generation of stars perhaps even prior to galaxy formation (see the exhaustive review by Carr [18]).

2 Mass-scale and IMF of Pop-III Stars

What were the mass-scale and the initial mass function (IMF) of Pop-III stars?

This is perhaps the most crucial question to pose, even before knowing the details of their structure and evolution, because it will decide the success or failure of the Pop-III idea itself. Since as nowadays there is no hope we can answer such a question on observational ground, all we know is merely hypothetical.

Three lines of arguments concur to cast light on this topic, which immediately lead us to the more subject of the kind of IMF holding in very early epochs of star formation both in the metal-free primordial medium and in primeval galaxies. They are the star forming process itself, the global properties of galaxies (both chemical and photometric), and the chemistry and mass content of hot gas in clusters of galaxies. The whole subject has bee recently discussed by Larson (1998) to whom the reader should refer for details.

Starting from the present-day IMF in the solar vicinity which can be described by a declining power law for masses above $1\,\mathrm{M}_\odot$ (Salpeter [88] law), flattening below $\simeq 0.5\,\mathrm{M}_\odot$, and possibly even declining below $\simeq 0.25\,\mathrm{M}_\odot$ [89], Larson [58] proposes the following analytical forms

$$\frac{\mathrm{dN}}{\mathrm{dlog\,M}} \propto \mathrm{m}^{-\alpha}\mathrm{exp}(-\frac{\mathrm{M_s}}{\mathrm{M}}) \qquad \text{or} \qquad \frac{\mathrm{dN}}{\mathrm{dlog\,M}} \propto (1+\frac{\mathrm{M}}{\mathrm{M_s}})^{-\alpha} \tag{1}$$

whose logarithmic slopes are $\mathrm{x} = \alpha - \mathrm{M_s}/\mathrm{M}$ and $\alpha(1+\mathrm{M_s}/\mathrm{M})^{-1}$, respectively, $\alpha = 1.35$ is the Salpeter case, and $\mathrm{M_s}$ is the mass-scale. With the first representation, the IMF approaches the Salpeter law [88] at large masses, peaks at $\mathrm{M_p} = \mathrm{M_s}/\alpha$, and falls exponentially at lower masses. With the second representation, the IMF recovers the Salpeter [88] law at high masses, but tends to become flat at lower masses. In this context the whole problem is simply reduced to understand whether α and $\mathrm{M_s}$ have always been the same or they have changed with time and hence physical conditions of the medium.

The star forming process. The bottom line of the problem is to find efficient cooling mechanisms in metal-free gas. In present-day galaxies, heavy elements or dust grains provide the most efficient cooling mechanism, whereas the cooling process in primordial gas is likely to be governed by hydrogen (atomic and molecular). According to Nakamura & Umemura [70], if hydrogen were to remain purely atomic, the primordial gas would cool down only to 10^4K because H atoms are poor radiators at low temperatures. It follows that the Jeans mass of such a cloud is much grater than the typical stellar mass. However, even a small fraction of hydrogen molecules provide a significant contribution to cooling through rotational and vibrational transitions, so that the temperature of primordial gas can go much lower than the 10^4K [80,77]. As a consequence of this, the Jeans mass can decrease to typical stellar values.

The mass-scale. Despite the many studies of the subject, the mass-scale of Pop-III stars has not yet converged. Carr [19] favored the possibility that Pop-III stars were more massive than say $10\,\mathrm{M}_\odot$, possibly in the range 10^2 to $10^5\,\mathrm{M}_\odot$. Similar suggestion was made by Hutchins [52], Silk [91], and Tholine [100] who indicated a minimum mass of 150-200 $\mathrm{M}_\odot$. In contrast, Calberg [14] and Palla et al. [77] argued that the Jeans mass can go down to a level of $\leq 0.1\,\mathrm{M}_\odot$. Yoshii & Saio [113], using the opacity limited fragmentation theory of Silk [91], estimate the peak mass of the IMF around 4-10 $\mathrm{M}_\odot$. Uehara et al. [102] show that the minimum mass is about $1\,\mathrm{M}_\odot$. Finally, Nakamura & Umemura [70] find that the typical mass of Pop-III stars is about $3\,\mathrm{M}_\odot$, which may grow to $16\,\mathrm{M}_\odot$.

The provisional conclusion we may get from all this is that the mass-scale is likely greater than say $1\,\mathrm{M}_\odot$ *and possibly in the range 1 to* $10\,\mathrm{M}_\odot$. *However, both lower and much higher values cannot be firmly excluded.*

E-Galaxies and intra-cluster medium. On different grounds, arguments have been gathered over the years to suggest that at early times the IMF was different from the present-day one in the solar vicinity. They stem from many attempts to explain in a coherent scenario a number of observational facts, among which we recall:

(i) The analog of G-Dwarf problem observed in the spectrum of E-galaxies [8] which hints that the relative percentage of old, metal-poor stars is small and likely compatible with early infall [97] or prompt enrichment [49].

(ii) The different increase of Mg_2 and $\langle \mathrm{Fe} \rangle$ passing from faint to bright E-galaxies is interpreted as an increase of the [Mg/Fe] with the galaxy mass [112], which could reflect a shorter star formation time-scale for the more massive galaxies.

(iii) In the present-day color-magnitude relation, E-galaxies (see for instance [13]) get redder at increasing luminosity (mass). Since Larson [57], this is explained by means of the SN driven galactic wind model, in which massive galaxies, ejecting their gaseous content later than the less massive ones, get higher mean metallicities and hence redder colors. This simply opposes to what inferred from the trend in [Mg/Fe].

(iv) In the space of central velocity dispersion Σ_0, effective radius R_e, and surface brightness I_e, E-galaxies are known to cluster around a plane called the *Fundamental Plane* (FP). Using the hypothesis of virialization and constancy of the so-called virial coefficients and suitable algebraic transformations, the FP seen edge-on can be represented by the relation $\log(M/L) = \beta\log M + \gamma$, otherwise known as the tilt of FP, where β and γ are positive constants and the dispersion is very small. Tilt and tightness of the FP have not yet received satisfactory explanations [32].

(v) E-galaxies have extended haloes of gas emitting in the X-ray band. Measurements of the Fe content from the ASCA data indicate a very low abundance, much lower (some time up a factor of 10) than the Fe content of the stellar populations in these galaxies as derived from integrated optical spectra [6]. The so-called *Iron Discrepancy* has so far eluded simple understanding.

(vi) The bulk of X-ray emission from clusters of galaxies is due to thermal bremsstrahlung in a hot gas (10^7 to 10^8 K) which is enriched in heavy elements. The abundance of Fe is roughly 1/3 solar [44], whereas the ratios of α elements with respect to iron, $[\alpha/\mathrm{Fe}]$, are more uncertain. They go from solar abundances [86], to higher than solar [15]. The recent ASCA data [69] yielded $[\alpha/\mathrm{Fe}] \simeq 0.2 \pm 0.3$ or in the case of oxygen $[\mathrm{O/Fe}] \simeq 0.48^{0.24}_{-0.55}$. However, more recent estimates favor again nearly solar values [56]. Typical values for the total amounts of iron and gas in several clusters [66] are $M_{Fe} \simeq 3\times10^{11}\,M_\odot$ and $M_g \simeq 4\times10^{14}\,M_\odot$ for Perseus, Coma, and A2199 clusters, and $M_{Fe} \simeq 1.5\times10^{10}\,M_\odot$ and $M_g \simeq 2\times10^{13}\,M_\odot$ for Virgo. Interpreting these data by means of the standard galactic wind model is a cumbersome affair. On one hand, the amounts of M_{Fe} and the possibility that $[\mathrm{O/Fe}] > 0$ seem to indicate a flatter IMF than the Salpeter case [48]. On the other hand, while the total M_{Fe} can be recovered, difficulties arise to account for M_g with standard models (see [48]).

The ability of a time-dependent IMF in alleviating if not solving the open questions listed above has been investigated in a number of studies, which differ for the kind of IMF that was adopted. For instance, [36] postulated a top-heavy IMF at early times. Chiosi et al. [30] adopted the theoretical IMF by Padoan et al. [76], whose analytical form is of the first type above, but both M_p and the logarithmic slope depend on the gas temperature, density, and velocity dispersion. This IMF reduces to the Salpeter law in ordinary conditions, but gradually shifts its M_p toward the high-mass end at increasing gas temperature, and decreasing gas density. Such conditions were likely met at early epochs (see also Larson [58]). Remarkably a modest increase in M_p form the present-day $\simeq 0.2\,M_\odot$ to about $1\,M_\odot$ at the early stages was strong enough to deeply change the standard scenario and to much improve upon agreement between theory and data (see [30] for all details).

Therefore it is likely that the IMF of Pop-III stars was much in favor of massive (not necessarily very massive) stars as amply discussed by Larson [58].

3 Main Stellar Kingdoms

The guide line of this presentation stems from what we know for ordinary metal abundance stars, which can be loosely classified in five groups depending on their initial mass, internal structure, and final fate.

Low Mass Stars (LMS). Leaving aside the objects of very low mass $\mathrm{M} \leq 0.07 - 0.08\,\mathrm{M}_\odot$ that fail core H-ignition, and the stars with mass in the range $0.1\,\mathrm{M}_\odot < \mathrm{M} < 0.5\,\mathrm{M}_\odot$ that after core H-burning fail central He-burning, LMS with mass lower than $\mathrm{M}_{\mathrm{HeF}} \simeq 2.0\,\mathrm{M}_\odot$ are characterized by He-flash in a strongly degenerate core. Soon after removing degeneracy, they burn helium quiescently, later evolve through the AGB phase, and eventually become White Dwarfs (WD).

Intermediate Mass Stars (IMS). They ignite hydrogen and helium non degenerately, but following central He-exhaustion develop an electron degenerate C-O core, and as AGB stars experience He-shell flashes or thermal pulses. The initial mass falls in the range $\mathrm{M}_{\mathrm{HeF}} < \mathrm{M} < \mathrm{M}_{\mathrm{up}} = 8 - 9\,\mathrm{M}_\odot$. Depending on the efficiency of mass loss during the RGB and AGB phases, stars lighter than $\mathrm{M}_{\mathrm{W}} \simeq 5 - 6\,\mathrm{M}_\odot$ become WD before the CO core mass has grown to the Chandraseckhar limit. Stars more massive than M_{W} may ignite central C-burning in highly degenerate conditions once the core mass has reached the Chandraseckhar limit with ensuing supernova explosion (C-deflagration or detonation). The mass interval for their existence can vanish if $\mathrm{M}_{\mathrm{up}} \to \mathrm{M}_{\mathrm{W}}$ as in models with convective overshooting.

High Mass Stars (HMS). The initial mass of HMS is grossly confined between 10 and $100\,\mathrm{M}_\odot$. They proceed through the whole series of nuclear burnings accompanied by strong neutrino cooling to the formation of an iron core. $Fe \to \alpha$, p, and n breakdown and electron-capture induce core collapse and consequent supernova explosion. Depending on several physical phenomena taking place during the collapse, these stars will leave either a Neutron Star or a Black Hole, if their initial mass is smaller or higher than about $30\,\mathrm{M}_\odot$ ([111] for details). The entire evolution of HMS is also affected by strong stellar winds from the surface [31].

Very massive stars (VMS). These stars are confined in the mass range $100 < \mathrm{M} < 5 \times 10^4\,\mathrm{M}_\odot$, They are found to be dynamically stable against general relativity effects, but pulsationally unstable during core H and He-burning phases (with associated strong mass loss) and finally to suffer pair instability during early stages of core oxygen burning, which lowering the adiabatic index Γ_1 below 4/3 induces core collapse and explosive O-burning. Many numerical calculations show that the final outcome is ultimately regulated by the mass of the carbon-oxygen core M_{CO} [108–111,37,72,9–13]. If $\mathrm{M}_{\mathrm{CO}} > 110\,\mathrm{M}_\odot$ the collapse cannot be halted and a Black Hole is formed. For $50\,\mathrm{M}_\odot < \mathrm{M}_{\mathrm{CO}} < 110\,\mathrm{M}_\odot$ complete thermonuclear disruption occurs. In stars with $\mathrm{M}_{\mathrm{CO}} \leq 50\,\mathrm{M}_\odot$, oxygen-burning does not set in until the center is too tightly bound to be destroyed by nuclear energy release. The inner part of the star, then burns on up to iron and perhaps joins the fate of less massive stars.

Super-massive stars (SMS). These objects directly collapse to black holes via general relativity effects or suffer total disruption due to explosive H-burning. The mass ranges in which the two alternatives are expected to occur are $M > 10^5\,M_\odot$ for total collapse and $M < 10^5\,M_\odot$ for explosive H-burning, depending upon the mass, initial metal content, and degree of rotation [4,5,42,43,45,46].

4 A Quick Review of Past Work on Pop-III Stars

The widely accepted ideas that only massive, very massive or even super-massive could form in primordial medium has long limited the study of Pop-III stars to objects more massive than say $100\,M_\odot$. However, over the years, the interest has also been turned towards more normal stars. Ezer & Cameron [39] first studied models of Pop-III stars in the mass range 5 to $200\,M_\odot$ from the pre main sequence till core H-exhaustion. In a subsequent paper Ezer [38] investigated the evolution of a $3\,M_\odot$ star up to the stage of core He-exhaustion. Cary [22] and Castellani & Paolicchi [25] computed zero age main sequence models in the mass range 2 to $20\,M_\odot$ and 1 to $8\,M_\odot$ respectively. The late phases of low mass stars remained almost unexplored till the early study by D'Antona [34] of a $1\,M_\odot$ star up to the stage of core He-flash, where for the first time the much less extended RGB was noticed (see also [25] for an earlier suggestion). Woosley & Weaver [107] followed the evolution at constant mass of a $200\,M_\odot$ star till the supernova explosion stage, thus allowing the first estimate of the contamination power of this type of star. Very massive Pop-III stars were first investigated by Bond et al. [10,11]. El Eid et al. [37] and Ober et al. [72] explored the mass range from 80 to $500\,M_\odot$, in presence of mass loss by stellar wind up to the stage of supernova explosion or collapse to a black hole. Similar study was undertaken by Klapp ([53,54]) for VMS in the mass range 500 to $10^4\,M_\odot$. These papers made it possible to get an estimate of the chemical yields both in the wind and explosive stages. Forieri [41] studied the evolution of massive Pop-III stars in mass range 10 to $100\,M_\odot$ up to the central He-exhaustion stage. These models were evolved at constant mass but in presence of convective overshoot. Castellani et al. [26] presented models for 10, 15, 25 $M_\odot$ stars from ZAMS to C-ignition. Chieffi & Tornambè [27] investigated the AGB phase of a 5 $M_\odot$ object. Fujimoto et al. [47] pointed out that threshold values for the core mass and CNO abundances exist for the occurrence of He-shell flashes during the AGB phase. Cassisi & Castellani [23] presented grids of models with masses in the range $0.7 \le M \le 15M_\odot$ and metallicity from $Z = 10^{-4}$ down to $Z = 10^{-10}$. The models were followed from ZAMS till He-flash, final cooling of the CO core or C-ignition as appropriate. Cassisi et al. [24] analyzed the thermal pulses of metal-deficient low mass stars. Finally, Marigo et al. [64] studied Pop-III stars in the mass range 0.8

to $100\,\mathrm{M}_\odot$. All the models are computed with convective overshooting and limited to HMS also with mass loss by stellar wind.

5 What About Mass Loss from Pop-III Stars?

Perhaps the most uncertain aspect of the evolution of Pop-III stars is mass loss by stellar wind. Two typical situations can be envisaged:
(1) Mass loss from HMS and VMS during their whole evolutionary history.
(2) Mass loss during the RGB and AGB phases of LMS and IMS.

Can what we know for normal-metallicity stars be extrapolated and safely used for Pop-III stars? This depends on the physical nature of the driving mechanism.

In HMS of normal metallicity (no matter whether low or high) mass loss at high effective temperature is due to radiation pressure on resonance lines of ions like CIV etc.., whereas that at low temperatures is likely caused by radiation pressure on dust grains and/or pulsational properties (see [31,61,40] for recent reviews). Furthermore, the body of observational and theoretical information allows us to establish empirical relations according to which the mass loss rates are seen to decrease with the metallicity.

On this ground one could perhaps argue that as long as the surface layers keep the original composition mass loss cannot occur. If and when the surface abundances are contaminated by mixing (diffusion, etc..) in heavy elements mass loss by the above mechanisms could be activated. However, the above reasoning would immediately fail, if other mechanisms (metallicity independent) concur to drive mass loss.

Given these premises, evolutionary models of zero-metal HMS have been calculated also in presence of mass loss using metal-independent mass-loss rates. For instance Klapp [53,54] adopted the empirical relation by Barlow & Cohen [7]

$$\dot{\mathrm{M}} = \mathrm{N}\frac{\mathrm{L}}{\mathrm{c}^2} \tag{2}$$

where N is a parameter ($\mathrm{N} \simeq 100$). El Eid et al. [37] and more recently Marigo et al. [64] made use of the relationship proposed long ago by Andriesse ([1], theoretical approach) and Chiosi ([28], empirical analysis)

$$\dot{\mathrm{M}} = \left(\frac{\mathrm{t_D}}{\mathrm{t_K}}\right)^{\mathrm{k}} \frac{\mathrm{LR}}{(1-\Gamma)\mathrm{GM}} \tag{3}$$

where $\Gamma = \sigma_{\mathrm{e}}\mathrm{L}/4\pi\mathrm{GcM}$ is the ratio of stellar to Eddington luminosity, $\mathrm{t_D}$ and $\mathrm{t_K}$ are the dynamical and thermal time-scales, and finally $\kappa \simeq 0.5$. This relationship was found to match the observed mass-loss rates of early type stars over large ranges of luminosities, effective temperatures, and evolutionary stages. It did not made use of the radiation pressure theory, but rather the non thermal energy storage in the stellar interiors (cf. [16] and the imperfect flow model of Andriesse [1]).

The case of VMS perhaps stands on more solid ground. These objects are in fact unstable to nuclearly energized pulsational instability [60,90,95], which instead of complete disruption could drive substantial mass loss [2,3,114,78,79]. It is worth recalling that nuclear energy generation always tends to destabilize a star, its effect being usually quenched by the stable overlying layers. In massive stars, Pop-III in particular, the nuclear energy source affects a large fraction of the mass, so that quenching may not be effective. The old linear analysis by Schwarzschild & Harm [90] set the stability limit at about $60\,M_{\odot}$, which was increased to $85\,M_{\odot}$ for zero-metal, and $90\,M_{\odot}$ for ordinary stars by more refined calculations [95]. Once formed, stars more massive than the above limits, being pulsationally unstable, may suffer from drastic mass loss bringing them below the stability limit on a time scale comparable to their core H-burning time scale (about 3×10^6 yr). The estimated mass loss rates are of the order of $10^{-4} - 10^{-5}\,M_{\odot}$/yr [2,3]. If so, VMS would lose a large fraction of their mass before H-burning completion. Finally, it reasonable to conceive that mass loss would continue after completion of core H-burning for two reasons at least: (i) Firstly, at the onset of shell H-burning, luminosities exceeding the Eddington value are likely met. This would cause the ejection of the residual envelope on very short (nearly dynamical) time scales (see for instance the case of the Pop-I $500\,M_{\odot}$ star by Bond et al. [10]). (ii) Secondly, the dominant He-core will itself be highly pulsational unstable. It is worth recalling that the maximum mass for the stability of pure He-stars is only $13\,M_{\odot}$ [95].

The RGB and AGB phases of low and intermediate mass stars are the most severe problem as we do not have observational hints nor solid theoretical arguments for the efficiency of mass loss during these stages. *Is the mass loss rate at the RGB tip similar to that in most metal-poor globular clusters? Is the rate along the AGB similar to that in ordinary stars? Can we apply the same algorithm proposed by Vassiliadis & Wood [105] based on the pulsational properties of these stars?* If the empirical relationships expressing the rate of mass loss as a function of basic stellar parameters are applied to Pop-III stars, very little mass is found to be lost during the RGB and AGB phases. *Does it mean that for these type of star only constant mass evolution is possible?*

Owing to all these uncertainties, we prefer to consider mass loss as a free parameter designed to exploring the effect of this phenomenon even in zero-metal stars.

6 Structure and Evolution of Pop-III Stars

Generalities. The major difference of zero-metal stars with respect to those of normal metal content (even down to very low values of Z) lies in the mechanism of nuclear energy generation. In fact owing to the lack of CNO nuclei, the pre-main sequence gravitational contraction cannot stop until the central temperature and density are high enough to allow the PP-chain to provide the energy budget. The PP-chain is indeed a poor thermostat as compared to the CNO-cycle as indicated by the path of central conditions. While the situation is normal for low mass stars where H-burning is always started by the PP-chain, this is not the case for higher masses where the CNO-cycle is the dominant source from the very beginning. It is worth recalling that the rule is fulfilled even for very small percentage of CNO nuclei.

The threshold abundance of ^{12}C at which the distinct behavior of zero metal stars appears is as low as 10^{-10} - 10^{-9} (or roughly equivalent $Z \simeq 10^{-10}$ - 10^{-9}). Starting from these values and higher the efficiency of CNO-cycle is fully sufficient to recover the standard behavior.

Core and Shell H-Burnings. Due to the small dependence of the PP-chain reaction rates on temperature, the balance of the energy output forces much higher temperatures and densities in the cores. The extension of convective core is smaller than in normal-metallicity stars.

Central temperatures and densities can reach such high values that the condition can be met for 3α burning of helium with subsequent production of ^{12}C and immediate activation of the CNO-cycle. In stars less massive than about $2.5\,M_\odot$, H-burning via CNO cycle becomes efficient only near the stage of central H-exhaustion ($X_c < 0.01$) or only during the subsequent shell H-burning [23,64]. In stars in the range $2.5 \leq M \leq 6\,M_\odot$ the production of ^{12}C and switch to CNO-cycle takes place when $X_c \leq 0.3$ or so [23,64]. The transition occurs earlier and earlier at increasing star mass [23,64]. This event manifests itself showing a loop in the HRD, which is pronounced in the case of low mass stars (up to $1.5\,M_\odot$), much less evident but still there at higher masses. The loop is missing in the range of massive stars. This feature, which most likely has no important observational consequences, is the signature of the energy source switching from PP-chain to CNO during the core and shell H-burning phase. See the evolutionary path in the HRD of stars of different mass shown in Fig.1 reproduced from [64].

There is another interesting point to note which is common to the classical models by Cassisi & Castellani [23] and the overshooting models by Marigo et al. [64]. The transition from PP-chain to CNO cycle in stars in the mass interval 2.5 to about $8\,M_\odot$ occurs when the central convective core has already started to recede in mass (actually in most cases) has almost disappeared. The onset of CNO-cycle reactivates central convection. This trend is also visible in low mass stars (0.9 to $1.2\,M_\odot$) where it may lead to the formation of a convective core (see [64]).

The H-burning shells of IMS extend over a large fraction of the star mass. In LMS and HMS it remains relatively thin although for different reasons: the density and temperature contrast between the core (degenerate) and the

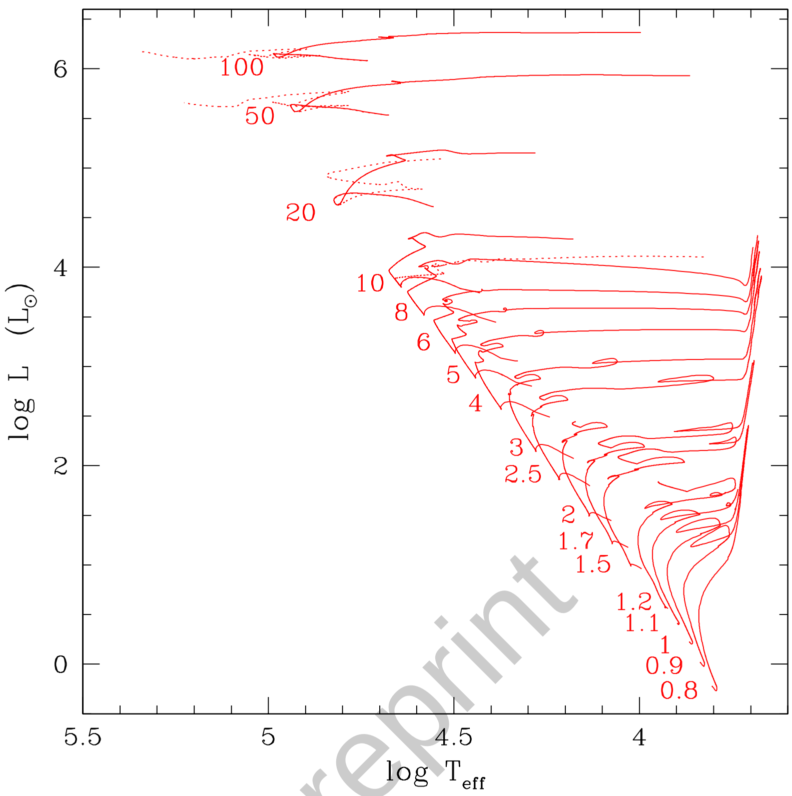

Fig. 1. The HRD of zero-metal stars with different mass reproduced from [64]. The solid lines are tracks evolved at constant mass, whereas the dotted lines are tracks with mass loss by stellar wind

expanding envelope in the former and the envelope erosion by stellar wind in the latter.

First dredge-up. The first dredge-up (along the RGB) is practically absent in all models. Only in stars with $M < 1\,M_\odot$ a very small amount of helium is brought to the surface (less than about $0.003\,M_\odot$).

Core and Shell He-Burnings. Core He-burning takes place in non degenerate conditions even in stars of rather low mass. Marigo et al. [64] find that M_{HeF} is as low as $\simeq 1.1\,M_\odot$ as indicated by the path of central conditions. At lower masses, core He-burning goes through the flash regime.

In normal stars of the same mass, stellar winds at the tip of the RGB would determine the mass of the stars during the core He-burning phase on the horizontal branch (HB). In stars of extremely low and/or zero-metal content the situation is much less clear. If for the sake of argument we apply the same algorithm used to derive the amount of mass to be lost passing from RGB to HB, i.e. the calibrated Reimers law

$$\dot{\mathrm{M}} = \eta \times \mathrm{A}\ \frac{\mathrm{LR}}{\mathrm{GM}} \tag{4}$$

where A contains the physical units and η is the calibrating parameter, the amount of lost mass would be small owing to the low luminosity and much bluer color (higher surface temperature, smaller radii) at the RGB tip. *Does it imply that the HB phase of zero-metal stars occurs at a mass nearly identical to that of progenitor star?*

HB models for stars with very low metallicity have been presented by Cassisi et al. [24]. The lowest considered metallicity is $\mathrm{Z} = 10^{-10}$. Even though the corresponding models with $\mathrm{Z} = 0$ have not yet been calculated, the Cassisi et al. [24] models are likely to be very close to those with no metals at all.

At the onset of He-burning in a shell, the contraction of the layers in which shell H-burning occurs makes the temperature of the latter increase and the CNO-cycle is once more activated in the H-burning shell. This causes a secondary loop in the HRD, which is well evident in stars with mass in the range 2.5 to $6\,\mathrm{M}_\odot$ and detectable in stars with mass in the interval 1.1 to $1.2\,\mathrm{M}_\odot$ (see the HRD of [64] shown in Fig.1).

The situation is not clear for stars in the range 1.2 to $2\,\mathrm{M}_\odot$ where core He-burning is complicated by a sort of *breathing convection* (see [29] for details of this kind of mixing in normal stars). The Marigo et al. [64] models show that during core He-burning the outer boundary of the convective core can get very close to the bottom of the H-burning shell. If the some H-rich material of the shell is mixed into the core immediately and burnt via the CNO cycle, a sort of flash may start which temporarily reduces the efficiency of He-burning and causes the recession of the convective core. The cycle tends to repeat itself likely giving rise to periodic H-flashes. All this is difficult to justify on physical grounds as it is much dependent on the type of mixing taking place at the border of the core. In contrast if mixing of H-rich material is suppressed, the evolution gets normal again, and the secondary loops at the onset of shell He-burning are recovered.

The mass limit M_{up}. The minimum mass, M_{up}, for non degenerate C-ignition for stars with $\mathrm{Z} = 10^{-10}$ has been set at about $7.3\,\mathrm{M}_\odot$ by Cassisi & Castellani [23]. For zero-metal models with overshooting, [64] provisionally confine M_{up} in the range 6 to $< 8\,\mathrm{M}_\odot$.

Second dredge-up. This is found to be efficient for stars with mass fro 2.5 to $8\,\mathrm{M}_\odot$. The surface composition is enriched almost only in He ($\mathrm{Y} = 0.32 \div 0.37$) and negligible in CNO elements (only 10^{-16} to 10^{-8} in abundance by mass).

The thermally pulsing AGB. LMS and IMS proceed toward the AGB phase, whose details are not yet fully understood. According to [27] a Pop-III $5\,\mathrm{M}_\odot$ star does not suffer from thermal pulses of the He-shell, and consequent third dredge-up, but in contrast evolve through a steady nuclear regime. The physical reason is found in the low abundance of CNO, which forces 3α reactions in the H-burning shell to produce the tiny fraction of C required to sustain the the CNO-cycle over-there. At the same time, 3α reaction occur in the He-shell, so that both shells (H and He) proceed at the same pace. The mass of the He-burning region does not increase with time a necessary condition for the onset of the thermal instability. The analysis by [47] has further clarified the problem. They pointed out that 3α reactions produce enough C to sustain the CNO-cycle provided that the core mass $\mathrm{M_c} > 0.5\,\mathrm{M_\odot}$. As a consequence of this, the stability of the He-shell changes when $\mathrm{M_c} \geq 0.7\,\mathrm{M_\odot}$. For core masses smaller than this limit the He-shell is thermally unstable, whereas it becomes stable above it. In addition to this, for $\mathrm{M_c} > 0.7\,\mathrm{M_\odot}$ there is a critical value of the metallicity in the envelope, above which He-flashes are recovered. Cassisi et al. [24] for a star of $0.8\,\mathrm{M_\odot}$ and $\mathrm{Z} = 10^{-10}$ report the occurrence of an unusually strong shell He-flash following the first re-ignition of the He-burning shell. In their model, He-burning grows so strong that a convective shell develops above it, which is large enough to interact with the H-burning shell. The estimated total luminosity $\mathrm{L_{He}} \simeq 2.5 \times 10^8\,\mathrm{L_\odot}$, enormously higher than the corresponding luminosity attained by a normal metallicity star ($\mathrm{L_{He}} \simeq 7.5 \times 10^4\,\mathrm{L_\odot}$). The physical response of the star to this sudden injection of energy is not understood (partial or total envelope ejection ?). Finally, Marigo et al. [64] report the occurrence of the first He-flash in some of their models namely the $1.5\,\mathrm{M_\odot}$ when $\mathrm{M_c} = 0.57\,\mathrm{M_\odot}$, and the $2.5\,\mathrm{M_\odot}$ when $M_c = 0.70\,M_\odot$. Uncertain is the case of $3.0\,\mathrm{M_\odot}$ when $M_c = 0.72\,M_\odot$ for which the He-flash is suspected. Finally no traces of this are noticed for the $4.0\,\mathrm{M_\odot}$ when $\mathrm{M_c} = 0.80\,\mathrm{M_\odot}$. This trend apparently conforms to [47]. Marigo et al. [64] stars of low mass do not yet extend beyond the RGB tip (core He-flash), so that the Cassisi et al. [24] violent shell He-flash cannot be confirmed.

Given these premises, one may infer that stars with a small total mass ($\leq 4\,\mathrm{M_\odot}$), being able to undergo the He-flash regime, may contribute to the production of ^{13}C and neutron-rich isotopes of light elements. The net efficiency will, however, depend on mass loss by stellar wind. Nothing can be said about $\mathrm{M_W}$ the maximum mass of WD progenitors. Star more massive than about $4\,\mathrm{M_\odot}$ will not experience the He-flash regime, and likely will proceed to C-ignition in highly degenerate core (SN explosion with consequent production of Ni and Fe).

HMS and VMS. Nothing special is noticed in the models of massive stars calculated by [64]. During the major nuclear phases (core H and He-burnings) they remain in the blue side of the HRD and do not show traces of surface pollution via dredge-up episodes. However thanks to mass loss they may expose nuclearly processed material to the surface. They build up CO cores linearly increasing with the initial star mass and likely obey the standard evolutionary scheme for HMS of normal composition. As far as the

VMS are concerned, the situation has remained unchanged with respect to the past because no recent stellar models have been calculated.

7 Stellar Yields

Since a detailed discussion of stellar ejecta and yields as a function of mass and metallicity is beyond the scope of the present paper, let us limit ourselves to a few general remarks.

As nowadays, estimating the nucleosynthetic enrichment by zero and very low metallicity stars is still hampered by the insufficient coverage of the space of parameters.

The task is marginally feasible in the range of massive and very massive objects. However, even in this case the uncertainty on the efficiency of mass loss during the so-called hydrostatic phases, does not allows us get safe estimates of the chemical yields in the wind.

The situations is better for the explosive yields if one amalgamates results for hydrostatic and explosive evolution and uses the mass of the CO core as the bridging parameter. It is worth recalling that in the range of massive stars, the M_{CO} versus M_i relation is a complicated function of the metallicity and mass loss during the previous stages.

To our knowledge, the most complete collection of stellar ejecta and yields for large ranges of stellar masses (0.9 to 1000 $M_\odot$) and chemical compositions ($0.0004 \leq Z \leq 0.05$) can be found in the series of papers by Marigo et al. [62,63] and Portinari et al. [81] to whom the reader should refer for all details. Suffice here to recall that for LMS and IMS the complete series of dredge-up episodes and the effect of envelope burning (whenever appropriate) are considered. For HMS the effect of mass loss by stellar wind and its dependence on the metallicity are taken into account not only during the wind phase but also on the M_{CO} versus M_i relation to properly scale the ejecta at final stage of supernova explosion. The same technique has been applied to VMS. Altogether this compilation represents a complete set of stellar yields of unprecedented homogeneity and self-consistency (see also Portinari 1999, this conference).

Preliminary ejecta from massive Pop-III stars are presented by [64] limited to the wind phase. A typical 50 $M_\odot$ ejects about 10 $M_\odot$ of ^{4}He, 0.1 $M_\odot$ of ^{12}C, 0.05 $M_\odot$ of ^{16}O, and 0.001 $M_\odot$ of ^{14}N. A 20 $M_\odot$ star ejects about 1 $M_\odot$ of ^{4}He and only minute traces of ^{12}C, ^{16}O, and ^{14}N. These values highly depend on the adopted rate of mass loss.

This study has by financed by the Italian Ministry of University, Scientific Research and Technology (MURST) under contract *Formazione ed Evoluzione delle Galassie* n. 9802192401.

References

1. Andriesse C.D., 1979, Astrophys. Space Sci. 61, 205
2. Appenzeller I., 1970a, A&A 2, 216
3. Appenzeller I., 1970b, A&A 5, 335
4. Appenzeller I., & Fricke K.J., 1972, A&A 21, 285
5. Appenzeller I., & Tscharnuter W., 1973, A&A 25, 125
6. Arimoto N., Matsushita K., Yshimaru Y, Osaki T., & Renzini A., 1997, ApJ 477, 128
7. Barlow M.J., & Cohen M., 1977, ApJ 213, 737
8. Bressan A., Chiosi C., & Fagotto F., 1994, ApJS94, 63
9. Bond J.R., 1981, ApJ 248, 606
10. Bond J.R., Carr B.J., & Arnett W.D., 1982, Nature 301, 584
11. Bond J.R., Carr B.J., & Arnett W.D., 1983, Nature 304, 514
12. Bond J.R., Arnett W.D., & Carr B.J., 1984, ApJ 280, 825
13. Bower R.G., Lucey J.R., & Ellis R.S., 1992, MNRAS 254, 601
14. Calberg R.G., 1981, MNRAS 197, 1021
15. Canizares C.R., Marert T.H., Donahue M.E., 1988, *Cooling Flows in Clusters and Galaxies*, eds. A.C. Fabian, (Kluwer: Dordrecht), p. 63
16. Cannon C.J., & Thomas R.N., 1977, ApJ 211, 910
17. Carr B.J., 1977, MNRAS 181, 293
18. Carr B.J., 1994, ARA&A 32, 531
19. Carr B.J., Arnett W.D., & Bond J.R., 1982, *Super-novae: a Survey of Current Research*, eds. M.J. Rees and R.J. Stoneham (Reidel: Dordrecht)
20. Carr B.J., Bond J.R., & Arnett W.D., 1984, ApJ 277, 445
21. Carr B.J., & Rees M.J., 1984, MNRAS 207, 585
22. Cary, N., 1974, Astrophys. Space Sci. 31, 3
23. Cassisi S., & Castellani V., 1993, ApJS 88, 509
24. Cassisi S., Castellani V., & Tornambè A., 1996, ApJ 459, 298
25. Castellani V., & Paolicchi P., 1975, Astrophys. Space Sci. 185, 196
26. Castellani V., Chieffi A., & Tornambè A., 1983, ApJ 272, 249
27. Chieffi A., & Tornambè A., 1984, ApJ 287, 745
28. Chiosi C., 1981, A&A 93, 163
29. Chiosi C., Bertelli G., Bressan A., 1992, ARA&A 30, 305
30. Chiosi C., Bressan A., Portinari L., & Tantalo R., 1998, A&A 339, 355
31. Chiosi C., & Maeder A., 1986, ARA&A 26, 329
32. Ciotti L., Lanzoni B., & Renzini A., 1996, MNRAS 282, 1
33. Cowie L.L., Songaila A., Kim T.S., & Hu E.M., 1995, AJ 109, 1522
34. D'Antona F., 1992, A&A 115, L1
35. Doroshkevich A.G., Zel'dovich Y.B., & Novikov I.D., 1967, Sov. Astr.-AJ 11, 231
36. Elbaz D., Arnaud M., & Vangioni-Flam E., 1995A&A 303, 345
37. El Eid M.F., Fricke K.J., & Ober W., 1983, A&A 119, 54
38. Ezer D., 1972, Astrophys. Space Sci., 18, 226
39. Ezer D., & Cameron A.G.W., 1971, Astrophys. Space Sci. 14, 399
40. Feast M.W., 1991, in *Instabilities in Evolved Super and Hyper-Giants*, eds. C. de Jager & H. Nieuwenhuijzen, Amsterdam
41. Forieri C., 1982, Master Thesis, University of Padova, Italy
42. Fricke K.J., 1973, ApJ 183, 941

43. Fricke K.J., 1974, ApJ 189, 535
44. Fukazawa Y., Makishima K., Tamura T. et al., 1998, PASJ 50, 187
45. Fuller G.M., Woosley S.E., & Weaver T.A., 1982a, Bull.AAS 14, 957
46. Fuller G.M., Fowler W.A., & Newman M.J., 1982b, ApJ 252, 715
47. Fujimoto M.Y., Iben I.Jr., Chieffi A., & Tornambè A., 1984, ApJ 287, 749
48. Gibson B.K., & Matteucci F., 1997, ApJ 475, 47
49. Greggio L., 1996, MNRAS 285, 151
50. Hartquist T.W., & Cameron A.G.W., 1977, Astrophys. Space Sci. 48, 145
51. Hogan C., 1983, MNRAS 202, 1101
52. Hutchins J.B., 1976, ApJ, 205, 103
53. Klapp J., 1983, Astrophys. Space Sci. 93, 313
54. Klapp J., 1984, Astrophys. Space Sci. 106, 215
55. Ikeuchi S., 1981, PASJ 33, 211
56. Ishimaru & Arimoto N., 1997, PASJ 49, 11
57. Larson R.B., 1974, MNRAS 166, 585
58. Larson R.B., 1998, MNRAS 301, 569
59. Layzer D., & Hively R.M., 1973, ApJ 179, 361
60. Ledoux P., 1941, ApJ, 94, 537
61. Maeder A., & Conti P.S., 1994, ARA&A 32, 227
62. Marigo P., Bressan A., & Chiosi C., 1996, A&A 313, 545
63. Marigo P., Bressan A., & Chiosi C., 1998, A&A 331, 564
64. Marigo P, Chiosi C., Girardi L., & Sarrubbi T., 1999, this conference.
65. Matteucci F., 1997, Fund. Cosmic Phys. 17, 283
66. Matteucci F., & Vettolani G., 1988, A&A 202, 21
67. Molaro P., & Bonifacio P., 1990, A&A 236, L5
68. Molaro P., & Castelli F., 1990, A&A 228, 426
69. Mushotzsky R.F., Lowenstein M., Arnaud M., Tamura T., Fukazawa Y., et al., 1996, ApJ 466, 686
70. Nakamura F., & Umemura M., 1999, ApJ 515, 239
71. Norris J.E., Peterson R.C., & Beers T.C., 1993, ApJ 415, 797
72. Ober W.W., El Eid M.F., & Fricke K.J., 1983, A&A 119, 61
73. Olive K.A., 1999, astro-ph/9901231
74. Ostriker J.P., & Cowie L.L., 1981, ApJ 243, L127
75. Ostriker J.P. & Gnedin N.Y., 1996, ApJ 472, L63
76. Padoan P., Nordlund A.P., & Jones B.J.T., 1997, MNRAS 288, 145
77. Palla F., Salpeter E.E., & Stahler S.W., 1983, ApJ 271, 632
78. Papaloizou J.C.B., 1973a, MNRAS 162, 143
79. Papaloizou J.C.B., 1973b, MNRAS 162, 162
80. Peebles P.J.E., & Dicke R.H., 1968, ApJ 154, 891
81. Portinari L., Chiosi C., & Bressan A., 1998, A&A 334, 505
82. Primas F., Molaro P., & Castelli F., 1994, A&A 290, 885
83. Puget J.L., & Heyvaerts J., 1980, A&A 83, L10
84. Rees M.J., 1978, Nature 275, 35
85. Renzini A., Ciotti A., D'Ercole A., & Pellegrini S., 1993, ApJ 419, 52
86. Rothenflug R., Vigroux L., Mushotsky R.F., & Holt S.S., 1984, ApJ 279, 53 1984,
87. Rowan-Robinson M., Negroponte J., & Silk J., 1979, Nature 281, 635
88. Salpeter E.E., 1955, ApJ 121, 161
89. Scalo J.M., 1998, in *The Stellar Initial mass Function*, ASP Conf. Ser. Vol. 142, eds. G. Gilmore & D. Howell, Astron. Soc. Pac., San Francisco, 201

90. Schwarzschild M., & Harm R., 1959, ApJ 129, 637
91. Silk J., 1977, ApJ 211, 638
92. Sneden C., Lambert D.L., & Whitaker R.W., 1979, ApJ 234, 964
93. Sneden C., Preston G.W., McWilliams A., & Searle L., 1994, ApJ 431, L27
94. Songaila A., & Cowie L.L., 1996, AJ 112, 335
95. Stothers R., & Simon N.R., 1970 ApJ 160, 1019
96. Talbot R.J., & Arnett W.D., 1971, Nature 229, 150
97. Tantalo R., Chiosi C., Bressan A., & Fagotto F., 1996, A&A 311, 361
98. Tegmark M., Silk, J., & Blanchard A., 1994, ApJ 420, 484
99. Tegmark M., Silk J., Rees M.J., Blanchard A., Abel T., & Palla F., 1997, ApJ 474, 1
100. Tholine J.E., 1980, ApJ 239, 417
101. Truran J., 1980, Nucleonica 25, 1472
102. Uehara H., Susa H., Nishi R., & Yamada M., 1996, ApJ 473, L95
103. Umemura M., Loeb A., & Turner E., 1993, ApJ 419, 459
104. van den Bergh S., 1962, AJ 67, 486
105. Vassiliadis E., & Wood P.R., 1994, ApJS 92, 125
106. White S., & Rees M.J., 1978, MNRAS 183, 341
107. Woosley S.E., & Weaver T.A., 1981, Ann. N.Y. Acad. Sci. 375, 357
108. Woosley S.E., & Weaver T.A., 1982a, *Essays in Nuclear Astrophysics*, eds. C.A. Barnes, D.D. Clayton, and D.N. Schramm (Cambridge Univ. Press: Cambridge), p. 377
109. Woosley S.E., & Weaver T.A., 1982b, *Super-novae: A Survey of Current Research* , eds. M.J. Rees and R.J. Stoneham (D. Reidel: Dordrecht), p. 79
110. Woosley S.E., & Weaver T.A., 1986, ARA&A 24, 205
111. Woosley S.E., & Weaver T.A., 1995, ApJS 101, 181
112. Worthey G., Faber S.M., Gonzáles J.J., 1992, 398, 69
113. Yoshii Y., & Saio H., 1986, ApJ 301, 587
114. Ziebarth K., 1970, ApJ 162, 947

The Evolutionary Properties of Low-Mass Pop III Stars Including Effects of External Pollution*

Santi Cassisi[1,2], Maurizio Salaris[2,3], Achim Weiss[2], and Helmut Schlattl[2]

[1]Osservatorio Astronomico di Collurania, Teramo, Italy
[2]Max-Planck-Institut für Astrophysik, Garching, Germany
[3]Liverpool John Moores University, Birkenhead, United Kingdom

Abstract. We investigate the evolution of low-mass metal-free Population III stars accounting for the most updated physical inputs and for atomic diffusion. In particular, we test the efficiency of pollution by the encounter with gas clouds, combined with particle diffusion, in order to verify if such mechanism could be a relevant external source of CNO-elements. The possibilities to discriminate between a Pop II and a polluted Pop III field star are also briefly discussed.

1 Introduction

It is widely accepted that the primordial gas from which the galaxies formed contained only hydrogen and helium. It is then natural to ask whether any of the first stars that formed from this material are still observable as "Population III" stars of ultralow or zero metallicity. The logical place to seek for such objects is, of course, in the halo of our Galaxy. However, even if the search for Population III stars has a rather long history, only a few stars of extremely low metallicity, $[Fe/H] \leq -4.0$ have been found ([5] and reference therein). This apparent dearth of extremely metal deficient stars and the observed abundances pattern in field halo stars have been, sometimes, shown to be consistent with the existence of a much larger group of Pop III stars which have been disguised by external pollution.

One can in fact expect that in a real world a very metal poor structure, traveling through the Milky Way, can accrete matter from the gas clouds it encounters. If this occurs, the accreted matter is mixed with the pristine material of the star in the surface convective zone, and then the heavy-elements abundances in this zone increase. Moreover, since it is well known that the peculiar evolutionary properties of Pop III stars are strongly related to the lack of CNO elements in the original stellar matter (see for instance [1] - hereinafter CC93 - and reference therein), the external pollution mechanism could have significant consequences also on the evolutionary history of the star if the CNO elements in the accreted matter should have the chance to

* Work supported by the Italian–German DAAD/Vigoni program

reach the H-burning layers. It is also important to analyze the temporal evolution of the surface heavy-element abundances in polluted stars, in order to check the possibility to yet identify a real Pop III star by means of its observed spectrum. Until now, all theoretical investigations devoted to study pollution in Pop III stars have provided some hints of the evolution of a polluted zero metal object by simply extrapolating the well-known behavior of "normal" Pop II stars ([2]). For these reasons we have decided to explore the theoretical scenario for Pop III stars accounting in a homogeneous and self-consistent framework for both atomic diffusion and external pollution.

2 The Evolutionary Computations

The evolutionary properties of extremely metal-poor stellar structures have been the subject of accurate investigations since the early 1970s (see CC93 and references therein). We refer to the quoted papers for a detailed description of the main evolutionary properties of Pop III objects, which also have been reviewed in this conference by Castellani and Chiosi.

In the present work, we decided to consider a "true" metal free ($Z = 0$) chemical composition and a helium abundance equal to $Y = 0.23$. The evolutionary computations have been carried out by adopting a nuclear network accounting for both H- and He-burning, but neglecting any possible unconventional nuclear-reaction branches ([6]). We have considered stellar masses ranging from $0.8M_\odot$ to $1.2M_\odot$, and all the evolutionary sequences have been followed from the initial Zero-Age Main Sequence until the ignition of He-burning at the tip of the Red Giant Branch. A detailed discussion on the physical inputs and the numerical treatment adopted in the computations can be found in [7].

For each mass we have considered two different cases without external pollution: one *without atomic diffusion*, which we denote as 'canonical' and one *with atomic diffusion*. The second case we call 'standard' following the contemporary definition of the physics for the standard solar model. In addition, we have computed some models taking into account both atomic diffusion *and* external He and heavy-element pollution.

2.1 The 'Standard' Scenario

The evolutionary paths of both the $1M_\odot$ canonical model and the standard one computed accounting for helium diffusion, are plotted in Fig. 1 along with some comparison tracks. Comparing our canonical model with the one by CC93 (dotted) we note the fine agreement between the two computations, until the early evolution along the sub-giant branch (SGB).

Fig. 1 highlights the evolutionary event, peculiar of true Pop III stars, which occurs during the transition to the RGB: a flash in the H-burning region, which leads to a blue loop in the H-R Diagram. The same result has

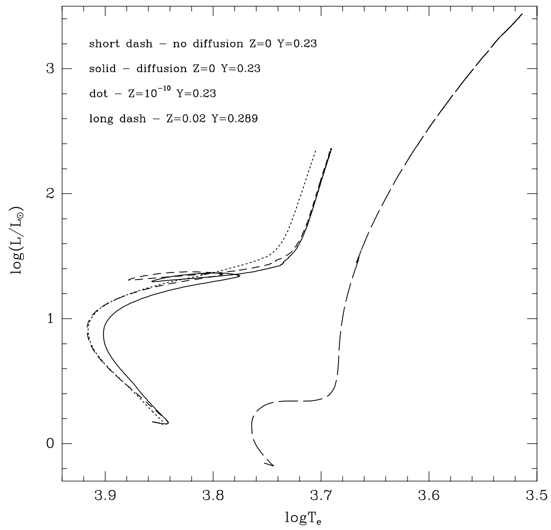

Fig. 1. The evolutionary paths in the H-R diagram for $1M_\odot$ stellar models, computed under different assumptions about the initial chemical composition: canonical metal-free model (short dashed), standard metal-free model accounting for atomic diffusion (solid), canonical Z=10^{-10} model computed by CC93 (dotted) and Z=0.02 one (long dashed). All sequences have been followed until the RGB tip.

been obtained also by [3] by computing a $1M_\odot$ metal-free model. The physical reasons for the occurrence of the flash is the following: close to the central H-exhaustion, the core strongly contracts, increasing temperature and density, thereby counterbalancing the effect of the continuous hydrogen depletion on the energy-production rate. Due to this increase in both central density and temperature, the efficiency of the 3α reaction is enhanced and thus, the number of carbon nuclei grows. As a consequence, the energy delivered by the CNO cycle strongly increases during this phase. A thermal runaway is produced and a flash occurs which produces the loop of the track in the H-R diagram. In this phase the star develops a convective core. The ensuing expansion of the inner stellar regions produces a significant decrease in both density and temperature, which reduces the 3α nuclear rate and, as a consequence, also the energy produced by the CN-conversion. When the central abundance of hydrogen drops to zero the convective core disappears ([7] for more details).

From the data plotted in Fig. 1, one can easily notice that the CNO flash along the SGB is missing in the CC93 computations, because they have assumed a non-zero primordial abundance of heavy elements: although very low ($Z = 10^{-10}$), this is sufficient to allow the CNO-cycle to operate, such that the central temperature remains low enough to avoid the thermal runaway. In this sense, *a metal abundance of the order of $Z = 10^{-10}$ seems to be a "critical" metallicity for getting the thermal runaway along the SGB.*

The comparison between the canonical and standard model accounting for atomic diffusion shows the expected changes. However, it is worth noticing that the efficiency of atomic diffusion during the MS evolution of low-mass stars increases when decreasing the metallicity, since the diffusion in the stellar envelopes is larger due to the thinner convective envelopes. Therefore, for fixed diffusion coefficients the effect of atomic diffusion is largest in metal-free stars. This is a quite important point to bear in mind when we will discuss the effect of external pollution on metal-free stars.

2.2 The 'Non-Standard' Scenario

One might explain the lack of objects with a Pop III metallicity by assuming that the surface has been metal-enriched by accretion of metal-rich material through encounters with interstellar gas clouds. This scenario we have investigated quantitatively. The amount of material accreted by a star depends on several parameters as, for instance, the relative velocity between the star and the gas cloud, the cloud parameters and so on. We explored, if and when atomic diffusion is able to bring CNO elements below the edge of the convective envelope and into the H-burning regions. We have used a very simple accretion model by assuming that instantaneous accretion of all the metal-rich matter has happened immediately before the star reached the ZAMS. By adopting this approach, we maximize the "efficiency" of the combination of both processes (accretion + diffusion). Following the estimates by [8], we have modified the chemical composition of the outermost $0.01 M_\odot$ of a model, by adopting as the chemical composition of the "accreted" matter $Z = 0.01$ and $Y = 0.25$.

In Fig. 2, we have plotted the evolutionary tracks in the H-R diagram for both the 'polluted' models and the standard one. The main result is that the accreted carbon never reaches the nuclear burning regions. The occurrence

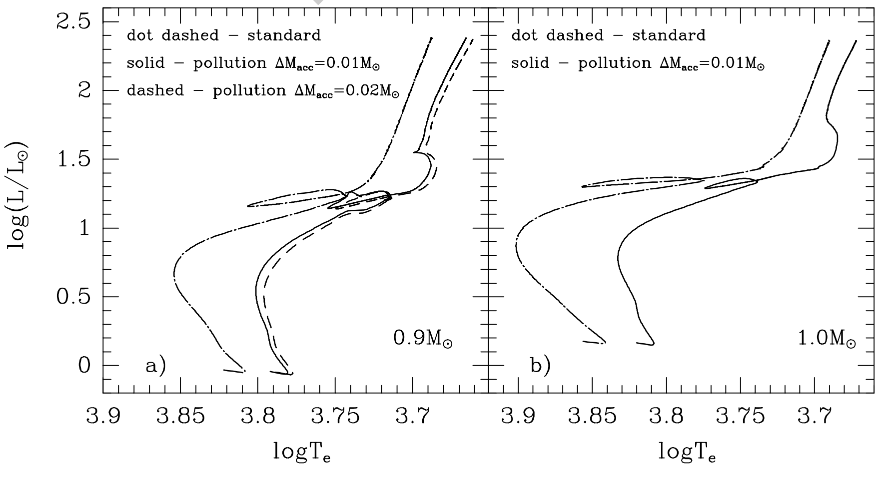

Fig. 2. (a) The evolutionary paths in the H-R diagram for a $0.9 M_\odot$ stellar structure, computed under different assumptions about the amount of accreted metal rich matter. (b) as (a) but for the $1 M_\odot$ model.

of the CNO-flash along the SGB – an event originated in the deep interior – is not affected at all by the accretion of metals. *This is an indirect proof that atomic diffusion is not able to bring CNO-elements into the nuclear burning region. Otherwise one would see an increase in the CNO-cycle burning rate during the previous MS-evolution, eventually developing into a thermal runaway.*

More details on the evolutionary properties can be found in Fig. 3: during the SGB evolution, a thin convective region of $\approx 0.02\,M_\odot$ appears in the envelope and basically all metals diffused during the MS evolution are dredged back to the surface (top panel). The increase in envelope metallicity is accompanied by a decrease in effective temperature (middle). Then the convective envelope goes even deeper, mixing therefore only matter with original zero metallicity; this results in a slight decrease of the surface abundances of the individual heavy elements. During the thermal runaway, $T_{\rm eff}$ increases and the convective envelope disappears, leaving the surface abundances unchanged for a short while. When the runaway stops and the star starts to climb up the RGB, the outer convection sets in again, this time reaching much deeper layers. At this point the surface metal abundances decrease even more (more primeval matter is mixed into the convective envelope), while the stellar track moves toward lower effective temperatures because of the progressively growing convective region. When the star is settling on its Hayashi track, the metal abundance in the convective envelope is still decreasing; this produces the "kink" which appears at the base of the RGB in Fig. 2. Up to this point our calculations indicate that diffusion is not able to transport the accreted metals into the nuclear burning regions. The last possibility for this occurrence takes place during the RGB evolution, where the hydrogen-burning shell might be able to pass through regions previously reached by the envelope convection at its maximum extension ($1^{\rm st}$ dredge-up). However, in all models we have computed, the distance in mass between the inner point reached by the convective envelope during its maximum penetration and the location of the hydrogen-burning shell at the He-flash is never less than $\approx 0.1 M_\odot$, so this possibility is completely ruled out. This evolutionary scenario is not significantly changed when accounting for a larger amount of metal-rich accreted matter (see Fig. 3).

3 Conclusions

We investigated the possibility that a low-mass Pop III star – due to accretion of metal-rich matter through encounters with molecular clouds – could increase its original amount of CNO elements in the core to a level which allows the ignition of the CN cycle, thus modifying its evolutionary behavior from the one characteristic of metal-free object to the one typical of extremely metal-poor stars. The main results can be summarized as follows:

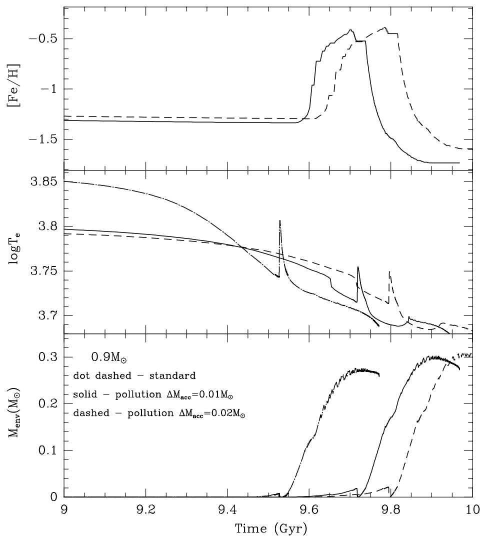

Fig. 3. Evolution of the surface abundance of iron, the effective temperature, and the size of the convective envelope for a $0.9M_{\odot}$ model computed taking into account different amounts of accreted metal-rich matter.

- Our calculations show that neither atomic diffusion during the MS phase nor outer convection during the RGB evolution, are able to bring CNO-elements into the nuclear burning region. So, in spite of the remarkable changes of the heavy-element abundances in the outer layers, the evolutionary behavior of a polluted Pop III star is always regulated by the original chemical composition;
- from the point of view of an 'external' observer it is extremely difficult to discriminate between a polluted Pop III field star and a very metal poor Pop II one; in spite of substantial differences in the core physical conditions and energy-production mechanisms, the evolution in the HRD is qualitatively quite similar;
- the analysis of the surface abundance ratios does not appear to be of very much help. This means that, if the chemical pollution of the stellar surface is effective, the still surviving Pop III stars could be all disguised as extremely Pop II stars with no chance to discriminate between "true" extremely metal-poor stars and polluted Pop III objects.

References

1. Cassisi, S. & Castellani, V. 1993, ApJS, **88**, 509
2. Fujimoto, M.Y., Iben, I.Jr. & Hollowell, D. 1990, ApJ, **349**,580
3. Fujimoto, M.Y., Sugiyama, K., Iben, I.Jr. & Hollowell, D. 1995, ApJ, **444**,175
4. Hollowell, D., Iben, I.Jr. & Fujimoto, M.Y. 1990, ApJ, **351**,245
5. Norris, J.E., Peterson, R.C. & Beers, T. 1993, ApJ, **415**, 797
6. Schlattl, H., Weiss, A., Cassisi, S. & Salaris, M. 2000, *this volume*
7. Weiss, A., Cassisi, S., Schlattl, H. & Salaris, M. 2000, ApJ, *in press*
8. Yoshii, Y. 1981, A&A, **97**, 280

Carbon Nucleosynthesis in Metal-Free Low-Mass Stars*

Helmut Schlattl[1], Achim Weiss[1], Santi Cassisi[2], and Maurizio Salaris[3]

[1] Max-Planck-Institut für Astrophysik, Garching, Germany
[2] Osservatorio Astronomico di Collurania, Teramo, Italy
[3] Liverpool John Moores University, Liverpool, UK

Abstract. We investigate possible nuclear chains for carbon production during the main-sequence phase of low-mass, initially metal-free stars with the help of an extended nuclear network. Though unconventional chains dominate during the early phases, only the familiar triple-α process is effective enough to produce carbon at a mass fraction level of 10^{-10}, which is then triggering operation of the CNO-cycle.

1 Nuclear paths to carbon in Pop III stars

In true Pop III stars, i.e. those with an initially vanishing metallicity of $Z = 0$, the CNO-cycle cannot operate due to the absence of carbon. This is the reason for an evolution different from Pop II stars. Primary carbon production *during hydrogen burning* is thus decisive for if, how and when Pop III stars begin to evolve as extreme Pop II stars. The critical mass fraction of carbon for the operation of the CNO-cycle is $X_C \approx 10^{-10}$.

The following possibilities for carbon synthesis in a hydrogen–helium–plasma exist:

1. triple-α process: operates spuriously at $7 \cdot 10^7$ K;
2. from minor constituents of pp-chains [1]: $^7\mathrm{Be}(\alpha,\gamma)^{11}\mathrm{C}(e^+\nu)^{11}\mathrm{B}(p,\gamma)^{12}\mathrm{C}$; $^7\mathrm{Li}(\alpha,\gamma)^{11}\mathrm{B}(p,\gamma)^{12}\mathrm{C}$; $^8\mathrm{B}(\alpha,p)^{11}\mathrm{B}(p,\gamma)^{12}\mathrm{C}$
3. hot pp-cycles [2]: e.g. $^8\mathrm{B}(p,\gamma)^9\mathrm{C}(\alpha,p)^{12}\mathrm{N}$

2 Network calculations and results

In order to evaluate which nuclear chains have to be taken into account in our full stellar evolution calculations (see Cassisi et al., this volume) we used a one-zone extended nuclear network [3], which contained all isotopes relevant for the pp- and CNO-chains and -cycles up to oxygen and fluorine. Reaction rates were taken from [4]. We took temperature and density profiles $T(t)$ and $\rho(t)$, needed as background for the nucleosynthesis calculations from our evolutionary calculations for the central conditions of stars of mass $M/M_\odot = 0.8,\ 1.0,\ 1.2$.

Figure 1 summarizes the evolution of C and N for the three models. We find that the chain $^7\mathrm{Be}(\alpha,\gamma)^{11}\mathrm{C}$ dominates for the largest part of main-sequence evolution, but produces carbon only up to $X_C \approx 10^{-13}$. During the

* Work supported by the Italian–German DAAD/Vigoni program

final phase of the main-sequence (low p-abundance; high T) triple-α begins to dominate and produces $X_C \approx 10^{-10}$. Other chains are irrelevant. Note that $0.8\,M_\odot$ appears to be the critical initial stellar mass to achieve the critical amount of X_C at any time.

To conclude, stellar evolution codes must treat hydrogen- and helium-burning simultaneously, such that C-production can take place in the presence of protons. The $^7\mathrm{Be}(\alpha,\gamma)^{11}\mathrm{C}$ chain dominates for the longest time but is not sufficiently productive. For low-mass Pop III stars it is sufficient to include the triple-α process to account for C-production.

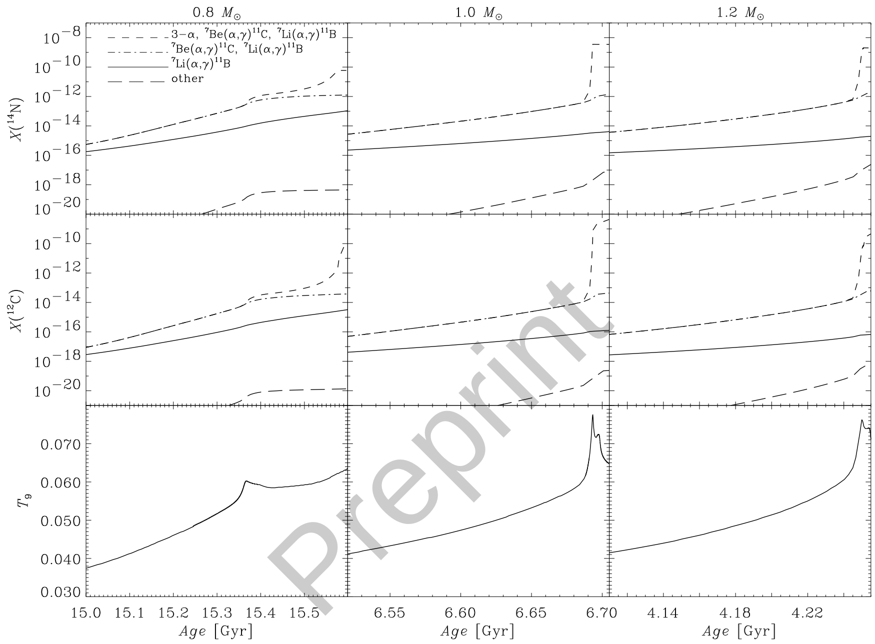

Fig. 1. Creation of $^{12}\mathrm{C}$ and ^{14}N as a function of time for the last phases of the main-sequence evolution of 3 stars of masses 0.8, 1.0 and 1.2 $M_\odot$. The three lines in each panel correspond to the production if all important processes – 3α, $^7\mathrm{Be}(\alpha,\gamma)^{11}\mathrm{C}$ and $^7\mathrm{Li}(\alpha,\gamma)^{11}\mathrm{B}$ – are included (dashed line), if 3α is excluded (dot-dashed), and if only the last one is considered (solid). Also shown is $T(t)$, which, together with $\rho(t)$, is taken from stellar evolution calculations and used as input for the network calculations.

References

1. Mitalas R. (1995) ApJ **290**, 273
2. Wiescher M., Görres J., Graff S. et al. (1989) ApJ **343**, 353
3. Weiss A., Truran J.W. (1990) A&A **238**, 178
4. Thielemann F.-K. (1996) REACLIB, `http://isotopes.lbl.gov/isotopes/astro/friedel.html`

Evolutionary Models of Zero Metallicity Stars

Paola Marigo, Cesare Chiosi, Léo Girardi, and Tiziana Sarrubbi

Department of Astronomy, University of Padova, Vicolo dell'Osservatorio 5, 35122 Padova, Italy

Abstract. We present new evolutionary models for zero-metallicity stars, covering a large range of initial masses (from 0.8 to 100 $M_{\odot}$). Models are computed with overshooting from stellar cores and convective envelopes, and assuming mass-loss from the most massive stars. We discuss the main evolutionary features of these stars, and provide estimates of the amount of newly-synthesized elements dredged-up to the stellar surface, and possibly lost by stellar winds from the most massive stars. Full details of these models will be given in Marigo et al. (2000, in preparation).

1 Model prescriptions

In our computations we adopt an initial helium content $Y = 0.23$. We consider the complete sets of reactions for the pp-chain and CNO tri-cycle, and the most important alpha-capture reactions for heavy elements up to Mg. Nuclear rates are taken from [3]. The nuclear network is implicitly solved for all the considered H- and He-burning reactions, and without any additional assumption for nuclear equilibria. Overshooting from stellar cores is applied according to the Bressan et al. formalism [1]. Mass-loss from massive stars ($M \geq 10 M_{\odot}$) is described according to [2]. Stellar evolution is calculated throughout the nuclear H-burning phase up to the He-flash at the RGB tip for low-mass models, and throughout nuclear H- and He-burning phases up to the beginning of the TP-AGB phase and carbon ignition for intermediate- and high-mass models, respectively.

2 Evolutionary features

Figure 1 presents the evolutionary tracks in the H-R diagram. The appearance of short-lived loops is caused by the ignition of the 3-α reaction during core and/or shell H-burning, leading to the first activation of the CNO-cycle. In the case of low-mass stars ($0.9 M_{\odot} \lesssim M \lesssim 1.2 M_{\odot}$) a loop develops near the end of central H-burning ($X_{\rm c} \sim 0.01$), whereas for more massive stars ($2.5 M_{\odot} \lesssim M \lesssim 6 M_{\odot}$) a similar feature also occurs at the formation of the He-shell.

As far as the critical stellar masses for non-degenerate nuclear ignition are concerned, we find that $M_{\rm Hef} \sim 1.1 M_{\odot}$ corresponds to the minimum initial mass for a star to avoid the He-flash, and $M_{\rm up} \sim 6.0 - 7.0 M_{\odot}$ the minimum initial mass for a star to avoid carbon deflagration.

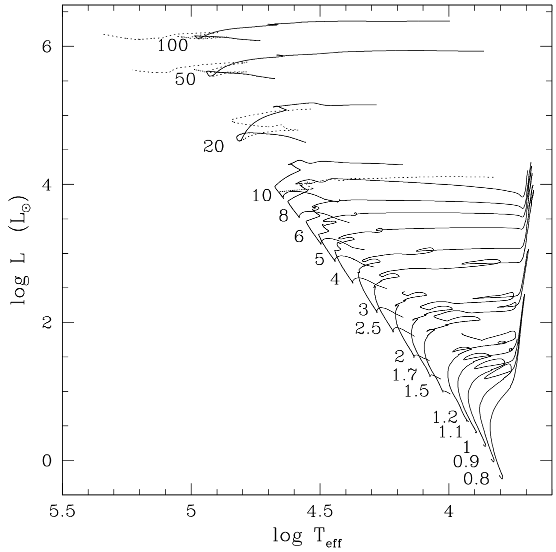

Fig. 1. HR diagram for the complete set of $Z = 0$ evolutionary tracks, from 0.8 to 100 $M_\odot$. Solid line: evolution at constant mass; dotted line: evolution with mass-loss

3 Surface chemical changes

The first dredge-up is practically absent in all models. Only for stars with $M < 1.0 M_\odot$ a very small amount (less than 0.003 $M_\odot$) of He is dredged-up to the surface. The second dredge-up is experienced by stars with $1.5 M_\odot < M < 8 M_\odot$, being quite efficient in models with $M \geq 2.5 M_\odot$. It turns out that the surface composition is enriched almost only in He (reaching $Y = 0.25$ – 0.37 at increasing stellar mass) and negligibly in CNO elements (10^{-16} – 10^{-8} in mass fraction).

Massive stars, with $10 M_\odot < M < 100 M_\odot$, do not show any trace of surface chemical pollution due to dredge-up episodes. Only models calculated with mass-loss may expose nuclearly processed material to the surface. With the adopted prescription for mass-loss, stellar winds are never able to strip off H-exhausted layers in models with $M \leq 20 M_\odot$. In these cases, at most, the H-burning shell is eaten up, with consequent surface enrichment in He and small amounts of CNO. For more massive models with $M \geq 50 M_\odot$, wind stripping is able to reach the CO-enriched region left by convective He-burning. In these cases, the corresponding yields of C and O are considerable ($\sim 0.1 - 1 M_\odot$).

References

1. Bressan A., Bertelli G., Chiosi C., (1981), A&A **102**, 25-30
2. Chiosi C., (1981), A&A **93**, 163-170
3. Caughlan G.R., Fowler W.A., (1988), Atomic Data Nucl. Data Tables **40**, 283

Evolution and Nucleosynthesis in Massive Stars of Zero Metallicity

Alexander Heger, Stan E. Woosley, and Richard Waters

Astronomy and Astrophysics Department, University of California, Santa Cruz, CA 95064, U.S.A.

Abstract. We follow the evolution of rotating, zero metallicity stars in the mass range $15-250\,\mathrm{M}_\odot$ from the zero-age main sequence to core collapse. Detailed nucleosynthesis is computed using a 199 isotope network complete up to germanium. In addition to the expected overabundance of alpha-isotopes in the final yields (compared to similar mass stars of solar metallicity), we find evidence for the production of primary $^{14}\mathrm{N}$. Stars more massive than $\gtrsim 100\,\mathrm{M}_\odot$ on the main sequence will encounter the electron-positron pair instability following helium burning. For currently favored values of nuclear cross sections and convection algorithm, we determine critical helium core masses for pulsational pair instability, prompt explosion, or prompt black hole formation of 45, 65, and $140\,\mathrm{M}_\odot$ respectively. Towards the upper end of the mass range that explodes, very large quantities of $^{56}\mathrm{Ni}$ are produced and the explosion should be extremely bright. The high mass models that make black holes might be potential progenitors of gamma-ray bursts (GRB) of enormous energy.

1 Introduction

We consider here the evolution of zero metallicity stars in the mass range $15-250\,\mathrm{M}_\odot$, that is, stars whose initial composition is given solely by the products of the Big Bang. These would be the very first stars to form in the universe and may have contributed to its reionization. Recent simulations (Norman, this volume; Abel, private communication) suggest that the first stars to form in the universe may have been quite massive with typical masses $\sim 100\,\mathrm{M}_\odot$ and perhaps more, hence we consider models well above the traditional $100\,\mathrm{M}_\odot$ limit.

It should be noted that zero metallicity is a singularity. Even a tiny amount of metals makes a qualitative difference in the evolution - in the way the star burns hydrogen, its entropy, and the binding energy of the presupernova star. The pp-chain is never sufficiently efficient to power massive stars [3], so stars of zero initial metallicity contract until central temperatures $\gtrsim 10^8\,\mathrm{K}$ are reached and CNO seed isotopes are produced by the triple-α process. By the end of central hydrogen burning such stars have $^{14}\mathrm{N}$ mass fractions $\gtrsim 10^{-7}$. As a consequence of this peculiar behavior in hydrogen burning, the post-main sequence entropy structure of stars of zero initial metallicity is different than that of stars having over 10^{-5} solar metallicity.

A major uncertainty, especially for the more massive stars considered here, is mass loss. Radiative mass loss is probably negligible for stars of such low metallicity (Kudritzki, this volume), but they still might lose an appreciable fraction of their mass because of nuclear-driven pulsations. The critical mass for the onset of the nuclear pulsational instability [2] is very uncertain ($90 \ldots 420\,\mathrm{M}_\odot$ for stars of solar metallicity [1]), and even more so, the resulting mass loss rates. At very low metallicity the temperature dependence of hydrogen burning and the gravitational potential at the surface of the star will be different and Appenzeller's estimates may need revision. Even for solar metallicity, the possibility exists for extremely massive supernova progenitors because the lifetime of stars $\gtrsim 100\,\mathrm{M}_\odot$ is only around $2-3\,\mathrm{Myr}$, comparable to their formation time. Thus such stars might still be accreting at the equator while losing mass at the pole at the same time. Because of these uncertainties, and for the sake of simplicity, we shall assume there is no mass loss for any of our zero metallicity models.

The evolution of these stars was followed with a 1D hydrodynamic stellar evolution code, KEPLER [9], from central hydrogen ignition till core collapse. A 199 isotope network was used to follow the nucleosynthesis [14]. For a few selected models, we continued the nucleosynthesis through the supernova explosion, simulated by mechanical energy input due to the movement of a piston located at the inner boundary [14]. Mixing induced by stellar rotation was also included in KEPLER as described in [5]. For the initial angular momentum of the rotating stars we assumed rigid rotation with a velocity that was 20 % Keplerian at the equator, comparable to what is observed for O-stars.

2 Nucleosynthesis and Production of Primary $^{14}\mathrm{N}$

For the assumed angular momenta the compact character of the low metallicity stars led to considerably faster rotation on the ZAMS. This induced stronger mixing due to circulation ($\tau_{\mathrm{circ}} \propto (\Omega_{\mathrm{crit}}/\Omega)^2$) and the envelopes of our stars became strongly enriched in helium. For solar metallicity, such stars would have become Wolf-Rayet stars, but without any metals Wolf-Rayet winds might be suppressed (Kudritzki, this volume).

As a consequence of helium enrichment and initial CNO-deficiency, hydrogen shell burning occured at comparatively low entropy and the envelope stayed compact and rapidly rotating. During the growth of the central helium-burning convective core, traces of carbon and oxygen were mixed into the hydrogen-burning shell due to meridional circulation. In our zero metallicity stars an enrichment of carbon/oxygen in the hydrogen-rich layers by a mass fraction as small as $\gtrsim 10^{-8}$ was already sufficient to dramatically increase the nuclear energy generation rate. In solar metallicity stars, for comparison, [5] found essentially no effect. Here we find that both, rapid rotation and higher mass favor the production of primary $^{14}\mathrm{N}$. In a $60\,\mathrm{M}_\odot$ star we found, even in the absence of rotation but owing to the shallow entropy gradient, the convective helium core can penetrate into hydrogen-rich layers and significantly produce $^{14}\mathsf{N}$. It should be noted though that even a mass fraction of 10^{-4} of $^{14}\mathsf{N}$ in the envelope, which would be a strong overabundance for a star of 10^{-4} solar metallicity, is still a gross underproduction in the final yields compared to solar values. However, in some of our more massive models we found nitrogen mass fractions of up to a few percent in the envelope.

Another important difference in the nucleosynthetic yields of the zero metallicity stars compared to solar metallicity stars is the strong dominance of the alpha-isotopes in the final yield after the explosion (e.g., [14]). More detailed results of this study will be presented in [6].

3 Pair Instability Supernovae (Hypernovae)

During the contraction phase towards central oxygen burning of helium cores of $\sim 42\,\mathrm{M}_\odot$ or more [10,13], the temperature in the center gets hot enough ($\gtrsim 3{\cdot}10^9\,\mathrm{K}$), while the density remains low, that the electron-positron pair instability is encountered. Pairs are created from the radiation field, turning some of the internal energy of the gas into rest mass of these particles. Therefore, γ drops below $4/3$ and the contraction is not stopped prior to the onset of central oxygen burning. This leads to explosive oxygen or even explosive silicon burning. When, and if, this burning produces enough energy, the infall is stopped and the core reexpands. An example for such an event could be SN 1997cy: Its light curve could be fit assuming $2\,\mathrm{M}_\odot$ of $^{56}\mathsf{Ni}$ [4], which could be easily produced in a hypernova, but would be hard to make in "common" core collapse supernova producing a compact remnant.

We reinvestigated the occurrence of the pair instability with recent input physics and followed the evolution of chemically homogeneous helium cores of 10^{-2} solar and "zero" metallicity stars where we assumed no wind mass loss (see above). For the lowest core masses the stars encounter several pulses of explosive burning, expelling matter from their surfaces in supernova-like outbursts after each pulse, until the mass of the helium drops below the critical mass. The star then continues an ordinary life of hydrostatic burning phases until iron core collapse. In this case, most probably a black hole (BH) forms. For *finite metallicity* ($Z \gtrsim 10^{-4}\,\mathrm{Z}_\odot$) the envelope usually is bound only loosely compared to the binding energy of the core and is already ejected during the first oxygen burning pulse.

For larger helium core masses, the stars are totally disrupted after a few pulses, i.e., the last pulse is violent enough to completely disrupt the star without leaving a compact remnant. For still larger masses, the star explodes in only one pulse. Finally, for core masses $\gtrsim 140\,\mathrm{M}_\odot$, the maximum central temperature becomes so high that the nuclei are photo-disintegrated into alpha-particles and nucleons. This consumes more energy than previously released by oxygen and silicon burning and the collapse continues directly

Table 1. Evolution of bare massive helium cores and of a zero metallicity star (last column). E_{51} is the explosion energy in 10^{51} erg.

mass / $M_\odot$	60	65	75	100	110	130	140+	150(ZAMS)
pulsations	yes	no	no	no	no	no	no	2
explosion	yes	prompt	prompt	prompt	prompt	prompt	BH	yes
E_{51}	2.74	5.43	12.4	41.6	55.8	87.1	–	16.7
^{12}C / $M_\odot$	4.27	4.30	4.24	3.93	3.99	3.89	–	0.91
^{16}O / $M_\odot$	41.2	43.5	46.1	41.9	38.9	29.9	–	33.1
^{20}Ne / $M_\odot$	3.57	3.92	4.38	4.13	3.74	3.47	–	1.28
^{24}Mg / $M_\odot$	2.12	2.39	2.98	2.80	3.80	3.73	–	1.38
^{28}Si / $M_\odot$	4.66	5.84	9.51	21.9	24.4	23.1	–	12.0
^{32}S / $M_\odot$	2.00	2.63	4.71	12.4	13.8	13.2	–	6.74
^{36}Ar / $M_\odot$	0.33	0.44	0.80	2.21	2.52	2.46	–	1.22
^{40}Ca / $M_\odot$	0.29	0.38	0.70	2.05	2.38	2.38	–	1.14
^{56}Ni / $M_\odot$	0.002	0.005	0.06	6.01	14.3	44.4	–	7.72

into a black hole. Our limit is slightly higher than that of [10] who found that the direct BH formation would occur already in a $130\,M_\odot$ helium core.

We computed complete stellar models for several stars of zero metallicity from the ignition of central hydrogen burning till either core collapse or disruption of the star. In contrast to the metal-enriched stars, the zero-metallicity stars carry a tightly bound envelope which prevents the (prompt) disruption in case of less energetic pair-instability flashes, i.e., for the lower-mass helium cores. A $150\,M_\odot$ star of our series developed a $\sim 71\,M_\odot$ helium core and disrupted the star at its third pulse. In contrast, the plain helium cores, which might be more representative for the helium cores of metal-enriched stars, show prompt disruption already at $\gtrsim 65\,M_\odot$.

The characteristic abundance pattern we found in our the $150\,M_\odot$ star after the explosion was dominated by alpha-isotopes, in particular ^{28}Si, ^{32}S, ^{36}Ar, and ^{40}Ca showed the highest production factors compared to solar abundances (Table 1). With the same measure the iron group isotopes were low by about a factor of two or more, despite the star produced about $7.5\,M_\odot$ of ^{56}Ni in the explosion. The latter changed for more massive stars which also produced considerably larger amounts of ^{56}Ni. ^{16}O and ^{24}Mg were, relative to solar abundance ratios, less abundant than ^{28}Si by a factor of ~ 10, ^{20}Ne by a factor of ~ 30, and ^{12}C by ~ 100. Below the iron group essentially only nuclei of the alpha chain were produced.

4 Conclusions and Outlook

One interesting result is that appreciable primary nitrogen might already be produced by the "The First Stars" (see also [13]). In particular, at zero metallicity, the entropy structure (and thus compactness) of the stars favors primary production of ^{14}N during the phase of central helium burning.

Second, several different regimes of the final outcome of massive stars of "zero" metallicity can be distinguished: At "low" masses $\lesssim 35\,\mathrm{M}_\odot$ (this limit is estimated on current results for stars of solar metallicities, assuming that the explosion mechanism is quantitatively not different), an explosion is launched by the collapse of the core that ejects (at least part of) the metal-enriched stellar mantle and envelope back into the interstellar medium. In the mass range $35\,\mathrm{M}_\odot \lesssim M \lesssim 100\,\mathrm{M}_\odot$ the neutrino-driven explosion is probably too weak to form an outgoing shock. A black hole forms and either consumes the whole star or, if there is adequate angular momentum, produces a jet that may make a GRB and explode the star [8,11]. Above $\sim 100\,\mathrm{M}_\odot$ the pair instability sets in and the stars may eject parts of their helium-enriched envelope. The metal abundance in this envelope, however, is $\lesssim 10^{-10}$ (by mass). For masses above $\sim 150\,\mathrm{M}_\odot$ the core (sometimes only after a few proceeding pulses) disrupts completely and the whole core is injected in the ISM. In case of helium core sizes beyond $\gtrsim 130\,\mathrm{M}_\odot$, i.e., initial masses $\gtrsim 250\,\mathrm{M}_\odot$, the nuclear photodisintegration leads to prompt formation of BHs and, again, either complete collapse or a jet powered explosion. These evolutionary paths neglect any possible mass loss.

In the latter case of BH formation, we found for the $150\,\mathrm{M}_\odot$ helium star that a moderate initial rotation rate of $\lesssim 10\,\%$ of Keplerian rotation (assuming an initially rigidly rotating core) is sufficient that the matter in the equatorial plane has larger specific angular momentum than that of the last stable orbit around a (moderately Kerr) BH of mass equal to the (spherical) mass coordinate. This may lead to disk formation, the initiation of a jet at the pole and, possibly, lead to a "Type III" collapsar [12,15]. The resulting equivalent isotropic energies might be as high as $\sim 10^{56}\,\mathrm{erg}$ (assuming beaming to $1\,\%$ of the sky). It is also possible that the collapse of a core with too much angular momentum to immediately become a Kerr black hole might produce, temporarily, a binary black hole with interesting implications for gravity wave astronomy.

As shown by others in these proceedings, the first stars may already have formed at red shifts of $15\ldots30$. However, the enormous luminosity of both the GRBs and the supernovae resulting from these stars might make them visible out to these distances [7]. Even without GRBs, the supernovae are very bright (cf. Table 1). For a rotating $250\,\mathrm{M}_\odot$ star, which developed a $130\,\mathrm{M}_\odot$ helium core and then produced $\sim 43\,\mathrm{M}_\odot$ of ^{56}Ni, [6] calculate a peak luminosity of $\sim 10^{44}\,\mathrm{erg\,s^{-1}}$ ($M_{\mathrm{bol}} = -21$) for about 150 days. Roughly the same peak luminosity and duration characterized the event with and without the hydrogen envelope, but the onset was delayed about 100 days and completely powered by ^{56}Co decay in the case of the bare helium core. Since the kinetic energy of the explosion was $9{\cdot}10^{52}\,\mathrm{erg}$, the interaction with circumstellar matter might also be quite brilliant.

Acknowledgments This research was supported, in part, by Prime Contract No. W-7405-ENG-48 between The Regents of the University of California and the United States Department of Energy, by the grants from the National Science Foundation (AST 97-31569 and INT-97-26315) and by the Alexander von Humboldt-Stiftung (FLF-1065004).

References

1. Appenzellt, I. (1986) in: *Luminous stars and associations in Galaxies*, eds. H. J. G. L. M. Lamers, C. W. H. De Loore, Reidel, Dordrecht, p. 55
2. Eddington, A. S. (1926) *The Internal Constitution of the Stars*, Cambridge, Cambridge, p. 200
3. Ezer, D., & Cameron, A. G. W. (1971) Ap. & Spac. Sci. **14**, 399
4. Germany, L. M., Reiss, D. J., Sadler, E. M., Schmidt, B. P., Stubbs, C. W. (1999) ApJ, submitted.
5. Heger, A., Langer, N., Woosley, S. E. (2000) ApJ **528**, in press
6. Heger, A., Woosley, S. E., Waters, R. (1999) ApJ, in preparation
7. Lamb, D. Q., & Reichart, D. E. 1999, submitted to ApJ, astro-ph/9909002
8. MacFadyen, A., Woosley, S. E. (1999) ApJ **524**, 262
9. Weaver, T. A., Zimmerman, G. B., Woosley, S. E. (1978) ApJ **225**, 1021
10. Woosley, S. E. (1986) in *Nucleosynthesis and Chemical Evolution*, Saas-Fee Advanced Course **15**, Geneva Observatoty, Sauverny-Versoix
11. Woosley, S. E. (1993) ApJ **405**, 273
12. Woosley, S. E., Heger, A. (1999) ApJ, in preparation
13. Woosley, S. E., Weaver, T. A. (1982) in *Supernovae: A Survey of Current Research*, eds. M. J. Rees and R. J. Stoneham, Dordrecht: Reidel, p. 79
14. Woosley, S. E., Weaver, T. A. (1995) ApJS **101**, 181
15. Woosley, S. E., MacFadyen, A. I., Heger, A. (1999) ApJ, submitted

Wind Models and Ionizing Fluxes of Massive Stars at Very Low Metallicity

Rolf-Peter Kudritzki[1,2]

[1] Munich University Observatory, Scheinerstr. 1, D–81679 Munich, Germany
[2] Max-Planck-Institut für Astrophysik, Karl-Schwarzschild-Str. 1, D–85748 Garching

Abstract. Wind Models of massive stars with metallicities in a range from 0.0001 to 1.0 solar are calculated using a new treatment of radiation driven winds with depth dependent radiative force multipliers and a comprehensive list of more than two millions of spectral lines in NLTE. The calculations yield mass-loss rates, wind momenta and wind energies as a function of metallicity and can be used to discuss the impact of stellar winds on the evolution of stellar populations in the early phases of galaxy formation.

Ionizing fluxes of hot stars depend crucially on the strengths of their stellar winds, which modify the absorption edges of hydrogen and helium (neutral and ionized) in the far UV. The new wind models are therefore also used to predict ionizing fluxes of massive stars as a function of metallicity.

1 Introduction

All hot massive stars have winds driven by radiation. These winds have substantial effects on the physics of stellar atmospheres by dominating the density stratification and the radiative transfer through the presence of their macroscopic transonic velocity fields (see [4] for a comprehensive review) and they modify the ionizing radiation of hot stars dramatically (see [1], [2], [3], [11]). Winds have an extremely important influence on the evolution of massive stars by affecting evolutionary time-scales, chemical profiles, surface abundances and stellar luminosities and they are vital for the evolution of galaxies by their input of energy, momentum and nuclear processed material to the ISM. In addition, stellar winds provide beautiful spectroscopic tools to investigate the physical properties of galaxies at high redshift through the analysis of broad stellar wind features easily detectable in the integrated spectra of starforming galaxies.

For our understanding of the evolution of galaxies and stars in the early phases of the universe it is, therefore, extremely important to investigate the properties of stellar winds at very low metallicity. Since these winds are initiated and maintained through absorption of photospheric photon momentum by UV metal lines, we expect their strengths to decrease with decreasing metallicity. [6] were the first to calculate wind models in metallicity range from solar to 0.1 solar and predicted that mass-loss rates scale with

$(Z/Z_\odot)^{0.5..0.8}$. [9] corroborated this conclusion by independent calculations. Spectroscopic studies of massive stars in the Magellanic Clouds confirm that the theoretical prediction is basically correct for metallicities ranging from solar down to 0.2 solar (see [8] for a review).

The objective of the project introduced here is to extend the theoretical work on stellar winds to metallicities significantly lower than those of the Magellanic Clouds to predict mass-loss rates, stellar wind momenta and energies and ionizing fluxes at very low metallicities applicable to the first generations of massive stars. For this purpose we have developed a new approach to calculate the wind dynamics. This approach is based on the improvements achieved during the last decade with regard to atomic physics and line lists (see [13]). We use the line list of 2.5 10^6 lines of 150 ionic species and apply analytical formulae (see [10], [16], [17], [15]) for a fast approximation of NLTE occupation numbers to calculate the radiative line acceleration, which is then represented by a new parameterization using depth dependent force multiplier parameters (see [5]; note that our present approach uses real model atmosphere fluxes instead of Planck functions for the photospheric irradiation of the wind). Because of the depth dependent force multipliers a new formulation of the critical point equations is introduced ([5]), which includes the old algorithm ([12]) in the limit of neglected depth dependence. In this way, wind models can be calculated within a few seconds on a workstation for every hot star with specified effective temperature, mass, radius and abundances.

2 First results

We have calculated wind models for very massive stars with masses between 100 and 300 solar masses and metallicities between 0.0001 and 1.0 solar in an effective temperature range from 40000 K to 60000 K. The following two subsections give a brief summary of the first results concerning stellar wind properties and ionizing fluxes. A more comprehensive paper is in preparation ([5]).

2.1 Stellar wind properties

At very low metallicities the mechanism of line driving becomes very inefficient and wind solutions can only be obtained very close to the Eddington limit, where the gravitational potential well is small enough. Fig. 1 demonstrates the behaviour of stellar wind momentum as a function of the distance to the Eddington limit. The analytical discussion of the hydrodynamic equations of radiation driven winds (see [7], [14], [4], [8]) predicts that the "modified stellar wind momentum" $\dot{M} v_\infty (R/R_\odot)^{0.5}$ depends strongly on stellar luminosity and metallicity and is only a weak function of stellar mass and, therefore Γ_{Edd}, the ratio of stellar luminosity to the Eddington luminosity. Fig. 1 reveals that this is true as long as the metallicities are not too small

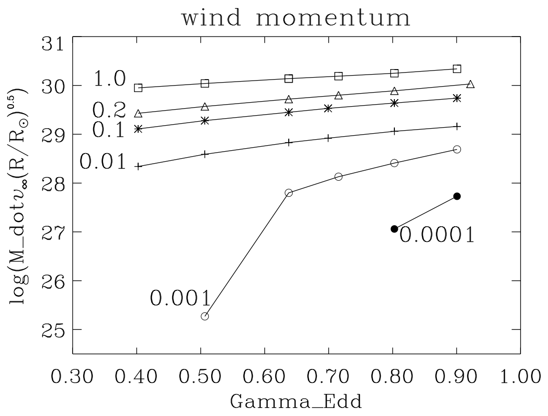

Fig. 1. Modified stellar wind momentum as a function Γ_{Edd}, the ratio of stellar luminosity to the corresponding Eddington luminosity for model sequences of different metallicity. Each sequence is labelled by its ratio of $Z/Z_\odot$. The effective temperature of the models is 50000 K and the luminosity is log $L/L_\odot = 6.26$. The variation of the Eddington luminosity is obtained by changes of the gravity.

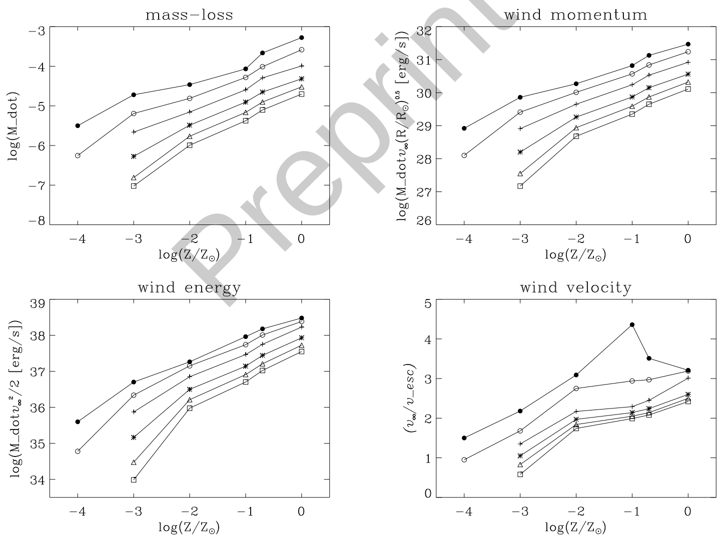

Fig. 2. Mass-loss rates, wind momenta, wind energies and wind velocities as a function of metallicity for model sequences of 300 (solid circles), 250 (circles), 200 (crosses), 150 (stars), 120 (triangles) and 100 (squares) solar masses. The effective temperature of the models is 50000 K.

(i.e. larger than or equal to 0.01). For very small metallicity, however, there is a sudden drop in wind momentum as we consider stars below a certain luminosity threshold.

Fig. 2 displays the metallicity dependence of the basic global stellar wind properties. As predicted by the analysis of the wind hydrodynamics (see references above) a power law describes the metallicity dependence very well except for the sharp drops, when Γ_{Edd} becomes too small at very low metallicity. The corresponding power law exponents are between 0.56 to 0.76 for the mass-loss rates, 0.63 to 1.0 for the wind momenta and 0.7 to 1.5 for the wind energies, respectively.

2.2 Spectra and ionizing fluxes

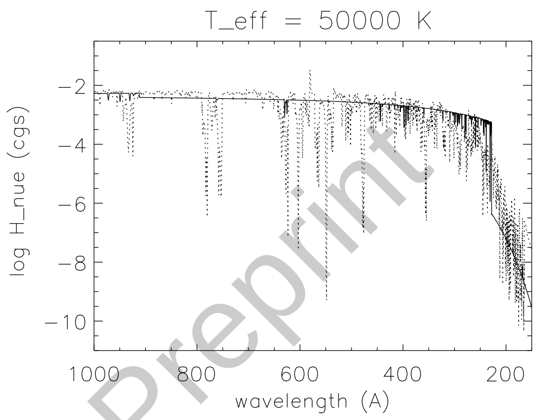

Fig. 3. FUV-fluxes of hydrodynamic NLTE model atmospheres for an effective temperature of 50000 K and metallicities of 0.2 (dashed) and 0.001 (solid) solar. The models have been calculated by T. Hoffmann and A.W.A. Pauldrach.

Fig. 3 compares the FUV spectra predicted by two hydrodynamic NLTE models calculated for a metallicity of 0.2 solar (corresponding to the SMC) and 0.001 solar. The influence of line blocking and line blanketing is still substantial at 0.2 but has practically disappeared at 0.001. The HeII absorption edge at 228 A is significantly stronger for the low metallicity model because of the reduced influence of the stellar wind (see [1], [2], [3] for an explanation of this effect).

Similar calculations for the full grid of models allow to predict the number of ionizing photons emerging from the stellar atmosphere as a function of metallicity. Fig. 4 shows that there is little influence on the ionization of hydrogen, neutral helium and ionized oxygen at these very high temperatures. The reason for this behaviour is the fact that close to the ionization edges

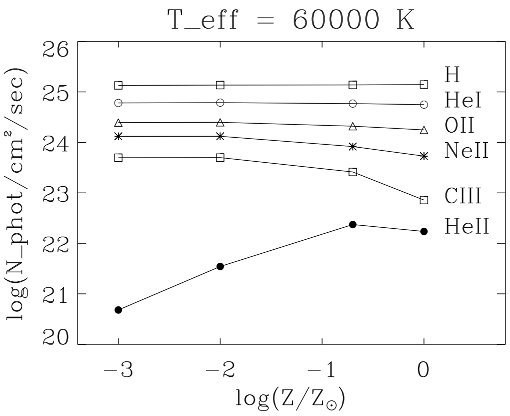

Fig. 4. Number of ionizing photons as a function of metallicity calculated for an effective temperature of 60000 K. The different sequences correspond to photons able to ionize H, HeI, OII, Ne II, CIII and HeII.

of these ions the effects of line blocking and line blanketing (together with the corresponding backwarming) cancel each other. However, the ionization of NeII and CIII is already marginally affected by metallicity, because the ionization edges of these ions are located in a spectral region with heavy line blocking. The effects on the ionization of HeII are dramatic.

3 Future work

The calculations presented here are only a first step of a large project to investigate stellar winds at very low metallicity. So far we have only calculated models in a very limited range of stellar masses and effective temperatures adopting simple estimates for the mass-luminosity relationship. The next step is to extend these calculations over the full HRD and to combine them in a self-consistent way with stellar structure and stellar evolution models. The results can then be used to develop comprehensive scaling relations for stellar mass-loss, wind momentum and energy as a function of stellar parameters and metallicity. These calculations will also provide ionizing fluxes, which can be used for population synthesis studies to understand the ionization of HII - regions in galaxies of different metallicites and with strong metallicity gradients and also to make predictions about the possible contribution of a very early population of massive stars to the re-ionization of the universe.

According to all our present experience gathered from theoretical and spectroscopic work, changes in metallicity are also accompanied by changes of the relative ratio of α-elements to iron-group-elements. So far, we have only varied the overall metallicity and have not investigated the influence of modifications in the abundance pattern. The recent work by [15] indicates that such modifications will have enormous repercussions on the properties of stellar winds. It will therefore be extremely important to investigate these effects as well.

The ultimate goal of calculations of this type is the spectral population synthesis at low metallicity corresponding to starbursting galaxies at very high redshift to be observed with NGST. The hot star group at Munich University Observatory is working hard towards this goal.

References

1. Gabler R., Gabler A., Kudritzki R.P., Pauldrach A.W.A., Puls J. (1989). A&A **226**, 162
2. Gabler R., Kudritzki R.P., Méndez R.H. (1991). A&A **245**, 587
3. Gabler R., Gabler A., Kudritzki R.P., Méndez R.H. (1992). A&A **265**, 656
4. Kudritzki R.P. (1998). Quantitative Spectroscopy of the Brightest Blue Supergiant Stars in Galaxies. Proc. 8th Canary Winter School, p. 149. Cambridge University Press
5. Kudritzki R.P. (2000). ApJ, in preparation
6. Kudritzki R.P., Pauldrach A.W.A., Puls J. (1987). A&A **173**, 293
7. Kudritzki, R.P., Pauldrach, A.W.A.,, Puls,J., & Abbott, D.C. (1989). A&A **219**, 205
8. Kudritzki R.P., Puls J. (2000) Winds from hot stars. Annual Review of Astronomy and Astrophysics **38**, in press
9. Leitherer C., Robert C., Drissen L. (1992). ApJ **401**, 596
10. Lucy L.B., Abbot D.C. (1993). ApJ **405**, 738
11. Najarro F., Kudritzki R.P., Cassinelli J.P., Stahl O., Hillier D.J. (1996). A&A **306**, 892
12. Pauldrach, A.W.A., Puls, J., & Kudritzki, R.P. (1986). A&A **164**, 86
13. Pauldrach, A.W.A., Lennon, M., Hoffmann, T.L., Sellmaier,F., Kudritzki, R.P., Puls, J. (1998). ASP Conference Series Vol. **131**, page 258 - 277
14. Puls, J., Kudritzki, R.P., Herrero, A., Pauldrach, A., Haser, S.M., Lennon, D.J., Gabler, R., Voels, S.A., Vilchez, J.M., Wachter, S., & Feldmeier, A. (1996). A&A **305**, 171
15. Puls J., Springmann U., Lennon M. (2000). A&AS, in press
16. Springmann, U. 1997, doctoral thesis, University of Munich
17. Springmann, U., Puls, J. (1998). ASP Conf. Series, Vol. **131**, p. 286 - 298

Model Atmospheres and Radiatively Driven Winds of Metal-Poor Stars

Ivan Hubeny[1], Thierry Lanz[1,2], and Sally Heap[1]

[1] NASA Goddard Space Flight Center, Greenbelt, MD 20771, USA
[2] Dept. of Astronomy, University of Maryland, College Park, MD 20742, USA

Abstract. We present a grid of non-LTE metal-line-blanketed hydrostatic model atmospheres for various effective temperatures, surface gravities (luminosities), and metallicities. The metallicities range from an essentially metal-free, primordial composition to a solar composition. For each model, we calculate the exact radiation force and compare to gravity acceleration. We thus find for each metallicity, the maximum surface gravity as a function of effective temperature required for the radiation force to exceed gravity and thus to initiate a radiatively-driven wind.

We investigate here the question whether hot massive stars at low metallicity have radiatively-driven winds. As it is well known, the wind can be initiated if the total radiation force acting on the atmospheric material (originating mostly by absorption of radiation in numerous metal lines) exceeds the force of gravity at the stellar surface. This work extends previous studies of the general behavior of radiatively driven winds which have concentrated on solar or near-solar metallicities pioneered by Abbott [1].

To obtain a sufficient condition for an initiation of a radiatively driven wind, we constructed a grid of plane-parallel static model stellar atmospheres for a range of effective temperatures, $T_{\rm eff}$, between 30,000 and 45,000 K (with step 5000 K), and for surface gravities, $\log g$, between 3.25 and 4.0 (with step 0.25), and for four metallicities, 1, 0.1, 0.01, and 0.001 times the solar metallicity. We used computer program TLUSTY [2]. In the present study, the following elements were treated in non-LTE: H, He, C, N, O, Si. For each model, we calculated the exact radiation acceleration and compared to the gravitational acceleration.

Fig. 1 summarizes the radiation pressure calculation for a grid of models between $T_{\rm eff} = 30,000$ and 45,000 K; $\log g$ between 3.25 and 4.0, and for four values of metallicity. The solar metallicity models do not have any problems to initiate a wind, which is a well-known phenomenon. The $Z = 0.1\,Z_\odot$ model will initiate a wind for lower surface gravities (higher luminosities); while for $Z = 0.01\,Z_\odot$ only models with low $\log g$'s produce enough line-radiation force. Therefore, stars with metallicity around or below 0.01 times the solar metallicity will have a radiatively driven winds only if close to the Eddington limit.

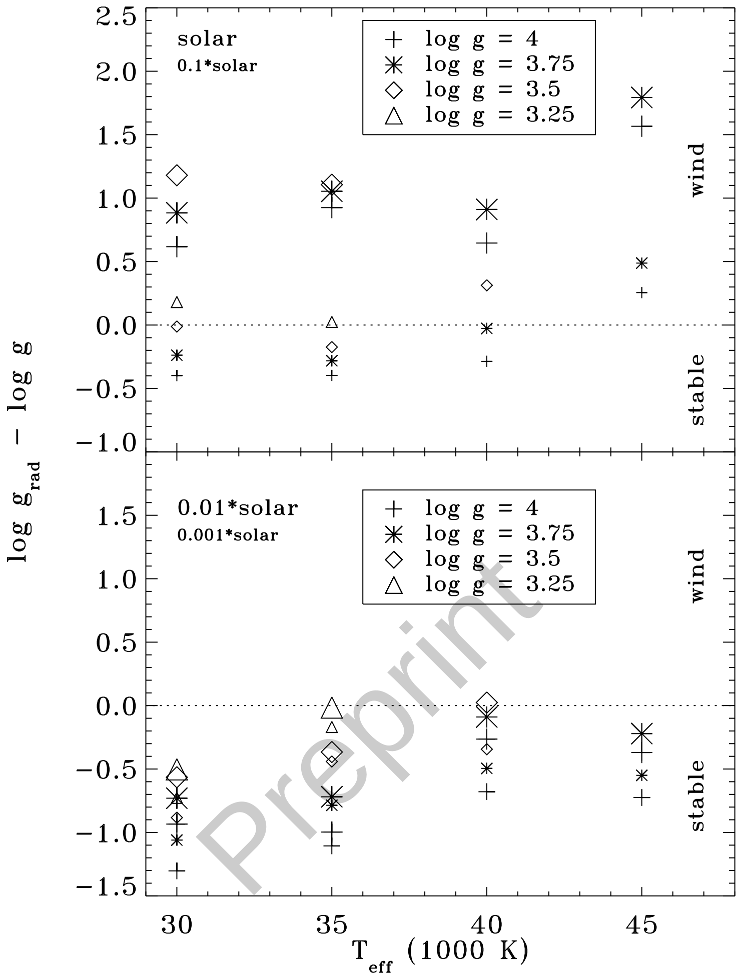

Fig. 1. Difference between radiative acceleration and gravity acceleration for a grid of non-LTE metal line-blanketed model atmospheres, for four different metallicities. Upper panel: solar metallicity (large symbols), 0.1× solar (small symbols). Lower panel: 0.01× solar metallicity (large symbols), 0.001× solar (small symbols).

References

1. Abbott, D.C., 1979, in Mass Loss and Evolution of O-Type Stars, ed P.S. Conti and C.W.H de Loore, 237
2. Hubeny, I., & Lanz, T., 1995, Astrophys. J. **439**, 875

Synthetic Stellar Clusters for Pop III

Gabriella Raimondo[1], Enzo Brocato[1], Santi Cassisi[1], and
Vittorio Castellani[2]

[1] Osservatorio Astronomico di Teramo, Teramo, Italy
[2] Università di Pisa, dip. di Fisica, Università di Pisa, Pisa, Italy

Abstract. We present preliminary results of an incoming theoretical work concerning the integrated properties of the Population III clusters of stars. On the basis of synthetic Color-Magnitude Diagrams, we provide a grid of optical and near-IR colors of Simple Stellar Populations with very low metallicity ($Z=10^{-10}$ and $Z=10^{-6}$) and age which spans from 10 Myr to 15 Gyr. A comparison with higher metallicities up to 0.006 is also shown, disclosing sizable differences in the CMD morphology, integrated colors and Spectral Energy Distribution (SED).

1 Metal deficient simple star populations

In the last two decades a great theoretical effort has been devoted to investigate the integrated properties of metal rich and metal poor star populations in the local universe [1,6] providing a modellization of integrated colors and spectra as a function of the IMF, age, chemical content etc... However, till now a complete evaluation of the integrated properties for first generation of stars which should directly form from matter emerged from the big bang is still missing.

As a part of a project devoted to investigate the integrated properties of stellar clusters in a homogeneous and complete framework ([2], Brocato et al. in preparation), we approach here the analysis of the spectro-photometric behavior of metal deficient star systems. By relying on the extended grid of evolutionary models for very metal poor stars ($Z=10^{-10}$ and $Z=10^{-6}$ with $Y=0.23$), including evolutionary phases from the MS up to the double shell burning, previously calculated [3,4] we performed synthetic population models for a wide range of age from 10 Myr to 15 Gyr adopting a Salpeter mass distribution (IMF).

Selected integrated colors in the optical and near-IR bands are reported in Fig. 1*a*. As expected from the synthetic CM Diagrams, the integrated colors become bluer and bluer as the metallicity decreases for the older cluster. Moreover, the younger clusters appear to show similar colors even with very different assumptions on metallicity (up to $Z=10^{-4}$), since the hotter and bluer stars dominate the spectral energy distribution.

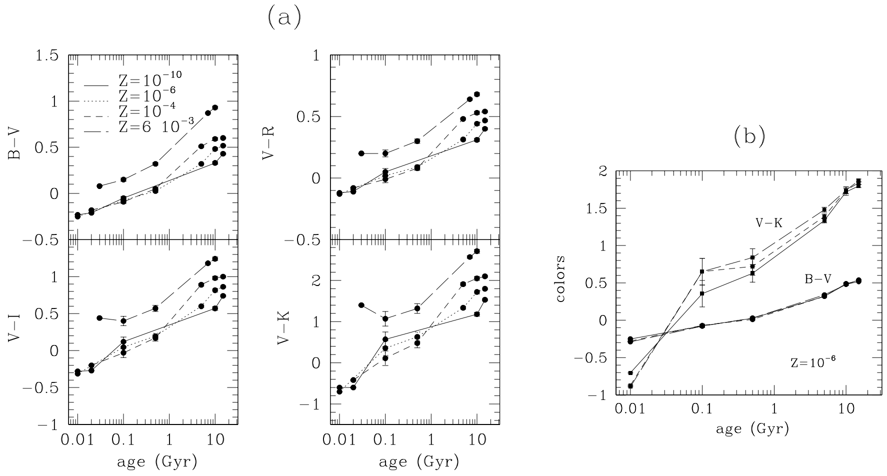

Fig. 1. (*a*) Integrated colors for four different star chemical contents: Z=10^{-10} (solid line), Z=10^{-6} (dotted line), Z=10^{-4} (dashed line) and Z=$6{\cdot}10^{-3}$ (long dashed line). (*b*) The variability in B−V and V−K colors calculated assuming: *i*) a power law with a Salpeter slope (solid line), *ii*) the Larson form with $M_p \sim 1.5M_\odot$ (dashed line) and *iii*) the Larson form with $M_p \sim 3M_\odot$ (long dashed line). Z=10^{-6} is adopted.

2 Effect of the IMF on the integrated colors

The long standing debate on the universality of the IMF is of particular relevance in the case of first star generation. Both theory and observation seem to suggest that the IMF has a typical power low at more massive stars and the deviation from this form should be confined at the lower part of the mass distribution. The thermo-dynamical conditions of primordial gas should imply a larger value of "mass-scale" (M_p) [5] compared to the present one (some tenth of solar mass), causing a deficiency of less massive stars. We investigate the effect of changing the IMF on the integrated colors adopting the analytic form suggested by Larson [5]: a Salpeter power law at larger masses, which peaks at M_p and falls exponentially at lower masses. We find (Fig. 1*b*) that the B−V color does not change for the three assumptions on the IMF. The V−K color shows the most evident variations, since it is strongly affected by the differences of the number of stars in the mass intervals.

References

1. Bressan, A., Chiosi, C., Fagotto F., 1994, ApJS **94**, 63
2. Brocato, E., Castellani, V., Raimondo G., Romaniello M., 1999, A&AS **136**, 65
3. Cassisi, S., Castellani, V., 1993, ApJSS **88**, 509
4. Cassisi, S., Castellani, V., Tornambè A., 1996, A&A **317**, 108
5. Larson, R., B., 1998, MNRAS **301**, 569
6. Leitherer K., et al. 1996, PASP **108**, 996

Chemical Yields from the First Stars

Laura Portinari

Dipartimento di Astronomia, Università di Padova
Vicolo dell'Osservatorio 5, I-35122 Padova (PD), Italy

Abstract. We examine the dependence of stellar yields on the metallicity Z of the stellar population. This effect may be important for the very first chemical enrichment from Population III stars, at very low Z. In the range of massive stars, mass loss rates varying with Z have remarkable effects. We also estimate chemical yields from Very Massive Objects (from 120 to 1000 $M_\odot$), which might have formed more easily in the very low-Z environment of the first stellar generations.

1 Introduction

Stellar model calculations show that the detailed structure and evolution of a star of given mass depends on its chemical composition; so we expect stellar yields as well to be influenced by metallicity. A homogeneous set of metallicity dependent yields, covering the whole stellar mass range, has been derived by the Padova group. Detailed results can be found in [23] (hereinafter PCB98) for massive and very massive stars and in [17,18] for low and intermediate mass stars. In this paper we will discuss the yields from massive and very massive stars; full details can be found in PCB98.

2 Yields from Massive Stars ($M = 6 - 120\,M_\odot$)

In the range of massive stars, quiescent mass loss has a strong influence on the yields, because (1) ejecta are directly released through the stellar wind, and (2) mass loss affects the final total and core mass and thus also, indirectly, the final supernova (SN). The efficiency of radiation pressure driven wind scales with metallicity ($\dot{M} \propto Z^{0.5}$ [14]). So, through the mass loss rate metallicity affects the mass and composition of the layers peeled off in the wind, as well as the final stellar mass M_{fin} and CO-core mass M_{CO} (Fig. 1). Notice how the most massive stars ($M \geq 40\,M_\odot$) in the high metallicity sets end up with similar, low final masses ($4 - 6\,M_\odot$). These stars go through a WR stage, where mass loss is efficient and strongly mass-dependent ($\dot{M} \propto M^{2.5}$ [15]): their mass decreases rapidly while $\dot{M}$ also decreases correspondingly, until they all reach very similar final masses. The switch to the WR stage at high masses produces a peak in M_{fin} and M_{CO}, which is less and less prominent, and corresponds to lower and lower initial masses, the higher the metallicity (Fig. 1). For the lowest Z, the peak mass falls in the range of very massive stars, where this behaviour is qualitatively extended (Sect. 3).

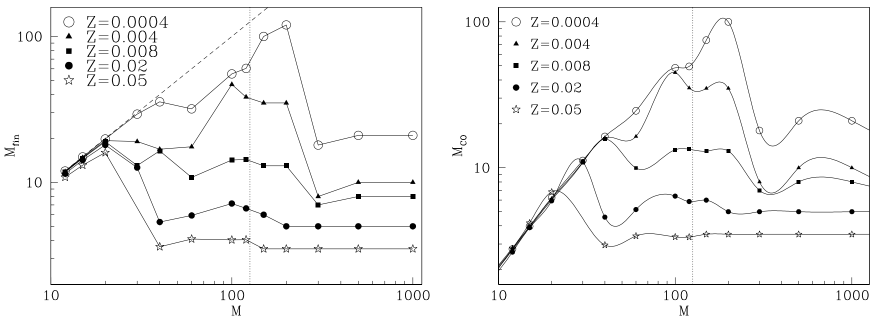

Fig. 1. *Left panel*: Final mass vs. initial stellar mass for five metallicities. The dashed line corresponds to constant mass evolution. The vertical dotted line separates massive stars with detailed stellar tracks (Sect. 2) from VMOs (qualitative calculations, Sect. 3). *Right panel*: Core mass vs. initial mass.

Basing on the Padova tracks [2,7,8] PCB98 calculated stellar yields of massive stars ($6 - 120\,M_\odot$) with mass loss for 5 sets of different metallicity, from $Z = 0.0004$ to $Z = 0.05$. The contribution to stellar yields from hydrostatic stages beyond He-burning and from explosive nucleosynthesis of *iron-core collapse* SN was estimated by matching our stellar pre-SN models with the SN yields by [26], on the base of the respective CO-core mass M_{CO}.

At the high mass end, *pair creation* (PC) SNæ are expected. Following [25], depending on the detailed mass the outome may be: partial explosion with ejection of some layers and the rest falling into a black hole ($M_{He} = 35 - 60\,M_\odot$), total thermonuclear explosion ($M_{He} = 60 - 110\,M_\odot$), complete collapse into a black hole ($M_{He} > 110\,M_\odot$); see also [10]. In our stellar models, mass loss inhibits the growth of so large cores, and PC SNæ are confined to the most massive stars in the lowest metallicity range ($M \geq 100\,M_\odot$ and $Z \leq 0.004$). The adopted SN yields for these PC cases are from [25].

The fractionary stellar yields of massive (and very massive, see Sect. 3) stars are shown in Fig. 2. At low metallicities, remnant masses can be very large due to low mass-loss rates: massive cores are built, leaving large remnants; and when most of the core mass falls into a black hole, little oxygen is released. For the largest masses ($M \geq 100\,M_\odot$), PC SNæ occur and the oxygen yields increase again, while remnant masses decrease.

For metallicities $Z \geq 0.008$ the effects of mass loss become apparent: for $M \geq 30\,M_\odot$, remnants are much smaller than in the low-Z sets, while helium and carbon yields increase because of the contribution of the wind.

For heavy elements (Si, S, Ca, Fe) the bulk of contribution generally comes from stars in the range $10 - 30\,M_\odot$.

3 Yields from Very Massive Stars ($M = 120-1000\,M_\odot$)

A primeval Population III of very massive objects (VMOs) was invoked in past years as a possible solution for the G-dwarf problem and for the non-zero metallicity of Population II stars, to form black holes which could account for Dark Matter and AGNs, to explain the reionization of the Universe, to produce primordial helium; for a review see [5]. Various stellar models for VMOs were therefore developed in the '80s [1,6,22,24,11,12].

VMOs might have formed more easily at the low metallicity of the early epochs, when the Initial Mass Function (IMF) was probably more top–heavy; e.g. [3–5]. But the interest for VMOs is not limited to extremely low-Z environments: the Pistol star with $M = 200 - 250\,M_\odot$ has been discovered in the Galactic Centre, where $Z \geq Z_\odot$ [9]; and other such objects are known within the Local Group [13]. Therefore, for any Z it is of interest to extend the grid of stellar yields beyond $M = 120\,M_\odot$, which we did in qualitative terms (PCB98).

Basing on the above mentioned papers on VMOs and on considerations of continuity with our stellar tracks for massive stars, we expect the structure and evolution of VMOs to be as follows. The H–burning lifetime of VMOs is $2 - 3\,Myr$, and H–burning takes place in the inner 50% of their initial mass. During H–burning VMOs undergo pulsational instability with violent mass loss, maybe as high as $10^{-3}\,M_\odot/yr$, independent on Z. Their mass therefore falls rapidly (in $10^5 - 10^6\,yrs$) below $120\,M_\odot$; from then on, they will end the phase of paroxysmal mass loss, enter the normal regime of radiation pressure driven wind and follow roughly the fate of a star of $100 - 120\,M_\odot$ for the corresponding Z. At very high masses, the (large!) H–burning core may be at some point revealed on the surface: the star then becomes a WR of very large mass and thus very large $\dot{M}$ (see Sect. 2), and decreases to a rather small final mass (Fig. 1). The core mass M_{CO} eventually drives the final SN explosion, as assumed for massive stars. In most cases the outcome is an iron–core collapse SN; only for very low Z a few PC SNæ are found.

This gross scenario gives us an analytical estimate of the yields of VMOs; for details see PCB98. The grid of stellar yields can thus be extended up to $1000\,M_\odot$ for the 5 metallicities; the results are shown in Fig. 2. For the lowest metallicity, $Z = 0.0004$, stars with $150 - 200\,M_\odot$ enter the regime of PC SNæ with complete thermonuclear disruption ($M_{CO} = 60 - 110\,M_\odot$) and large release of oxygen and heavy elements. If the IMF at low metallicities is skewed toward very high masses, these objects might contribute substantially to the very early chemical enrichment of galaxies (as pointed out also by [16]). At even larger masses, mass loss during the large WR stage reduces the final stellar and core mass to low values, so that the ejecta mainly consist of helium lost through the wind, with little production of metals.

This latter behaviour holds for all VMOs at higher Z, due to stronger mass loss in the radiation pressure wind phase (after they fall below $120\,M_\odot$).

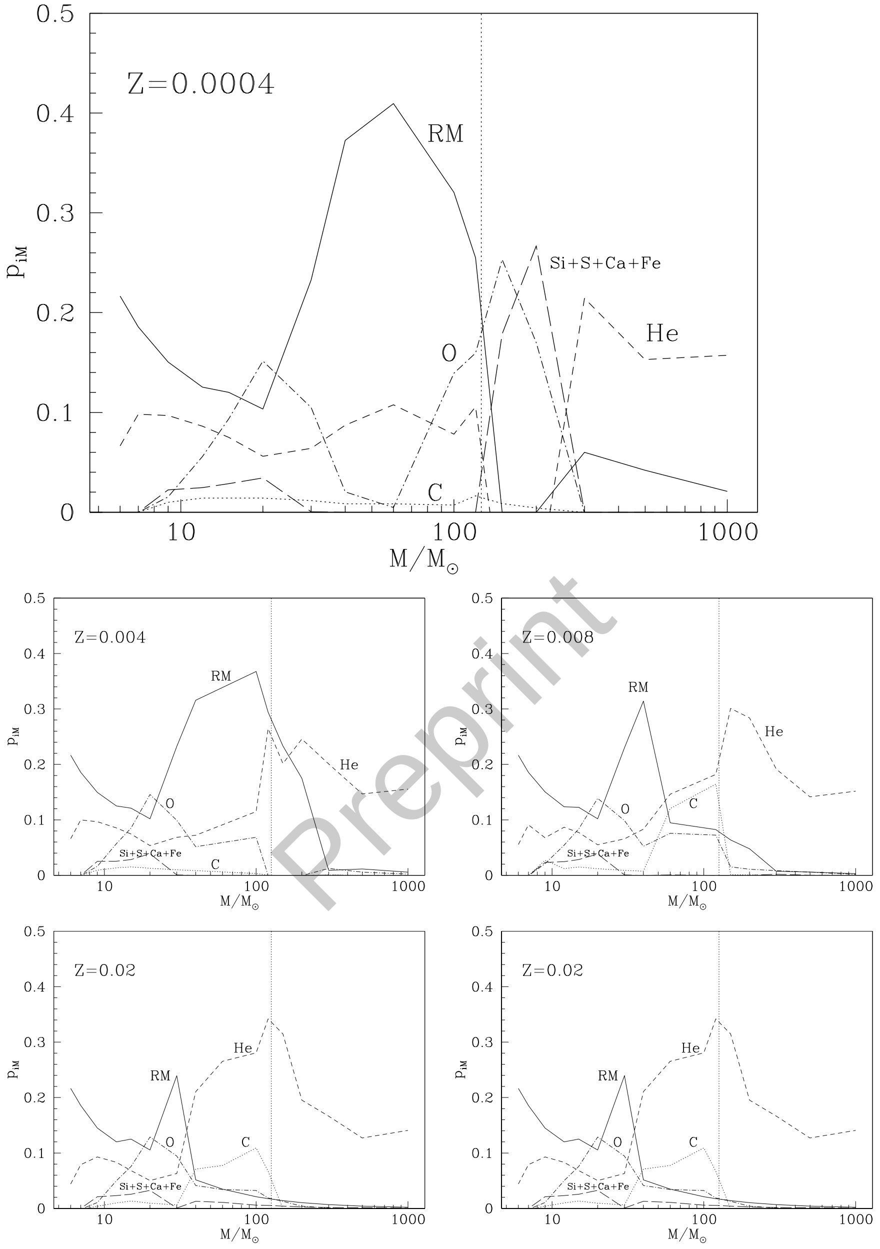

Fig. 2. Fractional remnant mass RM$=M_r/M$ and fractional stellar yields of a few elements for massive stars and VMOs of different metallicities. Solid line: RM; dashed line: helium yields; dotted line: carbon yields; dash-dotted line: oxygen yields; long-dashed line: heavy elements yields. The vertical dotted line separates massive stars with detailed stellar tracks (Sect. 2) from VMOs (qualitative calculations, Sect. 3).

Of course, the gross behaviour of VMOs is expected to depend on the efficiency of mass loss, which is basically unknown for the regime of pulsational instability typical of VMOs, and for very low Z in general [5]. What if the assumed mass loss rate in the violent phase is decreased, say, from 10^{-3} to $10^{-4}\,M_\odot/yr$? In most cases, such a mass loss rate is still fast enough to reduce the stellar mass below $120\,M_\odot$ in a short time, and then the overall evolution will remain substantially the same. Only for VMOs of $500-1000\,M_\odot$ the scenario will change: losing only $200-300\,M_\odot$ during their lifetime, they never become WR stars and result in a final core mass of ~ 250 and $500\,M_\odot$ respectively, ending up in a black hole collapse.

Calculations on stellar evolution and yields down to Z=0 are under way [19].

Acknlowledgements I acknowledge financial support from MPA during this conference. This study is financed by the Italian MURST, contract n. 9802192401.

References

1. Bond J.R., Arnett D.W., Carr B.J., 1984, ApJ 280, 825
2. Bressan A., Fagotto F., Bertelli G., Chiosi C., 1993, A&AS 100, 647
3. Bromm V., Coppi P.S., Larson R.B., this conference
4. Bromm V., Coppi P.S., Larson R.B., ApJL in press *(astro-ph 9910224)*
5. Chiosi C., 1999, this conference
6. El Eid M.F., Fricke K.J., Ober W.W., 1983, A&A 119, 54
7. Fagotto F., Bressan A., Bertelli G., Chiosi C., 1994, A&AS 104, 365
8. Fagotto F., Bressan A., Bertelli G., Chiosi C., 1994, A&AS 105, 29
9. Figer D.F., Najarro F., Morris M., McLean I.S., Geballe T., Ghez A.M., Langer N., 1998, ApJ 506, 384
10. Heger A., 1999, this conference
11. Klapp J., 1983, Ap&SS 93, 313
12. Klapp J., 1984, Ap&SS 106, 215
13. Kudritzki R.P., 1997, in *Stellar astrophysics for the Local Group*, A. Aparicio, A. Herrero, F. Sanchez (eds.), Cambridge University Press, p. 213
14. Kudritzki R.P., Pauldrach A., Puls J., Abbott D.C., 1989, A&A 219, 205
15. Langer N., 1989, A&A 220, 135
16. Langer N., Woosley S.E., 1996, ASP Conf. Ser. 98, 220
17. Marigo P., Bressan A., Chiosi C., 1996, A&A 313, 545
18. Marigo P., Bressan A., Chiosi C., 1998, A&A 331, 564
19. Marigo P., Chiosi C., Girardi L., Sarrubbi T., 1999, this conference
20. Nomoto K., 1984, ApJ 277, 791
21. Nomoto K., 1987, ApJ 322, 206
22. Ober W.W., El Eid M.F., Fricke K.J., 1983, A&A 119, 61
23. Portinari L., Chiosi C., Bressan A., 1998, A&A 334, 505 (PCB98)
24. Woosley S.E., Weaver T.A., 1982, in *Supernovae: a survey of current research*, M.J. Rees and R.J. Stoneham (eds.), p. 79
25. Woosley S.E., 1986, in *Nucleosynthesis and chemical evolution*, 16^{th} Saas-Fee Course, p. 1
26. Woosley S.E., Weaver T.A., 1995, ApJS 101, 181

Neutron Capture Nucleosynthesis in Early Galactic Environments

James W. Truran[1], John J. Cowan[2], Christopher Sneden[3],
Debra L. Burris[2], and Catherine A. Pilachowski[4]

[1] Department of Astronomy and Astrophysics, Enrico Fermi Institute, University of Chicago, Chicago, IL, 60637
[2] Department of Physics and Astronomy, University of Oklahoma, Norman, OK, 73019
[3] Department of Astronomy and Macdonald Observatory, University of Texas, Austin, TX, 78712
[4] Kitt Peak National Observatory, NOAO, Tucson, AZ, 85726

Abstract. The heavy elements formed by neutron capture processes have an interesting history from which we can extract useful clues to and constraints upon the star formation and nucleosynthesis history of Galactic matter. Of particular interest are the heavy element compositions of extremely metal-deficient stars. At metallicities [Fe/H] $\leq$ -2.5, the elements in the mass region past barium (A $\approx$ 140) have been found to be pure r-process products. The identification of an environment provided by massive stars and associated Type II supernovae as an r-process site seems compelling. Increasing levels of s-process enrichment with increasing metallicity reflect the delayed contributions from the intermediate mass stars that provide the site for s-process nucleosynthesis during the AGB phase of their evolution. We review recent observational studies of heavy element abundances in low metallicity stars and explore some implications of these results for nucleosynthesis and early Galactic chemical evolution.

1 Introduction

Element abundance patterns in very metal-poor halo field stars and globular cluster stars play a crucial role in guiding and constraining theoretical models of nucleosynthesis [1,2]. Nowhere is this more true than for the case of the neutron-capture processes that are understood to be responsible for the synthesis of the bulk of the heavy elements in the mass region A $\gtrsim$ 60: the s-process and the r-process. Nucleosynthesis theory identifies quite different astrophysical sites for these two distinct processes. r-Process nuclei are *primary* nucleosynthesis products, formed in an environment associated with the evolution of massive stars (M $\gtrsim$ 10 $M_\odot$) to supernova explosions of Type II and the formation of neutron star remnants. s-Process nuclei are understood to be products of neutron captures on preexisting silicon-iron "seed" nuclei, occurring both in the helium burning cores of massive stars and particularly in the thermally pulsing helium shells of asymptotic giant branch (AGB) stars. In this picture, the first heavy (A $\gtrsim$ 60) elements introduced into the interstellar gas component of our Galaxy are expected to have been r-process nuclei formed in association with massive stars, on timescales $\tau_* < 10^8$ years [3].

That the general features of this simple model are correct is confirmed by the finding that r-process contributions dominate the heavy element abundances in extremely metal-poor halo stars. This issue is discussed in the next section. The implications of trends in the heavy element abundances as a function of [Fe/H] for the early star formation history of the Galaxy and Galactic chemical evolution are then examined.

2 r-Process Nucleosynthesis at Early Galactic Epochs

Significant progress in our understanding of the site of operation of r-process nucleosynthesis has followed from studies of the abundances of elements from barium through bismuth in metal-poor stars. The heavy element abundance patterns for the two stars CS 22892-052 [4] and HD 115444 [5,6] are compared with the solar system r-process abundance distribution in Figure 1.

The robustness of the r-process mechanism operating in the early Galaxy is reflected in the close agreement of these two stellar patterns (which represent the nucleosynthesis products of, at most, a relatively small number of earlier stars) with the solar system r-process pattern (which represents the accumulated production of r-process elements over billions of years of Galactic evolution). Note the extraordinary agreement with solar system r-process abundances over this range, for the eighteen elements for which abundance data is available. These data provide conclusive evidence for the operation of an r-process at the earliest Galactic epochs that synthesizes the heavy r-process nuclei (barium and beyond), including the long lived isotope ^{232}Th critical to dating. The identification with massive stars seems compelling, although it is possible that neutron star mergers rather than a supernova environment may be responsible.

A critical question here involves the abundances of r-process nuclei less massive than barium. The incompatibility of the abundances of the short lived radioactivities ^{107}Pd and ^{129}I in early solar system matter with a model of "uniform production" that works well, for both the actinide chronometers and the short lived isotope ^{182}Hf, led Wasserburg *et al.* [7] to argue for a second r-process component for the mass region below A $\approx$ 140. Studies of abundances in the mass range from the iron region through barium in low metallicity stars can be expected to provide significant input in this regard.

3 Constraints on r-Process Nucleosynthesis Sites

r-Process abundances in low metal stars also provide an important further clue to the nature of the r-process site. The ratio [r-process/Fe] is displayed as a function of [Fe/H] for a large sample of halo and disk stars [8] in Figure 2.

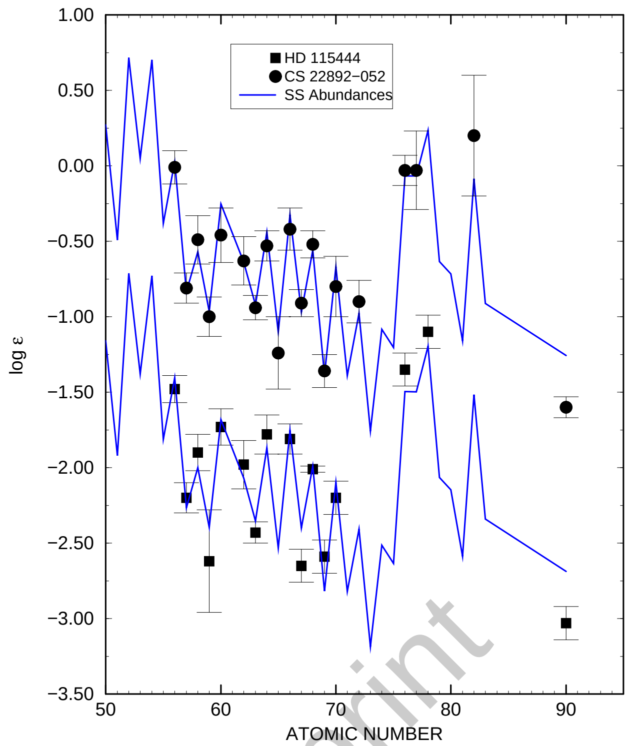

Fig. 1. The heavy element abundance patterns for the two stars CS 22892-052 and HD 115444 are compared with the scaled solar system r-process abundance distribution (solid lines) [4–6]

The increasing level of scatter of this ratio with decreasing metallicity, most pronounced at values below [Fe/H] ∼ -2.0, makes clear that not all early stars are sites for the formation of both r-process nuclei and iron. In the absence of other sources for either iron peak nuclei or r-process nuclei in the early Galaxy, this scatter is consistent with the view that the r-process operates in only a small fraction (∼ 1/10th to 1/50th) of the massive stars that produce iron [9]. Note again that this refers *only* to the nucleosynthesis sites for the heavy r-process isotopes (barium and beyond), and not to any possible site for the production of the lighter r-process nuclei.

4 Chemical Evolution of r-Process and s-Process Abundances

Studies of the time history of the heavy (neutron capture) elements have historically been driven by observations. Early trends in the s-process element patterns as a function of [Fe/H] by Pagel [16] motivated theoretical

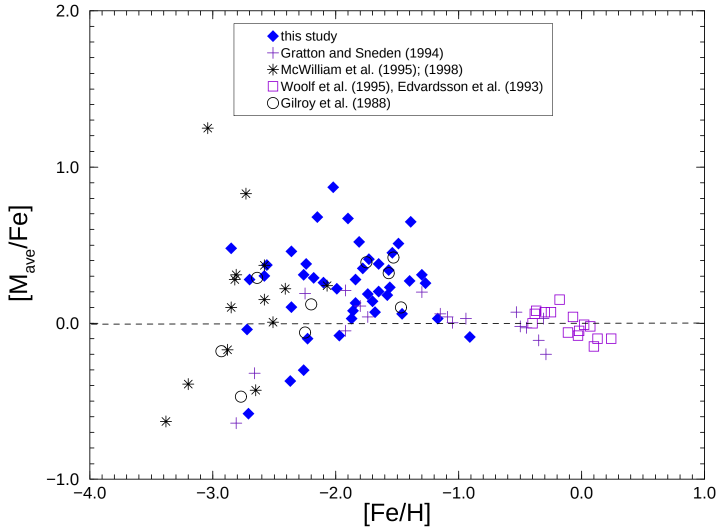

Fig. 2. The ratio [r-process/Fe] is displayed as a function of [Fe/H] for a large sample of halo and disk stars [8]. Data are from [10–15]

consideration of such trends in the context of models of Galactic chemical evolution [17]. The great increase in abundance data for metal-poor stars over the past decade has similarly motivated considerable theoretical activity [18–20]. The ratio [Ba/Eu], which reflects the ratio of s-process to r-process elemental abundances, is displayed in Figure 3 as a function of [Fe/H], for a large sample of halo and disk stars [8]. Note that at the lowest metallicities the [Ba/Eu] ratio is consistent with that for pure r-process matter. The subsequent increase in the [Ba/Eu] ratio with increasing [Fe/H] (i.e. increasing time) to its solar value reflects the input to the interstellar medium of the products of s-process nucleosynthesis in intermediate mass stars of lifetimes greater than those of the massive star sites of r-process nucleosynthesis.

5 Discussion and Conclusions

The observations reviewed in the previous sections provide great guidance to theoretical studies of r-process nucleosynthesis. They suggest: (1) the site of formation of the heavy r-process elements ($A > 130$-140) must be associated with events that occur very early in the history of our Galaxy; (2) the r-process mechanism that operates in this environment must be robust, in the sense that even a single nucleosynthesis event seems capable of producing an r-process abundance distribution closely in agreement with that found in solar system matter; (3) this early r-process component can only operate in a relatively small fraction (of order 1/10th to 1/50th) of the massive stars that produce iron; (4) a second r-process site/mechanism is required to account

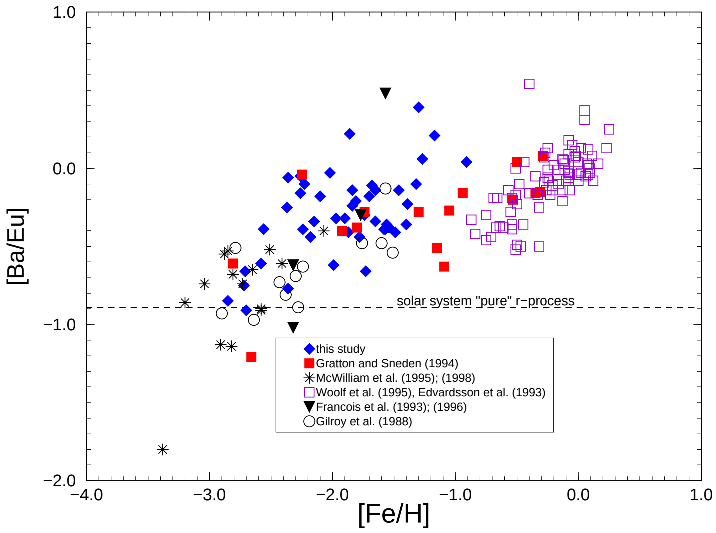

Fig. 3. The ratio [Ba/Eu], which reflects the ratio of s-process to r-process elemental abundances, is displayed as a function of [Fe/H] for a large sample of halo and disk stars [8]

for both the levels of ^{107}Pd and and ^{129}I in primordial solar system matter and the r-process nuclei in the mass range $80 < A < 130$-140 in solar matter; and (5) s-process contributions to barium and heavier nuclei are introduced into the ISM at later epochs than are r-process contributions.

References

1. Wheeler, J. C., Sneden, C., Truran, J. W. (1989) ARA&A **27**, 279-349.
2. McWilliam, A. (1995) ARA&A, **35**, 503-541.
3. Truran, J.W. (1981) A&A **97**, 391-393.
4. Sneden, C., McWilliam, A., Preston, G.W., Cowan, J.J., Burris, D.L., Armosky, B.J. (1996) ApJ **467**, 819-832.
5. Westin, J., Sneden, C., Gustafsson, B., Cowan, J.J. (1999) ApJ, in press.
6. Sneden, C., Cowan, J.J., Burris, D.L., Truran, J.W. (1998) ApJ **496**, 235-245.
7. Wasserburg, G.J., Busso, M., Gallino, R. (1996) ApJ **466**, L109-L113.
8. Burris, D.L., Pilachowski, C.A., Armandroff, T., Sneden, C., Cowan, J.J., Roe, H. (1999) ApJ, in press.
9. Truran, J.W., Fields, B.D., Cowan, J.J. (1999) preprint.
10. Edvardsson, B., Andersen, J., Gustafsson, B., Lambert, D. L., Nissen, P. E., Tomkin.J. (1993) A&A, **275**, 101.
11. Gilroy, K. K., Sneden, C., Pilachowski, C. A., Cowan, J. J. (1988) ApJ, **327**, 298.
12. Gratton, R., Sneden, C. (1994) A&A, **287**, 927.
13. McWilliam, A. (1998) AJ, **115**, 1640.

14. McWilliam, A., Preston, G. W., Sneden, C., Shectman, S. (1995) AJ, **109**, 2736.
15. Woolf, V. M., Tomkin, J., Lambert D. L. (1995) ApJ, **453**, 660.
16. Pagel, B.E.J. (1968) in *Origin and Distribution of the Elements*, ed. L.H. Ahrens (London, Pergamon Press), 195-204.
17. Truran, J.W., Cameron, A.G.W. (1971) A&SS **14**, 179-222.
18. Mathews, G.J., Bazan, G., Cowan, J.J. (1992) ApJ **391**, 719-731.
19. Ishimaru, Y., Wanajo, S. (1999) ApJ **511**, L33-L36.
20. Travaglio, C., Galli, D., Gallino, R., Busso, M., Ferrini, F., Straniero, O. (1999) ApJ **521**, 691-702.

Stellar and Nuclear-Physics Constraints on Two *r*-Process Components in the Early Galaxy

Bernd Pfeiffer[1], Karl-Ludwig Kratz[1], Ulrich Ott[2], Friedrich-Karl Thielemann[3], and Chris Sneden[4]

[1] Institut für Kernchemie, Universität Mainz, Mainz, Germany
[2] MPI für Chemie, Department for Cosmochemistry, Mainz, Germany
[3] Departement für Physik und Astronomie, Universität Basel, Basel, Switzerland
[4] Department of Astronomy, University of Texas, Austin, USA

Abstract. Stellar and nuclear-physics constraints on two r-process components are discussed in a site-independent approach to fit the $N_{r,\odot}$ pattern.

Recent astrophysical results indicate to the existence of (at least) two types of the rapid neutron capture process (r-process). The evidence is based on a variety of observations in different fields:
(a) the study of extinct radionuclides present in the early Solar System;
(b) isotope abundance anomalies observed in grains of circumstellar origin found in primitive meteorites;
(c) the continuing investigation of the elemental abundances in very metal-poor old halo stars, in particular the recent results of "low-Z" neutron-capture elements in CS22892-052.

Prominent among the radionuclides present in the early Solar System are the r-process products ^{129}I and ^{182}Hf, the former presence of which shows up as isotope abundance anomalies of their daughter nuclides. Wasserburg et al. [1] have argued that the observed abundance of ^{182}Hf (and the actinides) are consistent with uniform production throughout the history of the Galaxy up to about 10 Ma before formation of the Solar System, while that of ^{129}I is not. As a consequence, Wasserburg et al. [1] have argued for the existence of diverse supernova sources for the r-process.

Supporting evidence for complexity in the r-process comes also from the abundance pattern of trace tellurium in presolar diamond grains [2,3].

The strongest – because less model-dependent – indication for more than one type of r-process, however, comes from the observation of heavy neutron-capture element abundances [4–6] in very metal-poor Halo stars, especially in CS 22892-052: abundances of elements in the Pt peak and down to Ba (Z=56) are in remarkable agreement with the solar r-process pattern, while there seem to be lower abundances of "low-Z" neutron-capture elements.

An intersting feature of the abundances of the medium-heavy elements between Z=38 and 48 is their pronounced odd-even-Z staggering, which reflects nuclear-structure properties of the progenitor isotopes involved. All odd-Z elements from $_{39}$Y to $_{47}$Ag are clearly under-abundant compared to the (metallicity-scaled) solar pattern, whereas the even-Z elements ($_{38}$Sr – $_{48}$Cd) are closer to solar (see Fig. 1). Taking advantage of our site-independent approach to fit the $N_{r,\odot}$ pattern, we now can test under which stellar conditions the possible two r-processes have to run.

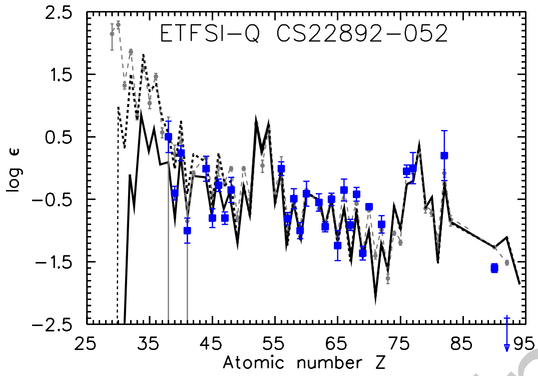

Fig. 1: Comparison between observed (squares) and calculated elemental r-abundances from CS 22892-052. The metallicity-scaled $N_{r,\odot}$ distribution is shown as dashed curve with filled circles, and the calculated one is superimposed as black curve. The abundance distribution for Z≥40 would be originating from the *main* r-process. The "residuals", $N_{r,\odot}$-$N_{r,main}$, would correspond to the second, *weak* r-process component (dotted curve).

When assuming that the abundances are a living record of the first (few) generation(s) of Galactic nucleosynthesis [7], the observed pattern beyond Z≃40 up to $_{92}$Th should most likely be produced by only one (or a few) r-process event(s) and site. This scenario (the *main* r-process) then produces the "low-Z" elements under-abundant compared to solar, and reaches the full solar values presumably around Z=50. Both, the general trend as well as the detailed structure of the "low-Z" abundances (40≤Z≤48) are nicely reproduced in our fit with the ETFSI-Q masses. At the same time, the good overall reproduction of the "high-Z" elements (beyond Z=56) is maintained [8]. Consequently, the abundance *"residuals"* at low Z will require a separate *weak* r-process component ($N_{r,weak}$=$N_{r,\odot}$–$N_{r,main}$) of yet unknown stellar site.

References

1. G.J. Wasserburg et., Ap. J. 466 (1996) L109
2. U. Ott, Ap. J. 463 (1996) 344
3. S. Richter et al., Nature 391 (1998) 261
4. C. Sneden et al., Ap. J. 496 (1998) 235
5. J.J. Cowan et al., 194^{th} AAS Meeting, Chicago (1999) #67.04
6. J. Westin et al., submitted to Ap. J. (1999)
7. J.J. Cowan et al., Ap. J. 521 (1999) 194
8. K.-L. Kratz et al., J. Radioanal. Nucl. Chem. 243 (2000), in print

Evolution and Nucleosynthesis of Metal-Free Massive Stars ⋆

Hideyuki Umeda, Ken'ichi Nomoto, and Takayoshi Nakamura

Department of Astronomy, and Research Center for the Early Universe, School of Science, University of Tokyo,
Bunkyo-ku, Tokyo 113-0033, Japan
E-mail: umeda@astron.s.u-tokyo.ac.jp; nomoto@astron.s.u-tokyo.ac.jp; nakamura@astron.s.u-tokyo.ac.jp

Abstract. We calculate presupernova evolutions and supernova explosions of massive stars ($M = 13 - 25M_{\odot}$) for various metallicities. We find the following characteristic abundance patterns of nucleosynthesis in the metal-free (Pop III) stars. (1) The α-nuclei (from C to Zn) are more efficiently produced than other isotopes, and the abundance pattern of α-nuclei can be similar to the solar abundance. In particular, near solar ratios of alpha elements/Fe might be a signature of Pop III which could produce a large amount of Fe. (2) The abundance ratios of odd Z to even Z elements such as Na/Mg and Al/Mg become smaller for lower metallicity. However, these ratios almost saturate below $Z \lesssim 10^{-5}$, and [Na, Al/Mg] ~ -1 for Pop III and low metal Pop II nucleosynthesis. This result is consistent with abundance pattern of metal poor stars, in which these ratios also saturate around -1. We suggest that these stars with the lowest [Na/Mg] or [Al/Mg] may contain the abundance pattern of Pop III nucleosynthesis. (3) Metal poor stars show interesting trends in the ratios of [Cr, Mn, Co/Fe]. We discuss that these trends are not explained by the differences in metallicity, but by the relative thickness between the complete and the incomplete Si burning layers. Large [Co/Fe] and small [Cr, Mn/Fe] values found in the observations are explained if mass cut is deep or if matter is ejected from complete Si burning layer in a form of a jet or bullets. (4) We also find that primary ^{14}N production occurs in the massive Pop III stars, because these stars have radiative H-rich envelopes so that the convective layer in the He-shell burning region can reach the H-rich region.

1 Introduction

Very metal poor stars provide important clues to investigate early cosmic and galactic chemical evolution because their abundance patterns would tell us what kind of stars (including the First Stars) contribute to form those patterns. We might be able to identify the signature of the First Stars and thus can learn how the universe and galaxies evolved chemically in its early phase. Such identification would be possible in the abundance pattern of an individual metal-poor star, because in early phase of the galaxy evolution the

⋆ This paper combines the review by K. Nomoto and the contributed talk by H. Umeda ejecta of each supernova may not have enough time to be uniformly mixed in the galaxy [4,34,36].

One example is the interesting trends of [Cr/Fe], [Mn/Fe] and [Co/Fe] with [Fe/H] [23–25,33]. Since the published SNe II yields [46] (hereafter WW95) and [39,13,40] are not consistent with these trends, one might suspect that these trends would be a signature of Pop III star yields.

Here we define the First Stars as metal-free (Pop III) stars. We evolve and explode massive metal-free stars as well as other metallicity stars including the metallicity dependent mass loss. We calculate nucleosynthesis to see what are the indications of the ejecta of the first stars. Previously, WW95 [46], Arnett [2], and Limongi et al. (LCS) [22] calculated nucleosynthesis of SNe II using for various metallicities down to metal-free, but these studies did not include mass loss and did not examine the dependence on the convective mixing.

In addition to the metallicity effects, we study the dependence on the explosion energy. This is because some recent supernovae have been recognized to be hyper-energetic (hypernovae) being more than 10^{52} ergs. The examples include SN 1998bw [11,17,45], SN 1997ef [18], and SN 1997cy [12,41]. These hypernovae are suggested to originate from quite massive stars, so that their nucleosynthesis may significantly contribute to the early cosmic and galactic chemical evolution.

Our results are also sensitive to the efficiency of convective mixing. Here we report mostly the case of low efficiency, and more complete results will be presented in a forthcoming paper.

2 Code and Method

We have developed a stellar evolution code which is based on Henyey type stellar evolution codes by Nomoto & Hashimoto (NH88) [27], [35], and [42]. We start calculations from the zero-age main-sequence through core collapse including metallicity dependent mass loss [8,20]. For example, the star of initially 25 $M_\odot$ with solar metallicity decreases its mass down to 21.5 $M_\odot$ before the explosion.

We adopt the OPAL opacity as a function of metallicity, $X(\mathrm{H})$, $X(\mathrm{C})$ and $X(\mathrm{O})$ [16]. This code runs a nuclear reaction network by Hix & Thielemann [15] for the calculation of nuclear energy generation and nucleosynthesis. For nucleosynthesis of H and He burning, 51 isotopes up to Si are included, and after He burning 240 isotopes up to Ge are included.

Schwartzshild criterion is adopted for convective stability criterion and diffusive convective mixing by Spruit [37] is adopted. In this work, a case for relatively slow mixing, $f_k = 0.05$ [35], is investigated. At the end of core helium burning, the central C/O ratio is largely influenced by the uncertain $^{12}\mathrm{C}(\alpha,\gamma)^{16}\mathrm{O}$ reaction rate [10]. The C/O ratio affects the abundances of Ne, Mg and Al, and also the Fe core mass.

In this work, the $^{12}C(\alpha,\gamma)^{16}O$ reaction rate is chosen to be 1.4 times the value given in Caughlan & Fowler (CF88) [6]. With this choice for the 25 $M_\odot$ model of Z=0.02, the central C/O ratio is 0.2 at the end of core helium burning, which is close to the NH88 models.

Using the presupernova models, we carry out 1D hydrodynamical simulations of SN II explosions with a PPM code which uses a small nuclear reaction network. Then the explosive nucleosynthesis is calculated as a post-processing using a larger reaction network of 300 isotopes up to Br as described in [39].

3 Presupernova Stellar Evolution

Figure 1 shows the H-R diagram of the 25 $M_\odot$ star with metallicity of $Z = 0, 0.001$, and 0.02. As shown in this figure, the star is more luminous for lower metallicity owing to the smaller opacity. The evolution in the H-R diagram of zero metal (Pop III) stars with 13 $M_\odot \lesssim M \lesssim 25$ $M_\odot$ are quite different from Pop I and II stars, because they do not evolve to red-giants before core collapse (e.g. [7]).

Figures 2 shows abundance distribution of presupernova stars. The H-rich envelope for $Z = 0.02$ is convective, while the H-rich envelope for $Z = 0$ is radiative. For $Z = 0$, only a small amount of CNO elements are produced in the H-rich layer, so that hydrogen burning is too weak to drive the expansion toward a red-giant.

For Pop I and II stars, lower metallicity leads to the formation of a more massive core because of the larger luminosity. One might expect Pop III stars have the largest cores because of this effect; however, the He core size is smaller than Pop II because of weak H-shell burning. In our model these two effects cancel out and the masses of the He and C-O cores are almost the same between $Z = 0$ and $Z = 0.02$ models (Fig. 2).

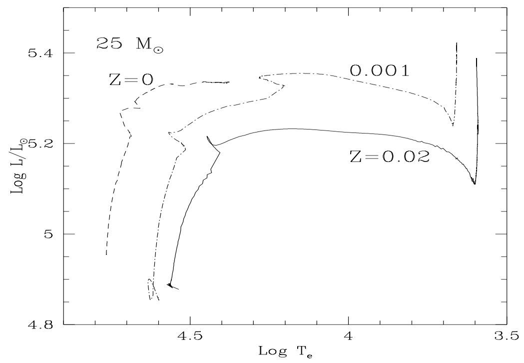

Fig. 1. The H-R diagram of the 25 $M_\odot$ stars with various metallicities.

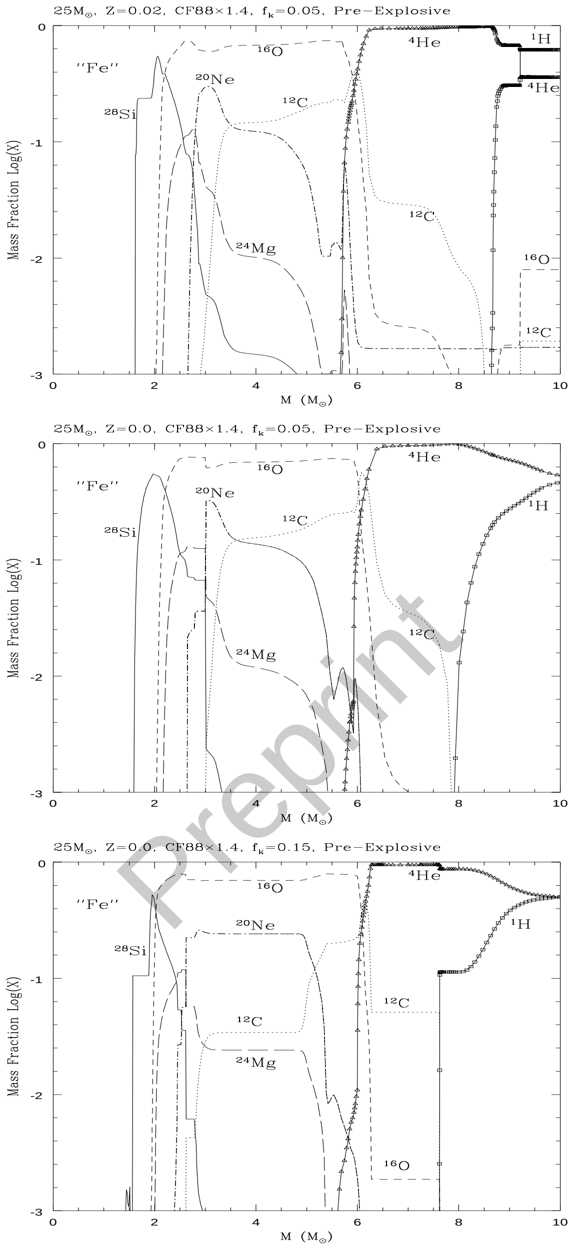

Fig. 2. Presupernova abundance distribution. The top and the middle panels show the cases with $Z = 0.02$ and $Z = 0$, respectively. The bottom one is the $Z = 0$ case with a more efficient convective mixing ($f_k = 0.15$) than others.

3.1 Fe Core Mass

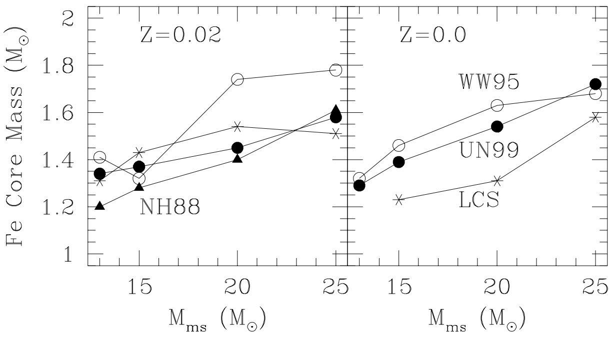

Fig. 3. The Fe core mass as compared with other works.

The Fe core mass is mostly determined by the He (or C-O) core mass, and the C/O ratio after the central helium burning. In general, a larger He (or C-O) core mass leads to a larger Fe core mass. The larger C/O ratio leads to weaker central O-burning and a smaller Fe core mass.

A more massive or lower (but non-zero) metallicity star tends to have a larger luminosity and hence a larger He (and C-O) core mass. Also the C/O ratio is smaller for a larger core mass. Therefore, the Fe core mass tends to be larger for a larger stellar mass and smaller metallicity, although its size also depends on the behavior of convection and these relations do not hold always.

Figure 3 summarizes the masses of the presupernova Fe cores compared with other works. We should note that all other works did not include mass loss.

Although opacity is smaller, Pop III stars have smaller core masses than Pop II stars for the same main-sequence mass because H-burning via the CNO cycle is weaker. Since the Pop II stars have larger cores than Pop I, the core masses of Pop III are closer to Pop I rather than Pop II. Note that this relation does not always hold since the core mass depends on the behavior of convection which is rather chaotic [5].

3.2 Y_e Distribution

The electron mole number Y_e is important for the explosive nucleosynthesis. In Figure 4 we show the distribution of Y_e in the presupernova model. This shows that Y_e is larger for zero metal stars than solar metallicity stars, because of smaller ^{22}Ne which is produced from ^{14}N.

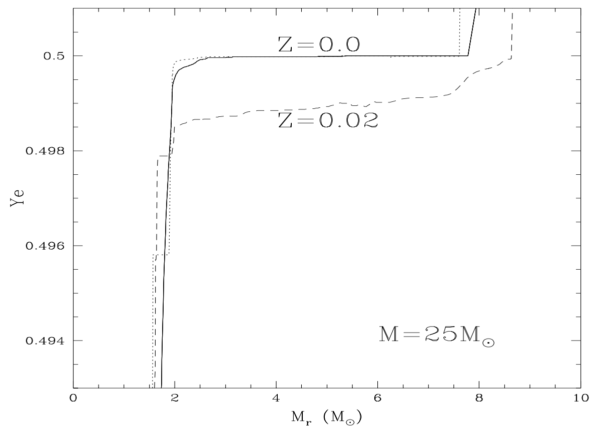

Fig. 4. Y_e distribution of the pre-explosive 25 $M_\odot$ stars for $Z = 0$ and 0.02. The solid and dotted lines corresponds to $f_k = 0.05$ and 0.15 models, respectively.

4 Explosive Nucleosynthesis

The general features of the explosive nucleosynthesis in SNe II are summarized as follows (e.g., [44,14,35,39]). The explosively produced elements depend mainly on the peak temperature attained through the passage of the shock. The region after the shock passage is radiation dominant, so that the peak temperature is approximately related to the stellar radius r and the deposited energy E^* as

$$T_9 = (E^*_{51})^{1/4}\ (r/3.16 \times 10^4\ \mathrm{km})^{-3/4}, \tag{1}$$

where E^*_{51} is the deposited energy in units of 10^{51} erg, T_9 is the peak temperature in 10^9 K. Therefore, assuming $E^*_{51} = 1$, explosive nuclear burning are classified into several cases according to T_9 (or r) at $T_9 = 5$ ($r = 3700$ km), $T_9 = 4$ ($r = 4980$ km), $T_9 = 3.3$ ($r = 6430$ km), and $T_9 = 2.1$ ($r = 11{,}800$ km). The relation between the presupernova radius r and the enclosed mass M_r depends on the progenitor's mass and metallicity (e.g., [28]).

4.1 Complete Silicon Burning and Neutron-Rich Species

For $T_9 > 5$, explosive silicon and oxygen burning leads to nuclear statistical equilibrium and produces mostly ^{56}Ni if $Y_\mathrm{e} > 0.49$, $T_9 < 8$, and $\rho < 10^8$ g cm^{-3}. Other iron peak elements are also produced owing to this high temperature but the final products depend on the time scale of the freezeout and initial distribution of Y_e.

For the inner region, α-rich freeze out occurs after complete silicon burning. Some ^{4}He remain even after the freezeout without recombining into the iron peak elements. In these regions, appreciable amount of radioactive nuclei, ^{56}Ni,^{57} Ni, and^{44}Ti, are produced. Also ^{56,57}Fe and ^{58,60,62}Ni are synthesized here. ^{60,62}Ni are originally produced as ^{60,62}Zn which decay as $^{60,62}\mathrm{Zn} \rightarrow ^{60,62}\mathrm{Cu} \rightarrow ^{60,62}\mathrm{Ni}$. These neutron-rich nuclei ($Y_{\mathrm{e}} = 0.484$ for ^{62}Zn and $Y_{\mathrm{e}} = 0.483$ for ^{58}Ni) are produced in the neutron-rich layers near the mass cut in SNe II as well as in Type Ia supernovae.

In smaller mass stars, a larger amount of neutron-rich elements ^{58}Ni, ^{60,62}Zn are produced near the mass cut. The mass cut is related to the amount of radioactive nuclei. The most important ones are ^{56}Ni and ^{57}Co ($^{57}\mathrm{Ni} \rightarrow ^{57}\mathrm{Co} \rightarrow ^{57}\mathrm{Fe}$) as actually observed in SN 1987A (e.g., [3,29] and the obtained ratio ^{56}Ni/^{57}Ni was used to infer the mass cut [20,21].

4.2 Incomplete Silicon Burning and Explosive Oxygen Burning

For $4 < T_9 < 5$, incomplete silicon burning and explosive oxygen burning produce mostly ^{28}Si,^{32}S,^{36}Ar and ^{40}Ca. Some ^{44}Ti and ^{56}Ni are also produced by incomplete silicon burning. Oxygen is burned up completely and ^{28}Si, ^{32}S and other α-particle nuclei are produced. The peak temperature is too low to produce iron peak elements.

For $3.3 < T_9 < 4.0$, explosive neon burning produces some amounts of ^{16}O,^{28}Si, and ^{32}S.

For $2.0 < T_9 < 3.3$, explosive carbon burning produces ^{20}Ne,^{24}Mg. However, the peak temperature is too low to change the initial abundances appreciably. For $T_9 < 2$, no significant explosive burning occurs. For the oxygen-rich layer with $2 < T_9 < 3$, where explosive neon and carbon burning take place, the p–process occurs via the photodisintegration of nuclei: (γ, p), (γ, n), (γ, α) (e.g., Rayet et al. [32]).

The inner part of the star where $T_9 > 2$ undergoes the explosive nucleosynthesis according to the above classification. The outer part, including most of the original oxygen-rich layer, is ejected without being processed by explosive nuclear burning. The ratio between the explosive and hydrostatic burning products is sensitive to the stellar mass.

5 Abundance Distribution

Figures 5–8 show the abundance distribution of some isotopes before and 10^3 sec after explosive nuclear burning for the 20 $M_\odot$ star with $Z = 0$ and 0.02. These figures show that $Z = 0$ and 0.02 models yield roughly the same amount of alpha nuclei which are produced during He and C-burnings such as ^{12}C, ^{16}O, ^{20}Ne, ^{24}Mg, and produced during explosive burning such as ^{40}Ca, ^{44}Ti, ^{52}Fe, ^{64}Ge. On the other hand, other elements produced during H, He and C-burnings such as ^{13}C, ^{14}N, ^{15}N, ^{23}Na, ^{27}Al, ^{31}P are much less abundant in the $Z = 0$ model compared with the $Z = 0.02$ model. This also can be seen in Figure 11.

As examples of these two types of species, we discuss the ejected masses of radioactive species ^{26}Al and ^{44}Ti (decays into ^{44}Ca), which are important for the Line Gamma-Ray astronomy. The ^{44}Ti mass is in general roughly independent of metallicity, but depends sensitively on the mass cut. In Figure 11, ^{44}Ti and all heavy elements with $A \geq 60$ appear to be much less abundant for $Z = 0$ than $Z = 0.02$. This is only because the mass cut is set to produce 0.07 $M_\odot$ ^{56}Ni for both cases despite the difference in the ^{56}Ni distribution; thus the abundances of those isotopes produced by complete Si burning relative to ^{56}Ni appear to be smaller for $Z = 0$ ($\sim 10^{-5}$ $M_\odot$) than $Z = 0.02$ by a factor of 2 - 4. We stress again that the ^{44}Ti mass is uncertain because it significantly depends on mass cut.

^{26}Al is produced in the H, He and C-burnings and the ejected mass is independent of mass cut, while its mass is smaller for smaller metallicity. For $Z = 0.02$, the ^{26}Al mass ranges from 1 $\times 10^{-5}$ $M_\odot$ to 8 $\times 10^{-5}$ $M_\odot$ for the 13 to 25 $M_\odot$ stars. For $Z = 0$, these masses range from 1 $\times 10^{-7}$ $M_\odot$ to 2 $\times 10^{-6}$ $M_\odot$.

6 Integrated Abundances Relative to the Solar Abundances

Figures 9-12 show the integrated abundances of stable isotopes in the ejecta relative to the solar values [1] for the stars of $M = 13 - 25$ $M_\odot$ and $Z = 0$ and 0.02. (Here we adopt the lower efficiency of mixing, $f_k = 0.05$.) Each yield is normalized to the solar ^{16}O value.

Figure 9 shows the yields from the solar metallicity stars. The explosion energy, i.e., the final kinetic energy, is assumed to be $E = 10^{51}$ erg and the mass cut is chosen to eject 0.07 $M_\odot$ ^{56}Ni. The abundance ratios are mostly consistent with the solar ratios from C to Ca, but show significant deviations from the solar ratios for heavier species. Further parameter study is necessary to see how the results depend on the metallicity, f_k, and the mass cut. The upper panel of Figure 13 shows that our result for $f_k = 0.05$ is roughly consistent with WW95, though our ^{12}C$(\alpha,\gamma)^{16}$O rate is smaller than WW95 by a factor of 1.2.

The results for the metal-free models are shown in Figure 10. A distinctive feature of the $Z = 0$ models compared with the $Z = 0.02$ models is that, alpha nuclei (from C to Zn) are much more abundant than others. In Figure 11 we show the yield ratios between $Z = 0$ and $Z = 0.02$. The most evident signature of the Pop III abundance pattern appears in the large isotopic ratios for the even Z elements (such as ^{13}C/^{12}C) and the deficiency of the odd Z elements such as ^{23}Na, ^{27}Al, and ^{31}P. We will come back to this point in Section 8. Comparison of our results with WW95 in the lower panel of Figure 13 shows that our model has smaller abundances of the even Z neutron-rich isotopes; this is probably because WW95 included neutrino irradiation effects which we do not.

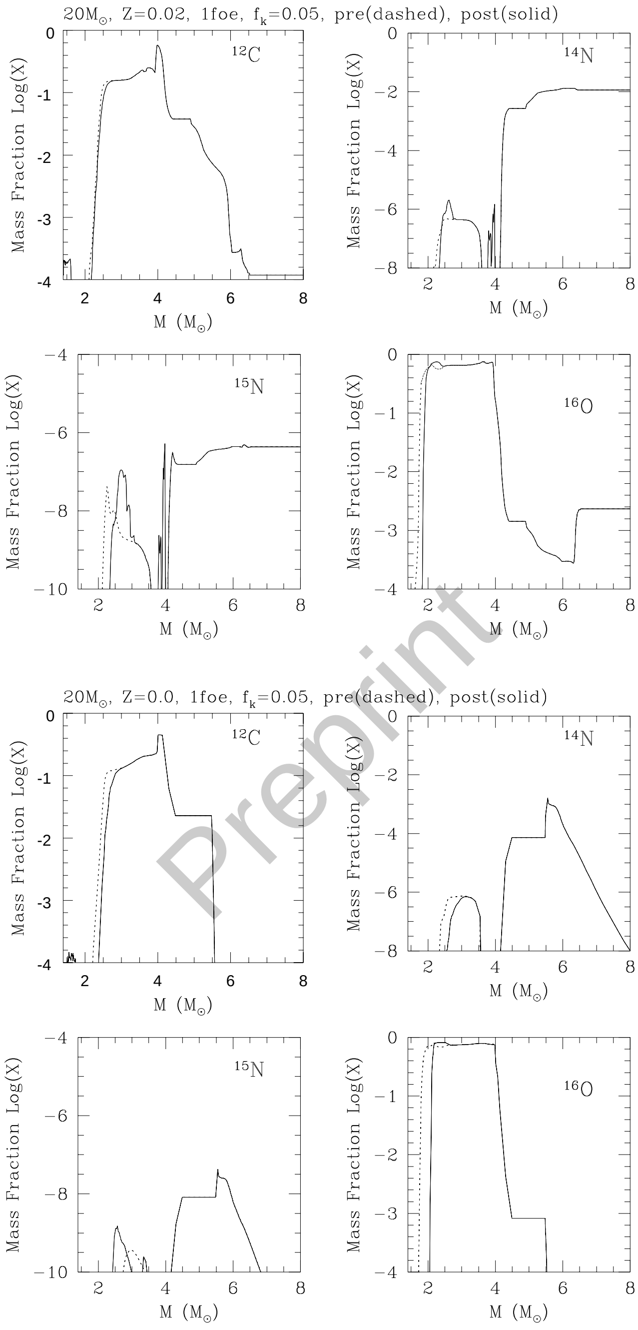

Fig. 5. Pre and post-explosive abundance distribution of ^{12}C, ^{14}N, ^{15}N, ^{16}O for $20M_{\odot}$, Z=0.02 (upper 4 panels) and Z=0 (lower 4 panels) models.

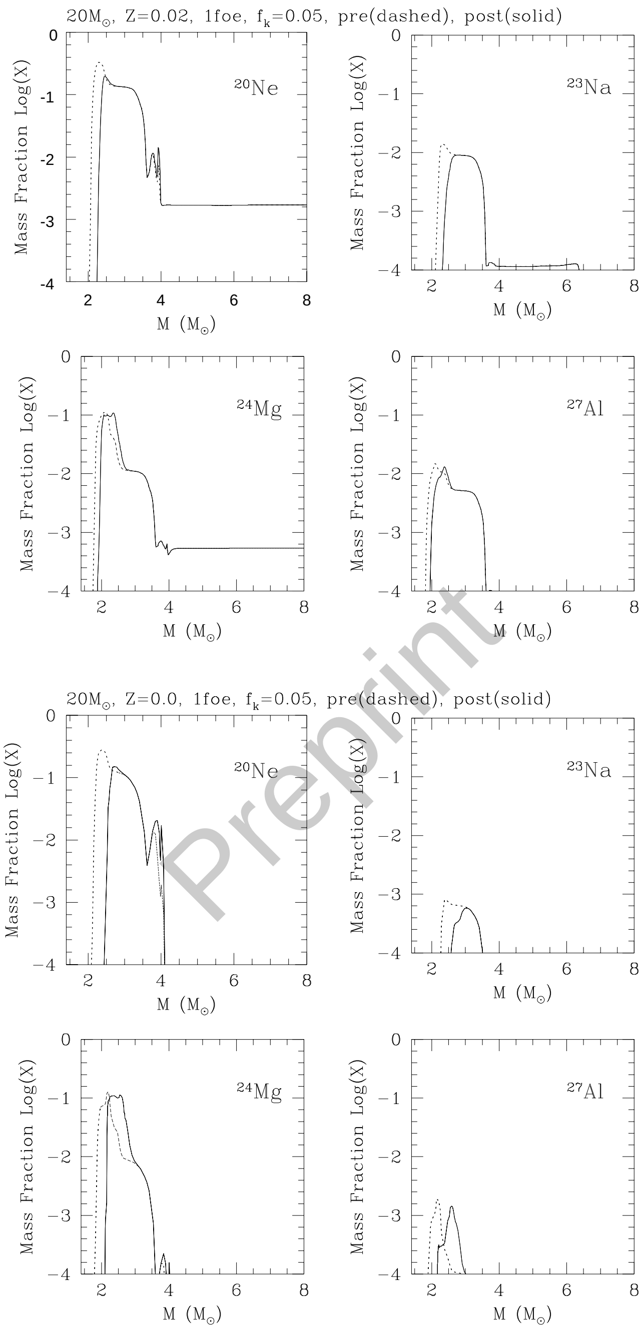

Fig. 6. Pre and post-explosive abundance distribution of ^{20}Ne, ^{23}Na, ^{24}Mg, ^{27}Al for the 20 $M_{\odot}$, $Z = 0.02$ (upper 4 panels) and $Z = 0$ (lower 4 panels) models.

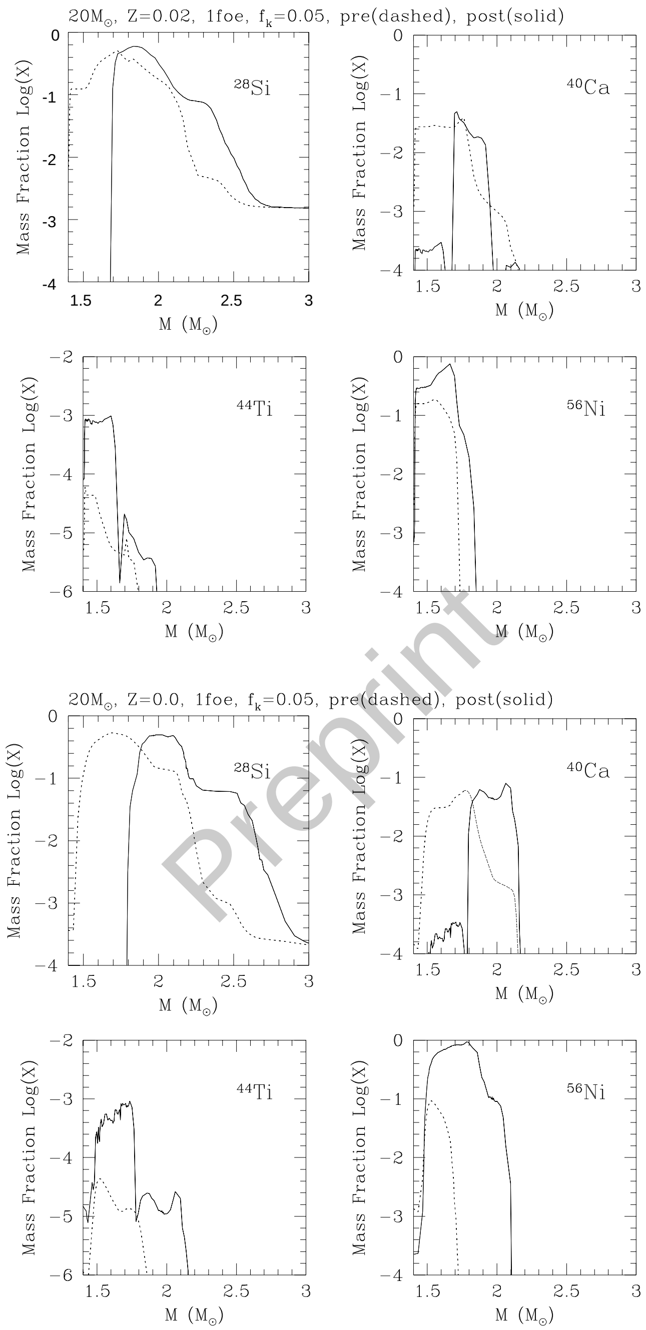

Fig. 7. Pre and post-explosive abundance distribution of ^{28}Si, ^{40}Ca, ^{44}Ti, ^{56}Ni for the 20 $M_\odot$, $Z = 0.02$ (upper 4 panels) and $Z = 0$ (lower 4 panels) models.

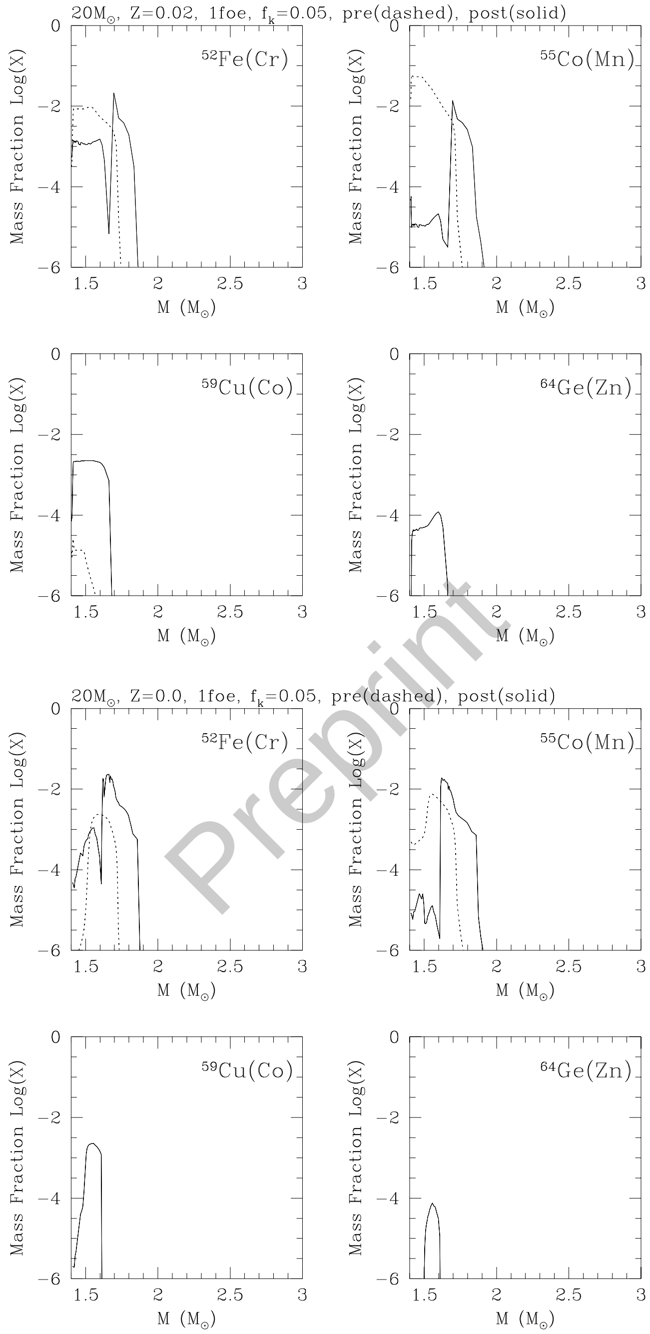

Fig. 8. Pre and post-explosive abundance distribution of ^{52}Fe, ^{55}Co, ^{59}Cu, ^{64}Ge for the 20 $M_{\odot}$, $Z = 0.02$ (upper 4 panels) and $Z = 0$ (lower 4 panels) models. These unstable isotopes are main sources to decay into Cr, Mn, Co and Zn, respectively.

Isotopes heavier than Si are mostly produced during explosive nucleosynthesis. The explosive nucleosynthesis depends on several parameters such as the explosion energy and mass cuts which are not well determined because of the uncertainty in the explosion mechanism. Some of the parameter dependences for $Z = 0$ are shown in Figure 12.

The difference in the bottom panel of Figure 10 and the top panel of Figure 12 is the mass cut. In the latter, deeper mass cut is chosen so that $[^{16}\mathrm{O}/^{56}\mathrm{Ni}] = 0$; then interestingly the abundance ratios for the even Z elements up to Zn can be roughly solar. Elements heavier than Zn might also be produced in the same way though we have not calculated.

The top, 2nd and 3rd panels of Figure 12 show the dependence on the explosion energy. The influence of the higher explosion energy is mainly to shift the distribution of the peak temperature outward. As a result, the location of the mass cut affects drastically the produced amount of ^{56}Ni. These figures show that Si and Ca are more abundant for a larger explosion energy.

Finally the effect of more efficient convective mixing is shown in the 2nd panel of Figure 12. It appears that this parameter choice ($f_k = 0.15$) is better to reproduce the solar abundance ratio for the even Z elements. However, we need further calculations for other masses and parameters in order to find general trends.

7 Cr, Mn, Co, and Zn

As mentioned in §1, recent high resolution abundance surveys discovered interesting trends of [Cr/Fe], [Mn/Fe] and [Co/Fe] with [Fe/H], that is, both [Cr/Fe] and [Mn/Fe] decreases as metallicity declines for [Fe/H] $= -2.4$ to -4.0 while [Co/Fe] increases [23–25,34]. One might suspect that these trends would be a signature of Pop III.

These trends could be explained with SNe II, if these abundance ratios strongly depend on metallicity. Figure 8 shows that the amount of iron peak elements produced by the explosive synthesis such as Cr, Mn, Co do not much depend on the initial stellar metallicity (even though Mn and Co have odd Z). Although Y_e for $Z = 0$ and 0.02 models is slightly different, these results show that the effect is not very large.

Therefore, other factors would be responsible to cause the above trends. In order to investigate the ratios [Cr/Fe], [Mn/Fe] and [Co/Fe] we look into the regions where these elements are produced. First of all, ^{56}Ni, which decays into the most abundant Fe isotope ^{56}Fe, is produced not only in the complete Si-burning region but also in the incomplete Si-burning region. ^{59}Cu, which decays into ^{59}Co, is produced in the complete Si-burning region.

^{52}Fe and ^{55}Co, which decay into ^{52}Cr and ^{55}Mn, respectively, are mostly synthesized in the incomplete Si-burning region. ^{52}Fe is also synthesized in the complete Si-burning region, but not a large amount. Note that ^{55}Mn

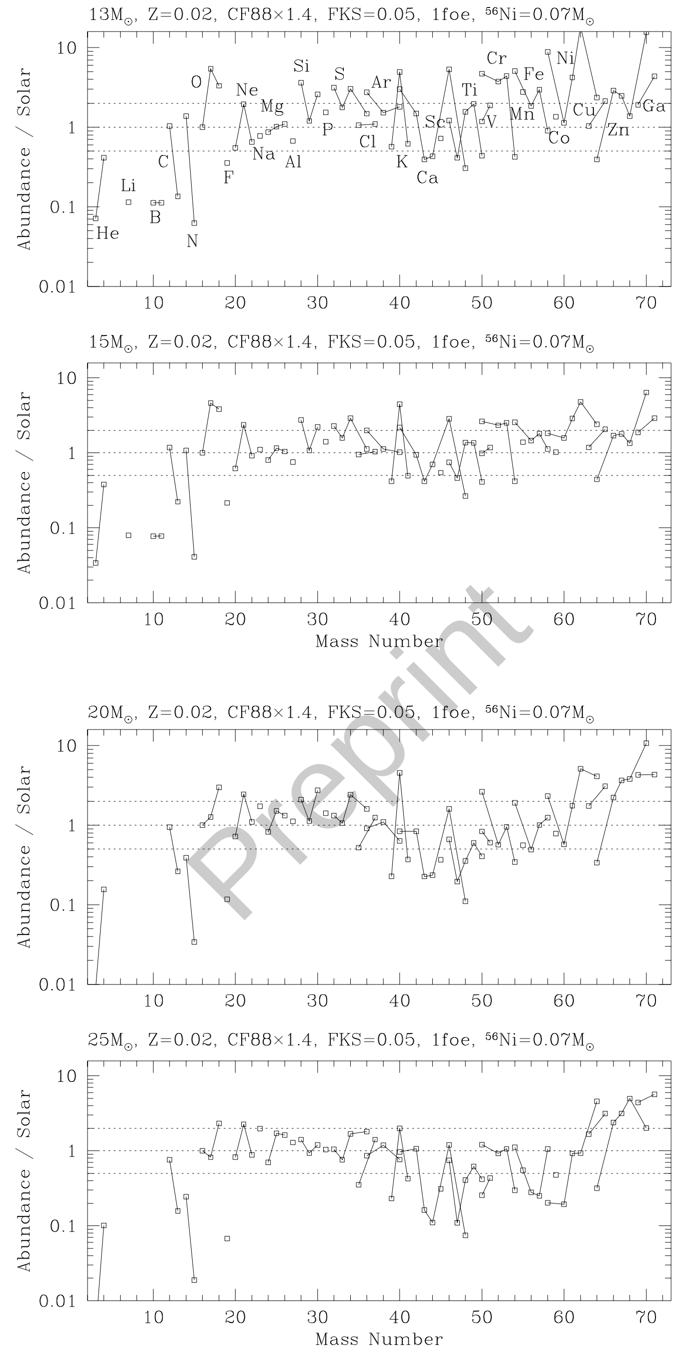

Fig. 9. Abundances for $Z = 0.02$, $M = 13 - 25\ M_\odot$ models normalized by the solar abundances.

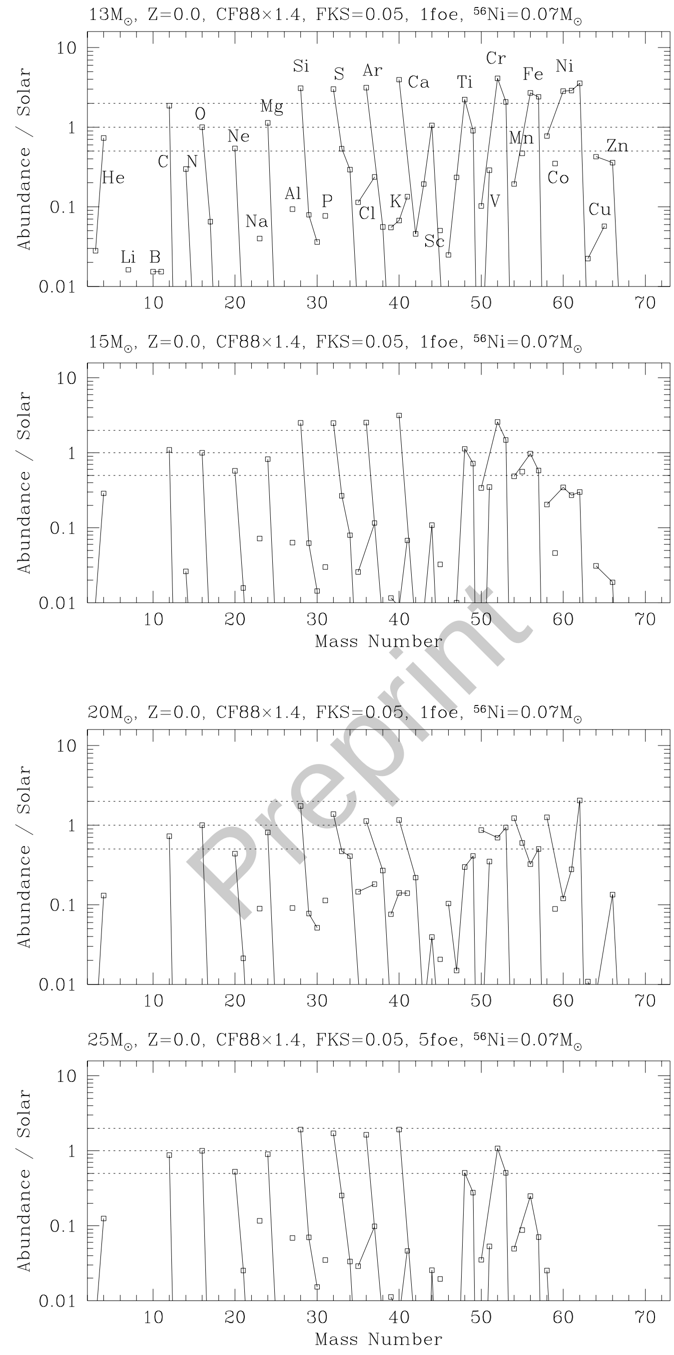

Fig. 10. Abundances for $Z = 0$, $M = 13 - 25\ M_\odot$ models normalized by the solar abundances.

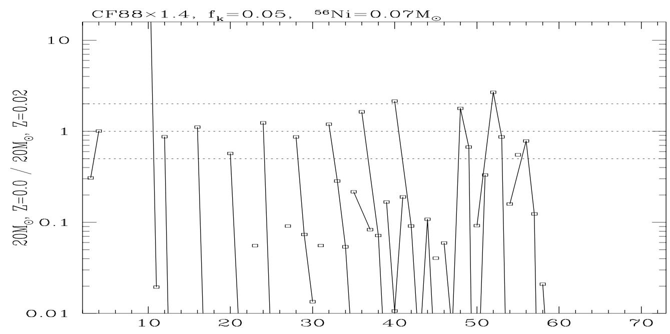

Fig. 11. Comparison of the 20 $M_\odot$ star yields between $Z = 0$ and 0.02.

and ^{59}Co are the only stable isotopes of these elements and therefore, their abundances are identical with the Mn and Co element abundances.

The above discussion suggests that the choice of the mass cut can affect the ratios [Cr/Fe], [Mn/Fe], and [Co/Fe]. For a deeper mass cut, the ejected mass of the complete Si-burning region is larger (i.e., the masses of Fe and Co are larger), while the ejected mass of the incomplete Si-burning region remains the same (i.e., the masses of Cr, Mn, and Fe are the same). Accordingly the ratios of [Cr/Fe] and [Mn/Fe] are smaller and [Co/Fe] is larger. For a mass cut at larger radii, these ratios show the opposite tendency. Therefore, specific choices of mass cuts in SNe II might explain the behavior of [Cr/Fe], [Mn/Fe], and [Co/Fe] in the metallicity range $-4 \leq$ [Fe/H] ≤ -2.5 [26].

The dependence of the abundance ratios on the mass cut is seen from the comparison between Figures 10 and 12. The relative thickness between the complete and the incomplete Si burning layers may also depend on the efficiency of convective mixing f_k.

Note also that Zn is produced from complete Si burning as seen in Figures 8. In order to reproduce [Zn/Fe] ~ 0 as observed in metal-poor stars, the ejection of relatively large amount of complete Si burning material is necessary as seen in Figure 12 and discussed in §6. This would occur if the mass cut is as deep as discussed above [26] or if such complete Si burning material is preferentially ejected in a form of a jet or bullets [42] from the deepest layer.

8 Pop III Characters in the Abundance Pattern

Massive Pop III stars no longer exist in the present universe. However, if Pop III supernovae induced the formation of low-mass stars, such stars should still alive and may be observable. Indeed some of the observed metal-poor halo stars may be such stars. If we can identify such stars, they are very useful in understanding the nucleosynthesis in the earliest universe. Also we may even be able to determine the typical mass range of Pop III stars by comparing theory with observed abundance pattern.

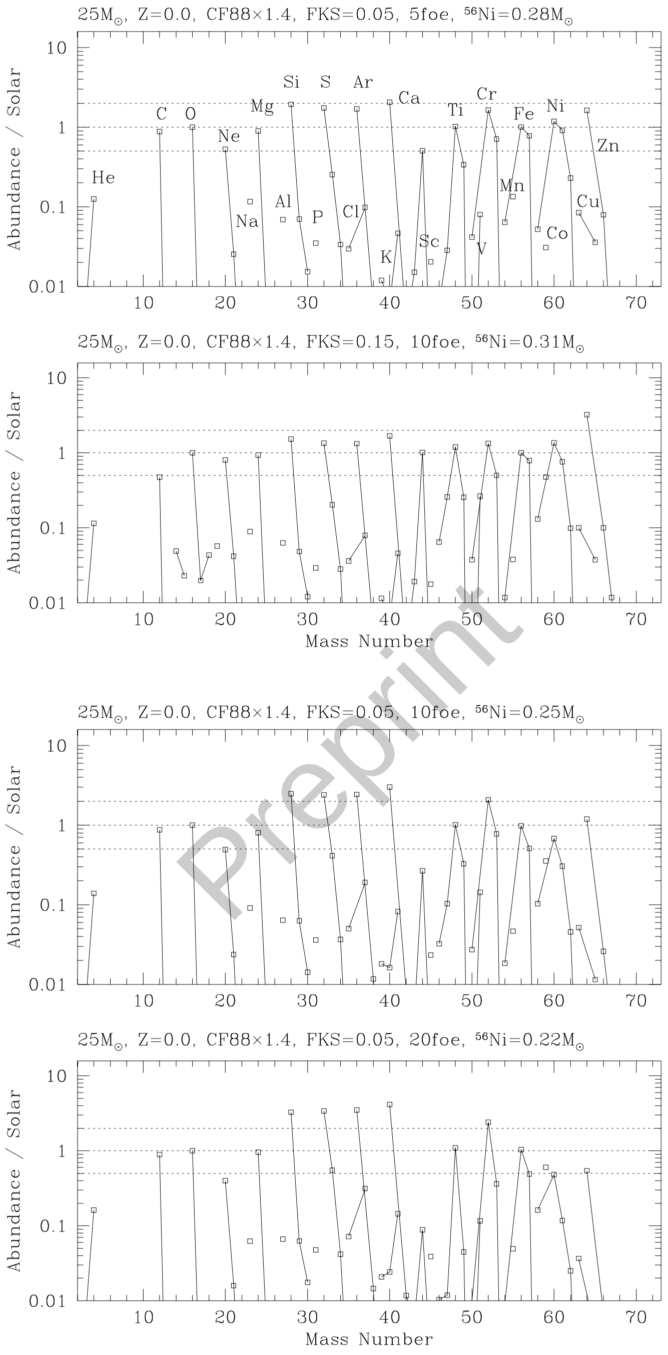

Fig. 12. Parameter dependence of the 25 $M_\odot$, $Z = 0$ model yields. From top to the bottom, explosion energy is varied as 5, 10, 10 and 20 foe (= 10^{51} erg). Mass cut is chosen for $[^{16}O/^{56}Ni] = 0$. The differences of the 2nd and 3rd panels are in the choice of convective mixing parameter f_k. Second one is a case for more efficient mixing.

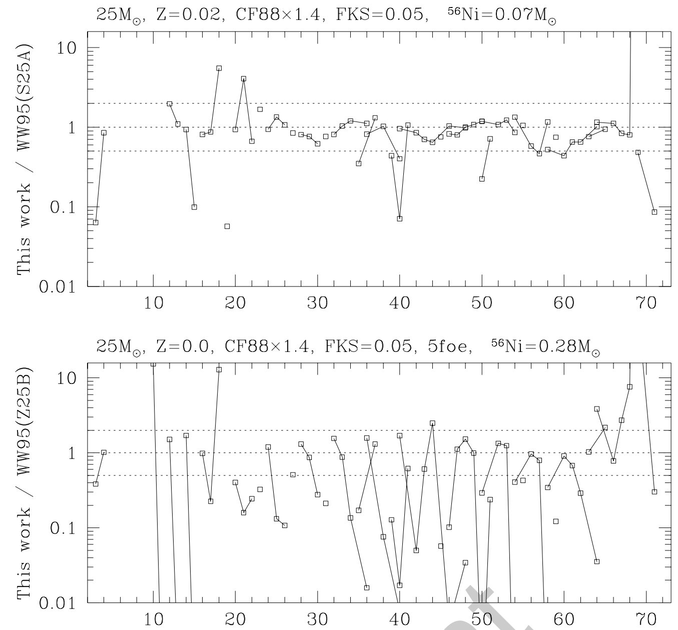

Fig. 13. Comparison of this work with Woosley & Weaver (1995), [46].

In the previous section we saw that the most distinctive features of the Pop III nucleosynthesis compared with Pop I and II are the abundance ratios in even Z isotopes (e.g., ^{12}C/^{13}C) and the deficiency of the odd Z elements such as ^{23}Na, ^{27}Al, and ^{31}P compared with even Z elements. In this section, we discuss in more detail the metallicity dependence of the abundance pattern to find specific characteristics of Pop III abundance pattern. As described above, yields from explosive nucleosynthesis depends on the non-well-understood properties of explosion such as the mass cut, mixing, etc. Therefore, we concentrate on the elements which are not sensitive to the explosive synthesis.

8.1 CNO Elements

In order to study the metallicity dependence of the yields in more detail, we calculate stellar evolution and explosive nucleosynthesis for the 20 $M_\odot$ models with $Z = 0.02$, 0.004, 0.001, 10^{-5} and 0. The integrated abundance ratio of some elements X to ^{24}Mg relative to the solar ratio are shown in Figures 14, where [X/Y]$\equiv \log_{10}(X/Y) - \log_{10}(X/Y)_\odot$. Here ^{24}Mg is used for normalization, because yield of ^{24}Mg is independent of mass cut and does not significantly depend on metallicity (e.g., 0.066, 0.054, 0.040, and 0.081 $M_\odot$ for

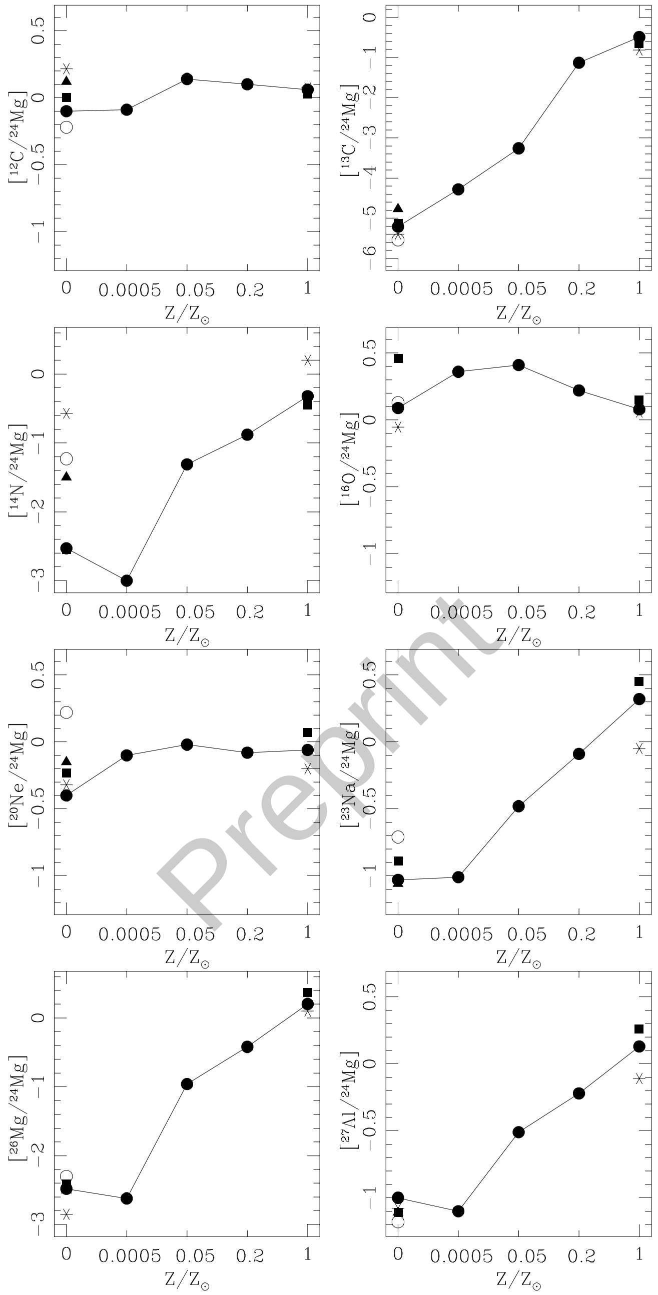

Fig. 14. Metallicity dependence of the integrated abundance ratio of elements X to ^{24}Mg relative to the solar ratio.

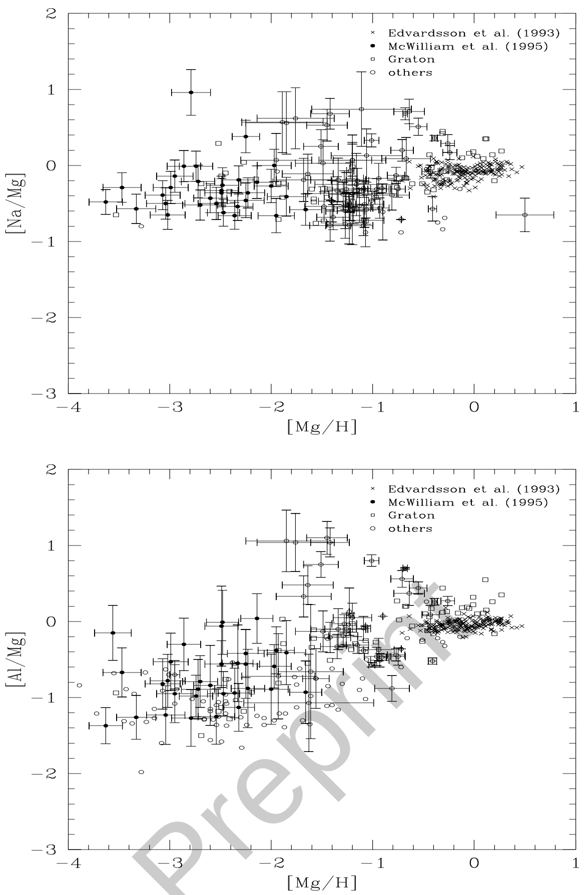

Fig. 15. Observed abundance ratios [Na/Mg] and [Al/Mg] in stars of the halo and the local disk.

$Z = 0.02, 0.004, 0.001$ and 0, respectively for the 20 $M_\odot$ models); furthermore observationally [^{24}Mg/H] appears to roughly correlate with metallicity [Fe/H] [36]. In these figures, the filled circles show the ratios for the 20 $M_\odot$ star. The asterisk, triangle, and square represent 13, 15, 25 $M_\odot$ models, respectively (only for Z=0 and 0.02), and open circle is the 25 $M_\odot$ $Z = 0$ model with more efficient convective mixing ($f_k = 0.15$).

These figures show that the abundance ratios for ^{12}C and ^{16}O are almost independent of metallicity (Z), while the ratios for ^{13}C and ^{14}N are smaller for smaller metallicity.

The result for ^{14}N yield is interesting. The [^{14}N/^{24}Mg] ratio decreases as metallicity gets smaller, but its metallicity dependence is sensitive to the stellar mass. For $Z = 0$, [^{14}N/^{24}Mg] is larger for less massive stars and its value for the 13 $M_\odot$ model is only 1/4 of the solar ratio. Therefore, primordial ^{14}N production from Type II supernovae may be significant. This ^{14}N production mechanism by these stars are similar to the suggestion in WW95. There, they commented that in some of their unpublished early calculations the convective He-shell penetrated into the H-layer with the consequent production of large amounts of primary ^{14}N. In our model also ^{14}N is produced in the He-burning shell during central C-burning. In this stage, the He-shell burning becomes strong enough to form a convective layer. This convective layer reaches the H-rich layer and the CNO-cycle operates to produce ^{14}N. In our model this mechanism is specific to the Pop III stars. For larger metallicity, the convective layer in the He-burning shell is hard to reach the H-rich region without overshooting because H-shell burning is so active to form a high entropy barrier. The ^{14}N production may be enhanced if we assume more efficient convective mixing as shown by the example in Figure 14 (open circle).

8.2 Odd Z Elements

The abundances of odd Z elements produced during C-burning such as ^{23}Na, ^{27}Al, and ^{31}P may be good indicators for the metallicity of the progenitor stars, because these elements are secondary and their abundances are expected to be smaller for smaller metallicity. Figure 14 shows that ^{23}Na and ^{27}Al abundances are smaller for smaller metallicity, in contrast to the primary elements such as ^{20}Ne and ^{24}Mg. These figures show, however, that the declines of [^{23}Na/^{24}Mg] and [^{27}Al/^{24}Mg] toward smaller metallicity almost saturate for $Z/Z_\odot \lesssim 5 \times 10^{-4}$. Hence it might be difficult to distinguish the Pop III abundance pattern from the abundance pattern of very low-metal Pop II stars only by these elements. Nevertheless we may say that the stars with the lowest [^{23}Na/^{24}Mg] and [^{27}Al/^{24}Mg] are most likely composed of the lowest metallicity SN ejecta.

Figure 15 shows the observed abundance ratios [Na/Mg] and [Al/Mg] in stars of the halo and the local disk [23,24,33,9]. The stars with the Pop III abundance pattern, if they exist, should belong to the low-metal stars ([Mg/H] $\lesssim -2$), but not necessarily the lowest metallicity stars because of the following reason. Such stars are composed of Pop III SNe ejecta mixed with interstellar matter (ISM). The amount of ISM mixed with the SN ejecta is estimated by Ryan et al. [34]. It depends on several uncertain factors but typically the metallicity of the mixed ejecta ranges from [Mg/H]~ -4 to -2 (see also [26,36]).

The observed patterns of [Na/Mg] and [Al/Mg] vs [Mg/H] are similar. For [Mg/H] $\lesssim -2$, the lower bounds are almost constant (~ -1) and upper bounds increase with [Mg/H]. The existence of the constant lower bounds is consistent with our results shown in Figures 14; it can be explained if these stars are composed of ejecta of Pop III or very low metal Pop II supernovae. Although only from these data it is hard to find the differences between the Pop III and the very low metal Pop II abundance, or the differences of progenitor masses, further theoretical and observational study may make discrimination possible.

8.3 Alpha Elements/Fe

In §6 and Figure 12, we discuss the cases with $[^{16}\mathrm{O}/^{56}\mathrm{Ni}] = 0$. These SNe produce a large amount of ^{56}Ni ($\sim 0.3 M_\odot$), which is comparable to hypernovae SN1998bw and SN1997ef [17,18] and even Type Ia supernovae [30].

In this connection, the abundance pattern of the very metal-poor binary CS22873-139 ([Fe/H] $= -3.4$) is interesting. This binary has only the upper limit to [Sr/Fe] < -1.5, thus being suggested to be a second generation star [31]. Although [Al/Fe] ~ -0.6 is too large for Pop III, other abundance features should be examined.

Interesting pattern is that this binary shows almost the solar Mg/Fe and Ca/Fe ratios. This would not mean that Type Ia supernovae contributed to the enrichment of Fe for such a metal-poor star. We rather suggest that the abundance pattern of this binary originates from hypernovae. Another feature of CS22873-139 is enhanced Ti/Fe ([Ti/Fe] $\sim +0.6$; [31]), which also seems to be the result from hyper-energetic or hyper-asymmetric explosion.

Since Pop III stars may consist of many massive stars that undergo hypernova-like explosions, [alpha element/Fe] ~ 0 could possibly be a signature of Pop III SNe.

9 Summary

We calculate pre-supernova evolutions and supernova explosions of massive stars ($M = 13 - 25 M_\odot$) for various metallicities. We find some characteristic abundance patterns of nucleosynthesis in the metal-free (Pop III) stars.

The most distinctive features of the Pop III nucleosynthesis compared with Pop I and II are that, for $Z = 0$, alpha nuclei (from C to Zn) are much more abundant than others. (The abundance pattern of α-nuclei can be similar to the solar abundance.) Therefore, by looking for the smallest isotopic ratios for the even Z elements (such as $^{13}\mathrm{C}/^{12}\mathrm{C}$) or the smallest abundance of odd Z elements in the metal-poor star abundances, we can find candidates of the stars having Pop III abundance pattern. Also, near solar ratios of alpha elements/Fe might be a signature of Pop III which could produce a large amount of Fe in hyper-energetic explosion.

The abundance ratios of odd Z to even Z elements such as Na/Mg and Al/Mg become smaller for lower metallicity. However these ratios almost saturate below $Z \lesssim 10^{-5}$, and [Na, Al/Mg] ~ -1 for Pop III and low metal Pop II nucleosynthesis. This result is consistent with abundance pattern of metal poor stars, in which these ratios also saturate around -1. We suggest that these stars with the lowest [Na/Mg] or [Al/Mg] may contain the abundance pattern of Pop III nucleosynthesis.

Metal poor stars show interesting trends in the ratios of [Cr, Mn, Co/Fe]. We discuss that these trends are not explained by the differences in metallicity, but by the relative thickness between the complete and the incomplete Si burning layers. Large [Co/Fe] and small [Cr, Mn/Fe] values found in the observations are explained if mass cut is deep or if matter is ejected from the complete Si burning layer in a form of a jet or bullets.

We also find that primary ^{14}N production occurs in the massive Pop III stars, because these stars have radiative H-rich envelopes so that the convective layer in the He-shell burning region can reach the H-rich region. Then primary ^{14}N production by NO-cycle can occur without overshooting.

Further study may make it possible to determine the metallicity and progenitor mass ranges of a SN which produced the metal-poor stars.

We would like to thank M. Hashimoto and H. Saio for providing us with the basis of the present evolutionary code. This work has been supported in part by the Grant-in-Aid for by COE Scientific research (07CE2002, 0980203) of the Japanese Ministry of Education, Science, and Culture.

References

1. Anders E., & Grevesse, N., 1989, Geochim. Cosmochim. Acta 53, 197
2. Arnett, W.D. 1996, Supernovave and Nucleosynthesis (Princeton Univ. Press)
3. Arnett, W.D., Bahcall, J.N., Kirshner, R.P., & Woosley, S.E. 1989, Ann. Rev. Astron. Ap., 27, 629
4. Audouze, J., & Silk, J. 1995, ApJ, 451, L49
5. Barkat, Z., & Marom, A. 1990, in Supernovae, ed. J.C. Wheeler et al. (World Scientific), 95
6. Caughlan, G.R., & Fowler, W.A., 1988, Atomic Data & Nucl. Data Tables, 40, 283 (CF88)
7. Castellani, V., Chieffi, A., & Tornambé 1983, ApJ, 272, 249
8. de Jager, C., Nieuwenhuijzen, H., & van der Hucht, K.A. 1988, A&AS, 72, 259
9. Edvardsson, B., Andersen, J., Gustafsson, b., Lamgert, D. L., Nissen, P. E., & Tomkin, J. 1993, A&Ap, 275, 101
10. Fowler, W.A. 1984, Rev. Mod. Phys., 56, 149
11. Galama, T.J. et al. 1998, Nature, 395, 670
12. Germany, L. et al. 1999, ApJ, submitted (astro-ph/9906096)
13. Hashimoto, M. 1995, Prog. Theor. Phys., 68, 795
14. Hashimoto, M., Nomoto K., & Shigeyama, T., 1989, A&A, 210, L5
15. Hix, W.R. & Thielemann, F.-K. 1996, ApJ, 460, 869
16. Iglesias, C.A., & Rogers, F.F., 1993, ApJ, 412, 752
17. Iwamoto, K., Mazzali, P.A., Nomoto, K., Umeda, H., Nakamura, T., et al. 1998, Nature, 395, 672
18. Iwamoto, K., Nakamura, T., Nomoto, K., Mazzali, P.A., Danziger, J., et al. 1999, ApJ, submitted (astro-ph/9807060)

19. Kudritzki, R.P., Pauldrach, A., Puls, J., & Abbott, D.C. 1989, 219, 205
20. Kumagai, S., Shigeyama, T., Nomoto K., et al. 1989 ApJ, 345, 412
21. Kumagai, S., Shigeyama, T., Nomoto K., Hashimoto, M., & Itoh, M. 1993, A&A, 273, 153
22. Limongi,M., Chieffi, A., & Straniero, O. 1998, in Nuclei in the Cosmos V, eds. N. Prantzos, S. Harissopulos (Editions Frontieres), 144; private communication (LCS)
23. McWilliam, A., Preston, G.W., Sneden, C., & Shectman, S. 1995a, AJ, 109, 2736
24. McWilliam, A., Preston, G.W., Sneden, C., & Searle, L. 1995b, AJ, 109, 2757
25. McWilliam, A. 1997, ARA&A, 35, 503
26. Nakamura, T., Umeda, H., Nomoto, K., Thielemann, F.-K., & Burrows, A. 1999, ApJ, 517, 193
27. Nomoto, K., & Hashimoto, M. 1988, Phys. Rep., 163, 13 (NH88)
28. Nomoto, K., Iwamoto, K., Tsujimoto, T., & Hashimoto, M. 1993, in Frontiers of Neutrino Astrophysics, ed. Y. Suzuki and K. Nakamura (Tokyo; Universal Academy Press), 235
29. Nomoto, K., Shigeyama, T., Kumagai, S., Yamaoka, H., & Suzuki, T. 1994, in Supernovae (Les Houche Session LIV), eds. S. Bludmann et al. (Elsever Science), 489
30. Nomoto, K., Thielemann, F.-K., & Yokoi, K. 1984, ApJ, 286, 644
31. Nordstrom, B. et al. 1999, in this volume
32. Rayet, M., Arnould, M., Hashimoto, M., Prantzos, N., & Nomoto, K. 1995, A&A, 298, 517
33. Ryan, S.G., & Norris, J.E. 1991, AJ, 101, 1835
34. Ryan, S.G., Norris, J.E., & Beers, T.C. 1996, ApJ, 471, 254
35. Saio, H., & Nomoto, K., 2000, in Computational Astrophysics: Stellar Physics, eds. Kudritzki, R., Mihalas, D., Nomoto, K., & Thielemann, F.-K. (New York: Springer), in press
36. Shigeyama, T. & Tsujimoto, T 1998, ApJ, 507, L135
37. Spruit, H.C. 1992, A&A, 253, 131
38. Thielemann, F.-K., Nomoto, K., & Hashimoto, M. 1994, in Les Houches, Session LIV ed. J. Audouze, S. Bludman, R. Mochkovitch & J. Zinn-Justin, 629
39. Thielemann, F.-K., Nomoto, K., & Hashimoto, M. 1996, ApJ, 460, 408
40. Tsujimoto, T., Nomoto, K., Yoshii, Y., Hashimoto, M., S. Yanagida, & Thielemann, F.-K. 1995, MNRAS 277, 945
41. Turatto, M., Suzuki, T., et al. 1999, ApJ, submitted (astro-ph/9910324)
42. Umeda, H. 1999, ApJ, in press (astro-ph/9911135)
43. Umeda, H., Nomoto, K., Yamaoka, H., & Wanajo, S. 1999, ApJ, 513, 861
44. Woosley, S.E., Arnett, W.D., & Clayton, D.D., 1973, ApJ, Suppl. 26, 231
45. Woosley, S. E., Eastman, R. G., & Schmidt, B.P. 1999, ApJ, 516, 788
46. Woosley, S.E., & Weaver, T., 1995, ApJS, 101, 181 (WW95)

Dependence of r-process Yields on the Progenitor Masses of Type II Supernovae

Shinya Wanajo[1], Kaori Otsuki[1], Toshitaka Kajino[1], and Yuhri Ishimaru[2]

[1] Division of Theoretical Astrophysics, National Astronomical Observatory, 2-21-1 Osawa, Mitaka, Tokyo 181-8588, Japan
[2] Department of Astronomy, University of Tokyo, 7-3-1, Hongo, Bunkyo, Tokyo 113-0033, Japan

Abstract. The r-process in Type II supernovae has been examined using a semi-analytic, general relativistic model of neutrino winds and a nuclear reaction network code. We found that the relatively high entropy ($\sim 140 N_{\mathrm{A}} k$) was obtained for the model of a massive proto-neutron star ($\sim 2 M_{\odot}$). Furthermore, the dynamical timescale of the wind was significantly short (~ 0.01 s) for the model of a high neutrino luminosity ($\sim 10^{52}$ ergs s^{-1}). These results imply that massive Type II supernovae are the site of r-process and the early times of the neutrino wind phases mainly contribute to its nucleosynthesis.

Recent observations of extremely metal poor stars show large dispersions in the abundances of neutron-capture elements[7][8][4][9]. This implies that these stars were formed by a few supernovae which had unique r-process yields[3][12]. Woosley et al.[14] have demonstrated that the neutrino winds from nascent neutron stars formed by Type II supernovae are a promising site for r-process. However, subsequent studies have shown serious difficulties, e.g., in obtaining enough entropy[10][6]. Otsuki et al.[5] have shown that general relativistic effects increase entropy and reduce dynamical timescale of neutrino winds (see also [6][1]). Furthermore, they suggested that the physical conditions for successful r-process were obtained for massive proto-neutron stars with high neutrino luminosity. In this paper, we present some nucleosynthesis results with the use of their models. In these models, the dynamical evolution of a neutrino wind is obtained with two parameter, the mass of the proto-neutron star M_{NS}, and the (constant) luminosity of electron neutrinos L_{ν}. We present the results of the following three models; (A) $M_{\mathrm{NS}} = 2.0 M_{\odot}$, $L_{\nu} = 10^{52}$ ergs s^{-1}, (B) $M_{\mathrm{NS}} = 2.0 M_{\odot}$, $L_{\nu} = 5 \times 10^{51}$ ergs s^{-1}, and (C) $M_{\mathrm{NS}} = 1.7 M_{\odot}$, $L_{\nu} = 10^{52}$ ergs s^{-1}. The r-process nucleosynthesis was calculated using a fully implicit network code with the data of nuclear reactions[11][2]. Neutrino capture on free nucleons was also included. As can be seen in Fig. 1, only the wind of a massive proto-neutron star with a high neutrino luminosity (model A) can obtain a robust physical condition for successful r-process, i.e., a high entropy ($\sim 140 N_{\mathrm{A}} k$) and a short dynamical timescale (~ 0.01 s). This imply that the r-process yields have a strong dependence on the progenitor masses of Type II supernovae, mainly originate from massive ones. We will present our results in more detail elsewhere[13].

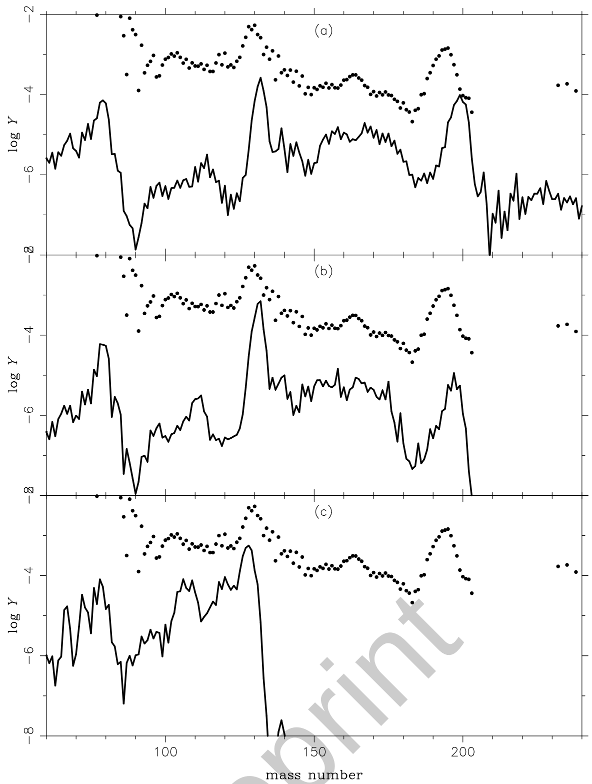

Fig. 1. Final r-process abundances for models A (a), B (b), and C (c), as a function of mass number. Also shown by *points* are the scaled solar r-process abundances.

References

1. Cardall, C. Y. & Fuller, G. M. 1997, ApJ, 486, L111
2. Cowan, J., Thielemann, F. -K., & Truran, J. W. 1991, Phys. Rep., 208, 267
3. Ishimaru, Y. & Wanajo, S. 1999a, ApJ, 511, L33
4. McWilliam, A. 1997, ARAA, 35, 503
5. Otsuki, K., Tagoshi, H., Kajino, T., & Wanajo, S. 1999, ApJ, in press
6. Qian, Y. -Z. & Woosley, S. E. 1996, ApJ, 471, 331
7. Ryan, S. G., Norris, J. E., & Beers, T. C. 1996, ApJ, 471, 254
8. Sneden, C., McWilliam, A., Preston, G. W., Cowan, J. J., Burris, D. L., & Armosky, B. J. 1996, ApJ, 467, 819
9. Sneden, C., Cowan, J. J., Debra, L. B., & Truran, J. W. 1998, ApJ, 496, 235
10. Takahashi, K., Witti, J., & Janka, H. -Th. 1994, A&A, 286, 857
11. Thielemann, F.-K. 1995, private communication
12. Tsujimoto, T., Shigeyama, T., & Yoshii, Y. 1999, ApJ, 519, L63
13. Wanajo, S, Otsuki, K., & Kajino, T. 1999, in preparation
14. Woosley, S. E., Wilson, J. R., Mathews, G. J., Hoffman, R. D., & Meyer, B. S. 1994, ApJ, 433, 229

A New Test of SN II Models and Their Predictions Regarding Nucleosynthesis: The Boron Isotopic Ratio

Luisa Rebull[1], Francesca Primas[2], and Douglas Duncan[1]

[1] University of Chicago, Chicago, IL, USA
[2] European Southern Observatory, Garching, Germany

1 Introduction

Type II supernovae (SNII) are expected to be the site of nucleosynthesis at very low [Fe/H]; one fairly robust prediction of SNII models is that ^{11}B is produced from ^{12}C via neutrino spallation. We can test these models by observing ^{11}B/^{10}B in low-metallicity stars.

Our first observation of the moderately metal-poor ([Fe/H]= -1.0) star HD 76932 placed a limit on its ^{11}B/^{10}B, but not a definite value, because possible blending from an unknown spectrum line could not be ruled out [1]. Hence, a strategy for better constraining the possible blending line is needed. The discovery of a halo star with a lower boron content than other similar stars (HD 160617 [2]) provides a wonderful opportunity to make the result definite.

2 Observations & Analysis: HD 76932

- Observed at λ2500 to have [Fe/H] = -1.0, $\log g$ = 4.0, $T_{\rm eff}$ = 6000 K, $\log \epsilon$ ($B_{\rm total}$)=1.82$\pm$0.2.
- All random errors measured to be much smaller than the isotopic splitting (25mÅ); systematic errors likely to be also $\ll$ 25 mÅ.
- If the 2089.55 Å absorption is entirely due to B, the B abundance as determined from λ2500 does not match the data.
- Larger abundance (within 1 σ) matches the data better.

3 Conclusions: HD 76932

- If λ2090 feature is entirely B, then:
  - best-fit abundance is $\log \epsilon$ (B)=2.07$\pm$0.25 dex, about 1 σ higher than the abundance from λ2500, $\log \epsilon$ (B)=1.82$\pm$0.20.
  - lower ^{11}B/^{10}B isotope ratios of 1:1 or 2.5:1 are ruled out, data most consistent with higher ratios of 4:1 or 10:1.

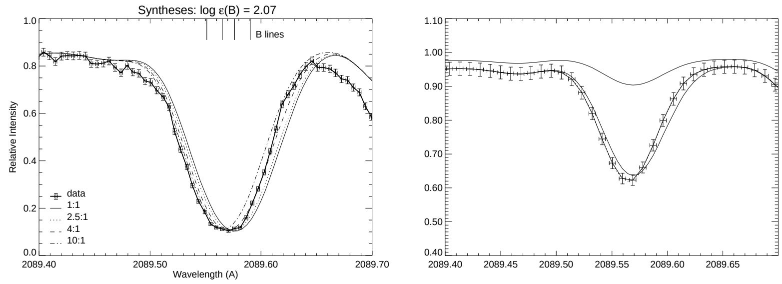

Fig. 1. Left panel: Isotopic fits at the higher B abundance – Enlargement of the B line (thicker line, with error bars denoting errors in both directions), and syntheses calculated with the larger B abundance, log ϵ ($B_{\rm total}$)=2.07, at a number of isotopic ratios. Shorter solid lines indicate the positions of the B lines as measured in the lab [3]. **Right panel:** Anticipated observations – Predicted B λ2090 profiles in HD 94028 and HD 160617 for $^{11}B/^{10}B$ isotopic ratios of 10:1 and 2.5:1. Error bars are those actually achieved in previous work on HD 76932.

  - Line shape matches 1:1 profile very well, but this would require an ad-hoc 7 mÅ wavelength shift. No obvious sources of such a shift were found, and the wavelengths are known to much better than this accuracy.
- If the λ2090 feature is B + blending line, then isotopic ratio can be either high or low.

4 Anticipated Observations

Primas [2,4] observed 7 new metal-poor stars for B (at λ2500). One of them, HD 160617, is deficient in B by $\sim$0.5 dex compared to other stars of similar temperature and metal abundance (T$\approx$ 5900 K, [Fe/H]~ -1.6). Observing and comparing two similar stars, HD 94028 and HD 160617, one of which lacks B, should immediately reveal which part of the feature at λ2090 is B, and which part blending metal lines. This should give a definite result for $^{11}B/^{10}B$ at metallcity [Fe/H]~ -1.6, an epoch when massive star SN should have dominated galactic nucleosynthesis. Then we can go back to the data for HD 76932 and obtain a firmer result for its isotopic ratio.

Data from an accepted HST STIS proposal to observe HD 94028 and HD 160617 at λ2090 are anticipated shortly.

References

1. Rebull, L. M., Duncan, D. K., Johansson, S., Thorburn, J. T., & Fields, B., 1998, ApJ, 507, 387
2. Primas, F., Duncan, D. K., & Thorburn, J. A., 1998, ApJL, 506, 51
3. Johansson, S. G., Litzen, U., Kasten, J., & Kock, M. 1993, ApJL, 403, 25
4. Primas, F., Duncan, D. K., Peterson, R. C., & Thorburn, J. A., 1999, A&A, 343, 545

Part IV

Feedback on the Environment

A New Model for Chemical Evolution of the Galactic Halo: Formulation and Applications

Takuji Tsujimoto[1], Toshikazu Shigeyama[2], and Yuzuru Yoshii[3]

[1] National Astronomical Observatory, Japan
[2] Reserch Center for the Early Universe, University of Tokyo, Japan
[3] Institute of Astronomy, University of Tokyo, Japan

1 A Model for Inhomogenous Chemical Evolution of the Galactic Halo

A model for Galactic chemical evolution, driven by supernova-induced star formation, is formulated and used to examine the nature of the Galactic halo at early epochs. In this model, new stars are formed following each supernova event, thus their abundance pattern is determined by the combination of heavy elements ejected from the supernova itself and those elements which are already present in the interstellar gas swept up by the supernova remnant. The end result is a prediction of large scatter in the abundance ratios among low-metallicity stars, reflecting a different nucleosynthesis yield for each Type II supernova (SN II) with a different progenitor mass. Formation of new stars is terminated when supernova remnants sweep up too little gas to form shells. We show from calculations based on the above scenario that (i) the observed [Fe/H] distribution for the Galactic halo field stars can be reproduced without effectively decreasing the heavy-element yields from SNe II by some manipulation required by previous models (e.g., via mass loss from the early Galaxy, or later mixing with "pristine" hydrogen clouds), (ii) the large observed scatter in the abundance ratio [Eu/Fe] for the most metal-poor stars can also be reproduced, and (iii) the frequency distribution of stars in the [Eu/Fe]−[Fe/H] plane can be predicted. Our model suggests that the probability of identifying essentially metal-free stars (Population III) in the local halo is around one in 10^{3-4}, provided that star formation in the halo is confined to individual gas clouds with mass of $10^{6-7}\,M_\odot$ and that the initial mass function of metal-free stars is not significantly different from the Salpeter mass function.

2 Production Site for *R*-process Element

If the astrophysical site for r-process nucleosynthesis in the early Galaxy is confined to a narrow mass range of SN II progenitors, with a lower mass limit of $M_{\rm ms} = 20M_\odot$, a unique feature in the observed distribution of [Ba/Mg] *vs.* [Mg/H] for extremely metal-poor stars can be adequately reproduced.

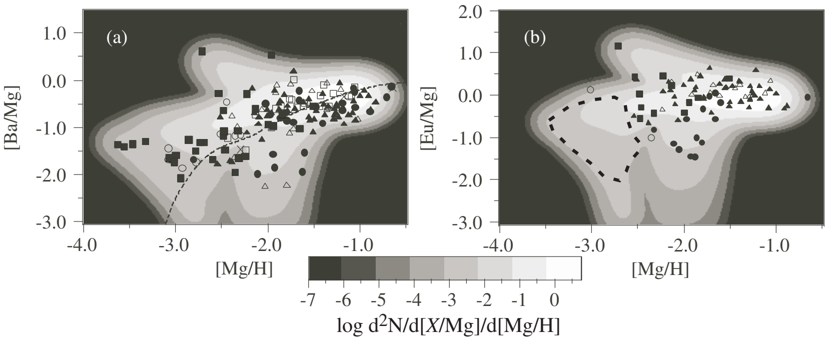

Fig. 1. (a) The frequency distribution of the long-lived stars in the [Ba/Mg]-[Mg/H] plane. The symbols represent the data taken from several references. For comparison, the result of the conventional one-zone chemical evolution model is shown by dashed line assuming the r-process site of $8 - 10\ M_\odot$ supernovae. (b) The same as (a) but for Eu. The dashed curve encloses the predicted region in which i-branch stars must exist.

We associate this feature, a bifurcation of the observed elemental ratios into two branches in the Mg abundance interval $-2.7 \leq$ [Mg/H] ≤ -2.3, with two distinct processes. The first branch, which we call the "y"-branch, is associated with the production of Ba and Mg from individual massive supernovae. The derived mass of Ba synthesized in SNe II is $8.5 \times 10^{-6} M_\odot$ for $M_{\rm ms} = 20 M_\odot$, and $4.5 \times 10^{-8} M_\odot$ for $M_{\rm ms} = 25 M_\odot$. We conclude that SNe II with $M_{\rm ms} \approx 20 M_\odot$ are the dominant source of r-process nucleosynthesis in the early Galaxy. An SN-induced chemical evolution model with this $M_{\rm ms}$-dependent Ba yield creates the y-branch, reflecting the different nucleosynthesis yields of [Ba/Mg] for each SN II with $M_{\rm ms} \gtrsim 20 M_\odot$. The second branch, which we call the "i"-branch, is associated with the elemental abundance ratios of stars which were formed in the dense shells of the interstellar medium swept up by SNe II with $M_{\rm ms} < 20 M_\odot$ that do *not* synthesize r-process elements, and applies to stars with observed Mg abundances in the range [Mg/H]< -2.7. The Ba abundances in these stars reflect those of the interstellar gas at the (later) time of their formation.

The existence of a [Ba/Mg] i-branch strongly suggests that SNe II which are associated with stars of progenitor mass $M_{\rm ms} \leq 20 M_\odot$ are infertile sources for the production of r-process elements. We predict the existence of this i-branch for other r-process elements, such as europium (Eu), to the extent that their production site is in common with Ba.

References

1. Tsujimoto, T., Shigeyama, T., Yoshii, Y. (1999) ApJ **519**, L63–L67
2. Tsujimoto, T., Shigeyama, T., Yoshii, Y. (1999) submitted to ApJ

A New Model for Chemical Evolution in the Galactic Halo: First Stars with Heavy Elements

Toshikazu Shigeyama[1] and Takuji Tsujimoto[2]

[1] Research Center for the Early Universe, Graduate School of Science, University of Tokyo, Bunkyo-ku, Tokyo 113-0033, Japan
[2] National Astronomical Observatory, Mitaka-shi, Tokyo, 181-8588, Japan

Abstract. It is demonstrated that abundance patterns in extremely metal-deficient stars with [Mg/H] $\lesssim -2$ are remarkably similar to those seen in the individual first generation supernova remnants. This suggests that most of the stars with [Fe/H] $\lesssim -2.5$ were made from individual supernova events.

1 Abundance patterns in extremely metal-poor stars

Older stars in the Galactic halo would show poorer abundances of heavy elements in their spectra if most of heavy elements were well mixed in the halo after they had been synthesized in massive stars and ejected by type II supernova (SN II) explosions. Reference [1] has shown that this age-metallicity relation is broken for recently observed extremely metal-poor stars with [Fe/H] < -2.5 [2], [3]. Instead it has been argued based on theoretical SN models that their abundance ratios with respect to Fe are consistent with a combination of those in two first generation SNe with differnet progenitor masses [4]. However, the Fe yields from the present SN models are still very uncertain [1].

2 Comparison with theoretical supernova remnants with different progenitor masses

The yields of heavy elements not influenced by the mass cut between the forming neutron star (or black hole) and the ejected envelope are expected to be more reliably calculated in SN II models than those influenced by the mass cut. Therefore the observed abundance ratios of [C/Mg] with respect to [Mg/H] can tell whether extremely metal-deficient stars were formed from individual SNe or from the well-mixed interstellar gas. The observed correlation of [C/Mg] with [Mg/H] [2] is shown in Fig. 1. The dashed curve in the same figure is the correlation of these ratios predicted from the one-zone Galactic chemical evolution model in which the gas is distributed uniformly and the heavy elements are well-mixed within the zone. Here we use the updated nucleosynthesis calculations by [5] for SN II yields and the results of

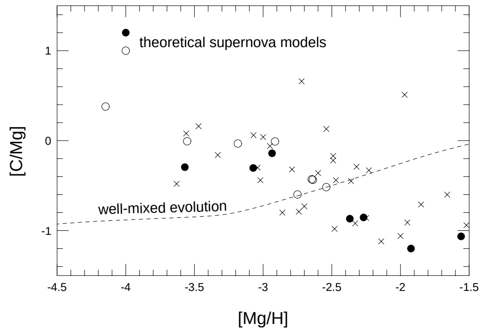

Fig. 1. Comparison of the observed abundance correlations (crosses) in halo field stars and those (circles) in theoretical supernova remnants with different progenitor masses.

[6] for the AGB star's yields. Details of the basic model ingredients can be found in [7]. This obvious disagreement with the observation indicates that the mixing of elements did not take place at that time. Figure 1 shows that the abundance correlations in theoretical SN models with different progenitor masses follow the observed correlation. Thus it is likely that most of the stars with [Fe/H]< -2.5 were formed from individual supernova remnants (SNRs). Since the ratio [Mg/H] is tightly correlated with the progenitor mass, the observed abundance patterns of extremely metal-poor stars enable us to construct yields of any observed heavy-element from each SN II [8], [9].

References

1. Shigeyama, T., Tsujimoto, T. (1998) Fossil imprints of the first-generation supernova ejecta in extremely metal-deficient stars. ApJ, **507**, L135–L139
2. McWilliam, A., et al. (1995) Spectroscopic analysis of 33 of the most metal poor stars. II. AJ, **109**, 2757–2799
3. Ryan, S. G., Norris, J. E., Beers, T. C. (1996) Extremely metal-poor stars. II. elemental abundances and the early chemical enrichment of the galaxy. ApJ **471**, 254–278
4. Audouze, J., Silk, J. (1995) The first generation of stars: first steps toward chemical evolution of galaxies. ApJ, **451**, L49–L52
5. Nomoto K., et al. (1977) Nucleosynthesis in type II supernovae. Nucl. Phys. **A616**, 79c–90c
6. van den Hoek, L. B., Groenewegen, M. A. T. (1997) New theoretical yields of intermediate mass stars.A&AS, **123**, 305–328
7. Yoshii, Y., Tsujimoto, T., Kawara, K. (1999) Age Dating of a High-Redshift QSO B1422+231 at Z = 3.62and Its Cosmological Implications. ApJ, **507**, L113–L116
8. Tsujimoto, T., Shigeyama, T. (1998) New insigths into the early stage of the galactic chemical evolution. ApJ **508**, L151–154
9. Tsujimoto, T., Shigeyama, T., Yoshii, Y. (1999) Chemical evolution of the Galactic halo through supernova-induced star formation and its iplication for Population III stars. ApJ, **519**, L63–L67

Light and Metals from Population III Stars

Jason Tumlinson

CASA, University of Colorado, Boulder, CO, 80309, USA

Abstract. We present zero-age models of Population III stars that demonstrate these stars have enhanced ionizing photon production relative to metal-enriched stars. We comment on the possibility that these stars reionized the universe and calculate a critical rate of metal-free star formation required to reionize H by $z = 5$. We speculate on the effects of our models on various other cosmological processes.

1 Model Population III Stars

Observational (Gunn – Peterson) constraints indicate that hydrogen was fully ionized by $z \sim 5$. The precise identity of the ionizing sources is still unknown, but *the apparent sharp decrease in the space density of quasars at $z \geq 3$ argues strongly in favor of stellar sources.*[1]

We have constructed static stellar structure and atmosphere models to calculate the ionizing photon yields from metal-free stars. A zero-age main sequence (ZAMS) appears in the left panel of Fig. 1. Model atmospheres have been calculated for each of these stars using the TLUSTY code [1].

Because they derive their energy from p-p burning, *these stars are uniformly hotter and smaller than their metal-enriched counterparts of equal mass.* As a result they emit much of their energy above 1 Ryd. Ionizing photon production increases by 50% for high mass (40 – 70 $M_\odot$) and by factors of 2 – 40 for moderate mass (10 – 30 $M_\odot$). The gains are 10^3 – 10^6 for photons above the He II edge at 54.4 eV, indicating that metal-free stars may contribute significantly to He II reionization before $z \sim 3$.

Using the model atmospheres and assuming a Salpeter IMF, we constructed a simple synthetic population to evaluate the ionizing photon production of metal-free stars per unit mass. Synthetic spectra of zero-age populations are displayed in the right panel of Fig. 1.

2 Reionization and Cosmological Effects

We calculate a critical rate of metal-free star formation necessary to reionize H in the IGM by $z = 5$. Assuming the IGM is reionized when the number of ionizing photons emitted in one recombination time is equal to the number of hydrogen atoms, this rate is 0.008 $M_\odot$ yr^{-1} Mpc^{-3}, consistent with the inferred SFR at $z = 5$ if 40% of ionizing photons escape into the IGM [3]. Metal-free star formation at this rate over the epoch $z = 5 - 10$ would enrich

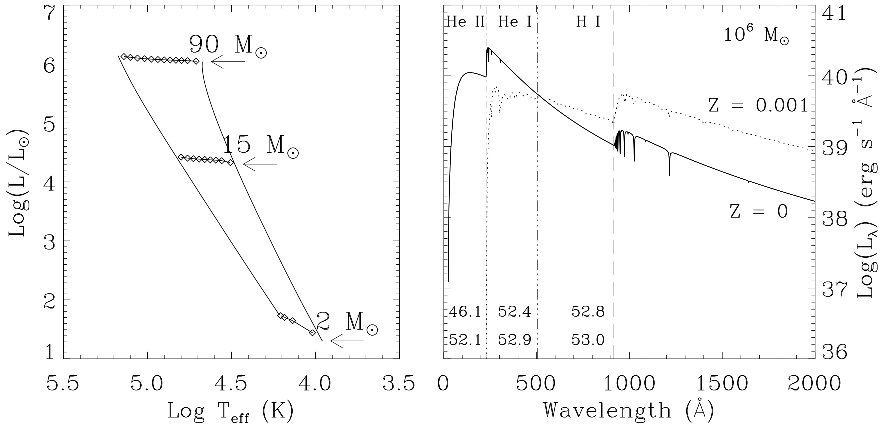

Fig. 1. Left panel: HR diagram for Pop I ($Z = Z_\odot$) and Pop III stars, where diamonds mark decades in Z down from $Z = 0.01$ to $Z = 0$ at selected masses. Right panel: Synthetic spectra of Pop II [2] and Pop III clusters of 10^6 M$_\odot$. The dashed lines mark the three photoelectric edges of H I, He I, and He II. The numbers to the left of each continuum represent the log of the ionizing photon production per unit time in that transition ($E \geq 13.6$, 24.4, and 54.4 eV from right to left).

the universe to a mean metallicity 20% of that observed in the most metal poor regions at $z \sim 3$, which have $\log(Z/Z_\odot) = -2.5$ (metal yields from [6]).

Assuming the ionizing spectra of clusters follow a power law, $L_\nu \propto \nu^{-\alpha}$, then α characterizes the effects of Pop III stars on the intergalactic radiation field. The Pop III cluster in Fig. 1 has a hard spectral index $\alpha_1 = -1.2$ in the range 1 – 4 Ryd and $\alpha_4 = 0.5$ for $h\nu \geq 4$ Ryd. For comparison, the Pop II cluster in Fig. 1 has $\alpha_1 = 1.0$ and negligible flux above 4 Ryd. Thus, metal-free stars could contribute harder radiation to the extragalactic spectrum than QSOs with intrinsic $\alpha_s = 1.8$ between 0.9 – 2.6 Ryd [5]. In addition, this hard intrinsic spectrum may be inconsistent with the observed IGM radiation field at $z \sim 3$. *At $z \sim 5$ this EUV spectrum is accessible to ground- and space-based instruments in the optical and near-UV.*

This proceeding summarizes work supported by astrophysical theory grants from NASA (NAG5-7262) and NSF (AST96-17073), and published in Tumlinson & Shull [4].

References

1. Hubeny, I., Lanz, T. 1995, ApJ, 439, 875
2. Leitherer, C., et al. 1999, ApJS, 123, 3
3. Madau, P., Mozetti, L., & Dickinson, M. 1998, ApJ, 498, 106
4. Tumlinson, J., & Shull, J. M. 1999, ApJL, submitted
5. Zheng, W., et al. 1997, ApJ, 475, 469
6. Woosley, S. E., & Weaver, T. A. 1995, ApJS, 101, 181

The Metallicity Enrichment of the First Generation Star of Our Galaxy

Jian Rong Shi[1,2], Gang Zhao[1,2], and Ye Lu[1,2,3]

[1] Beijing Astronomical Observatory, Chinese Academy of Sciences, Beijing 100012, China, sjr@yac.bao.ac.cn
[2] National Astronomical Observatories, Chinese Academy of Sciences, Beijing 100012, China, zg@orion.bao.ac.cn
[3] Department of Physics, Normal University of Huang Zhong, Wuhan 430079, China

Abstract. Zero metallicity stars may accrete a small amount of metal rich material of the ISM, which alters the metallicity of the stars. We calculated here that the expected degree $[Fe/H]$ of the metal enrichment of a $0.9M_{\odot}$ star may be $[Fe/H]_{*} \sim -5.43$ with a orbit like GL699 and $[Fe/H]_{*} \sim -7.45$ with a orbit like LDS519B.

1 The chemical evolution of the Galactic disk

We consider a multizone model for the chemical evolution of our Galaxy in which star formation, gas infall, and expanding supernova play a dominant role in determining the abundance of the various elements in the gas phase of the ISM. Here, we adopt Galactic chemical enrichment model used by [2], hereafter TWW95.

We have attempted to derive the evolution of the gas fraction with time as shown in TWW95 Fig. 7. And the metallicty $[Fe/H]$ of the ISM in our Galaxy as a function of time as shown in TWW95 Fig.2.

2 Metal enrichment for the zero metal FGS

When the first generation star (FGS) passes through the disk, the FGS accretes the ISM in it's vicinity in the disk, which alters it's evolution of elements abundance. The rate of accretion strongly depends on the relative velocity between the star and the gas of the disk. When the star of mass m moves through an interstellar gas with a relative velocity V_{rel}, the effective accretion radius ($r_b = Gm/c_s^2$) of a solar-type star ($m \sim 0.9M_{\odot}$) is much smaller than the disk thickness and the accretion process is similar to the three-dimensional problem considered by Bondy [1]. Then the accretion rate is

$$\dot{m} = 2.5\pi G^2 m^2 \rho_{ISM}(r,t) v_{rel}(t)^{-3}, \tag{1}$$

here, $\rho_{ISM}(r,t)$ is the gas density of ISM of the disk and $\rho_{ISM}(r,t) = \frac{\sigma_{ISM}(r,t)}{H}$. H is the thickness of the disk. From Eq.(1), we can get the accreting rate $\dot{m}$ against the time. The total accretion rate m_a is obtained by integrating equation $\dot{m}$ with the time that stars spend within the interstellar gas of the disk. The total accretion rate for the element E is

$$m_a(E) = \int_0^{t_old} 2.5\pi f G^2 m^2 \rho_{ISM}(E, r, t) v_{rel}(t)^{-3} dt \quad (2)$$

here, $f = 1$ when star pass through the disk, else $f = 0$. Assuming the age of FGS is $t \sim 14$ Gyr, H is taken from [3]. The total accreted mass through the ISM with a typical star of mass $0.9M_\odot$ and a orbit like GL699 is $m_a = 5.53 \times 10^{-10} M_\odot$, $m_a(Fe) = 6.53 \times 10^{-13} M_\odot$. And $m_a = 4.65 \times 10^{-12} M_\odot$, $m_a(Fe) = 6.31 \times 10^{-15} M_\odot$ for a star of mass $0.9M_\odot$ and a orbit like LDS519B. This accreted matter, although minuscule, can affect the elemental abundance in the surface convective zones for stars.

The degree of enrichment depends on the depth to which the accreted material is mixed. Here we assume that it is continuously mixed only in the convective envelope of a star with the mass of m_c, it means that we consider a closed surface connective region with no exchange of material with inner radiative core and no mass loss. According to [4], typical values for models without rotation range is $m_c \sim 10^{-4} M_\odot$, for $m \sim 0.9M_\odot$. Then the enriched abundance of FGS is

$$[Fe/H]_* \simeq log\left(\frac{m_a(Fe)/56}{m_c + m_a}\right) - log\left(\frac{N_\odot(Fe)}{N_\odot(H)}\right) \quad (3)$$

So the evolution of the relative enrichment abundance of FGS to the solar abundance for the above case are $[Fe/H] \sim -5.43$ and -7.45.

3 Conclusions

Our main results are: The metallicity abundance of the FGS (with mass $0.9M_\odot$) enriched by accreting the ISM with a orbit like GL699 amounts to $[Fe/H]_* \sim -5.43$. Then the absence of FGS which has the chemical composition inherited from the Big Bang could be explained by the hypothesis of enrichment of the FGS surface metal abundance due to accretion of metal-rich material.

Acknowledgments: This research work is supported by the National Natural Science Foundation of China.

References

1. Bondy, H., (1952), MNRAS, **112**, 195–
2. Timmes, F. X., Woosley, S. E., Weaver, T. A., (1995), ApJS, **98**, 617–658 (TWW 95)
3. Binney, J., Merrifled, M.,(1998), Galactic Astronomy, Princeton University Press, p568
4. Pinsonneault, M. H., Deliyannis, C. P., Demarque, P., (1992), ApJS, **78**, 179–203

Enrichment of Neutron-Capture Elements in Our Galaxy at the Early Epoch

Yuhri Ishimaru[1] and Shinya Wanajo[2]

[1] Department of Astronomy, University of Tokyo, 7-3-1 Hongo, Bunkyo-ku, Tokyo 113-0033, Japan
[2] Division of Theoretical Astrophysics, National Astronomical Observatory, 2-21-1 Osawa, Mitaka, Tokyo 181-8588, Japan

Abstract. Recent observations of halo stars show large dispersions in abundances, especially for neutron-capture elements. These dispersions may indicate that the inter-stellar medium was not mixed well at the early epoch. If star formations are induced by supernovae, chemical compositions of stars should be determined by each supernova yield. Under this assumption, we construct a new evolution model of our Galaxy. We examine distributions of stellar abundance ratios, and find the inhomogenious enrichment causes the observed dispersions. We also determine the origins of neutron-capture elements, by comparing our results with observations.

1 Introduction

The chemical compositions of long-lived stars provide us clues for the enrichment history of our Galaxy. Recent observations of metal-poor halo stars show intrinsic large dispersions in chemical abundances, especially for neutron-capture elements (eg., [1][2]; see also Fig. 1). These dispersions may indicate that the interstellar medium (ISM) was not mixed well at the very early epoch. In particular, the extremely high enhancement of [Eu/Fe] ($\simeq +1.7$) in CS 22892-052 strongly suggests mixing from a single supernova [3]. These facts imply that the heavy elements in metal-poor stars come from a few supernovae. If star formations are induced by supernova explosions, newly formed stars should contain the supernova products as well as metals in the ISM. With this assumption, we construct a new chemical evolution model of our Galaxy, and aim to understand the star formation history of our Galaxy at the beginning. This model can identify the supernovae which formed stars with enhanced abundances of specific elements. Thus, we also determine the origins of Eu, Ba, and Sr, as representatives of neutron-capture elements, by comparing our results with observations.

2 Inhomogeneous Chemical Enrichment Model

We assume star formations are induced by each supernova. Chemical compositions of newly formed stars are obtained by mass average of the 'snow-plowed' ISM and the supernova products. A supernova remnant is supposed

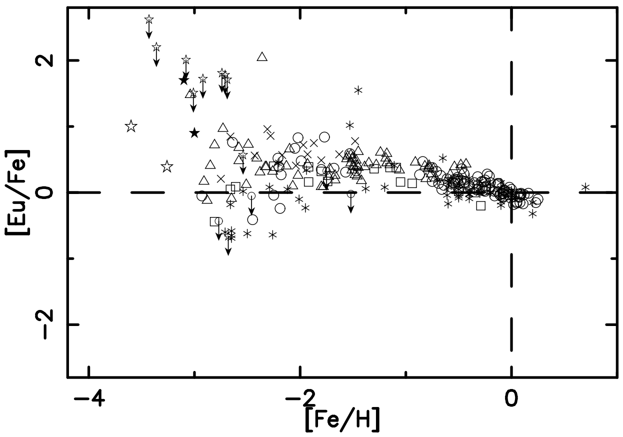

Fig. 1. Observational Data of [Eu/Fe] vs. [Fe/H] Relation: symbols refer to published observed data (for an explanation, see [4])

to expand spherically, until reaching the merge radius with the ISM (typically $\sim$ 100 pc; [5]). The chemical evolution of the ISM is calculated by a 1-zone model, losing gas through accretion onto the disk. Star formation and outflow rates are adjusted to fit to the observed [O/Fe] vs. [Fe/H] relation and the metallicity distribution of halo stars. Type Ia and type II supernova (SNII) products are taken from nuleosynthesis studies by Nomoto et al. [6][7]. We set the mass range of SNII progenitors as $8-60M_{\odot}$, but stars of $8-10M_{\odot}$ are assumed to produce no iron. Neutron-capture elements are produced by r-, main s-, or weak s-processes. R-elements are primary and are supposed to be produced by SNII, whereas s-elements are produced in AGB stars or SNII as secondary. The stellar mass ranges for the sites of each process are regarded as parameters. The masses of produced r-elements are assumed to be constant, regardless of progenitor mass. On the other hand, productivity of s-elements are given by functions of metallicity depending on neutron source; ^{13}C or ^{22}Ne [8].

3 Enrichment of Europium

Eu is regarded as a representative of r-process. Major candidates for r-process sites are 1) prompt shock of SNII of $8-10M_{\odot}$ with O-Ne-Mg cores ([9]; [10]), and 2) neutrino winds of SNII by massive stars $>10M_{\odot}$ (cf. [11]; [12]; [13]). Thus in models, masses of r-process sites are assumed as SNII of a) $8-10M_{\odot}$, b) $>30M_{\odot}$ and c) $>10M_{\odot}$. As shown in Figs. 2a and 2b, both cases can explain well the enhancement of Eu. In case of lower mass SNII, increases of [Eu/Fe] with [Fe/H] also appears. In future observations, if such low [Eu/Fe] stars are detected, we can determine the r-process site. On the other hand, as Fig. 2c, if all SNII produce Eu with similar yields, high [Eu/Fe] cannot be reproduced. In conclusion, the observed dispersions indicate that star formations are induced by SN explosions. In this case, the r-process site should be in SNII 1) which produces less Fe (a), or 2) whose number fraction is enough small (b).

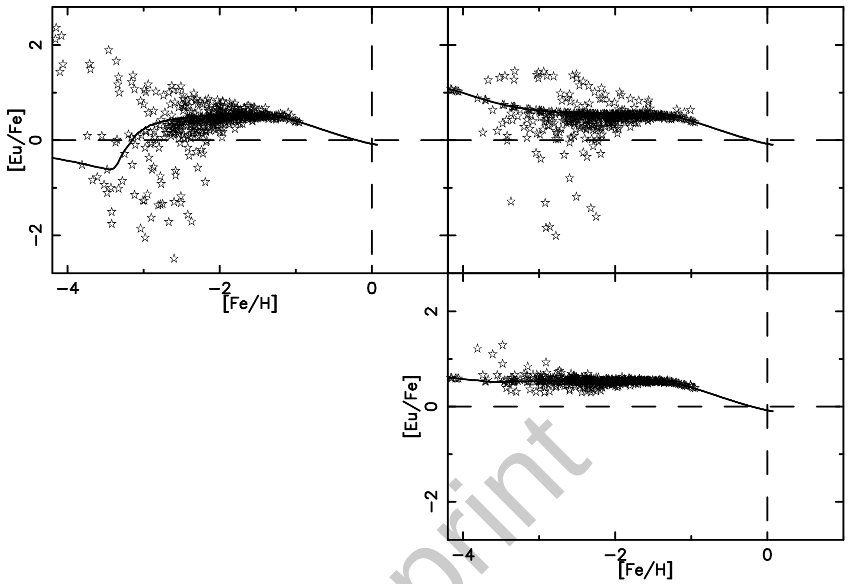

Fig. 2. Predicted [Eu/Fe] vs. [Fe/H] Relations: *stars* give abundances of each star and *solid lines* give the mean abundances of the ISM. the mass range of r-process sites are assumed as a) $8-10M_\odot$ *(top left panel)*, b) $>30M_\odot$ *(top right panel)*, and c) $>10M_\odot$ *(bottom right panel)*

4 Origin of Strontium

4.1 Problems in Strontium

Most of Ba and Sr are produced by main s-process and only $\sim 15\%$ of them come from r-process. Main s-elements are supposed to be produced in AGB stars. Thus, as clearly seen in Fig. 3a, the [Ba/Eu] ratios of very metal-poor stars suggest that Ba was produced by r-process at first and the Ba production by s-process increases later. If the origin of Sr is identical to Ba, [Sr/Eu] should show the similar trend with [Ba/Eu] and [Sr/Ba] should be constant throughout the Galactic evolution. However, as shown in Fig. 3b, a large spread is seen in [Sr/Ba] of very metal-poor stars. These strong Sr enhancements must indicate that part of Sr is produced by neither main s-process nor r-process. In the followings, we will discuss the third origin of Sr.

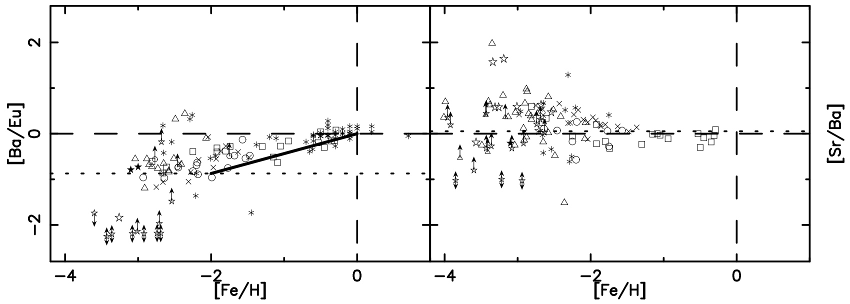

Fig. 3. Observed relations of a) [Ba/Eu] and b) [Sr/Ba] vs. [Fe/H]: symbols are the same as Fig. 1. *Dotted lines* give the solar-system r-fractions.

4.2 Candidates for the origin

It is known that part of Sr is produced through weak s-process. However, weak s-process requires ^{22}Ne as neutron source, which is a secondary element. Thus, the yield of Sr by weak s-process at [Fe/H]~ -3 is less than 1/100 at [Fe/H]~ -1. With such too low yields, weak s-process cannot be the cause of high enhancement of Sr in very metal poor stars. We will, then, suggest 'weak' r-process as a possible origin of Sr. While only specific SNe must be able to produce high mass elements (eg., Eu, Ba) by main r-process, lower mass elements like Sr may be produced by residual SNe as 'weak' r-process. Such two different sites of r-process has also been proposed from meteoritic studies ([14]; [15]).

4.3 Results

We assume that 50% of lower mass elements; $N < 54$ (Sr, Y, Zr), are produced by weak r-process, while high mass elements,$N > 54$ (Ba, Eu), are produced mostly by main r and only 5% of them come from weak r. The mass range of weak r are assumed as $20 - 30M_\odot$. As shown in Fig. 4a, dispersions in [Ba/Eu] is quite small, since the fractions of main r to weak r yields are the same between Ba and Eu. On the other hand, as clearly seen in Fig. 4b, large spread of [Sr/Ba] in metal-poor stars are caused by differences in weak r-process yields for Sr and Ba. Thus, these figures strongly suggest the existence of weak r-process as the origin of part of Sr.

5 Conclusion

We have constructed an inhomogeneous enrichment model of the Galactic Halo. The observed $\sim$ 300-fold dispersions in chemical abundances of metal-poor stars are explained by star formations induced by supernova explosions. Comparing the model predictions with observations, we have shown that r-elements must be produced by supernova of $8 - 10M_\odot$ or $\geq 30M_\odot$ stars.

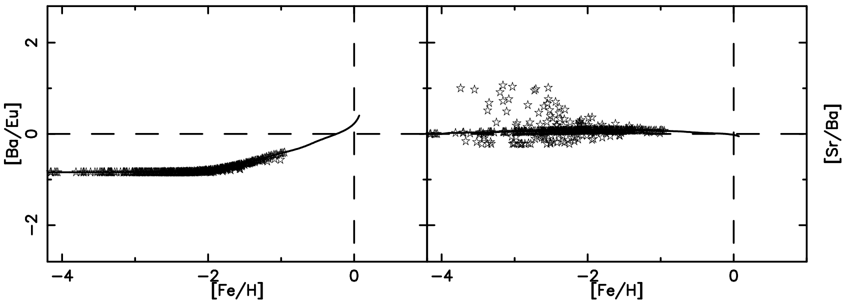

Fig. 4. a) [Ba/Eu] and b) [Sr/Ba] vs. [Fe/H] predicted by models with weak r-process. The mass ranges of main r- and weak r-process sites are assumed as SNII of $> 30M_{\odot}$ and $20 - 30M_{\odot}$ stars, respectively.

Especially, we have shown that the enhancements of [Sr/Ba] strongly suggest the existence of 'weak' r-process as origins of lower mass neutron-capture elements like Sr.

References

1. McWilliam, A., Preston, G. W., Sneden, C., & Searle, L. 1995, AJ 109, 2757
2. Ryan, S. G., Norris, J. E., & Beers, T. C. 1996, ApJ 471, 254
3. Sneden, C., McWilliam, A., Preston, G. W., Cowan, J. J., Burris, D. L., & Armosky, B. J. 1996, ApJ 467, 819
4. Ishimaru, Y., & Wanajo, S. 1999, ApJ 511, L33
5. Cioffi, D. F., McKee, C. F., & Bertschinger, E. 1988, ApJ 334, 252
6. Nomoto, K., et al. 1997a, Nucl. Phys. A 621, 467
7. Nomoto, K., Hashimoto, M., Tsujimoto, T., Thielemann, F. -K., Kishimoto, N., Kubo, Y., & Nakasato, N. 1997b, Nucl. Phys. A 616, 79
8. Mathews, G. J., Bazan, G., & Cowan, J. J. 1992, ApJ 391, 719
9. Hillebrandt, W., Nomoto, K., & Wolff, R. G. 1984, A&A 133, 175
10. Wheeler, J. C., Cowan, J. J., & Hillebrandt, W. 1998, ApJ 493, L101
11. Woosley, S. E., Wilson, J. R., Mathews, G. J., Hoffman, R. D., & Meyer, B. S. 1994, ApJ 433, 229
12. Takahashi, K., Witti, J., & Janka, H. -Th. 1994, A&A 286, 857
13. Otsuki, K., Tagoshi, H., Kajino, T., & Wanajo, S. 1999, ApJ in press
14. Wasserburg, G. J., Busso, M., & Gallino, R. 1996, ApJ 466, L109
15. Qian, Y. -Z. & Wasserburg, G. J. 1999, Phys. Rep., in press (astro-ph/9906259)

Metal-Poor Halo Stars as Tracers of ISM Mixing Processes During Halo Formation

Dominik Argast[1,2], Markus Samland[1], Ortwin E. Gerhard[1] and Friedrich-Karl Thielemann[2]

[1] Astronomisches Institut der Universität Basel, Venusstrasse 7, CH-4102 Binningen, Switzerland (argast@astro.unibas.ch)
[2] Institut für Physik der Universität Basel, Klingelbergstrasse 82, CH-4056 Basel, Switzerland (fkt@quasar.physik.unibas.ch)

Abstract. We discuss a stochastic halo formation model to compute the early chemical enrichment of the interstellar medium (ISM) of the halo. Contrary to 1-zone chemical evolution models, we are able to resolve local inhomogeneities in the ISM caused by single core-collapse supernovae. These inhomogeneities lead to different element abundance patterns in very metal-poor stars which can be seen as scatter in the abundances of halo stars with metallicities [Fe/H] < 2.0.

The early chemical evolution of the halo proceeds in different enrichment phases: At [Fe/H] < -3.0, the halo ISM is unmixed and dominated by local inhomogeneities caused by single core-collapse supernova (SN) events. For metallicities [Fe/H] > -2.0 the halo ISM is well mixed, showing an element abundance pattern integrated over the initial mass function. In the range $-3.0 <$ [Fe/H] < -2.0 a continuous transition from the unmixed to the well mixed ISM occurs. For some elements, like silicon, the scatter in the element-to-iron ratio [El/Fe] seen in the observations of metal-poor halo stars can be reproduced. On the other hand, the stellar yields of magnesium predict a scatter which, compared to the observations, is too large. This demonstrates the need for revised, self-consistent core-collapse SN yields.

1 The Model

Very metal-poor halo stars show a great diversity in their element abundances: the scatter in their element-to-iron ratios [El/Fe] is of order 1 dex. This scatter gradually decreases at higher metallicities until a mean element abundance is reached which corresponds to the [El/Fe] ratio of the stellar yields integrated over the initial mass function (IMF). The aim of our stochastic halo formation model is to understand the trends seen in the observations and to investigate how the metal-poor interstellar medium (ISM) in the halo evolves chemically.

Our model [1] is fully three dimensional and enables us to resolve local inhomogeneities in the ISM with a spatial resolution of 50 pc. All in all, we model a volume of $(2.5\ \mathrm{kpc})^3$, divided into 50^3 cells. Every cell of our grid contains detailed information about the enclosed ISM and the mass distribution of stars. We consider simultaneously the evolution of nine elements, the α-elements O, Mg, Si and Ca, the iron-peek elements Cr, Mn, Fe and Ni and the r-process element Eu.

Our initial conditions assume a halo ISM consisting of a homogeneously distributed single gas phase with primordial abundances and a density of 0.25 particles per cm^3, which gives a total mass of about $10^8\,M_\odot$ in a volume of $(2.5\ kpc)^3$. At each time-step 20 000 cells are chosen randomly and independently of each other and of the state of the enclosed ISM. Each selected cell may create a star with a probability proportional to the square of the local ISM density [2]. The mass of a newly formed star is chosen randomly from a Salpeter IMF. The lower and upper mass limits of the IMF are taken to be $0.1\,M_\odot$ and $50\,M_\odot$, respectively. Newly born stars inherit the abundance pattern of the ISM out of which they form, carrying therefore information about the state of the ISM at the place and time of their birth.

Stars in a range of $10-50\,M_\odot$ explode as core-collapse supernovae, resulting in an enrichment of the neighbouring ISM. Stellar yields are taken from Thielemann et al. [7] and Nomoto et al. [4] for all elements except Eu. Since there are no theoretical predictions of stellar Eu yields, we use the indirectly deduced yields of Tsujimoto & Shigeyama [8]. We do not include supernovae (SNe) of Type Ia, since we are only interested in the very early enrichment of the halo ISM, which is dominated by SNe of Type II. Of the stars with masses below $10\ M_\odot$, only the massive ones are assumed to evolve into planetary nebulae and to return slightly enriched material, while the low mass stars do not evolve significantly during the considered time.

Since the explosion energy of a core-collapse supernova (SN II) depends only slightly on the mass of its progenitor (see [9,7]), every SN II sweeps up a constant mass of about $5 \times 10^4\,M_\odot$ of gas [5,6]. Then the radius of the supernova (SN) remnant is computed from the local density of the ISM and lies typically between 100 pc and 200 pc. The ejecta of the SN II explosion and the swept up, enriched material are assumed to condense in a chemically well-mixed spherical shell. The material in the shell subsequently mixes with the ISM of the cells where the expansion of the remnant stopped. The star formation rate of cells influenced by the remnant will rise, since their density is higher than the average density of a cell and the probability to form a star is assumed to be proportional to the square of the local density. Stars which form out of material enriched by a single SN inherit its abundances and therefore show an abundance pattern which is characteristic for this particular progenitor mass.

The SN remnant expansion is the only dynamical process taken into account in our model. Therefore, this model has the least possible mixing of the ISM. This is the opposite limit as in the case of closed box models, which assume a complete mixing of the ISM at all times and are therefore not able to explain the scatter seen at low metallicities. We follow the evolution until the average iron abundance reaches [Fe/H] $= -1.0$. At this metallicity SN events of Type Ia, which we have not included in our model, would start to influence the ISM.

2 Results

Our calculations confirm that the incomplete mixing of the ISM during the halo formation plays a significant rôle in the early enrichment of the metal-poor gas. This can be seen in the [Si/Fe] and [Mg/Fe] ratios as function of [Fe/H], shown in Fig. 1 and Fig. 2. The dots show the [El/Fe] ratio of single model-stars. For comparison, observed metal-poor stars are represented by open squares. The numbered circles show the [El/Fe] and [Fe/H] ratios of a single SN II with the indicated mass. The [Fe/H] ratio in the shell of the SN remnants is determined by the mass of the exploding star and the $5 \times 10^4\,M_\odot$ of gas that are swept up by the shock front. This ratio represents the maximal abundance a *single* SN II can produce. On the other hand, the [El/Fe] ratio is determined solely by the stellar yields of a SN II and is independent of the mixing mass.

We divide the chemical enrichment process in the early evolution of the halo ISM into different enrichment stages: At very low metallicities ([Fe/H] < -3.0), only few stars exist, showing a considerable scatter in their [El/Fe] ratios which is given by the spread in metallicities of the SN models. The local inhomogeneities of the ISM begin to disappear when most of the gaseous SN remnants start to overlap. At the latest, this is the case when more or less every cloud in the halo was influenced at least once by a SN event, i.e. the total polluted mass is about equal to the total mass of the halo ISM. With the adopted mixing mass of $5 \times 10^4\,M_\odot$ this is the case at [Fe/H] ≈ -2.8. This metallicity gives an upper limit for the end of the early phase and the beginning of the transition to the well-mixed enrichment phase. The scatter in the metallicities gradually decreases from [Fe/H] $= -3.0$ to -2.0, reflecting the ongoing mixing process as more and more SNe pollute the ISM. At a metallicity of [Fe/H] > -2.0, the ISM can be considered well mixed, showing an IMF averaged abundance pattern as is observed in halo stars with a metallicity of $-2.0 <$ [Fe/H] < -1.0. Here we discuss only two of the nine elements considered in the model:

Silicon: The IMF averaged [Si/Fe] ratio and the scatter predicted by the stellar yields fit the observations perfectly, as shown in Fig. 1. The decrease in the scatter for higher metallicities and therefore the different enrichment phases of the halo ISM are clearly visible. At [Fe/H] < -3.0, the scatter in the model points reflects the scatter predicted by the stellar yields. During the transition from the unmixed to the well mixed ISM, in the range $-3.0 <$ [Fe/H] < -2.0, the scatter decreases steadily and consistent with observations, leading finally to the IMF averaged [Si/Fe] ratio at [Fe/H] > -2.0.

Magnesium: As can be seen in Fig. 2, the IMF averaged [Mg/Fe] ratio reproduces the mean abundance of the observed metal-poor stars nicely, with a deviation of less than 0.1 dex. However, the scatter in the data, although increasing at lower metallicities, does not match the large scatter of more than two dex predicted by the stellar yields. If we assumed a top-heavy IMF which favoured high-mass SNe, this problem could be solved. However, the

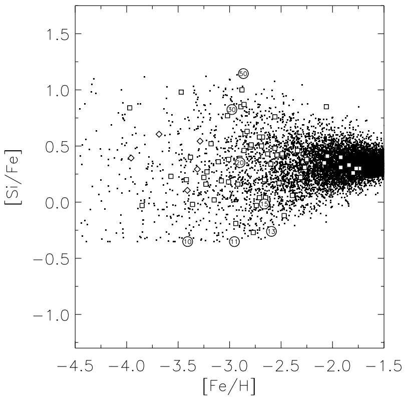

Fig. 1. Silicon-to-iron ratio [Si/Fe] as a function of metallicity [Fe/H]. Numbered circles depict stellar yields of SN II models of the indicated progenitor mass. Open symbols show observed stars, dots represent model stars

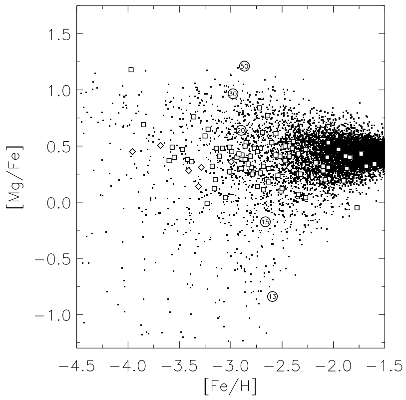

Fig. 2. The same as in Fig. 1 but for the [Mg/Fe] ratio. Note that there is no observed metal-poor star with [Mg/Fe] < 0.0, contrary to the model-stars which extend down to [Mg/Fe] < -1.0 because of the low Mg yields of 13 to 15 $M_\odot$ SNe

abundance pattern of the other elements should then also reflect this, which is not the case. This leaves us with two explanations: Either the stellar yields of Mg, or those of Fe are incorrect, or both. Since the exact location of the mass cut is not known, the actual Fe yields are not very well determined. Only the IMF integrated Fe-yields are constrained, but not necessarily their progenitor mass dependence [9,7]. In order to attain a fit to the observational data within our evolution model we would need to decrease the Fe yields of the 13 or 15 $M_\odot$ stars by a factor of six. Without adjusting Fe-yields for more massive stars, and assuming a standard Salpeter IMF, this would increase the IMF averaged [Mg/Fe] ratio by about 0.3 dex (a factor of two) and would therefore result in a much too high IMF averaged value. Moreover, every other abundance ratio would be affected by this change. On the other hand, the stellar yields of the α-element Mg could be too low for the 13 and 15 $M_\odot$ progenitors. The abundances of Mg are mainly determined in the hydrostatic burning phases; changing the Mg yields would therefore require to adjust the existing stellar models, which suffer from uncertainties in the theory of convection and the treatment of rotation.

3 Conclusion

In our stochastic chemical evolution model we have computed the evolution of the abundance in metal-poor halo stars for several elements (O, Mg, Si, Ca, Cr, Mn, Fe, Ni, Eu), and have investigated the mixing of the halo ISM.

At metallicities [Fe/H] < -3.0, the ISM is not mixed and is dominated by local abundance inhomogeneities caused by individual Type II SNe. A second phase at [Fe/H] > -2.0 is defined by a well mixed ISM with IMF averaged abundances. A continuous transition from the first to the second phase occurs between $-3.0 <$ [Fe/H] < -2.0.

We have found that the decrease of the observed abundance scatter with metallicity in metal-poor stars can be quantitatively reproduced only for some elements (Si, Ca, Eu). For most element ratios, with the employed nucleosynthesis yields and the adopted mixing mass, the observed decrease of the scatter is only qualitatively but not quantitatively reproduced. The predictions for O and Mg show a scatter which, compared to the observations, is too large, whereas the theoretical scatter in Ni is too small. Moreover, the observations of Cr and Mn show a decreasing trend with lower metallicity and only a different choice of mass cut as a function of progenitor mass [3] or as a function of metallicity would be able to rectify this. These problems argue strongly for a revision of the theoretical nucleosynthesis models and their extension to lower metallicities.

Nevertheless, the different enrichment phases of the halo ISM can be distinguished in every considered element and the rate of decrease of the abundance scatter with increasing metallicity is consistent with observations. This suggests that the early evolution of the halo ISM is indeed dominated by local chemical inhomogeneities whose importance gradually decreases as more and more SNe contribute to the enrichment of the metal-poor gas.

A more detailed discussion of the model and its results can be found in Argast et al. [1]. We would like to thank S. G. Ryan for helpful discussions and for providing us with some of the observational data. This work was supported by the Swiss Nationalfonds.

References

1. Argast, D., Samland, M., Gerhard, O. E., Thielemann, F.-K., 1999, submitted to A&A, astro-ph/9911178
2. Larson, R. B., 1988. In: R. E. Pudritz, M. Fich (eds.) Galactic and Extragalactic Star Formation. NATO ASI Series 232, 5, Kluwer, Dordrecht
3. Nakamura, T., Umeda, H., Nomoto, K., Thielemann, F.-K., Burrows, A., 1999, ApJ, 517, 193
4. Nomoto, K., Hashimoto, M., Tsujimoto, T., Thielemann, F.-K., Kishimoto, N., Kubo, Y., Nakasato, N., 1997, Nucl. Phys., A161, 79c13
5. Ryan, S. G., Norris, J. E., Beers, T. C., 1996, ApJ, 471, 254
6. Shigeyama, T., Tsujimoto, T., 1998, ApJ, 507, L 135
7. Thielemann, F.-K., Nomoto, K., Hashimoto, M., 1996, ApJ, 460, 408
8. Tsujimoto, T., Shigeyama, T., 1998, ApJ, 508, L151
9. Woosley, S. E., Weaver, T. A., 1995, ApJS, 101, 181

The EASE Scenario: Dynamical Study of the Supernova Phase

Geneviève Parmentier, Emannuel Jehin, Pierre Magain, Arlette Noels, and Anne Thoul

Institute of Astrophysics and Geophysics, University of Liège, Belgium

Abstract. We revisit the most often encountered argument against self-enrichment in globular clusters, namely the ability of a few number of supernovae to disrupt the proto-globular cloud. We show that, within the context of the Fall and Rees theory, primordial proto-globular cluster clouds may sustain several hundreds of Type II supernovae. Furthermore, the corresponding self-enrichment level is in agreement with galactic halo globular cluster metallicities.

1 The EASE Scenario

Accurate abundance determinations among a sample of 21 mildly metal-poor stars ([Fe/H]$\simeq -1$) have revealed the existence of two sub-populations of halo and thick disk field stars, namely Population IIa (hereafter PopIIa) and Population IIb (hereafter PopIIb). They differ by the behaviour of the s-process element versus the α element abundances. The PopIIa shows a correlation between the relative abundances of light s-process elements, e.g. Y, and α elements, e.g. Ti, with a slope smaller than one. The PopIIb presents a constant and maximum [Ti/Fe] value and varying values of [Y/Fe] starting at the maximum value reached by the PopIIa. Stars more metal-poor than [Fe/H]$=-1$ also follow these correlations, while the disk stars do not. Therefore, low metallicity stars do follow a universal relation described by the *two-branches diagram*, schematically illustrated in Fig. 1.

In [1], we have suggested a scenario which closely relates the origin of these stars to early globular cluster (hereafter GC) evolution. Indeed, GCs might provide halo and thick disk field stars through various dynamical processes, such as dislocation or *evaporation*. According to this scenario, PopIIa and PopIIb are related to two different stages of the GC's chemical evolution. In the first phase, some Type II supernovae (hereafter SNeII), from a first generation of metal-free stars, enrich the medium in heavy elements, notably in α elements. This is the *self-enrichment* process. In the second phase, low-mass stars *accrete* material ejected by AGB stars, enriching their surface in s-process elements. Depending on the time at which stars are ejected from GCs, during the first phase or after the onset of the second one, they will define either PopIIa or PopIIb. This is the scenario EASE, *Evaporation/Accretion/Self-Enrichment*. Both EASE chemical stages, namely self-enrichment and accretion, are also illustrated in Fig. 1. The major goal of this work is to perform a dynamical study of the first phase, the SNII phase.

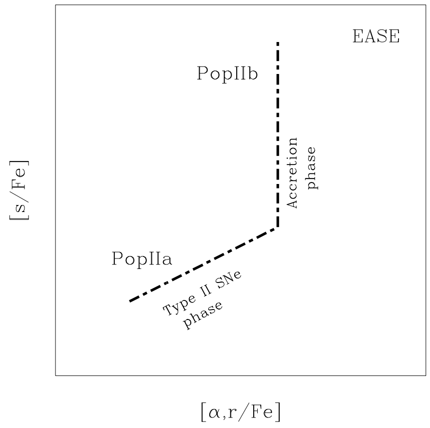

Fig. 1. EASE scenario

2 GC Formation Through Supershell Phenomenon

According to [2], the protogalaxy is a primordial two-phase medium, made up of cold and dense clouds embedded in a hot and diffused protogalactic background. A typical value for the temperature of the cold phase is 10^4 K, where the radiative cooling rate drops sharply in a metal-free medium. The cold clouds are supposed to be proto-globular cluster clouds (hereafter PGCCs), the progenitors of galactic GCs. We will describe them as isothermal spheres in hydrostatic equilibrium – their density profile $\varrho(r)$ scales therefore as r^{-2} – and assume that there is pressure equilibrium at the interface between the hot and the cold media. According to the Schmidt law, the denser the medium is, the quicker the stars will form. We therefore expect the formation of a first generation of stars in the PGCC central regions. After a few millions years, the massive stars of this first generation explode as SNeII. The blast waves associated with the explosions trigger the formation and the expansion of a supershell in which all the cloud material is swept. This supershell gets chemically enriched with the heavy elements released by the SNeII. Since the cloud has produced its own source of chemical enrichment, this phenomenon is called *self-enrichment*. In the supershell, in which all the cloud material gets compressed, the formation of a second generation of stars is triggered. This second generation forms a proto-globular cluster. In what follows, we restrict our analysis to *halo* GCs.

This scenario was proposed by [3] and further developed by [4] and [5]. However, even after these works, a recurrent argument has often been used against self-enrichment, namely the SN energetics. Since the binding energy of GCs today is of the same order of magnitude than the kinetic energy released by one SNII, several authors, e.g. [6], have concluded that a still gaseous proto-cluster could be immediately disrupted. Therefore, GCs could not be self-enriched. However, it is important to distinguish the kinetic energy released by the exploding stars from the kinetic energy effectively deposited in the Interstellar Medium (hereafter ISM). We therefore suggest another criterion for disruption : the equality between the binding energy of the cloud and the kinetic energy of the shell when all the cloud has just been swept ([7]).

3 PGCC Model

The density profile of an isothermal sphere in hydrostatic equilibrium is

$$\rho(r) = \frac{1}{4\pi}\frac{M}{R}r^{-2} \tag{1}$$

where M and R are its mass and its radius. The requirement of pressure equilibrium at the interface sets the value of M :

$$M = \sqrt{\frac{2}{\pi}}\left(\frac{kT}{\mu m_h}\right)^2 G^{-3/2} {P_{\mathrm{h}}}^{-1/2} \tag{2}$$

where k is the Boltzmann constant, T, the PGCC temperature, μ, its mean molecular weight (μ=1.2), G, the gravitational constant and P_{h}, the pressure value of the hot protogalactic background confining the PGCC.
In the same way, R and M are related by

$$R_{100} = \chi M_6^{1/3} \tag{3}$$

where M_6 is the cloud mass expressed in units of $10^6\,\mathrm{M}_\odot$ and R_{100}, its radius expressed in units of 100 pc. The parameter χ is related to P_{h} (expressed in dyne.cm^{-2}) by

$$\chi = \left(\frac{3.7\times10^{-12}}{P_{\mathrm{h}}}\right)^{1/3} . \tag{4}$$

Equations (1)–(4) define the medium through which the supershell will propagate.

4 Supershell Velocity

The equations describing the supershell motion were defined by [8]. Under the reasonable assumption of a constant rate of the SNII explosions, the supershell velocity v is also constant in time and can be deduced from

$$3v^3 + 3\left(\frac{kT}{\mu m_H} + \frac{GM}{2R}\right)v = 2\dot{E}_o\frac{R}{M} , \tag{5}$$

where $\dot{E}_o$ is the rate at which the SNII energy is supplied. The second and third terms on the left-hand-side account for the decelerating effects respectively provided by the pressure external to the shell and by the shell gravity. With the different hypothesis about PGCCs, (5) can be reduced to

$$v_{10}^3 + 1.4 v_{10} = \frac{N E_{51}}{\Delta t_6} \tag{6}$$

where v_{10} is the shell velocity expressed in units of $10\,\mathrm{km.s^{-1}}$, N is the total number of SNeII and Δt_6, the duration of the SNII phase.

5 Disruption Criterion

We now introduce our criterion for disruption, namely the equality between the kinetic energy of the ISM, therefore of the supershell, and the binding energy of the PGCC :

$$\frac{1}{2} v^2 = \frac{GM}{R} \ . \tag{7}$$

Combining (2), (3), (4) and (6), and assuming a duration of the SNII phase of 30 millions years, we obtain an estimation of the maximum number of SNeII a PGCC can sustain without being disrupted, i.e.,

$$N E_{51} = 200 \ . \tag{8}$$

6 Self-Enrichment Level

Is the dynamical limit defined above in agreement with the metallicities observed in galactic halo GCs ? To answer this question, we define relations between the mass of a primordial gas cloud and the number of SNeII necessary to reach a given final metallicity. We assume that each massive star whose mass m is at least $12\,\mathrm{M}_\odot$ releases a mass of metals given by $0.3\mathrm{m}-3.5$ (in units of one solar mass) [9]. The upper limit of the spectrum is assumed to be $60\,\mathrm{M}_\odot$. The stars whose mass is between 9 and $12\,\mathrm{M}_\odot$ release unsignificant amounts of heavy elements. However, their dynamical impact on the cloud must be considered and they are therefore included in the total number N of SNeII. In Fig. 2, the relations between Log M and N for three given metallicities, typical of the galactic halo ([Fe/H]$=-1$, -1.5 and -2) are shown, as well as the dynamical constraint defined in Sect. 5 for a protogalactic background pressure of $2.5\times10^{-10}\,\mathrm{dyne.cm^{-2}}$. We see that a metallicity of -1.5 can be reached through self-enrichment. Therefore, the self-enrichment process may provide a clue to the metal amounts observed today in galactic halo GCs.
An interesting consequence of this model is the dependence on the value of P_h of the location of the dynamical constraint among the iso-metallicity curves (see (2) and (8)). The higher the pressure is, the higher the final metallicity will be. Therefore, this model provides an explanation to the metallicity gradient observed throughout the Old Halo [10].

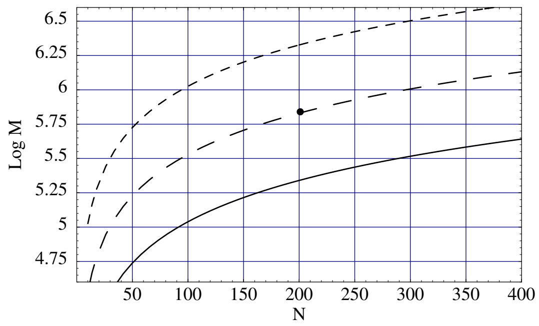

Fig. 2. Relations between the mass of the PGCC and the number of SNeII exploding in its central regions for three self-enrichment levels (*dashed curves*), from up to bottom, [Fe/H]= $-2, -1.5, -1$. The point represents the dynamical constraint described in the text for a hot protogalactic background pressure of 2.5×10^{-10} dyne.cm^{-2}

References

1. Jehin E., Magain P., Neuforge C., Noels A., Parmentier G., Thoul A.A. (1999) Abundance Correlations in Mildly Metal-Poor Stars. A&A **341**, 241–255
2. Fall S.M., Rees M.J. (1985) A Theory for the Origin of Globular Clusters. ApJ **298**, 18–26
3. Cayrel R. (1986) And if Population III were Population II. A&A **168**, 81–88
4. Brown J.H., Burkert A., Truran J.W. (1991) On the Formation of Globular Clusters. I. Dynamical Limits on Globular Cluster Metallicities. ApJ **376**, 115–122
5. Brown J.H., Burkert A., Truran J.W. (1995) On the Formation of Globular Clusters. II. Early Dynamical Evolution. ApJ **440**, 666–673
6. Meylan G., Heggie D.C. (1997) Internal Dynamics of Globular Clusters. A&AR **8**, 1–143
7. Parmentier G., Jehin E., Magain P., Neuforge C., Noels A., Thoul A.A. (1999) The Self-Enrichment of Galactic Halo Globular Clusters : a Clue to their Formation. Accepted for publication in A&A
8. Castor J., McCray R., Weaver R. (1975) Interstellar Bubbles. ApJ **200**, L107–L110
9. Woosley S.E., Weaver T.A. (1995) The Evolution and Explosion of Massive Stars. II. Explosive Hydrodynamics and Nucleosynthesis. ApJSS **101**, 181–235
10. Zinn, R. (1992) The Galactic Halo Globular Cluster Systems : Evidence for Accretion. In: Smith G.H., Brodie J.P.(Eds) The Globular Clusters-Galaxy Connection, Eleventh Santa Cruz Summer Workshop in Astronomy and Astrophysics, University of California, Santa Cruz, USA, July 19–29, 1992. Astronomical Society of the Pacific Conference Series, Volume 48, 38–47

The EASE Scenario: A New Origin for Metal-Poor Stars?

Emmanuel Jehin, Pierre Magain, Arlette Noels, Geneviève Parmentier, and Anne Thoul

Institut d'Astrophysique et de Géophysique, Université de Liège, 5 avenue de Cointe, 4000 Liège, Belgium

Abstract. We have analysed high resolution and high signal-to-noise spectra of 21 mildly metal-poor stars. The correlations between the relative abundances of 16 elements have been studied, with a special emphasis on the neutron-capture ones. This analysis reveals the existence of two sub-populations of field metal-poor stars which differ by the behaviour of the s-process elements versus the α and r-process elements. We suggest a scenario for the formation of metal-poor stars, which closely relates the origin of these stars to the evolution of globular clusters.

1 Introduction

Traditional abundance analyses of metal-poor stars consist in determining abundance ratios of chemical elements as a function of the overall metallicity ([Fe/H]). These trends are then compared to predictions from models of nucleosynthesis and chemical evolution of the Galaxy, in order to provide constraints on the sites and mechanisms for element synthesis.
However, many of these abundance ratios show rather considerable star-to-star scatter, so that they provide only weak constraints on the models. With the improvement of observing and spectroscopic analysis techniques, it is now possible to reduce considerably the observational uncertainties in the abundance determinations. With high quality data, we can therefore investigate the real cosmic scatter in the relative abundances at a given metallicity, and look for correlations between different elements.

2 Observations and results

We have performed [1] such an analysis for a sample of 21 unevolved metal-poor stars with one tenth of the solar metallicity. High resolution (65 000) and high signal-to-noise (200) spectra have been obtained with the Coudé Auxilliary Telescope (CAT) at the European Southern Observatory (La Silla, Chile). As we are especially interested in distinguishing minute variations from star to star, the analysis was carried out differentially inside the sample.

Looking for correlations between the element abundances, we found that the

α elements and the iron peak elements are well correlated with each other. The abundances of the rapid neutron-capture elements (r-process elements) are well correlated with those of the α elements, which is in agreement with the generally accepted idea that those elements are produced during the explosion of massive stars. For the slow neutron-capture elements (s-process elements), we find that the stars can be separated into two subpopulations. For those in Pop IIa, the abundances of the s-process elements vary little while that of the α elements increase up to a maximum value. The stars in Pop IIb show a large range in their s-process elements abundances, while they have a constant and maximum value for the abundances of the α elements. We called this behavior the " two-branches diagram ". When we add data coming from stars in other high quality studies, we observe that this behavior is well reproduced for stars with metallicities $<$ -0.6.

3 The EASE Scenario

We suggest a scenario for the formation and origin of the metal-poor stars, which provides an explanation for the relation described by the two-branches diagram. This scenario provides a link between the field halo stars (FHS) and globular clusters (GCs):
(1) FHS were born in (proto-) GCs;
(2) GCs have undergone a chemical evolution [2]; their evolution can be separated in two distinct phases;
(3) during the first phase, massive (first generation) stars in the proto-GC cloud evolve, ending their lives as supernovae and ejecting α elements and r-process elements into the ISM. A second generation of stars forms out of this enriched ISM. The proto-GC can become unstable and get disrupted, the lower-mass stars forming Pop IIa;
(4) during the second phase if the GC has survived, intermediate mass stars reach the AGB, ejecting s elements into the ISM through stellar winds or superwinds events; this matter can be accreted by the lower mass stars, enriching those stars in s elements [3];
(5) some of these low mass stars get dispersed in the halo when the GC is disrupted or evaporate from the GCs; they form Pop IIb FHS.

References

1. Jehin E., Magain P., Neuforge C., Noels A., Parmentier G., Thoul A. 1999, A&A 341, 241
2. Parmentier G., Jehin E., Magain P., Neuforge C., Noels A., and A. Thoul, 1999, A&A, in press
3. Thoul A., Jorissen A., Goriely S., Jehin E., Magain P., Noels A. and Parmentier G., 1999, in *Proceedings of the 35th Liège International Astrophysical Colloquium*, Eds. A.Noels et al., in press

Numerical Simulations of the Galaxy Formation

Kenji Bekki and Masashi Chiba

National Astronomical Observatory Mitaka, Tokyo 181-8588, Japan

Abstract. We numerically investigate whether the CDM model can reproduce reasonably well chemical, kinematical, and structural properties of the Galactic stellar halo.

1 Introduction

It is a longstanding and remarkable problem when and how the Galaxy was formed. In particular, the origin of structural, kinematical, and chemical properties observed in the Galactic metal-poor stellar halo components, which are generally considered to contain valuable information on the early dynamical evolution of the Galaxy, has been extensively discussed in terms of the collapse time scale of the Galaxy (e.g., [5,6]). Recent observational studies of the metal-poor stellar halo by the Hipparcos satellite have provided unprecedentedly wealthy data on the accurate proper motion of the halo components and thus revealed the detailed structural and kinematical properties of the halo. Comparing these up-to-date Hipparcos (and ground-based telescope) data by [4] and [1] with numerical results based on the Cold Dark Matter (CDM) model of galaxy formation, we discuss whether the CDM model can explain successfully the observed fundamental properties of the Galactic halo, and thereby assess the validity of the CDM model.

2 Model

We numerically investigate the chemodynamical evolution of a rigidly rotating homogeneous gas sphere with the initial mass of $6.0 \times 10^{11} M_{\odot}$ and the size of 45 kpc. The initial spin parameter, over-density, and gas mass fraction are set to be 0.08, 0.29 (corresponding to 2.5 σ peak for b=2 CDM spectrum), and 0.1, respectively. Interstellar gas is represented by the collection of discrete gas clouds (the so-called sticky particle method) and the star formation of the gas is modeled by using the Schmidt law with the exponent $n = 2$. We adopt an instantaneous mixing approximation with the chemical yield of 0.02 for the chemical evolution of each gas clouds and thereby solve time-evolution of metallicity of stellar and gaseous components of the Galaxy. Using this model, we particularly investigate the relation between orbital eccentricity, e, and metallicity, [Fe/H], for metal-poor halo components with [Fe/H] < -1.6. More details for the numerical model and results are given in [2].

3 Result

Figure 1 clearly shows that there is no correlation between e and [Fe/H], which is consistent with recent observational results by [3]. Figure 1 furthermore demonstrates that low-e ($e < 0.4$) and low metallicity ([Fe/H]< -1.6) halo stars can be successfully reproduced in the CDM model, which implies that dissipative merging between CDM sub-galactic clumps in the Galactic early evolution plays a vital role in determining the fundamental kinematics of the Galactic stellar halo. Star formation producing metal-poor halo components is rather extended ($\sim$ 2Gyr) in the present CDM model of the Galaxy formation, and consequently some metal-poor halo stars (in particular, those formed in later phase of the Galactic collapse) does not suffer so seriously from rapid change of gravitational potential of the collapsing Galaxy and thereby preserve initial (nearly) circular orbit. This is one of the essential reasons for the existence of the low-e and low metallicity halo stars. We here stress that although the standard CDM model can reproduce qualitatively the observed [Fe/H]-e relation of the Galaxy, it can not reproduce quantitatively the observed cumulative e distribution of stellar halos of the Galaxy [3].

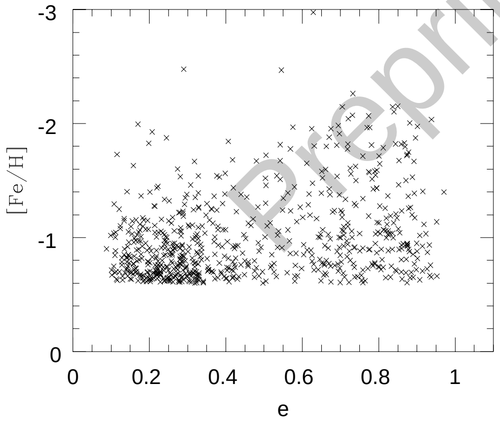

Fig. 1. [Fe/H]-e relation for metal-poor halo stars formed by dissipative merging between CDM sub-galactic clumps.

References

1. Beers, T. C., et al. (1999) AJ, in preparation.
2. Bekki, K., Chiba, M. (1999) in preparation.
3. Chiba, M., Beers, T. C., Yoshii, Y. (1999) AJ, in preparation
4. Chiba, M., Yoshii, Y. (1998) AJ, **115**, 168
5. Eggen, O. J., Lynden-Bell, D., Sandage, A.R. (1962) ApJ, **136**, 748
6. Searle, L., Zinn, R. (1978), ApJ, **225**, 357

Cosmological Reionization by Stellar Sources

Nickolay Y. Gnedin

University of Colorado, Boulder, CO 80303, USA

Abstract. I use cosmological simulations that incorporate an approximation of three-dimensional radiative transfer to investigate the process of the reionization of the universe by ionizing radiation from proto-galaxies. Reionization proceeds in three stages and occupies a large redshift range from $z \sim 15$ until $z \sim 5$. During the first, "pre-overlap" stage, H II regions gradually expand into the low density IGM, leaving behind neutral high density protrusions. During the second, "overlap" stage, that occurs in about 10% of the Hubble time, H II regions merge and the ionizing background rises by a large factor. During the third, "post-overlap" stage, remaining high density regions are being gradually ionized as the required ionizing photons are being produced.

Residual fluctuations in the ionizing background reach significant (more than 10%) levels for the Lyman-alpha forest absorption systems with column densities above $10^{14} - 10^{15}\,\mathrm{cm}^{-2}$ at $z = 3$ to 4.

1 Introduction

Existing ground based observations of the CMB on sub-degree angular scales suggest that the gas content of the universe was mostly neutral since recombination at $z \sim 1000$ until about $z \sim 100$ [1,2], because earlier reionization would have brought the last scattering surface to lower redshift, smoothing the intrinsic CMB anisotropy. At the same time we know that the universe is highly ionized since $z \approx 5$, from observations of the spectra of quasars with the highest redshifts [3–5]. This change of the ionization state of the universe from neutral to highly ionized is called *reionization*.

The understanding of the crucial role that the full 3D radiative transfer plays in the physics of reionization prompted the first attempts to develop numerical techniques to incorporate the radiative transfer into numerical simulations [6]. While they were able to develop an algorithm for an exact implementation of the full 3D radiative transfer into cosmological simulations, their algorithm is appropriate for following the radiation field in the case when there are only a few sources within the volume with the size of the mean free path of an ionizing photon. When the number of sources within this volume increases, as is the case after all H II regions overlap, their method becomes prohibitively expensive.

In this paper I adopt a somewhat different approach. Rather than trying to model the radiative transfer exactly, I develop an *approximation*, which is sufficiently fast computationally. I validate the adopted approximation on a series of spherically symmetric test cases, for which the full radiative transfer can be solved exactly at a modest computational expense.

Having developed the means to follow the full 3D spatially inhomogeneous and time-dependent radiative transfer, I apply them to modeling the process of reionization of the universe in a specific scenario when sources of ionizing radiation are stars (grouped into proto-galaxies).

2 Results

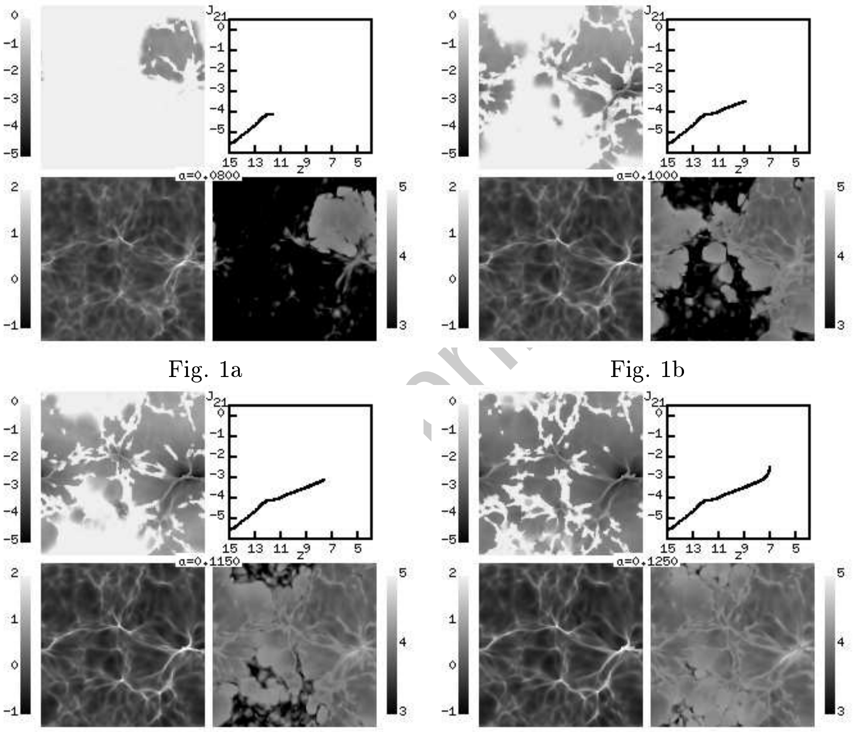

Fig. 1a Fig. 1b

Fig. 1c Fig. 1d

Fig. 1. A thin slice through the simulation volume at eight different epochs: (a) $z = 11.5$, (b) $z = 9$, (c) $z = 7.7$, (d) $z = 7$, (e) $z = 6.7$, (f) $z = 6.1$, (g) $z = 5.7$, (h) $z = 4.9$. Shown are neutral hydrogen (*upper-left*), gas density (*lower-left*), gas temperature (*lower-right*), and $\lg(J_{21})$ as a function of redshift (*upper-right*).

We can now look at a general description of the reionization process, as reflected in the simulations. In order to visualize the process, I show in Figure 1 a thin ($15h^{-1}$ comoving kiloparsecs deep) slice through the computational box taken at a random place. The three panels show in a logarithmic stretch

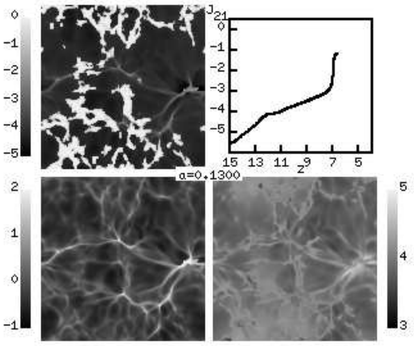

Fig. 1e

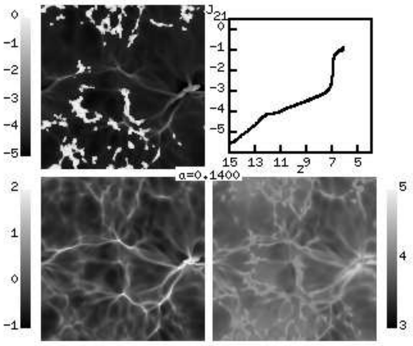

Fig. 1f

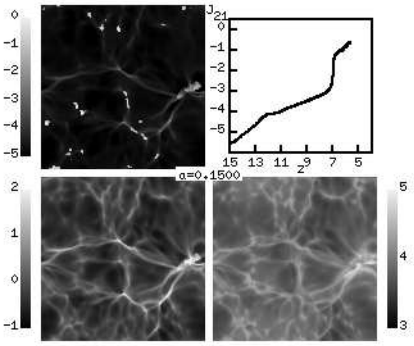

Fig. 1g

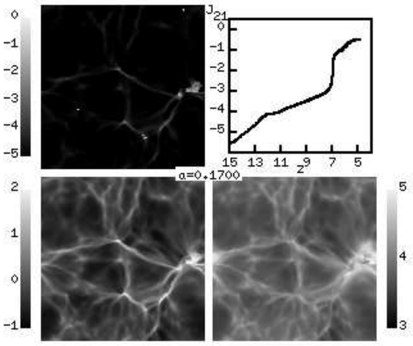

Fig. 1h

the neutral hydrogen (upper left panel), the gas density (lower left panel), and the gas temperature (lower right panel). The upper right panel shows the evolution of the ionizing intensity (logarithmically scaled) versus the redshift. The scale bars next to respective panels show the correspondence between the color and the numeric scale. The epoch as measured by the scale factor $a \equiv 1/(1+z)$ is labeled at the center of each plot.[1]

I can now describe the general features of reionization. The reionization starts (Fig. 1a) with ionization fronts propagating from proto-galaxies located in high density regions into the voids, leaving the high density outskirts of an object still neutral, because at high density the recombination time is very short, and there are not enough photons to ionize the high density regions. As an ionization front moves on with the H II region forming behind it, it leaves behind high density regions which require many more photons to get ionized than is available at that moment (Fig. 1a-d). This stage of the reionization process can be called "pre-overlap", and it extends over a considerable range of redshifts $\Delta z \sim 5$ around $z \sim 10$. During this time the high density regions

[1] An MPEG movie of the simulation and a preprint of the full paper are available at `http://casa.colorado.edu/~gnedin/GALLERY/rei_p.html`.

around the source are slowly becoming ionized, whereas high density regions far from the source remain neutral. The ionizing intensity at this time remains low and is slowly increasing with time. However, since the radiation field is highly inhomogeneous at this time, the ionizing intensity J_{21}, which is by definition a space-average, has only a formal meaning.

By $z \approx 7$ the H II regions start to overlap (Fig. 1d), with the result that the number of sources shining at an average place in the universe increases, and the ionizing intensity starts to rise rapidly. The process of reionization enters its second stage, the "overlap", which is quite rapid (Fig. 1d-e). As the ionizing intensity is rapidly increasing, the last remains of the neutral low density IGM are quickly eliminated, the mean free path increases by some two orders of magnitude (as explained below) over a Hubble time or so, and voids become highly ionized (neutral fraction of the order of 10^{-5}). The high density regions at this moment are still neutral, as the number of ionizing photons available is not sufficient to ionize them.

After the overlap is complete, the universe is left with highly ionized both low density regions and some of the high density ones (which happened to lie close to the source, where the local value of the ionizing intensity is higher than the spatial average). High density regions far from any source remain neutral. This stage can be called "post-overlap", and is well described by the semi-analytic model of Miralda-Escudé et al. [7]. As time goes on, and more and more ionized photons are emitted, the high density regions are gradually being eaten away (Fig. 1e-g), and the spatially averaged ionizing intensity J_{21} continues to rise slowly until it flattens out at $z \sim 5$ (Fig. 1g). The latter effect is however likely to be an artifact of a finite simulation box, as by this time the mean free path exceeds the box size by about a factor of 10 (as is shown below), and the simulation runs out of high enough density peaks, which would be present in the real universe (or a larger box simulation), and fails to reproduce the reality even on a semi-qualitative level.

Therefore, the recent argument of whether reionization is "fast" or "slow" (see, for example, [7] versus [8] or [9]) is, in large part, a question of terminology. If one considers the whole process of reionization, which consists of "pre-overlap", "overlap", and "post-overlap", one inevitably concludes that reionization is slow (i.e. taking place over a Hubble time or longer). However, if one looks only at the process of "overlap" and labels it reionization, then one concludes that reionization is fast.

2.1 Reionization and the Lyman-alpha forest

An important consideration that severely affects our ability to model the Lyman-alpha forest is how homogeneous the ionizing background is. Figure 2 shows the mean and rms fluctuation in the local ionizing background as a function of gas density at three values of redshift. As can be seen, there is essentially no evolution in the spatial distribution of the ionizing radiation in the low density regime, and gas with overdensities in excess of about 10

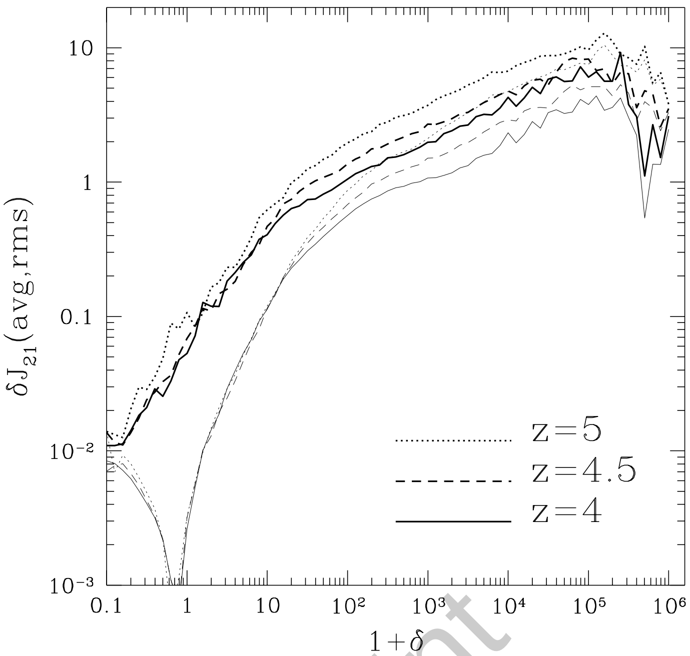

Fig. 2. A thin slice through the simulation volume at eight different epochs: (*a*) $z = 11.5$, (*b*) $z = 9$, (*c*) $z = 7.7$, (*d*) $z = 7$, (*e*) $z = 6.7$, (*f*) $z = 6.1$, (*g*) $z = 5.7$, (*h*) $z = 4.9$. Shown are neutral hydrogen (*upper-left*), gas density (*lower-left*), gas temperature (*lower-right*), and $\lg(J_{21})$ as a function of redshift (*upper-right*).

is subject to severe (more than 30%) inhomogeneities in the ionizing background.

References

1. Bond, J. R., & Jaffe, A. H. 1998, Phil. Trans. Royal Soc. Lon. A, in press (astro-ph 9809043)
2. Griffiths, L. M., Barbosa, D., & Liddle, A. D. 1998, MNRAS, in press (astro-ph 9812125)
3. Giallongo, E., D'Odorico, S., Fontana, A., McMahon, H. G., Savaglio, S., Cristiani, S., Molaro, P., & Treverse, D. 1994, ApJ, 425, L1
4. Williger, G. M. et al. 1994, ApJ, 453, L57
5. Songaila, A., Hu, E. M., Cowie, L. L., & McMahon, R. G. 1999, ApJ, 525, L5
6. Abel, T., Norman, M. L., & Madau P. 1999, ApJ, 523, 66
7. Miralda-Escudé, J., Haehnelt, M., & Rees, M. J. 1999, ApJ, in press (astro-ph/9812306)
8. Gnedin, N. Y., & Ostriker, J. P. 1997, ApJ, 486, 581
9. Madau, P., Haardt, F., & Rees, M. J. 1999, ApJ, 514, 648

The Impact of Pop III Stars on Reionization

Andrea Ferrara[1] and Benedetta Ciardi[2]

[1] Osservatorio Astrofisico di Arcetri, I-50125 Firenze, Italy
[2] Universita' di Firenze, I-50125 Firenze, Italy

Abstract. As the first stars form in the universe they produce radiation and synthesize heavy elements. The former process affects the reionization of the universe and it is regulated by a series of feedbacks involving the molecular hydrogen chemical network; the second one pollutes the intergalactic medium to the levels observed in the low column density Lyα forest. We quantify here the relevance of the first stars for both phenomena.

1 Introduction

Current models of cosmic structure formation based on CDM scenarios predict that the first stars in the universe form in tiny mini-galactic aggregates. These collapsed, luminous (PopIIIs) objects should form at redshift $z \approx 30$ and have a total mass $M \approx 10^6 M_\odot$ or baryonic mass $M_b \approx 10^5 M_\odot$ This conclusion is reached by requiring that the cooling time, t_c, of the gas is shorter than the Hubble time, t_H, at the formation epoch. In a plasma of primordial composition the only efficient coolant in the temperature range $T \leq 10^4$ K, the typical virial temperature of PopIII dark matter halos, is represented by H_2 molecules whose abundance increases from its initial post-recombination relic value to higher values during the halo collapse phase.

During the collapse, if fragmentation occurs, a stellar cluster is likely to be formed with a stellar mass, M_*, which depends on the (unknown) details of the star formation process. An educated guess, based both on the experimental data available for the Galaxy and on theoretical arguments, suggests that $M_* \approx 10^{2-3}$. The number of massive stars and supernovae produced depends on the postulated IMF; if the latter is not too steep, it is reasonable to expect that the Pop III star cluster will be a source of UV/ionizing photons, (explosive) energy and heavy element injection in the surrounding environment. Thus, reionization and metal enrichment of the intergalactic medium are intimately connected to and governed by the processes regulating star formation in the early universe, i.e. *radiative* (due to ionizing and H_2-photodissociating photons) and *stellar* (due to SN explosions) feedbacks.

2 Feedback Effects in the Early Universe

Reionization of the universe has occurred in a highly inhomogeneous way, as the first stars formed inside PopIII objects. Their ionizing radiation produced HII regions in the surrounding IGM, but their UV photons started to photodissociate H_2 molecules in the neighbor objects, thus preventing their collapse. This process is known as radiative feedback. However, even if some PopIIIs could form, their existence was not guaranteed: due to their low masses, a few SNe could blow away their gas and prevent further star formation. We define this process as stellar feedback. We discuss these two types of effects briefly below; a detailed description can be found in Ciardi, Ferrara, Governato & Jenkins ([1], CFGJ).

2.1 Radiative Feedback

In addition to the ionizing flux, the first objects will also produce UV radiation which could in principle introduce long range feedbacks on nearby collapsing halos. Particularly relevant is the soft UV background in the LW bands, as by dissociating the H_2, it could influence the star formation history of other small objects preventing their cooling.

Ciardi, Ferrara & Abel [2] have shown that the UV flux from these objects results in a soft (Lyman-Werner band) UV background (SUVB), J_{LW}, whose intensity (and hence radiative feedback efficiency) depends on redshift. At high redshift the radiative feedback can be induced also by the direct dissociating flux from a nearby object. In practice, two different situations can occur: i) the collapsing object is outside the dissociated spheres produced by preexistent objects: then its formation could be affected only by the SUVB ($J_{LW,b}$), as by construction the direct flux ($J_{LW,d}$) can only dissociate molecular hydrogen on time scales shorter than the Hubble time inside this region; ii) the collapsing object is located inside the dissociation sphere of a previously collapsed object: the actual dissociating flux in this case is essentially given by $J_{LW,max} = (J_{LW,b} + J_{LW,d})$. It is thus assumed that, given a forming Pop III, if the incident dissociating flux ($J_{LW,b}$ in the former case, $J_{LW,max}$ in the latter) is higher than the minimum flux required for negative feedback (J_s), the collapse of the object is halted. This implies the existence of a population of "dark objects" which were not able to produce stars and, hence, light.

To assess the minimum flux required at each redshift to drive the radiative feedback we have performed non-equilibrium multifrequency radiative transfer calculations for a stellar spectrum (assuming a metallicity $Z = 10^{-4}$) impinging onto a homogeneous gas layer, and studied the evolution of the following nine species: H, H^-, H^+, He, He^+, He^{++}, H_2, H_2^+ and free electrons for a free fall time. We can then define the minimum total mass required for an object to self-shield from an external flux of intensity $J_{s,0}$ at the Lyman limit, as $M_{sh} = (4/3)\,\pi\langle\rho_h\rangle R_{sh}^3$, where $\langle\rho_h\rangle = \langle\rho_b\rangle\Omega_b^{-1}$ is the mean dark matter density of the halo in which the gas collapses; R_{sh} is the shielding radius beyond which molecular hydrogen is not photodissociated and allowing the collapse to take place on a free-fall time scale.

Values of M_{sh} for different values of $J_{s,0}$ have been obtained at various redshifts and will be then used in the reionization calculations discussed below. Protogalaxies with masses above M_H for which cooling is predominantly contributed by Lyα line cooling will not be affected by the negative feedback studied here. The collapse of very small objects with mass $< M_{crit}$ is on the other hand made impossible by the cooling time being longer than the Hubble time. Thus the only mass range in which negative feedback is important lies approximately in $10^6 - 10^8 M_\odot$, depending on redshift. In order for the negative feedback to be effective, fluxes of the order of $10^{-24} - 10^{-23}$erg s^{-1} cm^{-2} Hz^{-1} sr^{-1} are required. These fluxes are typically produced by a Pop III with baryonic mass $10^5 M_{b,5} M_\odot$ at distances closer than $\simeq 21 - 7 \times M_{b,5}^{1/2}$ kpc for the two above flux values, respectively, while the SUVB can reach an intensity in the above range only after $z \approx 15$. This suggests that at high z negative feedback is driven primarily by the direct irradiation from neighbor objects in regions of intense clustering, while only for $z \leq 15$ the SUVB becomes dominant.

2.2 Stellar Feedback

Once the first stars have formed in the host protogalaxy, they can deeply influence the subsequent star formation process through the effects of mass and energy deposition due to winds and supernova explosions. While low mass objects may experience a blowaway, expelling their entire gas content into the IGM and quenching star formation, larger objects may instead be able to at least partially retain their baryons. However, even in this case the blowout induces a decrease of the star formation rate due to the global heating and loss of the galactic ISM. These two regimes are separated by a critical mass, M_{by}, explicitly calculated in CFGJ (see also [5]).

For the relatively small objects present during the reionization epoch $30 \geq z \geq 10$ the importance of these stellar feedbacks can hardly be overlooked. To understand the role of stellar feedback, let us consider a collapsed object with mass lower than M_{by}. Then the star formation is suddenly halted as the entire gas content is removed. In this case, the ionizing photon production will last only for a time interval of order $t_{OB} \approx 10^7$ yr, the mean lifetime of the massive stars produced initially; after this phase, the ionized gas around the source will start to recombine at a fast rate as a result of the highly efficient high z Compton cooling, rapidly decreasing the temperature inside the ionized region. Due to the short lifetime and recombination time scales, these object will only produce transient HII regions which will rapidly recombine and disappear. The blowaway mass depends weakly on the baryon-to-star conversion efficiency (approximately to the 1/4 power). At $z \approx 20$ objects with gas masses $\leq 10^7 M_\odot$ are blown away and the number of objects suffering blowaway decreases with redshift.

3 Reionization History Driven by Feedbacks

We have determined the spatial distribution of the ionizing sources from high resolution numerical N-body simulations within a periodic cube of comoving length $L = 2.55h^{-1}$ Mpc for a critical density cold dark matter model (Ω_0=1, h=0.5 with σ_8=0.6 at z=0). This allows us to describe the topology of the ionized and dissociated regions at various cosmic epochs and derive the evolution of H, He, and H_2 filling factors, soft UV background, cosmic star formation rate and the final fate of ionizing objects. There are three free parameters in the computation: f_b, the fraction of virialized baryons that is able to cool and become available to form stars, $f_\star$ the star formation efficiency, and f_{esc} the photon escape fraction from the proto-galaxy. The main results can be summarized as follows. For the reference case (Run A) presented by CFGJ, in which the values of the free parameters have been fixed at $f_b = 0.08, f_\star = 0.15, f_{esc} = 0.2$, galaxies are able to reionize the neutral atomic hydrogen by redshift $z\approx10$, while molecular hydrogen is completely dissociated at very high redshift ($z\approx25$). The reionization is basically driven by objects collapsed through H line cooling, while small mass PopIII stars play only a minor role and even in the absence of a radiative negative feedback they would not be able to reionize the IGM. Note that only about 2% of the stars observed at $z = 0$ is required to reionize the universe completely. This corresponds to an average IGM metallicity (assuming a Salpeter IMF) at redshift $z\approx10$ equal to $\langle Z\rangle \approx 3 \times 10^{-4} Z_\odot$. If SNae were the only source of kinetic energy for the metals, a highly inhomogeneous distribution would result at any redshift. Under these conditions we would expect most of the volume of the universe to remain at near-primordial composition, and the metals to be concentrated in relatively small pockets, in contrast with some recent observational results (for a discussion see [6]). Therefore, additional transport/mixing mechanisms as merging events [4] and turbulent diffusion [3] must be invoked to explain a more homogeneous level of enrichment.

References

1. Ciardi, B., Ferrara, A., Governato, F. & Jenkins, A. 1999, MNRAS, submitted (astro-ph/9907189)
2. Ciardi, B., Ferrara, A. & Abel, T. 1999, ApJ, in press
3. Ferrara, A., Pettini, M. & Shchekinov, Yu. 1999, MNRAS, submitted
4. Gnedin, N. Y. 1998, MNRAS, 294, 407
5. MacLow, M.-M. & Ferrara, A. 1999, ApJ, 513, 142
6. Pettini, M. 1999, in Chemical Evolution from Zero to High Redshift, ed. J. Walsh, & M. Rosa (Berlin: Springer), in press (astro-ph/9902173)

Zero Metallicity Stellar Sources and the Reionization Epoch

Paolo Cojazzi[1], Alessandro Bressan[2], Francesco Lucchin[1], and Ornella Pantano[3]

[1] Dipartimento di Astronomia, Università di Padova, Padova, Italy
[2] Osservatorio Astronomico, Padova, Italy
[3] Dipartimento di Fisica *G. Galilei*, Università di Padova, Padova, Italy

Abstract. We reconsider the problem of the cosmological reionization due to stellar sources and we focus our analysis on the basic parameters, such as stellar models and spectra, adopted for estimating the production rate of ionizing photons. In particular, we find that using suitable zero metallicity models instead of the very metal poor ones, commonly adopted, significantly modifies the reionization epoch.

1 The reionization model

Several analitycal and numerical works have estimated the reionization epoch and how this depends on the cosmological model and on the formation history of ionizing sources, which can be either stars or quasars. In this work we analyse how the properties of the stars, in particular the metallicity, could affect the reionization epoch. The overall dynamics of the reionization process is followed using the method outlined in [5]. The mass function of the dark matter halos is computed according to the Press-Schechter theory. In any halo with a total mass $M \geq 10^8\,[(1+z)/10]^{-3/2}$ M$_\odot$ a fraction f_* of the gas is converted into a *simple stellar population* (SSP). Only a fraction f_{esc} of the ionizing photons is able to escape from the haloes.

2 Very low metallicity stars

The first generation of stars forms from the primordial material, whose chemical composition is entirely dictated by the cosmological nucleosynthesis, which sets an upper limit of the CNO abundance by mass $Z_{CNO} \leq 10^{-9}$. These stars show a peculiar evolution because hydrogen burning initially can be only substained by the proton-proton cycle, and therefor their ZAMS is hotter than those of normal stars (see Fig. 1). We built our $Z = 0$ isochrones using the model of [2] up to $30\,\mathrm{M}_\odot$ and the models of [3] up to $100\,\mathrm{M}_\odot$. To compute the emissivity of the SSPs we used the Kurucz spectral library [6], adopting the lowest available metallicity data ($Z = 2 \times 10^{-7}$) for the zero-metal case, and a combination of Kurucz and 'CoStar' models [7] for highest metallicity here considered (4×10^{-3}).

The adopted initial metallicity has a significant impact on the reionization epoch. Table 1 depicts this effect in two different cosmological models.

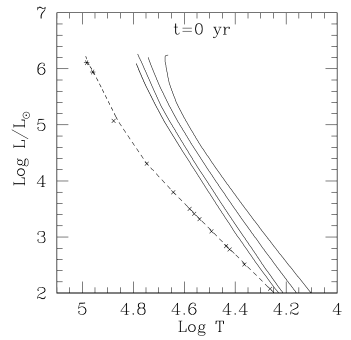

Fig. 1. Zero age main sequence for different initial chemical composition (lines and points). Starting from the rightmost one, the initial metallicity is Z=0.02, Z=0.004, Z=0.0004 [1], and Z=0.0001 [4]. The dashed line is our Z=0 isochrone. The points represent zero age main sequence models of PopIII stars and are: a) stars, 80 $M_\odot$ and 100 $M_\odot$ with Z=0 [3]; b) crosses, 0.7 $M_\odot$ - 15 $M_\odot$ Z=10^{-10} [2]

We see that, for the cases in which the reionization is late, the change in the reionization redshift moving from $Z = 0.004$ to $Z = 0$ is comparable with that obtained changing cosmological model.

Table 1. Reionization redshifts z_{rei} in a CDM model (Ω_0, Ω_Λ, Ω_b, h, $\sigma_{8h^{-1}\mathrm{Mpc}}$, n) = (1, 0, 0.05, 0.5, 0.52, 1) and in a ΛCDM model (Ω_0,Ω_Λ, Ω_b, h, $\sigma_{8h^{-1}\mathrm{Mpc}}$, n) = (0.3, 0.7, 0.03, 0.82, 0.93, 1).

		CDM				ΛCDM			
	f_*	0.015		0.150		0.015		0.150	
Z	f_{esc}	0.2	1	0.2	1	0.2	1	0.2	1
0.004		4.9	8.6	9.9	12.7	7.1	11.9	13.6	17.2
0.0001		5.2	8.8	10.1	12.8	7.5	12.1	13.8	17.4
0		6.1	9.4	10.7	13.3	8.6	13.0	14.7	18.0

References

1. Bertelli, G. *et al.*, 1994, A&AS **106**, 275
2. Cassisi, S., Castellani, V, 1993, ApJS **88**, 509
3. El Eid M.F., Fricke, K.J., Ober, W.W., 1983 A&A **119**, 54
4. Girardi, L. *et al.*, 1996, ApJS **117**, 113
5. Haiman Z., Loeb A., 1997, ApJ **483**, 21
6. Kurucz, R.L. 1992, Stellar Populations of Galaxies, eds. Barbuy, B., Renzini, A: Kluwer Academic Publishers
7. Schaerer, D., De Koter 1997 A&A **322**, 598

The Radiative Feedback from the First Stars and Quasars and the End of the Dark Age

Zoltan Haiman[1,2]

[1] NASA/Fermilab Astrophysics Center,
Fermi National Accelerator Laboratory, Batavia, IL 60510, USA
[2] Department of Astrophysical Sciences,
Princeton University, Princeton NJ 08544, USA

Abstract. In hierarchical models of structure formation, an early cosmic UV background (UVB) is produced by the small ($T_{\rm vir} \lesssim 10^4$K) halos that collapse before cosmological reionization. If the first collapsed halos harbor stars, then their UV flux below 13.6 eV photo–dissociates the molecular hydrogen H_2 in subsequently collapsing halos within a large sphere of influence. This causes a pause in the cosmic star–formation history: the buildup of the UVB and the epoch of reionization are delayed until larger halos ($T_{\rm vir} \gtrsim 10^4$K) collapse. In contrast, if the small halos harbor mini–quasars with hard spectra extending to ∼1keV, then their X–rays balance the effects of the UVB, the negative feedback does not occur, and reionization can be caused early on by the small halos.

1 Introduction

Recent high redshift observations have yielded estimates of the global star–formation history of the universe to redshifts as high as $z \sim 5$ [7,11]. However, some stellar activity must have taken place even at $z > 5$: the enrichment by heavy elements, as well as the reionization of the intergalactic medium (IGM), hints at early sources of metals and ionizing photons. Such ultra–high redshift objects are indeed expected in popular cosmological cold dark matter (CDM) models, which predict that the first virialized halos appear at redshifts as high as $z \sim 30$. It is natural to identify these halos as sites where the first stars or massive black holes appear, forming the first generation of "mini–galaxies" or "mini–quasars".

Because of the low virial temperatures ($T < 10^4$K) of the first halos, their H_2 molecule fraction determines whether they are able to cool and form any stars or black holes. As a result, the H_2 abundance inside these halos determines when the "dark age" ends: if there is sufficient H_2, it ends earlier; if H_2 is absent, it ends at the later redshift when the ~ 1000 times more massive halos collapse and cool via atomic H. Here, we study the H_2 abundance inside halos collapsing in a ΛCDM cosmology. The main question we address is: *Could the first collapsed dark halos, with masses near the Jeans mass, contribute to the reionization of the universe?* For a more detailed report on this work, we refer the reader to [5].

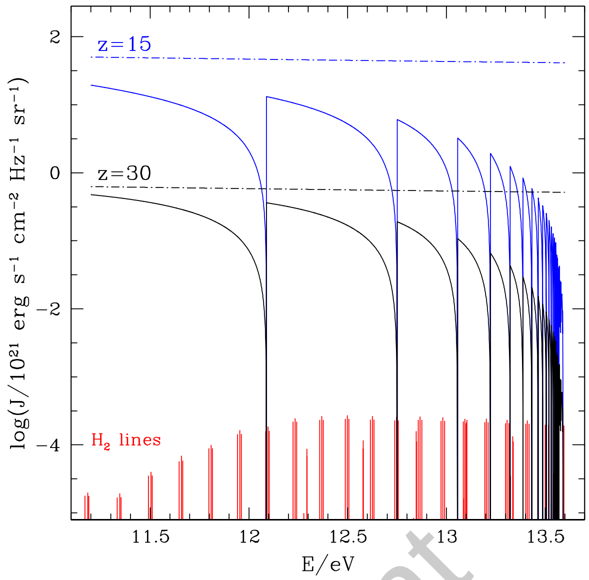

Fig. 1. The spectrum of the UV background at redshifts $z = 30$ and $z = 15$. The solid (dashed) lines show the spectrum after (without) absorption by neutral H in the high–redshift IGM. For reference, we show the location of the 76 lines of H_2.

2 Spectrum of the Early UV and X–ray Backgrounds

In any hierarchical model of structure formation, the radiation output associated with collapsed halos gradually builds up a cosmic UV background. If the first halos harbored black holes, in addition to (or instead of) stars, then the spectrum of the background extended into the X–ray regime [6], producing an early X–ray background (XRB). UV photons in the 11.18–13.6eV range can travel to a large fraction of the Hubble length across the IGM, and photo–dissociate molecular H_2 both in the IGM and inside other collapsed halos [4]. X–ray photons with energies above a few keV also travel to large distances, and photo–ionize H and He, as well as produce collisional ionization of H by fast photo–electrons. The resulting extra free electrons catalyze the formation of H^-, and therefore tend to increase the H_2 abundance. In order to assess the molecular fraction inside collapsed halos, it is necessary to quantify the spectrum of the background in the soft UV and X–ray bands. Consider an observer at redshift $z_{\rm obs}$, measuring the UVB at the local frequency $\nu_{\rm obs}$, where 11.18eV $< h\nu_{\rm obs} <$ 13.6eV. The photons collected at the frequency $\nu_{\rm obs}$ are arriving from sources located at $z_{\rm s} > z_{\rm obs}$, and have redshifted their original frequency $\nu_{\rm s} > \nu_{\rm obs}$. Because of the large optical depth of the IGM in the atomic Lyman series, effectively a "dark screen" blocks the view of all sources at redshifts above $z_{\max}$, defined as $(1+z_{\max})/(1+z_{\rm obs}) = \nu_{\rm i}/\nu_{\rm obs}$, where $\nu_{\rm i}$ is the frequency of the Lyman line closest to $\nu_{\rm obs}$. The cumulative effect of this absorption leads to a characteristic spectral shape for the early UVB, resembling a "sawtooth"[1], shown in a specific model (described below) in Figure 1. The shape of the early XRB is obtained in a more straightforward manner, by summing the spectra of individual sources (here assumed to be a power law with index -1), and including the opacity of the intergalactic H and He, which exponentially suppresses the flux to $\sim$1 keV.

3 H_2 Cooling Inside the First Halos

The H_2 Abundance in Collapsed Clouds. The radiative efficiency of a gas cloud by collisional excitations of H_2 molecules depends on the gas temperature, density, and H_2 abundance. Here we consider spherical clouds with density profiles of truncated isothermal spheres [10], composed of primordial H+He gas, with the initial abundances given by their post–recombination values [2]. We solve the time evolution of the chemical abundance profiles, when the cloud is illuminated by the external background. The initial conditions are specified by the virial temperature $T_{\rm vir}$, and collapse redshift $z_{\rm coll}$ of the cloud, and the amplitude of the UVB, J_{21}, as well as the XRB. The latter is obtained by assuming a power law spectrum above 13.6eV, including a multiplicative factor, $\epsilon_{\rm x}$, to characterize the ratio of X–ray to UV flux. For pure stellar sources, $\epsilon_{\rm x} = 0$; for typical quasar spectra (Elvis et al.), $\epsilon_{\rm x} \sim 1$. Values of $\epsilon_{\rm x}$ in–between 0 and 1 could describe either miniquasars with softer spectra, or a mixed population of stars and mini–quasars.

The evolution of $x_{\rm H_2}$ at the core of a cloud, chosen as an example, is shown by the solid curves in Figure 2. In the absence of any UVB, the H_2 fraction rises continuously, and reaches $10^{-3.5}$ in a Hubble time (top curve). When a UV flux with $J_{21} = 0.1$ is turned on (bottom solid curve), the H_2 fraction is suppressed. For higher fluxes, the suppression is even more pronounced. By performing similar calculations for clouds with virial temperatures and collapse redshifts in the ranges $10^2 < T_{\rm vir} < 10^4$K and $5 < z_{\rm coll} < 50$, we have found that the evolution shown in Figure 2 remains qualitatively the same. However, the level of flux required at which the H_2 molecules are photo–dissociated depends on the values of both $z_{\rm coll}$ and $T_{\rm vir}$. For defining a "critical flux" $J_{\rm crit}$, we assume that a cloud is able to form stars if the cooling time in the core becomes shorter than the time elapsed since the formation of the cloud.

If increasing amounts of X–rays are also added (middle two solid curves), then the H_2–suppression (relative to the dotted curve) is, as expected, less pronounced. By experimenting with different combinations of $z_{\rm coll}$ and $T_{\rm vir}$,

[1] We find that the overall effect of intergalactic molecular absorption is negligible.

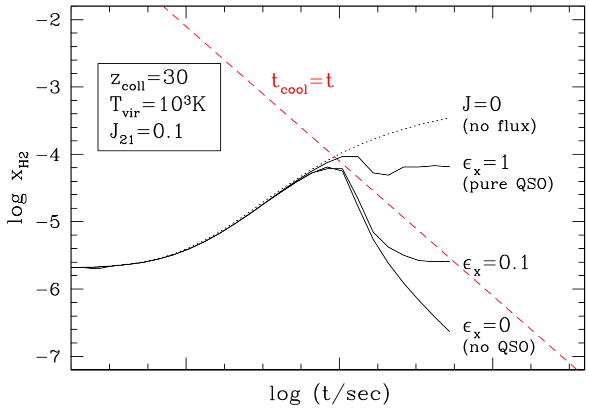

Fig. 2. Evolution of the H_2 abundance in the core of a truncated isothermal sphere. Also shown is the H_2 abundance at which the cooling time equals the time elapsed (short dashed line). The curve labeled J=0 shows the evolution in the absence of any flux. The label ϵ_x on the other curves is a measure of the X–ray/UV flux ratio, where $\epsilon_x = 0$ corresponds to a pure stellar spectrum with no X–rays, and $\epsilon_x = 1$ corresponds to a pure "mini–quasar" spectrum with a spectral index of -1.

we have found that the situation shown in Figure 2 is typical: a $\sim 10\%$ contribution by X–rays to the flux (e.g. the curve labeled $\epsilon_x = 0.1$ in fig.2) is sufficient to keep the H_2 fraction high enough to allow star formation. We therefore expect that if the early background had a non–negligible contribution from "mini–quasars" with hard spectra, extending to ~ 1 keV, then the negative H_2 feedback described here would not occur.

The Minimum UV Flux for Negative Feedback. In the example shown in Figure 2, $(z_{\rm coll}, T_{\rm vir}) = (30, 10^3{\rm K})$, the critical value of the UV flux to suppress starformation, $J_{\rm crit}$ can be read off directly from Figure 2 to be $J_{\rm crit} = 0.1$. In order to be able to investigate the evolution of the UVB in the Press–Schechter cosmological models, we have computed the evolution of clouds for a grid of values for $5 < z_{\rm coll} < 50$, and $2 < \log(T_{\rm vir}/{\rm K}) < 4$. For each pair of values, we have found the critical flux. We find that the resulting values are relatively low, $J_{\rm crit} \sim 10^{-1} - 10^{-3}$, depending on the collapse redshift and virial temperature. *Since these values of the flux necessary to prevent star–formation are 2–4 orders of magnitude below the minimum flux necessary to reionize the universe (i.e. one photon/baryon), a negative feedback necessarily turns on prior to reionization.* This robust conclusion holds unless there is an early XRB, as described above.

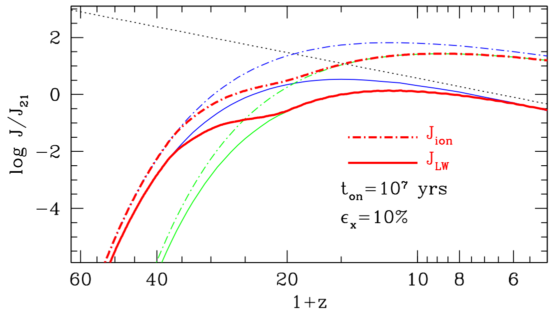

Fig. 3. Evolution of the background flux J at 13.6eV (dot–dashed lines) and the average flux in the LW bands (solid lines). In both cases, the bottom and top curve assume a constant $T_{\rm crit} = 10^{3.8}K$, and $10^{2.4}K$, respectively, and bracket our actual coupled solution, shown by the thick middle curve. The diagonal dotted line shows the minimum flux for reionization, corresponding to one photon per hydrogen atom. If early miniquasars produce an XRB, then the H_2 feedback does not occur.

4 H_2–Feedback and Cosmological Reionization

The next step is to compute the coupled redshift evolution of the background flux, the intergalactic H_2 fraction, and the mass–scale (expressed by the critical virial temperature $T_{\rm crit}[z]$) of the H_2 feedback. We assume that each halo that satisfies the star formation criterion has a constant star formation rate for $t_{\rm on}$ years, during which it turns a total fraction ϵ of its baryonic mass into stars with a Scalo IMF. We start from a high redshift, and take small redshift steps towards z=0. At each step, we sum the UV flux of all sources that are within the imaginary redshift screen $z_{\rm max}$, and satisfy our star formation criterion. Once the flux is obtained, we find the critical virial temperature numerically for the new flux J_{21} and redshift.

Our main results are shown in a model with $(t_{\rm on},\epsilon) = (10^7 \text{ yr}, 10\%)$ in Figure 3. The figure shows the evolution of the total ionizing flux produced by all sources at 13.6 eV ($J_{\rm ion}$) and the average flux in the LW bands, ($J_{\rm LW}$) The three solid curves show the evolution of $J_{\rm LW}$ in our model with feedback (middle curve), assuming that the critical virial temperature is fixed at $T_{\rm vir} = 10^{2.4}$K (upper curve), and at $T_{\rm vir} = 10^{3.8}$K (lower curve). These curves demonstrate that initially the small halos are allowed to form stars, there is no feedback, and the flux builds up as in the constant $T_{\rm vir} = 10^{2.4}$K case. At redshift $z \approx 35$, the feedback starts to be noticeable, as the flux builds up to $J_{\rm LW} \approx 10^{-2}$, and $T_{\rm crit}$ rises above $10^{2.4}$K. By redshift $z = 20$, $T_{\rm crit}$ reaches $10^{3.8}$K. The dot–dashed lines show the evolution of the ionizing flux, $J_{\rm ion}$; and the dotted line shows the minimum flux required for reionization (corresponding to one photon per hydrogen atom). As the figure shows, reionization in this model occurs at $z \sim 15$, and at this redshift the contribution from the small halos to $J_{\rm ion}$ is only $\sim$10%.

We have found that different choices for $t_{\rm on}$ and ϵ yield similar conclusions: the H_2 feedback suppresses star formation inside the small halos, and the contribution of the small halos to the reionizing flux is always below 10%, unless we include an XRB in addition to the UVB. If reionization occurs late, then the H_2 feedback makes less of a difference to the overall ionizing flux. The contribution from small halos to the reionizing flux is then small in any case, since by this late time, the collapsed baryon fraction, as well as the UV background, is dominated by the large halos. There is an indication from 3–D simulations that the efficiency in small halos might be unusually small ($< 1\%$, [1]). If the efficiency in small halos was intrinsically indeed much smaller than in large halos, then the contribution to the flux from the small halos would be again small, regardless of the H_2–feedback. We emphasize that the H_2 feedback generically occurs in any model without an XRB that satisfies the reionization constraint by $z = 5$, because the suppression of the H_2 abundance and star formation inside clouds requires a UV flux that is only a fraction $10^{-2} - 10^{-4}$ of the reionizing flux. As the UVB builds up to the reionizing level, it must necessarily first reach the level at which the H_2 feedback sets in. However, we find that if early miniquasars produce an XRB, at a flux level of $\sim 10\%$ of the UVB, then the H_2 feedback does not occur, and reionization can be caused early on by the small halos. The evolution of the small early halos is therefore distinctly different in stellar and mini–quasar models: this may help shed light on the question of what type of sources were responsible for ending the “dark age”, and reionized the Universe.

I thank my collaborators Tom Abel and Martin Rees with whom the work described here was carried out. Support for this work was provided by the DOE and NASA grant NAG 5-7092 at Fermilab.

References

1. Abel, T., Bryan, G. L., & Norman, M. L. 1998, in Proc. of the MPA/ESO Conference "Evolution of LSS: from Recombination to Garching", Garching, Germany, Aug. 1998, astro-ph/9810215
2. Anninos, P., & Norman, M.L. 1996, ApJ, 460, 556
3. Elvis, M., et al. 1994, ApJS, 95, 1
4. Field, G. B., Somerville, W. B., and Dressler, K. 1966, ARA&A 4, 207
5. Haiman, Z., Abel, T., & Rees, M. J. 2000, ApJ, in press, astro-ph/9903336
6. Haiman, Z., & Loeb, A. 1998, ApJ, 503, 505
7. Madau, P., et al. 1996, MNRAS, 283, 1388
8. Miralda-Escudé, J., Haehnelt, M., & Rees, M. J. 1999, ApJ, submitted
9. Press, W. H., & Schechter, P. L. 1974, ApJ, 181, 425
10. Shapiro, P. R., Iliev, I., & Raga, A. C. 1999, MNRAS, 307, 203
11. Steidel, C. C., et al. 1996, AJ, 112, 352

Temperature of the First H II Regions

Thomas Beckert[1,2]

[1] Harvard–Smithsonian Center for Astrophysics, Cambridge MA 02138, USA
[2] Institut für Theoretische Astrophysik, Tiergartenstr.15, 69121 Heidelberg, Germany

Abstract. The first stellar sources to reionize the interstellar and intergalactic medium during galaxy formation will ionize gas of primordial composition. Energy balance in these metal–free H II regions require gas temperatures between several times 10^4 K and a few times 10^5K. We can exclude higher temperature solutions based on a separate electron energy balance and lower temperatures from energy constrains at the ionization front.

1 Heating and Cooling in Metal–free H II Regions

H II regions ionized by massive stars with primordial abundancies of hydrogen and helium, but without heavier elements, are expected to be hotter than present day H II regions, in which hydrogen and helium account for up to 70% of the total cooling at temperatures of 10^4 K. Not all ionizing photons will be absorbed and converted into soft photons in the ionized region. Some will instead reach the actual boundary of the H II region and drive an ionization front into the surrounding neutral gas. A fraction $\exp(-\tau)$ of the ionizing stellar luminosity L_* is therefore consumed at the front for ionization and gas heating. We approximate the ionizing spectrum at the front by a Wien-law of temperature $T_{\rm eff}$. The gas heating is described by

$$L_{\rm hf} = 8\pi R_s^2 \frac{k^2 T_{\rm eff}^2 \nu_0^2}{hc^2} \exp\left[-\frac{\chi}{kT_{\rm eff}}\right] e^{-\tau} \tag{1}$$

where R_s is the stellar radius and χ the ionization energy. The number of ionizing photons in the H II region is reduced only by free-bound transitions, which equal the number of recombinations in ionization equilibrium [3]. The total energy balance for the initial ionizing photon luminosity is

$$L_*(1-e^{-\tau}) + L_{\rm hf} = L_{\rm ff} + L_{\rm fb} + L_{\rm bb} \tag{2}$$

$$\exp[-\tau] = \frac{V n_e n_i (\beta_{\rm tot} - \beta_1)}{N_{\rm Lyc}} \tag{3}$$

with the recombination rate $n_e n_i \beta_{\rm tot} - \beta_1$ from [4] in the Volume V of the H II region and the number $N_{\rm Lyc}$ of Lyman contiuum photons emitted by the star. The cooling in Eq. 2 is provided by free-free emision $L_{\rm ff}$, free-bound transitions [2] to exited states $n > 1$: $L_{{\rm fb},n>1} \approx 9.6\,10^{-21} V n_e^2 T^{-0.5} \langle g_{\rm fb}\rangle$ erg s^{-1} and cooling from bound-bound $L_{\rm bb} = 6.7\,10^{-21} V n_e^2 T^{-0.8}\,{\rm erg\,s^{-1}}$ emission, which we approximate by the Lyman-α luminosity .

2 Temperature in H II Regions

The balance Eq. 2 has one solution at high temperatures of several 10^6 K, where the cooling is dominated by free-free emission, and a second solution between 10^4 and a few 10^5 K, where the cooling is due to free-bound and bound-bound transitions [1]. In both cases the equilibrium temperature is very sensitive to density and volume of the H II region. The high temperature solution faces two severe problems in our context. First the expansion time for the ionization front driven by a massive star and the recombination time scale for reaching ionization equilibrium in a region of mean density $n_e = 10^2\,\mathrm{cm}^{-3}$ are both 10^6 years and a steady state will not be achieved. The second conjecture comes from the thermal balance of the electrons alone. At 10^6K the main cooling of free electrons is provided by free-free emission while the heating takes place at the ionization front and by reionization inside the H II region after recombination. The mean energy of a new free electron can be approximated by

$$\mathcal{E} \approx kT_{\mathrm{eff}} \frac{x-2}{x-1} \quad , \qquad x = \frac{\chi}{kT_{\mathrm{eff}}} \quad , \tag{4}$$

which holds for low effective stellar temperatures $kT_{\mathrm{eff}} \ll \chi$. The heating of electrons inside the ionized regions results in

$$L_{\mathrm{h}} = n_{\mathrm{e}} n_{\mathrm{i}} V \mathcal{E} (\beta_{\mathrm{tot}} - \beta_1) \tag{5}$$

and the free-free luminosity must balance the heating inside and at the ionization front

$$L_{\mathrm{ff}} = L_{\mathrm{h}} + L_{\mathrm{hf}} \quad . \tag{6}$$

This balance is satisfied to within a factor of two for the opacity factor $\exp(-\tau)$ present in Eq. 1 in case of the lower temperature solution. The electron energy balance Eq. 6 cannot hold for electrons of 10^6 K. We conclude that metal–free H II regions had temperatures of several times 10^4 K during their expansion and will cool down with the end of the first massive stars and subsequent metal enrichment.

References

1. Beckert T., Duschl W.J., Mezger P.G., 2000, submitted to A&A
2. Cooper J., 1966, Rep.Prog.Phys. **29**, 2
3. Rubin R.H., 1968, ApJ **154**, 391
4. Seaton M.J., 1959, MNRAS **119**, 81

Part V

Formation of the First Stars

Chemistry and Cooling of the Primordial Gas

Daniele Galli and Francesco Palla

Osservatorio Astrofisico di Arcetri, 50125 Firenze, Italy

Abstract. H_2 and HD molecules provide the cooling needed for the fragmentation and collapse of the first structures in the universe. In this review, we describe the main chemical and physical processes occurring in the primordial gas after the recombination epoch. We also highlight the areas where improvements in the determination of reaction rates and excitation coefficients are necessary to reduce the remaining uncertainties in the predictions of the numerical models. Finally, the interaction of primordial molecules with the CBR and the role of H_2 and HD cooling in the early universe are discussed.

1 The Cosmological Background

Models of structure formation are based on the growth of small primordial density fluctuations by gravitational instabilities. In both cold dark matter (CDM) and baryonic dark matter (BDM) cosmological models, the first objects predicted to go nonlinear are the smallest ones. In CDM models, it is expected that overdense regions with masses 10^5–10^7 $M_\odot$ would first collapse in the redshift range $10 \lesssim z \lesssim 100$ [1]. The crucial question is whether cooling will enable the baryonic clouds to dissipate their kinetic energy and collapse, to eventually become self-gravitating and form interesting objects such as a galaxy, a very massive object, a black hole, or a normal star (e.g. [2] [3]). For low mass objects, the smaller they are, the less efficiently they dissipate energy and cool. Thus, a detailed treatment of gas dynamical processes will predict the characteristic mass scale M_c such that objects with $M > M_c$ can cool rapidly, whereas smaller lumps will merely remain pressure-supported and not form anything luminous. In other words, *M_c is the mass scale of the first luminous objects.* In order to compute realistic values of M_c, both the abundances of the main molecular species and their cooling properties must be accurately known. It is the purpose of this contribution to review the main chemical and physical properties of the primordial gas in the post-recombination epoch.

2 The First Molecules

Saslaw & Zipoy [4] and Peebles & Dicke [5] were the first to realize the importance of gas phase reactions for the formation of the simplest molecule, H_2. They showed that trace amounts of molecular hydrogen, of order 10^{-6}–10^{-5}, could indeed form via the intermediary species H_2^+ and H^- once the radiation field no longer contained a high density of photons with energies above the threshold of dissociation (2.64 and 0.75 eV, respectively).

The presence of even a trace abundance of H_2 affects the cooling properties of the primordial gas which, in its absence, would be an extremely poor radiator: cooling by Ly-α photons is in fact ineffective at temperatures less than ~ 8000 K, well above the matter and radiation temperature in the post-recombination era. Since the evolution of primordial density fluctuations is controlled by the ability of the gas to cool down to low temperatures, it is very important to obtain a firm picture of the chemistry of the dust-free gas mixture, not limited to the formation of H_2, but also to other molecules of potential relevance (see [6] [7]).

2.1 Chemical Evolution of the Primordial Gas

The chemical composition of the primordial gas consists of e^-, H, H^+, H^-, D, D^+, He, He^+, He^{++}, Li, Li^+, Li^-, H_2, H_2^+, HD, HD^+, HeH^+, LiH, LiH^+, H_3^+, and H_2D^+. The fractional abundaces of these species are calculated as function of redshift, starting at $z = 10^4$ where He, H, D, and Li are fully ionized. The chemical and thermal evolution of the pregalactic gas can be followed by solving the set of coupled chemical rate equations of the form

$$\frac{\mathrm{d}n_i}{\mathrm{d}t} = k_{\mathrm{form}} n_j n_k - k_{\mathrm{dest}} n_i + \dots, \tag{1}$$

where k_{form} and k_{dest} are the formation and destruction reaction rates, and n_i is the number density of the reactant species i. The network includes $\sim$90 reactions with the rate coefficients taken from the most recent theoretical and experimental determinations (see the discussion in [8]). The evolution of the gas temperature T_{g} is governed by the equation

$$\frac{\mathrm{d}T_{\mathrm{g}}}{\mathrm{d}t} = -2T_{\mathrm{g}}\frac{\dot{R}}{R} + \frac{2}{3kn}[(\Gamma - \Lambda)_{\mathrm{Compton}} + (\Gamma - \Lambda)_{\mathrm{mol}}]. \tag{2}$$

The first term represents the adiabatic cooling associated with the expansion of the Universe, R being the scale factor. The other two terms represent respectively the net transfer of energy from the CBR to the gas (per unit time and unit volume) via Compton scattering of CBR photons on electrons

$$(\Gamma - \Lambda)_{\mathrm{Compton}} = \frac{4k\sigma_{\mathrm{T}} a T_{\mathrm{r}}^4 (T_{\mathrm{r}} - T_{\mathrm{g}})}{m_{\mathrm{e}} c} n_{\mathrm{e}}, \tag{3}$$

and via excitation and de-excitation of molecular transitions

$$(\Gamma - \Lambda)_{\mathrm{mol}} = \sum_k n_k \sum_{i>j} (x_i C_{ij} - x_j C_{ji}) h\nu_{ij}, \tag{4}$$

where C_{ij} and C_{ji} are the collisional excitation and de-excitation coefficients and x_i are the fractional level populations. For the molecular heating and cooling of the gas, the contribution of H_2 and HD should be considered (see Section 3). The temperature of the CBR is given by $T_r = T_0(1+z)$ with $T_0 = 2.726$ K [9].

The chemical network is completed by the equation for the redshift

$$\frac{dt}{dz} = -\frac{1}{H_0(1+z)^2\sqrt{1+\Omega_0 z}}, \tag{5}$$

where $H_0 = 100\,h$ km s^{-1} Mpc^{-1} is the Hubble constant and Ω_0 the closure parameter.

The density $n(z)$ of baryons at redshift z is

$$n(z) = \Omega_b n_{cr}(1+z)^3, \tag{6}$$

where $n_{cr} = 9.19 \times 10^{-6} h^2$ cm^{-3} is the critical density, and Ω_b is the ratio of the total to the critical density. This quantity is related to the baryon-to-photon ratio η by $\Omega_b = 3.66 \times 10^{-3} \eta_{10} h^{-2}$, with $\eta_{10} = 10^{10}\eta$.

2.2 Molecular Abundances After the Recombination Epoch

Since the seminal work of Peebles [10] and Zel'dovich et al. [11], several improvements in the process of H recombination have been introduced, but little has changed. One important correction has been introduced by the calculations of Sasaki & Takahara [12] who used the prescriptions for the rate of radiative recombination given by Grachev & Dubrovich This has led to a reduction of a factor 2–3 with respect to previous studies (e.g. [14]) in the abundance of electrons and H^+ at freeze-out. The lower residual ionization has a negative effect on the chemistry of the primordial gas in which electrons and protons act as catalysts in the formation of the first molecules. For an improved recombination calculation, see the recent work of Boschán & Bildtzinger [15] and Seager et al. [16] who find a delayed He I recombination and a 10% lower residual ionization fraction at freeze-out.

The chemical evolution of the gas in the expanding universe resulting from the solution of eqs. (1-6) is shown in Figure 1. The standard model is characterized by a Hubble constant $h = 0.67$ [17], a closure parameter $\Omega_0 = 1$, and a baryon-to-photon ratio $\eta_{10} = 4.5$ [18]. The initial fractional abundance of H, D, He and Li are taken from the standard big bang nucleosynthesis model of Smith et al. [19]. The residual ionization fraction at $z = 1$ for the standard model is [e/H] $= 3.02 \times 10^{-4}$.

The evolution of the abundance of H_2 follows the well known behaviour ([6] [20]) where the initial steep rise is determined by the H_2^+ channel followed by the contribution from H^- at $z \simeq 100$. The freeze-out value of H_2 is [H_2/H] $= 1.1 \times 10^{-6}$, a value somewhat lower than found in similar studies, as a consequence of the net reduction of the ionization fraction.

The formation of H_2^+ is controlled by radiative association and photodissociation at $z \geq 100$, whereas at lower redshifts there is a contribution from HeH^+ that explains the gentle rise up to [H_2^+/H_2] $\simeq 10^{-6}$. An

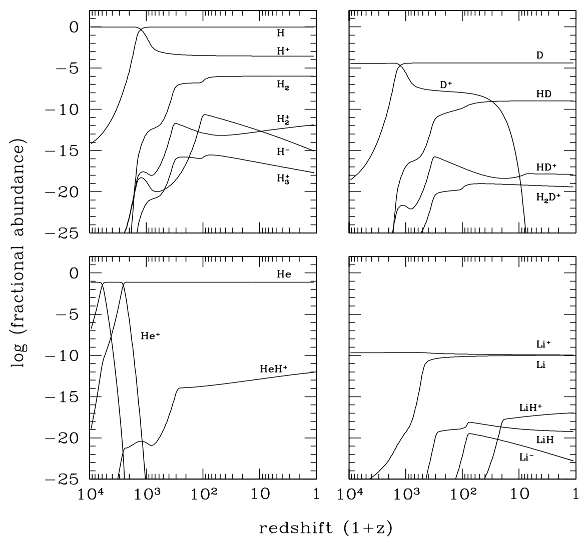

Fig. 1. The evolution of the chemical species considered in the standard model as a function of redshift. The four panels show the results for H (upper left), D(upper right), He (lower left), and Li (lower right). (From [8])

additional channel for H_2^+ formation is the associative ionization reaction $H + H(n=2) \rightarrow H_2^+ + e^-$ (see [21] and [22] for H_2 formation).

As for deuterium–bearing species, the only molecule formed in significant amount is HD, whose evolution with redshift follows closely that of H_2. However, its abundance at freeze-out is $[HD/H_2] \simeq 10^{-3}$, with an enhancement factor of $\sim$30 from the initial [D/H] abundance.

The main molecular species containing helium is HeH^+, formed by the radiative association of He and H^+. As emphasized by Lepp & Shull [6], this reaction is slower than the usual formation mode via association of He^+ and H, but since the abundance of He^+ is quite small, radiative association takes over. The HeH^+ ions are removed by CBR photons and at $z < 250$ also by collisions with H atoms to reform H_2^+. This explains the abrupt change in the slope of the curve of HeH^+ shown in Fig. 1. The final abundance is small, $[HeH^+/H] \sim 6 \times 10^{-13}$ at $z = 1$.

Finally, the chemistry of lithium is complicated, but the molecular abundances are indeed very small. The more abundant complex is LiH^+ whose formation is controlled by the radiative association of Li^+ and H [23]. As shown in Fig. 1, lithium remains more ionized at low redshifts and this explains why LiH is less abundant than LiH^+. At $z = 1$, the abundance of LiH^+ is $\simeq 10^{-17}$.

The final values of the molecular abundances depend on the choice of the cosmological parameters. Each model is in fact specified by three parameters η_{10}, Ω_0 and h. The observational (and theoretical) uncertainties associated with each of them are still rather large. The standard model is defined by the values of the cosmological parameters that better fit the abundances of the light elements. To gauge the effects induced on the chemistry network by changes in such parameters, Figure 2 displays the variation of the molecular abundances obtained for different values of η_{10}, Ω_0, and h. Note that the abundance of H_2 is the same in all cases, making this molecule a poor diagnostic of cosmological models. On the contrary, the abundance of HD molecules can vary by almost two orders of magnitude and is therefore a sensitive gauge. For the other species, however, a higher value of η_{10} implies a lower final abundance as a result of the lower initial value of each element predicted by the standard big bang nucleosynthesis which compensates for the higher total baryon density.

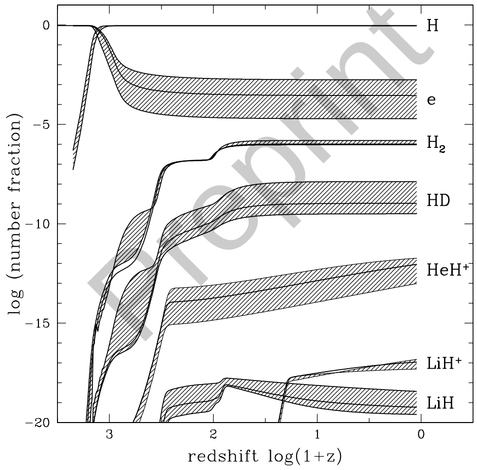

Fig. 2. The evolution of the most abundant molecular species as function of redshift (*solid* lines). The hatched area covers the range of variation of $\eta_{10} = 1$–10, $\Omega_0 = 0.1$–1, and $h = 0.3$–1. (From [24])

3 Cooling Functions for the Primordial Gas

Due to the absence of metals, the usual cooling processes that dominate in the interstellar medium are not present and the cooling by infrared emission of H_2 following collisional excitation by the gas is the most important mechanism in the early universe. However, since H_2 is homonuclear and does not possess a permanent dipole moment, the rovibrational transitions occur by electric quadrupole radiation and the emission is very inefficient. The large rotational constant (85.25 K) causes a large energy spacing of the rotational levels. Thus, the $J = 2$ state lies 510 K above the ground rotational level ($J = 0$), and $J = 3$ lies 815 K above $J = 1$. As a consequence, the cooling drops very sharply at lower temperatures. In the following subsection, we will describe the new developments in the computation of the cooling function due to H_2 and HD molecules.

3.1 H_2 Molecules

Since in some cases where H_2 plays a major role the gas temperature can reach more than one thousand degrees, it is not sufficient to consider only the ground ($v = 0$) vibrational state. The choice of the rovibrational H-H_2 collisional coefficients is very delicate, since the published data may vary up to factors of 50–100 according to different authors (see [25], [26], [27], [28]), and the resulting H-H_2 cooling functions may differ by considerable amounts.

For cosmological problems, one generally adopts the analytical H-H_2 cooling functions given by Hollenbach & McKee [29] [30] or Lepp & Shull [31]. These formulae appear now to suffer considerably from the limitations and uncertainties associated with the collisional coefficients available at the time. At low temperatures, the uncertainty is associated with the choice of the interaction potential, since it is very difficult, even nowadays, to calculate the potential in the interaction region to the requisite level of accuracy ($\sim 10^{-3}$ hartrees). However, recent improvements in the calculations employing both fully quantum mechanical methods ([28] [32]) and classical trajectory methods ([33] [34]) have greatly reduced the uncertainties in the cross-section and rate coefficients in the temperature interval 10^2 to 10^4 K (see [35]).

Several H-H_2 cooling functions are shown in Fig. 3 for two values of the the density, $n(\mathrm{H}) = 1\ \mathrm{cm}^{-3}$ and $n(\mathrm{H}) = 10^6\ \mathrm{cm}^{-3}$. Ortho- and para-$H_2$ were assumed in their equilibrium 3:1 ratio. The cooling functions given by Hollenbach & McKee [30] and Lepp & Shull [31], also shown in the figure, differ significantly from those recently computed by Forrey et al. [36] and Le Bourlot et al. [35], especially in the low-density limit, at both low and high temperatures. Of course, the differences disappear in the high density limit where the cooling function is computed in conditions close to LTE. The reduced cooling efficiency of H_2 molecules leaves its imprint on the determination of the characteristic mass scale of the first objects.

In considering the cooling by H_2, it is important not to neglect the effect of reactive collisions of H_2 with H or H^+ that cause ortho–para interchange and lead to a ratio out of the equilibrium value. In the conditions of the primordial gas with $H^+/H \gtrsim 10^{-4}$, the ortho–para exchange is dominated by collisions with protons, and cooling at low temperatures may occur primarily through the $J = 2 - 0$ transition of para-H_2. Le Bourlot et al. [35] have

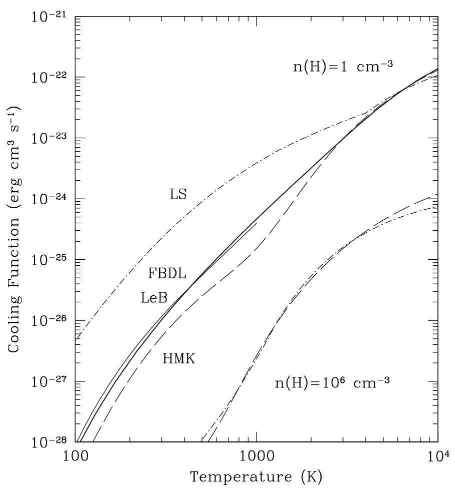

Fig. 3. Cooling function of H_2 for H-H_2 collisions for two values of the density. The thick solid curve shows the results of Le Bourlot et al. ([35]; LeBPF), while the thin solid line limited to $T < 1000$ K is from Forrey et al. ([36]; FBDL). The other curves give the cooling functions computed by Lepp & Shull ([31]; LS) and Hollenbach & McKee ([30]; HMK). (Adapted from [8])

calculated the variation of the ortho–para ratio as a function of temperature and density, and their results should be included in any realistic cosmological application.

3.2 HD Molecules

Due to its small dipole moment, $D = 8.3 \times 10^{-4}$ debyes, the energy spacing of the rotational levels of HD is large, but smaller than that of H_2. The lowest transition that can be excited in HD ($J = 1 - 0$) has an energy of 128 K, four times less than H_2. Therefore, HD molecules are important to enhance the cooling efficiency with increasing gas density and decreasing temperature.

The coefficients for inelastic scattering of HD by He and H_2 have been computed by Schaefer [37] for levels $J \leq 4$. Their values should be diveded by a factor 1.27 to account for the difference between the (HD,H) and (HD,He) interaction potentials (see [8]). Recently, Roueff & Flower [38] have computed rate coefficients for rotational transitions induced by collisions of HD with H atoms using fully quantum mechanical methods and an updated potential surface. Their calculations include levels up to $J = 9$ of the vibrational ground state and cover the temperature range 100 to 1000 K.

4 Interaction of Molecules with the CBR

The discussion of the previous sections has omitted the physical processes resulting from the interaction of the photons of the CBR with the primordial gas. Here, we briefly conclude by reviewing two specific issues: (a) the modification to the cooling function due to the presence of the background radiation field and (b) the Thomson scattering of CBR photons on trace molecules.

4.1 Heating vs. Cooling

The cooling functions described in Section 3 have been computed assuming that the temperature of the CBR is much smaller than the gas temperature. This approximation of course is valid at low redshifts, but becomes increasingly inaccurate at higher redshifts. Since most cosmological scenarios of structure formation begin at $z \simeq 100$, when $T_{\rm CBR} \simeq 300$ K, the level population of molecules is greatly affected by stimulated emission and absorption (see Capuzzo-Dolcetta et al. [39]).

For example, in the standard model of Sect. 2, the CBR temperature is always higher than, or equal to the matter temperature. Hence, the energy transfer function $(\Gamma - \Lambda)_{\rm mol}$ in eq. (4) becomes an effective heating source for the gas because the rate of collisional de-excitation of the rovibrational molecular levels is faster than their radiative decay ([40], [7]). As an illustration of the effects of accounting for the calculation of the level population in the presence of the CBR, we show in Figure 4 the net heat transfer function $(\Gamma - \Lambda)_{\rm H_2}$ computed at three selected redshifts. Note that for $T_{\rm gas} > T_{\rm CBR}$ the cooling function is significantly decreased from the value computed for $T_{\rm CBR} = 3$ K, because of the radiative depopulation of excited states. The sudden drop signals the condition when the two temperatures are equal. Finally, for $T_{\rm gas} < T_{\rm CBR}$ the function changes sign and becomes a heating term for the gas. Naturally, in cosmological simulations the heat transfer should be computed self-consistently at each redshift.

4.2 Thomson Scattering Due to Molecules

In addition to thermal absorption and emission, molecules of the primordial gas can also interact with the CBR via Thomson scattering. As pointed out by Zel'dovich et al. [11], the case for scattering is interesting since the cross-section for scattering of a harmonic oscillator is many orders of magnitudes larger than for free electrons. Although scattering occurs only in narrow spectral lines, the spectrum of molecular transitions contains several bands and the cumulative effect can give rise to appreciable continuum absorption.

Spatial anisotropies in the CBR can be produced by Thomson scattering of photons on molecules (or electrons) located in protoclouds moving with a peculiar radial velocity component $v_{\rm pec}$ (e.g. [41]). This process can create a

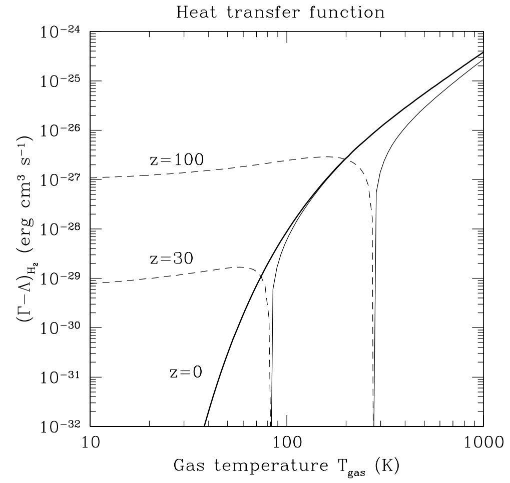

Fig. 4. The heat transfer function $(\Gamma-\Lambda)_{H_2}$ versus the gas temperature at selected redshifts. The solid line is computed ignoring the effects of the CBR ($z=0$). When $T_{\rm gas} > T_{\rm CBR}$ the heat exchange is a cooling term (solid portion of the two other curves). In the opposite case, the transfer becomes a heating source for the gas (dashed curves).

curtain that blurs primordial CBR anisotropies [42]. The level of secondary anisotropies in the CBR temperature at a frequency ν is simply

$$\frac{\Delta T}{T} = \frac{v_{\rm pec}}{c}\left(1-e^{-\tau_{\rm cl}}\right) \tag{7}$$

where $\tau_{\rm cl}$ is the optical depth through the cloud. The actual calculation of the resulting $\Delta T/T$ requires the solution of the radiative transfer equation in the moving cloud (see [43] for details).

In general, one can compute the total optical depth due to resonant Thomson scattering for all the relevant molecules, using the chemical evolution described in Sect. 2. This quantity is given by

$$\tau_{\rm tot} = \sum_i \int \sigma x_i n_b dl, \tag{8}$$

where σ is the Thomson cross section, normalized to the linewidth $\Delta\nu_D$ due to Doppler broadening, x_i is the fractional molecular abundance, and dl is the photon path length in the redshift interval dz. In order to evaluate (8), one has to compute the level population of each molecule.

LiH and H_2D^+ are promising molecules because of their large dipole moments ([42], [41]). However, their tiny final abundances (LiH/H$\simeq H_2D^+$/H$\simeq 10^{-19}$) yield negligible optical depths, $\tau_{\rm LiH} \simeq 10^{-10}$ at $\nu \simeq 30$ GHz and

$\tau_{\mathrm{H_2D^+}} \simeq 10^{-13}$ at $\nu \simeq 40$ GHz. The only trace molecule of some interest turns out to be $\mathrm{HeH^+}$ which, despite a freeze-out abundance of $\mathrm{HeH^+/H} \simeq 10^{-12}$, has a maximum optical depth of $\tau_{\mathrm{HeH^+}} \simeq 10^{-5}$ at $\nu \simeq 50$ GHz due to the excitation of rotational transitions. The variation of the total optical depth due to Thomson scattering on $\mathrm{HeH^+}$ is shown in Figure 5. From eq. (7), we see that even for $v_{\mathrm{pec}} \sim 300$ km s^{-1}, the resulting spatial variations of the CBR temperature are only $\Delta T/T \sim 10^{-8}$. On the other hand, the expected spectral distortion of the CBR should affect all angular scales smaller than the angular diameter of the horizon by an amount $(1 - e^{-\tau_\nu}) \simeq 10^{-5}$. Since ongoing CBR anisotropy experiments in the 10-50 GHz frequency range reach a sensitivity of $\sim 10\,\mu$K, and the fluctuations measured on degree scales are of order $\sim 100\,\mu$K, it is not completely out of the question that one may eventually be able to search for $\mathrm{HeH^+}$ at high redshifts.

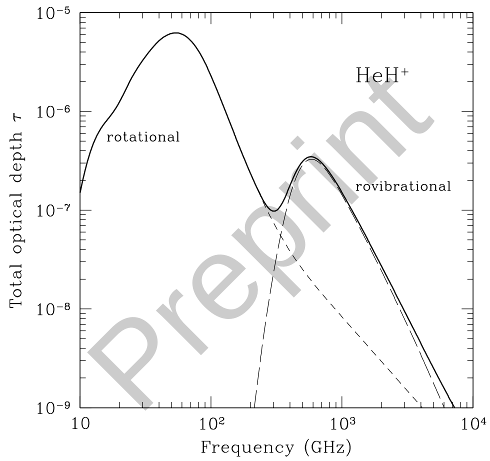

Fig. 5. Optical depth of the universe generated by Thomson scattering of the CBR photons on $\mathrm{HeH^+}$ molecules. The contribution of rotational and rovibrational transitions to the total (*solid* line) is shown by the *dashed* curves.

4.3 How Small Were the First Cosmological Objects?

This important question is fully addressed in the multidimensional numerical simulations presented by Norman et al. and Bromm et al. in these proceedings. Here, we consider a particular issue related to the choice of the initial conditions for fragmentation and collapse calculations. The relevant question is: how much molecular cooling is needed for a gas cloud to be able to cool in a

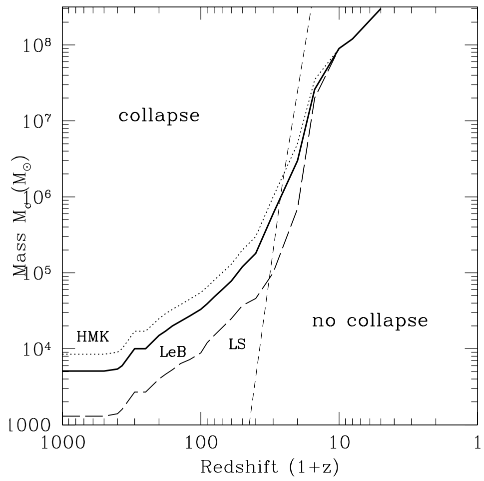

Fig. 6. The minimum mass needed to collapse. The function M_c is plotted as a function of virialization redshift for standard CDM (Ω =1, Ω_b =0.06, h =0.5). The three curves are for different H_2 cooling functions, labeled as in Fig. 3. Only lumps whose parameters (z_{vir}, M_c) lie above these curves can collapse and form luminous objects. The dashed line corresponds to 3σ peaks in standard CDM, normalized to σ_8 =0.7, so such objects with baryonic mass $\Omega_b \times 2 \times 10^6 M_\odot \sim 10^5 M_\odot$ can form at z =30. (Adapted from [45] [46])

Hubble time? Haiman et al. [44] and Tegmark et al. [45] have provided an answer to the question of the formation of H_2 using an approximate method for the halo density profile and following the growth of an isolated density peak that is spherically symmetric. The critical H_2 fraction satisfies the condition that the cooling and the Hubble timescales must be equal. This fraction is given by

$$f_{H_2} \approx 2 \times 10^{-4} \left(\frac{h\Omega_b}{0.03}\right)^{-1} z_{100}^{-3/2} \left(1 + \frac{10T_3^{7/2}}{60 + T_3^4}\right) e^{512/T} \tag{9}$$

where the last two terms on the left hand side come from an approximation to the cooling function obtained by [29]. The H_2 fraction required exceeds typical initial abundances ($\sim 10^{-4}$) for all redshifts z <200 when the temperature is less than $\sim 10^4$ K. Therefore, the low-mass high-redshfit clouds can cool and collapse only if additional H_2 is produced. This can happen during the virialization phase of an overdense region that grows and goes nonlinear.

As a rule of thumb, Tegmark et al. [45] find that if the virial temperature is high enough to produce an H_2 fraction of order 5×10^{-4}, then the cloud will collapse. Computing the density, temperature and H_2 abundance in virialized lumps as a function of $z_{\rm vir}$, they find that the minimum baryonic mass, $M_b =$

$\Omega_b M_c$, is strongly redshift dependent, dropping from 10^6 $M_\odot$ at $z \sim 15$ to 5×10^3 $M_\odot$ at $z \sim 100$. The resulting minimum mass for collapse is shown in Figure 6. The solid line has been computed using the cooling function of Le Bourlot et al. [35], but the qualitative behavior is the same for all functions. For $z > 100$, M_c decreases less rapidly with redshift as the CMB photons inhibit H_2 formation through the H^- channel. For $z > 200$, the H_2^+ channel for H_2 formation becomes effective, driving M_c down toward $M_c \sim 10^3 M_\odot$. With a standard CDM power spectrum with $\sigma_8 = 0.7$, this implies that a fraction 10^{-3} of all baryons may have formed luminous objects by $z = 30$, which could be sufficient to reheat the universe.

References

1. Cen, R., Ostriker, J.P., Peebles, P.J.E. 1993, ApJ, 415, 423
2. Couchman, H.M.P., Rees, M.J. 1986, MNRAS, 221, 53
3. de Araújo, J.C.N., Opher, R. 1991, ApJ, 379, 461
4. Saslaw, W.C., Zipoy, D. 1967, Nature, 216, 967
5. Peebles, P.J.E., Dicke, R.H. 1968, ApJ, 154, 891
6. Lepp, S., Shull, J.M. 1984, ApJ, 280, 465
7. Puy, D., Alecian, G., Le Burlot, J., Léorat, J., Pineau des Fôrets, G. 1993, AA, 267, 337
8. Galli, D., Palla, F. 1998, AA, 335, 403
9. Mather, J.C., Cheng, E.S., Cottingham, D.A. et al. 1994, ApJ, 420, 439
10. Peebles, P.J.E. 1968, ApJ, 153, 1
11. Zel'dovich, Ya.B., Kurt, V.G., Suyaev, R.A. 1968, Zh. Eksp. Teoret. Fiz., 55, 278. English transl., 1969, Sov Phys JETP, 28, 146
12. Sasaki, S., Takahara, F. 1993, PASJ, 45, 655
13. Grachev, S.I., Dubrovich, V.K. 1991, Astrophysics, 34, 124
14. Peebles, P.J.E. 1993, Principles of Physical Cosmology (Princeton Univ. Press: Princeton), chapter 6
15. Boschán, P., Biltzinger, P. 1998, AA, 336, 1
16. Seager, S., Sasselov, D.D., Scott, D. 1999, ApJ, in press
17. van den Bergh, S. 1989, Astron. Astrophys. Rev., 1, 111
18. Galli, D., Palla, F., Ferrini, F., Penco, U. 1995, ApJ, 443, 536
19. Smith, M.S., Kawano, L.H., Malaney, R.A. 1993, ApJS, 85, 219
20. Black, J.H. 1991, in Molecular Astrophysics, ed. T.W. Hartquist (Cambridge: Cambridge Univ. Press), 473
21. Rawlings, J.M.C., Drew, J.E., Barlow, M.J. 1993, MNRAS, 265, 968
22. Latter, W.B., Black, J.H. 1991, ApJ, 372, 161
23. Dalgarno, A., Lepp, S. 1987, in IAU Symp. 118 Astrochemistry, eds. M.S. Vardya & S.P. Tarafdar (Dordreht: Reidel), 109
24. Palla, F., Galli, D., Silk, J. 1995, ApJ, 451, 44
25. Mandy, M.E., Martin, P.G. 1993, ApJS, 86, 199
26. Sun, Y., Dalgarno, A. 1994, ApJ, 427, 1053
27. Flower, D.R. 1997a, MNRAS, 288, 627
28. Flower, D.R. 1997b, J Phys B, 30, 1
29. Hollenbach, D., McKee, C.F. 1979, ApJS, 41, 555

30. Hollenbach, D., McKee, C.F. 1989, ApJ, 342, 306
31. Lepp, S., Shull, J.M. 1983, ApJ, 270, 578
32. Flower, D.R. 1998, MNRAS, 297, 334
33. Boothroyd, A.I., Keogh, W.J., Martin, P.G., Peterson, M.R. 1996, J Chem Phys, 104, 7139
34. Tiné, S., Lepp, S., Dalgarno, A. 1998, in Molecular Hydrogen in the Early Universe, eds. E. Corbelli, D. Galli & F. Palla, Mem Soc Astr It, 69, 345
35. Le Bourlot, J., Pineau des Fôrets, G., Flower, D.R. 1999, MNRAS, 305, 802
36. Forrey, R.C., Balakrishnan, N., Dalgarno, A., Lepp, S. 1997, ApJ, 489, 100
37. Schaefer, J. 1990, AAS, 85, 1101
38. Roueff, E., Flower, D.R. 1999, MNRAS, 305, 353
39. Capuzzo-Dolcetta, R., Di Fazio, A., Palla, F. 1991, AAS, 88, 451
40. Khersonskii, V.K. 1986, Astrophysics, 24, 114
41. Maoli, R., Melchiorri, F., Tosti, D. 1994, ApJ, 425, 372
42. Dubrovich, V.K. 1993, SvA Lett, 19, 53
43. Bougleux, E., Galli, D. 1997, MNRAS, 288, 638
44. Haiman, Z., Rees, M.J., Loeb, A. 1997, ApJ, 476, 458
45. Tegmark, M., Silk, J., Rees, M.J., Blanchard, A., Abel, T., Palla, F. 1997, ApJ, 474, 1
46. Abel, T., Anninos, P., Norman, M.L., Zhang, Y. 1998, ApJ, 508, 518

The First Stars: Where Did They Form?

Jordi Miralda-Escudé[1,2]

[1] University of Pennsylvania, David Rittenhouse Laboratory, 209 St. 33rd St., Philadelphia PA 19104-6396 jordi@llull.physics.upenn.edu
[2] Alfred P. Sloan Fellow

Abstract. Several emerging links between high-redshift observational cosmology, and the Galactic fossil evidence found in the kinematics, metallicities and ages of Milky Way stars are discussed. In a flat Cold Dark Matter model with $\Omega \simeq 0.3$ that agrees with present large-scale structure observations, the oldest stars in the Milky Way should have formed in the first halos where gas was able to cool, at $z \simeq 20$. These earliest, weakly bound dwarf galaxies probably turned only a small fraction of their gas to stars, which should be metal-poor. However, the merging rate in the early universe was much faster than the present one, so massive halos with more efficient star formation and metallicities up to the highest values present today in the bulge could have formed less than 10^9 years after the oldest stars. The mean metallicity produced in the universe by a given redshift is related to the mean surface brightness of star-forming galaxies above this redshift, and also to the reionization epoch if galaxies were the dominant sources of ionizing radiation. The biased distribution of the early dwarf galaxies where the first stars formed should result in an age gradient with radius of the low-metallicity stars in the Milky Way, with the oldest ones concentrated in the bulge and the youngest in the outer halo.

1 Introduction

Interest in observations of the Galactic fossil evidence contained in the spatial distribution and metallicities of stars was for a long time driven by phenomenological models of the formation of the Galaxy. The first model [8] proposed a monolithic and rapid collapse forming the halo first and then the disk. A second one [22] suggested instead a more gradual collapse of gas clumps to form the halo. In modern cosmology, the formation of the Galaxy must be viewed in its cosmological context, where the large-scale structure theories for the initial fluctuations that collapsed to galaxies are tested with observations of the Cosmic Microwave Background, galaxy clustering and evolution, gravitational lensing, Lyα forest absorption, etc. These ab initio theories should also predict in principle the statistical characteristics of the formation of a typical galaxy like the Milky Way (such as the number of clumps that merged to form our Galaxy at different times and their contents in gas and stars). In practice, many of these predictions are uncertain due to the large dynamic range involved, and the complexity of physical processes like radiative cooling, thermal instability and star formation. We should nevertheless attempt to identify predictions that circumvent these uncertainties.

I review the ideas for galaxy formation in CDM models in §2, discussing the formation of the first stars in §3, and where they are now in §4.

2 Galaxies at $z > 5$

I will use here the Cold Dark Matter model with $\Omega = 0.3$, $\Lambda = 0.7$, $H_0 = 65\mathrm{km\,s^{-1}\,Mpc^{-1}}$, $\Omega_b h^2 = 0.019$, and normalization $\sigma_8 = 0.9$. This model seems to fit basically all available observations of large-scale structure, [30], and of Type Ia supernovae as distance indicators [18,20].

In any large-scale structure models hypothesizing the presence of dark matter that can cluster on small scales, gravitational collapse starts with low-mass halos, which then grow in mass by merging with each other and accreting the remaining diffuse matter. The abundances of halos as a function of redshift is easily visualized in Figure 1, where the three thick solid lines give the velocity dispersion (right vertical axis) or virial temperature of the gas (left vertical axis) of a halo collapsing at redshift z from a $(1, 2, 3) - \sigma$ fluctuation, in the model adopted here, calculated in the Press-Schechter model [19,3]. The lower line represents the typical object present at a given redshift, while the upper line gives the most massive objects, containing only about 0.3 % of the mass of the universe if the fluctuations are Gaussian. This upper line indicates, for example, that at $z = 3$ the most massive clusters should not have velocity dispersions in excess of $400\,\mathrm{km\,s^{-1}}$. The thin dotted lines are of constant halo mass, increasing in steps of factors of 10.

Also shown as thick dotted lines are the halos where the radiative cooling time of the gas equals the Hubble time, for three values of the gas metallicity. Above these lines, the halo gas does not have enough time to cool, and therefore cannot form galaxies (e.g., [32]). Notice that the gas could still cool in the central parts of these halos, corresponding to massive clusters, owing to the higher density near the center; but we know observationally that star formation does not occur in large amounts in these cooling regions around central cluster galaxies, for reasons that are not understood [9].

After the intergalactic medium was reionized (at $z > 5$), galaxies could only form in halos with $\sigma \gtrsim 30\,\mathrm{km\,s^{-1}}$, because photoionization heats the gas, raises the Jeans scale, and makes line-cooling inefficient in objects that collapse only marginally above the Jeans scale (e.g., [29]). Thus, the lower thick solid line in Figure 1 shows that most of the gas in the universe had to stay in diffuse form until $z < 2$, which is confirmed in numerical simulations of the Lyα forest [14,35].

Up to redshifts of ~ 4, it was possible to form galaxies with a total mass similar to a typical L_* galaxy today. At that time, galaxies of this size should have formed by the cooling of all the gas in some of the most massive halos that existed, and can be identified with the luminous Lyman break galaxies (e.g., [26]). But at higher redshifts, the maximum mass of galaxies must rapidly decline. For example, at $z = 8$, galaxies formed from $3 - \sigma$

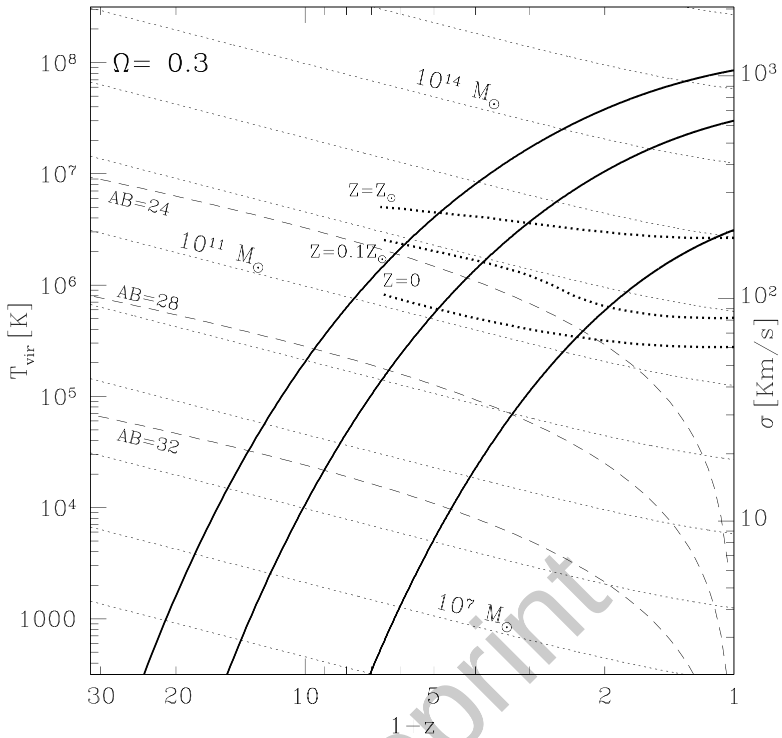

Fig. 1. Velocity dispersion of halos collapsed from $(1, 2, 3) - sigma$ fluctuations at each redshift (*solid thick lines*. See the text for description of other lines.

fluctuations should be 100 times less massive than at $z = 4$ in Figure 1. Even if starbursts at high redshift occur on shorter timescales or are more efficient than at low redshift, the rapid decline in galaxy mass should most likely cause a similar decline in galaxy luminosities at $z > 5$.

The mean UV surface brightness of high-redshift galaxies can be related to the mean metallicity that their stars produced and to the number of ionizing photons that were emitted [24,13,15]. We know that the universe had to be reionized before $z = 5$. If star-forming galaxies were the main sources responsible for reionization, then at least one ionizing photon per baryon had to be emitted. More likely, several ionizing photons were needed since most photons could have been absorbed locally by the interstellar gas in the emitting galaxies, and the intergalactic gas can also recombine several times before $z = 5$. For every ten ionizing photons emitted per baryon in the universe by stars, the mean metallicity rises by $10^{-2} Z_{\odot}$, and the galaxies containing the stars contribute 32 AB magnitudes per square arc second to the sky surface brightness in a redshifted UV band to the red of the Gunn-

Peterson trough [15], where galaxies can most easily be observed at high redshifts. The heavy elements produced by this first generation of galaxies could be the ones that are observed at $z \sim 3$ in the diffuse Lyα forest gas [25], and in some of the lowest metallicity stars we observe at present.

The dashed lines in Figure 1 indicate the AB magnitude of a starburst galaxy that forms in a halo of velocity dispersion σ at redshift z (in a rest-frame UV band to the red of the Gunn-Peterson trough), assuming the optimistic case where all the halo gas turns to stars on a timescale of the order of the age of the universe (this simple model is described in more detail in [15]). This shows that typical galaxies at redshift $z = 10$ are not likely to be brighter than $AB = 30$, and are probably even fainter if star formation is less efficient (converting only a small fraction of the halo gas into stars).

3 The Very First Stars

The first objects where gas is able to cool in the universe correspond to the high peaks of the density field collapsing on scales of $\sim 10^7 M_\odot$, at $z \sim 20$ in the model of Fig. 1 (see [4]). In halos with temperatures $T \gtrsim 1000$ K the gas cools effectively through the rovibrational levels of a small fraction of molecular hydrogen, formed from the primordial ionization fraction via H^- [21,17,28]. We also see in this Figure that these early halos merge very rapidly, with the virial temperatures of $3 - \sigma$ peaks increasing from 2000 K (where molecular cooling is first rapid enough to lead to the first stars) to 8000 K (where atomic line cooling is already effective) over the short interval from $z = 19$ to $z = 16$.

Recently the first simulations of the formation of the first objects which compute the formation of the molecular hydrogen, with high enough resolution to identify the site where the cooled gas concentrates to form stars, have been performed ([1,2,16]. These simulations show that once the gas cools fast enough, it becomes self-gravitating and forms a cooling flow in the halo center (notice that because of the rapid merging rate there should often be several "halo centers" or density peaks in a given collapsed object). Obviously the gas at the center cools fastest and will collapse first. At the center of the cooling flow, the cloud becomes optically thick and fully molecular by three-body reactions, on a time short compared to the evolutionary timescale of the halo, and this should cause the rapid cooling and collapse of a central core with a mass of 100 to $1000 M_\odot$ [2,16].

There is much uncertainty about the type of stars that will form first in the center of this cooling flow [27,12,6,23]: Will the first stars be massive? Will many stars be formed by rapid fragmentation? What differences in the star formation process will be caused by the absence of heavy elements and magnetic fields? If low-mass stars formed at the same time as the first massive stars in these low-mass halos, then there should be some stars with zero metallicity at present; otherwise, all low-mass stars will have a minimum metallicity generated by the first supernovae.

Even if rapid fragmentation led to the formation of a large number of low-mass stars first, it is clear that massive stars should eventually form in the first low-mass halos. As long as the formation of stars does not release much energy, gas will continue to cool and accumulate in the center, and continued accretion of more gas at the bottom of the potential cannot be stopped until a sufficiently massive star is formed to heat and expel the gas around it. A single massive star will produce about 10^{63} ionizing photons, about the same as the number of atoms in a halo containing $10^6\, M_\odot$ of baryons. Several massive stars need to form to maintain the entire halo ionized, since the recombination time at the virial radius of $\sim$ 100 pc is typically 10^5 years. The evolution after the formation of massive stars is likely to be very similar to that of molecular clouds in our Galaxy: their lifetimes are not much longer than 10^7 years, as they are destroyed after the formation of a few O stars, turning only 1% to 10% of their mass into stars [33,34,11,5]. Molecular clouds and the first halos to form stars have similar baryonic masses, and if anything the first halos are less dense and their low metallicity should reduce cooling, making them easier to be heated and dispersed by ionization and supernova explosions compared to Galactic molecular clouds. Every supernova explosion produces a few solar masses of metals which, if spread over $10^6 M_\odot$ of gas in a halo, will raise the metallicity by $\sim 10^{-4} Z_\odot$.

Whereas in the Milky Way a destroyed molecular cloud disperses in the atomic medium, and the gas probably forms molecular clouds again when it crosses another spiral arm shock [11], in the first collapsed halos the gas can be expelled in a wind, and can later collapse again into a more massive object as the sequence of mergers continues. A self-regulated star formation process can then start, where new halo mergers produce new starbursts which are stopped when enough energy is produced by ionizing radiation and supernovae to disperse the gas again.

4 Where Are the First Stars?

The self-regulation of star formation in galaxies naturally leads to the idea that the gas metallicity in a halo will depend mostly on the velocity dispersion. Gas in weakly bound halos will be heated and dispersed easily after the formation of a very small number of massive stars, but in more strongly bound halos star formation can proceed faster, since the energy output of stars is insufficient to drive a strong wind, and heated gas is quickly recycled into new molecular clouds. Since the metallicity depends on the overall fraction of the gas that has been turned to stars, it should reflect the efficiency of star formation in each halo.

The earliest stars formed at $z \simeq 20$ should clearly be metal-poor. However, in any models where the spectrum of the rms density fluctuation flattens at small scales (as in CDM), the velocity dispersions increase very fast at early epochs. Thus, by $z = 9$, $3-\sigma$ peaks (which contain 0.3% of the mass) are already halos with $\sigma = 50\,\mathrm{km\,s^{-1}}$, similar to the LMC, which could therefore have characteristic metallicities $\sim 0.1 Z_{\odot}$, and solar metallicities can generally be produced as soon as sufficiently massive objects have collapsed in any model [10,7]. At the same time, stars with the lowest metallicities will not all form at the highest redshifts: most of them will form when the low velocity dispersion halos collapse from $1-\sigma$ peaks, at $z < 9$. Reionization can in fact stop much of the gas in the universe from collapsing and forming stars until it becomes part of a system with $\sigma \gtrsim 30\mathrm{km\,s^{-1}}$, implying that most stars at the lowest metallicities would form at $z < 2$ for the model of Figure 1.

Because the age difference between $z = 20$ and $z = 9$ is only about 400 million years, the prediction that the *very oldest* stars should all be metal-poor will be difficult to test. Until ages for the oldest stars are not measured with accuracies greater than $\sim 10^9$ years, we should expect essentially no correlation between age and metallicity [31].

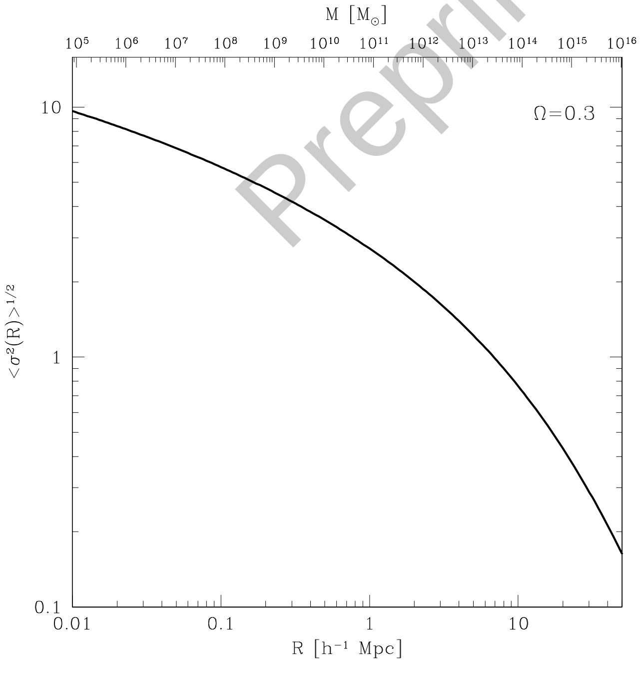

Fig. 2. Rms density fluctuation linearly extrapolated to the present time on spheres of radius R and mass M.

Another interesting feature of CDM-like theories is the strong bias of collapsed objects on small scales, which should cause the oldest low-metallicity stars to be more abundant in the central parts of galaxies and clusters. Figure 2, showing the rms density fluctuation (linearly extrapolated to the present) as a function of the smoothing scale for the same CDMΛ model used in Fig. 1, serves to illustrate the idea. We consider a $10^7 M_\odot$ halo collapsing from a $3-\sigma$ peak at $z = 18$ as the typical site where the oldest stars were formed. On average, $3-\sigma$ peaks contain 0.3% of the mass; however, this fraction should change in different environments, being high within a massive galaxy or cluster that collapsed early, and low in a low-mass galaxy that collapsed late, owing to the bias effect [31]. As an example, consider the condition that the halo of the Milky Way has recently reached a mass of $10^{12} M_\odot$, collapsing from a $1-\sigma$ fluctuation on this scale. Now, we find from Figure 2 that the ratio of the rms fluctuation on the scales of $10^{12} M_\odot$ and $10^7 M_\odot$ is 0.3, so the overdensity due to a $1-\sigma$ fluctuation on $10^{12} M_\odot$ already provides 10% of the total overdensity needed for a $3-\sigma$ peak at the scale of $10^7 M_\odot$. At the same time, the rms fluctuations on scales $10^7 M_\odot$ that are independent of the smoothed fluctuations on $10^{12} M_\odot$ are reduced by a factor $1-(1/3)^2 = 8/9$. Thus, given the condition of being part of the Milky Way halo at present, the abundance of objects of $10^7 M_\odot$ formed at $z = 18$ should actually correspond to a density peak $(3-0.3)\cdot(9/8)^{1/2} = 2.86$ times the rms, or an abundance about 50% higher than the average. On the other hand, in a massive galaxy collapsing on the same scale of $10^{12} M_\odot$ from a $3-\sigma$ peak at $z = 5$ (likely to be part of a cluster today), the abundance of the $10^7 M_\odot$ objects collapsed at $z = 18$ should correspond to $(3-0.9)\cdot(9/8)^{1/2} = 2.23-\sigma$ peaks, or an abundance ~ 10 times higher than the average.

Of all the galaxies that formed within the region that has collapsed to the Milky Way today, the ones that ended up merging into the bulge were the ones that formed in a region with a high overdensity on the scale of the bulge mass (this assumes that the bulge collapsed before the Galactic disk was formed, which is supported by the existence of bulge stars with much lower metallicities than the minimum disk metallicities). Therefore, they should also contain the largest abundance of the oldest low-metallicity stars, due to the same bias effect discussed above. On the other hand, the low-metallicity stars in the Local Group dwarfs, and in the outer parts of the Milky Way halo (if they resulted from the disruption of satellite dwarfs) obviously did not merge into a massive galaxy until they fell recently to the Milky Way halo, so they were formed in underdense regions on the scale of the bulge mass, and they are likely to have formed from low peaks at low redshift. They should consequently have low-metallicity stars that are younger than in the bulge of the Milky Way and M31.

This prediction is uniquely characteristic of large-scale structure theories, since in earlier models it was assumed that the low-metallicity stars formed in the early generations that produced the heavy elements in the bulge would still be found in the outer halo, and would therefore be the oldest stars, with the gas being enriched as it collapsed further toward the center. These predictions are discussed here at a very qualitative level, but improved numerical simulations of galaxy formation combined with chemical-enrichment models are likely to make these more quantitative in the near future.

References

1. Abel, T., Anninos, P., Norman, M. L., & Zhang, Y. 1998, ApJ, 508, 518
2. Abel, T., Bryan, G., & Norman, M. L. 1999, in *H2 in Space*, eds. F. Combes, G. Pineau des Forêts, Cambridge University Press.
3. Bond, J. R., Kaiser, N., Cole, S., & Efstathiou, G. 1991, ApJ, 379, 440
4. Blumenthal, G. R., Faber, S. M., Primack, J. R., & Rees, M. J. 1984, Nature, 311, 517
5. Carpenter, J. M., Snell, R. L., & Schloerb, F. P. 1995, ApJ, 450, 201
6. Carr, B. J., Bond, J. R., & Arnett, W. D. 1984, ApJ, 277, 445
7. Cen, R., & Ostriker, J. P. 1999, ApJ, 519, L109
8. Eggen, O. J., Lynden-Bell, D., & Sandage, A. R. 1962, ApJ, 136, 748
9. Fabian, A. C., Nulsen, P. E. J., & Canizares, C. R. 1991, A&A Rev, 2, 191
10. Gnedin, N., & Ostriker, J. P. 1997, ApJ, 486, 581
11. Heyer, M. H., & Terebey, S. 1998, ApJ, 502, 265
12. Kashlinsky, A., & Rees, M. J. 1983, MNRAS, 205, 955
13. Madau, P., & Shull, J. M. 1996, ApJ, 457, 551
14. Miralda-Escudé, J., Cen, R., Ostriker, J. P., & Rauch, M. 1996, ApJ, 471, 582
15. Miralda-Escudé, J., & Rees, M. J. 1998, ApJ, 497, 21
16. Norman, M. L. 1999, these proceedings
17. Peebles, P. J. E., & Dicke, R. H. 1968, ApJ, 154, 891
18. Perlmutter, S., et al. 1998, Nature, 391, 51
19. Press, W. H., & Schechter, P. 1974, ApJ, 193, 437
20. Riess, A. G., et al. 1998, AJ, 116, 1009
21. Saslaw, W. C., & Zipoy, D. 1967, Nat, 216, 967
22. Searle, L, & Zinn, R. 1978, ApJ, 225, 357
23. Silk, J. 1983, MNRAS, 205, 705
24. Songaila, A., Cowie, L. L., & Lilly, S. J. 1990, ApJ, 348, 371
25. Songaila, A., & Cowie, L. L. 1996, AJ, 112, 335
26. Steidel, C. C., Adelberger, K. L., Giavalisco, M., Dickinson, M., & Pettini, M. 1999, ApJ, 519, 1
27. Takeda, H., Sato, H., & Matsuda, T. 1969, Prog. Theor. Phys., 41, 840
28. Tegmark, M., Silk, J., Rees, M. J., Blanchard, A, Abel, T., & Palla, F. 1997, ApJ, 474, 1
29. Thoul, A., & Weinberg, D. H. 1996, ApJ, 465, 608
30. Wang, L., Caldwell, R. R., Ostriker, J. P., & Steinhardt, P. J. 1999, ApJ, in press (astro-ph/9901388).
31. White, S. D. M., & Springel, V., these proceedings.
32. White, S. D. M., & Rees, M. J. 1978, MNRAS, 183, 341
33. Williams, J. P., & McKee, C. F. 1997, ApJ, 476, 166
34. Williams, J. P., Blitz, L., & McKee, C. F. 1999, in *Protostars and Planets IV*
35. Zhang, Y., Meiksin, Anninos, P., & Norman, M. L. 1998, ApJ, 495, 63

First Structure Formation and the First Stars

Michael L. Norman[1], Tom Abel[2], and Greg Bryan[3]

[1] University of Illinois, Urbana, IL 61801
[2] Harvard University, Cambridge, MA 02138
[3] MIT, Cambridge, MA 02138

Abstract. We discuss the results of recent 3D simulations of first structure formation in relationship to the formation of the first stars. On the basis of a new, high-resolution AMR simulation (spatial dynamic range = 3×10^7), we conclude that the first stars are likely to be massive.

1 First Cosmological Objects

Hierarchical theories of structure formation such as Cold Dark Matter (CDM) and its variants have been very successful in accounting for the existence of galaxies, galaxy clusters and cosmological large scale structure in the low redshift universe [10,26]. The cynic would say that this is what they were invented to do. However, the models also make definite predictions at earlier epochs and on different mass scales which can be checked observationally. Some proof that these models are *essentially correct* is the remarkable agreement achieved between the observed and predicted properties of the Lyman alpha forest at $2 < z < 4$ (e.g. [37,31]) — something the models were not designed to do. Encouraged by this agreement, we may ask: *what were the first objects to form in such models?*

Assuming the CDM power spectrum extends to very small mass scales, the first cosmological objects to form are small dark matter halos collapsing from small scale density fluctuations at high redshift ($z \sim 30$) [15,35]. Halos whose mass is significantly less than the cosmological Jeans mass $M \sim 10^{4-5} M_{\odot}$ would not be able to trap the baryonic fluid, and hence not form astrophysical objects. Conversely, halos of approximately this mass or greater would be expected to form highly condensed objects (stars, black holes, etc.) provided the gas can cool and transport angular momentum. At the temperatures and densities prevailing in such halos, the primordial gas cools inefficiently by collisional excitation of H_2 molecules which exist in low abundance. As described in more detail below, H_2 forms via nonequilibrium gas phase reactions in which the tiny post-recombination electron abundance acts as a catalyst.

This chemistry, combined with the nonlinear dynamics of halo formation and mergers, makes this epoch of structure formation exceedingly complex and interesting. We have termed this epoch *first structure formation*, and have explored it numerically in recent papers [3,4,11,22]. Here we review our numerical methodologies and findings, and discuss their implications to the first stars.

2 Relevance to First Stars

First structure formation is relevant to the theme of this conference as it is likely that the first stars are formed as a byproduct. Note this is not a theoretical certainty since it has been variously argued that the first objects are not stars in the usual sense, but rather objects at both extremes of the mass spectrum, ranging from supermassive black holes [34] to Jupiter sized "clumpuscules" [14]. Since the mass function of the first objects is not known, much of the theoretical literature consists of making various assumptions about the primordial mass function (PMF) and working out the cosmological consequences. Carr, Bond & Arnett [12] presented a comprehensive review of the prevailing ideas as of 1984, many of which are still relevant today. Couchman & Rees [15] placed the matter in a modern cosmological framework. Both papers highlighted the impact of massive stars and possibly very massive objects (VMOs) on heating, ionizing and enriching the pregalactic medium with heavy elements.

A few authors have attempted to compute the PMF from first principles: Silk [33] argued for a flat PMF between $0.1 - 100 M_\odot$ on the basis of a linear analysis of thermal instability in a primordial gas near the critical density for H_2 formation via three body reactions. Padoan, Jimenez & Jones [29] applied the statistical model for star formation of [28] to primordial globular cluster formation, and found a PMF slightly shallower than the Miller-Scalo IMF [20] with a lower cutoff of $0.2 M_\odot$.

Given the theoretical uncertainties, let us pose the following question: *do stars form in the first nonlinear structures in hierarchical models?* Indications from our recent numerical simulations is that they do. In this paper, we follow our historical developments which lead us toward this conclusion.

3 $\mathbf{H_2}$ Formation and the Minimum Mass to Cool

After recombination, the universe is filled with a neutral, metal-free gas of H and He and trace amounts of D and Li. How can such a gas cool to form stars? Long ago it was realized that small amounts of molecular hydrogen will form in a primordial gas via two reaction pathways: the H^- channel (McDowell 1961):

$$H + e^- \rightarrow H^- + h\nu, \tag{1a}$$

$$H^+ + H \rightarrow H_2 + e^-. \tag{1b}$$

and the H_2^+ channel [32]:

$$H + H^+ \rightarrow H_2^+ + h\nu, \tag{2a}$$

$$H_2^+ + H \rightarrow H_2 + H^+. \tag{2b}$$

At high redshifts $z > 100$ the fragile H^- molecule is photodissociated by the CMB, and thus the H_2^+ channel dominates the production of H_2 . At lower

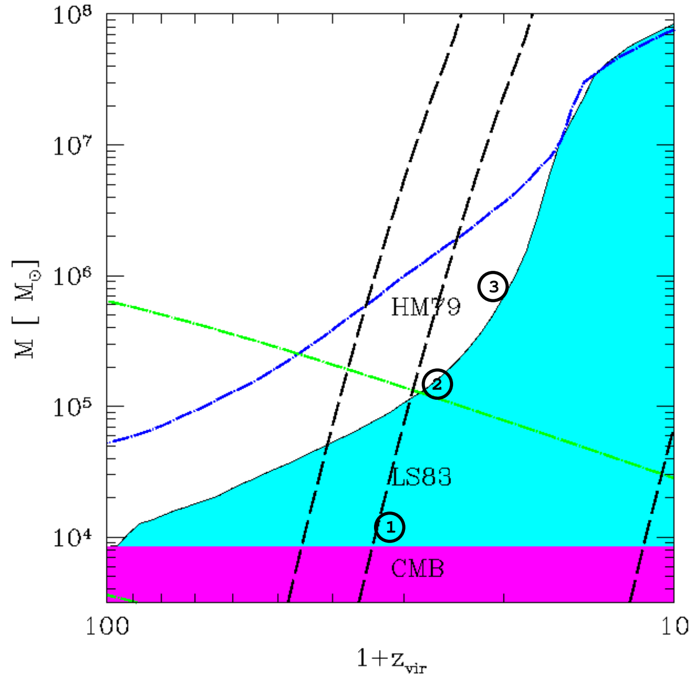

Fig. 1. The horizontal dark shaded region shows the mass scale for which the virial temperature equals the CMB temperature. The light blue shaded area (labeled LS83) represents the domain of parameters for which collapsed structures cannot cool. This curve is computed assuming a spherical collapse model as in [35], except we use the [18] H_2 cooling function. Only above the light shaded area are structures believed to be able to collapse and cool via H_2 . The three heavy dashed lines plot the collapse redshift given by linear theory for the standard CDM spectrum for $1\sigma, 3\sigma$, and 4σ perturbations. The green dot-dashed line represents the Jeans mass at $18\pi^2$ times the background density. The heavy dot-dashed line labeled HM79 is the minimum mass line computed by [35] based on the cooling function by [17]. The circled numbers denote the evolution of the halo discussed in the text.

redshifts, the situation is reversed and the H^- channel dominates. We see from Eq. (1) that free electrons catalyze the formation of H_2 via the H^- channel. Where do they come from? Well, the post-recombination primordial gas is not totally neutral. This is because the recombination time is longer than the cooling time in such a diffuse gas, and the electron abundance is out of equilibrium at a given temperature. Detailed nonequilibrium calculations show that there is a residual ionization fraction of about $x_e \sim 10^{-4}$ at $z \sim 100$ [16]. This is enough to form H_2 with an abundance of $f_{H_2} \equiv n_{H_2}/n_H \sim 10^{-6}$.

As gas concentrates in the potential wells of dark matter halos, the H_2 fraction increases according to a simple analytic result [3]. In the absence of an external UV background at gas temperatures below 6000 K, one can integrate the rate equations for the free electron and H_2 fractions in a collapsing gas cloud to get:

$$
\begin{aligned}
f_{H_2}(t) &= f_{H_2}(t=0) + \frac{k_{PA}}{k_{rec}} ln(x_0 n_H k_{rec} t + 1) \\
&= f_{H_2}(t=0) + 1.0 \times 10^{-8} T_{vir}^{1.53} ln(t/t_{rec} + 1), \qquad (3)
\end{aligned}
$$

where $k_{PA}, k_{rec}, t_{rec}, x_0$, and n_H are the rate coefficients of photo-attachment of H^- and recombination to neutral hydrogen, the initial recombination timescale, ionized fraction, and neutral hydrogen number density, respectively. Given the H_2 cooling function, one can ask at what concentration will the cooling time be less than the Hubble time for a spherical top hat perturbation of mass M collapsing at redshift z? This analysis was first carried out by [1] and later by [35], who found a rather universal result: $f_{H_2}(crit) \sim 5 \times 10^{-4}$. Fig. (1) shows the locus of critical cloud masses as a function of redshift for two choices of the cooling function, which is still somewhat uncertain (for a recent discussion of the uncertainties, see [36]. As can bee seen, extremely rare 4σ peaks of mass $\gtrsim 5 \times 10^4 M_\odot$ will collapse and cool at $z \sim 40$, whereas more typical 2.5σ fluctuations of mass $\gtrsim 5 \times 10^5 M_\odot$ will collapse and cool at $z \sim 25$. The evolution of such a peak described in detail below is shown by the circled numbers in Fig. 1.

4 Simulating First Structure Formation

First structure formation is a well-posed problem both physically and computationally, since for a given cosmogony the thermodynamic properties, baryon content, and chemical composition are specified for the entire universe at high redshifts, at least in a statistical sense. Futhermore, the dominant physical laws are readily identified: the general theory of relativity describing the evolution of the background spacetime geometry and particle geodesics, the Euler equations governing the motion of the baryonic fluid in an expanding universe, and the primordial kinetic rate equations determining the chemical processes. Radiation backgrounds, save the CMB, are entirely absent prior to first structure formation in standard models. The complete set of equations governing first structure formation in a cosmological framework are given in [7].

Unlike traditional star formation calculations, which are plagued by a lack of knowledge of appropriate initial conditions, the initial conditions for first structure formation calculations are well defined—namely, a Gaussian random field of density fluctuations characterized by a power spectrum whose shape can be computed theoretically. The amplitude of the fluctuations is constrained by observations on a variety of scales and redshifts [13,23,26]. In the calculations described here, we assume a cluster normalized standard cold dark matter (SCDM) model with the following parameters: $H_0 = 50$ km/s, $\Omega_0 = 1, \Omega_b = 0.06, \sigma_8 = 0.7$.

As in all star formation calculations, resolving the relevant length scales is the principal technical challenge. A simple estimate of what is required is to compare the baryonic Jeans length at a typical collapse redshift of 25 to the solar radius:

$$\frac{\lambda_J}{r_\odot} = 5.7pc(1+z)^{-1/2}/r_\odot \equiv 5 \times 10^7 \tag{4}$$

Adding a couple more decades in scale to model the cosmological environment brings the total spatial dynamic range to around 10^{10}. This is easily achievable in 1D spherical symmetry with logarithmic or adaptive grids. However, the all-important effects of hierarchical mergers, tidal forces, and fragmentation all demand 3D simulations. Until recently, such dynamic ranges were impossible to achieve in 3D.

We have developed two high-resolution, 3D numerical codes for solving the first structure formatiion equations set forth in [8]. The first, more primitive code HERCULES [7], uses fixed nested Eulerian grids for an effective resolution of 512^3 in regions of interest. This code was used to carry out the first self-consistent simulations of first structure formation [3] in which we verified the predictions of [35] and quantified the cooled mass fraction in primordial halos. The second, more powerful code ENZO [11,21], utilizes an adaptive hierarchical mesh of arbitrary depth to achieve unprecedented resolution wherever it is needed.

Using adaptive mesh refinement (AMR), we have previously reported the results of a simulation of first structure formation which achieved a spatial dynamic range of 262,144 [4,35,22]. Here we update that result with a new simulation which achieves an additional factor of 128 in resolution for a total spatial dynamic range of 3×10^7. While not 10^{10}, this is sufficient to characterize the properties of the collapsing protostellar cloud core. The calculation is done in a comoving box 128 kpc on a side. The starting redshift is z=100. At the stopping redshift z=19.1, the range of resolved scales is $6.4kpc \gtrsim \ell \gtrsim 2^{-4}pc$. The mass resolution in the initial conditions within the refined region are 0.53(8.96) $M_\odot$in the gas (dark matter). The refinement criteria ensure that: (1) the local Jeans length is resolved by at least 4 grid zones, and (2) that no cell contain more than 4 times the initial mass element (0.53 $M_\odot$).

5 Core Formation

To illustrate the physical mechanisms at work during the formation of the first cosmological object in our simulation, we show the evolution of various quantities in Fig. 5. The top panel of this plot shows the virial mass of the largest object in the simulation volume. We divide the evolution up into four intervals. In the first, before a redshift of about 33 (point 1 in Fig. 1), the

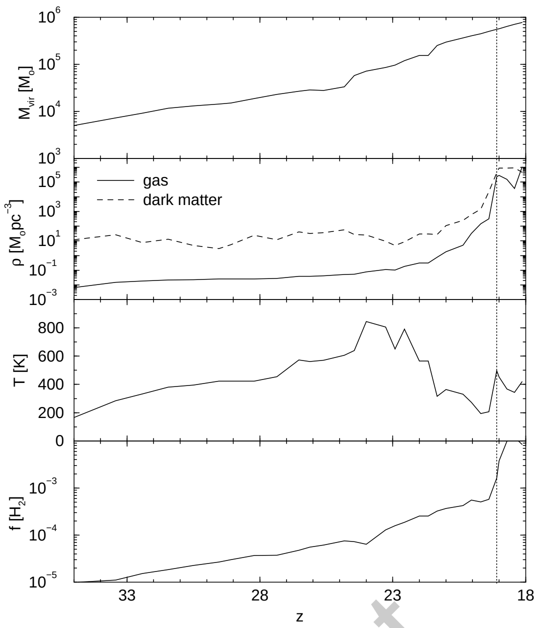

Fig. 2. The top panel shows the evolution of the virial mass of the most massive clump as a function of redshift. The remaining panels show the density (both dark and baryonic), the temperature, and the molecular hydrogen mass fraction at the central point of that clump. The central point is defined as the point with the highest baryon density. Finite gas pressure prevents baryons from clumping as much as the dark matter at redshifts $\gtrsim$ 23. Cooling begins in earnest once the H_2 fraction reaches a few $\times 10^{-4}$, lowering the central Jeans mass. At $z \sim 19$ a dense core begins to form and collapse with characteristic mass $\sim 200\ M_\odot$.

Jeans mass in the baryonic component is larger than the mass of any non-linear perturbation. Therefore, the only collapsed objects are dark-matter dominated, and the baryonic field is quite smooth.

In the second epoch, $23 < z < 33$, as the non-linear mass increases, gas becomes trapped in the gravitational potential wells of the dark matter halos. However, this gas is not sufficiently dense to cool and the primordial entropy of the gas prevents dense cores from forming. This is shown in the second frame of Fig. 2 by a large gap between the central baryonic and dark matter densities (note that while the central dark matter density is limited by resolution, the baryonic is not, so the true difference is even larger). As mergers continue and the mass of the largest clump increases, its temperature also grows, as shown in the third panel of this figure. The H_2 fraction also increases (bottom panel).

By $z \sim 23$ (point 2 in Fig. 1), enough H_2 has formed (a few $\times 10^{-4}$) that cooling begins to be important. During this third phase, the central temperature decreases and the gas density increases. However, the collapse is quasistatic rather than a runaway freefall because around this point in the evolution, the central density reaches $n \sim 10^4$ cm^{-2}, and the excited states of H_2 are in LTE. This results in a cooling time which is nearly independent of density rather than in the low–density limit where $t_{cool} \sim \rho^{-1}$ (e.g. [18]).

Finally, at $z \sim 19$ (point 3 in Fig. 1), a very small dense core forms and reaches the highest resolution that we allowed the code to produce. We follow the collapse to a final central density of 10^{12} cm^{-3}, well above the critical density for the formation of H_2 via 3–body reactions (see [30]). These reactions are included, as well as an escape probability treatment of radiative transfer of the molecular line radiation ([3]) which becomes important at these densities. Finite word length and the lack of an appropriate equation of state forced the termination of the calculation at this point.

6 Core Structure

The structure of the cloud at the end of the calculation is shown in Fig. 4. The quantity plotted is the logarithm of the baryon overdensity $\rho/ < \rho >$ on a slice passing through the densest cell at z=19.1. Proceeding from large scales to small scales we see: (6 kpc)–the filamentary cosmological density field, with a dense halo at the intersection of several filaments; (600 pc)–a virialized halo with $M_{vir} \sim 4 \times 10^5$ $M_\odot$ and $r_{vir} \sim 100$ pc; (60pc)–a dense baryonic core in the center of the cooling halo. From scales of a few pc on down, the core is self-gravitationally bound and collapsing.

Despite the non-spherical structure of the cloud, mass-weighted spherical averages of various quantities centered on the density maximum provide insight into the physical processes governing the formation and evolution of the core. A schematic based on a careful analysis of these radial profiles is shown in Fig. 4.

Jagged lines in Fig. 4 indicate approximate radii where the material makes a kinematic, thermodynamic, or other significant physical transition. Proceeding form large to small radii, we have the virialization shock ($r_{vir} \approx 100$ pc); the cooling radius ($r_{cool} \approx 25$ pc), defined where the gas temperature reaches its maximum value $T_{vir} \sim 1000K$; the radius where the gas reaches the minimum temperature allowed by H_2 cooling $\sim$ 200K ($r_{T_{min}} \approx 5$ pc); the radius where the H_2 level population enters LTE ($r_{LTE} \approx .5$ pc) defined where $n = 10^4$ cm^{-3}; and the radius where 3–body H_2 formation reactions become important ($r_{3H} \approx 10^{-2}$ pc), defined where $n = 10^8$ cm^{-3}.

In the settling zone, the H_2 number fraction rises from 7×10^{-6} to near $f_{H_2}(crit)$. Here H_2 cooling is negligible. Inside $r_{T_{max}}$, a cooling flow is established reducing the gas temperature to T_{min}. At $r_{T_{min}}$, the sound crossing time becomes substantially shorter than the cooling time. This suggests that inside this radius the core is contracting quasi–hydrostatically on the cooling time scale, which approaches its constant high–density value at small radii.

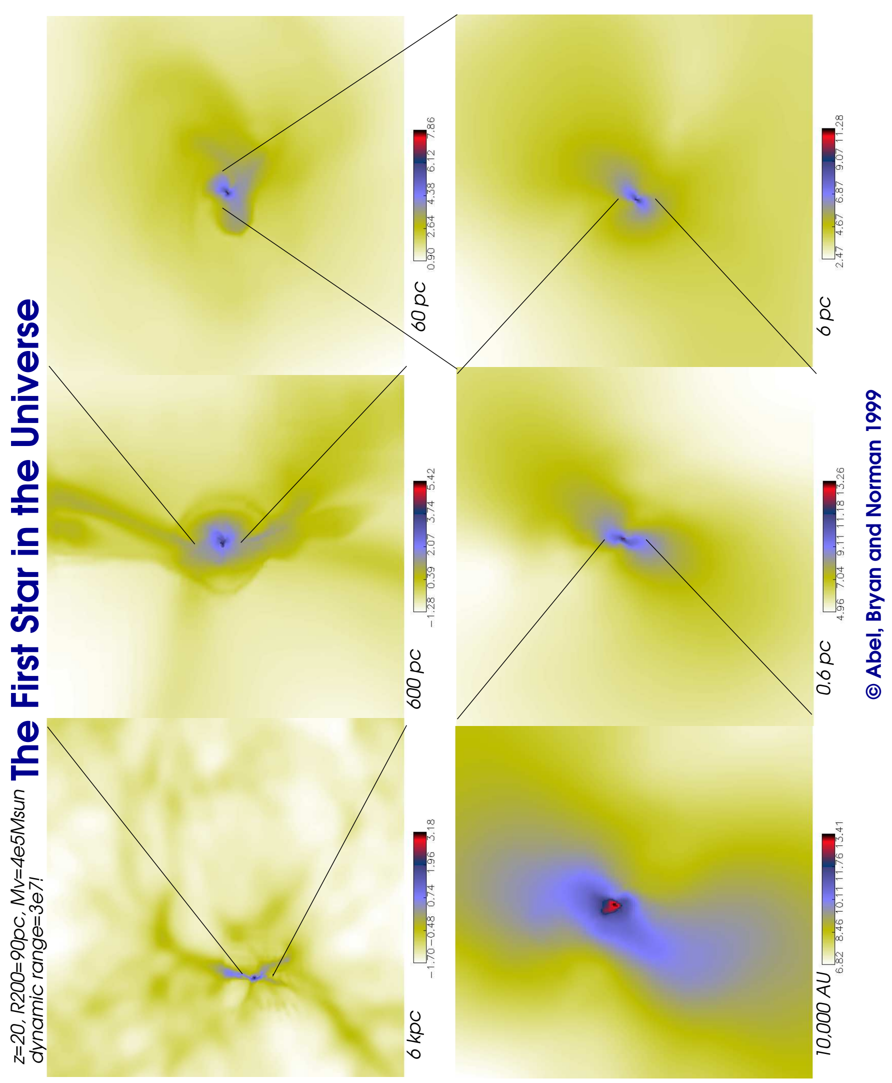

Fig. 3. Million-fold zoom showing the multiscale structure of a primordial protostellar cloud core in the center of a low mass halo at z=19.1. Plotted is the logarithm of the baryon overdensity on a slice passing through the densest structure on the grid. Zoom proceeds clockwise from upper left. Linear scales are proper. The smallest grid cell in the center of the cloud core in the last frame is 2^{-4} pc = 43 AU.

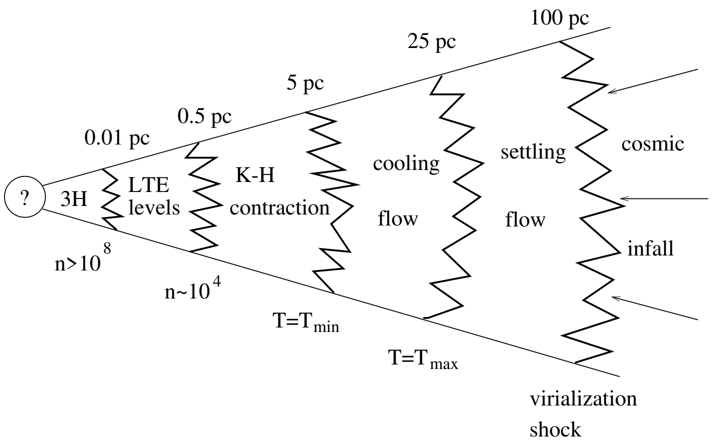

Fig. 4. Schematic of the structure of the primordial protostellar cloud core based on spherical averages around the density maximum at z=19.1. Jagged lines demarkate different physical regions.

This constant cooling time of $\sim 10^5$ years sets the time scale of the evolution of the fragment until it can turn fully molecular via three body associations. Inside $r \sim 0.3$ pc, the enclosed baryonic mass of $\sim 200 M_\odot$ exceeds the local Bonnor-Ebert mass, implying this material is gravitationally unstable. However, due to the inefficient cooling, its collapse is subsonic. The radius where $M > M_{BE}$ defines our protostellar cloud core.

7 Fragmentation?

Inside r_{3H} atomic hydrogen is completely converted into H_2 via the 3–body reaction. This increases the cooling rate sufficiently to initiate a freefall collapse in the central part of the core. What will be the fate of this collapsing cloud? Omukai & Nishi [24] have simulated the evolution of a collapsing, spherically symmetric (1D) primordial cloud to stellar density including all relevant physical processes. Coincidentally, their initial conditions are very close to our final state. Our results agree with theirs where our solutions overlap. Based on their results, we can say that if the cloud does not fragment, a massive star will be formed. Adding a small amount of angular momentum to the core does not change this conclusion [9], who found a dynamical bar mode instability efficiently transports angular momentum outward in a 3D simulation of galactic protostellar collapse. A third possibility is that the cloud breaks up into low mass stars via thermal instability in the quasi-hydrostatic phase. Silk [33] has argued that, due to the enhanced cooling from the 3–body produced H_2 , fragmentation of this core might ensue and continue until individual fragments are opacity limited (i.e. they become opaque to their cooling radiation). We do not see any evidence of this. Our code, which resolves the Jeans mass everywhere and at all times, would not suppress the growth of these instabilities if they exist.

Rather, inspection of the density distribution on the smallest resolvable scales shows a centrally concentrated, object of mass $\sim$ 10 $M_\odot$ collapsing supersonically with $v_r \sim$ -4 km/s. The local free fall time is a few hundred years. The protostar is embedded in a flattened nebula with a pronounced one-arm spiral structure, suggesting an operative angular momentum transport mechanism.

8 Implications

The direct implications of our results are that the first stars, here defined to be those which form in a gas of zero metallicity, are massive. Here massive means of order the gravitationally unstable core which forms them $\sim$ 200 $M_\odot$. Where does this mass scale come from? We argue that it comes from the peculiar properties of a gas cooling solely through H_2 line excitation, which sets a minimum temperature for the gas of a few hundred K. The other factor is that above $n_{LTE} \approx 10^4$ cm^{-3}, the cooling time becomes independent of density, meaning that gravitationally bound clouds will evolve quasi-statically until the onset of 3–body production of H_2 at much higher densities.

The Bonnor-Ebert mass at $n = n_{LTE}$ and $T = T_{min}$ is 240 $M_\odot$, close to our simulated core mass. We suggest that cold gas in the centers of primordial low mass halos fragments into cores of this mass, each of which forms a massive star (10-100 $M_\odot$), or possibly a binary. These stars would be strong sources of UV radiation prior to supernova and/or black hole formation. Recent analyses [19,25] show that the UV radiation from a single O star per halo will destroy H_2 both locally and globally, quenching further star formation by this mechanism. Due to the low binding energy of the parent halo, metals ejected by the supernova explosion would be returned to the pre-galactic medium. Pockets of enriched gas collecting in the cores of more massive halos formed by subsequent mergers would form stars of various metallicities in the familiar but complicated way we have been studying for decades in Galactic molecular clouds. A key question, which must await further numerical investigations, is whether there is a pause in the star formation history of the universe, or rather a smooth transition from the formation of the first stars to the "next stars" as suggested by simulations of [27].

References

1. Abel, T. 1995, Thesis, University of Regensburg, Germany
2. Abel, T., Anninos, P., Zhang, Y., Norman, M.L. 1997, NewA, 2, 181
3. Abel, T., Anninos, P., Norman, M.L., Zhang, Y. 1998a (AANZ), ApJ, 508, 518.
4. Abel, T., Bryan, G.L., Norman, M.L. 1998b, in Proc. of the MPA/ESO Conference "Evolution of LSS: from Recombination to Garching", astro-ph/9810215

5. Abel, T., Bryan, G.L., Norman, M.L. 2000, ApJ, submitted.
6. Abel, T., Stebbins, A., Anninos, P., Norman, M.L. 1998b, ApJ, 508, 530.
7. Anninos, P., Norman, M.L., & Clarke, D. A. 1994, ApJ, 436, 11
8. Anninos, P., Zhang, Y., Abel, T., Norman, M.L. 1997, NewA, 2, 209
9. Bate, M. 1998. ApJL, 508, 95
10. Bertschinger, E. 1998. ARAA, 36, 599
11. Bryan, G.L., Norman, M.L. 1997, in *Computational Astrophysics*, eds. D.A. Clarke and M. Fall, ASP Conference #123
12. Carr, B.J., Bond, J.R., Arnett, W.D. 1984, ApJ, 277, 445
13. Croft, R., et al. 1999, ApJ, 520, 1
14. Combes, F. & Pfenniger, D. 1998, J. Ital. Astron. Soc., 69, 413
15. Couchman, H. M. P. & Rees, M. J. 1986. MNRAS, 221, 53
16. Galli, D. & Palla, F. 1998, J. Ital. Astron. Soc., 69, 337
17. Hollenbach, D. & McKee, C. F. 1979, ApJS, 342, 555
18. Lepp & Shull 1983
19. Haiman, Z., Abel, T. & Rees, M. J. 1999, ApJ, in press (astroph/9903336)
20. Miller, G. & Scalo, J. 1979, ApJS, 41, 413
21. Norman, M.L., Bryan, G.L. 1999, in *Numerical Astrophysics 1998*, eds. S. Miyama & K. Tomisaka, Kluwer, 19
22. Norman, M. L., Abel, T. & Bryan, G. L. 1999. in "After the Dark Ages: When Galaxies were Young", Eds. S. Holt & E. Smith, AIP Conference Proceedings 470, AIP Press, 58
23. Nusser, A. & Haehnelt, M. 1999, MNRAS, 303, 179
24. Omukai, K. & Nishi, R. 1998. ApJ, 508, 1410
25. Omukai, K. & Nishi, R. 1999. ApJ, 518, 64
26. Ostriker, J. P. 1993. ARAA, 31, 689
27. Ostriker, J. P. & Gnedin, N. 1996. ApJ, 472, L63
28. Padoan, P. 1995, MNRAS, 277, 377
29. Padoan, P., Jimenez, R. & Jones, B. 1997, MNRAS, 285, 711
30. Palla, F., Salpeter, E.E., Stahler, S.W. 1983, ApJ, 271, 632
31. Rauch, M. 1998. ARAA, 36, 267
32. Saslaw, W. C. & Zipoy, D. 1967, Nature, 216, 967
33. Silk, J. 1983, MNRAS, 205, 705
34. Silk, J. 1998, J. Ital. Astron. Soc., 69, 363
35. Tegmark, M., Silk, J., Rees, M.J., Blanchard, A., Abel, T., Palla, F. 1997, ApJ, 474, 1
36. Tiné, S., Lepp, S. & Dalgarno, A. 1998, J. Ital. Astron. Soc., 69, 345
37. Zhang, Y., Anninos, P., Norman, M. & Meiksin, A. 1997. ApJ, 485, 496

The Destruction of Molecular Hydrogen

Simon Glover

Institute for Astronomy, University of Edinburgh, Royal Observatory,
Blackford Hill, Edinburgh EH9 3HJ

Abstract. We examine the chemical reactions responsible for destroying the main primordial coolant, H_2, and show that the most important reaction at low temperature is collisional dissociation by neutral hydrogen. Since the formation rate is proportional to the ionization fraction, while the destruction rate is not, this has the consequence of significantly limiting the amount of H_2 that can form in low ionization gas, and hence the ability of such gas to cool.

1 The Dominant H_2-Destroying Reactions

In CDM-based cosmological models, the first gravitationally bound gas clouds form on small scales, with typical virial temperatures significantly below the temperature at which hydrogen line cooling becomes ineffective. At these low temperatures, cooling is dominated by the rotational and vibrational transitions of H_2.

In the absence of dust, H_2 forms only slowly, via the intermediate ions H^- and H_2^+ [1]. Of the reactions responsible for destroying H_2, only three are found to be important:

$$\mathrm{H_2 + H^+ \rightarrow H_2^+ + H} \ , \tag{1a}$$

$$\mathrm{H_2 + H \rightarrow 3H} \ , \tag{1b}$$

$$\mathrm{H_2 + e \rightarrow 2H + e} \ . \tag{1c}$$

We have investigated the relative importance of these reactions. We find that:

- At low temperatures, none of the reactions are significant. For gas temperatures below 1000 K it is a good approximation to ignore them.
- Between 1000 K and 10^4 K, collisional dissociation by neutral hydrogen dominates. This occurs despite the fact that the charge transfer reaction is significantly faster because the H_2^+ produced by the latter will very quickly reform H_2.
- At temperatures above 10^4K, collisional dissociation by electrons becomes important, as does charge transfer, the H_2^+ no longer surviving for long enough to form H_2.

2 Consequences for Gas Cooling

The formation rate of H_2 is directly proportional to the ionization fraction. In the temperature range where reaction (1b) dominates, this implies that the maximum H_2 abundance is also proportional to the ionization fraction. This can have important consequences for the thermal evolution of the gas.

We plot in Fig. 1 the limiting abundance as a function of temperature for representative ionization fractions of 10^{-2} and 10^{-4}. We also plot the minimum abundance of H_2 required for a uniform overdensity with $\delta = 200$ at $z = 50$ to be able to cool in less than its own dynamical timescale.

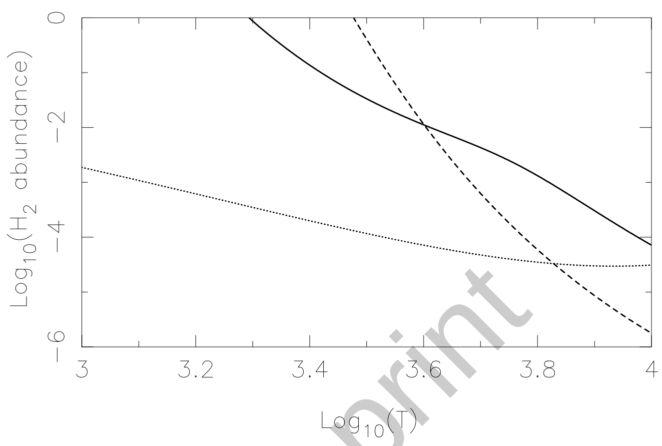

Fig. 1. The limiting H_2 abundance as a function of temperature for ionization fractions of 10^{-2} (*solid line*) and 10^{-4} (*dashed line*), compared with the minimum fraction needed for efficient cooling at $z = 50$ (*dotted line*)

In the high ionization case, the limiting abundance is high enough that the gas can still cool efficiently. In the low ionization case, however, gas above a critical temperature $T_c \simeq 7000\,\mathrm{K}$ cannot cool efficiently. Moreover, the required abundance is quite insensitive to large shifts in temperature, so a small decrease in the ionization can result in a large decrease in T_c.

As a consequence, the ability of hot primordial gas to cool efficiently depends to a large extent on its previous dynamical history. For example, gas reaching this temperature from above will typically have a high ionization fraction, and will continue to be able to cool efficiently. On the other hand, gas heated to this temperature from below will preserve its post-recombination ionization fraction, similar to our low ionization case, and thus will not cool.

References

1. Hirasawa, T., Aizu, K., Taketani, M., (1969), Progr. Theor. Phys. **41**, 835

Fragmentation of Primordial Gas Clouds: On the Mass of the First Stars

Fumitaka Nakamura[1] and Masayuki Umemura[2]

[1] Niigata University, 8050 Ikarashi-2, Niigata, Japan
[2] University of Tsukuba, Tsukuba, Japan

Abstract. We study the gravitational contraction and fragmentation of filamentary primordial gas clouds by means of one-dimensional (1D) and two-dimensional (2D) hydrodynamical simulations. The cloud evolution is computed from the central proton density $n_c \sim 10^2 - 10^6$ cm^{-3} up to $\sim 10^{11-12}$ cm^{-3}. From the 1D simulations, it is found that the radial contraction decelerates after the central density reaches $\sim 10^4$ cm^{-3}, beyond which the LTE populations are achieved for the rotational levels of hydrogen molecules. When the central density reaches 10^{11-12} cm^{-3}, the cloud becomes optically thick to the H_2 lines. Therefore, the radial contraction almost stops at that stage. From the 2D simulations, it is found that the fragmentation takes place during the stages at which 10^4 cm$^{-3} \lesssim n_c \lesssim 10^{11-12}$ cm^{-3} because the radial contraction becomes slower. The fragment mass depends on the initial model parameters such as the central density and temperature. For the higher initial temperature and higher initial density, the fragment mass is lower. Then, the maximum and minimum masses are estimated as 10^3 $M_\odot$ and $1 \sim 2$ $M_\odot$, respectively. If one fragment collapses into one star, then the masses of the first stars are expected to range from $1 - 2$ $M_\odot$ to $\sim 10^3$ $M_\odot$, which are low-mass deficient compared to the Pop I stars. The effect of HD cooling is also discussed.

1 Introduction

Based on the standard big bang cosmology, the first stars should form from metal-deficient gas. Hitherto, many authors have considered the formation processes of primordial stars from metal-deficient gas ([6,4] and references therein). The first stars could play an important role in the early evolution of galaxies or the formation of massive black holes (e.g., [5,3,7,9]). In addition, they may be responsible for the chemical pollution of the intergalactic medium that has recently been inferred from metallic absorption in the Lyα forest seen in quasar light. It is thus important to study the formation processes of the first stars and estimate the masses of the first stars.

In a bottom-up theory like the CDM model, it is expected that overdense regions with masses of $10^{5-8} M_\odot$ would first collapse at the redshift $z \sim 10 - 10^2$ and that the first stars would form there. Such objects are heated by shocks to $T > 10^3 - 10^4$ K. Just after shock formation, however, the gas temperature descends to $T \sim 10^2 - 10^3$ K because of the H_2 line cooling which is the most efficient cooling process in primordial gas.

Numerical simulations have also shown that such an object collapses or fragments into filamentary clouds [8,1,2]). The first stars would have formed from such filamentary clouds.

In this paper we thus study the fragmentation of filamentary primordial gas clouds with 1D and 2D hydrodynamical simulations coupled with non-equilibrium processes for H_2 formation.

2 Model

The initial model of a filamentary cloud is the same as that of [4]; we consider an infinitely long cylindrical gas cloud in which the density is uniform along the cylinder axis. We assume that the gas consists of hydrogen and helium. The distributions of the temperature and abundances are assumed to be spatially uniform at the initial state.

The initial density distribution is expressed as $\rho = \rho_0 \left(1 + r^2/R_{\rm cyl}^2\right)^{-2}$ and $R_{\rm cyl} = \sqrt{2fkT_0/(\pi G \rho_0 \mu m_{\rm H})}$. This model is specified by three parameters: the central density ρ_0, the temperature T_0, and the radius in units of the equilibrium radius $\sqrt{f}$. The parameter f is also equal to the ratio of the gravitational force to the pressure force. We adopt $f = 2$ for a typical model.

In the models calculated in this paper, the gas temperature does not exceed 10^4 K. Thus, we only take into account thermal processes by H_2. We consider line cooling by rotational and vibrational transitions, cooling by collisional dissociation, and heating by H_2 formation. To compute the H_2 line cooling rate, we first determine the level populations at the rotational and vibrational excitations and estimate the optical depths for all the transitions. We consider 21 rotational and 3 vibrational levels for H_2. We then apply a photon escape probability method for each transition.

We solved hydrodynamical equations in the cylindrical coordinates with a second-order upwind TVD code based on Roe's method.

3 Numerical Results of 1D Simulations

In this section we examine the radial contraction of the filamentary clouds with 1D simulations. These calculations are basically the same as those of [4]. In the following we focus on the evolution of physical quantities on the axis. See [4] for more details (e.g., the radial distributions of the physical quantities).

We calculated 21 models by choosing the parameters n_0, f, and T_0 to be $n_0 = 10^2, 10^3, \ldots, 10^6$ cm^{-3}, $f = 2$, and $T = 300$, 500, 1000 K, respectively.

As a typical example, we show the evolution of the model with $n_0 = 10^2$ cm^{-3}, $T_0 = 300$ K, and $f = 2$. The electron and H_2 number fractions are initially set to 5×10^{-5} and 10^{-4}, respectively. Figure 1 shows the evolution of the temperature (*solid line*), the contraction time ($t_{\rm cont} \equiv \rho/\dot{\rho}$: *solid line*), the free-fall time ($t_{\rm ff} \equiv 1/\sqrt{4\pi G \rho_c}$: *dotted line*), and the cooling time [$t_{\rm cool} \equiv 3nkT/(2\Lambda)$: *dashed line*] as a function of the central density [$n_c \equiv \rho_c/(\mu m_H)$]. During the contraction, the temperature stays nearly constant at $T \sim 300$ K. The cloud collapses in a cooling time. The contraction time becomes longer than the free-fall time after the central density reaches a critical density of H_2, $n_{\rm cr} \sim 10^{3-4}$ cm^{-3}, beyond which the LTE populations are achieved

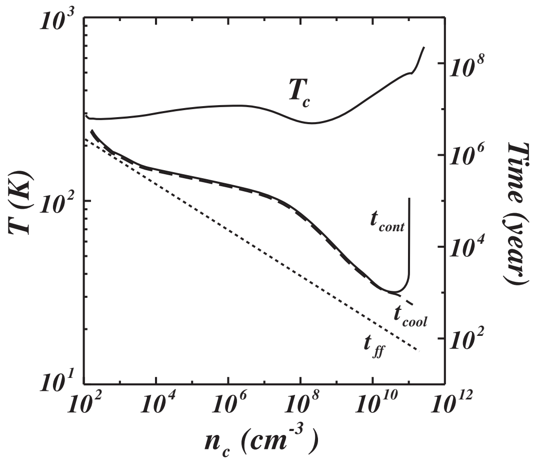

Fig. 1. Evolution of the temperature (T_c, *solid curve*), the contraction time ($t_{\rm cont}$, *solid curve*), the cooling time ($t_{\rm cool}$, *dashed curve*), and the free-fall time ($t_{\rm ff}$, *dotted curve*) at the center for the model with $(n_c, T_c, f) = (10^2 {\rm cm}^{-3}, 300{\rm K}, 2)$.

for the rotational levels of hydrogen molecules. (For $n < n_{\rm cr}$, the H_2 line cooling rate is nearly proportional to n^2, while for $n > n_{\rm cr}$, it is proportional to n; i.e., $t_{\rm cool} \propto n^{-1}$ for $n < n_{\rm cr}$ and $t_{\rm cool} \propto$ const. for $n > n_{\rm cr}$ when the temperature is nearly constant. Thus, the cooling time gets longer than the free-fall time for $n > n_{\rm cr}$.). Thereafter, the contraction proceeds quasi-statically. The fragmentation along the z-axis is expected to occur for $n > n_{\rm cr} = 10^{3-4}$ cm^{-3} because the radial contraction is appreciably retarded.

The evolution of the other models with different parameters is qualitatively similar to that of the model in Figure 1. In the next section we pursue the fragmentation processes of clouds with 2D simulations and evaluate the masses of the fragments.

4 Numerical Results of 2D Simulations

To estimate the masses of the fragments, we explored the evolution of collapsing filamentary clouds by means of 2D simulations. To pursue the fragmentation processes, white-noise density fluctuations were added in the clouds. For all the models presented below, the grid number was set to 1024×1024. We calculated ~ 100 models with different initial parameters and amplitudes of the fluctuations.

Figure 2 shows a typical example of the 2D simulations. This figure shows the cross-sections of the cloud at four different stages. The model in Figure 2 has the same initial parameters as that of Figure 1. In this model we added white-noise density fluctuations which have the initial amplitudes of $\delta_0 \equiv \delta\rho/\rho = 10^{-2}$. In spite of the small density fluctuations, the filamentary cloud fragments into several cores whose masses are estimated to be nearly $\sim 10^3 M_\odot$.

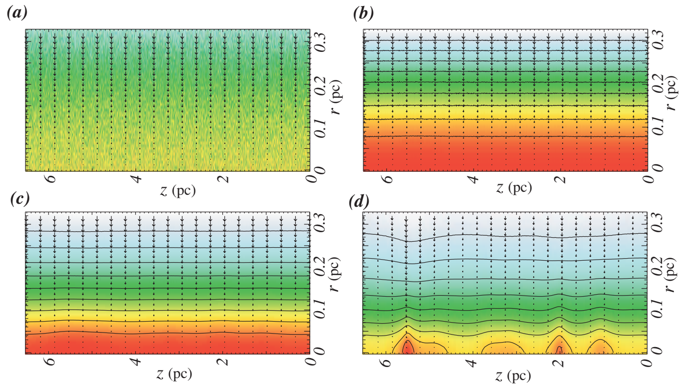

Fig. 2. Density and velocity distributions in the r-z plane for the model with $(n_c, T_c, f) = (10^2\mathrm{cm}^{-3}, 300\mathrm{K}, 2)$. At the initial state, the white-noise fluctuations of $\delta\rho/\rho = 10^{-2}$ are added. Panels (a) through (d) show the cross-sections at the stages at which (a) $n_{\max} = 10^4$ cm^{-3}, (b) $n_{\max} = 10^5$ cm^{-3}, (c) $n_{\max} = 10^6$ cm^{-3}, and (d) $n_{\max} = 10^7$ cm^{-3}, where $n_{\max}$ is the maximum density on the z-axis.

Figure 3 shows the distribution of the averaged fragment mass derived from the 2D calculations. The abscissa denotes the initial central density. The ordinate denotes the averaged fragment mass. The solid lines denote the contour of the fragment mass. For comparison, we show the lines at which the cooling time balances the free-fall time. When the filamentary cloud forms by gravitational instability, the initial physical quantities of the cloud are likely to be comparable to those on the line.

The averaged fragment mass depends on the initial parameters, which are especially sensitive to the initial temperature. For higher temperature or higher density, the fragment mass becomes lower. The fragmentation takes place during the stages at which 10^4 cm^{-3} $\lesssim n_c \lesssim 10^{11-12}$ cm^{-3} because the radial contraction becomes slower. Then, the maximum and minimum masses are estimated as 10^3 and $1 \sim 2$ $\mathrm{M}_\odot$, respectively.

5 Effect of HD Cooling

For several models calculated in §3 and §4, we recalculated the fragmentation processes of the filamentary clouds by varying the initial H_2 fraction and taking into account the effect of HD cooling. We confirmed that the numerical results presented in the above sections are nearly independent of those effects as long as the initial H_2 fraction is less than 10^{-3}. Therefore, we conclude that HD cooling is not important for the formation of the first stars in a standard CDM model, in which the first collapsed objects have masses of $10^5 - 10^8$ $\mathrm{M}_\odot$ (In such objects the H_2 fraction reaches 10^{-3} at most.). HD cooling can play an important role in the fragmentation of the clouds with higher initial H_2 fraction ($\sim 10^{-2}$) and/or lower initial density (see also Uehara's paper on

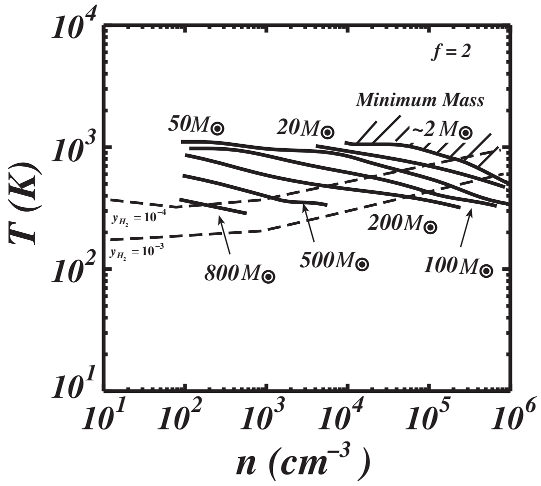

Fig. 3. Distribution of the averaged fragment mass on $\log n_0 - \log T_0$ plane. The abscissa denotes the initial central density, while the ordinate denotes the averaged fragment mass. The solid lines denote the contour of the fragment mass. For comparison, we show the lines at which the cooling time balances with the free-fall time. In this figure the amplitudes of the fluctuations are set to be $\delta\rho/\rho = 10^{-2}$.

these proceedings). In a standard CDM model, such situations are realized in the case of the contraction of the clouds with masses greater than 10^9 $M_\odot$.

6 On the Mass of the First Stars

The 2D simulations indicate that the fragment masses are in the range of $1 \sim 2M_\odot \lesssim M \lesssim 10^3 M_\odot$. If one fragment collapses into one star, then the masses of the first stars are expected to be basically in the same range as those of the fragments. Therefore, the first stars are expected to be low-mass deficient compared to the present-day stars.

References

1. Abel T., Anninos P. A., Norman M. L., & Zhang Y. 1998, ApJ, 508, 518
2. Bromm, V., Coppi P., & Larson R. B. 1999, submitted to ApJL
3. Haiman Z., Rees M. J., & Loeb A. 1997, ApJ, 476, 458
4. Nakamura F., & Umemura M. 1999, ApJ, 515, 239
5. Ostriker J. P., & Gnedin N. Y. 1996, ApJ, 472, L63
6. Palla F., Salpeter E. E., & Stahler S. W., 1983, ApJ, 271, 632
7. Tegmark M. et al. 1997, ApJ, 474, 1
8. Umemura M. 1993, ApJ, 406, 361
9. Umemura M., Loeb A., & Turner E. 1993, ApJ, 419, 459

On the Formation of Primordial Stars and Pop III Luminous Objects

Ryoichi Nishi[1], Hajime Susa[2], and Kazuyuki Omukai[1]

[1] Kyoto University, Kyoto 606-8502, Japan
[2] University of Tsukuba, Tsukuba 305-8571, Japan

Abstract. We investigate the formation site of the primordial stars, the formation process of them and the feedback on the host clouds. First, the 'cooling diagram' for cosmological low mass objects is shown. We assess the cooling rate taking into account the contribution of H_2, which is not in chemical equilibrium generally. Next, we show the results of the hydrodynamical simulation for primordial star formation, which includes radiative transfer and the chemistry of H_2. Moreover, the feed back by the first generation massive stars is considered. The main feedback consists of two different processes, UV radiation from the stars and energy input by SNe. Finally, we investigate the formation condition of luminous objects and the mass of the Pop III luminous objects is estimated to be several times $10^7 M_\odot$.

1 Introduction

For the present day star formation, it is usually assumed that the host cloud evolves isothermally [2]. On the contrary, for the primordial star formation, the host cloud is not in the thermal equilibrium because of the weak cooling source. So we must investigate the thermal evolution of the primordial gas cloud. Moreover, weak cooling makes the feedback efficient. The main feedback consists of two different processes, UV radiation from the stars and energy input by SNe. Through ionization of H and dissociation of H_2, UV radiation have negative feedback on the further star formation in the host clouds. By the way, SNe can disrupt the host clouds before they become luminous, because the energy input of the explosion is comparable with the typical binding energy of host clouds. Here, we investigate the formation of primordial stars and evolution of primordial host clouds systematically.

2 Cooling Diagram

The formation of cold dense clouds, where the primordial stars are formed, is basically understood by the comparison between free-fall time and the cooling time. The 'cooling diagram' originally introduced by [11] and [13] shows the region where cooling time is shorter than the free-fall time on ρ-T plane, and vice versa. In this section, we present the cooling diagram on ρ-T plane including H_2 cooling [5]. With this diagram, we can predict whether a cloud virialized at $z = z_{\rm vir}$ with virial temperature $T_{\rm vir}$ cools.

In order to estimate the cooling rate at $T < 10^4$K, we need the fraction of H_2. The number fraction of H_2 is not generally in equilibrium for $T < 10^4$ K in the epoch of galaxy formation. Using recent reaction rates and the cooling rate of H_2 [1], we estimate the fraction of H_2. There are four important time scales, dissociation and formation time of H_2, cooling time, and recombination time, respectively. Comparing these time scales we can estimate the fraction of H_2 and cooling efficiency for cosmological low mass objects (Fig. 1a.).

There are three different star formation sites and the star formation process is probably different. (1) The cloud in the region $t_{\rm ff} < t_{\rm cool} < H^{-1}$ cools faster than the Hubble expansion, but cannot collapse dynamically, initially. (2) The cloud in the region $t_{\rm cool} < t_{\rm ff}$ cools faster than the free fall time and can collapse dynamically. (3) The first collapse of the cloud with the virial temperature higher than about 10^4 K is highly dynamical and the ionization at the bounce epoch is important (e.g., [12,17,15]).

3 Dynamical Collapse of Primordial Protostellar Clouds

In this section we show the results of the hydrodynamical calculation of primordial protostellar clouds and the formation of stellar cores [8] .

The collapse proceeds almost self-similarly and is analogous to the Larson-Penston similarity solution [3,10] until the central region reaches the stellar density. The density profile outside the core is very resemble to $\rho \propto r^{-2.2}$, which correspond to the effective adiabatic index is 1.1.

After the central part of the cloud contracts almost adiabatically to some extent, a hydrostatic core with very small mass ($\sim 5 \times 10^{-3} M_\odot$) forms at the center. At that time, the central number density and temperature are $\sim 10^{22}$ cm^{-3} and $\sim 3 \times 10^4$ K. These values are almost the same as those of present-day stellar cores at the formation epoch. But before the formation of the stellar core, no transit core is formed, in contrast to the case of present-day star formation.

The mass accretion rate is estimated as

$$\dot{M}_* = 8.3 \times 10^{-2} M_\odot \ \mathrm{yr}^{-1} \left(\frac{t}{1 \ \mathrm{yr}}\right)^{-0.27}, \tag{1}$$

$$= 3.7 \times 10^{-2} M_\odot \ \mathrm{yr}^{-1} \left(\frac{M_*}{M_\odot}\right)^{-0.37}. \tag{2}$$

The estimated mass accretion rate is very large and diminishes with time. The main reason for this large mass accretion rate is that the temperature of primordial gas clouds ($\sim 10^3$ K) is higher (which is the result of weak cooling) than that of the present-day molecular clouds (~ 10 K). The final stellar mass is expected to be large because of this large mass accretion rate.

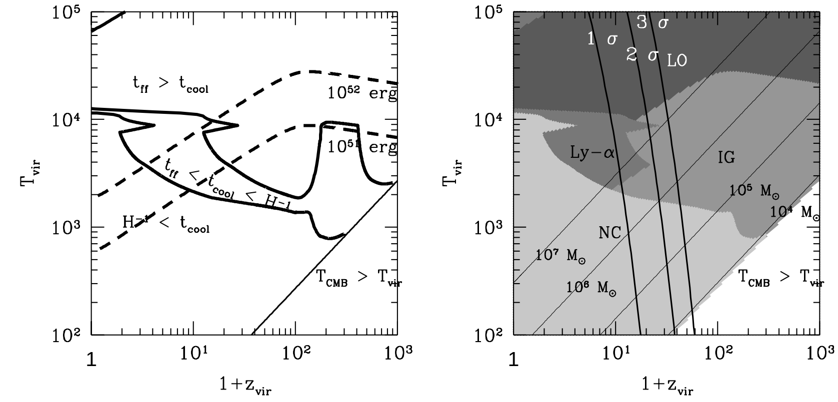

(a) (b)

Fig. 1. (a) Cooling diagram is plotted on the $(1 + z_{\rm vir})$-$T_{\rm vir}$ plane. The thick solid lines divide the plane into three regions. In the region denoted as $t_{\rm ff} > t_{\rm cool}$, cooling proceeds faster than the collapse. The narrow region denoted as $t_{\rm ff} < t_{\rm cool} < H^{-1}$, the cloud cools faster than the Hubble expansion, but cannot catch up with the free-fall. The clouds in the lower region cannot cool. Two dashed lines denote the boundary below which virialized clouds are destroyed by SN explosions. The lines correspond to the cases that the total energy of SNe is 10^{51} erg and 10^{52} erg. (b) $(1 + z_{\rm vir})$-$T_{\rm vir}$ plane is divided into five regions. In the lower region ($T_{\rm CMB} > T_{\rm vir}$ and the region denoted as "NC"), clouds cannot cool. In the region denoted as "IG", clouds will be disrupted by the SNe. Clouds in the region "Ly-α" will not be destroyed by the SN. The region denoted as "LO" represents the clouds which could be luminous objects. The thick solid three lines marked as 1σ, 2σ, and 3σ represent the location that the density perturbations in standard CDM cosmology should virialize. The mass of the clouds are constant along the thin solid four lines which cross the panel from lower left to upper right. (From [5].)

4 Feedback by the First Generation Massive Stars

In this section we investigate feedback by the first generation massive stars. The feedback effects considered here are UV radiation from the stars and energy input by SNe.

4.1 Star Formation Regulation by UV Radiation

Around an OB star, hydrogen is photoionized, and an HII region is formed. Ionizing photons hardly escape from the HII region, but photons whose radiation energy are below the Lyman limit can get away. Such FUV photons photodissociate molecular hydrogen, and a photodissociation region (PDR) is formed just outside the HII region. It is shown that H_2 is dissociated in such a large region that the whole of an ordinary low mass cloud is influenced by one O5 type star [9]. This indicates that FUV radiation from one or a few OB stars prohibits the whole small pregalactic cloud from H_2 cooling and quenches subsequent star formation in it.

For low metallicity clouds, if metallicity is lower than about 10^{-2} of the solar metallicity, the host cloud depletes main coolant (H_2) by one O5 type star [7]. This indicates that stars do not form efficiently before the metallicity becomes larger than about 10^{-2} of the solar metallicity. When the metallicity is lower than this value, star formation can occur only after previous massive star died. If these massive stars died with SN explosion, we can consider that SN-induced star formation is the only star formation process, since stars can form only after SN explosion.

4.2 Disruption of the Host Cloud by SNe

After massive first generation stars form, evolution of the host clouds become slower because of strong regulation by UV radiation as the previous section [5]. Thus, next generation stars are hardly formed before the first generation stars die. Subsequent SNe might disrupt the gas binding before significant amount of total gas transferred into stars. We derived the cloud disruption condition by SNe, with the assumption that the cloud is spherical and the density is constant, for the simplicity.

On the cooling diagram (Fig. 1a.), the boundaries ($v_{\rm esc} = v_{\rm tot}$) are superimposed for two cases. These lines are obtained with the assumption that the input thermal energy from the SNe is 10^{51} erg and 10^{52} erg, respectively. The input energy almost reflects the number of the SNe. The values 10^{51} erg and 10^{52} erg represent the case of single SN and 10 SNe, respectively. The former should corresponds to the clouds in $t_{\rm ff} < t_{\rm cool} < H^{-1}$, because they will have a runaway collapsing central core. The core evolves much faster than the envelope and will be a massive star, probably, followed by a single SN. The latter case represents the clouds in $t_{\rm ff} > t_{\rm cool}$. They will have a shocked pancake, and the cooled region will fragment into stars. That's why they should have multiple SNe.

5 Formation of Pop III Luminous Objects

Considering the previous investigations, the clouds in the region LO in Fig. 1b. can survive. The mass of the clouds are fairly massive (virial temperature is higher than about 10^4 K) and they evolve into luminous objects through following processes (see [6]): (1) By pancake collapse of an overdense region or collision between subclouds in a potential well, a quasi-plane shock forms (e.g., [14]). (2) If the shock-heated temperature is higher than $\sim 10^4$ K, the post-shock gas is ionized and cooled efficiently by H line cooling. After it is cooled bellow 10^4 K, H_2 is formed fairly efficiently and it is cooled to several hundred K by H_2 line cooling (e.g., [12,15]). (3) The shock-compressed layer fragments into cylindrical clouds when $t_{\mathrm{dyn}} \sim t_{\mathrm{frag}}$ (eg., [17]). (4) The cylindrical cloud collapses dynamically and fragments into cloud cores when $t_{\mathrm{dyn}} \sim t_{\mathrm{frag}}$ [16,4]). (5) Primordial stars form in cloud cores [8]. (6) Since the gravitational potential of the cloud is deep enough, subsequent SNe cannot disrupt the cloud. Star formation regulation by UV radiation is also weak because of highly flattened configuration of the host cloud. (7) Next generation stars can form efficiently and the cloud evolves into a luminous object.

The lower limit of the Pop III luminous objects mass is estimated to be several times $10^7 M_{\odot}$ (Fig. 1b.). Smaller objects may be disrupted by the SNe before they become luminous.

References

1. Galli D., Palla F. (1998) AA **335**, 403
2. Hayashi C., Nakano T. (1965) Prog. Theor. Phys. **34**, 754
3. Larson R. B. (1969) MNRAS **145**, 271
4. Nakamura F., Umemura M. (1999) ApJ **515**, 239
5. Nishi R., Susa, H. (1999) ApJL **523**, L64
6. Nishi R., Susa H., Uehara H., Yamada M., Omukai K. (1998) Prog. Theor. Phys. **100**, 881
7. Nishi R., Tashiro, M. (2000) in preparation
8. Omukai K., Nishi R. (1998) ApJ **508**, 141
9. Omukai K., Nishi R. (1999) ApJ **518**, 64
10. Penston M. V. (1969) MNRAS **144**, 425
11. Rees M. J., Ostriker J. P. (1977) MNRAS **179**, 541
12. Shapiro P. R., Kang H. (1987) ApJ **318**, 32
13. Silk J. (1977) ApJ **211**, 638
14. Susa H., Uehara H., Nishi R. (1996) Prog. Theor. Phys. **96**, 1073
15. Susa H., Uehara H., Nishi R., Yamada M. (1998) Prog. Theor. Phys. **100**, 63
16. Uehara H., Susa H., Nishi R., Yamada M., Nakamura T. (1996) ApJL **473**, L95
17. Yamada M., Nishi R. (1998) ApJ **505**, 148

Collapse and Fragmentation of Rotating Primordial Clouds

Toru Tsuribe

Kyoto University, Sakyo-ku, Kyoto, 606-8502, Japan

Abstract. The collapse of rotating primordial clouds is investigated using three-dimensional hydrodynamical calculations to answer whether the fragmentation takes place during the runaway core collapse of quasi-spherical knots. It is found that a collapsing core is well approximated by the polytropic gas with $\gamma = 1.1 - 1.2$ between $100 \lesssim n \lesssim 10^8$ even if the rotation is included. The condition that a cloud becomes flattened enough to fragment is found to be $M_{\rm T} \gtrsim 6 \times 10^6 M_\odot$ for $z_{\rm vir} \sim 30$ in the CDM model. Smaller subclumps that collapse inside larger dark matter halo is not expected to fragment during the core collapse.

1 Introduction

Recently, the collapse of the low-mass primordial clouds ($T_{\rm vir} \gtrsim 10^3 K$) with hydrogen molecular cooling is investigated in the context of first stars in the CDM model for structure formation (e.g., [1]). The calculation of non-linear growth of the cosmological spherical perturbations revealed that the fraction of molecular hydrogen necessary for the collapse beyond the virialization are provided only after the shock formation inside the virialized dark matter halo [2]. According to the three-dimensional calculations with realistic initial conditions, the first collapsing regions are found to be spherical knots at the intersection of filaments [3].

The formation of the first generation of stars can be divided into the following three stages: (1) the fragmentation triggered by the dark matter fluctuation to form a virialized halo and to attract gas into it, (2) the runaway core collapse and fragmentation of the self-gravitating baryonic components inside the shocks, and (3) collision and merging of clumps to form larger systems. In this paper, we investigate the second process, i.e., the condition of the fragmentation during the core collapse.

2 Numerical Calculations and Results

Hydrodynamics is calculated by the three-dimensional SPH-like code with the accurate shock capturing method using Riemann solver. Checking the resolution conditions that is necessary for valid numerical results for fragmentation problems carefully, we calculated the collapse of a single density peak using $N = 10^5$ particles for baryonic component (see [4] for isothermal clouds).

Non-equilibrium primordial chemistry of 18 reactions for H, H^-, H^+, H_2, H_2^+, and e^- within each smoothed particles are solved by the implicit scheme during the hydrodynamical calculations.

As initial states, we adopt an isolated quasi-spherical cloud core with or without dark matter halo. When we include a dark matter, virialized uniform background dark matter halo is used. This approximation is valid for the small mass clouds in which the collapse of the baryonic component is slow due to the effect of the pressure gradient and dark matter had already virialized when baryonic component infalls onto it. In some cases, an initial density central concentration is taken into account. Calculations are started from two kinds of initial epochs that corresponds to an initial density and temperature: (1) maximum expansion epoch $z_{\max} \sim 60$ and (2) the minimum temperature epoch in the center when the temperature is decreased to about 200K by the H_2 cooling. In both cases, the initial radial velocity was assumed to be zero. We consider the evolution until the three-body reaction dominates and clouds are optically thin during the whole stage in the calculation. Angular momentum distribution is set to be the same as that of rigidly rotating uniform sphere.

As a result, the critical mass $M_T = 3 - 6 \times 10^6 M_\odot$ that divides fragmentation and single core formation is found. When we consider other collapse redshift, above mass becomes different value according to its virial temperature. The fragmentation condition is mainly determined by the ratio of the pressure gradient force to the gravitational force inside the shocks when the temperature becomes minimum. In the core that has large ratio of the thermal energy to the gravitational energy ($\gtrsim 0.5$), the fragmentation does not take place. The dependence on the spin parameter is found to be weaker than that of the virial temperature. Instead, a collapsing cloud core generates a central spiral arm and collapses further keeping its self-similar profile, even if the rotation exists.

References

1. Tegmark, M., Silk, J., Rees, M. J., Blanchard, A., Abel, T., & Palla, F. 1997, ApJ, 474, 1
2. Haiman, Z., Thoul, A., & Loeb, A. 1996, ApJ, 464, 523
3. Abel, T., Anninos, P., Norman, M. L., & Zhang, Y. 1998, ApJ, 508, 518
4. Tsuribe, T. & Inutsuka, S. 1999, ApJ, 523, L155

The Effect of Spin on the Fragmentation of Primordial Gas

Volker Bromm, Paolo S. Coppi, and Richard B. Larson

Yale University, New Haven CT 06520, USA

Abstract. We discuss the sensitivity of the fragmentation of primordial gas to the initial amount of angular momentum. The collapsing halos correspond to the sites of the very first stars in a CDM-like model of structure formation. The gas fragments into clumps of $\sim 10^3 M_\odot$ which subsequently grow in mass up to $\sim 10^4 M_\odot$. This result is very robust, and the initial amount of spin mainly plays a role in shaping the resulting clump mass spectrum.

To elucidate the nature of the very first stars (the so-called Population III), one has to investigate the fragmentation of primordial, metal-free gas. Although the search for Population III stars has proven elusive so far, upcoming CMB anisotropy probes (MAP/Planck) will study their signature, and NGST might be able to directly see them. We explore the physics of primordial star formation by means of three-dimensional simulations of the dark matter (DM) and gas components, using Smoothed Particle Hydrodynamics. In the context of hierarchical models of cosmic structure formation, the first stars are expected to form in virialized DM halos of mass a few times $10^6 M_\odot$ at redshift $z \sim 30$. The gas dissipatively settles into the center of the DM potential, and forms a very filamentary, lumpy disk. At this stage, the gas has attained typical temperatures of $200 - 300$ K, and densities of $n \sim 10^{3-4}$ cm^{-3}, which correspond to a Jeans mass of $\sim 10^3 M_\odot$. This result is very robust, being determined by the microphysics of H_2 cooling. The gravitationally unstable gas fragments into high-density clumps ($n > 10^8$ cm^{-3}) with masses close to M_J. Subsequently, these clumps experience a complex history of tidal disruption, competitive accretion, and merging with other clumps. We address the sensitivity of the fragmentation to differences in the initial amount of spin (Figs. 1 and 2). The case with less initial spin has a more concentrated morphology with more mass incorporated in heavy clumps ($M > 10^4 M_\odot$). For details and references see [1].

Support from the NASA ATP grant NAG5-7074 is gratefully acknowledged.

References

1. Bromm, V., Coppi, P. S., & Larson, R. B. 1999, ApJL, in press

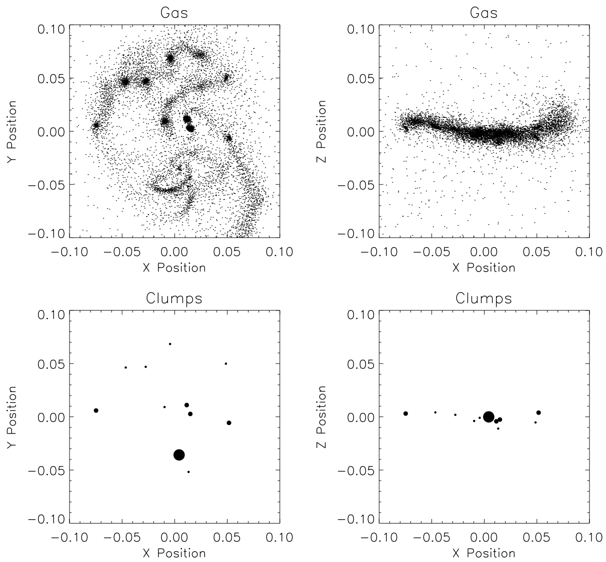

Fig. 1. Situation at $z = 29$ with initial spin $\lambda = 0.05$. The (proper) length of the box is 30 pc. *Left Panels:* Face-on view. *Right Panels:* Edge-on view. The four increasing dot sizes denote increasing mass scale: $10^2 - 10^3 M_\odot$, $10^3 - 5 \times 10^3 M_\odot$, $5 \times 10^3 - 10^4 M_\odot$, and $M > 10^4 M_\odot$.

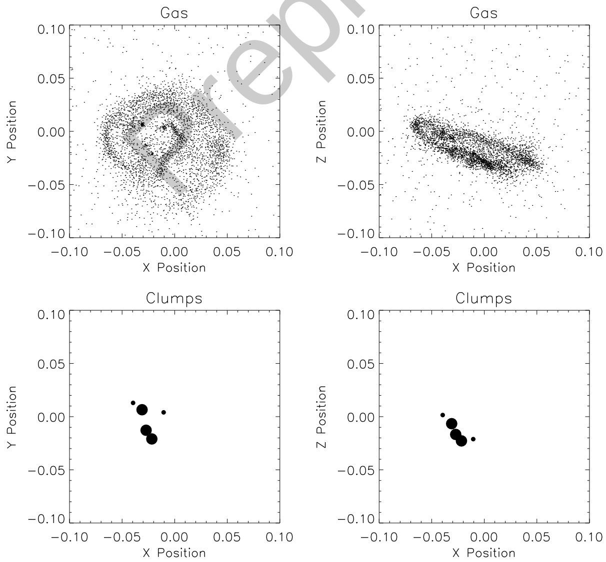

Fig. 2. Same as Fig. 1, but for initial spin $\lambda = 0.025$. More mass is incorporated into high-mass clumps, compared to the case in Fig. 1.

Protostellar Collapse with Various Metallicities

Kazuyuki Omukai

Department of Physics, Kyoto University, Sakyo-ku, Kyoto 606-8502, Japan

Abstract. The thermal and chemical evolution of gravitationally collapsing protostellar clouds are investigated focusing attention on their dependence on metallicity. The size of the stellar core at the formation is found to be the same regardless of the gas composition of the parent cloud.

1 Introduction

The distinction between the star formation in galaxy formation epoch and that in present-day star forming regions mainly resides in the difference of the composition of gas that stars are made from. Metallicity and, therefore, the gas to dust ratio is lower for earlier star formation. In present-day star forming regions, protostellar clouds remain roughly 10K in a wide range of densities owing to efficient dust emission (e.g., [1]) in the course of contraction. Whereas the collapse of metal-free protostellar clouds, which is relevant for the first star formation in the universe, is induced by radiative cooling owing to molecular hydrogen lines, and their temperatures are about 1000K (e.g., [2] [3]). In this paper, we aim to fill the gap between the protostellar collapse of primordial and present-day interstellar gas, and study the collapse of slightly metal polluted clouds.

2 Calculations

We consider a homogeneous spherical cloud with mean metallicity Z. The dust-to-gas ratio is assumed to be proportional to the mean metallicity. We calculate the time evolution of the central density, temperature and chemical composition.

In addition to compressional heating, we include cooling owing to (i) atomic and molecular line radiation ([CI], [CII], [OI], H_2, CO, OH, and H_2O) (ii) energy transfer between the gas and the dust grains, which will be emitted as infrared radiation from the grains, (iii) continuous radiation from the gas, and (iv) cooling and heating associated with chemical reactions.

We solve nonequilibrium chemistry involving the 4 elements H, He, C and O, that contains major 45 species.

Figure 1 displays the evolutionary trajectories of protostellar clouds whose metallicities are $z = 0, 10^{-6}, 10^{-4}, 10^{-2}, 1$.

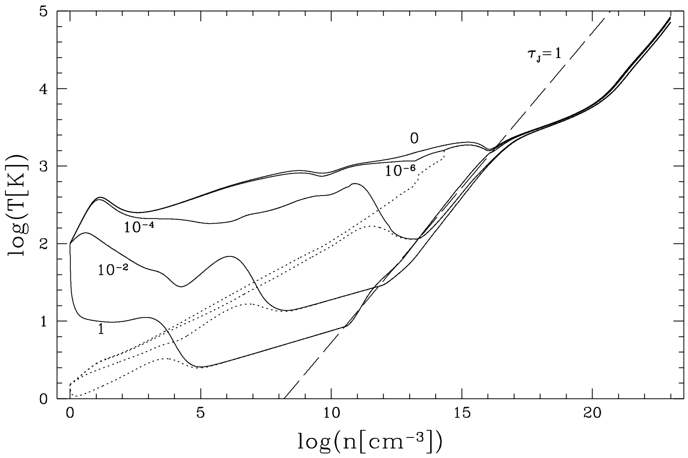

Fig. 1. The evolutionary trajectories of protostellar clouds with different metallicities. The solid curves show the temperature of the clouds with metallicity $Z/Z_{\odot} = 0, 10^{-6}, 10^{-4}, 10^{-2}, 1$ from the top to bottom. The dotted curves show the grain temperature for the same clouds. The dashed line marked "$\tau_{\rm J} = 1$" represents the line L in the text (Eq.(1)).

We set the initial condition to be $T = 100$K, $n = 1\text{cm}^{-3}$, $y(e) = 1 \times 10^{-4}$, $y(\text{H}_2) = 1 \times 10^{-6}$. The evolution of the clouds is summarized as follows. While the clouds are transparent to continuous radiation, the temperature of clouds with lower metallicity is higher since their radiative cooling rates are lower for the same density and temperature. However, after the clouds become opaque and begin adiabatic contraction, their evolutionary trajectories converge to a line that is determined only by physical constants. This line (L) can be expressed as [4];

$$\text{L}: \quad T = \left(\frac{k^3}{12\sigma^2 m_{\rm p}}\right)^{1/5} n^{2/5}. \tag{1}$$

Thereafter, the trajectories coincide with each other regardless of their metallicity. Consequently, the physical dimension of the stellar core at the time of formation is the same for clouds with any composition.

References

1. Hayashi, C., & Nakano, T. (1965) Prog. Theor. Phys. **34**, 754
2. Matsuda, T., Sato, H., & Takeda, H. (1969) Prog. Theor. Phys. **42**, 219
3. Palla, F., Salpeter, E. E., & Stahler, S. W. (1983) Astrophys. J. **271**, 632
4. Omukai, K. (1999) submitted to Astrophys. J.

Does Deuterium Enable the Formation of Primordial Brown Dwarfs?

Hideya Uehara and Shu-ichiro Inutsuka

National Astronomical Observatory, 181-8588, Japan

Abstract. We investigate thermal and dynamical evolutions of a primordial gas cloud whose mass is much higher than the cosmological Jeans mass using an updated deuterium chemistry. Such a cloud collapses to form a shock and fragment.

At first we investigate molecule formation in a primordial shock. Our numerical model, including an updated deuterium chemistry [1,3], is based on that of[2]. Figure 1 shows the evolution of fractional abundances as a function of temperature. When the postshock cooled sheet fragments due to gravitational instability (i.e. when the cooling timescale becomes equal to the free-fall timescale), the fractional H_2 and HD abundances become $\sim 10^{-2}$ and 10^{-5}, respectively. These molecular fractions are $10^3 - 10^4$ times higher than the results of molecule formation in the expanding universe after recombination (see e.g. [3]). These enhanced molecular fractions would have significant effects on the subsequent evolution of fragments.

In order to see subsequent evolution of a fragment, we performed one-dimensional simulation of a spherical and acylindrical cloud, of which initial conditions are derived from results of shock calculations. The evolution of the central density and temperature is shown in Figure 2. It is found that, in case of a cylindrical collapse, the cooling by HD molecules keeps the temperature of the cloud less than 100 K and the cloud evolves almost isothermally. When the cloud becomes optically thick to the HD line emission ($\sim 10^{10}\mathrm{cm}^{-3}$) , Jeans mass becomes less than $0.1M_{\odot}$. This fact suggests the formation of primordial brown dwarfs, which are one of the possible candidates for massive compact halo objects (MACHOs), in primordial gas clouds.

References

1. Galli, D., & Palla, F. (1998) A&A, **335**, 403
2. Kang, H., & Shapiro, P. R. (1992) ApJ **386**, 432
3. Stancil, P. C., Lepp, S., & Dalgarno, A. 1998 ApJ, **509**, 1

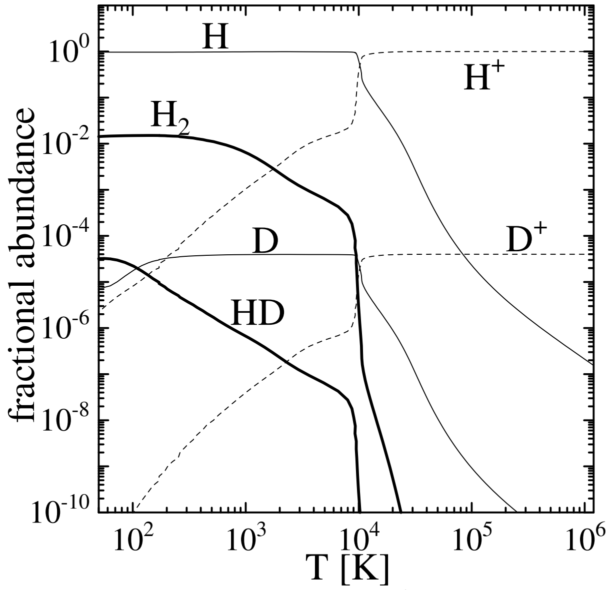

Fig. 1. Fractional abundances as a function of temperature for shock velocity 300km/s.

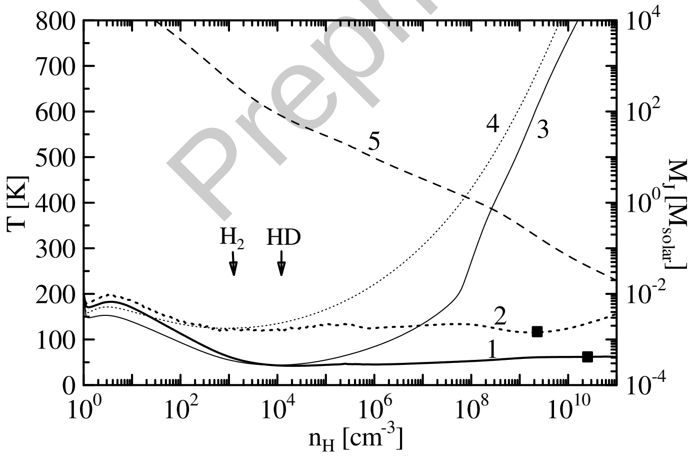

Fig. 2. The evolution of the central density and temperature of a cloud. The lines labeled with 1 and 2 represent a cylindrical cloud with and without HD cooling, respectively, 3 and 4 represent a spherical cloud with and without HD cooling, respectively. The arrows labeled H_2 and HD represents the critical density for H_2 and HD molecules, respectively. The filled squares on the lines show the density at which the optical depth to the most effective line emission becomes unity. The line labeled with 5 represent the Jeans mass for a cylindrical cloud with HD cooling (corresponding to line 1).

Part VI

Observational Clues from Galaxies at High z or Low Z

Local Dwarf Galaxies: Windows on Life at High z with Low Z

Mario Mateo

Dept. of Astronomy, University of Michigan, 821 Dennison Bldg., Ann Arbor, MI 48109-1090, mateo@astro.lsa.umich.edu

Abstract. In modern hierarchical galaxy formation scenarios, the smallest objects form first and merge to produce larger structures. In this review, I summarize some of the properties of the currently smallest dwarf galaxies of the Local Group and discuss whether they represent surviving examples – or close analogs – of the original galaxy building blocks of the early Universe.

1 Introduction: The Problem with Fossils

Paleontologists understand well that their fossil record offers a distorted picture of early life on earth. Some animals are found more or less where they fell, more or less complete, more or less in a state that reflects some common life activity. But this is uncommon. Instead, most fossils are distributed far from where the animals lived originally, and may be physically mixed up with fossils of other species from their own or other eras. Most importantly, *no fossil is the actual animal!* Minerals have replaced bone; impressions of bodies within rock have recorded form; footprints have survived to remind us of the living, breathing creatures that are now gone.

My aim in this paper is to illustrate how dwarf galaxies can serve as fossils that help illuminate the formation era of the first stars and galaxies. However, like paleontologists, we must remain acutely aware that the galaxy fossil record represents a modified view of what the early Universe was like. We should not *a priori* expect to find the chronologically first star – nor their remnants – within any existing dwarf system. We should not even expect to find any of the first galaxies. But, as I argue below, it may be reasonable to identify some nearby dwarfs as the closest surviving links to the types of systems within which the first stars formed in the earliest days of the Universe.

2 A Primer on Local Group Dwarfs

I will concentrate on dwarf galaxies of the Local Group (LG) because (a) we have the most complete and uniform basic data for these galaxies, and (b) because the sample of well-studied LG dwarfs is now sufficiently large that we may be able to confidently extract statistically useful information.

In this section, I focus on some very general properties that may or may not be directly relevant to the study of the first stars.

Table 1 provides a list of all LG galaxies, including the four newest additions discovered since I compiled a similar table in a recent review [21]. Three of the new systems are certain satellites of M31 (And V, VI, and VII) and were discovered by [4,5,19]. A fourth galaxy, Cetus, was discovered very recently [28]; the limited information on that system is also listed in Table 1. The original sources for data for the other galaxies listed in Table 1 can be found in [21].

The distributions of galaxies in the Local Group is not uniform: four distinct groups are apparent. The two larger galaxies, M31 and the Milky Way, serve as the nuclei to two of these subgroups. NGC 3109, itself a dwarf system, is the dominant member of the third subgroup. The remaining galaxies are distributed in a much more extended, amorphous, and very large system that I call the 'Local Group Cloud'. The groups exhibit a very clear parent/satellite segregation: The early-type systems are strongly concentrated about the larger galaxies, while the late-type irregulars dominate the areas further from the deepest potential wells within the group. Apart from NGC 205 and Sagittarius (Sgr), no galaxies lie closer than about 50 kpc from the two large systems. Interestingly, these two exceptions exhibit evidence of severe tidal interactions with their parents. The luminosity function of the Local Group is fit well with a Schechter law for systems brighter than $M_V \sim -15$ (see [21]). Globular clusters are found in nearly every Local Group dwarf with $M_V \leq -14.5$.

3 Dwarf Galaxies as the Sites of the First Stars

I will now focus on three specific areas that may be directly relevant to the question of whether existing dwarfs represent systems in which first stars formed: chemistry, star-formation history and dark-matter content. However, before I embark on this I must stress two issues. First, what definition should be used for 'first stars'? I counted no fewer than eight during our three-day conference, including five in one talk [6]! For the purposes of this paper, 'first stars' refers to the process of star formation – whenever or wherever it may have occurred – that occurs under the same conditions that *the* chronologically first star formed. Because these conditions – and particularly the accumulation of enough material for stars to form – may have taken significantly longer in some regions of the local Universe than in others, we cannot rule out that some 'first stars' formed considerably late in the early history of the Universe. They may even be forming now in some environments (e.g. I Zw 18; but see [2]). The second point I want to emphasize is that the dwarf galaxies we see today are obviously 'survivors' of the process of large-galaxy formation. We can confidently expect that the majority of primordial star-forming systems are now gone, or they have merged to form larger galaxies.

Table 1. Local Group Members

Galaxy	Type	Sub-Group	Dist kpc	L $10^6 L_\odot$	M $10^6 M_\odot$	$\overline{[Fe/H]}$	$\sigma_{[Fe/H]}$
M31	SbI-II	M31	770	25000	700000	—	—
Milky Way	Sbc	MW	8	8300	350000	—	—
M33	ScII-III	M31	840	3000	30000	—	—
LMC	IrrIII-IV	MW	49	2100	20000	—	—
SMC	IrrIV-V	MW	58	580	1000	—	—
WLM	IrrIV-V	LGC	925	500	150	−1.5	[0.3]
M32	E2	M31	805	380	2120	−1.1	0.7
NGC 205	E5p/dSph-N	M31	815	370	740	−0.8	0.5
NGC 3109	IrrIV-V	N3109	1250	160	6550	−1.5	[0.3]
IC 10	dIrr	M31	825	160	1580	−1.1	[0.3]
NGC 185	dSph/dE3p	M31	620	130	130	−1.2	0.4
NGC 147	dSph/dE5	M31	725	130	110	−1.1	0.4
NGC 6822	IrrIV-V	LGC	490	94	1640	−1.2	0.5
IC 5152	dIrr	LGC	1590	70	400	−0.9	[0.3]
IC 1613	IrrV	M31	700	64	795	−1.3	[0.3]
Sextans A	dIrr	N3109	1440	56	395	−1.9	[0.3]
Sextans B	dIrr	N3109	1345	41	885	−1.2	[0.3]
Sagittarius	dSph-N	MW	24	18	—	−1.0	0.5
Fornax	dSph	MW	138	16	68	−1.3	0.6
Pegasus	dIrr/dSph	LGC	955	12	58	−1.0	[0.3]
EGB 0427+63	dIrr	M31	1300	9.1	—	−1.7	[0.3]
SagDIG	dIrr	LGC	1060	6.9	9.6	−1.9	[0.3]
And VII	dSph	M31	770	5.7	—	−1.4	[0.3]
UKS2323-326	dIrr	LGC	1320	5.3	—	—	—
Leo I	dSph	MW	250	4.8	22	−1.5	0.3
And I	dSph	M31	805	4.7	—	−1.5	0.3
Leo A	dIrr	MW	690	3.0	11	−2.0	0.3
And II	dSph	M31	525	2.4	—	−1.6	0.5
Sculptor	dSph	MW	79	2.2	6.4	−1.8	0.3
Antlia	dIrr/dSph	N3109	1235	1.7	12	−1.8	0.3
And VI	dSph	M31	830	1.4	—	−1.5	0.3
LGS 3	dIrr/dSph	M31	810	1.3	13	−1.8	0.3
And III	dSph	M31	760	1.1	—	−2.0	0.2
And V	dSph	M31	800	1.0	—	−1.5	[0.3]
Phoenix	dIrr/dSph	MW	445	0.9	33	−1.9	0.5
DDO 210	dIrr/dSph	LGC	800	0.8	5.4	−1.5	[0.3]
Tucana	dSph	LGC	880	0.6	—	−1.7	0.3
Leo II	dSph	MW	205	0.6	9.7	−1.9	0.3
Cetus	dSph	LGC?	80	0.6	—	—	—
Sextans	dSph	MW	86	0.5	19	−1.7	0.2
Carina	dSph	MW	101	0.4	13	−2.0	0.1
Ursa Minor	dSph	MW	66	0.3	23	−2.2	0.2
Draco	dSph	MW	82	0.3	22	−2.0	0.5

But, like fossils, present-day dwarfs may represent our most direct links to these early objects.

3.1 The Chemical Properties of Local Group Dwarfs

Over the past 15 years there has been steady progress in the determination of reliable abundances of the stellar and nebular components of local dwarfs. For many early-type systems, mean abundances and abundance spreads have been estimated from greatly improved color-magnitude (CM) diagrams (e.g. [17]). Deep photometric studies are able to account for the (slight) effect of an age spread – also common in nearly all local dwarfs – on photometrically derived abundances. Some studies (e.g. [14]) have used specialized photometric systems to obtain more precise photometric abundances. Spectroscopic stellar abundances remain relatively rare and, owing to the faintness of the stars, are generally based on low-dispersion observations. One notable exception is the recent study of Shetrone et al. [24] who obtained Keck HIRES echelle spectra of four stars in the Draco dSph. More high resolution spectral observations can be expected from HIRES and, in the near future, from UVES (VLT) and MIKE (Magellan). Nebular abundances can be derived reliably when care is taken to observe emission lines that constrain HII-region electron temperatures. These observations generally provide Oxygen abundances, though abundances of He – of cosmological importance – and elements such as Nitrogen and Sulfur are also sometimes reported (see [21] for a detailed summary). Nebular and stellar abundance estimates are both available in ten LG galaxies; these systems indicate that the [O/Fe] $\sim +0.4$.

There are three key points to stress from these abundance studies. First, no LG dwarf exhibits a mean Fe or O abundance lower than about 230 times solar ([Fe/H] $\gtrsim -2.5$). In this sense there is a dwarf G(alaxy) problem reminiscent of the more famous dwarf G problem of the solar neighborhood revealing itself as a distinct lack of galaxies of extremely low mean metal abundance. This is illustrated in Fig. 1 which shows the cumulative abundance distribution of all LG dwarfs. Interestingly, one of the four stars observed by [24] has a very low mean abundance but still far higher than one would expect for a true 'Pop III' object. The second point is that the LG dwarfs seem to exhibit a correlation of abundance with luminosity such that the dimmest systems are the most metal weak [25,11]. It is not clear if dSph and dIrr galaxies obey the same correlation [21]; at a given luminosity dSph galaxies appear to be more metal rich by about 0.5 dex compared to dIrrs. Could this mean that dSph galaxies are more chemically evolved than their dIrrs cousins? Finally, the galaxies with photometric and spectroscopic stellar abundance estimates exhibit significant metallicity spreads which do not appear to correlate with total luminosity.

Côté et al. [9] have modeled the formation of the halo and bulge via the accretion of dwarf-like subcomponents. They note that the metallicity distributions of the halo and bulge – and their associated globular clusters –

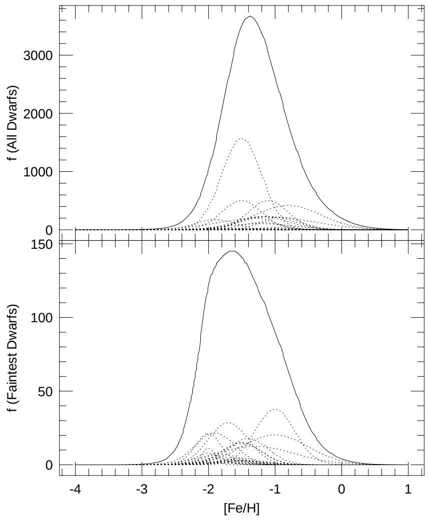

Fig. 1. The summed metallicity distributions (solid lines) for all dwarf galaxies (*upper panel*; systems located below the first horizontal line in Table 1) and for all dwarfs less luminous than the Sagittarius dwarf (*lower panel*; systems located below the second horizontal line in Table 1). The individual galaxy metallicity distributions are shown as dotted lines based on the data in Table 1. Each galaxy's normalization is proportional to its luminosity; the ordinate units are arbitrary.

can be understood from the distribution of chemical abundances of present-day local dwarfs.

3.2 The Star-Formation Histories of Local Group Dwarfs

Because of their relative proximity, the local dwarfs offer a unique opportunity to study their star-formation histories in some detail. The key tool of these studies are the new, deep CM diagrams that are possible with good CCD detectors on large telescopes. Recent studies have exploited large CCD mosaics to study the SFHs over most of the projected areas of many nearby systems [17]. Generally, observed CMDs are compared with synthetic diagrams based on assumed SFHs and the known photometric completeness and uncertainty distributions (e.g. [13]), though some recent studies have investigated non-parametric approaches [15]. The best available data (both in terms of photometric precision *and* in numbers of stars in the CMDs) provide ages of individual star-forming episodes precise to about 10-20%.

Though the results from these studies differ in detail for individual galaxies, some robust results have begun to emerge:

- The stars in even some of the least luminous local galaxies formed over a very large time interval extending from the era of the oldest stars to the present;
- Nearly all local dSph galaxies contain ancient stars as revealed by the presence of RR Lyr stars, ancient, metal-poor giants, or turnoff stars with luminosities comparable to those in globular clusters;
- The SFHs of all of the dwarfs are demonstrably different from one another;
- Star formation 'bursts' or episodes with durations of $\lesssim$ 10Myr to 2+ Gyr are common within local dwarfs;
- There is growing evidence that the SFHs vary spatially in many dwarfs [3,17]).

Unavane et al. [27] and Mateo [20] discussed whether galaxies with similar properties could have conceivably constructed the Galactic halo. Both papers concluded that some fraction – ranging from 10-50– of the halo could be composed of stars from galaxies similar to local dwarfs. The key uncertainty is the timing: if most of the dwarf accretion occurred very early in the evolution of our Galaxy, then few of the intermediate-age populations we see in local dwarfs would have been injected into the halo (the galaxies would have been disrupted before these populations could have formed). If the Galactic accretion process was more extended – the existence of Sagittarius implies that this may be the case – then it seems very likely that dwarfs with multiple star-formation episodes would have dissolved over time into the halo. The presence of some intermediate-age stars in the halo [23] could be explained in this manner.

These complex SFHs raise some interesting problems. As noted above, the local dwarfs obey a global luminosity-metallicity relation, consistent with simple models in which the star-formation in these galaxies is dominated by single episodes where the metallicity is regulated by winds in dark-matter dominated systems [10]. But the actual SFHs are far more complex than this sort of model requires; it is truly surprising that dwarfs obey any sort of relation between luminosity and abundance. The lack of gas in many of the nearby dSph galaxies is also surprising given their active SFHs. Some recent studies [8,26] suggest that some individual dwarfs of the outer halo do indeed have associated gas. Blitz et al. [7] have proposed that some high velocity HI clouds may reside in the outer halo, either associated with known dwarfs or with heretofore unidentified systems. Such clouds could supply the raw material needed to form stars in distant, seemingly isolated dwarfs, but only if individual dwarfs retain extended gas reservoirs over very long periods of time, or that gas accretion can occur in dwarfs of the outer halo. The complex SFHs of dwarfs may also imply that these small galaxies are themselves the products of mergers of even smaller systems with distinct SFHs (see [17]).

3.3 The Dark-Matter Content and Masses of Local Group Dwarfs

Since Aaronson's [1] pioneering study, many people have worked hard to measure the internal kinematics of local dwarfs. As summarized by Mateo [21], the majority of these galaxies now have either well-measured stellar or nebular kinematic data; in a few cases, both sorts of data are now available. Many of the possible pitfalls in the acquisition – inadequate precision, binary contamination, velocity 'jitter' in luminous giants, small samples – and interpretation – velocity anisotropy, the relative distributions of visible and dark matter, tidal effects – have either been overcome with better data or are now sufficiently well understood that we can be confident of the principal results. These include:

- The minimum observed central velocity dispersion in any local dwarf is about 6-7 km/s, despite samples of high-quality spectral observations that could resolve much smaller dispersions;
- Dwarf masses derived under the assumption that mass follows light reveals an apparent minimum galactic mass of about $2 \times 10^7 M_\odot$ [21]. If the mass is more extended than the visible matter (Fig. 2), then this value represents a lower limit.

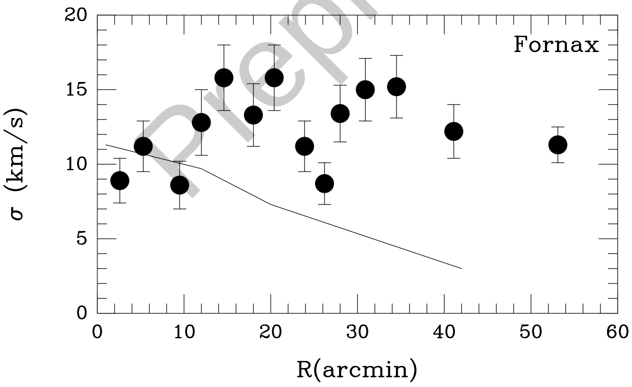

Fig. 2. The radial velocity dispersion profile for the Fornax dSph galaxy. Each point represents 16 independent stellar kinematic measurements. The solid line shows the profile expected for a system in which mass follows light for an isotropic velocity distribution. These data imply that the dark halo of Fornax is considerably more extended than the visible material or that the velocity anisotropy varies in such a way as to mimic an extended $\rho \propto r^{-2}$ halo.

Ferrara & Tolstoy [12] interpret this second point differently. In their models the lower mass limit corresponds to the smallest dark halo that can retain a significant baryonic component. Less massive dark halos may exist, but they will not be associated with a visible stellar component. Either way, stars forming in the lowest-mass galaxies seem to require galactic nurseries with $M \gtrsim 10^7 M_\odot$.

One of the fundamental problems with all models of halo formation via the accretion of systems similar to present-day dwarfs has to do with the inability to account for all the mass in the halo. For example, the models of Côté et al. [9] do an excellent job of accounting for the baryonic content and the metallicity distributions of the Galactic halo and bulge and their corresponding globular clusters. But they fail by many orders of magnitude to account for the halo mass. If present-day dwarfs are true fossils of the systems from which the Galaxy formed, then many had to be 'dark', supplying only mass but essentially no stars. It is clear that we need to measure the *mass function* of dwarf halos, but if most of these are dark, this may prove to be extremely difficult.

4 Summary and Future Prospects

There is now compelling evidence that systems similar to present-day dwarfs played a significant role in the formation of the Galactic halo and bulge [18,9,16]); surveys are underway to identify further streams in the halo (e.g. [22]) with the ultimate aim of quantifying the fraction of the halo that formed from distinct accretion events. There is also little doubt that present-day local dwarfs are analogs of these early galactic building blocks. However, the galaxies that survived to the present day did so by virtue of some accident of birth, such as a favored orbit, or because they formed at a chronologically later time than the systems that have already accreted. Consequently, it is by no means clear that any of the stars found in existing dwarf galaxies qualify as candidates for the chronologically 'first stars'. The truly earliest galaxies – the ones that have formed the bulk of the Galactic halo and bulge – were probably separate entities for only a very short time before becoming subsumed by the proto-Galaxy.

Nonetheless, the present-day dwarfs probably do tell us a lot about the environments in which these first stars formed. We can, for example, conclude that the first stars probably did form within dark halos with masses no smaller than about $10^7 M_\odot$ (though see [12] for their different interpretation of the significance of this limit). As such, the models of Dekel & Silk [10] may represent a good picture of how these first stellar populations evolved. In particular, the massive halos would have allowed considerable self-enrichment that would have quickly polluted the recently pristine ISM and all subsequently formed stars. The small sizes would have also guaranteed that this enrichment was prompt; a single supernova could not only provide enough metals to significantly raise the abundance of the entire mass of the ISM, but the small sizes of these 'pre-galaxies' would have helped ensure that these metals would be distributed throughout the star-forming regions. The fact that many of the surviving dwarfs have experienced multiple episodes of star formation is direct evidence that these environments are conducive – perhaps necessary – to star formation within the Galactic halo.

I have already noted that future high-resolution spectrographs should quickly revolutionize our understanding of the chemical enrichment histories of the existing dwarfs and of field halo stars. I expect that these sorts of studies will conclusively identify stars that are at most one type-II supernova removed from the epoch when the first stars formed; chronologically, perhaps only a few tens of millions of years removed from this epoch. These same instruments will allow us to pursue kinematic studies of unprecedented detail as well. With such data it may be possible to identify kinematically distinct populations within dwarfs – perhaps remnants of mergers at the dwarf-galaxy scale – and to better understand the distribution and masses of dark halos in these systems. These observations may provide us with the best possible fossil record of what the dark halos of the original galactic sub-structures were like, and hence give us our best opportunity to compare observations with theories of structure formation. It should all be very exciting, not only for what we will learn that constrains our current ideas, but especially for the surprises that are sure to come.

References

1. Aaronson, M. 1983, ApJ, 266, L11.
2. Aloisi, A., Tosi, M. & Greggio, L. 1999, AJ, 118, 302.
3. Aparicio, A., Dalcanton, J., Gallart, C. & Martinez-Delgado, D. 1997, AJ, 114, 1447.
4. Armandroff, T., Davies, J. & Jacoby, G. 1998, AJ, 116, 2287.
5. Armandroff, T., Jacoby, G. & Davies, J. 1999, AJ, 118, 1220.
6. Beers, T. 1999, this volume.
7. Blitz, L., Spergel, D., Teuben, P., Hartmann, D. & Burton, B. 1999, ApJ, 514, 818.
8. Carignan, C. Beaulieu, S., Côté, S., Demers, S. & Mateo, M. 1998, AJ, 116, 1690.
9. Côté, P., Marzke, R., West, M. & Minniti, D. 1999, preprint.
10. Dekel, A. & Silk, J. 1986, ApJ, 303, 39.
11. Durrell, P., Harris, W., Geisler, D. & Pudritz, R. 1996, AJ, 112, 972.
12. Ferrara, A. & Tolstoy, E. 1999, preprint (astro-ph/9905280).
13. Gallart, C., Aparicio, A., Bertelli, G. & Chiosi, C. 1996, AJ, 112, 1950.
14. Grebel, E. 1997, Rev Mod Astron, 10, 29.
15. Hernandez, X., Valls-Gabaud, D. & Gilmore, G. 1999, MNRAS, 304, 705.
16. Helmi, A., White, S., de Zeeuw, T. & Zhao, H.-S. 1999, Nature, 402, 53.
17. Hurley-Keller, D., Mateo, M. & Grebel, E. 1999, ApJ, 523, L25.
18. Ibata, R., Gilmore, G. & Irwin, M. 1994, Nature, 370, 194.
19. Karachentseva, V. & Karachentsev, I. 1998, A&AS, 127, 409.
20. Mateo, M. 1996, in *The Formation of the Galactic Halo ... Inside and Out*, eds. H. Morrison & A. Sarajedini, p. 434.

21. Mateo, M. 1998, ARAA, 36, 435.
22. Morrison, H., Mateo, M., Olszewski, E., Harding, P., Dohm-Palmer, R., Freeman, K., Norris, J. & Morita, M. 1999, preprint.
23. Preston, G., Beers, T. & Shectman, S. 1994, AJ, 108, 538.
24. Shetrone, M., Bolte, M. & Stetson, P. 1998, 115, 1888.
25. Skillman, E., Kennicutt, R. & Hodge, P. 1989, ApJ, 347, 875.
26. St.-Germain, J., Carignan, C., Côté, S. & Oosterloo, T. 1999, AJ, 118, 1235.
27. Unavane, M., Wyse, R. & Gilmore, G. 1996, MNRAS, 278, 727.
28. Whiting, A, Irwin, M. & Hau, G. 1999, BAAS, 194, 110.02.

Blue Compact Dwarf Galaxies – Home to the Latest of the First Stars?

Regina E. Schulte-Ladbeck[1], Ulrich Hopp[2], Mary M. Crone[3], and Laura Greggio[2,4]

[1] University of Pittsburgh, Pittsburgh, PA 15260, USA
[2] Universitätssternwarte München, München, FRG
[3] Skidmore College, Saratoga Springs, NY 12866, USA
[4] Osservatorio Astronomico di Bologna, Bologna, Italy

Abstract. We review single-star photometry with the Hubble Space Telescope (HST) of five well resolved Blue Compact Dwarf (BCD) galaxies. Three BCDs exhibit well populated red giant branches. These galaxies are therefore at least 1-2 Gyr old, and possibly older than 10 Gyr. For two BCDs, the available HST data do not go deep enough to reveal the red giant branch. We argue that over a wide range of possible galaxy distances, the color-magnitude diagrams of these BCDs are nevertheless consistent with showing the evolved descendants of intermediate-mass stars on the asymptotic giant branch. Such stars are nucleosynthetic sites of nitrogen and carbon production. Their identification in BCDs contradicts recent conclusions that BCDs must be young galaxies in which primary production of these elements takes place exclusively in massive stars, and implies that BCDs are unlikely to be home to newly formed metal-free stars. Color-magnitude diagrams of BCDs thus point to difficulties in decoding star-formation histories of starburst galaxies from the metallicities of the ionized gas.

1 Introduction

Whether Blue Compact Dwarf (BCD) galaxies are "young" galaxies which are forming their very first stars at the present epoch, or "old" galaxies which made their first generation of stars at high redshift and are currently experiencing a burst of star formation, has remained an open question in spite of considerable observational effort over the past thirty years (e.g. [8,10,9]). The discovery of H-II galaxies forming their first stars in the local Universe, or of any pristine H-I clouds that are still awaiting the formation of their first stars, would present a key test for models of galaxy formation [2].

The possibility that BCDs are genuinely young galaxies was immediately raised when they were first recognized [8]. BCDs have high star-formation rates and low abundances indicated by their ionized gas. Their metallicities (oxygen abundances) range from about 1/5 to 1/50 of solar (e.g. [10]). While their H-I reservoirs are large, BCDs could not have sustained star-formation at the present rate for a long time, and they would have self-enriched the gas in H-II regions much beyond what is observed. Therefore, BCDs must either be young galaxies, or old galaxies presently undergoing one of only a few starbursts.

Near-IR color-magnitude diagrams (CMD) are particularly sensitive to the intermediate-age and old stellar content of BCDs. Several near-IR CMDs of BCDs with metallicities in the range from 1/10 to 1/20 of solar are presented in Fig. 1. The BCDs exhibit well-populated red giant branches. They are therefore at least 1-2 Gyr old, and may contain a truly ancient stellar substratum. For these BCDs, the detection of red giants with HST, in combination with ground-based observations of faint background sheets that extended far beyond the starburst regions covered by the small field of the NICMOS camera 2, support the conclusion that they are old galaxies.

Abundance determinations have also been used to probe the star-formation histories of BCDs. Massive stars feed metal-enriched gas back into the interstellar medium of galaxies, strongly influencing their chemical enrichment histories. Because massive stars live only for a few Myr before exploding as supernovae and returning chemically processed material, the first starburst in a BCD might almost instantaneously enrich its local environment. Kunth & Sargent [5] suggest that I Zw 18, famous for being the most metal-poor galaxy in the nearby Universe ($\sim Z_\odot/50$), could presently experience its first burst and exhibit the low-end cut-off for BCD metallicities. Indeed, many searches have not turned up any BCDs with metallicities below that of I Zw 18.

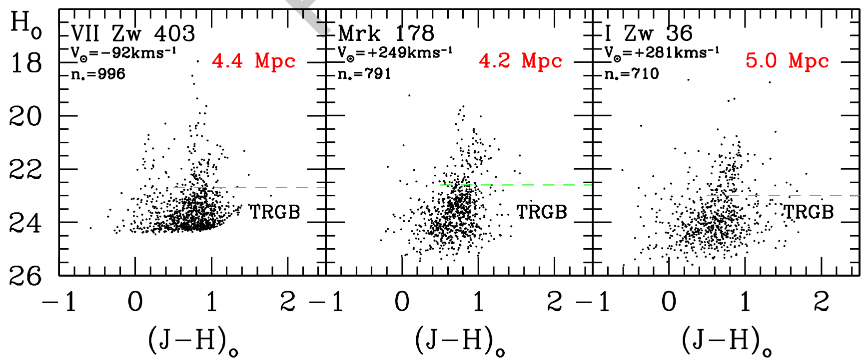

Fig. 1. Near-infrared CMDs based on observations with the NICMOS camera 2 aboard HST. Owing to Wien's law, the J and H-bands are more sensitive than optical passbands for the detection of red giants. All three BCDs exhibit well-developed giant branches. They are not primeval galaxies. The distance estimates for Mrk 178 and I Zw 36 are preliminary; future refereed papers will provide more careful distance determinations.

There has been substantial literature related to the physical processes which may determine the observed chemical enrichment history of BCDs. These processes include infall of pristine gas, selective metal-enhanced outflow of processed gas, time-delayed production of elements, and allowing material to "hide" in unobserved stages of ionization. The interested reader is referred to [11], as well as to the contributions by Pilyugin and Pettini in this volume.

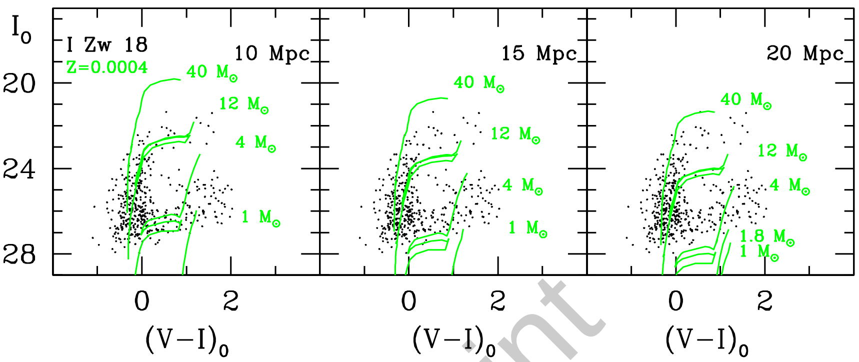

Fig. 2. The CMD of I Zw 18 from the data of [1]. Stellar-evolution tracks from the Padova library are overlayed for a stellar metallicity that corresponds to that of the ionized gas. Aloisi et al. adopted a distance of 10 Mpc and showed that the present burst is not the first to occur. Recently, [4] have suggested that the distance to I Zw 18 could be larger, namely 20 Mpc. We therefore also show the tracks shifted to cover the new range of possible distances. Nevertheless, the stellar content of I Zw 18 is consistent with the presence of intermediate-mass stars. These stars have ages of a few hundred Myr and are possible sources of nitrogen and carbon enrichment of the interstellar medium of I Zw 18.

2 The Origin of Nitrogen

Here we address one of the controversial features of enrichment in BCDs: the question of whether or not massive stars are responsible for *all* of their primary nitrogen, as recently concluded by [3]. These authors observe that the N/O versus O/H ratios for BCDs with metallicities below $\sim Z_{\odot}/20$ are constant, with little scatter. Interpreting this as evidence in favor of both oxygen and nitrogen synthesis in the same massive stars, they conclude that these galaxies are "primeval", in the sense that they are currently forming their very first generation of stars out of pristine gas.

We find that the CMDs of two of the most metal-poor BCDs, I Zw 18 and SBS 1415+437, show evidence for the presence of evolved intermediate-

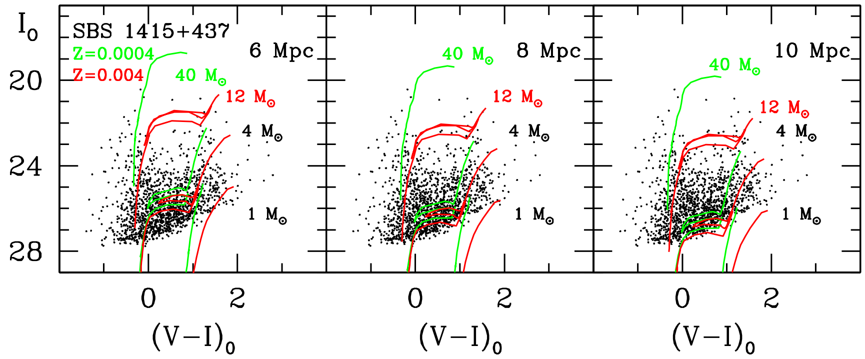

Fig. 3. We re-reduced the archival HST data of SBS 1415+437. This CMD contains about twice as many sources as the original reduction presented by [10]. The data do not go deep enough in the V-band to include the red giant branch. We show two sets of tracks that bracket the gas abundance. It can be seen that for quite a range of possible distances, the CMD of SBS 1415+437 provides evidence for the presence of intermediate-mass stars with ages of a few hundred Myr.

mass stars, even if we take into account the vast uncertainty in their distances (cf. Fig. 2 and 3). Intermediate-mass stars are considered to be nucleosynthetic sites for the production of nitrogen via hot-bottom burning in the asymptotic-giant-branch phase of stellar evolution [7]. The presence of evolved intermediate-mass stars allows the alternate conclusion that nitrogen is not exclusively synthesized in massive stars, and that BCDs have produced stars for at least a few hundred Myr. This alternative requires that the constancy of the N/O versus O/H ratios for low O/H values has some other cause. Pilyugin [6], for example, recently worked out a scenario to simultaneously account for the nitrogen abundances in BCDs and the very low N/Si ratios observed in damped Lyα systems. This scenario *requires* the nitrogen to be produced by intermediate-mass stars in BCDs; the constancy of N/O for low O/H is due to the fact that BCDs are observed after the cumulative effect of previous star-formation episodes has enriched their interstellar medium but before the oxygen released by massive stars formed in the present burst has mixed to become detectable in the H-II regions.

3 Conclusions

Five Blue Compact Dwarf galaxies are resolved well enough with HST to yield deep photometry of individual stars.

- HST data reveal the presence of red giants in three BCDs: Mrk 178 ($\sim Z_\odot/10$), I Zw 36 ($\sim Z_\odot/15$), and VII Zw 403 ($\sim Z_\odot/20$). These galaxies are therefore at least 1-2 Gyr old, and possibly contain a truly ancient population. The optical CMD of VII Zw 403 allows a photometric determination of the mean *stellar* abundances of the red giants, $<$[Fe/H]$> =$ -1.92 [9]. While this is low, it is perfectly consistent with a Population II type abundance. HST data are not deep enough to allow distance determinations for SBS 1415+437 ($\sim Z_{\odot}/20$) and I Zw 18 ($\sim Z_{\odot}/50$) using the tip-of-the-red-giant-branch method.

- All BCDs observed with HST — even those with extremely low O/H — show evidence for asymptotic-giant-branch stars, the older, evolved descendents of intermediate-mass stars. These stars contribute to the carbon and nitrogen enrichment of the interstellar medium through their winds. Therefore, the constancy of the N/O (and C/O) ratios at low O/H does not indicate that only SNeII enriched the gas of low metallicity dwarfs. Other explanations for this behaviour have to be found; and the conclusion that extremely metal-poor BCDs are "primeval" galaxies should not be considered a definitive argument.
- While the exact age of the oldest stellar component of BCDs cannot be determined with the present data, future observations with the ACS on HST and the NGST will allow the stellar content in BCDs to be probed to deeper limiting magnitudes. This will clarify the age of the oldest stars and yield the redshift of formation for several nearby BCDs.

Based on observations made with the NASA/ESA Hubble Space Telescope obtained from the Space Telescope Science Institute, which is operated by AURA, Inc., under NASA contract NAS 5-26555. We acknowledge financial support of NASA grants as well as SFB 375.

References

1. Aloisi, A., Tosi, M., Greggio, L. 1999, AJ, 118, 302
2. Briggs, F.H. 1997 PASA, 14, 37
3. Izotov, Y.I., Thuan, T.X. 1999, ApJ, 511, 639
4. Izotov, Y.I., Papaderos, P. Thuan, T.X., Fricke, K.J., Foltz, C.B., Guseva, N.G. 1999, A&A, astro-ph/9907082
5. Kunth, D., Sargent, W.L.W. 1986, ApJ, 300, 496
6. Pilyugin, L.S. 1999, A&A, 345, 428
7. Renzini, A., Voli, M. 1981, A&A 94, 175
8. Searle, L., Sargent W.L.W. 1972, ApJ, 173, 25
9. Schulte-Ladbeck, R.E., Hopp, U., Crone, M.M., Greggio, L. 1999, ApJ, in press
10. Thuan, T.X., Izotov, Y., Foltz, C.B. 1999, ApJ, in press
11. van Zee, L., Salzer, J.J., Haynes, M.P. 1998, ApJL, 1

On the Origin of Nitrogen in Low-Metallicity Galaxies

Blue Compact Galaxies versus Damped Lyα Absorbers

Leonid S. Pilyugin

Main Astronomical Observatory of National Academy of Sciences of Ukraine, Goloseevo, 03680 Kiev-127, Ukraine, (e-mail pilyugin@mao.kiev.ua)

Abstract. Recently a remarkably small scatter in the N/O ratios for the HII regions in low-metallicity blue compact galaxies (BCG) has been found. It lead to the conclusion that N is produced by massive stars. Conversely, the N/Si ratios in damped Lyα absorbers (DLA) show a large scatter. This provides support for the time-delay model of nitrogen production in intermediate-mass stars, nitrogen production in massive stars being not required.

Here it has been tested whether these observational data are compatible with each other and with the existing ideas on the chemical evolution of galaxies. We find that it is possible to reconcile the constancy of N/O ratios in low-metallicity BCGs and the scatter of N/Si ratios in DLAs under the assumptions that a significant part of nitrogen is produced by intermediate-mass stars, and previous star formation events are responsible for measured heavy element abundances of HII regions in BCGs.

1 Introduction

The theoretical stellar yields of nitrogen are rather uncertain. It has been found [21], [14], [15], [23] that nitrogen production takes place in intermediate-mass stars, but the mass range of the nitrogen-producing stars and the predicted amount of produced nitrogen depend on poorly known parameters. The theoretical yields of nitrogen by massive stars are also poorly known. The schematic sketch of the time variation of N/O ratio in the interstellar medium of the system after three successive star formation bursts is shown in Fig. 1a. Since the bulk of oxygen is produced by short-living massive stars and part of nitrogen is produced by relatively long-living intermediate-mass stars, there is a temporary decrease of the N/O ratio after star formation event. The value of the N/O decrease depends on the contribution of intermediate-mass stars to the nitrogen production and on the initial metallicity of gas where the star formation event takes place. The N/O ratio corresponding to the early stage (before ejecta of intermediate - mass stars) of the first star formation event is a lower limit for the global N/O ratios, Fig. 1a. Strictly speaking, the constancy of N/O ratio during the early stage of the first star formation event will take place if stellar nitrogen yields $Y_N(M_S)$ and oxygen yields $Y_O(M_S)$ are related by the following equation $Y_N(M_S) = const \times Y_O(M_S)$.

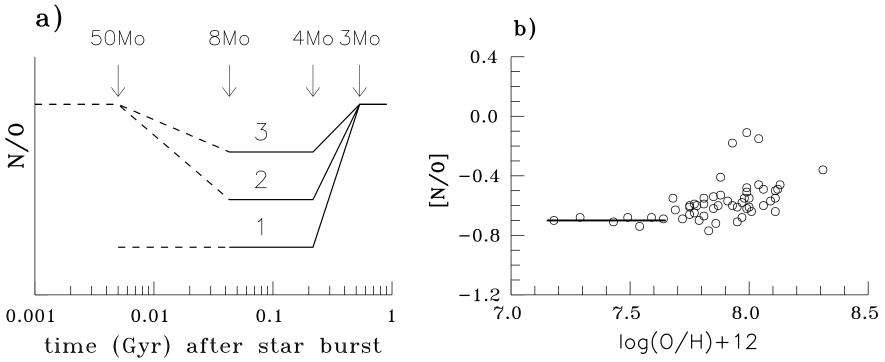

Fig. 1. a) The schematic sketch of the time variation of N/O ratio in the interstellar medium of system after three successive star formation bursts. Every curve is labeled with number of star burst. The dashed part of every curve corresponds to the period of existence of a giant HII region. **b)** The observed N/O – O/H diagram for blue compact galaxies. The data are taken from [6].

Since the theoretical yields of nitrogen are rather uncertain, an "empirical" approach (analysis of the relation of N/O with O/H) has been widely used to study of the origin of nitrogen ([3], [11], [16], [4], [17], [18], [24], [13]; among others). However, two diametrically oposite conclusions about nitrogen origin have been recently made within the framework of empirical approach. Izotov and Thuan [22], [6] have found a remarkably small scatter in the N/O ratios of the HII regions in low-metallicity (with 12+logO/H $\leq$ 7.6) BCGs, Fig. 1b. They concluded that these galaxies are presently undergoing their first burst of star formation, and that nitrogen in these galaxies is produced by massive stars only. If it is the case, the N/O ratio observed in low-metallicity BCGs would be a lower limit for the global N/O ratios. This is in conflict with the fact that the nitrogen to α-element abundance ratios measured in some DLAs are well below than the value observed in low-metallicity BCGs ([12], and references therein), Fig. 2a. Then the question arises whether the constancy of the N/O ratios in low-metallicity BCGs and and the scatter of the N/Si ratios in DLAs are compatible with each other and with the existing ideas on the chemical evolution of galaxies.

2 Possible Interpretation of Nitrogen Abundances in BCGs and DLAs

Here we will demonstrate that the constancy of the N/O ratios in low-metallicity BCGs and the scatter of the N/Si ratios in DLAs can be reconciled under the assumptions that a significant part of nitrogen is produced by intermediate-mass stars, and the previous star formation events are responsible for heavy element abundances observed in the HII regions of the BCGs. (Since oxygen abundance measurements are not available for DLAs, $[N/S]$ or $[N/Si]$ ratios are considered instead of $[N/O]$. This is justified by the fact that there is no reason to believe that the relative abundances of O, S and Si which are all produced in Type II supernovae are different from solar in DLAs.)

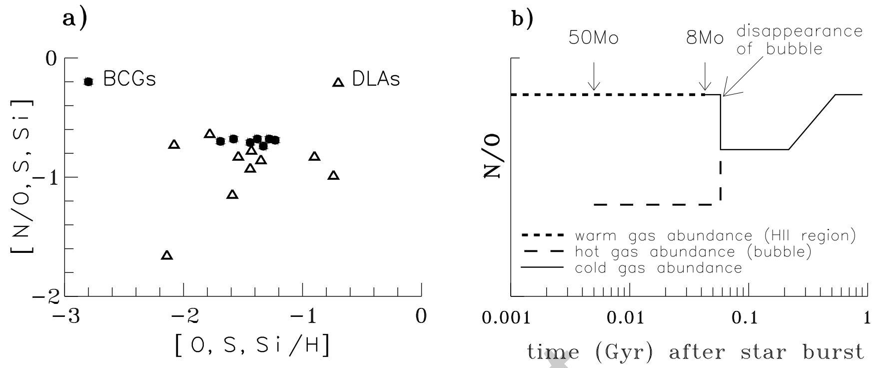

Fig. 2. a) The observed N/O – O/H diagram for low-metallicity blue compact galaxies (data are taken from [6]) and damped Lyα absorbers (data are taken from [12]). **b)** The schematic sketch of the time variation of N/O ratio in different phases (hot, warm, and cold) of the interstellar medium in the case when products of massive stars are in high stages of ionization and do not mix immediately into HII region.

The assumption that previous star formation events are responsible for the observed heavy element abundances in BCGs is equivalent to saying that the element abundances of HII regions in BCGs are not yet polluted by the stars of the present star formation event, and that their abundances reflect the average N/O in the galaxy, which results from cumulative previous star formation. Kunth & Sargent [10] suggest that the heavy elements produced by massive stars in the current star formation burst mix immediately into HII regions, i.e. the giant HII regions are self-enriched. However, it is possible that the nucleosynthetic products of massive stars are in high stages of ionization and do not make appreciable contribution to the element abundance as derived from optical spectra [8], [7]. Indeed, the oxygen abundance in SBS 0335-052 has been measured within the region of 3.6 kpc [5]. There is a supershell of radius $\sim$ 380 pc. There is no difference in oxygen abundances inside and outside the supershell as it should be expected since $\sim$ 1500 supernovae are required to produce this supershell [5]. Other star-forming galaxies, which are chemically homogeneous despite the presence of multiple massive star clusters, are reported by [9]. This can be considered as evidence that the nucleosynthetic products of massive stars in giant HII regions are hidden from optical spectroscopic searches because they are predominantly found in a hot, highly – ionized superbubble. It should be noted however that some fraction of supernova ejecta can mix with dense clouds changing their chemical composition. If such cloud survives and produces a subgroup of stars shortly, the star formation region will have sub-generations of stars with different chemical composition. This seems to be the case in the Orion star formation region [2], [20].

If the suggestion that the heavy elements ejected by massive stars are in hot superbubble for some time and do not mix immediately into the giant HII region is correct, the time variation of the N/O ratio in the warm gas phase after star formation event is different from that presented in Fig. 1a. Hot and warm gas phases have different chemical compositions. The chemical composition of warm gas remains unaltered and is equal to the average chemical composition in the galaxy. A temporary decrease of the N/O ratio takes place in cold gas phase after disappearence of bubble. Fig. 2b illustrates the time behaviour of N/O in different phases (hot, warm, and cold) of the interstellar medium.

With this behaviour of the N/O ratio, the nitrogen abundances measured in BCGs and DLAs can be interpreted in the following way. The low-metallicity BCGs are systems with a small amount of old underlying stellar population over which the current star formation burst is superposed; only the stars from the previous star formation event(s) are responsible for the observed chemical composition in the giant HII regions in these galaxies. In other words, the abundances mesured in giant HII regions in BCGs reflect the average N/O in the galaxy, which results from cumulative previous star formation. The DLA observations sample the general ISM at random times along random lines of sight and may or may not see a region where a star formation event occured in a recent past. The DLAs with low nitrogen to α-element ratios correspond to systems probed less than around 1 Gyr after the last local star formation event, but after a time sufficient for disappearance of the superbubble and mixing of the freshly produced heavy elements in the interstellar medium. Conversely, the DLAs with nitrogen to α-element ratios close to that in low-metallicity BCGs correspond to systems in which the time interval after last star formation event is sufficiently large for intermediate-mass stars to have substantially enhanced the nitrogen to α-element abundance ratios.

The more detailed discussion can be found in [19]

3 Conclusions

If a significant part of nitrogen is produced by intermediate-mass stars, it is possible to reconcile the observational data for BCGs and DLAs.

If nitrogen is mainly produced by massive stars, the observational data for BCGs and DLAs are incompatible with each other. Since the low nitrogen to α-element abundance ratios obtained in some DLAs are not beyond question [6], the possibility that nitrogen measured in low-metallicity BCGs is produced by massive stars cannot however be completely excluded.

The best way to find the lower limit of N/O ratio and hence the amount of nitrogen produced by massive stars would be to determine the N/O ratios in galactic halo stars. Unfortunately, at the present state their N/O ratios cannot be determined with a precision better than a factor 2 or 3. The only firm conclusion is that nitrogen has a strong primary component [1].

Acknowledgements. I would like to thank Drs. N.G. Guseva and Y.I. Izotov for fruitful discussions. I thank the Organizing Committee of the MPA/ESO workshop for the financial support of my participation in the meeting. This research was supported in part by INTAS grant No 97-0033.

References

1. Carbon D.F., Barbuy B., Kraft R.P., Friel E.D., Suntzeff N.B. (1987) PASP **99**, 335
2. Cunha K., Lambert D.L. (1994) ApJ **426**, 170
3. Edmunds M.G., Pagel B.E.J. (1978) MNRAS **185**, 77p
4. Garnett D.R. (1990) ApJ **363**, 142
5. Izotov Y.I., Lipovetsky V.A., Chaffee F.H., Foltz C.B., Guseva N.G., Kniazev A.Y. (1997) ApJ **476**, 698
6. Izotov Y.I., Thuan T.X. (1999) ApJ, **511**, 639
7. Kobulnicky H.A. (1999) astro-ph 9901260
8. Kobulnicky H.A., Skillman E.D. (1997) ApJ **489**, 636
9. Kobulnicky H.A., Skillman E.D. (1998) ApJ **497**, 601
10. Kunth D., Sargent W.L.W. (1986) ApJ **300**, 496
11. Lequeux J., Peimbert M., Rayo J.F., Serrano A., Torres-Peimbert S. (1979) A&A **80**, 1979
12. Lu L., Sargent W.L.W., Barlow T.A. (1998) ApJ **115**, 55
13. Marconi G., Matteucci F., Tosi M. (1994) MNRAS **270**, 35
14. Marigo P., Bressan A., Chiosi C. (1996) A&A **313**, 545
15. Marigo P., Bressan A., Chiosi C. (1998) A&A **331**, 564
16. Matteucci F., Tosi M. (1985) MNRAS **217**, 391
17. Pilyugin L.S. (1992) A&A **260**, 58
18. Pilyugin L.S. (1993) A&A **277**, 42
19. Pilyugin L.S. (1999) A&A **287**, 387
20. Pilyugin L.S., Edmunds M.G. (1996) A&A **313**, 792
21. Renzini A., Voli M. (1981) A&A **94**, 175
22. Thuan T.X., Izotov Y.I., Lipovetsky V.A. (1995) ApJ **445**, 108
23. van den Hoek L.B., Groenewegen M.A.T. (1997) A&AS **123**, 305
24. Vila-Costas M.B., Edmunds M.G. (1993) MNRAS **265**, 199

On the Evolutionary Status of I Zw 18

Yuri Izotov[1], Polichronis Papaderos[2], Trinh Thuan[3], Klaus Fricke[2], Craig Foltz[4], and Natalia Guseva[1]

[1] Main Astronomical Observatory of National Academy of Sciences of Ukraine, Goloseevo, 252650 Kiev-22, Ukraine
[2] Universitäts–Sternwarte, Geismarlandstrasse 11, D–37083 Göttingen, Germany
[3] Astronomy Department, University of Virginia, Charlottesville, VA 22903, USA
[4] Multiple Mirror Telescope Observatory, University of Arizona, Tucson, AZ 85721, USA

Abstract. We analyze existing HST and ground-based observations in order to put constraints on the distance to the most metal-deficient blue compact dwarf (BCD) galaxy known, I Zw 18. We find that the distance to I Zw 18 should be as high as 20 Mpc, twice the previously accepted distance, to explain simultaneously the properties of the massive stellar population inferred from colour-magnitude diagrams, the high ionization state of the gas and presence of WR stars in the main body, and the ionization state of the C component. An age of stellar populations in I Zw 18 with new adopted distance is ≤ 100 Myr.

1 The Distance to I Zw 18

A distance of 10 Mpc to I Zw 18 has generally been adopted (e.g. [1]) for the analysis of HST colour-magnitude diagram. At this distance the brightest stars observed in the main body and in the C component have absolute V magnitudes fainter than –8 and –6 mag respectively [1,2]. If that is the case, comparison with evolutionary tracks implies that the most massive stars in the main body and C component would have masses less than 15 $M_\odot$ and 9 $M_\odot$ respectively. This conclusion is in contradiction with the observed ionization state of I Zw 18. Indeed, the equivalent width of the Hβ emission line expected from a stellar population having an upper mass limit of 15 $M_\odot$ is $<$ 10 Å, while the observed Hβ equivalent widths in the NW and SE components lie in the range 60 – 130 Å, implying the presence of stars with masses $\geq$ 40 – 50 $M_\odot$. If the upper stellar mass limit of 9 $M_\odot$ for the C component is correct, then ionized gas should not be present in this component because of the lack of O and early B stars. But Hα and Hβ are clearly observed (e.g. [3,4]) in the C component. Thus, late O and early B stars with masses as high as 15 $M_\odot$ must be postulated in the C component.

The real distance to I Zw 18 appears to be considerably larger. We base our estimate of the distance to I Zw 18 on two firm observational results: 1) the presence of ionized gas in the C component and 2) the presence of WR stars in the NW component. Concerning the ionized gas in the C component, the distance should be increased to a value of $\sim$ 20 Mpc. Increasing the distance by a factor of 2 would make the most massive stars more luminous by a factor of 4 and push the mass upper limit to $\sim 15\ M_{\odot}$. These more massive stars would then provide enough ionizing photons to account for the observed emission lines in the C component. Concerning the WR stars, they have been seen both spectroscopically and photometrically in the NW component of I Zw 18, in the region where the brightest post-main-sequence stars are located. The existence of WR stars implies the presence of very massive stars in the NW component. It was found in [5] using Geneva stellar evolutionary tracks for massive stars with enhanced stellar wind and with heavy element mass fraction $Z = 0.0004$ that the minimum initial mass M_{min} for stars evolving to WR stars to be $\sim 90\ M_{\odot}$ and that the WR stage is very short-live, being only ~ 0.8 Myr, if the instantaneous burst model is adopted. These models do not take rotation into account, which may decrease M_{min}, but probably by not more than a factor of 1.5. Thus the observation of WR stars in the NW component implies the presence of post-main-sequence massive stars with $M \geq 40 - 60\ M_{\odot}$ and with lifetimes $\leq 3 - 5$ Myr. To accomodate this small time scale, we are forced again to increase the distance of I Zw 18 to ~ 20 Mpc. Increasing the distance would increase the luminosity of all stars and the location of the brightest stars in the CMD of the main body can be accounted for by isochrones with age as short as ~ 5 Myr.

2 On the Age of the Resolved Stellar Population in I Zw 18

An appreciable number of faint red sources with $V = 26 - 27$ mag and $(V - I) = 1 - 2$ mag was found in [1]. With our new distance of 20 Mpc, these sources have absolute I magnitude of –6.5 mag, or 2 mag brighter than the absolute I magnitude of older and fainter AGB stars. Because of their high luminosities, these red stars cannot be interpreted as old AGB stars as proposed in [1]. Rather, it is more likely that they are young stars with an age of ~ 100 Myr.

References

1. Aloisi A., Tosi M., Greggio L. (1999) AJ **118**, 302–322
2. Hunter D. A., Thronson H. A., Jr. (1995) ApJ **452**, 238–252
3. Izotov Y. I., Thuan T. X. (1998) ApJ **497**, 227–237
4. van Zee L., Westpfahl D., Haynes M. P., Salzer J. J. (1998) AJ **115**, 1000–1015
5. de Mello D. F., Schaerer D., Heldmann J., Leitherer C. (1998) ApJ **507**, 199–209

The First Stars: Clues from the Spectra of QSOs and High Redshift Galaxies

Max Pettini

Institute of Astronomy, Madingley Road, Cambridge CB3 0HA, England

Abstract. It has recently become possible to measure directly the abundances of several chemical elements in a variety of environments at redshifts up to $z \simeq 5$. In this review I summarise the latest observations of Lyman break galaxies, damped Lyman alpha systems and the Lyman alpha forest with a view to uncovering any clues which these data may offer to the first episodes of star formation. The picture which is emerging is one where the universe at $z = 3$ already included many of the components of today's galaxies—even at these early times we see evidence for Populations I and II stars, while the 'smoking gun' for Population III objects may be hidden in the chemical composition of the lowest density regions of the IGM, yet to be deciphered.

1 Introduction

The aim of this talk is to consider the information on the first episodes of star formation in the universe provided by studies of element abundances at high redshift. This is very much a growth area at present. Thanks largely to the new opportunities offered by the Keck telescopes and their VLT counterparts in the southern hemisphere, we find ourselves in the exciting position of being able, for the first time, to measure the abundances of a wide range of chemical elements directly in stars, H II regions, cool interstellar gas and hot intergalactic medium, all observed when the universe was only $\sim 1/10$ of its present age. Our simple-minded hope is that, by moving back to a time when the universe was young, clues to the nature, location, and epoch of the first generations of stars may be easier to interpret than in the relics left today, some 11 Gyrs later. As can be seen from Figure 1, our knowledge of element abundances at high redshift is still very sketchy. Given the limitations of space, in this review I shall focus primarily on results obtained in the last year on the different components of the high z universe shown in Figure 1.

2 Lyman Break Galaxies

Undoubtedly, one of the turning points in extragalactic astronomy in the 1990s has been the realisation that high redshift galaxies can be found in large numbers using a highly efficient photometric selection technique based on the passage of the Lyman edge—at the rest wavelength of 912 Å—through

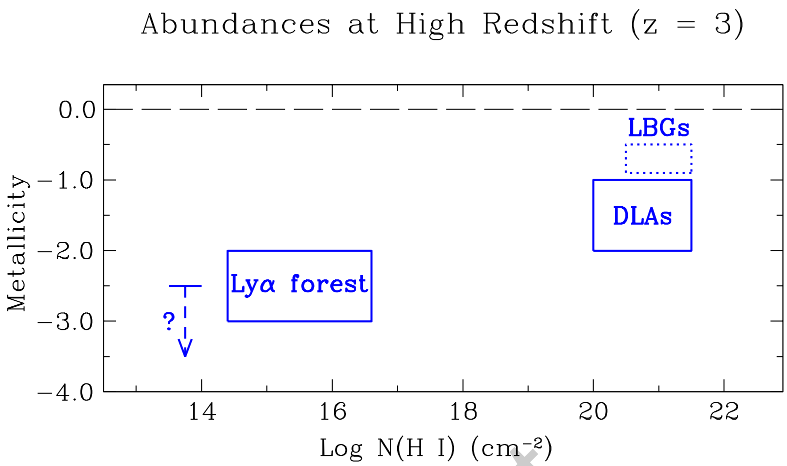

Fig. 1. Summary of our current knowledge of abundances at high redshift. Metallicity is on a log scale relative to solar, and N(H I) is the column density of neutral hydrogen measured in the Lyα forest, damped Lyα systems and Lyman break galaxies.

the U-band. After many years of fruitless searches (targeted mainly to Lyα emission which turned out to be a less reliable marker than anticipated), we have witnessed a veritable explosion of data from the *Hubble Deep Fields* and ground-based surveys. Galaxies with *measured* redshifts in excess of $z \simeq 2.5$ now number in the many hundreds (the 1000 mark is just around the corner); such large samples have made it possible to trace the star formation history of the universe over most of the Hubble time and to measure large-scale properties of the population, most notably their clustering and luminosity functions ([1], [2], [3] and references therein).

However, for a quantitative study of many of the physical properties of Lyman break galaxies, even the light-gathering power of the world's largest telescopes is not enough and we have to rely on gravitational lensing to boost the flux to levels where their spectra can be recorded with sufficiently high resolution and signal-to-noise ratio. This is the case for the $z = 2.73$ galaxy MS 1512-cB58, an L^* Lyman break galaxy fortuitously magnified by a factor of ~ 30 by the foreground cluster MS 1512+36 at $z = 0.37$ [4], [5]. Somewhat ironically, our Keck spectrum of cB58 [6] is one of the best examples of the ultraviolet spectrum of a starburst galaxy *at any redshift*, thanks to the combined effects of gravitational lensing, redshift, and collecting area of the Keck telescopes.

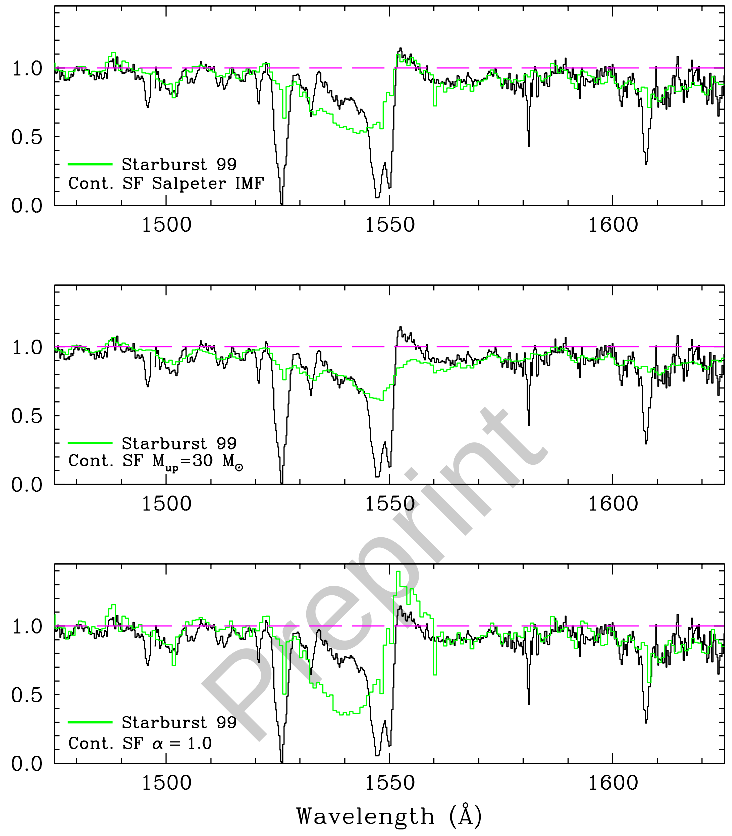

Fig. 2. Comparisons between *Starburst99* [7] population synthesis models with different IMFs (green lines—grey in the black and white version of the figure) and the Keck spectrum of MS 1512-cB58 analysed by Pettini et al. [6] in the region near the C IV doublet (black histogram).

At $z \simeq 3$ optical wavelengths correspond to the rest-frame far-UV, where we see the integrated light of short-lived O and early B stars. Such spectra are most effectively analysed with population synthesis models, the most sophisticated of which is *Starburst99* developed by the Baltimore group [7]. In Figure 2 we compare *Starburst99* model predictions for different IMFs with our data in the region of the C IV $\lambda\lambda 1548, 1550$ doublet. It is important to realise that the comparison only refers to *stellar* spectral features and does not include the *interstellar* lines, readily recognisable by their narrower widths (these IS lines are much stronger in cB58, where we sample the whole ISM of the galaxy, than in the models which are based on libraries of nearby Galactic O and B stars). With this clarification, it is evident from Figure 2 that the spectral properties of at least this Lyman break galaxy are remarkably similar to those of present-day starbursts—a continuous star formation model with a Salpeter IMF provides a remarkably good fit to the observations. In particular, the P-Cygni profiles of C IV, Si IV and N V are sensitive to the slope and upper mass limit of the IMF; the best fit in cB58 is obtained with a standard Salpeter IMF with slope $\alpha = 2.35$ and $M_{\rm up} = 100 M_{\odot}$ (top panel of Figure 2). IMFs either lacking in the most massive stars or, conversely, top-heavy seem to be excluded by the data (middle and bottom panels of Figure 2 respectively).

The only significant difference between the observed and synthesised spectrum is in the optical depth of the P-Cygni absorption trough which is lower than predicted (top panel of Figure 2). This is likely to be an abundance effect, since an analogous weakening of the absorption is seen in OB stars with mass loss in the Magellanic Clouds (e.g. [8]) and is also predicted by stellar wind theory (e.g. [9]). In future, when the libraries of stellar spectra in *Starburst99* are expanded to include Magellanic Cloud stars (a project which is already underway), it may be possible to calibrate the optical depth of C IV absorption with Carbon abundance and use this feature to deduce the metallicity of high redshift star-forming galaxies. For the moment, we conclude on the basis of a qualitative comparison that the metallicity of the young stellar population in cB58 is similar to that in the LMC, where [C/H]$\simeq -0.6$. Weak interstellar lines of Sulphur, Silicon, and Nickel are consistent with this abundance estimate.

2.1 Moving to the Infrared

Very recently, the successful commissioning of NIRSPEC on Keck II and ISAAC on VLT1 have made it possible to extend spectroscopic studies of Lyman break galaxies to the near infrared which, at $z \simeq 3$, includes the familiar optical emission lines from H II regions on which much of our knowledge of local star-forming galaxies is based. As indicated by exploratory observations with UKIRT [10], detecting these lines is a challenging task even with large telescopes, and in general we are restricted to studying the brightest examples of Lyman break galaxies, with $L \gtrsim L^*$. Figure 3 shows an example of such data. Application of the familiar R_{23} method [11] indicates that abundances of about 1/3 solar may be typical; this includes cB58 for which Teplitz et al. [12] deduced [O/H] $\simeq -0.5$, in good agreement with the UV analysis discussed above.

The combination of (rest-frame) optical and UV observations gives insights into several other properties of LBGs, apart from chemical abundances.

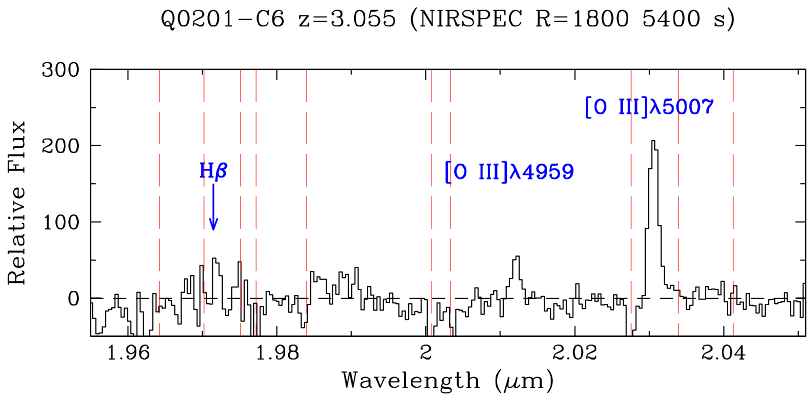

Fig. 3. K-band spectrum of the Lyman break galaxy Q0201-C6. The dashed vertical lines indicate the locations of OH emission lines from the night sky; although the lines have been subtracted out the spectrum remains very noisy at these wavelengths. It is thus essential to select LBGs at redshifts which place the nebular lines of interests in the gaps between OH emission, as is the case here.

The widths of the emission lines are likely to be better indicators of the underlying masses than the interstellar absorption lines which, being sensitive to very low column densities, can be broadened by gas accelerated to high velocities by supernovae and stellar winds associated with the star-formation activity. In the dozen or so objects studied so far, we measure velocity dispersions $\sigma \simeq 60 - 120$ km s^{-1}; $\sigma \simeq 80$ km s^{-1} seems to be typical. As shown in the recent study by Kobulnicky & Gebhardt [13], this is the value which one may expect from a disk galaxy (viewed at a random inclination) rotating at ≈ 150 km s^{-1}. Indeed there are hints in two cases that we may be seeing the rotation curve directly in spatially resolved [O III]λ5007 emission lines. Kinematical masses in excess of a few times 10^{10} $M_\odot$ are indicated.

Finally, the relative velocities of nebular emission lines, interstellar absorption lines, and Lyα can be explained as resulting from large scale outflows with velocities of up to several hundred km s^{-1}. In cB58 Pettini et al. [6] deduced a mass outflow rate $\dot{M} \simeq 60$ $M_\odot$ yr^{-1}, comparable to the rate at which gas is being turned into stars. Such galactic 'superwinds' seem to be a common feature of starburst galaxies at all redshifts, and may well be the mechanism which self-regulates star formation, distributes metals over large volumes and allows the escape of ionizing photons into the intergalactic medium.

In summary, all the information available so far is consistent with the notion that Lyman break galaxies are already well developed systems at $z \simeq 3$, with stellar populations, chemical abundances and kinematics very much in line with those of the more massive star-forming galaxies in the local universe. Of necessity, the best studied examples are at the bright end of the luminosity function; thus, perhaps we should not be surprised to find that their properties are relatively uniform. What is interesting is that galaxies at such an advanced stage of evolution were already in place at the relatively early epochs corresponding to $z = 3 - 4$; it therefore seems most natural to associate these objects with the progenitors of today's elliptical galaxies and bulges of spirals, as proposed by Steidel et al. [14].

3 Damped Lyman-α Systems

These are the absorption systems with the highest column density of neutral hydrogen, $N(\mathrm{H~I}) \geq 2 \times 10^{20}$ cm^{-2}, seen in the spectra of QSOs and they provide us with the best opportunity to measure accurately the abundances of a wide range of elements at high redshift. The reason is simple: QSOs can be several hundred times brighter than Lyman break galaxies at the same redshift. Surveys with HIRES on Keck I have produced data of exquisite quality—a 10% accuracy in the determination of interstellar gas-phase abundances is achievable with only modest efforts [15], [16].

This makes it all the more frustrating that a clear connection between DLAs and galaxies has yet to be established. In principle, selecting galaxies by their H I absorption cross-section should provide a more representative sampling of the field population at a given redshift than conventional magnitude limited surveys, either in the continuum or emission lines. Thus one may conjecture that DLAs pick out galaxies from the whole luminosity function, particularly if H I cross section has only a mild dependence on galaxy luminosity [17], and that Lyman break galaxies may just be the most luminous DLAs at $z \simeq 3$ ([6], [18], [19]). While this interpretation is attractive in its simplicity, we must face up to the fact that it cannot readily account for the most recent observations of DLAs which find no significant evolution of either the gas mass or the metallicity ([20], [21], [22]) over a redshift interval ($z \simeq 0.5 - 4$) during which most of today's stars were apparently formed (see Figure 5 of [23]). Possibly, existing samples of damped Lyα systems are subject to subtle selection effects of their own and may preferentially trace a particular stage in the evolution of galaxies, when the gas has an extended distribution and only moderate surface density, and the metal—and therefore dust—content is low. There is both theoretical [24] and observational [25], [26] evidence in support of this picture.

These latest developments do not detract from our interest in damped Lyα systems. First, as emphasised repeatedly by Fall and collaborators (e.g. [27]), the column density-weighted mean metallicity of DLAs is probably the best

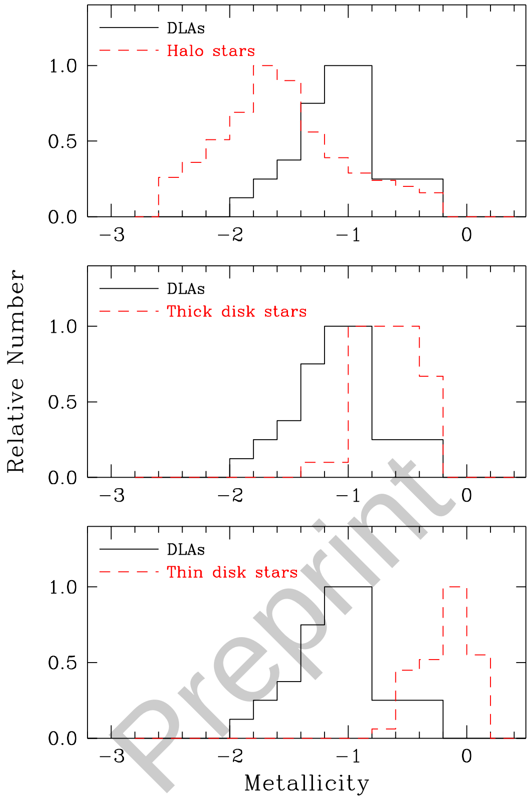

Fig. 4. Metallicity distributions, normalised to unity, of DLAs at $z \simeq 2-3$ and of stars belonging to the disk and halo populations in the Milky Way. See [30] for references to the sources of data and further deatils.

measure we have of the degree of metal enrichment reached by the universe at a given epoch, *irrespectively of the precise nature of the absorbers*. Thus, values of $[\langle Z_{\rm DLA} \rangle]$ at different redshifts (so far most effectively deduced from the abundance of Zn [21]) are essential reference points for models of global chemical evolution ([28], [29]). The only uncertainty which remains to be resolved for a full use of this information is the degree to which existing samples of DLAs are biased against sight-lines sufficiently dusty to obscure the background QSOs; this is a question which we are in the process of exploring by examing the statistics of damped systems in radio selected QSOs. At redshifts $z \simeq 2-3$ the metallicity distribution of known DLAs is intermediate between those of stars in the halo and thick disk of the Milky Way; at this epoch most of the galaxies giving rise to damped systems were clearly less evolved chemically than the stellar population forming the thin disk of our Galaxy (see Figure 4).

Second, DLAs present us with the opportunity to extend local studies of the relative abundances of different elements to unexplored regimes and to earlier epochs. Potentially, DLAs have an important role to play here in complementing the information so far obtained from observations of Galactic stars and nearby H II regions and providing fresh clues both to the origin of different stellar populations and to the stellar yields. For example, Pettini, Lipman, & Hunstead [31] and Lu, Sargent, & Barlow [32] showed that in DLAs it is possible to follow the behaviour of the (N/O) ratio to lower metallicities than those probed up to now (IZw18 still remains the most metal-poor star-forming region known in our vicinity). Their results appear to lend support to the idea of a delayed production of primary nitrogen by intermediate mass stars, although this interpretation has been challenged more recently ([33], [34]—see also [35]) and more observations are clearly required in order to settle the issue.

The latest application of this technique involves Silicon (an α-capture element) and Manganese. In Figure 5 (reproduced from [40]) the abundances of these two elements in damped Lyα systems of different metallicities are compared with analogous data for stars in the disk and halo of our Galaxy. The DLAs considered are those where less than 50% of Si, Mn, and Fe is locked up in dust grains, so that the total (gas+dust) abundances can be recovered with minimum uncertainty. The first-order conclusion is that the DLA values roughly follow the local trends, but there are notable differences too, as we now discuss.

The rise of [Si/Fe] from to solar to between +0.3 and +0.4 as the metallicity drops to [Fe/H]$= -2$ (top panel of Figure 5) is the well-known overabundance of the α-elements commonly attributed to the delayed production of additional Fe by Type Ia supernovae. While some DLAs do show enhanced [Si/Fe], we also find counter-examples of near-solar abundance of Si at metallicities in the range [Fe/H]$\simeq -1$ to -2. Current wisdom would interpret such cases as arising in galaxies where star formation has proceeded slowly, or in bursts, so that there has been sufficient time for Fe to build up to solar abundance relative to Si, while the overall metallicity remained low. Corroborating evidence for this interpretation may be provided by deep imaging of the absorbers, if they are found to be low surface brightness or dwarf galaxies.

Turning to Mn (lower panel of Figure 5), the strong decrease in [Mn/Fe] towards low metallicities is now well documented, but its origin is unclear. Two possibilities have been proposed and both have problems with the DLA data, at least at face value. If the stellar trend is due to a metallicity depen-

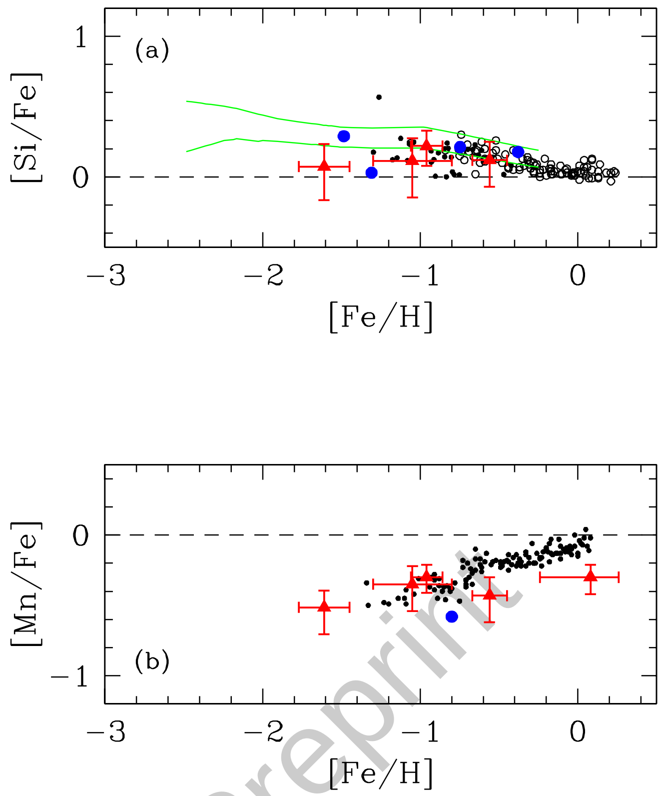

Fig. 5. Metallicity dependence of the abundances of Si and Mn. Small dots are values in Galactic stars from [36] and [37] for Si and [38] for Mn. The continuous thin lines in the top panel show the range (upper and lower quartiles) spanned by the compilation of measurements in halo stars by Ryan, Norris, & Beers [39]. The other symbols refer to damped Lyα systems.

dent yield of Mn in massive stars, it is difficult to explain the one DLA with [Mn/Fe] $\simeq -0.3$ at solar [Fe/H]. On the other hand, enhanced (relative to Fe) production of Mn in Type Ia supernovae cannot explain DLAs with low [Mn/Fe] and near-solar [Si/Fe] of which there are at least two examples.

In concluding this section, it is important to stress the preliminary nature of the above conclusions which are based on the comparison of very few measurements in DLAs with a much larger body of stellar data. One of the lessons from stellar work is that there is considerable scatter, both observational and instrinsic, in the relative abundances of different elements so that most trends only become apparent when a large set of measurements has been assembled. Thus Figure 5 should be taken as no more than an illustration of the issues which can be addressed with surveys of element abundances in damped systems. Although work on element ratios in high redshift galaxies is still a long way behind its counterpart in Galactic stars, future observations with UVES in particular may well play a decisive role in resolving some outstanding questions on the origin of elements.

4 The Lyman-α Forest

The final component of the high redshift universe considered in this review is the all-pervading intergalactic medium which manifests itself as fluctuating absorption bluewards of the Lyα emission line of every QSO. Observationally, the term Lyα forest is used to indicate the bulk of discrete Lyα absorption lines with column densities in the range $10^{16} \gtrsim N(\mathrm{HI}) \gtrsim 10^{12}$ cm^{-2}; since this gas is highly ionised, it may account for most of the baryons at $z \simeq 3$ [41]. Hydrodynamical simulations have shown that the Lyα forest is a natural consequence of structure formation in a universe dominated by cold dark matter and bathed in a diffuse ionising background (e.g. [42]). In this picture, the physics of the absorbing gas is relatively simple and the run of optical depth $\tau(\mathrm{Ly}\alpha)$ with redshift can be thought of as a 'map' of the density structure of the IGM along a given line of sight. At low densities, where the temperature of the gas is determined by the balance between photionisation heating and adiabatic cooling, $\tau(\mathrm{Ly}\alpha) \propto (1+\delta)^{1.5}$, where the δ is the overdensity of baryons $\delta \equiv (\rho_\mathrm{b}/\langle\rho_\mathrm{b}\rangle - 1)$. At $z = 3$ $\tau(\mathrm{Ly}\alpha) = 1$ corresponds to a region of the IGM which is just above the average density of the universe at that time ($\delta \approx 0.6$).

The lack of associated metal lines was originally one of the defining characteristic of the Lyα forest and was interpreted as evidence for a primordial origin of the clouds [43]. As it is often the case, subsequent improvements in the observations have shown this to be an oversimplification and in reality weak metal absorption, principally by C IV, is present at the redshift of most Lyα clouds down to the detection limit of the data [44]. The degree of metal enrichment implied is relatively high, ([C/H]$\simeq -2.5$ with a scatter of perhaps a factor of ~ 3 [45]), in the sense that stars with significantly lower metallicities are known to exist in the halo of our Galaxy.

It is not easy to understand how the low density IGM came to be polluted so uniformly by the products of stellar nucleosynthesis at such an early epoch. While, as explained above, we see directly the outflow of metal-enriched gas in 'superwinds' from Lyman break galaxies at the same redshift, most of this gas is not expected to travel far from the production sites, because it is either trapped by the gravitational potential of the galaxies, if they are sufficiently massive, or is confined by the pressure of the hot IGM [46]. Whether an early episode of pre-galactic star formation is required depends on whether C IV lines continue to be seen in Lyα clouds of diminishing H I column density. Current limits are for $N(\text{H I}) \gtrsim 3 \times 10^{14}$ cm^{-2} (some 75% of such Lyα clouds have associated C IV absorption [44]) corresponding to moderately overdense gas ($\delta \gtrsim 10$) which in the simulations is preferentially found in the vicinity of collapsing structures and may thus reflect local, rather than universal, metal pollution.

The detection of C IV lines when $N(\text{H I}) \lesssim 1 \times 10^{14}$ is a challenging task, even with a 10-m telescope, because we are dealing with observed equivalent widths $W_\lambda(1550) \lesssim 2.5$ mÅ. A possible approach in these circumstances is to try and recover such a weak signal from a statistical treatment of many lines which individually are below the detection limit. Unfortunately, different analyses have reached conflicting conclusions [47], [48]. Furthermore, a recent reappraisal of the techniques with the help of extensive simulations of the spectra has indicated that many subtle effects, such as small random differences between the redshifts of Lyα and C IV absorption, make the interpretation of the results far from straightforward [49].

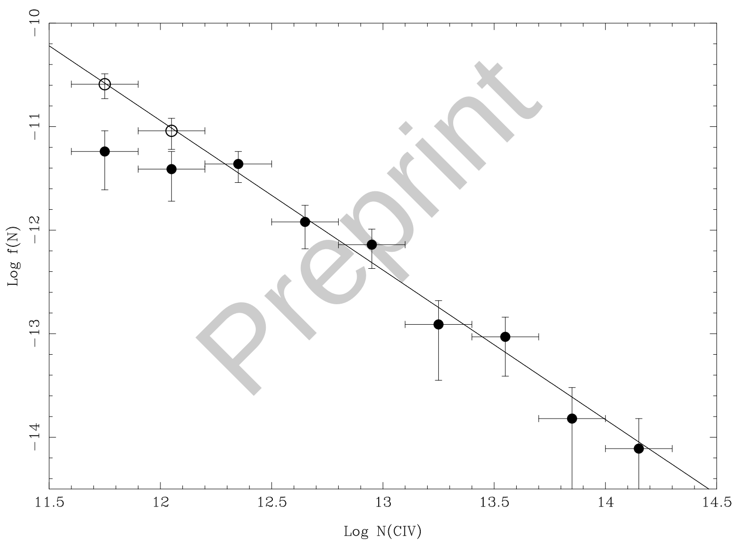

Fig. 6. C IV column density distribution in Q1422+231 at $\langle z \rangle \simeq 3.15$ (reproduced from [50]); $f(N)$ is the number of C IV systems per column density interval and per unit redshift path. The filled circles are the data grouped into bins of 0.3 in log N(C IV) for display purposes. The line shows the best fitting power-law slope $\alpha = 1.44$, assuming the distribution to be of the form $f(N)dN = BN^{-\alpha}dN$. The open circles show the values corrected for incompleteness at the low column density end; the correction factors were estimated with the aid of simulations which showed that only $\sim 43\%$ and $\sim 23\%$ of C IV lines with log $N(\text{C IV}) = 12.05$ and 11.75 respectively are typically recovered from the data. Once these correction factors are introduced, there is no indication of a turnover in the column density distribution down to the lowest values of N(C IV) reached up to now.

A more direct way to tackle the problem is to push the detection limit further by securing spectra of exceptionally high signal-to-noise ratio; as for Lyman break galaxies this is most effectively achieved with the aid of gravitational lensing. In this way Ellison et al. [50] were able to reach S/N= $200-300$ in the C IV region between $z = 2.91$ and 3.54 of the gravitationally lensed QSO Q1422+231 after adding together data recorded over several nights with HIRES on Keck I.

As can be seen from Figure 6, the number of weak C IV lines continues to rise as the signal-to-noise ratio of the spectra increases and any levelling off in the column density distribution presumably occurs at $N(\text{C IV}) < 5 \times 10^{11}$ cm^{-2}. This limit is one order of magnitude more sensitive than those reached previously. In other words, we have yet to find any evidence in the Lyα forest for regions of the IGM which are truly of primordial composition or have abundances as low as those of the most metal-poor stars in the Milky Way halo. Pushing the sensitivity of this search even further is certainly one of the goals for UVES on VLT2.

5 Conclusions

This review has covered a lot of ground reflecting the fast pace of progress in the study of element abundances at high redshift, now set to accelerate further with the forthcoming availability of new, efficient spectrographs on Keck, VLT, Subaru and Gemini. The picture which is emerging is that of a universe at $z = 3$ with many of today's characterstics already in place. At this epoch, Lyman break galaxies resembled closely today's star-forming galaxies dominated by Population I stars, damped Lyα systems exhibited mostly Population II chemical abundances, and the low density Lyα forest may well have been the repository of the first heavy elements synthesised by Population III stars. This does not necessarily imply a one-to-one correspondence between these objects then and now, given the substantial time interval available for evolution. It is likely that Lyman break galaxies, which at $z = 3$ trace the highest peaks in the underlying mass distribution, have through subsequent mergers evolved into today's massive ellipticals and bulges to be found preferentially in rich clusters. It is also plausible that the gas giving rise to at least some high redshift damped Lyα systems has turned into the stars of today's spiral galaxies. And the heavy elements ejected into the IGM by the first stars which formed in low mass collapsed structures have by now presumably been augmented by the much more substantial metal-enriched outflows from successive generations of stars in more massive galaxies. Thus the lack of a clear age-metallicity relationship in our own Galaxy is reflected on a much larger scale by the universe as a whole—old does not necessarily mean metal-poor, as emphasised by Richard Larson in his concluding remarks at this conference. While it is important to continue to search for the chemical signatures of the first stars in the low density IGM, we shall probably have to wait for *NGST* to see these objects directly as supernovae at $z > 10$.

I should like to acknowledge my collaborators in the various projects described in this talk, particularly Chuck Steidel, Sara Ellison, Kurt Adelberger, David Bowen, Len Cowie, Jean-Gabriel Cuby, Mark Dickinson, Mauro Giavalisco, Alan Moorwood, Joop Schaye, Alice Shapley and Toni Songaila. I am very grateful to the organisers of this timely and stimulating meeting for inviting me, and to the European TMR network on 'The Formation and Evolution of Galaxies' for financial support.

References

1. Madau, P., Ferguson, H.C., Dickinson, M.E., Giavalisco, M., Steidel, C.C., & Fruchter, A. 1996, MNRAS, 283, 1388
2. Steidel, C.C., Adelberger, K.L., Dickinson, M., Giavalisco, M., Pettini, M., & Kellogg, M. 1998, ApJ, 492, 428
3. Steidel, C.C., Adelberger, K.L., Giavalisco, M., Dickinson, M., & Pettini, M. 1999, ApJ, 519, 1
4. Yee, H.K.C., Ellingson, E., Bechtold, J., Carlberg, R.G., & Cuillandre, J.-C. 1996, AJ, 111, 1783
5. Seitz, S., Saglia, R.P., Bender, R., Hopp, U., Belloni, P., & Ziegler, B. 1998, MNRAS, 298, 945
6. Pettini, M., Steidel, C.C., Adelberger, K.L., Dickinson, M., & Giavalisco, M. 2000, ApJ, in press (astro-ph/9908007)
7. Leitherer, C., et al. 1999, ApJS, 123, 3
8. Lennon, D.J. 1999, Rev. Mex. Astr. Ap., in press
9. Kudritzki, R.P. 1998, in Stellar Astrophysics for the Local Group, ed. A. Aparicio, A. Herrero, & F. Sánchez (Cambridge: CUP), 149
10. Pettini, M., Kellogg, M., Steidel, C.C., Dickinson, M., Adelberger, K.L., & Giavalisco, M. 1998, ApJ, 508, 539
11. Pagel, B.E.J., Edmunds, M.G., Blackwell, D.E., Chun, M.S., & Smith, G. 1979, MNRAS, 189, 95
12. Teplitz, H.I. et al. 2000, ApJ, in press
13. Kobulnicky, H.A., & Gebhardt, K. 2000, AJ, in press (astro-ph/9911361)
14. Steidel, C.C., Giavalisco, M., Pettini, M., Dickinson, M. & Adelberger, K.L. 1996, ApJ, 462, L17
15. Lu, L., Sargent, W.L.W., Barlow, T.A., Churchill, C.W., & Vogt, S.S. 1996, ApJS, 107, 475
16. Prochaska, J.X., & Wolfe, A.M. 1999, ApJS, 121, 369
17. Steidel, C.C., Dickinson, M., & Persson, S.E. 1994, ApJ, 437, L75
18. Steidel, C.C., Pettini, M., & Hamilton, D. 1995 D. AJ, 110, 2519
19. Djorgovski, S.G., Pahre, M.A., Bechtold, J., & Elston, R. 1996, Nature, 382, 234
20. Rao, S.M., & Turnshek, D.A. 2000, ApJ, submitted (astro-ph/9909164)
21. Pettini, M., Ellison, S.L., Steidel, C.C., & Bowen, D.V. 1999, ApJ, 510, 576
22. Prochaska, J.X., & Wolfe, A.M. 2000, ApJ, submitted
23. Pettini, M. 1999, in Chemical Evolution from Zero to High Redshift, ed. J. Walsh & M. Rosa (Berlin: Springer), 233

24. Mo, H.J., Mao, S., & White, S.D.M. 1999, MNRAS, 304, 175
25. Le Brun, V., Bergeron, J., Boissé, P., & Deharveng, J.M. 1997, A&A, 321, 733
26. Rao, S.M., & Turnshek, D.A. 1998, ApJ, 500, L115
27. Fall, S.M. 1996, in The Hubble Space Telescope and the High Redshift Universe, ed. N. Tanvir, A. Aragon-Salamanca, & J.V. Wall (Singapore: World Scientific), 303
28. Prantzos, N., & Silk, J. 1998, ApJ, 507, 229
29. Pei, Y.C., Fall, S.M., & Hauser, M.G. 1999, ApJ, 522, 604
30. Pettini, M., Smith, L.J., King, D.L., & Hunstead, R.W. 1997, ApJ, 486, 665
31. Pettini, M., Lipman, K., & Hunstead, R.W. 1995, ApJ, 451, 100
32. Lu, L., Sargent, W.L.W., & Barlow, T.A. 1998, AJ, 115, 55
33. Centurión, M., Bonifacio, P., Molaro, P., & Vladilo, G. 1998, ApJ, 509, 620
34. Izotov, Y.I., & Thuan, T.X. 1999, ApJ, 511, 639
35. Pilyugin, L.S. 1999, A&A, 346, 428
36. Edvardsson, B., Andersen, J., Gustaffson, B., Lambert, D.L., Nissen, P.E., & Tomkin, J. 1993, A&A, 275, 101
37. Nissen, P.E., & Schuster, W.J. 1997, A&A, 326, 751
38. Nissen, P.E., Chen, Y.Q., Schuster, W.J., & Zhao, G. 2000, A&A, submitted
39. Ryan, S.G., Norris, J.E., & Beers, T.C. 1996, ApJ, 471, 254
40. Pettini, M., Ellison, S.L., Steidel, C.C., Shapley, A.E., & Bowen, D.V. 2000, ApJ, in press (astro-ph/9910131)
41. Rauch, M. 1998, ARA&A, 36, 267
42. Weinberg, D.H., Katz, N., & Hernquist, L. 1998, in ASP Conf. Series 128, Origins, ed. C.E. Woodward, J.M. Shull, & H.A. Thronson (San Francisco: ASP), 21
43. Sargent, W.L.W., Young, P.J., Boksenberg, A., & Tytler, D. 1980, ApJS, 42, 41
44. Songaila, A., & Cowie, L.L. 1996, AJ, 112, 335
45. Davé. R., Hellsten, U., Hernquist, L., Katz, N., & Weinberg, D. 1998, ApJ, 509, 661
46. Ferrara, A., Pettini, M., & Shchekinov. Y. 2000, MNRAS, submitted
47. Lu, L., Sargent, W.L.W., Barlow, T.A., & Rauch, M. 1998, ApJ, submitted (astro-ph/9802189)
48. Cowie, L.L., & Songaila, A. 1998, Nature, 394, 44
49. Ellison, S.L., Lewis, G.F., Pettini, M., Chaffee, F.H., & Irwin, M.J. 1999, ApJ, 520, 456
50. Ellison, S.L., Songaila, A., Schaye, J., Cowie, L.L., & Pettini, M. 2000, ApJ, submitted

Evidence for Large Scale Structure in the Lyα Forest at $z > 2.6$

Gerard M. Williger[1], Alain Smette[1], Cyril Hazard[2,3], Jack A. Baldwin[4], and Richard G. McMahon[2]

[1] Code 681, NASA/GSFC, Greenbelt MD, USA
[2] IOA, U. Cambridge, England
[3] Dept. of Astronomy, U. Pittsburgh, PA, USA
[4] CTIO, La Serena, Chile

Abstract. We present a search for spatial and redshift correlations in a 2 Å resolution spectroscopic survey of the Lyα forest at $2.15 < z < 3.37$ toward ten QSOs within a 1° diameter field. We find a 3.2σ signal for correlations of the Lyα absorption line wavelengths between different lines of sight over $2.60 < z < 3.26$. We conclude that a significant fraction of the Ly-α forest arises in structures whose correlation length extends at least over 30 arcmin ($\sim 26\ h^{-1}$ comoving Mpc at $z = 2.6$ for $H_0 \equiv 100h$ km s^{-1} Mpc^{-1}, $\Omega = 1.0$, $\Lambda = 0$).

In this paper, the Lyα forest toward ten $2.36 < z < 3.44$ QSOs within a 1° diameter field near the SGP is used as a probe for the existence of $\sim 30h^{-1}$ comoving Mpc scale structures transverse to the lines of sight.

The data consist of the 10 highest signal to noise ratio spectra covering the Ly-α forest that were obtained during a parallel study [1] on the large scale structure revealed by C IV absorbers, in front of 25 QSOs at $z > 2$ within a $\simeq 1°$ diameter field; details of the observations and reductions are presented in the same work. The instrumental resolution was ~ 2 Å, which allows us to resolve lines with a velocity difference of $\Delta v > 140$ km s^{-1} at $z = 3$. The signal to noise ratio per 1 Å pixel reaches up to 40 between the Lyα and Ly β emission lines. We stress the homogeneity of the instrumental set-up, of the reduction process and of the line list preparation procedures. The angular separation between any two lines of sight ranges from 6.1 to 69.2 arcmin ($5.2h^{-1}$ to $52.7h^{-1}$ comoving Mpc). Between two and seven lines of sight probe any given redshift over $2.155 < z < 3.258$.

We calculated the two point correlation function in velocity space for Lyα absorbers along *different* lines of sight, to search for extended structures in the plane of the sky. To create control samples, we simulated the data directly from the Lyα absorber distribution functions in HI column density and Doppler parameter as recently determined using Keck–HIRES spectra [2]. Our simulated spectra have the same resolution and signal to noise ratio as the observed data; between 100 and 1000 spectra were used to form control samples. We used the same software to search automatically for absorption lines in the simulated spectra as we did for the observed data [1].

Limiting the line redshifts to the range $2.60 < z < 3.26$ reveals an overdensity of line pairs at the 3.2σ significance level (Figure 1). The probability of finding such an excess in *any* bin is $P = 0.0012$. The origin of the correlation is mysterious if the result is taken at face value, that is, if the excess of pairs really occurs at $50 < \Delta v/\mathrm{km\,s^{-1}} < 100$, and does not actually peak at $0 < \Delta v/\mathrm{km\,s^{-1}} < 50$. We find that the blending of several Lyα lines due to the low spectral resolution can account for the observed Δv of the correlation peak if the signal to noise ratio is not very good. This was done by modifying the generation of the simulated spectra, by adding a common set of lines to each line of sight, whose redshift is modified by a Gaussian distributed velocity dispersion δv. These simulations show that it is unlikely that the signal that we detect is a statistical fluke; on the contrary, it probably indicates that a significant number of lines are common between the different lines-of-sight with probable $\delta v > 100$ km s^{-1}. The comparison between Lyα absorbers on such wide angular scales provides a unique tool to probe the evolution of large scale structure at high redshift. A writeup of this work is elsewhere [3].

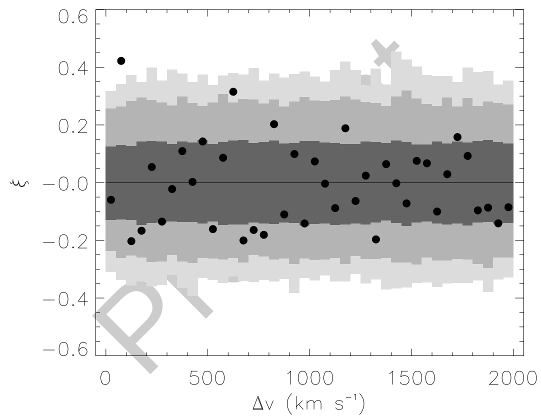

Fig. 1. The two point correlation function $\xi(\Delta v)$ for the observed lines, with rest equivalent width threshold $W_0 \geq 0.1$ Å and covering $2.60 < z < 3.26$, with a 3.2σ feature at $50 < \Delta v/\mathrm{km\,s^{-1}} < 100$. Only pairs between *different* lines of sight are counted. The dark, medium, light shadings signify the 68%, 95%, 99% confidence limits determined by 1000 Monte Carlo simulations as described in the text

References

1. Williger, G.M., Hazard, C., Baldwin, J.A., McMahon, R.G. 1996, ApJS, 104, 145
2. Kim, T.-S., Hu, E. M., Cowie, L. L., & Songaila, A., 1997, AJ, 114, 1
3. Williger, G.M., Smette, A., Hazard, C., Baldwin, J.A., McMahon, R.G. 1999, ApJ, in press, astro-ph/9910369

Galactic Chemical Evolution and Damped Lyman α Absorbers

Helmut Meusinger and Rajko Thon

Thüringer Landessternwarte Tautenburg, D-07778 Tautenburg, Germany

Abstract. We discuss inferences of a special type of Galactic chemical evolution models for damped Lyman α absorber systems (DLAS) at intermediate and high redshift. The agreement between model predictions and the observed properties of DLAS strongly depends on the existence of a dust extinction bias in the DLAS sample. The redshift evolution of the mean Zn abundance in DLAS is reasonably fitted by the models, especially if there is a bias due to dust extinction. However, the predicted abundance scatter is too small at intermediate redshifts. Moreover, the models predict a factor of about two more disks at $z = 0$ than are observed in normal spiral galaxies.

1 Galactic Evolution Models

We have studied chemical evolution models for the Galactic disk which are based on the following essential ideas: A primordial disk is formed 12 Gyr ago during the self-similar contraction of baryonic matter in an isothermal sphere of a mixture of baryonic matter and cold dark matter [5]. The models include secular infall of external gas of primordial composition with parameters determined from chemical evolution constraints from the local disk. The gas within the disk is redistributed by radial gas flows due to viscosity and due to infall. Star formation and viscosity are linked to the same processes, expressed by a correspondence between the timescales, $t_\nu \approx t_*$ [1]. We have tested a wide range of descriptions both for the viscosity and the star formation rate. The chemical evolution description takes into account the contribution from type Ia supernovae. Element production rates from supernovae are taken from [4,3]. The models provide a reasonable fit to a large set of observed global properties of the Galactic disk and of spiral disks in general [6]. Due to the characteristic evolution of the radial profiles (e.g. the viscous spreeding of the gaseous disk) the viscously evolving disks are interesting objects with regard to their properties as absorbers at high redshift.

2 Comparison of Model Disks with DLAS

DLAS have been considered the best candidates for high-redshift progenitors of the disks in normal present-day spiral galaxies. If this is true, DLAS provide an important diagnostic tool for the investigation of early evolution of galaxies.

We have analysed predictions from the viscous Galactic evolution models for the evolution with redshift of the HI gas column density and the Zn abundance in QSO absorber systems [2]. The redshift-Zn abundance relation of DLAS is remarkably flat, which seems to be in disagreement with the age-metallicity relation from stars in the local Galactic disk. We performed Monte Carlo simulations to allow for random orientations and random distances of the disks from the line of sight. The observed shape of the frequency distribution of HI column densities is roughly reproduced only by few model parameter combinations. The fit is substantially improved, however, for all models after a mass spectrum of absorber galaxies is accounted for corresponding to the luminosity function of spiral galaxies.

Though some observed properties of the DLAS sample are roughly reproduced by the models, there remain serious discrepancies. Furhermore, the model predictions strongly depend on the role of dust at high z. Notably, the simulations provide an acceptable fit to the observed mean metallicity-redshift relation if an extinction bias is taken into account. However, the predicted abundance scatter is much too small and a deficiency of high column density systems is expected for $z \leq 1.5$. In any case, the models predict too a high number density of absorber galaxies at $z = 0$ if the gas column density distribution of DLAS at high z is matched.

3 Conclusions

A better agreement between model predictions and observations is expected if DLAS are assumed to be associated with various galaxy types, including in particular low surface brightness galaxies. The observed H I column density distribution at low z is obviously explained by the contribution of galaxies having high gas densities but low metallicities.

References

1. Lin, D. N. C., Pringle, J. E. 1987, ApJ **320**, L 87–L 91
2. Meusinger, H., Thon, R. 1999, Astron Astrophys., in press.
3. Nomoto, K., Hashimoto, M., Tsujimoto, T., Thielemann, F.-K., Kishimoto, N., *et al.* 1997a, Nuclear Physics A **616**, 79–90
4. Nomoto, K., Iwamoto, K., Nakasato, N., Thielemann, F.-K., Brachwitz, F. *et al.* 1997b, Nuclear Physics A **621**, 467–476
5. Olivier, S. S., Primack, J. R., Blumenthal, G. R. 1991, MNRAS **252**, 102–115
6. Thon, R., Meusinger, H. 1998, Astron. Astrophys. **338**, 413–434

The HeII Gunn–Peterson Effect

Sara R. Heap[1], Ivan Hubeny[1,2], Alain Smette[1,2], and Gerard Williger[1,2]

[1] NASA's Goddard Space Flight Center, Greenbelt MD 20771, USA
[2] NOAO, Tucson AZ

Abstract. The UV background at a given redshift is representative of the starlight and QSO-light generated in earlier redshifts. It holds key information on the populations of stars and QSO's at high redshift. We have used observations of the He II Gunn-Peterson (G-P) effect along the line of sight to Q 0302–003 at $z = 3.286$ to constrain the spectral energy distribution of the UV background spectrum over the redshift range, $z = 2.78 - 3.28$. Assuming that stars have softer spectra than do QSO's, we used the softness of the UV background to discriminate between these two possible classes of ionizing sources. We find that stars appear to be significant contributors to the UV background at $z > 3$, but below $z = 3$, there is a hardening of the UV background suggestive of an increased contribution by QSO's.

1 Observations

We used the Space Telescope Imaging Spectrograph (STIS) on-board Hubble to obtain an ultraviolet spectrum (1145–1720 Å) of Q 0302–003 at $z = 3.286$ [2]. The spectrum, shown in both panels of Fig. 1, clearly delineates the Gunn–Peterson He II Lyα absorption trough produced by He^+ ions along the line of sight over the redshift range $z = 2.78 - 3.28$. Measurements of the residual intensity in the G-P trough indicate a generally high He II Lyα opacity at $z > 3.0$. For example, at $z \approx 3.15$, $\bar{\tau} \geq 4.8$. Even at the redshift $z \sim 3.18$ of the Dobrzycki-Bechtold void, $\bar{\tau} = 4.5$.

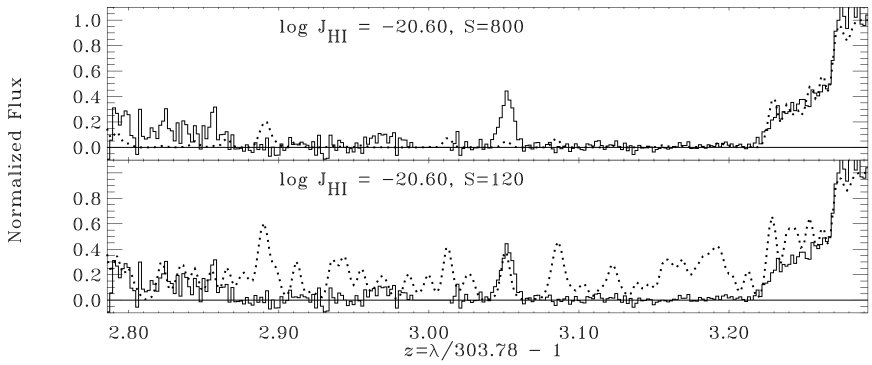

Fig. 1. Observed Spectrum of Q 0302–003 vs. Models (dashes)

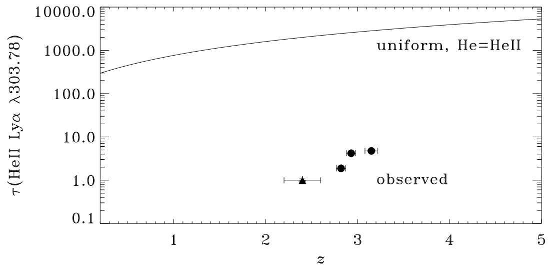

Fig. 2. Models vs. Observed Optical Depths

At redshifts $z < 2.87$, the He II Lyα opacity is significantly lower: $\bar{\tau} = 1.88$. Such a reduction in opacity is consistent with Songaila [3] report of a rapid hardening of the UV background spectrum at $z < 3$. Fig. 2 compares our measured opacities along with the measurement of Davidsen et al. [1] (1996) at $z = 2.4$ to the expected opacities for a uniform IGM in which all helium is He II. The observed He II Lyα opacities pale in comparison to what they would have been had no ionizing sources been present at $z \geq 3$. Over 99% of helium in the IGM must be fully ionized by z=3. This observation brings up the question of what kind of sources – stars or QSO's – were responsible for ionizing He^+.

2 Sources of the UV Background at $z \sim 3$

We computed model spectra for different intensities and shapes of the UV background. Fig. 1 shows two models, which are described by $J_{\rm HI}$, the intensity at the H I Lyman limit, and by the softness parameter, S, which is defined as the ratio of the H I to He II photo-ionization rates: $S \equiv \Gamma_{HI}/\Gamma_{He\,\rm II}$. The model spectrum shown in top panel assumes a rather soft UV backgound ($S \simeq 800$) characteristic of stars. The model is able to match the observations over most of the G-P region surveyed by STIS, suggesting that stars make a significant contribution to the UV background at $z \sim 3$. The model does not match the high-transmission region around $\lambda 1230$ ($z = 3.05$). As shown in the bottom panel, a hard background is required to reproduce this spectral feature. We suggest that the high transmission likely arises in a region where helium is doubly ionized by a discrete local source, quite possibly an AGN.

References

1. Davidsen, A.F., Kriss, G.A., & Zheng, W. 1996, Nature, 380, 47
2. Heap, S.R., Williger, G., Smette A., I. Hubeny, et al. 1999, ApJ in press
3. Songaila, A. 1998, AJ, 115, 2184

Part VII

A New View of the First Stars

Where Are the First Stars Now?

Simon D.M. White and Volker Springel

Max-Planck-Institute for Astrophysics, Garching bei München, Germany

Abstract. We use high-resolution simulations to show that the current standard paradigm for the growth of structure in the Universe predicts the formation of a galaxy like our own to differ substantially from the classic ELS and Searle/Zinn pictures. On scales larger than the Local Group, the earliest star formation was extremely inhomogeneous, suggesting that the high redshift intergalactic medium should have large-scale abundance variations. The very oldest stars should be found today in the central regions of rich galaxy clusters. In the Milky Way's bulge and stellar halo little correlation is expected between age and metallicity. Some of the lowest metallicity stars may be relatively young. Many of the oldest stars may have high metallicity. Spheroid stars were formed before and during halo assembly, the oldest now lying preferentially at small radii, while low metallicity stars lie preferentially at large radii. The bulk of the Milky Way's stellar spheroid came from a small number of progenitors. It should show little spatial structure in the inner 5 to 15 kpc, but consist at each point of a superposition of hundreds of 'cold' streams. Such streams have been detected in the Solar neighborhood.

1 Introduction

Over the last two decades a standard paradigm has emerged for the origin and evolution of structure in the Universe. The basic ingredients of this picture are the following.

- The Universe has expanded from a hot, dense and smooth state. This Hot Big Bang is observed directly in the CMB at an age of 300,000 years. It is checked by the Planckian nature of the CMB spectrum back to an age of a few months, and by the abundances of the light elements back to an age of a few minutes.
- The observed near-homogeneity and isotropy were produced by an early phase of inflationary expansion.
- The dominant matter component today is some unseen form of nonbaryonic, weakly interacting dark matter.
- All observed structure originated from quantum zero-point fluctuations during inflation. These produced a gaussian field of density fluctuations with a near-Harrison-Zel'dovich power spectrum showing no characteristic features on scales relevant to galaxies and larger structures.
- Present structure grew by gravitational amplification of these small initial fluctuations.
- Galaxies formed by cooling and condensation of gas in the cores of heavy halos produced by nonlinear hierarchical clustering of the dark matter.

The current "consensus" version of this model imagines a flat Universe in which baryons contribute a few percent of the closure density, cold dark matter contributes about one third, and an effective cosmological constant contributes the rest. This model is consistent with current data on the distance scale, acceleration, large-scale structure and galaxy populations of the Universe. It should be definitively tested by the next generation of CMB experiments, in particular by the MAP and Planck Surveyor satellites.

Strong points of such CDM models are that they provide fully specified initial conditions, and that the nonlinear growth of structure in the dominant component, the dark matter, can be simulated accurately on scales larger than a kiloparsec or so. Below this scale nongravitational processes undoubtedly play a major role in shaping galaxies. Recent work has grafted phenomenological modelling of gas cooling, star-formation, feedback, and stellar evolution onto high resolution N-body calculations of dark matter clustering [7]. This has made it possible to simulate cosmologically representative volumes with sufficient resolution to follow the formation and evolution of individual galaxies. Here we present preliminary results from an extension of this work to much higher resolution. We trace the detailed formation history of individual objects and of their immediate environment, showing results for a rich galaxy cluster and for a system like the Milky Way. A much more detailed account of the results for clusters will be published shortly as Springel et al (in preparation).

2 The Simulations

The simulations discussed here were carried out using a parallel tree-code called Gadget [13] on the Cray T3E at the Garching Computing Centre of the Max Planck Society. Initial conditions were taken from a ΛCDM simulation already analysed by Kauffmann and collaborators [7]. This simulation assumes $\Omega_o = 0.3$, $\Lambda = 0.7$, $h = 0.7$ and $\sigma_8 = 0.9$. The second most massive cluster ($M_{vir} = 5.6 \times 10^{14} h^{-1} M_\odot$) at $z = 0$ was placed at the origin of coordinates and a surrounding spherical region of radius $70h^{-1}$Mpc was isolated for resimulation with Gadget. The initial mass distribution between 21 and $70h^{-1}$Mpc was represented at relatively low resolution by 3×10^6 particles. In the inner region, where the original simulation had 2.2×10^5 particles, we created new initial conditions with 4.5×10^5, 2.0×10^6, 1.3×10^7 and 6.6×10^7 particles. With increasing mass resolution along this sequence we included extra initial fluctuations on scales beyond the Nyquist frequency of the original simulation, and we decreased the force softening to give improved spatial resolution. We then ran all four simulations to $z = 0$ and compared results with each other and with the original simulation. In the largest resimulation there are about 20 million particles within the virial radius of the final cluster and the gravitational softening radius is $0.7h^{-1}$kpc. This is the highest resolution simulation of a rich galaxy cluster ever carried out.

The particle data for all these simulations were dumped at intervals of 0.06 in $\ln(1+z)$. We then implemented the semianalytic galaxy formation recipes of Kauffmann et al [7] on merging trees constructed from these outputs. A major improvement is possible as a result of the increased resolution of the present simulations. The dark halos of most of the more massive galaxies remain identifiable as self-bound substructures within the cluster. In the highest resolution simulation there are almost 5000 such "galaxy halos" within the virial radius of the final cluster. By keeping track of such substructures we are able to follow the dynamical evolution of galaxies within clusters and it is no longer necessary to use semianalytic recipes to track galaxy merging. Apart from this change we follow the procedures of Kauffmann et al exactly, using their "ejection" prescription for the fate of reheated gas, and setting the parameters regulating star formation and feedback so that the observed I-band Tully-Fisher relation and cold gas fraction are reproduced for spiral galaxies outside the cluster. This requires parameter choices very similar to those used by Kauffmann et al.

3 Cluster Results

We begin by showing that our modelling of galaxy formation, although adjusted to reproduce the properties of spiral galaxies outside the cluster, also reproduces well the observed properties of the galaxy populations within clusters. The uppermost panel of Fig. 1 compares the observed Tully-Fisher relation [2] with the predicted relation for isolated Sb/Sc galaxies; the linewidth and Hubble type are defined here as in Kauffmann et al [7]. The star formation and feedback efficiencies were tuned to reproduce this relation as well as possible, but it is still striking that adjusting two parameters can produce an excellent fit to the slope and scatter of the observations. It is much more remarkable, however, that with *no* additional parameters the model produces a cluster luminosity function which is similar in normalisation and shape to observed luminosity functions, and a morphology-radius relation within the cluster which is also like that observed. Note that in contrast to earlier work, this latter success is achieved without tuning any parameter related to merging rates.

Given that this simulation produces a reasonably good fit to the galaxy populations in and around rich clusters, it is interesting to examine in detail its predictions for the history of star formation. In our highest resolution simulations the smallest resolved objects have a total mass of about $5 \times 10^8 M_\odot$, corresponding to a total initial baryon mass of $5 \times 10^7 M_\odot$ although their mass in stars is at least 10 times smaller. The latter difference arises because feedback is assumed to make star formation inefficient in low mass objects. Thus we resolve the formation of stellar systems similar in mass to large globular star clusters.

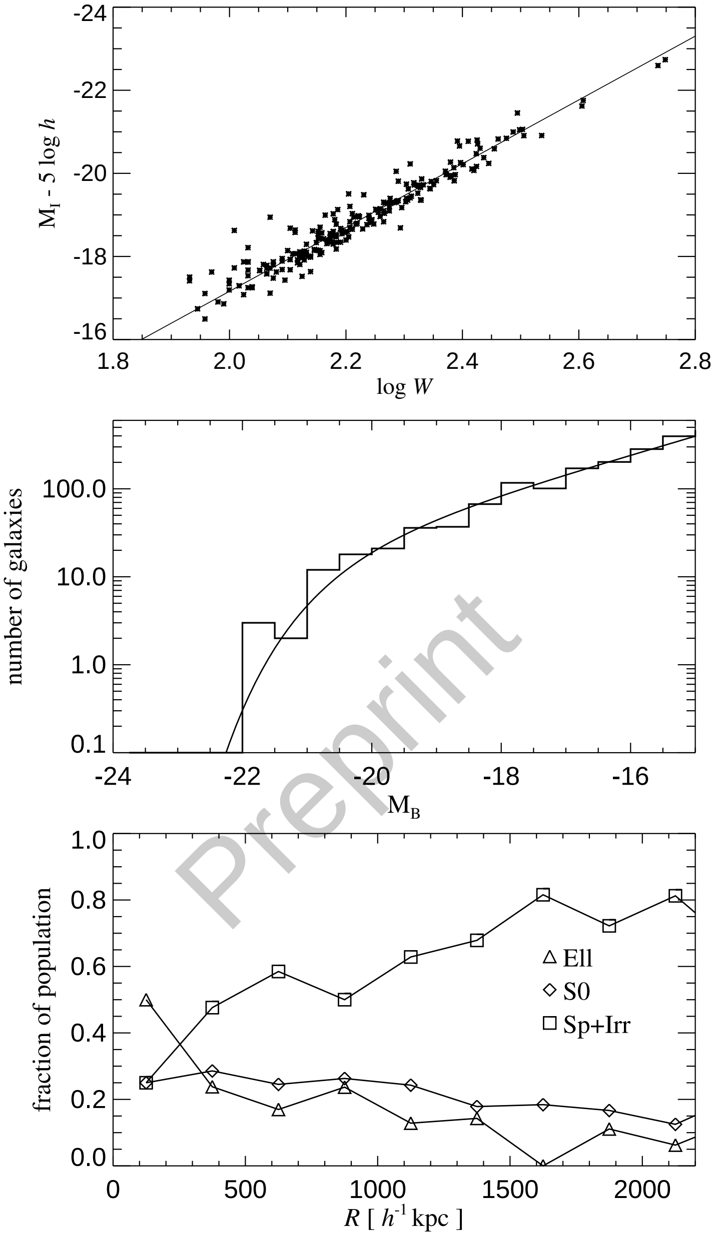

Fig. 1. *Top* I-band Tully-Fisher relation for isolated Sb/Sc galaxies outside the cluster. The straight line is the mean observed relation from [2]. *Middle* Number of galaxies within the virial radius of the cluster as a function of their absolute magnitude in the B-band. The Schechter fit shown has a faint end slope, $\alpha = -1.2$. *Bottom* Fraction of galaxies brighter than $M_B = -16.5$ in each of three morphology classes as a function of distance from cluster centre.

A first striking effect is the bias towards earlier formation for stars which end up inside the cluster. Thus half the stars which lie within the final virial radius form before $z = 4$ while half the stars outside this radius form after $z = 2$. The first 1.5% of stars in cluster galaxies have already formed by $z = 13$ while one has to wait until $z = 7.5$ to form a similar fraction of the stars outside the cluster. Note that formation is still biased in the cluster's vicinity but outside its virial radius [9]. Thus the first 1.5% of the stars in a "typical" region of the Universe would form even later.

In the upper right panel of Fig. 2 we show a projection at $z = 13$ of the galaxies in a cube of comoving side $10h^{-1}$Mpc centred on the barycentre of the material of the future cluster. The area of each symbol is proportional to the stellar mass of the galaxy. This distribution is clearly extremely inhomogeneous, with almost all the stars lying on or close to a single filament of comoving scale about $10h^{-1}$Mpc. Clearly the heavy elements produced by these "first stars" are very unlikely to be well mixed through the IGM. In the lower left panel we show where these same stars are at $z = 0$; the area of each symbol is here proportional to the mass of "first stars" which the corresponding galaxy contains. This can be compared to the plot at upper left which shows the distribution of all the stars at the end of the simulation, symbol area now corresponding to total stellar mass. Clearly the first stars are concentrated in a relatively small number of galaxies and these galaxies tend to lie close to the cluster centre. In fact, at $z = 0$ more than half of all the "first stars" lie within $100h^{-1}$kpc of cluster centre, whereas fewer than 10% of all cluster stars lie at such small radii.

Because of these strong bias effects the first stars in different regions of the Universe are predicted to form at very different times; some may still be forming today in weak structures in "voids". For many purposes it is more interesting to define the first stars not as those which formed first in time, but as those which formed from the least processed gas. In hierarchical cosmogonies the degree of processing of gas is closely related to the mass of the object in which it is found. For example, in the simulations analysed here gas which has never been part of a virialised object at all, or never part of an object with virial temperature exceeding $\sim 10^4$K, has never been associated with star formation and could plausibly have zero heavy element abundance. Such effects may be reflected in the strong observed correlation between the mean metal abundance of galaxies and their stellar mass. We illustrate the possible distribution of the "lowest metallicity" stars in the lower right panel of Fig. 2. This shows the distribution at $z = 0$ of the 1.5% of cluster stars which formed in the lowest mass dark halos. These stars are still primarily part of the lowest mass galaxies and their radial distribution within the cluster is similar to that of all the stars. Half of this subset of stars formed after $z = 3.9$, and their age distribution is very similar to that of clusters stars as a whole. Low metallicity stars in clusters are no older than the average.

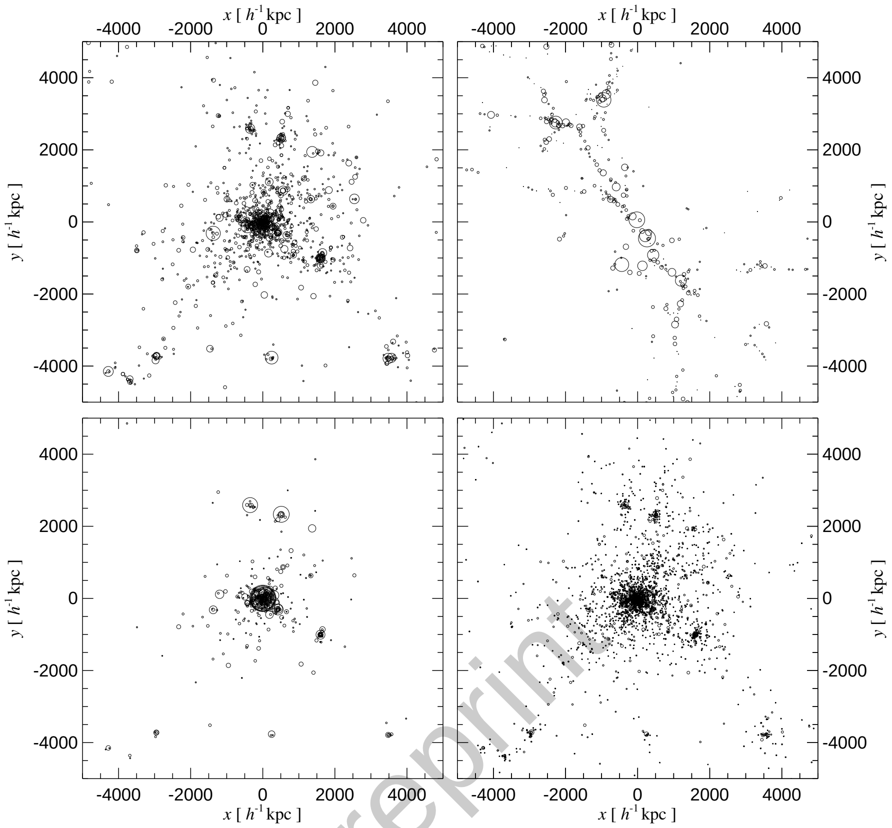

Fig. 2. Projections of the galaxy distribution in a cube of comoving side $10h^{-1}$Mpc. The upper right image is at $z = 13$ when 1.5% of the stars in final cluster have formed. The other three images are at $z = 0$. The upper images show all galaxies in the cube with symbol area proportional to stellar mass. The lower two images show only galaxies containing stars which were among either the first 1.5% (left) or the 1.5% formed in the lowest mass halos (right). In these lower images symbol size is proportional to the mass of the relevant stellar population.

4 "Milky Way" Results

Rather than running a new simulation of the assembly of a "Milky Way" halo, we here take a short cut by scaling our cluster simulations down by a factor of 7 in both size and velocity, corresponding to a factor of 343 in mass and to unchanged dynamical times. Both theoretical [8] and numerical [10] results suggest that such a scaling should give a good approximation to the dark matter evolution of a "typical" halo, except that assembly is shifted to somewhat lower redshifts. We run our semianalytic machinery on these rescaled simulations (using the same parameters as before) to obtain predictions for the star formation history within a "Milky Way" halo.

The results are illustrated in Fig. 3 which can be compared directly with Fig. 2. The shift in temperature (by a factor 49) caused by our rescaling produces large changes in cooling and feedback. Most star formation occurs at late times in the central disk. Within the final galaxy's halo about 80% of all stars are in the disk, 16% are in the bulge, and only 3% are part of other objects, more than half of those in a single satellite. Only by $z = 6.9$ has our model Milky Way made 1% of its stars. Figure 5 of ref. [11] suggests that this should be increased to $z \sim 10$ to account for the bias towards late assembly just noted. Despite the much higher effective resolution of the rescaled simulation, this redshift is still well below the 1% formation redshift of stars in the cluster of the last section.

The upper right panel of Fig. 3 shows the initial distribution of these "first" stars to be very inhomogeneous – most are in a handful of progenitor galaxies. By $z = 0$ they are quite centrally concentrated; 60% are within 10 kpc, with even older stars being even more centrally concentrated. On the other hand, if low metallicity stars are identified as those formed in the lowest mass dark halos, only 16% of the lowest metallicity 1% lie within 10 kpc, and lower metallicity stars are predicted to be even less centrally concentrated. These "low metallicity" stars have a median formation redshift of $z = 5.5$, much higher than the formation redshift of "typical" stars. Most are part of intact (60%) or disrupted (30%) dwarf satellites; only 10% are part of the central bulge. We return to these numbers in the next section.

5 Discussion

The results shown above demonstrate that if current structure formation theories are correct, the oldest stars should be found at the centres of rich clusters. Furthermore the distribution of the first stars was inhomogeneous on the (comoving) scale of *present-day* large-scale structure. As a result, enrichment of the intergalactic medium at high redshift must have been extremely patchy. If we want to find the oldest stars in the local universe we should look near the centre of M87, not in our own Galactic halo or in intergalactic space. Unfortunately they may be indistinguishable from the enormous background of slightly younger stars. On the other hand, the lowest metallicity stars (assumed here to be those that formed in the lowest mass objects) are distributed on large scales in a similar way to the general stellar population.

On smaller scale, similar effects imply that the classic monolithic collapse [1] and inhomogeneous assembly [12] pictures are of little help in interpreting the age and metallicity distribution within the Galactic bulge and halo. The oldest stars are predicted to be in the inner halo or bulge, and will be very difficult to distinguish from the dominant, somewhat younger population. Lower metallicity populations are expected to have more extended distributions, but there is no strong correlation between metallicity and age. Some

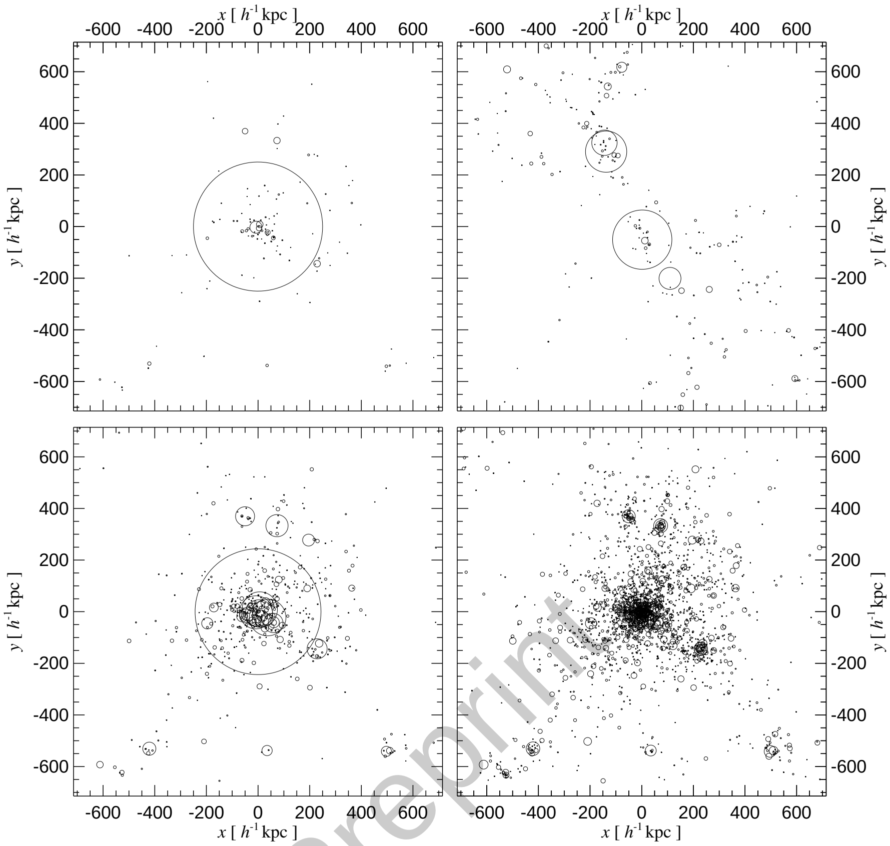

Fig. 3. Projections of the galaxy distribution in a cube of comoving side $1.4h^{-1}$ Mpc around a "Milky Way" halo. The upper right image is at $z = 5.4$ when 1% of the final stars have formed. The other three are at $z = 0$. The illustrated quantities are as in Fig. 2 except that the lower plots show the 1% "earliest" and 1% "lowest metallicity" stars.

low metallicity stars may be quite young, and indeed may continue to form today in low mass, isolated dwarf galaxies.

The rich internal structure predicted for dark matter halos in these CDM models is, as Fig. 1 demonstrates explicitly, in very satisfying agreement with the observed galaxy populations in rich clusters. Ben Moore and his collaborators [10] have emphasised that the situation is less clear for the Milky Way. Most of the low metallicity stars in our simulation are in the stellar halo rather than the bulge, but twice as many reside in satellites as in the diffuse component. In the real Galaxy more are in the diffuse halo than in satellites. This may be because the cores of many low mass halos survive undisrupted in our model, while the Milky Way can disrupt dwarfs even from relatively weakly bound orbits, as the example of Sagittarius clearly shows

[5]. It is uncertain whether this is a serious shortcoming of CDM models or may be resolved by more detailed dynamical modelling of the formation and evolution of satellites. The luminosity function we predict for satellites is *not* in obvious conflict with observation.

In our Milky Way model most of the spheroidally distributed stellar mass is contributed by the bulge of the central galaxy. As in other hierarchical models, these stars formed in the gaseous disks of a small number of relatively massive progenitors prior to or during their merger, and before the formation of the present disk [6]. The disruption of Sagittarius-like dwarfs contributes relatively few stars to the bulge.

If the stellar spheroid of the Milky Way was indeed assembled in this way, one may ask whether its current structure should retain any trace of its inhomogeneous origin. Inside the Solar circle, where most of the spheroid stars reside, orbital times are so short that the spatial distribution of debris from a 10 Gyr old merger is expected to show few sharp features. In phase-space, however, it may still occupy a small fraction of the accessible region, being confined to a kinematically cold sheet which wraps many times around the Galaxy. Such structure may be detectable with sufficiently good kinematic data; the stars in the neighborhood of any given point will not be distributed uniformly through velocity space but will be confined to a few hundred cold streams [3]. A recent analysis of the velocities of nearby metal-poor giants, based on combined ground-based and Hipparcos data, has detected two such streams in the Solar neighborhood [4]. These appear to be debris from a galaxy like Fornax or Sagittarius, destroyed roughly 10 Gyr ago. This is, perhaps, the first direct evidence for hierarchical assembly of the stellar halo.

We thank G. Tormen for help in creating initial conditions and G. Kauffmann for help in implementing semianalytic recipes.

References

1. Eggen, O. J., Lynden-Bell, D. & Sandage, A. R. 1962, ApJ, 136, 748 (ELS)
2. Giovanelli, R et al 1997, AJ, 113, 53
3. Helmi, A. & White, S. D. M. 1999, MNRAS, 307, 495
4. Helmi, A., White, S. D. M., DeZeeuw, P. T., & Zhao, H. S. 1999, Nature, 402, 53
5. Ibata, R. A., Gilmore, G. & Irwin, M. J. 1995, MNRAS, 277, 781
6. Kauffmann, G. 1996, MNRAS, 281, 487
7. Kauffmann, G., Colberg, J. G., Diaferio A. & White, S. D. M. 1999, MNRAS, 303, 188
8. Lacey, C. G. & Cole, S. 1993, MNRAS, 262, 627
9. Lemson, G. & Kauffmann, G. 1999, MNRAS, 302, 111
10. Moore, B. et al 1999, ApJ, 524, L19
11. Navarro, J. F., Frenk, C. S. & White, S. D. M. 1997, ApJ, 490, 493
12. Searle, L. & Zinn, R. 1978, ApJ, 225, 357
13. Springel, V. 1999, in preparation

Observational Constraints on the Nature of the First Stars – Final Comments

Timothy C. Beers

Department of Physics & Astronomy, Michigan State University,
E. Lansing, MI 48824 USA

Abstract. I briefly summarize a number of the astrophysical avenues of exploration which were presented in the FIRST STARS meeting. I then consider a "call to action," from the observer's point of view, which I believe will result in a much deeper understanding of the nature of the first generations of stars (possibly including Population III) to have formed in the Milky Way.

1 Introduction

Observational constraints on the nature of the first generations of stars to have formed in the Milky Way, and indeed in the Universe, have benefited enormously from a flurry of recent activity, but the picture astronomers have outlined to date remains far from complete. As is clear from the number and variety of contributions made at this conference, explorations of the history of star formation in the Galaxy are expanding their scope, both in the quantity and quality of the data which are presently being obtained. It is further evident, from the range of applications which have been discussed, that the importance of this knowledge for many areas of astrophysical research is becoming better recognized by the general astronomical community. In this brief summary, I endeavor to at least touch on a few of the areas which strike me as the most exciting in the near term, that is, those most likely to yield new results quickly. I close with an admittedly biased view of what steps must be taken next to accomplish some of the lofty goals which those at the conference have mentioned as particularly important.

2 A Brief Summary

Sitting in the audience at the conference, and perusing the many interesting posters which were on display, I was struck by the realization that, depending on ones previous exposure to the many astrophysical problems discussed, it was a non-trivial matter to separate what I would call "continuing progress" from "Great Leaps Forward" (GLF). Since space is limited I confine my remarks to a number of areas which, in my view, qualify as bona-fide GLF.

2.1 Searches for Population III

A decade ago only a handful of stars were known with metallicities close to [Fe/H] = −3.0, and perhaps a little lower, but large samples of stars with abundances below 1/1000th of the Solar value were not available. Today, thanks to the labors of many astronomers, this situation has changed dramatically ([1]; Beers, this volume, p. 3). There are now ~ 100 stars known to exhibit such extremely low abundances, and on the order of 500 stars with [Fe/H] below the metallicity of the lowest Galactic globular cluster ([Fe/H] = −2.5). To the extent that a non-detection qualifies as a GLF, the fact that NO SINGLE STAR has been identified (other than a debatable claim for the inferred metallicity of a C-enhanced binary) with abundance approaching the primordial level (for practical reasons, [Fe/H]≤ -6.0) is surely an important constraint on our picture of the FIRST STARS to have formed in the Galaxy. Plans to continue the, thus far, unsuccessful searches for Population III have been described by Christlieb et al. (this volume, p. 49), and are touched upon again below.

2.2 Kinematics of Stellar Populations

Chiba (this volume, p. 77) nicely summarizes the GLF which is taking place in this arena, with his discussion of a large sample ($N \sim 2000$) of *non-kinematically* selected metal-deficient stars in the thick disk and halo of the Milky Way, many of which now have available space motion information (see [2]). Those who have worried about the effects which kinematic bias might have on our picture of the formation and evolution of the early Galaxy can now explore a sample which is free of this particular limitation. The plot of [Fe/H] vs. eccentricity which Chiba shows (his Figure 2) serves as a clear reminder of the fallacies which can arise from biased sample selection.

The exciting discovery of a stellar debris stream comprised of relatively bright low-metallicity stars in the solar neighborhood described by White (this volume, p. 327), using data from the catalog described by Chiba, certainly qualifies as a GLF. Debris streams such as this are predicted to occur in great number if our present ideas of the heirarchical assembly of the Galaxy are correct, so it is particularly gratifying that at least one such stream is now known. Others will surely be found soon, as the database of metal-deficient stars with well-measured radial velocities, abundances, distances, and proper motions expands.

2.3 Confrontation with Numerical Modeling

Though not strictly an *observational* GLF, the continued refinement of theoretical and numerical approaches to the simulation of ever-more realistic models for the formation and evolution of galaxies has reached the point that one can usefully compare model predictions of stellar abundances, spatial distiributions, and kinematics with the wealth of observational data which is now in hand (e.g., Bekki & Chiba, p. 206; Bromm et al., p. 275; Miralda-Escude, p. 242; all this volume). One might expect that this "rush toward realism" will only accelerate in the near future.

2.4 The Ages of the First Stars

The notion that the abundance of heavy metals such as Fe, at least in some average sense, are useful predictors of the *age* of an ancient stellar population, is giving way to the more likely picture that metals trace the environment and vigor of star formation, rather than the precise point in time that it has taken place. This realization, observational aspects of which are addressed in the contributions of Fuhrmann (this volume, p. 68) and Korn & Gehren (this volume, p. 75), surely qualifies as a GLF, assuming it is true! Astronomers must seek additional, well-calibrated, estimators of stellar ages which can be applied to stars of the thick disk and halo. A number of possibilities have been mentioned, including using light elements formed by the interaction of the ISM with early Galactic cosmic rays [8], as well as the use of radioactive chronometers ([3]; Truran 1999, private communication), but further study will be required.

2.5 The Importance of CNO for the First Stars

Even a casual glance through the proceedings of this conference reveals a growing appreciation of the roles that carbon, nitrogen, and oxygen are likely to play in controlling the ultimate fate of the presumed Population III stars. Both from the theoretical (Cassisi et al., p. 111; Castellani, p. 85, both this volume; [4]; Schlattl et al., this volume, p. 117) and observational (Hill et al., this volume, p. 62; [5,6]; Ryan, this volume, p. 37) standpoints, it appears safe to say that at least the seeds of a GLF in this area may already have been planted.

3 A Call to Action – An Observer's Manifesto

In my other contribution to this volume (p. 3), I outlined several pathways to discovery (hopefully of Population III, but certainly of stars *related* to Population III) which should prove useful in the near future. Astronomers in attendance at the FIRST STARS meeting (and many others who have participated in related endeavors as members of collaborative efforts) have strong vested interest in the successful completion of the plans I suggest below. I realize that, at least for many in the likely audience of this proceedings, I am "preaching to the choir," but so be it. History suggests that the first steps toward a GLF often falter, and sometimes halt altogether, without the vocal support of people who wish to make most immediate use of the results. We are, of course, a representative subset of "those people."

I suggest the we strongly consider the following three goals as necessary, and achievable, tasks to be accomplished over the course of the next five years.

3.1 Astronomers Identify 1,000 "Bright" Stars with [Fe/H]≤ -3.0

There are those who would argue that we have already discovered enough extremely low-metallicity stars in the Galaxy, and that searches for additional members of this population should wait until we have completed exhaustive study of the existing stars. Such an assertion is not only short sighted, but demonstrably incorrect.

It has taken several decades of extensive collaborative efforts (generally with 1.5m-2m class telescopes) to identify the list of ~ 100 stars with [Fe/H] < -3.0 that are presently known. By the time this proceedings is published, many of those stars will have been subjected to intensive high-resolution spectroscopic analysis with new generation 8m-class telescopes. Two years hence ALL of these targets will have been exhausted, and new questions will have formed in the minds of astronomers which can only be addressed by expanding the sample of targets by *at least* a factor of ten. Now is the time for formulating plans to accelerate our searches for the most metal-deficient stars. In my view, this is best accomplished using 4m-class telescopes to obtain medium-resolution spectroscopic follow-up of *well-selected* candidates. Given the speed of modern spectrograph/detector combinations, a collaborative effort using four 4m telescopes could complete a reconnaissance of 10,000 or more candidates with apparent magnitudes in the range $14.5 < B < 16.5$ over a period of the next three years, and require no more than a total of 14 nights (two weeks) per year, per telescope, in the effort, for example:

$$\left[\frac{1\ \mathrm{spectrum}}{10\ \mathrm{minutess}}\right]\left[\frac{600\ \mathrm{minutes}}{\mathrm{night}}\right]\left[\frac{14\ \mathrm{nights}}{\mathrm{telescope/year}}\right][3\ \mathrm{years}]\,[4\ \mathrm{telescopes}] = 10,080\ \mathrm{stars}$$

If candidates are chosen from a survey with effective yield (EY) for stars with [Fe/H] < -3.0 exceeding 10%, we will reach our goal. In all likelihood, time would not be granted unless the EY can be demonstrated to be 25% or better, in which case we will MORE than meet our goal, perhaps sufficiently quickly that less time will be required. The first step, clearly, is to put a number of survey techniques "to the test," such as has been described by Christlieb et al. (this volume, p. 49) in their discussion of the Hamburg/ESO survey selection algorithms.

3.2 Astronomers Complete High-Resolution Spectroscopic Analysis of 1,000 stars with [Fe/H]< -2.5

The combination of 8m telescopes and sensitive UV/optical/near IR spectrographs and detectors means that high signal-to-noise spectroscopy of a star of apparent magnitude $B = 14.5 - 16.5$, at a resolving power on the order of $R = 60,000$, is achievable in no more than a few hours of integration time. This *needs* to be done for as many stars as is practical, but I would imagine at least for $\sim 1,000$ stars with [Fe/H]≤ -2.5. As is clear from the contributions of several authors at this meeting (e.g., Ryan, p. 37; Shigeyama et al., p. 183, both this volume), constraints on the nature of the first generations of stars rely as much on accurate, quantitative, estimates of the scatter in their abundances as on the identification of the general trends.

Furthermore, as one subdivides samples of metal-deficient stars into smaller and smaller "bins" (in order to test specific questions which rely on samples of stars with quite specific characteristics – e.g., the stars which [7] used to tightly constrain the behavior of lithium at very low abundances), one runs the risk of running out of a sufficient number of tracers to explore the problems of interest. I look forward to a time when it will no longer be required that each and every astronomer with a clever idea they wish to explore has to propose high-resolution study of yet another sample of $\sim 20 - 30$ low-metallicity stars (the effective limit imposed by time allocation committees for present 4m telescopes) in order to examine its validity. Small samples DO have a place in this vision – they are suitable for exploration of the *exceptional* cases, not for establishing general behaviors.

3.3 Astronomers Establish a Center for Elemental Abundance Data Analysis

Observers have already heard the grumblings from the theoreticians. Those who seek to model the chemical evolution of the Galaxy, based on the ever increasing database of spectroscopically determined elemental abundances – a database which becomes less and less manageable, let alone readily interpretable by non-specialists, over time – are in dire need of a central storehouse of this information. We, as a community, should take steps to ameliorate these well-founded concerns before the comparative trickle of elemental abundance data becomes a raging torrent. Picture a time in the near future when every spectrum taken (at least of the sort I have advocated obtaining above) will yield abundance information for $N \sim 30$, or more, important elemental species, molecules, and, in some cases, isotopes. Then multiply this by 1,000 or more stars. The prospect is daunting.

There exists no present means for *separate groups of astronomers*, let alone individuals, to sensibly deal with the multitude of issues which must be considered on the path one takes from spectrum to inferred abundances, let alone do so in a self-consistent and homogeneous manner, and present results which can be combined with those of others to form the "systematics-minimized" database we require to understand the "fossil history" of star formation in the Galaxy. It is equally as important to fully, and correctly (as best as is possible), exploit the precious information which is encoded in our spectra as it is to obtain the data in the first place.

This suggestion does *not* mean that we must compromise our personal preferences for how data might be analysed. It *does* mean that we need a central facility to develop and maintain the reduction and analysis tools which are needed to make best use of our data. It makes little sense to expend effort on obtaining the most exquisite data if it is to be subjected to "piecemeal" analysis.

Over time, as our understanding of the physics of stars improves, things change. Model atmospheres change, line lists change, temperature scales change, oscillator strengths change, estimates of surface gravity change, reference abundances change (witness the debates over the Solar abundance of Fe in recent years). How can we efficiently deal with this problem? One possibility would be the development of a web-based form, similar in structure to those which already exist in some areas of astronomy – e.g., *Vizier*, or *Skyview*, which provide ready access to far-flung catalogs of information in an organized manner – but dedicated to providing well-tested (and consistent) analysis of high-resolution spectroscopic data. At the very least, a secure "first pass" analysis of data would be obtainable in a straightforward manner, and tabulations of the changes in derived abundances which result from different input assumptions made in the analysis could be returned to the user, and passed along to the "consumer" of the information. It would then be a trivial, rather than impractical, exercise to place data from a variety of groups on a single, homogeneous system.

If this suggestion were adopted, as the database of available spectroscopic information grows the tools with which it is analysed would be kept up to date, and available to all. Such a facility would require, I would imagine, no more than one or two full time personnel to manage, but its benefits would be reaped by a large number of spectroscopists, and an even larger body of non-specialists, worldwide.

There are other goals which could be appended to this manifesto, of course, including some which might be done in parallel to the above, but if we could accomplish these first few, I believe we would be well prepared for undertaking the studies required for the next GLF in the ongoing search for evidence of Population III.

References

1. Beers, T.C. (1999a) Third Stromlo Symposium: The Galactic Halo, eds. B. Gibson, T. Axelrod, M. Putman (ASP, San Francisco), 165, p. 206
2. Beers, T.C., Chiba, M., Yoshii, Y., Platais, I., Hanson, R.B., Fuchs, B., Rossi, S. (1999b) AJ, (submitted)

3. Cowan, J.J., Pfeiffer, B., Kratz, K.-L., Thielemann, F.-K., Sneden, C., Burles, S., Tytler, D., Beers, T.C. (1999) ApJ 521, 194
4. Fujimoto, M., Aikawa, M., Iben, I., Jr. (1999) Third Stromlo Symposium: The Galactic Halo, eds. B. Gibson, T. Axelrod, M. Putman (ASP, San Francisco), 165, p. 243
5. Norris, J.E., Ryan, S.G., Beers, T.C. (1997) ApJ 488, 350
6. Rossi, S., Beers, T.C., Sneden, C. (1999) Third Stromlo Symposium: The Galactic Halo, eds. B. Gibson, T. Axelrod, M. Putman (ASP, San Francisco), 165, p. 268
7. Ryan, S.G., Norris, J.E., Beers, T.C. (1999) ApJ, 523, 654
8. Suzuki, T.K., Yoshii, Y. (2000), in preparation

The First Stars: Final Remarks

Richard B. Larson

Department of Astronomy, Yale University, New Haven, CT 06520-8101, USA

How did star formation begin in the universe? Can we make any credible predictions, and can we find any traces of the first stars? We have only recently begun to be able to address these questions in any depth, thanks to a rapidly developing understanding of the history of the universe and to increasingly powerful instruments, and our efforts to answer them have formed the subject of this stimulating first conference on "The First Stars". In these final remarks, I shall try to summarize from a theorist's perspective some of the questions that have been addressed here, and offer some brief comments on what we may have learned so far.

How did the first stars form? In the standard hot-big-bang picture, essentially no heavy elements were produced during the big bang, and the first stars must therefore have formed without any heavy elements. This changes and simplifies the physics of star formation compared with the present situation, since the important physical processes then involve only various forms of hydrogen; the cooling of the first star-forming clouds, for example, is controlled by molecular hydrogen. The thermal behavior of the first collapsing clouds is becoming relatively well understood, thanks to the work of several groups as reported here, and a general conclusion is that the first star-forming clouds must have been hotter than present-day molecular clouds by one or two orders of magnitude in temperature. This higher temperature means that thermal pressure must have been more important for early star formation than it is at the present time, and also that the Jeans mass must have been higher for similar cloud pressures or densities. Even in non-standard cosmologies, the amount of heavy elements that can be produced during the big bang is still very small, and probably too small to change the conclusion that heavy elements played no important role in the formation of the first stars.

When and where did they form? Recent progress in cosmology has narrowed the class of popular models to several variants of the standard CDM model which predict that the first collapsed structures formed at redshifts between about 20 and 50 and had masses between about 10^5 and $10^8\,\mathrm{M}_\odot$. The work reported here has mostly focused on a 'typical' case in which the first 3σ density peaks collapsed at a redshift of ~ 30 and formed bound structures with masses of the order of $10^6\,\mathrm{M}_\odot$. In this case, the first population III stars are predicted to have formed at a redshift of ~ 30 in small systems whose total masses were of the order of $10^6\,\mathrm{M}_\odot$ and whose baryonic masses were of the order of $10^5\,\mathrm{M}_\odot$. The formation of metal-free stars need not have occurred only at such high redshifts, however; lower-amplitude primordial density peaks still unenriched in heavy elements could have continued to collapse and form metal-free stars at smaller redshifts, and the formation of metal-free stars could conceivably have continued until much more recent times in the least dense and most slowly evolving 'backwaters' of the universe.

What were their typical masses? In the detailed simulations reported here, the dark matter in the first collapsing structures virializes to form small dark halos, while the baryonic matter settles into flattened configurations in which the Jeans mass is of the order of $10^3\,\mathrm{M}_\odot$. This result does not seem to depend very much on the details of the simulations, but only a few cases have been studied so far. Studies of present-day star formation suggest that the Jeans mass may play an important role in determining typical stellar masses, and the simulations reported here also suggest this, showing the formation of a small number of dense collapsing gas clumps whose typical mass is of the order of $10^3\,\mathrm{M}_\odot$. A considerable mass range for the clumps is also suggested, extending from less than $10^2\,\mathrm{M}_\odot$ to more than $10^4\,\mathrm{M}_\odot$. Little tendency is found for these clumps to fragment into smaller objects as the simulations are pushed to higher densities, in agreement with our understanding of present-day star formation which suggests that the outcome of the collapse of Jeans-mass clumps is the formation of at most a small multiple system, so it seems likely that the first stars were indeed typically very massive.

Were any low-mass population III stars formed? Fragmentation to much smaller masses can occur if some of the gas collapses into thin filaments, as indeed happens in some simulations. The fragmentation of such filaments is ultimately limited by the onset of high opacity to the cooling radiation, and in metal-free gas the lower mass limit set by opacity is comparable to the Chandrasekhar mass and somewhat above one solar mass. This is an important result because it means that no metal-free stars should remain visible today; all such stars should by now have evolved. This may explain why we now see no metal-free stars, although it is not yet clear whether we can argue the inverse, namely that the fact that we see no metal-free stars means that the first stars formed must have been exclusively massive. Similar effects may explain why we apparently see fewer than expected extremely metal-poor stars, and it will be interesting to study the effect of a finite but low metallicity on star formation to see whether there is a threshold metallicity above which significant numbers of low-mass stars can form.

What effects did they have? The apparent reionization of the universe at a redshift larger than 5 could in principle have been caused by a small number of massive population III stars formed at high redshifts, but the ionization history of the universe was probably more complex than this, and the effects of the first stars may initially have been rather local and limited by negative feedback effects. One such feedback effect might have been the dissociation of hydrogen molecules by UV radiation before most of the gas became ionized; this might have suppressed further star formation by removing the possibility of cooling by molecular hydrogen. Star formation might have picked up again when larger regions of the universe collapsed and created systems with more internal structure and densities high enough to provide self-shielding from the dissociating UV radiation. Simple predictions of ionization effects are not possible in this more complex situation, but a general expectation illustrated by numerical simulations is that the low-density parts of the universe became ionized first and that the denser regions took longer to become ionized.

How did metal enrichment begin? The first stars must also have produced the first heavy elements. Stars more massive than about $200\,\mathrm{M}_\odot$ are predicted to collapse completely to black holes, and therefore they should not contribute to heavy-element production. But stars with masses between about 100 and $200\,\mathrm{M}_\odot$ are predicted to disrupt entirely due to the pair-production instability, so stars in this mass range are plausible candidates for the first sources of heavy elements. Stars with smaller masses, perhaps between 40 and $100\,\mathrm{M}_\odot$, may again collapse to black holes and not contribute to nucleosynthesis, but still smaller stars with masses between 10 and $40\,\mathrm{M}_\odot$ may produce type II supernovae and provide a second source of heavy elements, if significant numbers of such stars were formed. It is less straightforward to understand how the heavy elements produced by these stars became mixed into the surrounding medium and incorporated into subsequent generations of stars; not until this had happened could the formation of stars of finite metallicity begin. The dispersal and mixing of heavy elements is a complex process, and it was almost certainly not as efficient as has usually been assumed in simple models of the chemical evolution of the universe; chemical enrichment may initially have been quite localized. Supernova-driven winds and galaxy mergers may have contributed to dispersing the heavy elements, but the universe may well have remained chemically very inhomogeneous up to the present time.

Where are the first stars or their products now? If the first stars typically had masses of the order of $10^3\,\mathrm{M}_\odot$, they would mostly have collapsed into black holes with masses of this order. Simulations that keep track of the locations of the first stars or their remnants show that these first condensed objects, which formed in the densest parts of the universe, typically became incorporated through successive mergers in systems of larger and larger size, and typically ended up in the inner parts of present-day large galaxies. If significant numbers of black holes with masses of 10^3 or even $10^4\,\mathrm{M}_\odot$ were present at early times in the inner parts of large galaxies, they might have played a role in the formation of the central supermassive black holes of AGNs. One of the remnants of the early population III stars might have served as a seed for building up a supermassive black hole by accretion, or many of them might have merged into a single much larger black hole because of strong gravitational drag effects in the dense environment of a forming galactic nucleus. Conceivably, most of the first stars or their remnants could have ended up in the central black holes of AGNs!

The heavy elements produced by the first stars may also have ended up mostly in the inner parts of large galaxies. Heavy-element abundances in galaxies are observed to increase towards their centers, and also to increase systematically with galactic mass. Neither of these trends is fully explained by standard models, but both might be explainable if heavy elements produced by the first stars contributed significantly to the observed abundances. The innermost parts of the largest galaxies were the first regions to make stars and heavy elements, and if the first stars formed were predominantly massive, high abundances of heavy elements could have been produced in these regions. The high metallicities of some quasars might also be explainable in this way.

Were they closely related to the oldest observed stars? The hypothetical 10^6-$M_\odot$ systems that formed the first stars probably cannot be identified with any observed systems, and they probably did not form the oldest observed stars because they would have been too short-lived and too weakly bound to retain any gas or heavy elements. The first systems capable of self-enrichment were probably larger systems formed somewhat later by the collapse of larger-scale cosmological structures. These early star-forming systems may have resembled dwarf galaxies, but they probably cannot be identified with observed dwarf galaxies like those in the Local Group since the latter objects inhabit low-density regions and are actually relatively young systems, being dominated in many cases by stars of intermediate age. Thus the observed dwarfs may have been 'stragglers' that formed relatively late in low-density regions of the universe, and not the birthplaces of the first stars. Globular clusters, another once-popular candidate for the sites of the first star formation, are almost certainly not primordial self-enriched objects, since their internal chemical homogeneity cannot be explained without very contrived assumptions unless they were formed in larger pre-existing systems that provided an environment for chemical enrichment and mixing to take place.

How did the first observed stars form? A notable property of the dwarf galaxies in the Local Group is that they appear to have a minimum mass of about $2 \times 10^7\ M_\odot$, regardless of how faint or metal-poor they may be. This may be the minimum mass that a galaxy needs to retain gas and heavy elements, and thus to allow continuing star formation and self-enrichment to occur. In fact, this mass is about the minimum required for a galaxy to bind ionized gas at a temperature of 10^4 K; retaining ionized gas is necessary to sustain star formation and chemical enrichment because massive stars quickly ionize the surrounding medium as soon as they form, and the interstellar gas in a typical galaxy goes through many cycles of ionization and recombination before being incorporated into stars. This cycling process also plays an important role in chemical enrichment, since the heavy elements produced by supernovae are probably dispersed and mixed mainly in an ionized medium.

Many complex astrophysical processes must therefore have occurred prior to the formation of the first observed stars, and star-forming systems at least as massive as present-day dwarf galaxies may have been required. These early star-forming systems might also have been the birthplaces of the first globular clusters. However, nearly all of them would by now have been destroyed by being merged into larger galaxies, and the globular clusters may be their only surviving remnants.

What can we learn from element abundances? Much attention has been given at this meeting to chemical abundances in old stars, but this subject has many intricacies, and their implications for our understanding of early star formation and galaxy evolution are not yet very clear. Some of the abundance patterns in very metal-poor stars seem compatible with element synthesis in predominantly massive stars, and this might be consistent with enrichment by an initial metal-free population consisting mostly of massive stars; however, the origin of the heavy elements in these very metal-poor stars cannot yet be identified with certainty.

We are just beginning, in any case, to appreciate the true complexity of the chemical enrichment of galaxies and the universe. Clearly it is completely misleading to imagine that heavy-element abundances are correlated in any simple way with time and can be used as a clock; instead, it is clear that the densest parts of the universe and of individual galaxies evolved more rapidly and became chemically enriched much earlier than the less dense regions. The universe must therefore have evolved in a chemically highly inhomogeneous way; "old" and "metal-poor" are not synonymous. Even in the solar neighborhood in our own Galaxy, chemical enrichment must have been a very non-uniform process, since the metallicities of nearby stars and clusters show a large scatter and only a weak trend, if any, with age. All of the standard models of chemical evolution fail badly to account for these observations, and we need to go back to the drawing board with these models because our present understanding of this subject is still primitive.

So, much has been learned, but much remains to be done. It is an encouraging sign of progress that we have even been able to make a start in answering some of the questions mentioned above. Let us look forward to many more fruitful meetings as we continue the quest to understand the first stars.

List of Participants*

Name	Affiliation and E-Mail
Tom Abel	MPA tabel@cfa.harvard.edu
Yann Alibert	CRAL-ENS yalibert@ens-lyon.fr
Christine Allen [P]	Instituto de Astronomia, UNAM, Mexico allen@venus.astroscu.unam.mx
Johannes Andersen	Astronomical Obs., Copenhagen University ja@astro.ku.dk
Dominik Argast [C]	Astronomisches Institut der Universität Basel argast@astro.unibas.ch
Isabelle Baraffe	Ecole Normale Superieure ibaraffe@ens-lyon.fr
Thomas Beckert [P]	Center for Astrophysics tbeckert@cfa.harvard.edu
Timothy Beers [R,S]	Michigan State University beers@pa.msu.edu
Dominik Bomans	Ruhr-Univ. Bochum bomans@astro.ruhr-uni-bochum.de
Volker Bromm [P]	Yale University, Dept. of Astronomy volker@astro.yale.edu
Margaret Burbidge	University of California, San Diego mburbidge@ucsd.edu
Fillipina Caputo	Osservatorio Astronomico di Roma, Monteporzio caputo@coma.mporzio.astro.it
Santi Cassisi [C,P]	Osservatorio Astronomico Teramo cassisi@astrte.te.astro.it
Vittorio Castellani [R]	Physics Dept., University of Pisa vittorio@astr18pi.difi.unipi.it
Tzu Chia	MPA chia@mpa-garching.mpg.de
Masashi Chiba [T]	National Astronomical Observatory of Japan chibams@gala.mtk.nao.ac.jp
Cesare Chiosi [R]	Dept. of Astronomy, Univ. of Padova chiosi@pd.astro.it

* The letters in square brackets indicate whether the participant gave a [C]ontributed, [T]argetted [R]eview, or [S]ummary talk, or contributed a [P]oster paper.

Norbert Christlieb [P]	Hamburger Sternwarte `nchristlieb@hs.uni-hamburg.de`
Paolo Cojazzi	University of Padova `cojazzi@pd.astro.it`
Thierry Contini	ESO `tcontini@eso.org`
Paolo S. Coppi	Yale University, Dept. of Astronomy `coppi@astro.yale.edu`
Stefano Cristiani	ESO/ECF `scristia@eso.org`
Antonaldo Diaferio	MPA `diaferio@mpa-garching.mpg.de`
Wolfgang Duschl	Inst. für Theoretische Astrophysik, Heidelberg `wjd@ita.uni-heidelberg.de`
Andrea Ferrara [C]	Osservatorio Astrofisico Arcetri `ferrara@arcetri.astro.it`
Patrick François	ESO `fpatrick@eso.org`
Katherine Freese [C]	University of Michigan `ktfreese@umich.edu`
Klaus Fuhrmann [T]	Universitäts-Sternwarte München `fuhrmann@usm.uni-muenchen.de`
Thomas Gehren	Universitäts-Sternwarte München `gehren@usm.uni-muenchen.de`
Sergio Gelato	University of Durham `Sergio.Gelato@Durham.ac.uk`
Leo Girardi	Dept. of Astronomy, Univ. of Padova `lgirardi@pd.astro.it`
Ami Glasner	The Hebrew University Jerusalem `ami@saba.fiz.huji.ac.il`
Simon Glover [P]	Inst. for Astronomy, Univ. of Edinburgh `scog@roe.ac.uk`
Nick Gnedin [T]	University of Colorado - Boulder `gnedin@casa.colorado.edu`
Martin Groenewegen	MPA `groen@mpa-garching.mpg.de`
Martin Haehnelt	MPA `haehnelt@mpa-garching.mpg.de`
Zoltan Haiman [C]	Fermilab `zoltan@astro.princeton.edu`
Sara R. Heap [P]	NASA/Goddard Space Flight Center `heap@srh.gsfc.nasa.gov`

Alexander Heger [C]	UCO/Lick, Univ. of California at Santa Cruz `alex@ucolick.org`
Miguel Angel Herrera	Instituto de Astronomia, UNAM `mike@astroscu.unam.mx`
Vanessa Hill [T]	ESO `vhill@eso.org`
Matthias Hoeft	TU-Berlin `hoeft@kalium.physik.tu-berlin.de`
Ulrich Hopp	Universitäts-Sternwarte München `hopp@usm.uni-muenchen.de`
Ivan Hubeny [P]	NASA Goddard Space Flight Center `hubeny@tlusty.gsfc.nasa.gov`
Yasufumi Ikeda	Hokkaidou Univ. Dept. of Phys. `ikeda@phys.hokudai.ac.jp`
Yuhri Ishimaru [C]	Inst. of Astronomy, Univ. of Tokyo `ishimaru@mtk.ioa.s.u-tokyo.ac.jp`
Garik Israelian [C]	Instituto de Astrofisica de Canarias `gil@ll.iac.es`
Yuri Izotov [P]	Main Astronomical Observatory, Ukraine `izotov@mao.kiev.ua`
Hannah Jang-Condell	Harvard University `hjang@cfa.harvard.edu`
Karsten Jedamzik [C]	MPA `jedamzik@mpa-garching.mpg.de`
Emmanuel Jehin [P]	Universite de Liege `jehin@astro.ulg.ac.be`
Tae-Sun Kim	Institute for Astronomy (ESO) `tsk@ilya.ifa.hawaii.edu`
Andreas Korn [P]	Universitäts-Sternwarte München `akorn@usm.uni-muenchen.de`
Rolf-Peter Kudritzki [T]	Universitäts-Sternwarte München `kudritzki@usm.uni-muenchen.de`
Miriam E. Rengel Lamus	CIDA, Venezuela `mrengel@cida.ve`
Richard B. Larson [S]	Yale University, Dept. of Astronomy `larson@astro.yale.edu`
Francesco Lucchin	Astronomy Dept., University of Padova `lucchin@pd.astro.it`
Paola Marigo [P]	Dept. of Astronomy, Univ. of Padova `marigo@pd.astro.it`
Simone Marri	MPA `marri@mpa-garching.mpg.de`

Mario Mateo [R]	University of Michigan `mateo@astro.lsa.umich.edu`
Helmut Meusinger [P]	Thüringer Landessternwarte Tautenburg `meus@tls-tautenburg.de`
Friedrich Meyer	MPA `frm@mpa-garching.mpg.de`
Jordi Miralda-Escude [C]	University of Pennsylvania `jordi@llull.physics.upenn.edu`
Houjun Mo	MPA `hom@mpa-garching.mpg.de`
Palle Moller	ESO `pmoller@eso.org`
Fumitaka Nakamura [C]	Niigata University, Japan `fnakamur@ed.niigata-u.ac.jp`
Emma Nasi	Univ. Astronomical Observatory, Padova `nasi@pd.astro.it`
Ryoichi Nishi [C]	Physics Dept., Kyoto University `nishi@tap.scphys.kyoto-u.ac.jp`
Ken'ichi Nomoto [R]	University of Tokyo `nomoto@astron.s.u-tokyo.ac.jp`
Birgitta Nordström [P]	Niels Bohr Inst. for Astr., Phys., & Geophys. `birgitta@astro.ku.dk`
Michael Norman [R]	NCSA, University of Illinois `norman@ncsa.uiuc.edu`
Kaz Omukai [P]	Dept. of Physics, Kyoto University `omukai@tap.scphys.kyoto-u.ac.jp`
Francesco Palla [R]	Osservatorio Astrofisico di Arcetri `palla@arcetri.astro.it`
Ornella Pantano [P]	Physics Dept., University of Padova `pantano@pd.infn.it`
Genevieve Parmentier [C]	Institute of Astrophys. & Geophys. of Liege `g.parmentier@ulg.ac.be`
Max Pettini [R]	Institute of Astronomy, Cambridge `pettini@ast.cam.ac.uk`
Bernd Pfeiffer [P]	Institut fuer Kernchemie, Univ. Mainz `pfeiffer@vkcmzd.chemie.uni-mainz.de`
Leonid Pilyugin [C]	Main Astronomical Observatory, Ukraine `pilyugin@mao.kiev.ua`
Tomasz Plewa	Copernicus Astronomical Center, Poland `tomek@mpa-garching.mpg.de`
Laura Portinari [C]	Dept. of Astronomy, Univ. of Padova `portinari@pd.astro.it`

Francesca Primas [C]	ESO `fprimas@eso.org`
Michael Rauch	ESO `mr@eso.org`
Luisa Rebull [P]	University of Chicago `rebull@boron.uchicago.edu`
Johannes Reetz	Universitäts-Sternwarte München `reetz@usm.uni-muenchen.de`
Alvio Renzini	ESO `arenzini@eso.org`
Emanuele Ripamonti	Universita di Milano `emanuele@merate.mi.astro.it`
Martino Romaniello	ESO `mromanie@eso.org`
Sean Ryan [R]	Institute of Astronomy, Cambridge `sgr@ast.cam.ac.uk`
Maurizio Salaris	John Moores University, Liverpool `ms@staru1.livjm.ac.uk`
Tiziana Sarrubbi	University of Padova `sarrubbi@pd.astro.it`
Helmut Schlattl	MPA `schlattl@MPA-Garching.MPG.DE`
Regina Schulte-Ladbeck [C]	University of Pittsburgh `rsl@phyast.pitt.edu`
Peter Shaver	ESO `pshaver@eso.org`
Toshikazu Shigeyama [P]	Dept. of Astronomy, Univ. of Tokyo `shigeyama@astron.s.u-tokyo.ac.jp`
François Spite [R]	Observatoire de Paris `Francois.Spite@obspm.fr`
Christian Straka	Inst. für Theoretische Astrophysik, Heidelberg `cstraka@ita.uni-heidelberg.de`
Eline Tolstoy	ESO `etolstoy@eso.org`
Jim Truran [C]	University of Chicago `truran@nova.uchicago.edu`
Takuji Tsujimoto [P]	National Astronomical Observatory, Japan `taku.tsujimoto@nao.ac.jp`
Toru, Tsuribe [P]	Dept. of Physics, Kyoto University `tsuribe@tap.scphys.kyoto-u.ac.jp`
Jason Tumlinson [P]	University of Colorado, Boulder `tumlinso@casa.colorado.edu`

Hideya Uehara [P]	National Astronomical Observatory, Japan uehara@th.nao.ac.jp
Hideyuki Umeda [C]	Univ. of Tokyo umeda@iron.astron.s.u-tokyo.ac.jp
Shinya Wanajo [P]	National Astronomical Observatory, Japan shinya.wanajo@nao.ac.jp
Kerstin Weis	Inst. für Theoretische Astrophysik, Heidelberg kweis@ita.uni-heidelberg.de
Achim Weiss [P]	MPA weiss@mpa-garching.mpg.de
Simon White [R]	MPA swhite@mpa-garching.mpg.de
Gerard Williger [P]	NASA Goddard Space Flight Ctr. williger@tejut.gsfc.nasa.gov
Naoki Yoshida	MPA naoki@mpa-garching.mpg.de
Simone Zaggia	ESO szaggia@eso.org
Gang Zhao [P]	Beijing Astronomical Observatory zg@orion.bao.ac.cn
Houri Ziaeepour	ESO houri@eso.org

Author Index